
Evaluation of Hypotheses for the Cause of the 1886 Charleston Earthquake

Final Report

Prepared by R. M. White/LEI
L. T. Long/GIT

Law Environmental, Inc.

Georgia Institute of Technology

Prepared for
U.S. Nuclear Regulatory Commission

8911080428 891031
PDR NUREG
CR-5269 R PDR

AVAILABILITY NOTICE

Availability of Reference Materials Cited in NRC Publications

Most documents cited in NRC publications will be available from one of the following sources:

1. The NRC Public Document Room, 2120 J Street, NW, Lower Level, Washington, DC 20555
2. The Superintendent of Documents, U.S. Government Printing Office, P.O. Box 37082, Washington, DC 20013-7082
3. The National Technical Information Service, Springfield, VA 22161

Although the listing that follows represents the majority of documents cited in NRC publications, it is not intended to be exhaustive.

Referenced documents available for inspection and copying for a fee from the NRC Public Document Room include NRC correspondence and internal NRC memoranda; NRC Office of Inspection and Enforcement bulletins, circulars, information notices, inspection and investigation notices; Licensee Event Reports; vendor reports and correspondence; Commission papers; and applicant and licensee documents and correspondence.

The following documents in the NUREG series are available for purchase from the GPO Sales Program: formal NRC staff and contractor reports, NRC-sponsored conference proceedings, and NRC booklets and brochures. Also available are Regulatory Guides, NRC regulations in the *Code of Federal Regulations*, and *Nuclear Regulatory Commission Issuances*.

Documents available from the National Technical Information Service include NUREG series reports and technical reports prepared by other federal agencies and reports prepared by the Atomic Energy Commission, forerunner agency to the Nuclear Regulatory Commission.

Documents available from public and special technical libraries include all open literature items, such as books, journal and periodical articles, and transactions. *Federal Register* notices, federal and state legislation, and congressional reports can usually be obtained from these libraries.

Documents such as theses, dissertations, foreign reports and translations, and non-NRC conference proceedings are available for purchase from the organization sponsoring the publication cited.

Single copies of NRC draft reports are available free, to the extent of supply, upon written request to the Office of Information Resources Management, Distribution Section, U.S. Nuclear Regulatory Commission, Washington, DC 20555.

Copies of industry codes and standards used in a substantive manner in the NRC regulatory process are maintained at the NRC Library, 7920 Norfolk Avenue, Bethesda, Maryland, and are available there for reference use by the public. Codes and standards are usually copyrighted and may be purchased from the originating organization or, if they are American National Standards, from the American National Standards Institute, 1430 Broadway, New York, NY 10018.

DISCLAIMER NOTICE

This report was prepared as an account of work sponsored by an agency of the United States Government. Neither the United States Government nor any agency thereof, or any of their employees, makes any warranty, expressed or implied, or assumes any legal liability of responsibility for any third party's use, or the results of such use, of any information, apparatus, product or process disclosed in this report, or represents that its use by such third party would not infringe privately owned rights.

Evaluation of Hypotheses for the Cause of the 1886 Charleston Earthquake

Final Report

Manuscript Completed: May 1989
Date Published: October 1989

Prepared by
R. M. White, Law Environmental, Inc.
L. T. Long, Georgia Institute of Technology

Law Environmental, Inc.
112 Townpark Drive
Kennesaw, GA 30144

Subcontractor:
Georgia Institute of Technology
Atlanta, GA 30332

Prepared for
Division of Engineering
Office of Nuclear Regulatory Research
U.S. Nuclear Regulatory Commission
Washington, DC 20555
NRC FIN B8291
NRC Contract No. NRC-04-85-112

ABSTRACT

This report describes a geophysical/geological investigation of the earth's crust at seismogenic depths in the Charleston, South Carolina, area. This investigation was made for the purpose of narrowing the range of theories that have been used to explain the historic 1886 Charleston earthquake (Modified Mercalli Intensity $I_0 = X$). Since a number of these theories are based on only a portion of the available data, we have established a comprehensive data set in order to allow these hypotheses to be subjected to the entire data set.

Specifically, we combined existing and new gravity, magnetic and topographic data in grids of 128 km, 256 km and 1028 km on a side centered on Charleston. Seismic, geologic and drilling data were collected and summarized. A magnetotelluric survey consisting of 12 soundings interpreted to depths of over 40 kilometers defined the bottom of the rigid crust with assistance from seismic reflection and other data.

A geologic model of the crust in the area of Charleston was constructed and it defined the locations of Triassic/Jurassic basins and Paleozoic plutons in greater detail than has previously been achieved.

Three-dimensional regional crustal stress modeling used topographic and density variability as stress sources and also included horizontal stresses due to plate spreading at the mid-Atlantic ridge. The modeling was performed over a 1028 x 1028 km region and implied ordinary stress conditions in the Charleston area.

Two-dimensional local stress modeling used the geologic model as input and showed stress amplification related to: variability of the depth to the base of the rigid crust, Triassic/Jurassic basins, and mafic intrusives (although the stress amplification due to the intrusives is not great).

Finally, the comprehensive data set, together with the results of the geologic and stress modeling, were used to evaluate hypotheses as to Charleston's seismicity. The results of this study strongly support the intersections of Mesozoic Basin border faults, whose locations may have been controlled by the presence of rigid Paleozoic mafic plutons, as the most likely location for Charleston-type earthquakes. The study infers that the spatial association of seismicity with plutons in the Charleston area may be due to the plutons' role in controlling the location of faults rather than due to stress amplification. This study showed evidence for significant change in thickness of the rigid crust, which may also limit possible locations for 1886 Charleston-size earthquakes to areas of thicker rigid crust.

TABLE OF CONTENTS

	<u>Page Number</u>
ABSTRACT	iii
LIST OF FIGURES	ix
ACKNOWLEDGEMENTS	
EXECUTIVE SUMMARY	1
1. INTRODUCTION	5
2. HYPOTHESES FOR CAUSES OF THE 1886 CHARLESTON, SOUTH CAROLINA EARTHQUAKE	8
2.1 Introduction	8
2.2 Crustal Stress and Rheology	8
2.2.1 Crustal Stress	8
2.2.2 Rheological Properties of Continental Crust	8
2.3 Hypotheses	9
2.3.1 Hypotheses Associated with Faults	11
2.3.1.1 Reactivation of Horizontal (or Decollement) Faults	11
2.3.1.2 Reactivation of Northeast- Striking Near-Vertical Faults	12
2.3.1.3 Reactivation of Mesozoic Basin Border Faults	14
2.3.1.4 Reactivation of Northwest- Striking Near-Vertical Faults	14
2.3.1.5 Faults Associated with Base- ment Province Boundaries	16
2.3.1.6 Ductile Shear Zone (Lower Crust)	16
2.3.1.7 Intersecting Structural Trends	16
2.3.2 Hypotheses Concerning Structures Other Than Faults	17
2.3.2.1 Topographic and Density Anomaly Loads	17
2.3.2.2 Brunswick Suspect Terrane	17
2.3.2.3 Stress Amplification Near Plutons	18

3.	PROJECT APPROACH	26
4.	GEOPHYSICAL AND GEOLOGICAL DATA	28
4.1	Gridded Data	28
4.1.1	Grid Definitions and Data Consolidation	28
4.1.2	Gravity	37
4.1.2.1	EPRI Gravity Data	37
4.1.2.2	Merging and Compilation of Data	38
4.1.2.3	Acquisition of New Gravity Data	39
4.1.2.4	Image Processing of Gravity and Magnetic Data	39
4.1.3	Magnetic Data	40
4.1.4	Geodetic Data	40
4.1.5	Availability of Gridded Data	41
4.1.6	Satellite Imagery	41
4.2	Magnetotelluric Soundings	41
4.2.1	Introduction	41
4.2.2	Principles of the Magnetotelluric Method	42
4.2.3	Magnetotelluric Data	46
4.2.4	Modeling Results	46
4.2.4.1	One-Dimensional Modeling	47
4.2.4.2	Two-Dimensional Modeling	54
4.3	Seismic Refraction and Reflection Studies	63
4.4	Geologic Data	65
5.	GEOLOGIC MODEL	73
5.1	Current State of Knowledge	73
5.2	Modeling Approach	73
5.3	Modeling Process	85
5.4	Results	98
6.	REGIONAL CRUSTAL STRESS	112
6.1	Introduction	112
6.2	Current State of Crustal Stress Knowledge	112
6.2.1	Regional Stress Data	112
6.2.1.1	In-Situ Stress Measurements	112
6.2.1.2	Earthquake Focal Mechanisms	113

6.2.2	Sources of Crustal Stress	113
6.2.2.1	Renewable Crustal Stresses	113
6.2.2.2	Non-Renewable Crustal Stresses	114
6.2.3	Rheological Properties of Continental Crust	115
6.2.4	Interpreted Regional Stress	115
6.3	Theory of Three-Dimensional Stress Modeling	116
6.4	Application of the Regional Stress Model to the Charleston Area	119
6.5	Modeling Results	122
7.	LOCAL STRESS MODELING	130
7.1	Theory of Two-Dimensional Stress Modeling	130
7.2	Elastic Properties of Crustal Rock	132
7.3	Modeling Results	142
8.	HYPOTHESIS TESTING	147
8.1	Considerations in Hypothesis Testing	147
8.2	Testing Hypotheses for Causes of the 1886 Charleston, S.C. Earthquake	147
8.2.1	Reactivation of Horizontal (or Decollement) Faults	147
8.2.2	Reactivation of Mesozoic Basin Border Faults	148
8.2.3	High Angle Faults not Associated with Mesozoic Basins	148
8.2.4	Intersecting Structural Trends	150
8.2.5	Faults Associated with Basement Province Boundaries	150
8.2.6	Ductile Shear Zones in the Lower Crust	151
8.2.7	Brunswick Suspect Terrane	151
8.2.8	Topographic and Density Anomaly Loads	151
8.2.9	Stress Amplification Near Plutons	152
8.3	Conclusion	154
BIBLIOGRAPHY.....		159

APPENDIX A: POTENTIAL DATA ACQUISITION AND ANALYSIS

CONTENTS.....	A-i
LIST OF FIGURES.....	A-ii
ABSTRACT.....	A-iii
1. DOCUMENTATION OF CHARLESTON AREA DATA SETS AND COMPUTER PROGRAMS.....	A-1-1
2. PRINCIPAL FACTS FOR CHARLESTON AREA GRAVITY.....	A-2-1
3. DEFINITION OF DATA GRIDS FOR CHARLESTON STUDY.....	A-3-1
4. DETAILS OF MAGNETIC ANOMALY MAP.....	A-4-1
5. BIBLIOGRAPHY.....	A-5-1
6. PROGRAM LISTINGS.....	A-6-1

APPENDIX B-1: MAGNETOTELLURIC SOUNDINGS NEAR CHARLESTON,
SOUTH CAROLINA, VOLUME I METHOD

LIST OF FIGURES.....	B-1-iii
LIST OF TABLES.....	B-1-iii
CHAPTER 1.	B-1-1
CHAPTER 2.	B-1-3
CHAPTER 3. INSTRUMENTATION.....	B-1-28
CHAPTER 4. CALIBRATION AND VERIFICATION OF PROPER SYSTEM OPERATION.....	B-1-31
CHAPTER 5. FINAL PLOTS AND TABLES.....	B-1-39
CHAPTER 6. CHARLESTON, SOUTH CAROLINA FIELD AREA.....	B-1-52
ACKNOWLEDGEMENTS.....	B-1-54
REFERENCES.....	B-1-55

APPENDIX B-2:	MAGNETOTELLURIC SOUNDINGS NEAR CHARLESTON, SOUTH CAROLINA, VOLUME II: SOUNDINGS (Available on request, see P. 41)	
APPENDIX B-3:	MAGNETOTELLURIC SOUNDINGS IN THE CHARLESTON, SOUTH CAROLINA AREA.....	B-3-1
APPENDIX B-4:	TWO-DIMENSIONAL MAGNETOTELLURIC MODELS OF THE CHARLESTON, SOUTH CAROLINA DATA SET..	B-4-1
APPENDIX C:		
ACKNOWLEDGEMENTS.....		C-i
LIST OF TABLES.....		C-iv
LIST OF ILLUSTRATIONS.....		C-v
SUMMARY.....		C-xi
CHAPTER		
I. INTRODUCTION.....		C-1
II. PHYSICAL MODEL AND MATHEMATICAL EQUATIONS.....		C-8
III. CRUSTAL STRUCTURES OF THE SOUTHEASTERN UNITED STATES.....		C-23
IV. SEISMICITY AND STRESS OF THE SOUTHEASTERN UNITED STATES.....		C-28
V. COMPUTED STRESS FIELD.....		C-33
VI. CONCLUSIONS AND DISCUSSIONS.....		C-44
FIGURES.....		C-48
BIBLIOGRAPHY.....		C-89

LIST OF FIGURES

Figure 2-1.	Meizoseismal area of 1886 Charleston earthquake and recent earthquake epicenters near Charleston, South Carolina.	10
Figure 2-2.	Faults interpreted to be associated with the Charleston, South Carolina earthquake zone.	13
Figure 2-3.	Exposed and inferred Mesozoic Basins (from earlier studies), and Brunswick suspect terrane (from Wheeler and Bollinger, 1984).	15
Figure 4-1.	Location of grid points relative to sample area. The sample area consists of nine grid points.	30
Figure 4-2.	Relative locations of rotated reference axes.	30
Figure 4-3.	Location of data grids. See Tables 4-1 and 4-2 for grid sizes and corner coordinates.	34
Figure 4-4.	Relative location of grid points.	36
Figure 4-5.	Locations of Magnetotelluric Stations. See Table 4-3 for station coordinates.	43
Figure 4-6.	Example plot of apparent resistivities and frequencies for magnetotelluric station ANW. See Appendix B for explanations and other data.	45
Figure 4-7.	Apparent resistivity curves for all sites. The upper curve at each site is R_{ho-max} (solid line) and the lower curve is R_{ho-min} . Each curve is in its correct geographical position. The scale of all the curves is identical and is presented for the upper left curve only. (Taken from Young, <u>et al.</u> , 1986).	48
Figure 4-8.	The boundary of the step offset in the bottom of the resistive layer from one-dimensional MT interpretations. The locations of selected earthquake epicenters are shown. Also shown are the locations of COCORP seismic reflection lines.	49
Figure 4-9.	Impedance ellipses at each site. Data from 85 sec and 455 sec are shown at each site, as indicated in the upper left. The solid line indicates the on-diagonal MT impedance tensor, Z_{xy} , as a function of rotation angle and the dashed line indicates the off-diagonal element Z_{xx} . (Taken from Young, <u>et al.</u> , 1986).	51

- Figure 4-10. Magnetic field transfer functions for 85 sec. The directions are plotted with the directions reversed according to convention and thus should point towards conductors. The dots indicate station locations. The solid lines indicate the real component of magnetic transfer function and the dashed line (shorter) indicates the imaginary component. Data for station CHS is ten times larger than the graphical value. (Taken from Young, et al., 1986). 52
- Figure 4-11. Geophysical cross sections from one-dimensional MT modeling of effective impedance at each station (triangle). The layers are labeled with their interpreted resistivity in ohm-m. The cross section locations can be seen in Figure 4-8. The approximate hypocenters are from Tarr (1977). (Taken from Young, et al., 1986). 53
- Figure 4-12. Two-dimensional solution I for the Charleston MT data. This cross section crosses Figure 4-13. See Figure 4-16 for locations. The numbers are interpreted resistivity in ohm-m. The stations are shown as inverted triangles. 55
- Figure 4-13. Two-dimensional solution I for the Charleston MT data. See Figure 4-16 for locations. The numbers are interpreted resistivity in ohm-m. The stations are shown as inverted triangles. 56
- Figure 4-14. Two-dimensional solution II for the Charleston MT data. This cross section crosses Figure 4-15. See Figure 4-16 for locations. The numbers are interpreted resistivity in ohm-m. The stations are shown as inverted triangles. 57
- Figure 4-15. Two-dimensional solution II for the Charleston MT data. See Figure 4-16 for locations. The numbers are interpreted resistivity in ohm-m. The stations are shown as inverted triangles. 58
- Figure 4-16. Location of two-dimensional magnetotelluric solutions (Figures 4-12 through 4-15). 59
- Figure 4-17. Comparison of MT model to COCORP profile (Schilt, et al., 1983). The shading of the top represents shallow conductive material. The bold line represents the boundary between resistive and conductive rocks at depth. The station locations are shown by triangles at the top. The location of the COCORP lines are shown in Figure 4-20. 60

Figure 4-18.	Comparison of MT model to COCORP profile (Schilt, <u>et al.</u> , 1983). The shading of the top represents shallow conductive material. The bold line represents the boundary between resistive and conductive rocks at depth. The station locations are shown by triangles at the top. The location of the COCORP lines are shown in Figure 4-20.	61
Figure 4-19.	Comparison of MT model to COCORP profile (Schilt, <u>et al.</u> , 1983). The shading of the top represents shallow conductive material. The bold line represents the boundary between resistive and conductive rocks at depth. The location of the COCORP lines are shown in Figure 4-20.	62
Figure 4-20.	Location of seismic reflection lines near Charleston, South Carolina.	64
Figure 4-21.	Location of boreholes which provided information for modeling. USGS deep boreholes at Clubhouse Crossroads are labeled CC1, CC2 and CC3.	66
Figure 5-1.	Image of Bouguer gravity anomaly field, 1 km grid. Higher values appear lighter, lower values appear darker.	75
Figure 5-2.	Image of vertical second derivative of Bouguer gravity data.	76
Figure 5-3.	Image combining Bouguer gravity field and vertical second derivative (Figures 5-1 and 5-2).	77
Figure 5-4.	Shaded-relief image of Bouguer gravity data. Source of illumination is to north.	78
Figure 5-5.	Shaded relief image of Bouguer gravity data. Source of illumination is to east.	79
Figure 5-6.	Image of magnetic-anomaly data, 1 km grid. Higher values appear lighter, lower values appear darker.	80
Figure 5-7.	Image of vertical second derivative of magnetic-anomaly data.	81
Figure 5-8.	Image combining magnetic anomaly data and vertical second derivative (Figures 5-6 and 5-7).	82
Figure 5-9.	Shaded-relief image of magnetic-anomaly data. Source of illumination is to south.	83

Figure 5-10.	Shaded relief image of magnetic anomaly data. Source of illumination is to east.	84
Figure 5-11.	Sample cross section of geologic model.	86
Figure 5-12.	Modeling sequence diagram. This figure shows the sequence of modeling and the appropriate figures depicting a particular modeling stage.	88
Figure 5-13.	Bouguer gravity anomaly map of the Charleston, S.C. area. Contour interval is 2 milligals.	89
Figure 5-14.	Magnetic anomaly map for Charleston area. Contour interval is 100 gammas.	90
Figure 5-15.	Structural contour map of the "J" seismic horizon as used in the geologic model. Contours are depth in kilometers.	91
Figure 5-16.	Gravity field after removal of the effects of the material above the "B" seismic horizon (including the "J" seismic horizon). Contour interval is 2 milligals.	93
Figure 5-17.	Gravity field after removal of the effect of material above the "B" seismic horizon (including the "J" horizon) and removal of the effect of a tilt of the mantle. Contour interval is 2 milligals.	94
Figure 5-18.	Gravity/magnetic forward model of a pluton as modeled by the MAGGRAV computer program (Figure 5-20 for location).	95
Figure 5-19.	Gravity/magnetic forward model of a pluton as modeled by the MAGGRAV computer program (Figure 5-20 for location).	96
Figure 5-20.	Location of MAGGRAV cross sections (Figures 5-18 and 5-19).	97
Figure 5-21.	Location of interpreted mafic plutons used for the geologic model. Also shown is recent seismic activity.	99
Figure 5-22.	Gravity field computed from model. Compare this figure with Figure 5-13 which is the measured gravity field. Contour interval is 2 milligals.	100
Figure 5-23.	Structural contour map of the "B" seismic horizon. Contours are depth in kilometers.	102

Figure 5-24.	This is an isopach map of the Triassic/Jurassic rocks which are interpreted as being all rock between the "J" and "B" seismic horizons. Contours are thickness in kilometers.	103
Figure 5-25.	Map indicating depth to the base of the rigid crust.	104
Figure 5-26.	Cross section through A-A' (Figure 5-29) showing the geologic model.	105
Figure 5-27.	Cross section through B-B' (Figure 5-29) showing the geologic model.	106
Figure 5-28.	Cross section through C-C' (Figure 5-29) showing the geologic model.	107
Figure 5-29.	Location of cross sections shown in Figures 5-26 through 5-28.	108
Figure 6-1.	Average stress orientations for the eastern United States from source parameter and stress measurements. (From Law Engineering Testing Co., 1986).	117
Figure 6-2.	Interpreted stress regime for the eastern United States. (From Law Engineering Testing Co., 1986).	118
Figure 6-3.	Vertical displacements and principal axes for the stress ellipsoid in a plate with a flat cylinder surface load in the center of the computation grid. The open circles are tension axes and the solid dots are pressure axes.	120
Figure 6-4.	Location of 1028 km x 1028 km grid used for regional stress modeling.	121
Figure 6-5.	Contour plot of Bouguer Gravity Anomalies. Contour interval is 10 milligals.	123
Figure 6-6.	Local stress field of the Coastal Plain and the eastern continental margins centered at Charleston, South Carolina at 10 km depth. The stress difference is shown in units of MPa (from Kuang, 1987).	124
Figure 6-7.	The corresponding SNPPSA plots (the Schmidt Net Projection of Principal Stress Axis). The open circle stands for the maximum extensional (S_1 or T) axis, the solid circle represents the maximum compressive (S_3 or P) axis and the dot is the intermediate axis (S_2 or B) axis (from Kuang, 1987).	125

Figure 6-8.	The total stress field which combines the local field (Figure 6-6) with a 30 MPa N80°E regional horizontal compression (from Kuang, 1987).	126
Figure 6-9.	The corresponding SNPPSA plots (the Schmidt Net Projection of Principal Stress Axis). The open circle stands for the maximum extensional (S_1 or T) axis, the solid circle represents the maximum compressive (S_3 or P) axis and the dot is the intermediate axis (S_2 or B) axis (from Kuang, 1987).	127
Figure 7-1.	Schematic cross section of typical crust in the Charleston area showing elastic constants used in two-dimensional stress modeling.	131
Figure 7-2.	Node map used for the two-dimensional stress model (1 of 3).	133
Figure 7-3.	Node map used for the two-dimensional stress model (2 of 3).	134
Figure 7-4.	Node map used for the two-dimensional stress model (3 of 3).	135
Figure 7-5.	Relative principal stress magnitude from the two-dimensional stress model (1 of 3).	136
Figure 7-6.	Relative principal stress magnitude from the two-dimensional stress model (2 of 3).	137
Figure 7-7.	Relative principal stress magnitude from the two-dimensional stress model (3 of 3).	138
Figure 7-8.	Relative maximum shear stress from the two-dimensional stress model (1 of 3).	139
Figure 7-9.	Relative maximum shear stress from the two-dimensional stress model (2 of 3).	140
Figure 7-10.	Relative maximum shear stress from the two-dimensional stress model (3 of 3).	141
Figure 7-11.	Effect of pressure and temperature on compressional velocity. (From Steinhart and Meyer, 1961; modified after Birch, 1960).	143
Figure 8-1.	Contour map of the top of crystalline rock (the "B" seismic horizon) and recent seismicity. Contours are in kilometers.	149
Figure 8-2.	This figure shows the location of plutons used in the geologic model and recent seismicity.	153

ACKNOWLEDGMENTS

This project was a team effort with Law Environmental, Inc. and Georgia Institute of Technology as the primary team members. Consultants from Michigan Technological University, Virginia Polytechnical Institute and State University, and the University of North Carolina also played significant roles.

Georgia Institute of Technology, under L. T. Long, provided the lead on potential field data assimilation, collection and processing, and stress modeling both regional and local. Jean-Claude Mareschal of Georgia Institute of Technology contributed significantly to the stress modeling and also the the magnetotelluric investigations.

J. R. Butler of the University of North Carolina was the senior geologist on the team and provided overview and assistance in interpreting the crustal geology of the Charleston area.

Charles T. Young of Michigan Technological University collected the magnetotelluric data and assisted in its interpretation.

John K. Costain of Virginia Polytechnical Institute and State University provided an overview and evaluation of the existing seismic reflection data and interpretations.

The achievements of this project were accomplished through the hard work, perservance and talents of the following people:

Sidney S. Brandwein
J. Robert Butler
John M. Callahan
John A. Chulick
Mary E. Chulick
John K. Costain
Charlotte E. Cutter
John J. Dwyer
Andreas Georgiopoulos
Thomas C. Holmes
Mark Kitchen
Jian Kuang
Paul Lagace
L. Timothy Long
Jean-Claude Mareschal
Mark Parker
E. Radford
J. C. Rogers
Robert M. White
Charles T. Young
Karl-Heinz Zelt
Ernst G. Zurflueh

EVALUATION OF HYPOTHESES FOR THE CAUSE OF THE
1886 CHARLESTON EARTHQUAKE

EXECUTIVE SUMMARY

This project performed in response to the need to reduce the uncertain in estimating seismic risk to nuclear facilities in the eastern United States, due to the lack of definition for the cause of the 1886 Charleston earthquake. Specifically, the purpose of this study was to test existing hypotheses as to the cause of the 1886 earthquake by way of a geophysical/geological investigation.

Our approach to this project was to gather a comprehensive set of existing data and collect new data where needed. These data were used to construct geologic and stress models which would be used to test the various extant hypotheses concerning the origins of the 1886 Charleston earthquake.

As indicated, a major effort involved the collection and processing of existing data. We used gravity, magnetic, seismic and geologic data. Additional data were collected, primarily gravity and magnetotelluric measurements. Figure 4-3 shows the location of the three data grids that were used for gravity, magnetic and topographic data. The largest, 1028 km on a side, was used for regional crustal stress modeling. The intermediate grid, 256 km on a side, provided boundary conditions and continuity to the third grid, 128 km on a side and containing the Charleston area. The detailed grid was developed to allow potential field modeling of the crust in the Charleston area. As a product of this project the data sets for all three grids and their supporting software are available.

We collected and analyzed magnetotelluric (MT) sounding data as part of this project. Twelve MT soundings were conducted with effective depths of interest greater than 40 kilometers. Figure 4-5 shows the location of the MT soundings and Figures 4-12 through 4-15 show two equivalent two-dimensional interpretations of the data. As is common with electrical soundings a unique solution was not found. We prefer solution I (Figures 4-12 and 4-13) because its results are corroborated by existing seismic results and seismicity data. This solution gives shallow electrically conductive layers corresponding to Coastal Plain sediments in the upper kilometer and then a deep resistive layer to depths of 10 to 23 kilometers where a conductive zone is reached. Figures 4-17, 4-18 and 4-19 compare our preferred solution to interpreted COCORP reflection profiles. Our high resistivity zone corresponds to crust which is without reflections and the top of the deep low resistivity zone corresponds to the beginning of numerous short reflectors. This depth is also equivalent to the maximum depth of earthquakes in the region. The MT solution shows a 13 km variation in the depth to what we interpret to be the bottom of

the rigid crust and has a significant effect on the results of our local stress modeling.

We developed a geologic model of the 128 x 128 km area around Charleston which interprets the lithology, structure, geologic history and physical properties of the entire crust. We used three-dimensional gravity modeling constrained by seismic, drilling, MT and geologic data. Two-dimensional magnetic/gravity modeling was used in conjunction with the three-dimensional gravity modeling. We used image processing computer techniques developed for remote sensing data to manipulate the gravity and magnetic data to great advantage. Figures 5-1 through 5-10 show the results of this technique.

The geologic modeling is described in detail in Chapter 5. The results are summarized by Figure 5-11 which shows an interpretation along a generalized northwest-southeast striking profile through the study area. A wedge of Coastal Plain sediments (Quaternary through Cretaceous) thickens toward the coast and is underlain by a thin Jurassic basalt called the "J" horizon. The "J" horizon is a series of flows covering almost all of the study area. Triassic to early Jurassic sediment-filled basins are immediately below the Jurassic basalt. The lithology of the Triassic/Jurassic rocks is not well known locally but using information from other similar nearby basins and Clubhouse Crossroads Test Hole #3 as a guide, we arrive at a mix of clastic sediments (sandstones, siltstones, shales, argillites, etc.) and perhaps basalt flows.

Crystalline rock underlies the Triassic/Jurassic rock. The crystalline rock may consist of quartz-rich metamorphic rock intruded by mafic or ultramafic plutons. The igneous rocks are thought to be gabbroic in composition and Paleozoic in age, thus predating the basin development.

The crystalline rock appears to continue with uniform character to depths of between 10 and 23 kilometers. This depth range corresponds to the maximum hypocentral depths of seismicity. Below 10 to 23 km the physical properties as observed in COCORP reflection profiles appear to change. In the lower crust the COCORP reflection images of the crust change from being seismically transparent to displaying numerous short reflectors. Also, the rock of the lower crust becomes more electrically conductive. We interpret these phenomena to indicate a rigid upper crust underlain by a viscoelastic lower crust.

The crust/mantle boundary is located at a depth of about 28 to 30 km and is interpreted to become more shallow toward the coast.

Figures 5-15, 5-23 and 5-25 are structural maps of key horizons; namely, the "J" seismic horizon, the "B" seismic horizon, and the bottom of the rigid crust. Figure 5-24 is an isopach map of Triassic/Jurassic rock and Figure 5-21 locates

the plutons. Figures 5-26 through 5-28 are cross sections through the study area. Figure 5-29 shows the location of the cross sections.

Three-dimensional regional stress modeling was conducted in the Charleston area using topographic and gravity anomaly loading as stress sources and also including horizontal stresses due to plate spreading at the mid-Atlantic ridge. This stress modeling technique was developed initially at Georgia Institute of Technology and they applied the technique to the southeast as part of this project. The Charleston area was interpreted to have ordinary stress conditions.

Two-dimensional finite-element stress modeling was performed for the local Charleston area. The nature of our geologic modeling process allowed us to construct an appropriate crustal cross section, using appropriate elastic parameters (Figure 7-1). The results of our two-dimensional stress modeling allow several significant conclusions to be drawn (Figures 7-5 through 7-10): the Coastal Plain and Triassic sediments seem to be effectively isolated from the compressive crustal stress; the maximum shear stress is increased in the upper crystalline basement at the interface with the Triassic sediments; the sudden decrease in depth of the rigid crust to the west and north increases the maximum shear stress above the rise; and finally the mafic plutons have a mild effect on the stress in the crust immediately surrounding the pluton.

The testing of hypotheses for the cause of the 1886 Charleston earthquake is the main result of this project. Several important models produced by this project were considered when evaluating the viability of each hypothesis. The results of the geologic model, the regional stress model, and the local two-dimensional stress model were used in conjunction with information from the literature and other pertinent projects to evaluate each hypothesis.

Several hypotheses were considered to be viable:

- o Reactivation of Mesozoic Basin Border Faults: includes northeast- and northwest-striking faults. We found that recent seismicity is located where the boundaries of Mesozoic Basins intersect (Figure 8-1). Our geologic model has located the border faults with sufficient accuracy to make this conclusion.
- o Stress Amplification Near Plutons: Plutons are found to also coincide with recent seismicity and with Mesozoic Basin boundary intersections (Figure 8-2). Our study infers that plutons only mildly amplify stress in the rigid crust in the Charleston area. We suggest that these Paleozoic plutons may have controlled the Mesozoic extensional faulting in such a way as to be at the intersection of Mesozoic Basin border faults. The spatial association of recent

earthquakes and plutons may be explained by the previous hypothesis.

- o Brunswick Suspect Terrane: may be seismogenic within areas near Mesozoic Basin border fault intersections. This terrane is a large area containing the Charleston region whose crustal geology is similar to that of the Charleston region, that is, containing Mesozoic basins and Paleozoic plutons, and having a similar tectonic history and a similar current stress regime.
- o High-Angle Faults not Associated with Mesozoic Basins: also seem to have some potential as possible sources of the Charleston earthquake.

The following hypotheses are not considered viable:

- o Reactivation of Horizontal (or Decollement) Faults
- o Landward Extension of Blake Spur Fracture Zone
- o Topographic and Density Anomaly Loading (Barosh's hypothesis of extensional tectonics)
- o Faults Associated with Basement Province Boundaries.

The following hypothesis remains unevaluated or undecided:

- o Ductile Shear Zones in Lower Crust.

The results of this study indicate that the hypothesis of reactivation of Mesozoic Basin border faults is strongly supported, specifically at the intersections of Mesozoic Basin border faults near buried mafic plutons. These conditions are not necessarily restricted to the Charleston area. This hypothesis implies locations for the occurrence of a Charleston-type event in other areas of the eastern U.S.

There appear to be strong differences in the thickness of the rigid crust which also may constrain the location of Charleston-type earthquakes to areas of thicker crust. This would limit the maximum earthquake magnitude in areas of thinner crust such as the Bowman seismic zone, thus excluding a Charleston-size event.

CHAPTER 1

INTRODUCTION

This project was performed in response to the need to reduce the uncertainty in estimating seismic risk to nuclear facilities in the East due to the lack of understanding of the cause of the 1886 Charleston earthquake. Specifically, the purpose was to develop geophysical and geological information that would permit defining the cause of seismicity near Charleston, South Carolina, or narrowing down the range of theories that may explain it. Such a study should allow more specific prediction as to the likelihood and location of future large earthquakes in the East.

A large and damaging earthquake occurs when a major portion of the earth's rigid crust, with a thickness of 10 to 20 km, fails along one or more planes. Such crustal failure occurred in 1886 in the vicinity of Charleston, South Carolina. The transient manifestation of failure, the earthquake vibrations, were felt over most of the eastern United States and caused extensive damage in Charleston and significant damage in most of South Carolina and parts of neighboring Georgia and North Carolina. The potential for a recurrence of such a devastating event at Charleston or elsewhere in the eastern United States and the impact of such an event on critical facilities has motivated the recent resurgence of studies of the cause of the 1886 Charleston earthquake.

Today even after extensive study and review during the last 15 years (Gohn, 1983; Rankin, 1977; Hays and Gori, 1983; Dewey, 1985; Talwani, 1986) there is still no consensus on the cause of this event. The more permanent manifestations such as fault displacements have eluded detection and the causative fault is still not unequivocally identified. Without direct evidence for the plane of failure and with no consensus on the cause of the Charleston earthquake, recent investigations into the cause of the Charleston earthquake have sought data from almost all of the domain of geological and geophysical techniques.

The objective of this project is to clarify possible causes of seismicity at Charleston. An overwhelming proportion of the existing literature fails in this aspect; perhaps because most recent studies represent evaluations of limited types of data by individual scientists or are directed toward proving specific hypotheses. A notable exception is the classic study by Dutton (1889).

The many individually excellent studies of the last 15 years have vastly improved and increased the quality and quantity of appropriate data. As individual efforts, they have contributed many ideas, concepts and hypotheses relevant to the cause of the Charleston seismicity. As most of the hypotheses are derived from specific data sets, those same data sets will, of course, support the hypothesis. In order to avoid or at least

minimize the contamination of the results of this study by such circular arguments, we have established a single comprehensive and homogeneous data set against which to compare and test the leading hypotheses for the cause of the Charleston earthquake. The data set has been evaluated for completeness and significance to assure its usefulness.

Because many hypotheses are vague or poorly defined, the design of appropriate tests for validity using the data set is difficult. In this project each hypothesis was recast in terms of the basic physical principles that govern the stress system or strength inhomogeneities allegedly responsible for the seismicity.

Dewey, J. W., "Review of Recent Research on the Seismotectonic, of the Southeastern Seaboard and an Evaluation of Hypotheses on the Source of the 1886 Charleston, South Carolina, Earthquake", USNRC Report NUREG/CR-4339, August, 1985

Dutton, C. E., "The Charleston Earthquake of August 31, 1886", U.S. Geological Survey Annual Report, No. 9, p. 203-528, 1889

Gohn, G. S., Studies Related to the Charleston, South Carolina, Earthquake of 1886 - Tectonics and Seismicity, U. S. Geological Survey Professional Paper 1313, 375 p., 1983

Hays, W. W., and P. L. Gori, A Workshop on the 1886 Charleston, South Carolina, Earthquake and its Implications for Today, U. S. Geological Survey Open-File Report 83-843, 508 p., 1983

Rankin, D. W., Studies Related to the Charleston, South Carolina Earthquake of 1886 - A Preliminary Report, U. S. Geological Survey Professional Paper 1028, 204 p., 1977

Talwani, P., "Current Thoughts on the Cause of the Charleston, South Carolina Earthquakes", South Carolina Geology, Vol. 29, No. 2, p. 19-38, 1986

CHAPTER 2

HYPOTHESES FOR CAUSES OF THE 1886 CHARLESTON, SOUTH CAROLINA EARTHQUAKE

2.1 Introduction

A primary goal of this project was to assimilate and evaluate all available pertinent information to allow evaluation of the hypotheses for causes of the 1886 Charleston, South Carolina earthquake. This chapter describes the hypotheses to which this information was applied. It includes those hypotheses for the cause of the Charleston earthquake currently given credibility. Each hypothesis is described in terms of fundamental physical processes relating to crustal stress and rheology.

2.2 Crustal Stress and Rheology

An earthquake occurs when an accumulation or concentration of stress is released by sudden failure. The earthquake process can be initiated with a change in strength or an increase in deviatoric stress. In either case, the earthquake will only occur if significant deviatoric stress exists in the rock; hence, in this compilation of hypotheses, the source of stress will be emphasized if it has been specified by the author(s) of the hypotheses.

2.2.1 Crustal Stress

The state of stress at depths of major earthquakes cannot be measured directly, and near the earth's surface it can be measured only with difficulty. The current lack of understanding of the changes in the rheology of geologic materials with depth accounts for the largest portion of the uncertainty in the state of stress. Hypotheses on the origins of lithospheric stress have been related to processes at the boundaries of a lithospheric plate or to local sources in the interior of a plate. Processes at the plate boundary generate homogeneous regional stresses. In contrast, stresses from local sources in the interior of a plate will be inhomogeneous. The magnitudes of plate boundary and internally-derived stresses can be similar. Chapter 6 discusses the possible sources of crustal stress in detail.

2.2.2 Rheological Properties of Continental Crust

At crustal depths of less than 20 to 30 km, structural failure occurs as brittle failure or by frictional sliding (Meissner and Strehlau, 1982). Stresses at these depths are limited by the elastic strength of the rock or by the shear strength on existing planes of weakness. Lubrication of existing planes of weakness can reduce the shear strength to a few tens of MPa in contrast to a rock strength of typically 1000 MPa (Kanamori, 1980).

In the lower crust and upper mantle, geologic materials can deform by viscous or plastic mechanisms. In viscous materials, the maximum allowable stress is determined by the strain rate. Increased water content and temperature can decrease the viscosity and decrease the maximum possible stress. Thus, as the temperature increases with depth, the viscosity and maximum stress decrease with depth. Areas in the crust with high heat flow and higher temperatures have reduced capability to retain stresses.

The combination of failure by frictional sliding at shallow depths and viscous relaxation in the lower crust results in a high-strength stress channel at depths of 5 to 25 km in the middle crust (Meissner and Strehlau, 1982). The thickness of the channel as determined by crustal temperature is consistent with observed distributions of mid-plate earthquakes.

The strength of the crust, based on a combination of rheological arguments and estimates from earthquake stress drops, ranges from 10 to 150 MPa (Kanamori, 1980). However, this range can be modified significantly by small-scale geologic inhomogeneities which can vary widely in strength and deformation properties even at shallow depths.

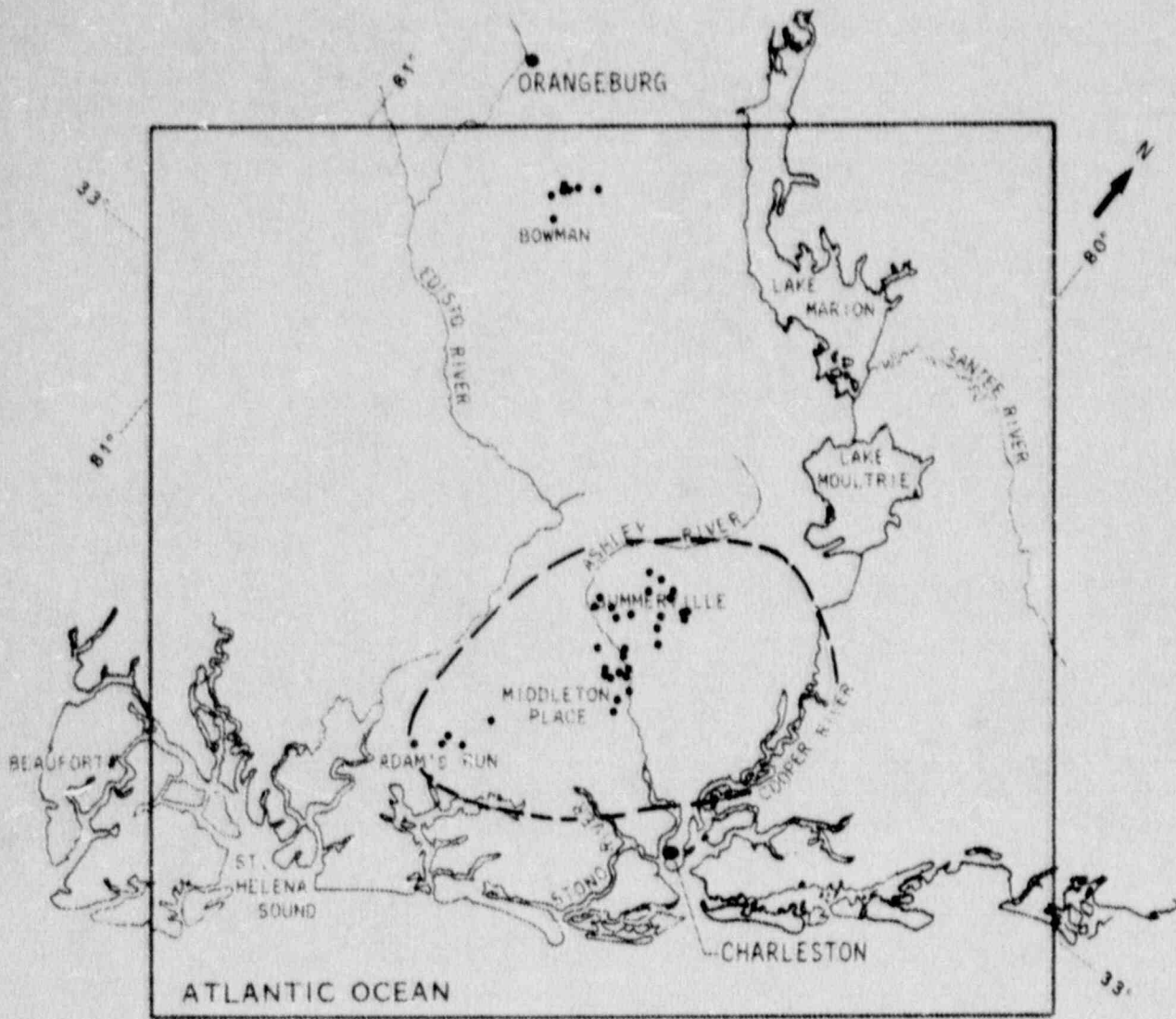
Costain et al., (1987) have recently suggested that diffusion of pore pressure transients to seismogenic depths from changes in ground water levels is a triggering mechanism for intraplate seismicity. This suggestion may be applied to many of the hypotheses for causes of the 1886 Charleston earthquake, but it does not effect the validity of any individual hypothesis.

2.3 Hypotheses

Many explanations for the Charleston earthquake are simply features observed or suspected in regional geophysical or geological data. The source of stress is seldom identified and only a structure, usually a suspected fault providing a crustal strength anomaly, is suggested as the feature along which movement occurred during the Charleston earthquake.

In seismology, an earthquake is traditionally associated with a fault. At Charleston, the causative fault has proved elusive and no consensus has developed in favor of a single structure. The seismicity data have been of little help (Tarr, et al., 1981) since instrumentally located earthquakes in the epicentral area of the 1886 Charleston shock have occurred in three distinct zones: Middleton Place-Summerville (the most active zone), Bowman, and Adam's Run (Tarr and Rhea, 1983). Seismic monitoring to date has shown an absence of seismic activity between the zones, implying the absence of active structure connecting the zones. Many investigators assume that the present activity at the Middleton Place-Summerville zone is directly related to the 1886 event (Figure 2-1).

Dewey (1985) and Talwani (1984, 1986a) both summarize and



LEGEND

• EARTHQUAKE EPICENTER [SOURCE: TARR AND RHEA (1983)]

— 1886 CHARLESTON EARTHQUAKE MEIZOSEISMAL AREA
[SOURCE: BOLLINGER (1977)]

Figure 2-1. Meizoseismal area of 1886 Charleston earthquake and recent earthquake epicenters near Charleston, South Carolina.

analyze hypotheses for the cause of the 1886 Charleston, South Carolina, earthquake.

2.3.1 Hypotheses Associated With Faults

Because a fault can be identified without understanding the source of stress that caused failure, many of the proposed hypotheses presented are descriptions of faults without an associated mechanism. In most cases, a regional stress field is assumed to be responsible for the earthquake. The following are classes of faults identified as possible candidates for the Charleston earthquake fault. In some cases, a mechanism is suggested, but the emphasis is on the existence of the presumed or interpreted fault. The hypothesized faults seem to have two major sources of inference: seismic reflection data and earthquake hypocenters (Figure 2-1).

As more earthquake data have been accumulated over the years, many faults and fault orientations have been interpreted. Unfortunately, the increase in data has yielded more hypotheses, not fewer.

2.3.1.1 Reactivation of Horizontal (or Decollement) Faults

It has been suggested that the 1886 earthquake has resulted from normal displacement on a low-angle decollement fault underlying much of the southeastern seaboard near Charleston (Seeber and Armbruster, 1981a, 1981b). More generally, aseismic slippage on a mid-crustal detachment surface could produce seismogenic stresses in the upper crust (Seeber, 1983). Stresses caused by this slippage might cause earthquakes on moderately or steeply-dipping faults.

Interpretations of deep crustal seismic reflection data in the Piedmont of South Carolina and Georgia suggest the existence of a nearly horizontal decollement surface (Cook *et al.*, 1979; Cook *et al.*, 1981; Harris and Bayer, 1979). However, the extension of this feature from the Piedmont across the Coastal Plain has been questioned (Iverson and Smithson, 1982) and the decollement may not exist near Charleston.

The decollement surface could be reactivated by gravity sliding or by compressional forces of unspecified origin (Seeber and Armbruster, 1981b; Armbruster and Seeber, 1981).

Behrendt, *et al.* (1981, 1983), Brehrendt, (1983) and Hamilton (1981) associate earthquakes with movement along a decollement with possible secondary seismicity associated with northeast-striking high-angle reverse faults. Local stress release along the decollement results in reverse faulting along features that are rooted in the decollement. Seeber and Armbruster (1986) use revised aftershock reports of the 1886 Charleston earthquake to show a large aftershock area and increased regional seismicity. They imply that shallow-dipping faults

could explain the intensity effects and aftershock distribution.

As discussed by Behrendt *et al.* (1983), listric faults that are believed to be rooted in the decollement include: Cooke Fault (b), Helena Banks Fault, Gants Fault, and Drayton Fault (Figure 2-2).

2.3.1.2 Reactivation of Northeast-Striking Near-Vertical Faults

Most versions of this hypothesis attribute the cause of the 1886 earthquake to reactivated reverse fault motions on northeast-striking faults which had predominantly normal motion in the tensional Mesozoic stress regime (Wentworth and Mergner-Keefer, 1981, 1983; Wentworth, 1983). Similar faults are considered responsible for much of the low-level seismicity elsewhere in the eastern Seaboard. Behrendt *et al.* (1983) attribute the cause of the 1886 event to reverse activation of Mesozoic listric normal faults related to a decollement as mentioned in the previous hypothesis.

Taber (1914) was perhaps the first to suggest a northeast-striking fault in the crystalline basement. He proposed that the fault was near Woodstock, S.C. and this hypothesized feature has become known as the "Woodstock Fault" (Figure 2-2). No new evidence for this fault has been found and its justification may have been derived from the intensity-defined dual "epicentrum" described by Dutton (1889).

Northeast-striking reverse faults are observed at many locations in the Piedmont, particularly near the edge of the Coastal Plain, and some have been demonstrated to have Cenozoic movement (York and Oliver, 1976; Prowell, 1983); however, none of these faults exhibit active seismicity.

Wentworth and Mergner-Keefer (1981b, 1983) suggested that Cenozoic reverse faults are responsible for the Atlantic margin seismicity as well as being a cause of the Charleston Earthquake. They also suggest that these faults probably follow older discontinuities, especially early Mesozoic normal faults. They conclude that northeast-striking reverse faulting produced the 1886 Charleston earthquake; furthermore, they hypothesized that recent events on northwest-trending structures are due to temporary changes in the local stress field caused by the strain release of the 1886 main shock.

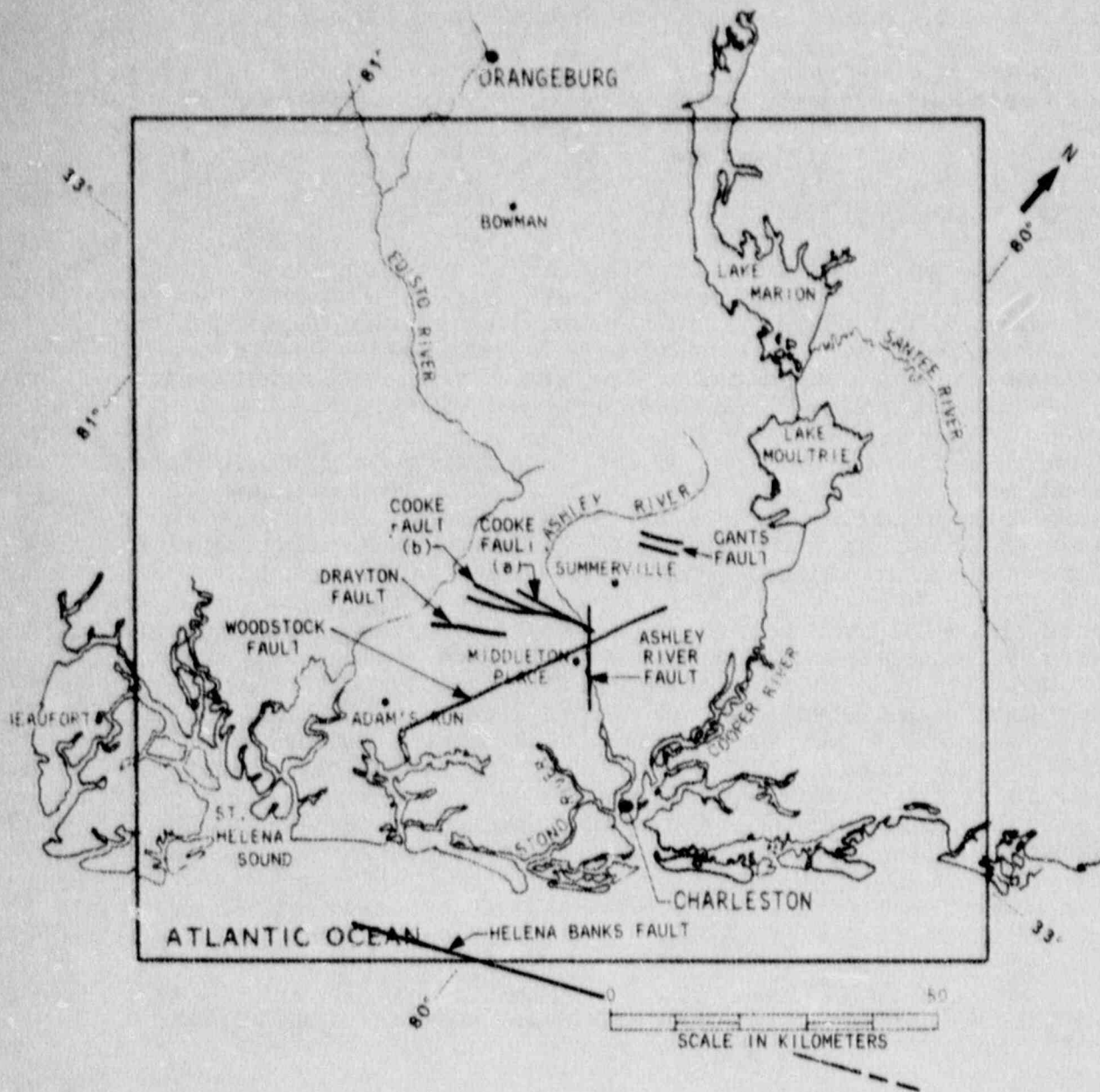


Figure 2-2. Faults interpreted to be associated with the Charleston, South Carolina earthquake zone.

2.3.1.3 Reactivation of Mesozoic Basin Border Faults

This hypothesis suggests that the 1886 earthquake occurred on either northeast or northwest-striking border faults on buried Mesozoic basins. Illies (1982) proposed that large earthquakes could occur as northwest-striking strike-slip shear zones resulting from stress concentrations associated with northeast-trending buried Mesozoic basins.

Behrendt *et al.* (1981a, 1981b, 1983) and Behrendt (1983) proposed that the Charleston earthquake occurred on a northeast-striking listric fault near the southeast edge of the Jedburg Mesozoic basin (Figure 2-3). Behrendt also proposed that movement on the decollement results in reverse faulting along features that are rooted in the decollement.

Tarr and Rhea (1983) suggest that one segment of the Middleton Place-Summerville seismic zone is based on "activation of an unhealed east-northeast-striking border fault bounding a horst on the southeast and a graben of Triassic or Jurassic age to the northwest." Other segments are interpreted to be activation of "nearly vertical, northwest-striking faults on contacts, possibly at the edges of diabase dikes, crossing the Triassic or Jurassic border fault" described above.

Behrendt and Yuan (1986) associate the Gants-Cooke fault zone with the Jedburg basin as a source of the 1886 earthquake. An unnamed fault associated with the Branchville basin is attributed to the Bowman earthquake cluster. These faults show mostly strike-slip motion in a northeast maximum horizontal compressive stress field.

2.3.1.4 Reactivation of Northwest-Striking Near-Vertical Faults

Normal or strike-slip faults have been inferred from alignments of geophysical anomalies associated with basement rocks (Rankin, 1976; Talwani, 1983).

Inshore extensions of oceanic fracture zones have been proposed as an explanation for some of the northwest-trending features (Fletcher and Sykes, 1977; Sbar and Sykes, 1973; Talwani and Howell, 1976; Fletcher, *et al.* 1978; Sykes, 1978; Barosh, 1983). However, results of extensive and detailed geophysical investigations offshore from South Carolina (for summary see Behrendt, *et al.* 1983; Klitgord, *et al.* 1983; Dillon and McGinnis, 1983) have indicated no evidence that the Blake Spur Fracture Zone exists northwest of about 150 km offshore from Charleston.

Talwani (1982) proposed the Ashley River Fault as a shallow northwest-striking fault related to the extension of the Blake Spur Fracture Zone. This was based on earthquake hypocenters. Talwani and Poley (1984), Poley (1984), and Poley and Talwani (1984) examined leveling data in the Charleston region and

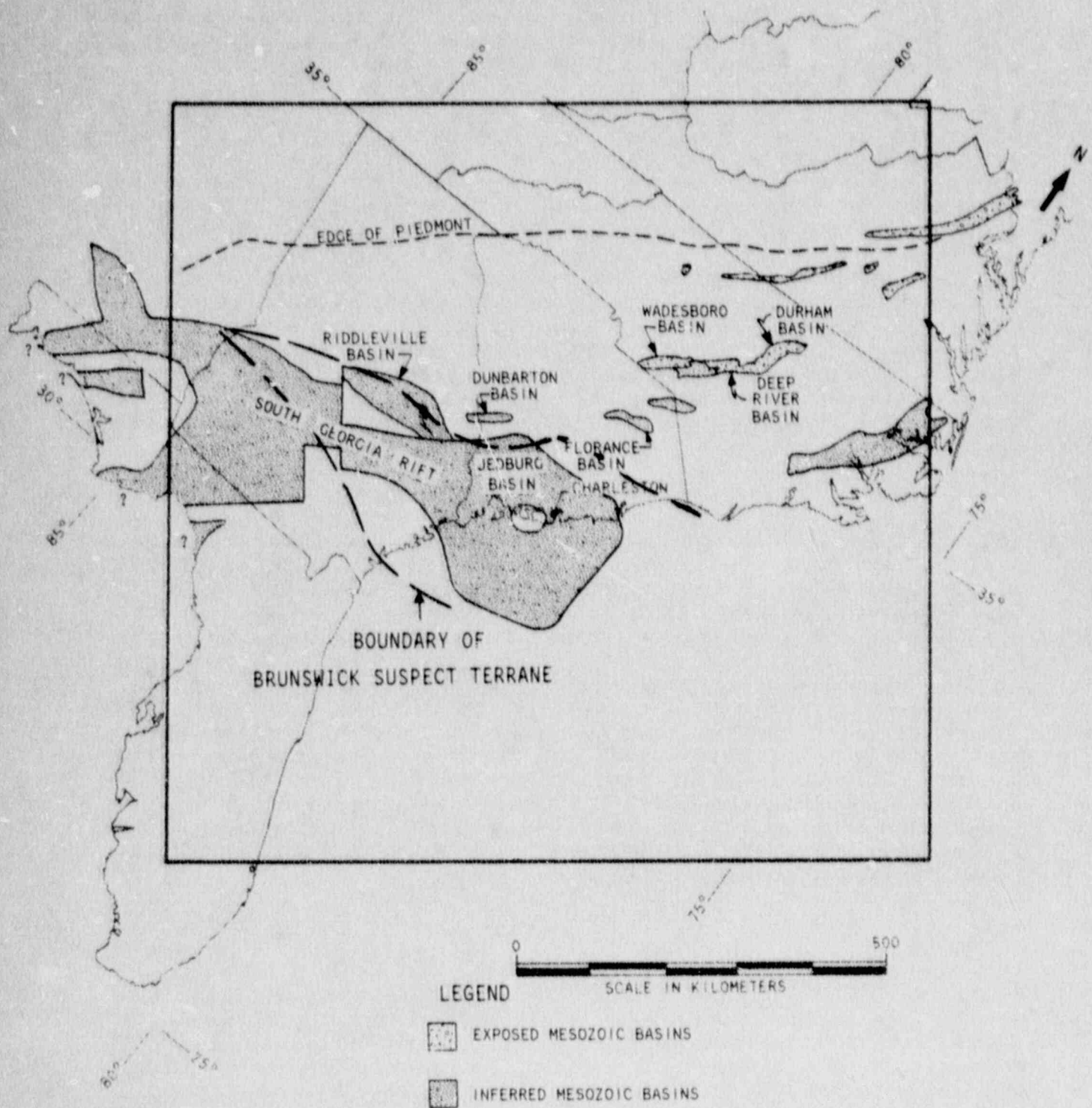


Figure 2-3. Exposed and inferred Mesozoic Basins (from earlier studies), and Brunswick suspect terrane (from Wheeler and Bollinger, 1984).

found an apparent vertical displacement occurring at an average rate of 2-3 mm/yr at a location coincident with the approximate location of the Ashley River fault.

Weems (1985) presented evidence from shallow drilling for structure in shallow coastal plain sediments. In the Mount Holly quadrangle, a northwest-trending lineament exists across which Oligocene sediments drape down to the southwest; intensity data suggest that the epicenter of the Charleston 1886 earthquake was beneath this feature.

In an earthquake relocation analysis using more than 50 earthquakes, Shedlock (1987) has refined a three-dimensional velocity model and significantly reduced hypocenter errors resulting in a north-south trending zone of seismicity between Middleton Place and Summerville. Single-event and composite fault-plane solutions using the new locations and new polarity data cannot resolve whether there is strike-slip or normal faulting.

2.3.1.5 Faults Associated With Basement Province Boundaries

Northwest-trending offsets in gravity and magnetic anomalies define crustal blocks 60-70 km wide with apparent displacements. The blocks provide a model that Talwani (1983) has used to propose a northwest-trending zone of crustal weakness extending northwest from Charleston.

2.3.1.6 Ductile Shear Zone (Lower Crust)

Zoback (1983) suggested that there are antecedent ductile shear zones in the lower crust which concentrate deformation and thus concentrate stresses in the upper crust. Laboratory rock deformation evidence suggest that such zones could exist in the lower crust. Earthquakes caused by such a mechanism would concentrate in areas of weakness in shallow brittle crust in the vicinity of these ductile zones.

2.3.1.7 Intersecting Structural Trends

Talwani et al. (1979) suggested that the seismicity in the South Carolina Coastal Plain and in the Central Virginia seismic zone was occurring at localized zones of weakness formed at the intersection of an older pre-existing zone of weakness. In the case of the Charleston area, this involves the intersection of the Blake Spur Fracture Zone with the boundary faults of Triassic basins.

The proximity of the Charleston earthquake of 1886 to an area of widespread Mesozoic rifting and to the Blake Spur fracture zone suggest that earthquake activity along the southern Atlantic Coastal Plain may be related to old zones of weakness that were reactivated during the Mesozoic opening of the Atlantic Ocean.

Bollinger (1983) hypothesized that the source zone for the 1886 Charleston earthquake is localized by the intersection of at least two seismogenic structures, one trending northwest and the other trending northeast. The faulting in 1886 was on the northeast structure. Ninety years later, the aftershock activity has shifted to the northwest element. The variable trends in the few isoseismal maps that are available for the intervening period could reflect activity on one or the other of these two structures.

Tarr and Rhea (1983) characterized the seismicity of the Coastal Plain as occurring in clusters. They believe that contemporary seismicity in the Charleston area occurs in clusters because the weakest places in the crust are located at the intersections of unhealed border faults and cross faults with contact zones in the basement (of Triassic or Jurassic age).

More recently, Talwani (1986b) has suggested that the Charleston earthquake was caused by stress buildup at a locked intersection of the Ashley River Fault and the Woodstock fault. Both faults are defined by earthquake epicenters and are supported by some gravity and magnetic data. Events on the Woodstock fault show strike-slip motion and are deeper than the strike-slip event on the Ashley River Fault.

2.3.2 Hypotheses Concerning Structures Other Than Faults

The following hypotheses are not directly related to a fault or class of faults.

2.3.2.1 Topographic and Density Anomaly Loads

Barosh (1983) suggested that adjustments on shallow local structures due to vertical movements brought about by continued opening of the North Atlantic basin appear to be the cause of the seismicity of the southeastern United States. The main activity seems related to the relative subsidence at the inner edge of embayments within the Coastal Plain. The embayments overlie older grabens that have apparently played a significant role in controlling their location.

2.3.2.2 Brunswick Suspect Terrane

The existence of seismic zones that are spatially and temporally stationary suggest that there is some type of spatial selectivity in the accumulation and release of strain energy in the Southeast. Suspect terranes are defined as internally homogeneous geologic provinces of orogenic belts with features that contrast sharply with those of nearby provinces (Williams and Hatcher, 1982). These contrasts include differences in stratigraphy, structure, mineral deposits, paleomagnetic signatures, and metamorphic and plutonic histories. Wheeler and Bollinger (1984) suggested that the Charleston area lies in the Brunswick suspect terrane

of Williams and Hatcher (1982) and this terrane is more conducive to seismic activity (Figure 2-3).

2.3.2.3 Stress Amplification Near Plutons

There is evidence from many sources (Long and Champion (1977), Kane (1977), McKeown (1978), and Barstow et al. (1981)) that there is a spatial association between mafic (and ultramafic) plutons and local seismicity. It is hypothesized that mafic intrusions tend to concentrate stress along their margins because of property contrasts between the pluton, surrounding altered country rock, and unaltered country rock. Ravat et al. (1987) found that some mafic intrusives strengthen surrounding rock by alteration, thereby concentrating local stresses. They also found that these mafic plutons dislocate rather than amplify local stress fields.

Kane (1977) and Campbell (1978a, 1978b) proposed that stress amplification is caused by serpentinization of ultramafic plutons. The amount of stress which could be concentrated is a function of the effective rigidity moduli of the contrasting materials. The serpentinized mafic body is substantially weaker than the surrounding material. This yields the "hole in a plate" model where stresses are concentrated at the edges of the zone of weakness. In contrast, Yang and Aggarwal (1981) have hypothesized that the presence of unfaulted plutons inhibits earthquake activity.

- Armbruster, J. G., and L. Seeber, "Seismicity and Back-slip on the Detachment of the Southern Appalachians", Abstract, Eos, Transactions, American Geophysical Union, Vol. 62, p. 403, 1981
- Barosh, P. J., "Use of Seismicity and Tectonic Framework to Define the Seismic Hazard in the Region Encompassing Charleston, South Carolina", in Proceedings of Conference XX, A Workshop on "The 1886 Charleston, South Carolina, Earthquake and its Implications for Today", United States Geological Survey Open-File Report No. 83-0843, p. 380-390, 1983
- Barstow, N. L., K. G. Brill, Jr., O. W. Nuttli, and P. W. Pomeroy, "An Approach to Seismic Zonation for Siting Nuclear Electric Power Generating Facilities in the Eastern United States", USNRC Report NUREG/CR-1577, 1981
- Behrendt, J. C., "Did Movement of a Northeast Trending Listric Fault near the Southeast Edge of the Jedsburg Triassic-Jurassic(?) Basin Cause the Charleston, South Carolina, 1886 Earthquake?", in Proceedings of Conference XX, A Workshop on "The 1886 Charleston, South Carolina, Earthquake and its Implications for Today", United States Geological Survey Open-File Report No. 83-843, p. 126-131, 1983
- Behrendt, J. C., R. M. Hamilton, H. D. Ackermann, and V. J. Henry, "Cenozoic Faulting in the Vicinity of the Charleston, South Carolina, 1886 earthquake", Geology, Vol. 9, No. 3, p. 117-122, 1981b
- Behrendt, J. C., R. M. Hamilton, H. D. Ackermann, V. J. Henry, and K. C. Bayer, "Marine Multichannel Seismic-Reflection Evidence for Cenozoic Faulting and Deep Crustal Structure near Charleston, South Carolina", in G. S. Gohn, Studies Related to the Charleston, South Carolina, Earthquake of 1886 - Tectonics and Seismicity, U.S. Geological Survey Professional Paper 1313, p. J1-J29, 1983
- Behrendt, J. C., R. M. Hamilton, and P. Pomeroy, "New Multichannel Seismic Reflection Profiles in South Carolina and Implications Concerning the Origin of the Charleston 1886 Earthquake", Abstract, Earthquake Notes, Vol. 52, No. 3, p. 9, 1981a
- Behrendt, J. C., and A. Yuan, "Strike Slip on Reactivated Triassic (?) Basin Boundary Fault Zones as Sources of Earthquakes Near Charleston, S.C.", in J. E. Beavers, Proceedings, Third U.S. National Conference on Earthquake Engineering, (Earthquake Engineering Research Institute, El Cerrito, CA), p. 43-54, 1986

- Bollinger, G. A., "Reinterpretation of the Intensity Data for the 1886 Charleston, South Carolina Earthquake", in D. W. Rankin, Studies Related to the Charleston, South Carolina Earthquake of 1886 - A Preliminary Report, U. S. Geological Survey Professional Paper 1028, p. 33-42, 1977
- Bollinger, G. A., "Speculations on the Nature of Seismicity at Charleston, South Carolina", in G. S. Gohn, Studies Related to the Charleston, South Carolina Earthquake of 1886 - Tectonics and Seismicity, U.S. Geological Survey Professional Paper 1313, p. T1-T11, 1983
- Bollinger, G. A. and R. L. Wheeler, "The Charleston, South Carolina, Seismogenic Zone, Terrane Decoupling and Horizontal Versus Vertical Source Geometry", in Proceedings of Conference XX, A Workshop on "The 1886 Charleston, South Carolina, Earthquake and its Implications for Today", U. S. Geological Survey Open-File Report No. 83-0843, p. 132-136, 1983
- Campbell, D. L., "Investigation of the Stress-Concentration Mechanism for Intraplate Earthquakes", Geophysical Research Letters, Vol. 5, No. 6, p. 477-479, 1978a
- Campbell, D. L., "Stress-concentration Mechanism for Earthquakes in the Charleston, South Carolina, Area", Geological Society of America, Abstracts with Programs, Vol. 10, No. 4, p. 161, 1978b
- Chowns, T. M. and C. T. Williams, "Pre-Cretaceous Rocks Beneath the Georgia Coastal Plain: Regional Implications", in G. S. Gohn, Studies Related to the Charleston, South Carolina, Earthquake of 1886 - Tectonics and Seismicity, U. S. Geological Survey Professional Paper 1313, p. L1-L42, 1983
- Cook, F. A., D. S. Albaugh, L. D. Brown, S. Kaufman, and J. E. Oliver, "Thin-Skinned Tectonics in the Crystalline Southern Appalachians: COCORP Seismic Reflection Profiling of the Blue Ridge and Piedmont", Geology, Vol. 5, p. 563-567, 1979
- Cook, F. A., L. D. Brown, S. Kaufman, J. E. Oliver, and T. A. Petersen, "COCORP Seismic Profiling of the Appalachian Orogen Beneath the Coastal Plain of Georgia", Geological Society of America Bulletin, Part I, Vol. 92, p. 738-748, 1981
- Costain, J. K., G. A. Bollinger, and J. A. Speer, "Hydroseismicity: A Hypothesis for the Role of Water in the Generation of Intraplate Seismicity", Seismological Research Letters, Vol. 58, 1987

- Daniels, D. L., I. Zietz, and P. Popenoe, "Distribution of Subsurface Lower Mesozoic Rocks in the Southeastern United States, As Interpreted From Regional Aeromagnetic and Gravity Maps", in G. S. Gohn, Studies Related to the Charleston, South Carolina, Earthquake of 1886 - Tectonics and Seismicity, U. S. Geological Survey Professional Paper 1313, p. K1-K24, 1983
- Dewey, J. W., "A review of Recent Research on the Seismotectonic of the Southeastern Seaboard and an Evaluation of Hypotheses on the Source of the 1886 Charleston, South Carolina, Earthquake", USNRC Rep. NUREG/CR-4339, 1985
- Dillon, W. P. and L. D. McGinnis, "Basement Structure Indicated by Seismic-Refraction Measurements Offshore from South Carolina and Adjacent Areas", in G. S. Gohn, Studies Related to the Charleston, South Carolina, Earthquake of 1886 - Tectonics and Seismicity, U. S. Geological Survey Professional Paper 1313, p. 01-07, 1983
- Dutton, C. E., "The Charleston Earthquake of August 31, 1886", U. S. Geological Survey Annual Report No. 9, p. 203-528, 1889
- Fletcher, J. B., M. L. Sbar, and L. R. Sykes, "Seismic Trends and Travel Time Residuals in Eastern North America and Their Tectonic Implications", Geological Society of America Bulletin, Vol. 89, p. 1656-1676, 1978
- Fletcher, J. B. and L. R. Sykes, "Earthquakes Related to Hydraulic Mining and Natural Seismic Activity in Western New York", Journal of Geophysical Research, Vol. 82, No. 26, p. 3767-3780, 1977
- Hamilton, R. M., "Geologic Origin of Eastern United States Seismicity", in J. E. Beavers, Proceedings of Earthquakes and Earthquake Engineering: The Eastern United States, (Ann Arbor Science Publishers, Inc., Ann Arbor, MI), p. 3-23, 1981
- Harris, L. D. and K. C. Bayer, "Sequential Development of the Appalachian Orogen Above a Master Decollement - A Hypothesis", Geology, Vol. 7, p. 568-572, 1979
- Illies, J. H., "Der Hohenzollerngraben and Intraplatten-Seismizität Infolge Vergitterung Lamellarer Scherung mit Einer Riftstruktur," Oberrhein, Geol. Abh., Vol. 31, p.47-78, 1982
- Iverson, W. P. and S. B. Smithson, "Master Decollement Root Zone Beneath the Southern Appalachians and Crustal Balance", Geology, Vol. 10, No. 5, p. 241-245, 1982

- Kanamori, H., "The State of Stress in the Earth's Lithosphere", in Dziewonski, A. M., and Boschi, E., Physics of the Earth's Interior, Proceedings of the International School of Physics "Enrico Fermi" Course, (North-Holland Pub. Co., New York), p. 531-554, 1980
- Kane, M. F., "Correlation of Major Eastern Earthquake Centers with Mafic/Ultramafic Masses", in D. W. Rankin Studies Related to the Charleston, South Carolina, Earthquake of 1886 - A Preliminary Report, Geological Survey Professional Paper 1028, p. 199-204, 1977
- Klitgord, K. D., W. P. Dillon, and P. Popenoe, "Mesozoic Tectonics of the Southeastern United States Coastal Plain and Continental Margin", in G. S. Gohn, Studies Related to the Charleston, South Carolina, Earthquake of 1886 - Tectonics and Seismicity, U.S. Geological Survey Professional Paper 1313, p. P1-P15, 1983
- Long, L. T., and J. W. Champion, Jr., "Bouguer Gravity Map of the Summerville-Charleston, South Carolina Epicentral Zone and Tectonic Implications", in D. W. Rankin Studies Related to the Charleston, South Carolina, Earthquake of 1886 - A Preliminary Report, U. S. Geological Survey Professional Paper 1028, p. 151-166, 1977
- McKeown, F. A., "Hypothesis: Many Earthquakes in the Central and Southeastern United States are Causally Related to Mafic Intrusive Bodies", U. S. Geological Survey Journal of Research, Vol. 6, p. 41-50, 1978
- Meissner, R., and J. Strehlau, "Limits of Stress in Continental Crusts and the Relation to the Depth-Frequency Distribution of Shallow Earthquakes", Tectonics, Vol. 1, p. 73-89, 1982
- Poley, C. M., and P. Talwani, "Vertical Tectonics in the South Carolina Coastal Plain", Abstract, Eos, Transactions, American Geophysical Union, Vol. 65, p. 190, 1984
- Popenoe, P. and I. Zietz, "The Nature of the Geophysical Basement Beneath the Coastal Plain of South Carolina and Northeastern Georgia", in D. W. Rankin, Studies Related to the Charleston, South Carolina, Earthquake of 1886 - A Preliminary Report, U. S. Geological Survey Professional Paper 1028, p. 119-137, 1977
- Prowell, D. C., "Index of Faults of Cretaceous and Cenozoic Age in the Eastern U.S.", U.S. Geological Survey Miscellaneous Field Study Map, M.F. 1269, 2 sheets, 1983
- Rankin, D. W., "Appalachian Salients and Recesses: Late Precambrian Continental Breakup and the Opening of the Iapetus Ocean", Journal of Geophysical Research, Vol. 81, No. 32, p. 5605-5619, 1976

- Ravat, D. N., L. W. Brailes, and W. J. Hinze, "Earthquakes and Plutons in the Midcontinent-Evidence From the Bloomfield Pluton, New Madrid Rift Complex", Seismological Research Letters, Vol. 58, No. 2, p. 4-52, 1987
- Sbar, M. L. and L. R. Sykes, "Contemporary Compressive Stress and Seismicity in Eastern North America; An Example of Intraplate Tectonics", Geological Society of America Bulletin, Vol. 84, p. 1861-1881, 1973
- Seeber, L. and J. G. Armbruster, "The 1886 Charleston, South Carolina Earthquake and the Appalachian Detachment", Journal of Geophysical Research, B, Vol. 86, No. 9, p. 7874-7894, 1981a
- Seeber, L. and J. G. Armbruster, "Large Strain Effects of the 1886 South Carolina Earthquake", in Proceedings of Conference XX, A Workshop on "The 1886 Charleston, South Carolina, Earthquake and its Implications for Today", U. S. Geological Survey Open-File Report 83-0843, p. 142-149, 1983
- Seeber, L. and J. G. Armbruster, "The 1886-1889 Aftershocks of the Charleston, South Carolina, Earthquakes: A Widespread Burst of Seismicity", Journal of Geophysical Research, Vol. 92, p. 2663-2696, 1986
- Shedlock, K. M., "Seismicity Near Charleston, South Carolina - 1974 to Present", Abstract, Eos, Transactions, American Geophysical Union, Vol. 68, No. 16, p. 363, 1987
- Sykes, L. R., "Intraplate Seismicity, Reactivation of Pre-existing Zones of Weakness, Alkaline Magmatism, and Other Tectonism Postdating Continental Fragmentation", Reviews of Geophysics and Space Physics, Vol. 16, p. 621-687, 1978
- Taber, S., "Seismic Activity in the Atlantic Coastal Plain Near Charleston, South Carolina", Bulletin of the Seismological Society of America, No. 4, p. 108-160, 1914
- Talwani, P., "Internally Consistent Pattern of Seismicity Near Charleston, South Carolina", Geology, Vol. 10, No. 12, p. 654-658, 1982
- Talwani, P., "Intraplate Earthquakes, Block Tectonics, Aeromagnetic and Gravity Anomalies; or Why We Have Earthquakes at Charleston, S.C.", Geological Society of America Abstracts With Programs, Vol. 15, No. 2, p. 64, 1983
- Talwani, P., "Orientation of Stress in Southeastern United States", Geological Society of America Abstracts with Programs, Vol. 16, p. 202, 1984

- Talwani, P., "Seismotectonics of the Charleston Region", in J. E. Beavers, Proceedings, Third U. S. National Conference on Earthquake Engineering: the Eastern United States, (Earthquake Engineering Research Institute, El Cerrito, CA), p. 15-24, 1986
- Talwani, P., "Current Thoughts on the Cause of the Charleston, South Carolina Earthquakes", South Carolina Geology, Vol. 29, p. 19-38, 1986a
- Talwani, P., D. C. Amick, and R. Logan, "A Model to Explain the Intraplate Seismicity in the South Carolina Coastal Plain", Abstract, Eos, Transactions, American Geophysical Union, Vol. 60, p. 311, 1979
- Talwani, P. and D. Howell, "Crustal Structure of South Carolina - Some Speculations at Symposium of the Atlantic Continental Margin", Geological Society of America, Abstracts with Programs, Vol. 8, p. 284, 1976
- Talwani, P. and C. M. Poley, "Vertical Tectonics in the Charleston, S.C. Area", Abstract, Earthquake Notes, Vol. 55, p. 30, 1984.
- Tarr, A. C. and S. Rhea, "Seismicity Near Charleston, South Carolina, March 1973 to December 1979", in G. S. Gohn, Studies Related to the Charleston, South Carolina, Earthquake of 1886 - Tectonics and Seismicity, U. S. Geological Survey Professional Paper 1313, p. R1-R17, 1983
- Tarr, A. C., P. Talwani, S. Rhea, D. Carver, and D. Amick, "Results of Recent South Carolina Seismological Studies", Bulletin of the Seismological Society of America, Vol. 71, p. 1883-1902, 1981
- Weems, R. E., "Possible Subsurface Structures in Coastal Plain Sediments Near Charleston, S.C.", Abstract, Earthquake Notes, Vol. 55, p. 27, 1985
- Wentworth, C. M., "Reverse Faulting as the Source of Earthquakes Along the Eastern Seaboard of the United States; Problems and Needed Research", in Proceedings of Conference XX, A Workshop on "The 1886 Charleston, South Carolina, Earthquake and its Implications for Today", U. S. Geological Survey Open-File Report 83-0843, p. 117-125, 1983
- Wentworth, C. M. and M. Mergner-Keefer, "Reverse Faulting Along the Eastern Seaboard and the Potential for Large Earthquakes", in J. E. Beavers, Proceedings of Earthquakes and Earthquake Engineering: Eastern United States, (Ann Arbor Science Publishers, Ann Arbor, MI), p. 109-128, 1981a

- Wentworth, C. M. and M. Mergner-Keefer, "Regenerate Faults of Small Cenozoic Offset; Probable Earthquake Sources in the Southeastern United States", U. S. Geological Survey Open-File Report 81-0356, 37 p., 1981b
- Wentworth, C. M. and M. Mergner-Keefer, "Regenerated Faults of Small Cenozoic Offset; Probable Earthquake Sources in the Southeastern United States", in G. S. Gohn, Studies Related to the Charleston, South Carolina Earthquake of 1886 - Tectonics and Seismicity, Geological Survey Professional Paper 1313, p. S1-S20, 1983
- Wheeler, R. L. and G. A. Bollinger, "Seismicity and Suspect Terranes in the Southeastern U.S.", Geology, Vol. 12, p. 323-326, 1984
- Williams, H. and R. D. Hatcher, Jr., "Suspect Terranes and Accretionary History of the Appalachian Orogen", Geology, Vol. 10, p. 530-536, 1982
- Yang, J. and Y. P. Aggarwal, "Seismotectonics of Northeastern United States and Adjacent Canada", Journal of Geophysical Research, Vol. 86, p. 4981-4998, 1981
- York, J. E. and J. E. Oliver, "Cretaceous and Cenozoic Faulting in Eastern North America", Geological Society of America Bulletin, Vol. 87, p. 1105-1114, 1976
- Zoback, M. D., "Intraplate Earthquakes, Crustal Deformation, and In-Situ Stress", in Proceedings of Conference XX, A Workshop on "The 1886 Charleston, South Carolina, Earthquake and its Implications for today", U. S. Geological Survey Open-File Report 83-0843, p. 169-178, 1983

CHAPTER 3

PROJECT APPROACH

The purpose of this project was to develop geophysical and geological information that would permit defining the cause of seismicity near Charleston, South Carolina, or reducing the number of theories that may explain it. Our approach to this project was to gather a comprehensive set of existing data and collect new data (primarily gravity and magnetotelluric measurements) where needed. These data were used to construct geologic and stress models which would be used to test the various extant hypotheses concerning the origins of the 1886 Charleston earthquake.

As indicated, a major effort of this project involved the collection and processing of new and existing potential field data as well as magnetotelluric data, seismic data, and geologic information. This involved establishing data formats and computer programs to allow easy evaluation of the information gathered. Existing and new potential field data were then accumulated and made compatible with the common data base, which would be available for use by other researchers. Chapter 4 describes this data gathering and formatting process.

The collected data were used to develop a geologic interpretation of the crust in the Charleston area. The interpreted crustal geology was used both in producing a crustal stress model and in directly testing hypotheses. The process of producing the geologic model using the variety of available data is detailed in Chapter 5.

As part of our hypothesis evaluation, we wanted to be able to consider the state of stress in the crust in the Charleston region. Our approach to this was to model both the regional and local stress fields.

The regional three-dimensional model considered topography and crustal density differences as causes of stress in the crust, and also considered stresses due to the horizontal plate-spreading force originating at the mid-Atlantic ridge. This large scale regional modeling was done mainly to determine if the state of stress in the Charleston area was very different from surrounding areas. This regional stress modeling is described in Chapter 6.

The two-dimensional local stress model was a finite element model whose geometry and physical properties were determined from our geologic model. The purpose of this model was to determine perturbations in the stress field in the Charleston area. The local stress modeling is described in Chapter 7.

The final step in this project was to use the available data, together with our geologic and stress modeling results, to critically examine the existing hypotheses for the cause of the

Charleston earthquake which were presented in Chapter 2. The results of this analysis are given in Chapter 8.

CHAPTER 4

GEOPHYSICAL AND GEOLOGIC DATA

Information accumulated for the testing of hypotheses for the sources of the 1886 Charleston earthquake is presented in this chapter. The sources of the data, their manipulation, and the final format and availability are also discussed. The data are divided into four sets. The first set consists of data which can be gridded: gravity, magnetics, ground elevation and bathymetry, and satellite imagery. The second set consists of magnetotelluric soundings and modeling performed specifically for this project. The third set consists of seismic reflection and refraction interpretations compiled to help constrain the crustal model. The fourth set consists of geologic information collected from various sources.

Most geophysical studies of the epicentral zone of the 1886 Charleston earthquake have collected, analyzed, and presented data in a manner which best displays that type of data. It is the goal of this study to accumulate many types of geophysical data. Different data types such as potential data, landsat images, magnetotelluric soundings, and geologic information are best presented in significantly different and often incompatible formats. Hence, the first objective of this study of data relevant to the Charleston earthquake was to establish a single appropriate format for all data. The format would permit the direct comparison of a variety of data types and permit the use of analysis techniques for multiple data sets on a common data base. The second objective was to accumulate existing data and make it compatible with the common data base. In most cases, this requires a change in format and a merging of data sets from different sources. A third objective was to provide a mechanism to update the data when new data become available and to assess the accuracy of the data. The fourth objective was to present the collected data in a format appropriate for distribution.

4.1 Gridded Data

This section discusses data which can be represented by discrete points. The description of gridding and analysis common to all gridded data is discussed first, followed by the specific information concerning gravity, magnetics, elevations, bathymetry and Landsat data.

4.1.1 Grid Definitions and Data Consolidation

The use of a two-dimensional planar representation of data on an ellipsoidal surface is inherently non-conformal. The distortion of distances, directions, and areas will depend on the projection. A variety of projections (including Lambert conic, Universal Transverse Mercator, Albers equal area) have been used for the data available to this study. A direct comparison of data on different projections is difficult.

While the dimensions of a grid may be the same, the grid points do not coincide with the same location on the earth's surface. In order to compare data which were originally in different projections, all the data should be referenced to a grid in the same projection. The Landsat data are conventionally displayed using the Universal Transverse Mercator projection. In terms of the amount of computational effort required to effect conversion among projections, the Landsat data would be the most difficult because there are more than 16 million data points. For this reason we have chosen the Universal Transverse Mercator projection (zone 17) to map latitude and longitude to a plane surface on which a uniform rectangular grid can be defined. Other projections, for example the Albers Equal Area Conic projection, are more common and more appropriate for large study areas such as the eastern United States. However, the largest area of interest in this study has a longitudinal dimension of about 1500 km and the distortion at this distance related to the Universal Transverse Mercator (UTM) projection is significantly less than the precision necessary for the data presented in the large grid. In the case of the largest grid, the area extends beyond zone 17 but the zone is fixed at 17 for consistency even outside of zone 17. FORTRAN subroutines for converting UTM coordinates to latitude and longitude and back are given in Appendix A.

The interpolation of scattered data into a rectangular grid was accomplished by a weighted average over a limited area. The weighted average, which is limited to a small area, allows the grid to be easily updated any time new data are available. The computational implementation to the weighted average is also efficient and stable.

The values at each grid point were determined by the weighted average of all data points falling within an area defined by a square with three grid points on a side (Figure 4-1). The weights are a function of distance and decrease with increasing distance between the grid point and the data point. The data points are transformed from their original coordinate system to the Universal Transverse Mercator projection. After the grid area surrounding a data point is identified, the surrounding 16 grid points are found. For each grid point the distance to the data point is computed. Then the weighting function is calculated by the following equation,

$$\bar{w}_i = \sum_{i=1}^{16} w_i$$

where:

$w_i = [1/(1+(r_i/dx))]$, the weight function

$dx =$ grid point separation

$r_i =$ distance from data point to grid point

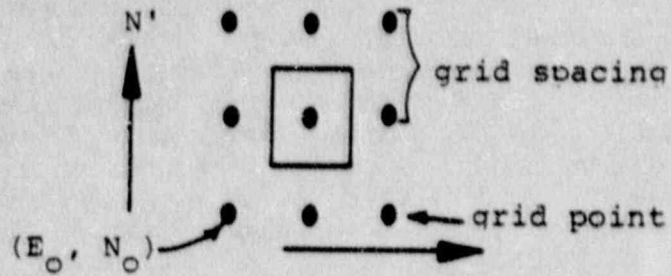


Figure 4-1. Location of grid points relative to sample area. The sample area consists of nine grid points.

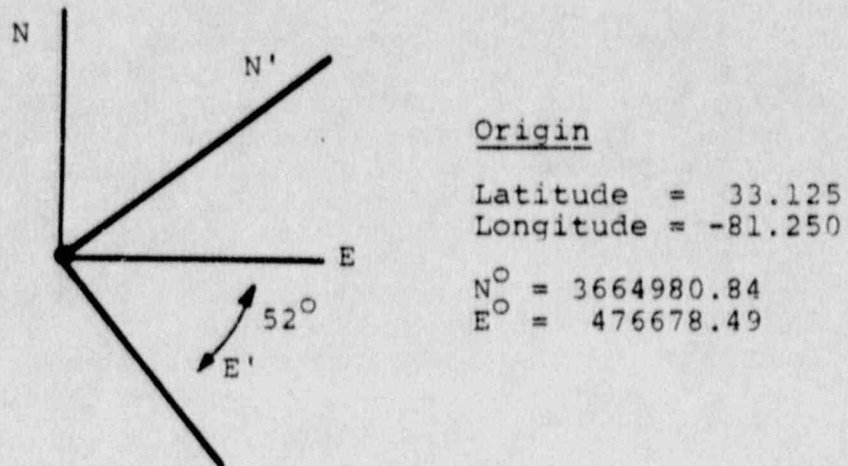


Figure 4-2. Relative locations of rotated reference axes.

The spacing between the grid points is set to the grid separations for this study (i.e., 1 km, 4 km, 8 km, 31.25 m). The individual weights are normalized. Hence, the significance of the weights is that they are equivalent to the number of points contributing to a grid point or the density of data for the area represented by one grid point. With this distance-dependent weight, significantly greater weight is given to the closer grid points. Since data points near the edge of the grid area do not have 16 surrounding grid points, two extra rows (or columns) were added at the four edges of the grid for convenience in programming. These values are preserved for the addition of new data to the grid but are excluded from the grids used in analysis. The program used to generate the grid is found in Appendix A, and is called program SNGGRID.

The gridding technique employed in program SNGGRID works best when the data density is uniform and similar to the density of the grid. In areas where the data are most dense, an averaged and smoothed value is given at the grid point, simulating the average effect of the field surrounding the grid point and not just the value at the grid point. The average is preferable to the point value for modeling since it better represents the block corresponding to the grid point. In areas of equivalent density, the gridded data represent a smoothing of the original data within a radius equivalent to the grid spacing. For the more difficult condition of areas which lack data, the gridding technique does not provide information and the values remain zero. For these conditions, a program to expand the radius of smoothing was developed. This program, AB, considers each point at which the weight (equivalent number of points) fell below a criterion determined by the distance and weighting function suggesting that less than three points contributed to the value. For those points, the area was expanded until the equivalent of six points contributed to the value and the weighted average recomputed. This is equivalent to choosing a larger grid increment and interpolating between grid points.

Four data grids were used; each data grid was centered about the epicentral zone of the 1886 Charleston earthquake. The grids are all square in the Universal Transverse Mercator projection and are rotated clockwise 52 degrees about the point (33.125°N , 81.25°W) which corresponds to the points (1,1) in the 128 x 128 point grid with 1.0 km spacing called grid 1 (Figure 4-2). The other grids are centered on this grid exactly and have sides of 256 points at 4.0 km spacing (grid 2), 128 points at 8.0 km spacing (grid 3), and 4096 points at 31.25 m spacing (grid 4). Table 4-1 and Table 4-2 contain grid sizes and corner coordinates, respectively. Figure 4-3 shows the grid locations.

The locations in the rotated system are found by the following steps:

Table 4-1. Size of the four grids.

Grid No.	Pts./Side	Side Length (km)	Grid Interval	Data
1	128	128	1.0 km	gravity ¹ , topography ² , magnetics ³
2	64	256	4.0 km	gravity ⁴ , magnetics ⁵ , topography ⁶
3	128	1028	8.0 km	gravity ⁴ , topography ⁶ , magnetics ⁵
4	4096	128	.03125 km	Landsat ⁷

¹ Gravity data from Georgia Institute of Technology, Virginia Poly and State University, U.S. Geological Survey, University of So newly acquired data.

² Topography from gravity surveys.

³ Magnetics from USGS/SEG.

⁴ Gravity from EPRI.

⁵ Magnetics from EPRI.

⁶ Topography from EPRI.

⁷ Proprietary data from EOSAT.

Table 4-2. Corner coordinates of grids.

Grid No.	X	Y	N (feet)	E (feet)	Latitude (°N)	Longitude (°W)
1	1	1	3,664,980	476,678	33.1250	81.2500
1	128	1	3,564,903	554,867	32.2211	80.4177
1	1	128	3,743,170	576,756	33.8277	80.1705
1	128	128	3,643,092	654,945	32.9168	79.3430
2	1	1	3,675,753	388,949	33.2167	82.1916
2	64	1	3,477,173	544,095	31.4301	80.5360
2	1	64	3,830,899	587,527	34.6180	80.0453
2	64	64	3,632,320	742,674	32.8038	78.4084
3	1	1	3,741,590	-147,254	33.6190	87.9710
3	128	1	2,940,971	478,258	26.5908	81.2183
3	1	128	4,367,102	653,365	39.4417	79.2178
3	128	128	3,566,483	1,278,877	31.9683	72.7695
4	1	1	3,665,064	475,999	33.12574	81.25729
4	4096	1	3,564,224	554,784	32.21497	80.41865
4	1	4096	3,743,850	576,839	33.83385	80.16958
4	4096	4096	3,643,009	655,624	32.91597	79.33577

The relative positions of the grid corners can be seen in Figure 4-3.

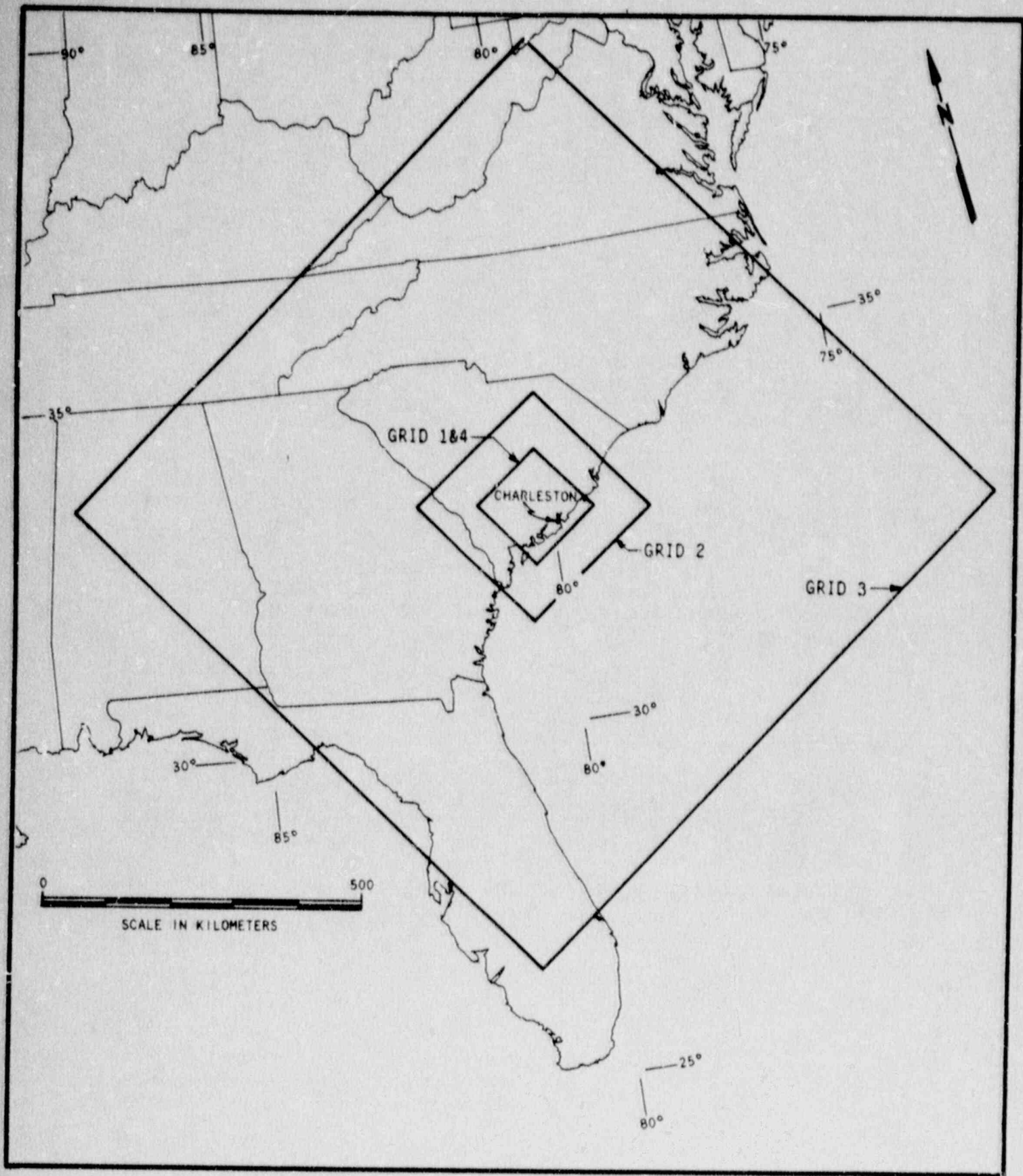


Figure 4-3. Location of data grids. See Tables 4-1 and 4-2 for grid sizes and corner coordinates.

1. Transform latitude and longitude to UTM zone 17 (i.e. to N,E).
2. Shift origin to grid point (1,1) at (N_0, E_0) .
3. Rotate axes clockwise 52 degrees to primed coordinate system.
4. Find index of grid point closest to the data point.

Computer programs to transform latitude and longitude to UTM zone 17 are given in Appendix A. The equations for step two, the translation, and step three, the rotation, are combined as follows:

$$E' = (E - E_0) \cdot \cos(A) - (N - N_0) \cdot \sin(A)$$

$$N' = (E - E_0) \cdot \sin(A) + (N - N_0) \cdot \cos(A)$$

where A is positive clockwise.

The new primed axes (N', E') represent a clockwise rotation of the old axes (N, E) about (N_0, E_0) .

Within each grid, a grid point represents data in a square area centered over the grid point and with sides equal to the grid spacing (Figure 4-1). The relative locations of the grid points in each of the four grids are shown in Figure 4-4.

The 64 x 64 point grid (grid 2) with dimensions of 256 km is centered on the reference grid. In the rotated system, the grid reference point (1,1) for the 64 x 64 point grid is located at $N' = -62.5$ km and $E' = -62.5$ km.

The 128 x 128 point grid with 8 km grid interval and dimensions of 1024 km is also centered on the reference grid. For grid 3 the grid reference point (1,1) for the 128 x 128 point 8 km grid is located at $N' = -444.5$ km and $E' = -444.5$ km.

The Landsat data have 4096 x 4096 points which can be divided into 64-512 x 512 point units for convenient display. Each unit of 512 x 512 points covers an area of side length 16 km or an area of 256 square km. The pixels were rectified to the 128 x 128 point 1.0 km grid points such that each 1.0 km grid point is surrounded by four areas of 16 x 16 pixels. The pixels are 31.25 meters apart and the origin is at the point $N' = -484.375$ m, $E' = -484.375$ m in grid 4.

The index (IX, IY) of the grid points closest to a specified latitude and longitude coordinate (or UTM coordinate position) can be obtained from the following equations:

$$IY = 1 + \text{Int}[(N' - R(I) + DY(I)/2.0)/DY(I)]$$

$$IX = 1 + \text{Int}[(E' - R(I) + DX(I)/2.0)/DX(I)]$$

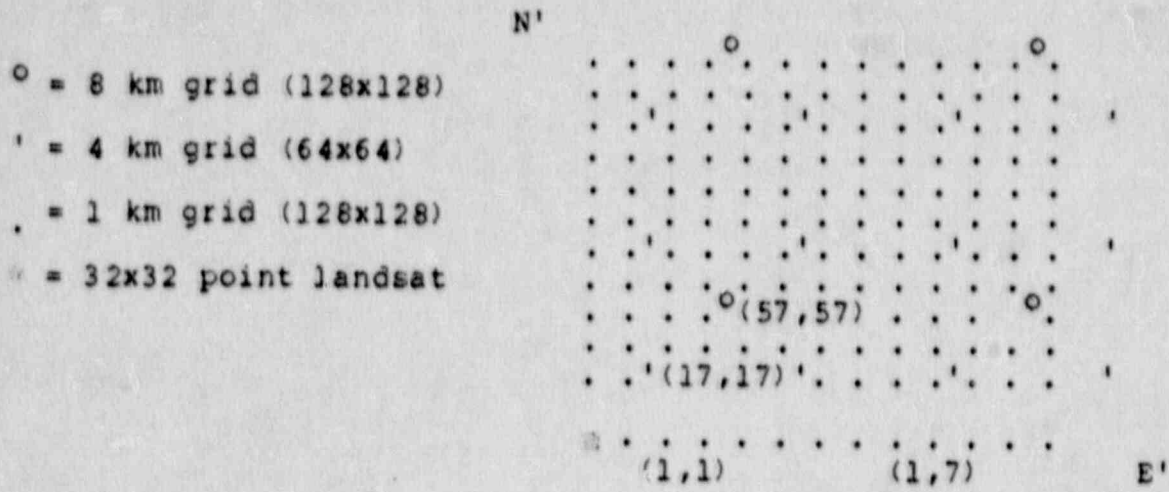


Figure 4-4. Relative location of grid points.

(Int[] truncates fractional part of number)

where $R(I)$ is the origin in the primed system of the I th grid, DX or DY is the grid point spacing of the I th grid, and in this study $DX(I) = DY(I)$.

4.1.2 Gravity

The gravity data accumulated for this study were taken from several sources. For grids 2 and 3, the Bouguer gravity values were provided by the Electric Power Research Institute (EPRI). Grid 1 consisted of Bouguer gravity values from the Georgia Institute of Technology, the U.S. Geological Survey, Virginia Polytechnic Institute and State University, and new field data.

4.1.2.1 EPRI Gravity Data

EPRI acquired gravity data from the Defense Mapping Agency (DMA). These points were converted into a digital gridded set. Onshore data consist of Bouguer gravity anomaly values computed using a density of 2.67 g/cm^3 , and the offshore data consist of free-air gravity anomaly values.

All computations were performed using the International Gravity Standardization Net of 1971 (Morelli, 1974) and the 1967 Geodetic Reference System formula for theoretical gravity (International Association of Geodesy, 1971).

The initial data set acquired by EPRI was first screened to eliminate redundant values, then terrain-corrected in areas that had substantial relief, and finally edited to remove erroneous values. Even though the data have been extensively edited, a few incorrect values unknown to authors may still be present in the data set. Terrain corrections were computed at radial distances from station locations ranging from .895 km (Hammer zone F) to 166.7 km (Hayford zone 0) using a density of 2.67 g/cm^3 . The final corrected data were then transformed from geodetic coordinates to ground kilometers using an Albers equal-area projection with a central meridian of 96 degrees and standard parallels of 29.5 degrees and 45.5 degrees.

A gridding program (Webring, 1981) based on a minimum curvature procedure (Briggs, 1974) was used to produce values spaced at 4 km intervals. The program used a search radius of 40 km to determine values at grid positions in areas of sparse data. This distance was sufficient to calculate values at all grid locations inside the boundaries of the data. This procedure extrapolated the data out to the search radius around the irregular boundaries of the data, and, therefore, these extrapolated values should be used with caution.

Since a rectangular grid is produced from irregularly spaced data, there are many grid locations around the edges of the data beyond the search radius where no values were calculated. These grid locations were arbitrarily assigned a value of 9999.

The above description applies to EPRI procedures. For purposes of this study, the EPRI data were converted to our gridding system.

4.1.2.2 Merging and Compilation of Data

All the data incorporated in the 1 km grid for gravity data were carefully examined. Duplicate points and points which were inconsistent with neighboring points were removed before generating the grid. The programs designed to remove duplicate points, CLEAN, and the program designed to identify inconsistent data, CLERR, are given in Appendix A.

Program CLEAN was designed to identify duplicate and virtual duplicate points. Each new point was compared to a sorted listing of the gravity points and those pairs that were closer than a distance of 0.2 km were listed for examination. One of these was removed. The choice was based on the value of the Bouguer Anomaly. Duplicate points were common because the same data were often obtained from multiple sources. This duplicity was easily identified on basis of identical gravity values and survey designations. In a few cases, the same data were reduced using two different international gravity formula. The difference in the value of gravity allowed choice of the data referenced to the IGSN 71 datum. When the same location was sampled by two different surveys, the choice of value to use was more difficult. In general, we chose the value most consistent with neighboring points. In some surveys, data were obtained at closely spaced intervals along lines. Such data tend to bias values computed by a weighted average technique. In order to minimize the bias and provide a data set with more uniform data distribution, data points were removed from the line. In essence, points closer than 0.2 km were considered duplicates and selectively removed.

Program CLERR was designed to identify values that were anomalous or inconsistent. Each point tested was removed from the data set and the eight nearest points were found. These points were then used to estimate by a weighted average method the value and uncertainty at the point. Any point that deviated more than one standard deviation from the extrapolated value was considered as a possible error or inconsistent value. These values were examined for a possible correction. If correction was not possible and the apparent error could not be explained by gradients in the data, the value was considered in error and removed.

The largest block of data was obtained from the files of Georgia Tech. This block includes detailed survey areas near the epicenter of the 1886 earthquake (Champion, 1975) and the 1972 Bowman earthquake (McKee, 1974). It also includes a selection of detailed line data and existing regional data. U.S. Geological Survey data (Phillips and Davis, 1985) made available to the study expanded the Georgia Tech data to the west, northwest, and north. Data from the Virginia Polytechnic

Institute and State University complemented the USGS data. University of South Carolina data which cover the northern corner of the study area were not made available to us. Consequently, based on the existing coverage, it was decided to extend the data area to the east and to fill in major gaps between the USGS and Georgia Tech, Bowman area data. The only remaining significant areas of sparse data would be in areas of difficult access near the coast and lake or swamp areas to the north.

4.1.2.3 Acquisition of New Gravity Data

The goal in gravity data acquisition was to provide data sufficient to complete a grid with a uniform 1.0 km spacing between points and 128 points on each side (Grid 1, Table 4-1). The grid was rotated to follow the coastline and maximize the land area. Such a grid requires 16,384 points and only about 3150 points were available. Since we budgeted for only about 600 new data points, it was important to use those 600 points in areas of sparse coverage near the epicenter of the 1886 Charleston earthquake. Hence, areas of new data were chosen to expand the areas of existing coverage in the central portion of the grid.

Standard methods of gravity data acquisition and reduction were followed. Data reduction used the program GRAVUN on file at the Georgia Institute of Technology, School of Geophysical Sciences. Data were obtained along lines at a spacing of less than 0.5 km or as regional data at a 1.0 km spacing. Corrections were applied for earth tides and drift. These techniques are outlined in Champion (1975). Appendix A lists the surveys. All surveys were made with LaCoste-Romberg gravity meter number 668. All data are tied to the Branchville state base. Temporary base station values are also given in Appendix A. Point plots and format information can be found in Appendix A.

4.1.2.4 Image Processing of Gravity and Magnetic Data

The image processing of gravity and magnetic data was performed on the image processing system at Georgia Institute of Technology. The system was developed by Earth Resources Data Analysis Systems (ERDAS) of Atlanta, Georgia. It was designed primarily for the analysis of satellite imagery, and has the capability of displaying raw data as various false colors or shades of gray. Three bands of data may be examined at one time, each band being given one of three colors (red, blue or green). The intensity level of the color at each grid point is controlled by the data value associated with that grid point. If the same data set is used on all three bands, the data values are associated with shades of gray. Various operations may be performed on the resulting image, including intensity stretching, which improves contrast, and level slicing, which can isolate certain select data values.

For this study our 1 km gravity and magnetic grids were converted to imagery data files. In addition, the vertical second derivatives were calculated for both data sets, and these grids were also converted. Finally, the shaded-relief technique (Dods, *et al.* 1985) was used to examine the gravity and magnetic data as pseudo-topography under a variety of false sun-angles. The results and uses of these various operations are given in Chapter 5.

4.1.3 Magnetic Data

The magnetic data came from two sources: the Electric Power Research Institute (EPRI) and a joint U.S. Geological Survey and Society of Exploration Geophysicists project (USGS/SEG). EPRI data were used for grids 2 and 3 and USGS/SEG data were used for grid 1. Both sets required conversion to our gridding systems.

For EPRI, the continental U.S. residual magnetic anomaly data were acquired from the Phoenix Corporation. They were sampled at 2 minute intervals and were located using coordinates in decimal degrees. The locations were transformed to kilometers. After this, the 1975 IGRF reference field (updated to 1977.19) was added back into the grid. Then the 1975 DGRF reference field (updated to 1977.19) was subtracted from the grid. This resulted in residual magnetic values related to the 1975 DGRF. This is the condition of the data set as we received it from EPRI. We further modified the data by converting it to our gridding systems.

The magnetic data acquired for grid 1 were assembled by the U.S. Geological Survey and the Society of Exploration Geophysicists (1982). There were six sources for the data in the area of study. All consisted of airborne magnetic recording with flightline spacing of 1/2 to 1 mile. Elevations were 400 to 500 feet above ground (Appendix A).

Flight altitudes were not continued upward or downward to a common value. These data are total-intensity aeromagnetic-anomaly data. These anomaly data were referenced to various magnetic field datums; however, an attempt was made (USGS SEG 1982) to adjust most anomaly data to a common magnetic-field datum (Fabiano and Peddie, 1969; Barraclough and Fabiano, 1978).

As indicated earlier, grid 1 magnetic data were also loaded into the EPDAS image processing system at Georgia Institute of Technology.

4.1.4 Geodetic Data

Topographic or elevation data were obtained from EPRI and from elevations taken from gravity field work. The data received from EPRI were sampled at intervals of two minutes of longitude and one minute thirty seconds latitude to produce a grid of 4

km spacing. The locations were computed to kilometers. For our use, the topography for EPRI was converted to our gridding system. The EPRI data set was used in grids 2 and 3. Grid 3 was supplemented by offshore bathymetry data digitized from bathymetry maps.

For grid 1, elevations were provided by measurements taken from U.S.G.S. quadrangle maps from gravity data acquisition. These elevations were gridded and smoothed for our use.

4.1.5 Availability of Gridded Data

Gridded magnetic, gravity, or topographic data on grids 1 through 3 can be purchased from Georgia Institute of Technology for a handling and shipping fee. Purchasing information can be obtained from:

Charleston Earthquake Program
Department of Geology and Geophysics
Georgia Institute of Technology
Atlanta, Georgia 30332-0340

4.1.6 Satellite Imagery

Satellite imagery from the Landsat thematic mapper series was bought from EOSAT. The image was selected for the highest quality, least cloud cover, and best sun angle. The Landsat data have been gridded with 4096 points on a 128 km side. This yields over 16 million points with 31.25 meters between each point.

4.2 Magnetotelluric Soundings

Magnetotelluric sounding information, in contrast to the gridded data in the previous section, is presented as field data (Appendix B) and as one-dimensional and two-dimensional interpretations.

4.2.1 Introduction

As part of this study, twelve magnetotelluric (MT) soundings were conducted near Charleston, South Carolina. The MT method is a geophysical technique that measures subsurface resistivity by passively measuring the electrical currents induced in the earth by fluctuations in the earth's magnetic field.

The primary purpose of the soundings was to produce information at seismogenic depths that would help constrain the geologic crustal model. A secondary purpose was assessment of the usefulness and cost-effectiveness of the magnetotelluric method for collecting resistivity data at seismogenic depths in the Charleston area. Audio-frequency magnetotelluric and other electrical sounding data have been collected in the Charleston area by the U.S. Geological Survey (Campbell, 1977). This previous study investigated to depths of only 1.6 km.

Remote reference tensor MT measurements were conducted under our supervision by Michigan Technological University near Charleston, South Carolina during October and November, 1985. A real-time magnetotellurics apparatus manufactured by Phoenix Geophysics of Willowdale, Ontario was used to make deep soundings. The results of these soundings were used to help model deep crustal structure in the area surrounding the epicentral zone of the 1886 Charleston, South Carolina earthquake. Figure 4-5 shows the location of the 12 soundings which occupy two lines crossing at Summerville, South Carolina. Table 4-3 gives the names and coordinates of the stations.

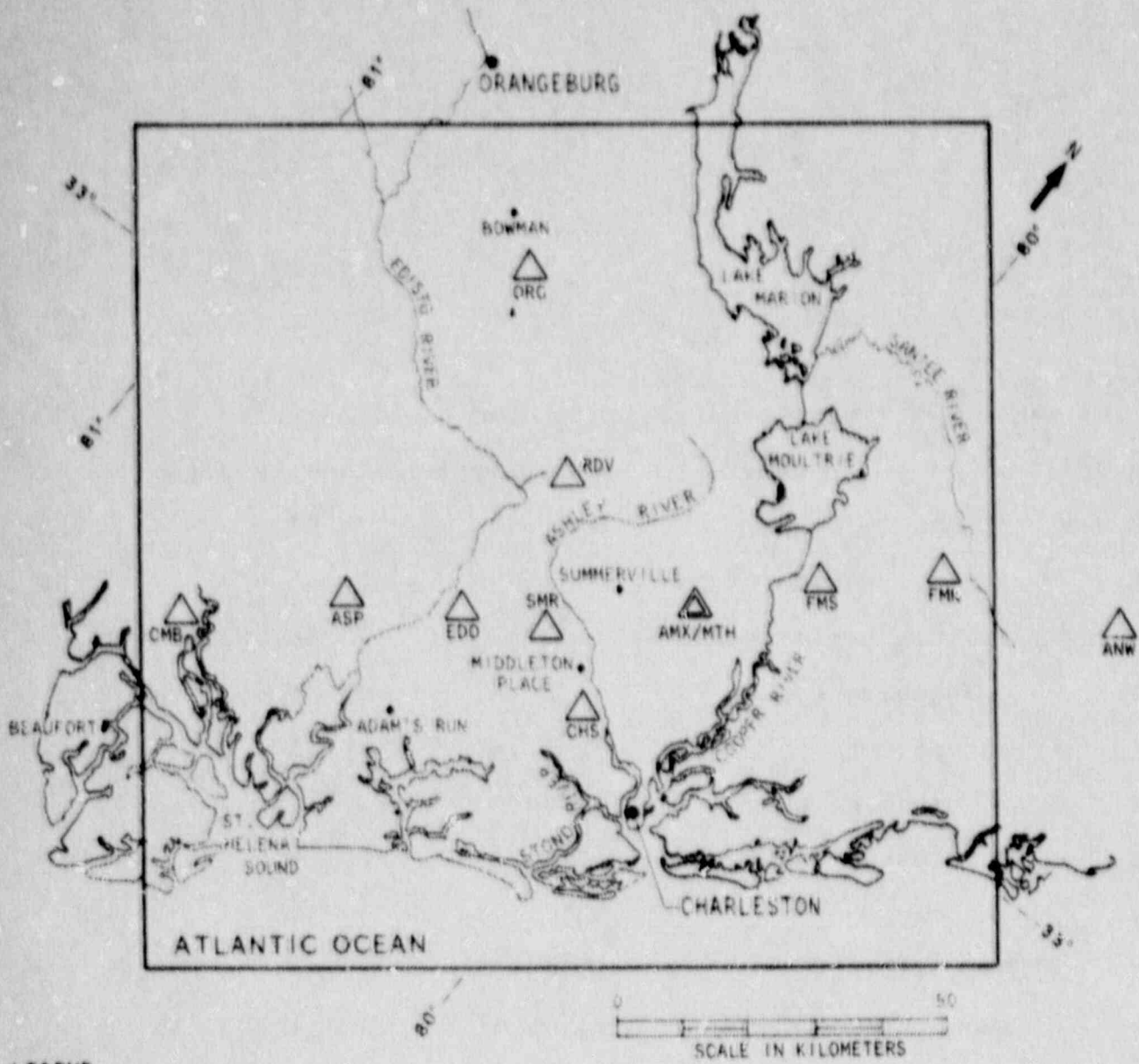
Tensor magnetotellurics (MT) uses natural time-varying electric and magnetic fields to determine the surface impedance of the earth. From the impedance at one or more sites, a resistivity cross section can be estimated which can be interpreted for geologic structure. MT has the advantage of great depths of penetration (tens of kilometers), high lateral resolution, and no need for a man-made signal source. The primary disadvantages are the complicated recording apparatus necessary and the sophisticated data analysis. Details on the recording apparatus, magnetotelluric theory, data, and data analysis can be found in the section titled "Magnetotelluric Soundings Near Charleston, South Carolina Volume I: Principles" in Appendix B.

Sites for MT soundings were chosen to have as little cultural noise as possible (cultural noise includes power line interference, mining operations, logging operations, etc.). The general locations were chosen to give the best data, the deepest crustal structure, and maintain a safe distance from the (highly conductive) Atlantic Ocean. The stations form two lines, one parallel to the coast and one perpendicular to the coast.

4.2.2 Principles of the Magnetotelluric Method

The MT method uses natural transient electric and magnetic fields to determine the surface electromagnetic impedance of the earth. These fields are generated by the flow of charged particles in the ionosphere and by distant lightning storms. The electromagnetic impedance expresses an assumed linear relationship between the applied magnetic field and the resulting electric field. The observation depth of a given measurement is dependent upon the frequency of the detected signal and upon the subsurface resistivity. Low frequency electromagnetic waves penetrate deeper than high frequency waves. Waves of a given frequency penetrate deeper into resistive rocks than into conductive rocks. The impedance is usually expressed as apparent resistivity and plotted as a function of period. An example can be seen in Figure 4-6. The rest of the sounding data can be found in Appendix B.

Remote reference recording was used during this survey; two horizontal components of electric field and three orthogonal



LEGEND
 △ MAGNETOTELLURIC STATION

Figure 4-5. Locations of Magnetotelluric Stations. See Table 4-4 for station coordinates.

Table 4-3. Magnetotelluric station coordinates.

Site Code	Site Code	Latitude ($^{\circ}$ N)	Longitude ($^{\circ}$ W)
AMX/MTH	Alumax	33 $^{\circ}$ 04'	80 $^{\circ}$ 04'
FMS	Francis Marion South	33 $^{\circ}$ 11.5'	79 $^{\circ}$ 55.5'
FMN	Francis Marion North	33 $^{\circ}$ 18'	79 $^{\circ}$ 46.5'
ORG	Orangeburg County	33 $^{\circ}$ 17.5'	80 $^{\circ}$ 36.5'
ASP	Ashepoo	32 $^{\circ}$ 47.5'	80 $^{\circ}$ 31'
CMB	Combahee River	32 $^{\circ}$ 38'	80 $^{\circ}$ 43'
CHT	Charleston County	32 $^{\circ}$ 51.5'	80 $^{\circ}$ 06.5'
ANW	Andrews	33 $^{\circ}$ 23.5'	79 $^{\circ}$ 30'
RDV	Ridgeville	33 $^{\circ}$ 06'	80 $^{\circ}$ 21.5'
SMR	Summerville	32 $^{\circ}$ 55.5'	80 $^{\circ}$ 14'
EDO	Edisto River	32 $^{\circ}$ 52'	80 $^{\circ}$ 21.5'

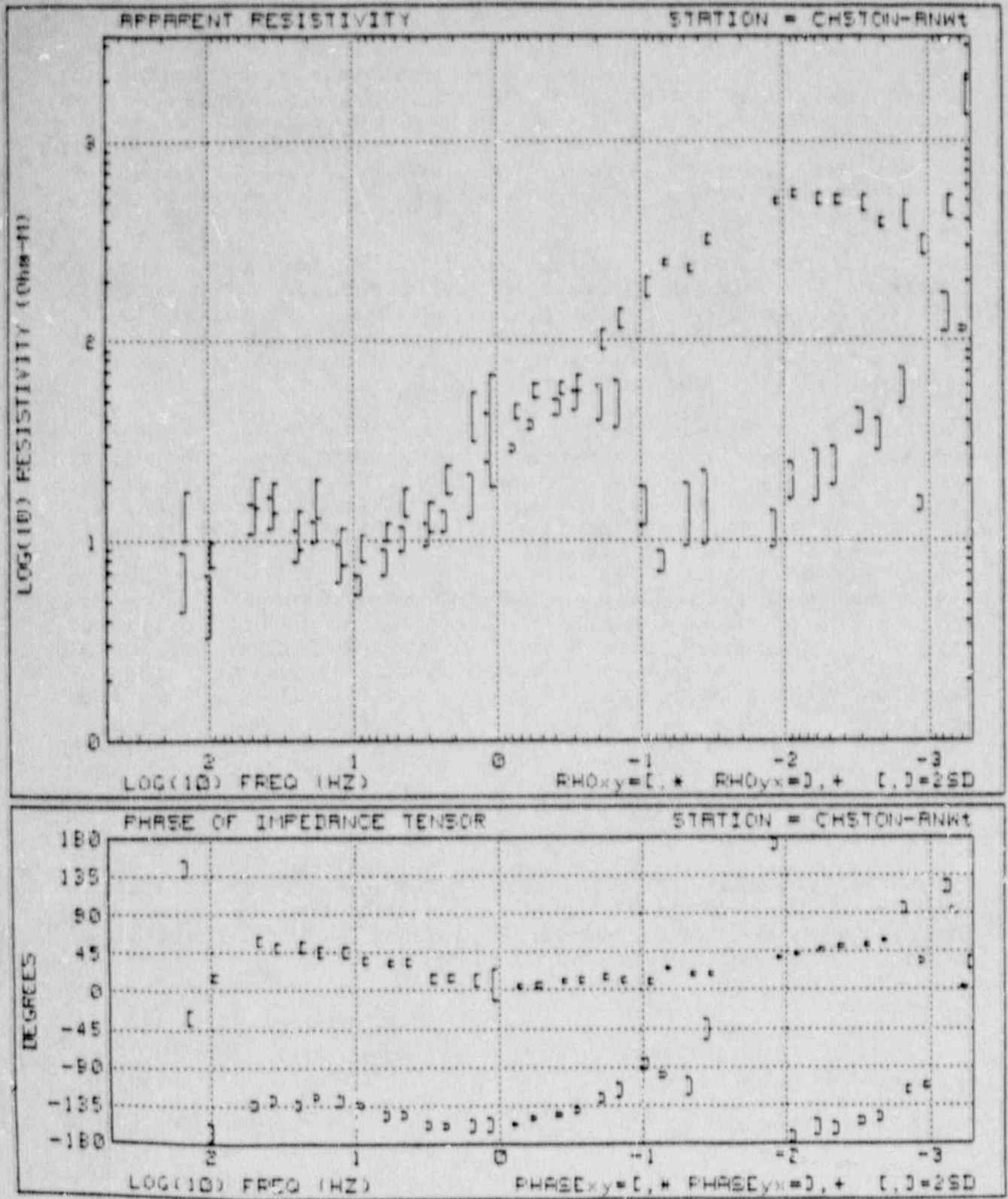


Figure 4-6. Example plot of apparent resistivities and frequencies for magnetotelluric station ANW. See Appendix B for explanations and other data.

components of magnetic field were recorded at the survey station; and, simultaneously, two components of reference magnetic field at a station a few hundred meters away were also recorded. The reference field was used to improve the signal-to-noise ratio. Coincident signals were considered to be correct and non-coincident signals were assumed to be noise. This procedure reduces the effects of circuit noise or local ground vibrations.

The horizontal electric and magnetic fields are used to determine the impedance tensor which is usually mathematically rotated with respect to the principal axis. The direction of principal axis (impedance maximum) and the ratios of the maximum to minimum impedance express the electrical resistivity structure in the subsurface at the site.

The vertical component of the magnetic field is used to define a magnetic field transfer function which is also used to reveal the resistivity structure of the area. If the earth consists only of flat layers, there will be only uniform currents, but if there is a more complicated structure, electric current will concentrate in conductors. The magnetic field of a concentrated current curls around the current, as described by the right hand rule; thus, a horizontal current concentration will have a vertical magnetic field component on either side of it. The ratio of the vertical magnetic field to horizontal magnetic field components, known as the magnetic transfer function, is a tensor consisting of phasors. The axes of this tensor can be mathematically rotated to maximize one component, thereby finding the direction perpendicular to the orientation of the current concentration. More detail on this technique can be found in Appendix B.

4.2.3 Magnetotelluric Data

The magnetotelluric (MT) data were reduced in the field and lab by Michigan Technological University. The data are presented in the section "Magnetotelluric Soundings Near Charleston, South Carolina Volume II: Data" in Appendix B.

4.2.4 Modeling Results

Magnetotelluric data were analyzed using one-dimensional (1-D) and two-dimensional (2-D) techniques. Preliminary 1-D modeling was prepared as part of this project by C. T. Young and J. C. Rogers of Michigan Technological University (Appendix B-1). Additional 1-D modeling was performed by J. C. Mareschal of the Universite du Quebec a Montreal. Initial two-dimensional modeling was performed by C. T. Young and M. R. Kitchen. Final 2-D modeling and magnetotelluric interpretation was conducted by Law Environmental personnel.

4.2.4.1 One-Dimensional Modeling

The 1-D modeling consisted of Bostick one-dimensional inversion (Bostick, *et al.* (1977)). This computation converts apparent resistivity data to a continuous resistivity versus depth function. The computation is an approximate method of converting field measurements to apparent resistivity versus depth. Details on this technique are given in Appendix B.

One-dimensional modeling and interpretations were discussed by Young, *et al.* (1986); the following discussion incorporates their work. Figure 4-7 presents apparent resistivity curves for each site. The data have been rotated at each site to obtain maximum and minimum values. Typically, at a given site, the maximum and minimum resistivities are nearly identical at short periods, indicating a locally flat layered earth.

The apparent resistivities generally drop at intermediate periods, rise at longer periods and drop at the longest periods. This sequence reflects the variation of resistivity with depth. The maximum and minimum apparent resistivity curves diverge with increasing period, indicating that the earth should be modeled in two or three dimensions at these frequencies.

The models show four layers. The top layer is moderately conductive (12 to 312 ohm-m) with thickness ranging from 200 to 400 m. The second layer is very conductive (1 to 4 ohm-m) with thickness ranging from 200 to 400 m. These two layers correspond to coastal sediments. This is underlain by a high resistivity layer (3000-20000 ohm-m) which is very thick (5 to 18 km). These high resistivities are typical of continental igneous rock, especially dry granite. Below this thick resistive layer, the model consists of an infinitely deep half-space which is moderately conductive (77 to 373 ohm-m). The bottom of the resistive layer shows a step offset, and is shallower to the northwest and northeast. The offset is indicated by dashed line on the map of Figure 4-8. The resistive layer corresponds to a region of no seismic reflections on the COCORP profiles. Both the electrical and seismic properties of the resistive layer are consistent with granite or other igneous or metamorphic lithology, where there are no extensive boundaries to reflect energy.

Compared to the COCORP profiles, the deep interface in the MT cross section corresponds to the transition from the reflection-free zone above 5 seconds to a zone of gently dipping discontinuous reflectors below. The presence of reflectors and the moderate resistivities of the bottom half-space are consistent with lower strength rock. Both COCORP and MT data indicate a general gentle southward dip.

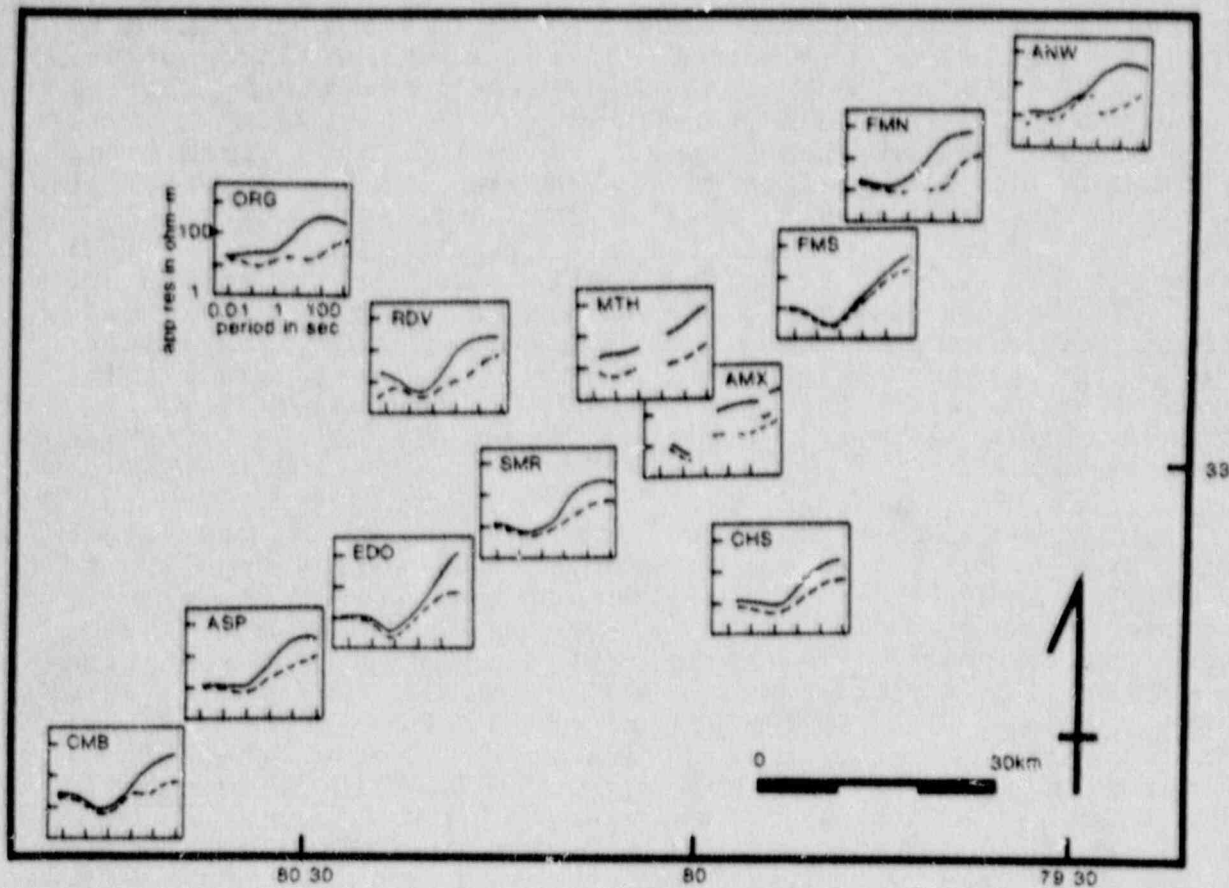
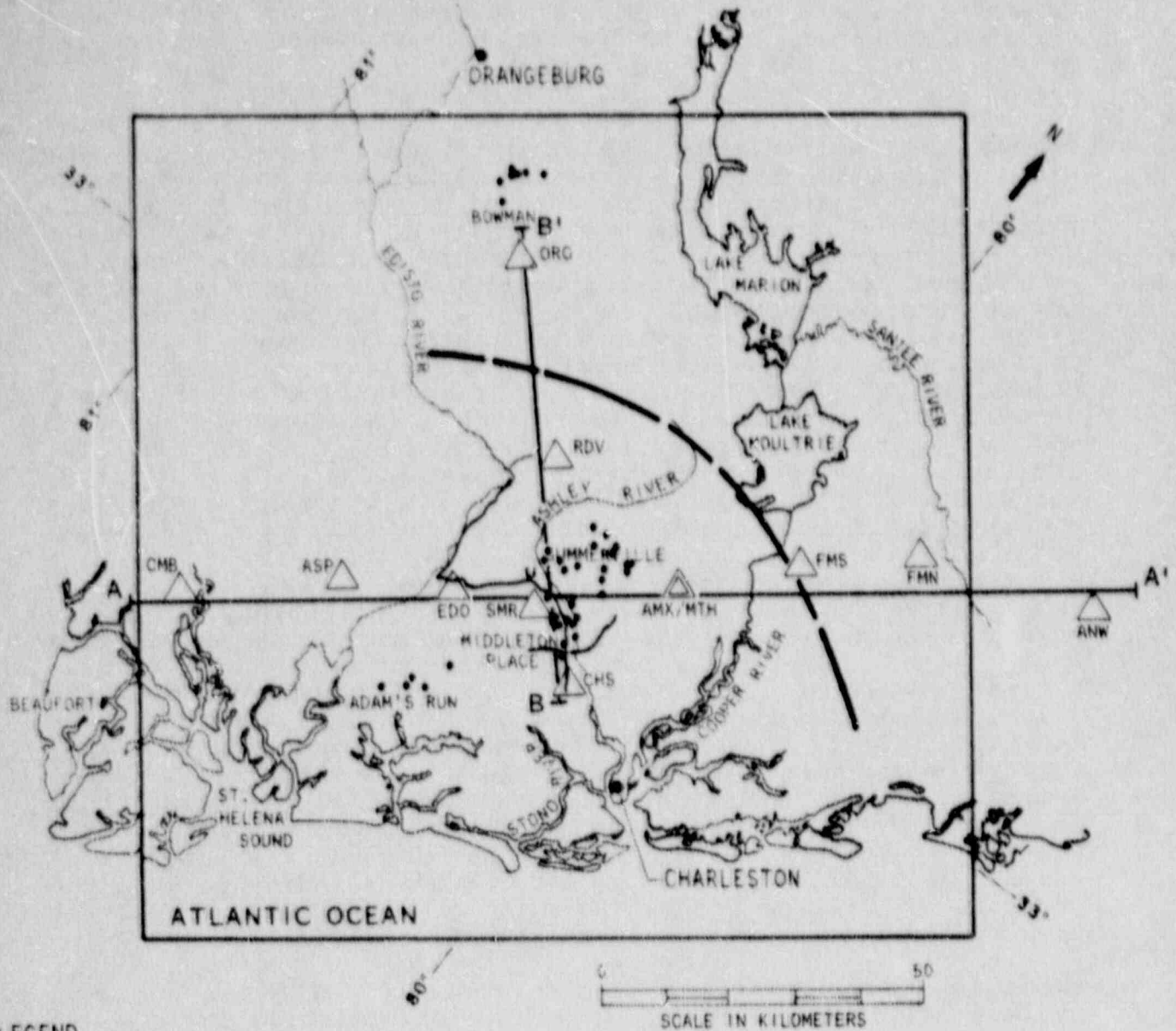


Figure 4-7. Apparent resistivity curves for all sites. The upper curve at each site is Rho-max (solid line) and the lower curve is Rho-min. Each curve is in its correct geographical position. The scale of all the curves is identical and is presented for the upper left curve only. (Taken from Young, *et al.* 1986).



LEGEND

- △ MAGNETOTELLURIC STATION
- RECENT EARTHQUAKE EPICENTERS [SOURCE: TARR AND RHEA (1983)]
- A ——— CROSS SECTIONAL PROFILES
- BOUNDARY DETERMINED BY MT SURVEY
- ~~~~~ COCORP PROFILES

Figure 4-8. This figure shows the boundary of the step offset in the bottom of the resistive layer from 1-D interpretations. The locations of selected earthquake epicenters are shown. Also shown are the locations of COCORP seismic reflection lines.

In order to gain meaningful information in the crust beneath the MT stations, it was necessary to extend the modeled profiles beyond the stations.

In addition to layered models, MT data can also reveal inhomogeneities and structural grain by anisotropy diagrams and transfer function maps. Figure 4-9 illustrates polar impedance diagrams to indicate the anisotropy of the impedance tensor. Data from two frequencies are displayed, $T = 85$ sec and 455 sec. These frequencies have a depth of penetration appropriate to regional studies. At each station, two polar diagrams are presented at each frequency. The polar figure drawn with solid lines indicates anisotropy of the diagonal impedance term, Z_{xy} . This quantity represents the electric field in the x direction generated by a magnetic field at right angles to it (the y direction). If the earth is isotropic (no electrical fabric and no nearby inhomogeneities), Z_{xy} should plot as a circle. Similarly, the polar diagram, drawn with a dashed line, represents Z_{xx} , the electric field in the x direction due to a magnetic field in the x direction. For an isotropic earth with no inhomogeneities, Z_{xx} should be zero. The Z_{xy} polar plot makes a peanut shape for a two dimensional earth with its long axis indicating the principal axis of anisotropy, and Z_{xx} should go to zero along the principal axis. Z_{xx} polar diagrams that are not zero along the principal axes indicate a three dimensional earth. The data in Figure 4-9 indicate that the principal axes at most sites are parallel to the Atlantic coast (NE-SW) at both 85 sec and 455 sec, and that the degree of three dimensionality is small. The only exceptions are site AMX, which was near an aluminum smelting facility that generated significant magnetic field interference, and at site FMS, where the recording was terminated due to an electrical storm. Analysis of MT data in other regions indicated that the presence of a large conducting body of water does not affect the results (Young, personal communication, 1987).

These impedance orientations are consistent with either large scale electrical anisotropy in the thick resistive layer shown in Figure 4-11 or with a two-dimensional structure approximately parallel to the sea coast.

As described earlier, the transfer function relating the vertical magnetic field to the horizontal electric field reveals concentrations of current in the crust. These transfer functions, also termed induction vectors, are presented in Figure 4-10 for a period of 85 seconds. The dot indicates the station locations, the solid line indicates the direction and magnitude of the maximum of real part of the transfer functions while the dashed line indicates the maximum of the imaginary part of the transfer function. The directions are plotted reversed, so that the lines point toward the current concentrations. Transfer functions are not reported for stations near population concentrations, because the data quality was poor there, presumably due to interference. The induction vectors shown in Figure 4-10 generally point toward

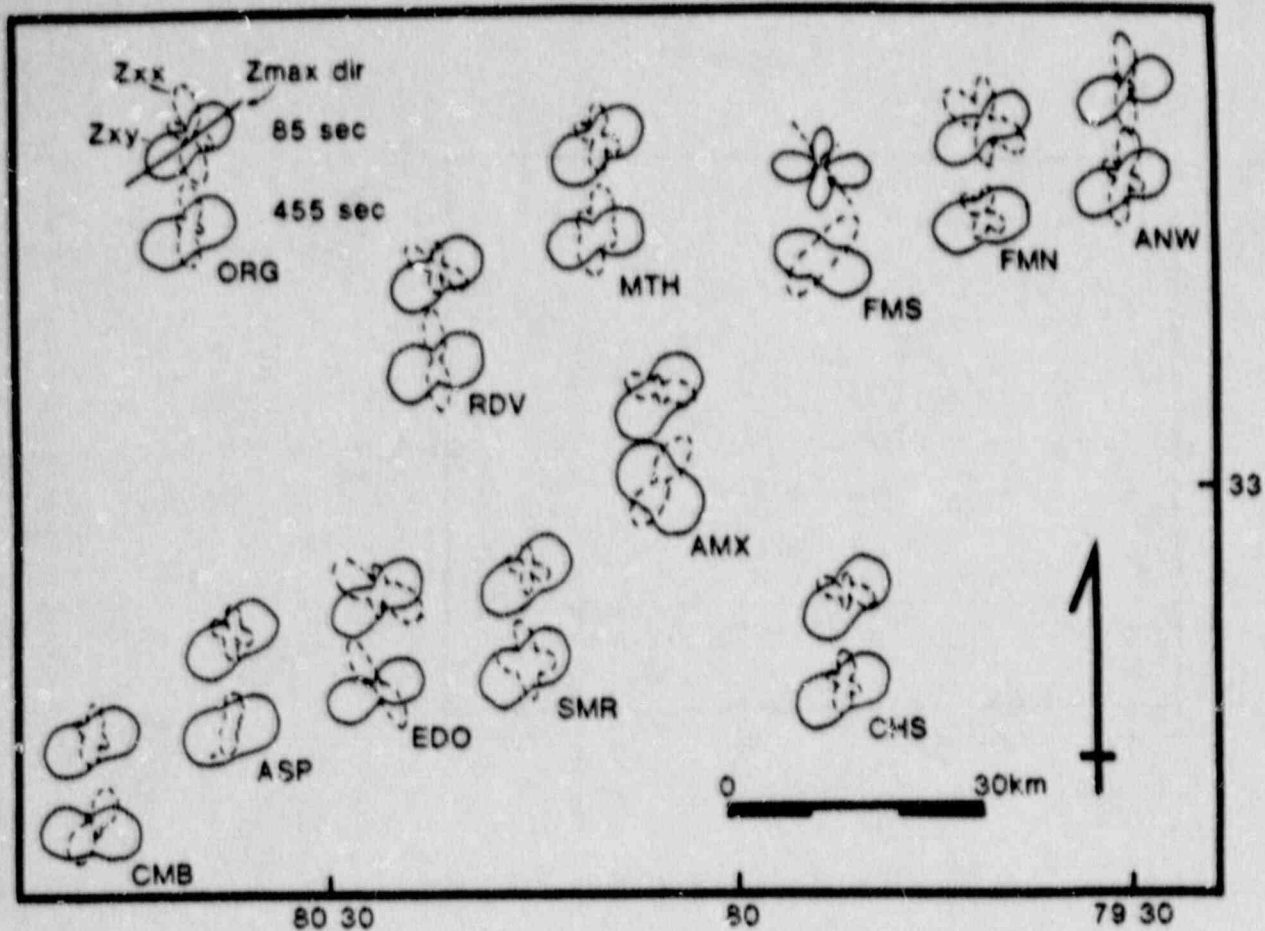


Figure 4-9. Impedance ellipses at each site. Data from 85 sec and 455 sec are shown at each site, as indicated in the upper left. The solid line indicates the on-diagonal MT impedance tensor, Z_{xy} , as a function of rotation angle and the dashed line indicates the off-diagonal element Z_{xx} . (Taken from Young, et al. 1986).

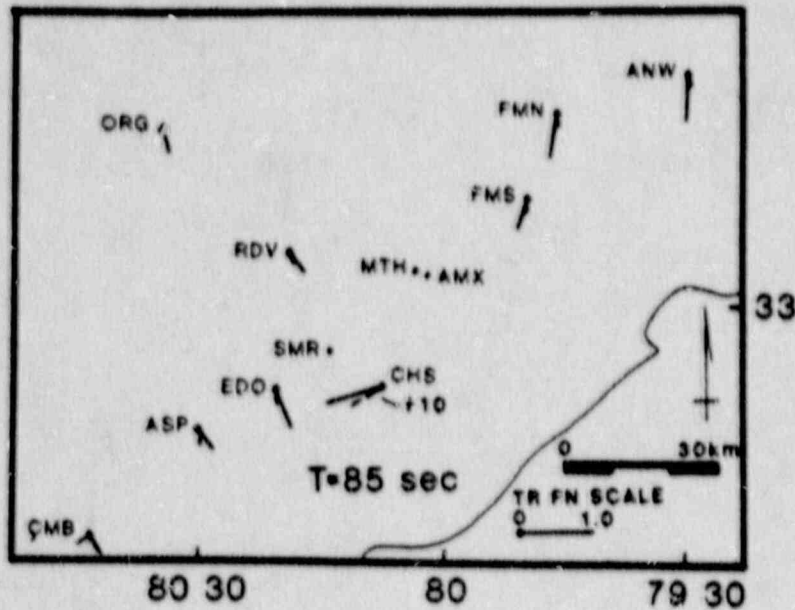


Figure 4-10. Magnetic field transfer functions for 85 sec. The directions are plotted with the directions reversed according to convention and thus should point towards conductors. The dots indicate station locations. The solid lines indicate the real component of magnetic transfer function and the dashed line (shorter) indicates the imaginary component. Data for station CHS is ten times larger than the graphical value. (Taken from Young, *et al.* 1986).

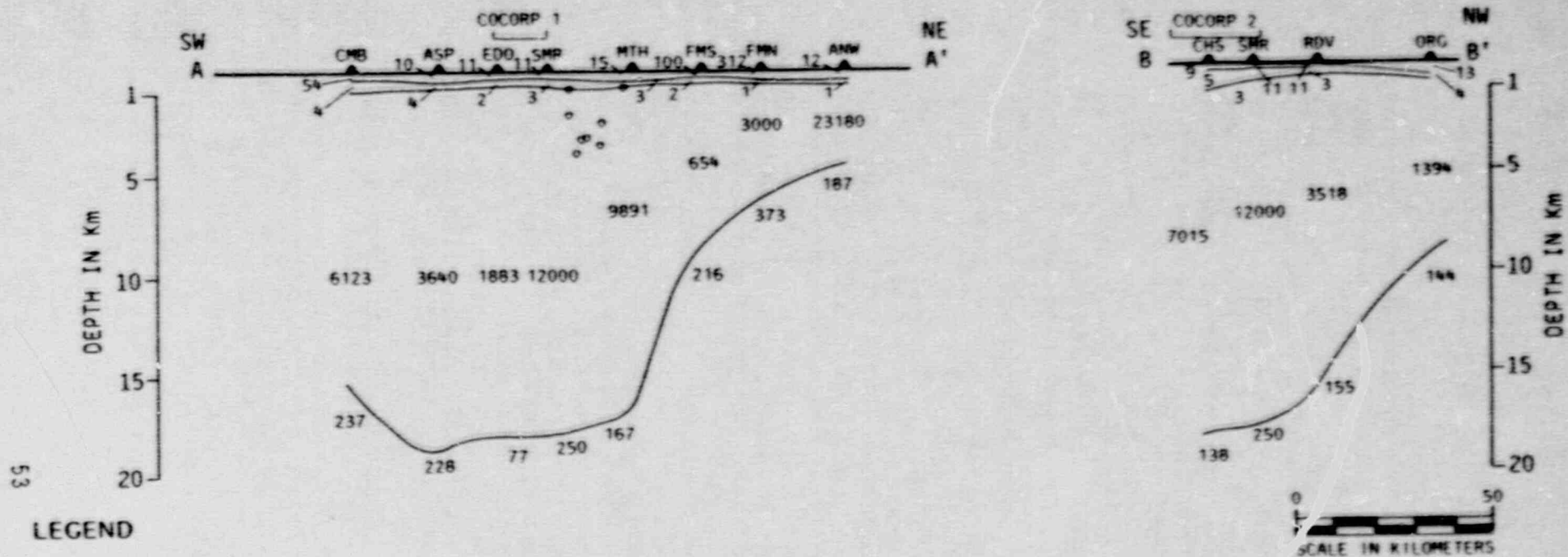


Figure 4-11. Geophysical cross sections from one-dimensional MT modeling of effective impedance at each station (triangle). The layers are labelled with their interpreted resistivity in ohm-m. The cross section locations can be seen in Figure 4-8. The approximate hypocenters are from Tarr, 1977. (Taken from Young, *et al.*, 1986).

the coast, except for station CHS which was probably affected by currents induced in power transmission lines or pipelines.

The one-dimensional magnetotelluric soundings were preliminarily interpreted by layered models and interpreted as profiles. The resulting cross-sections indicated a sequence of conductive sediments, overlying a thick resistive layer interpreted as crystalline rock. The bottom half-space is relatively conductive (Figure 4-11). At the time of the initial data collection Young and Kitchen proposed that the deep relatively conductive layer could be interpreted as a very deep sedimentary trough. J. C. Mareschal suggested water-filled secondary porosity in crystalline rock as an alternate interpretation. One purpose of the MT survey was to contribute to the data accumulated to yield a geologic interpretation which was consistent with all data and not one or two sets. Impedance anisotropy and other indicators of two- and three-dimensionality indicate that higher order models are desired to account for some data characteristics. The one-dimensional geologic interpretations should be considered interesting but not as robust as the final interpretation.

4.2.4.2 Two-Dimensional Modeling

Two-dimensional modeling was performed by C. T. Young and M. R. Kitchen of Michigan Technological University. One-dimensional modeling is appropriate for the Charleston data to depths of about 1 km. Below these depths, the data cannot be adequately resolved by one-dimensional techniques. Two-dimensional techniques are more appropriate. For an elongated sedimentary basin with a lateral offset, the maximum resistivity curve at each site provides a more accurate representation of the crustal structure than using other modeling techniques such as adjacent one-dimensional models (Hermance, 1982). The two-dimensional models presented here for the Charleston MT data agree with this assertion, and agree with the one-dimensional models determined earlier for the maximum resistivity curve at each site. Two-dimensional models fitting a given data set are not necessarily unique. The non-uniqueness is not as severe as in gravity modeling, because the depth penetration of MT is clearly controlled by the frequency of observation. We present here two alternate models which fit the data set equally well.

A two-dimensional solution for the Charleston MT data is shown in Figures 4-12 and 4-13. The numbers shown are interpreted resistivities in ohm-m. An alternative solution is shown in Figures 4-14 and 4-15. These figures show two sets of perpendicular profiles. The locations of the profiles are shown in Figure 4-16. It can be seen that the near-surface structure is the same while deeper portions of the models differ. The two models shown here were used to constrain the geologic model developed using potential field data and other information. The MT interpretation shown in Figures 4-12 and 4-13 compares well with COCORP cross sections (Figures 4-17, 4-18 and 4-19). Of interest at this point is the correspondence

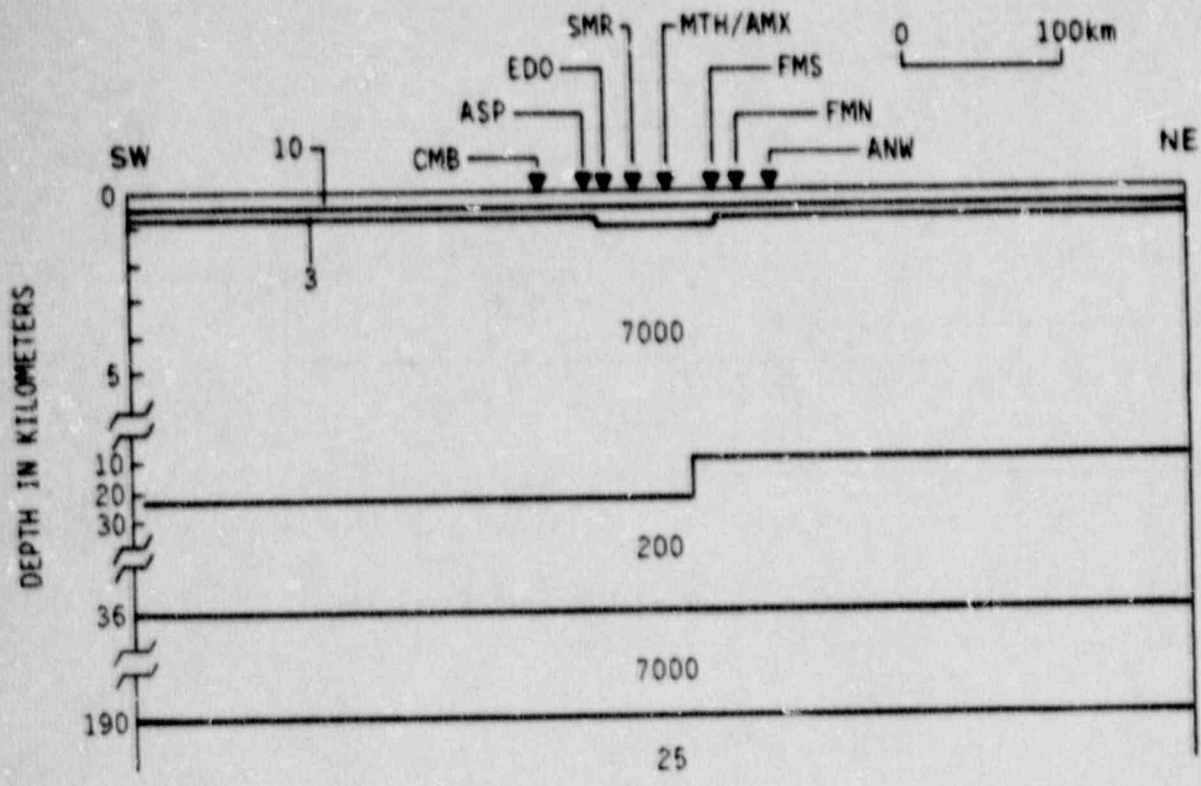


Figure 4-12. Two-dimensional solution I for the Charleston MT data. This cross section crosses Figure 4-13. See Figure 4-16 for locations. The numbers are interpreted resistivity in ohm-m. The stations are shown as inverted triangles.

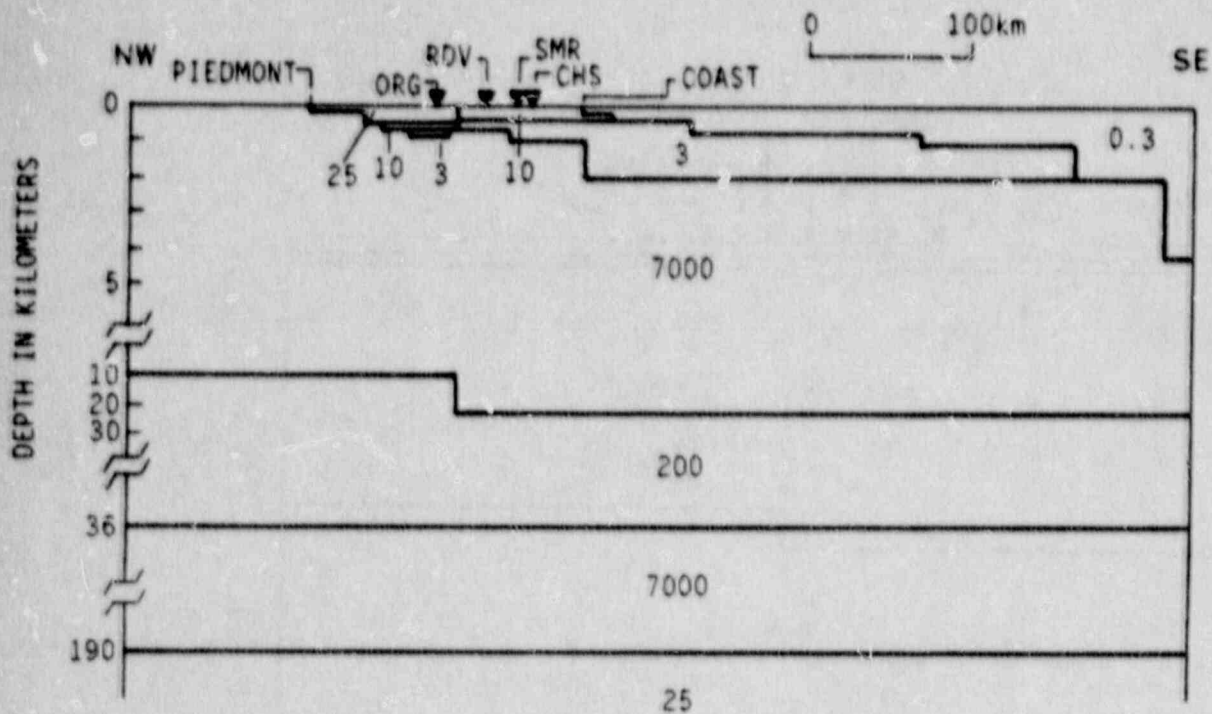


Figure 4-13. Two-dimensional solution I for the Charleston MT data. See Figure 4-16 for locations. The numbers are interpreted resistivity in ohm-m. The stations are shown as inverted triangles.

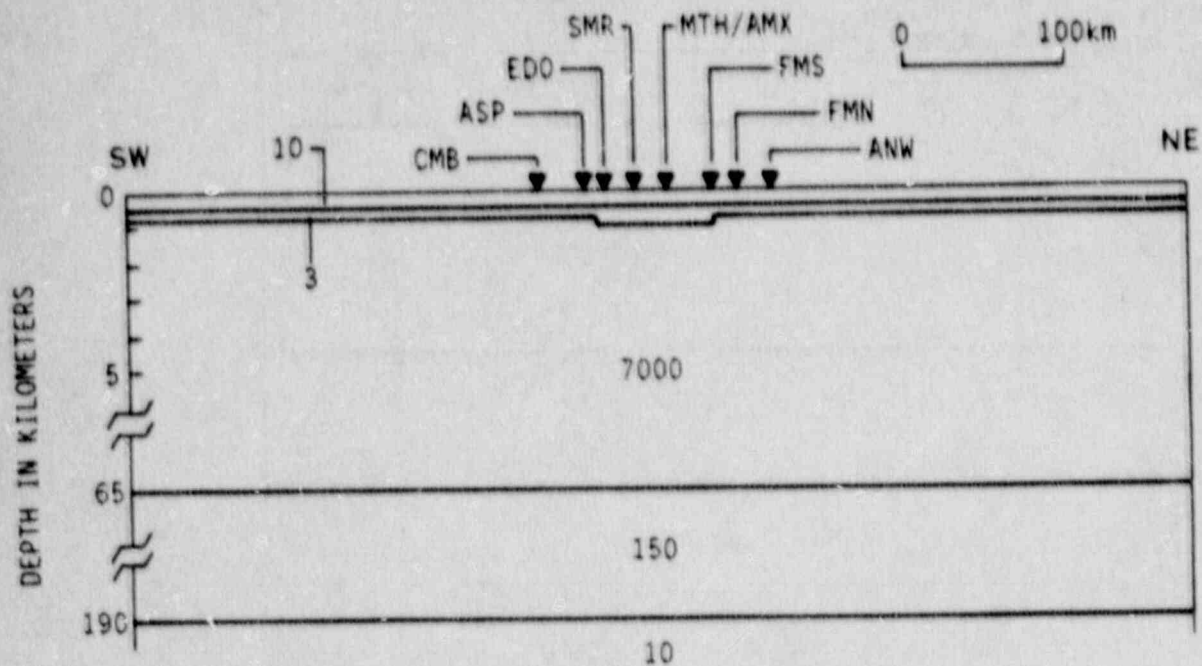


Figure 4-14. Two-dimensional solution II for the Charleston MT data. This cross section crosses Figure 4-15. See Figure 4-16 for locations. The numbers are interpreted resistivity in ohm-m. The stations are shown as inverted triangles.

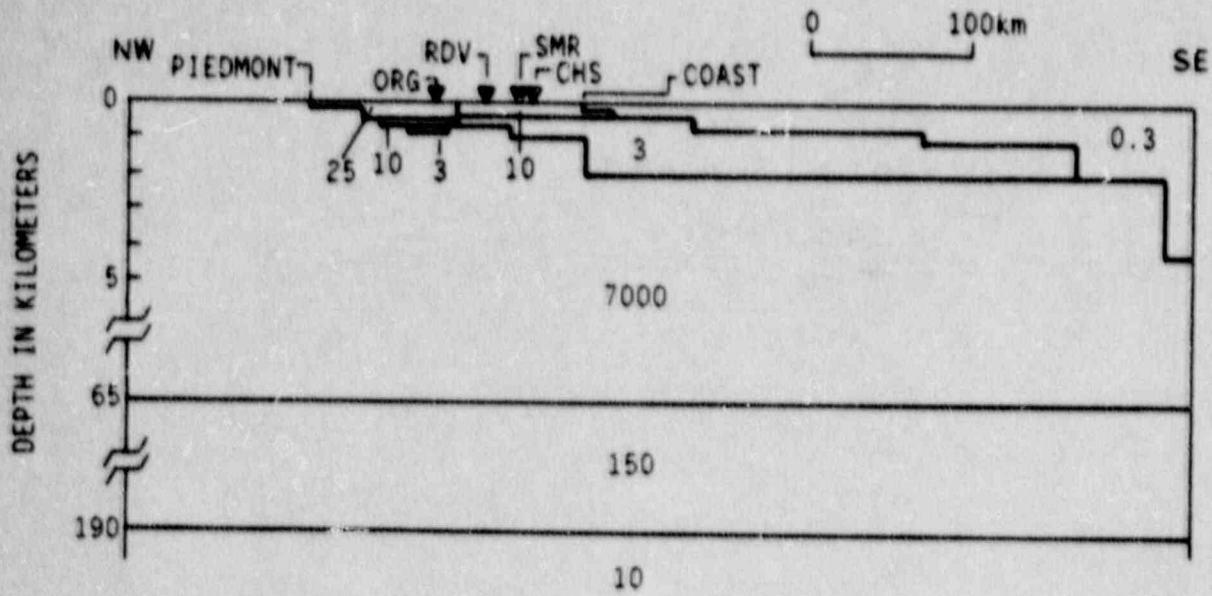


Figure 4-15. Two-dimensional solution II for the Charleston MT data. See Figure 4-16 for locations. The numbers are interpreted resistivity in ohm-m. The stations are shown as inverted triangles.

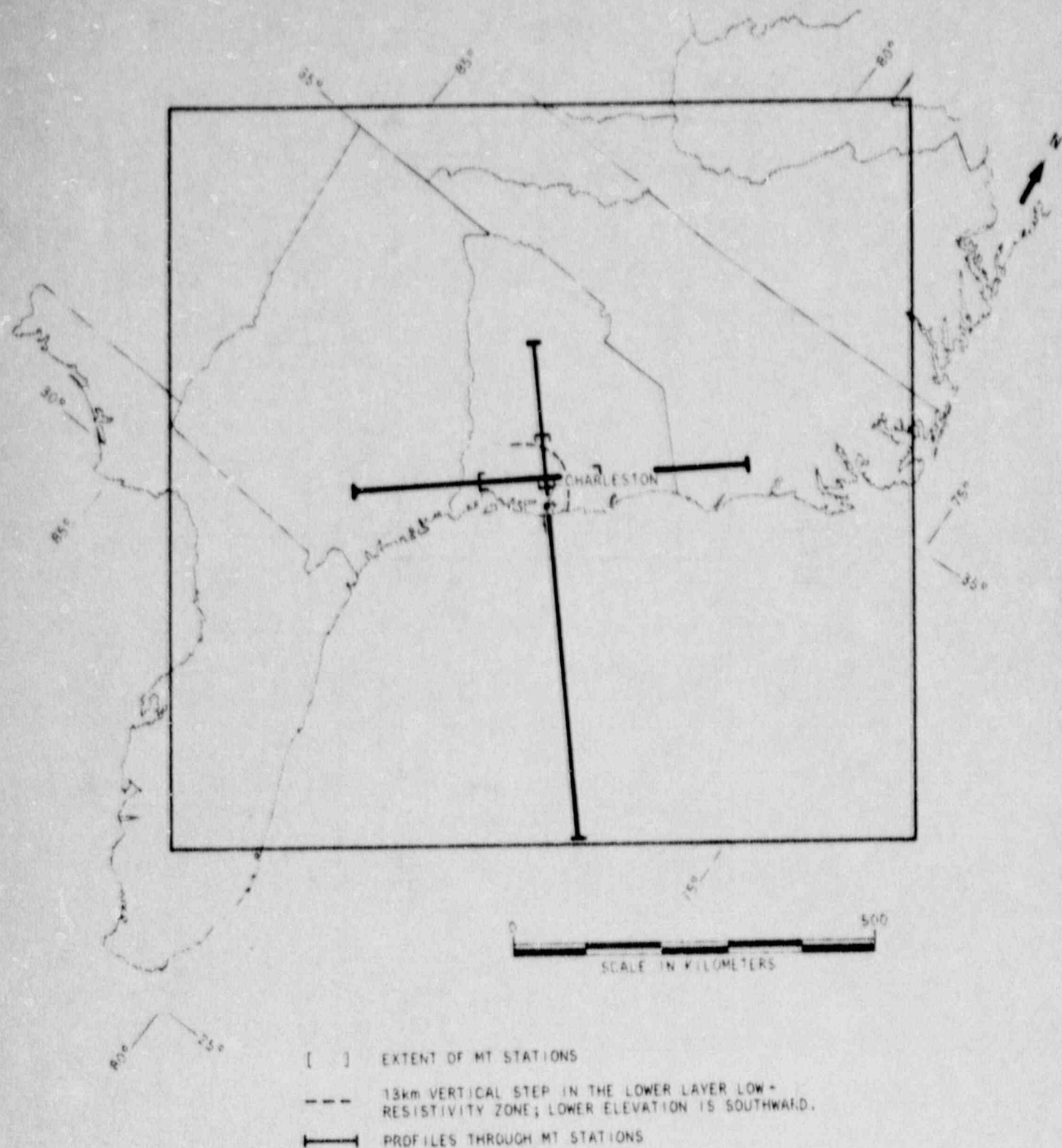


Figure 4-16. Location of two-dimensional magnetotelluric solutions (Figures 4-12 through 4-15).

SOUTHWEST NORTHEAST

COCORP 1

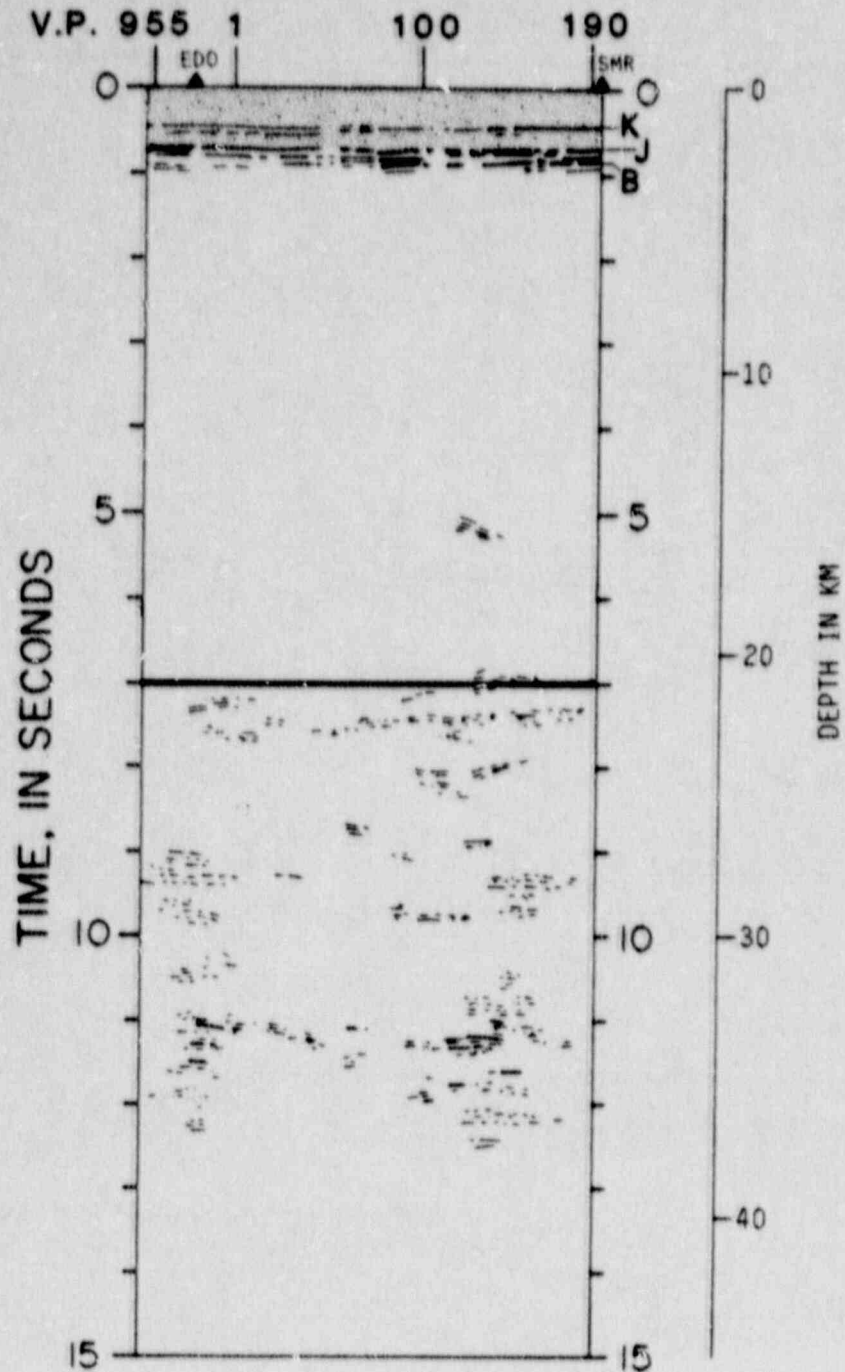


Figure 4-17. Comparison of MT model to COCORP profile (Schilt, *et al.*, 1977). The shading of the top represents shallow conductive material. The bold line represents the boundary between resistive and conductive rocks at depth. The station locations are shown by triangles at the top. The location of the COCORP lines are shown in Figure 4-20.

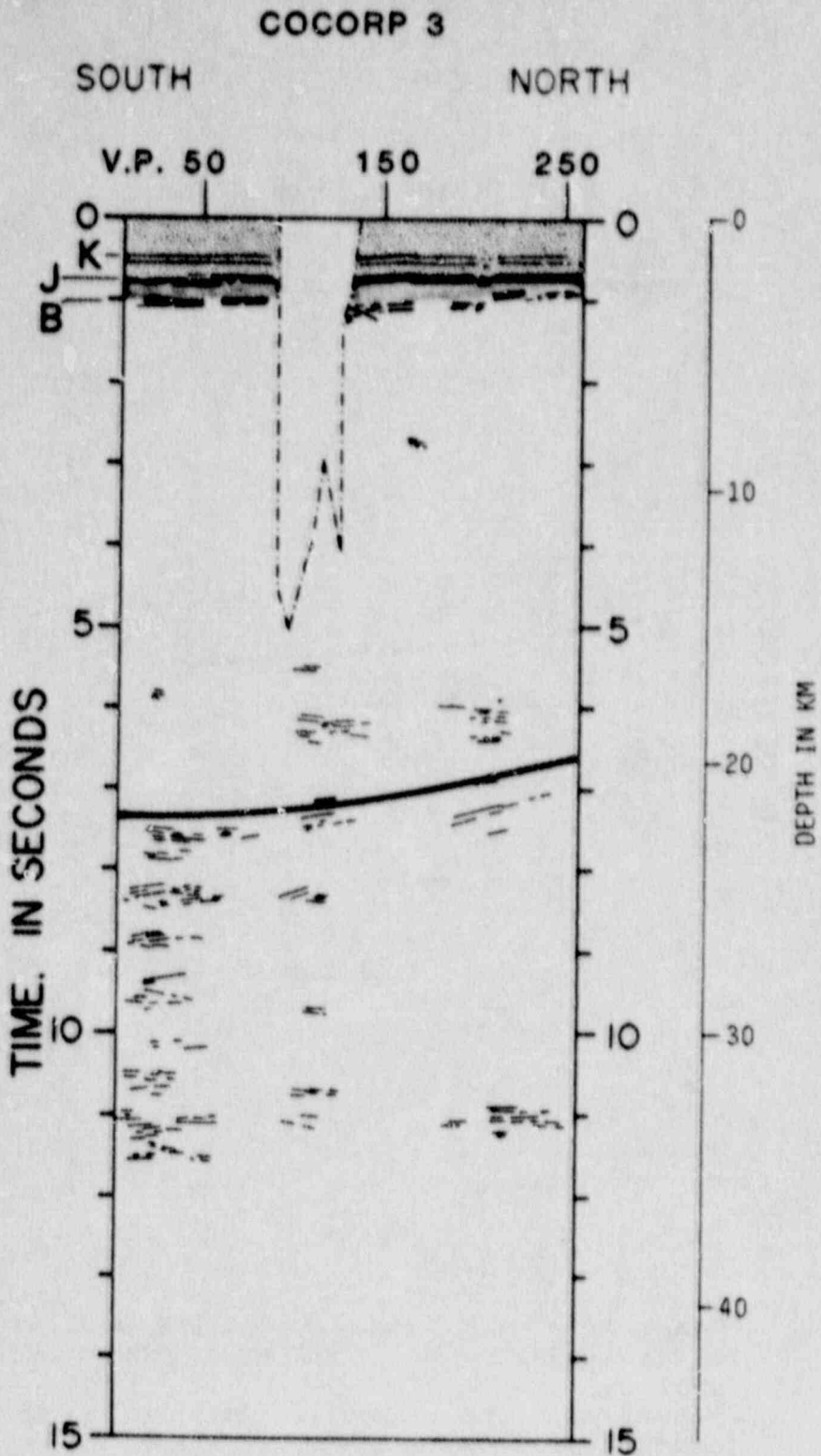


Figure 4-19. Comparison of MT model to COCORP profile (Schilt, et al., 1983). The shading of the top represents shallow conductive material. The bold line represents the boundary between resistive and conductive rocks at depth. The location of the COCORP lines are shown in Figure 4-20.

of the lower resistivity lower layer with the zone of discontinuous reflections in the COCORP cross sections. Because of this correspondence model I is preferred.

4.3 Seismic Refraction and Reflection Studies

In order to develop a realistic crustal model for the Charleston area, seismic reflection and refraction information was used to define depths to interfaces and depths to basement. Refraction velocities and reflection data were used as an aid to interpreting lithology and density of material present for constraining gravity modeling.

Existing interpretations of seismic reflection and refraction data were used. Five reflection interpretations were selected and are as follows:

- 1) COCORP - The interpretation we used is given in Schilt, et al., (1983). Four lines totaling 72 kilometers, Vibroseis data with a record length of 20 seconds. Display package consisting of location map, ISO velocity plot and CDP stacked prints at 3 scales available.
- 2) GSI - The interpretation is given in Hamilton, et al., (1983). Ten lines totaling 140 kilometers, Vibroseis data with a record length of 3 seconds. Data package consisting of 9 magnetic tapes, shot point maps, microfilm with statics, and test in U.S.G.S. Open File Report 82-311.
- 3) Seisdata - A line drawing interpretation of the data is given by Behrendt (1985). Part of Southeastern overthrust survey, Line 4 passes through the area of interest.
- 4) Yantis - A location map, profile sections and interpretations are given in Yantis, et al., (1983). Three lines totaling 7 kilometers, explosive source and a record length of 1 second.
- 5) Virginia Tech - Interpretation of this data is in preparation for publication. Although under revision, a copy of the report was furnished by Costain (Coruh, et al. (1982). Five lines totaling 51 kilometers, Vibroseis data with a record length of 2 seconds.

Although the reflection coverage near Charleston is fairly dense, most of it has been poorly processed and interpretations are not universally accepted. The location of the reflection lines are given in Figure 4-20.

Most of the reflection profiles were interpreted by their authors primarily to find faulting. Our use of the reflection data is, first, to locate near-horizontal layering to constrain gravity modeling, and, second, to locate horizontal changes in lithology and faulting. The first use does not tax the data to

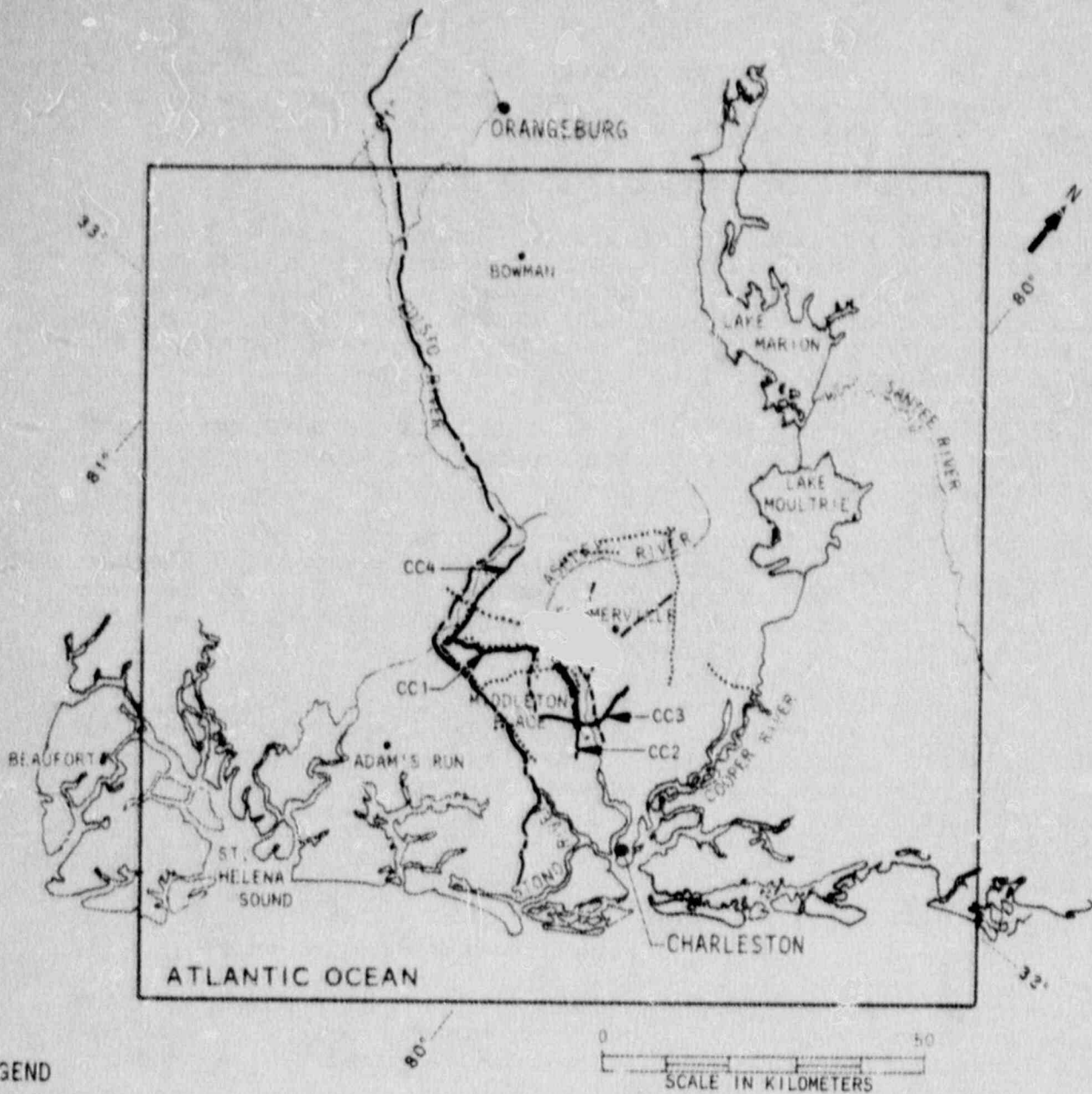


Figure 4-20. Location of seismic reflection lines near Charleston, South Carolina.

the extent that the second does. All of the reports of onshore reflection surveys give cross sections in time not depth, though approximate depths are given in the text. All lines show a strong reflection at the base of upper Cretaceous sediments at a depth of approximately 750 meters. In most areas, this is interpreted to be the top of a widespread basalt layer. Generally one or two continuous reflectors are seen in the Coastal Plain sediments. The "Yantis" interpretation does not go deeper than the basalt. The "GSI" and "Virginia Tech" interpretations show a reflector interpreted to be the surface of crystalline basement at approximately 1 sec (1-2 km), and some reflectors from 1 to 3 seconds deep which may indicate structure.

The COCORP data give the deepest penetration. The basalt (approximately 0.7 seconds, 750 meters) and basement (approximately 1.0 seconds, 1600 meters) have good continuity. Few coherent reflections are seen from 1.5 to 6 seconds (approximately 18 kilometers). There are many short discontinuous reflections from 6 to 11 seconds. Some of these reflections are speculated to be from meta-sedimentary rocks buried by Appalachian thrusting (Schilt *et al.*, 1983). However, no reflections which correlated with southern Appalachian thrust faults were found. More coherent reflections seen at 10.5 to 11.5 seconds (32 to 34 kilometers) are postulated to be from the crust-mantle transition zone.

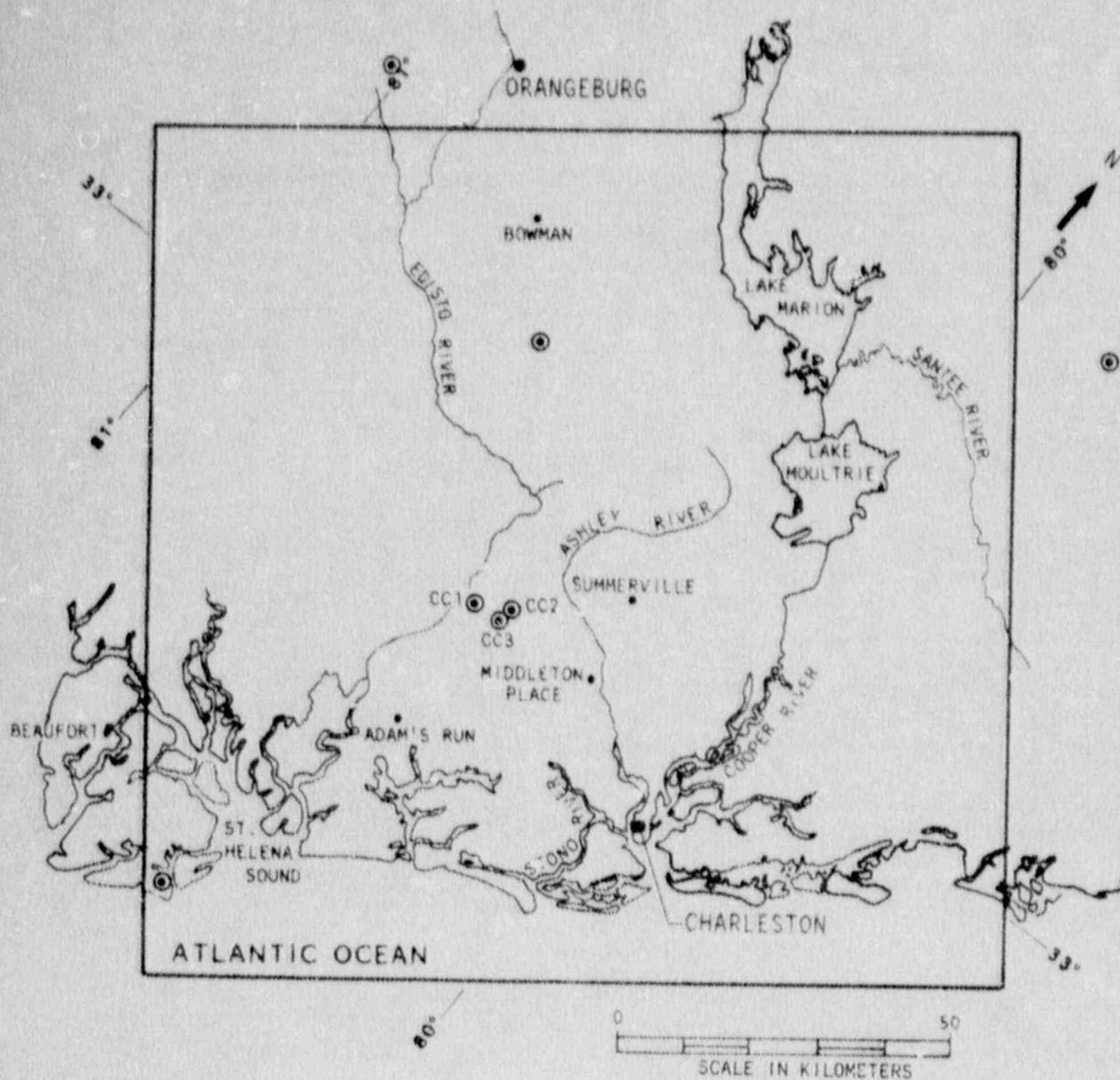
Refraction: The seismic refraction survey interpreted by Ackermann (1979) gave elevation contours for the pre-Cretaceous surface (-500 to -1000 meters) which is interpreted to be equivalent to the top of basalt where present. Elevation contours for crystalline basement (-800 to -2200 meters) are also given.

Reports of three marine surveys were used. The reflection survey by Behrendt *et al.* (1983) gives a structure contour, in time, of the top of basalt. They also give line drawing interpretations and a hypothetical crustal model. The second reflection survey by Dillon *et al.* (1983) outlines two deep sedimentary basins. They present depth sections on three seismic lines, depth contours of a post-rift unconformity which the basalt layer overlies, and depth and isopach maps for both Jurassic and Cretaceous sediments. The marine refraction survey by Dillon and McGinnis (1983) restates information from the reflection survey.

Several other sources of refraction data were examined. These included Talwani (1977), Smith, *et al.*, (1987), and Woollard *et al.* (1957).

4.4 Geologic Data

The geologic data are based on information from surface geologic maps, numerous shallow drill holes, and a few deep drill holes, and on geological interpretations of aeromagnetic maps, gravity maps, and seismic profiles. The tectonic



◎ BOREHOLE

Figure 4-21. Location of boreholes which provided information for modeling. USGS deep boreholes at Clubhouse Crossroads are labeled CC1, CC2 and CC3.

interpretations are based on our data plus recently published tectonic summaries.

General surface geology is shown by McCartan et al. (1984) for the area from Charleston to Orangeburg, South Carolina (map scale 1:250,000). Other near-surface features (thickness of overburden and contours on top of the Cooper Formation and Santee Limestone) are shown at the same scale from the same area by Force (1978a, 1978b). More detailed geologic maps for parts of the area (scales 1:24,000 to 1:49,000) are by Cameron et al. (1984), Malde (1959), and Weems and Lemon (1984a, 1984b). These maps are based partly on power-auger drilling to depths generally less than 25 meters. Many of the drilling logs are published; others are on open file with the U.S. Geological Survey and the South Carolina Geologic Survey. Aspects of the near-surface stratigraphy are published by McCartan et al. (1980), Sanders et al. (1982), and Weems et al. (1982).

The landforms and near-surface stratigraphy of the region have been interpreted in terms of cycles of submergence and emergence as the shoreline shifted during geologic time. Classic papers on the origin of terraces and scarps are by Cooke (1936) and Doering (1960). Much work in the Coastal Plain has been done by D. J. Colquhoun and his associates (1965, 1969, 1974; Colquhoun et al. 1972). A recent atlas of the South Carolina Coastal Plain (Colquhoun et al. 1983) compiles and summarizes much geologic work on the surface features, subsurface stratigraphy, structure, and aquifers.

Discussions of deep subsurface stratigraphy and interpretations of geophysical maps are given in U.S. Geological Survey Professional Papers 1028 and 1313. The three deep boreholes near Clubhouse Crossroads provide the deepest borehole information available in the Charleston area (about 790 to 1150 m below the surface) (Figure 4-21). Well logs and other data are listed by Gohn et al. (1978) and Valentine (1982).

Regional tectonic interpretations include a discussion of terranes in the Appalachian orogenic belt by Williams and Hatcher (1983), which includes a description of the Brunswick terrane, in which the Charleston area is situated. A recent summary volume on the western North Atlantic contains several papers pertinent to tectonic evolution of the Charleston area, for example Klitgord and Schouten (1986) and Tucholke and McCoy (1986).

- Ackermann, H. D., "Exploring the Charleston, South Carolina, Earthquake Area with Seismic Refraction - A Preliminary Study", in D. W. Rankin, Studies Related to the Charleston, South Carolina, Earthquake of 1886 - A Preliminary Report, U. S. Geological Survey Professional Paper 1028, p. 167-175, 1977
- Barraclough, D. R. and E. B. Fabiano, "Grid Values and Charts for the International Geomagnetic Reference Field-1975", U.S. Department of Commerce, National Technical Information Service PB-276630, 139 p., 1978
- Behrendt, J. C., "Interpretation From Multichannel Seismic-Reflection Profiles of the Deep Crust Crossing South Carolina and Georgia From the Appalachian Mountains to the Atlantic Coast", U. S. Geological Survey Map, MF 1656, 3 sheets, 1985
- Behrendt, J. C., R. M. Hamilton, H. D. Ackermann, V. J. Henry, and K. C. Bayer, "Marine Multichannel Seismic-Reflection Evidence for Cenozoic Faulting and Deep Crustal Structure Near Charleston, South Carolina", in G. S. Gohn, Studies Related to the Charleston, South Carolina, Earthquake of 1886 - Tectonics and Seismicity, U. S. Geological Survey Professional Paper 1313, p. J1-J29, 1983
- Bostick, F. S., H. W. Smith, and J. E. Boehl, "Magnetotelluric and DC Dipole-Dipole Soundings in Northern Wisconsin", Electrical Geophysics Research Laboratory Technical Report, University of Texas at Austin, 1977
- Briggs, I. C., "Machine Contouring Using Minimum Curvature", Geophysics, Vol. 39, p. 39-48, 1974
- Cameron, C. C., E. R. Force, and A. E. Grosz, "Geologic Map of the Hell Hole Bay, Wambaw Swamp, Little Wambaw Swamp, and Wambaw Creek Wildernesses, Berkeley and Charleston Counties, South Carolina", U.S. Geological Survey Map MF-1556-A, 1984
- Campbell, D. L., "Electric and Electromagnetic Soundings near Charleston, South Carolina - A Preliminary Report", in D. W. Rankin, Studies Related to the Charleston, South Carolina, Earthquake of 1886 - A Preliminary Report, U. S. Geological Survey Professional Paper 1028, p. 189-198, 1977
- Champion, J. W., Jr., "A Detailed Gravity Study of the Charleston, South Carolina, Epicentral Zone", Master's Thesis, Georgia Institute of Technology, 97 p., 1975
- Colquhoun, D. J., "Terrace Sediment Complexes in Central South Carolina", in Guidebook, Atlantic Coastal Plain Geological Association, Field Conference 1965, University of South Carolina, Columbia, 62 p., 1965

- Colquhoun, D. J., "Geomorphology of the Lower Coastal Plain of South Carolina", Division of Geology, South Carolina State Development Board, MS. 15, 36 p., 1969
- Colquhoun, D. J., "Cyclic Surficial Stratigraphic Units of the Middle and Lower Coastal Plains, Central South Carolina", in R. W. Oaks and J. R. DuBar, Post-Miocene Stratigraphy, Central and Southern Atlantic Coastal Plain, Utah State University Press, p. 179-190, 1974
- Colquhoun, D. J., T. A. Bond, and D. Chappel, "Santee Submergence, Example of Cyclic Submerged and Emerged Sequences", in B. W. Nelson, Environmental Framework of Coastal Plain Estuaries, U. S. Geological Society of America Memoir 133, 619 p., 1972
- Colquhoun, D. J., I. D. Woollen, D. S. Van Nieuwenhuise, G. G. Padgett, R. W. Oldham, D. C. Boylan, P. D. Howell, and J. W. Bishop, "Surface and Subsurface Stratigraphy, Structure, and Aquifers of the South Carolina Coastal Plain", Report for Department of Health and Environmental Control, Ground Water Protection Division, published through the Office of the Governor, State of South Carolina, Columbia, South Carolina, 78 p., 1983
- Cooke, C. W., "Geology of the Coastal Plain of South Carolina", U. S. Geological Survey Bulletin, Vol. 867, 196 p., 1936
- Coruh, C., J. K. Costain, J. H. Behrendt, and R. A. Hamilton, "Mesozoic Faulting in the Charleston, South Carolina Region: New Evidence from Seismic Reflection Data", unpublished, 1982
- Dillon, W. P., K. D. Klitgord, and C. K. Paull, "Mesozoic Development and Structure of the Continental Margin off South Carolina", in G. S. Gohn, Studies Related to the Charleston, South Carolina Earthquake of 1886 - Tectonics and Seismicity, Geological Survey Professional Paper 1313, p. N1-N16, 1983
- Dillon, W. P., and L. D. McGinnis, "Basement Structure Indicated by Seismic-Refraction Measurements Offshore From South Carolina and Adjacent Areas", in G. S. Gohn, Studies Related to the Charleston, South Carolina Earthquake of 1886 - Tectonics and Seismicity, U. S. Geological Survey Professional Paper 1313, 01-07, 1983
- Dods, S. D., D. J. Tesky, and P. J. Hood, "The New Series of 1:1,000,000-Scale Magnetic Anomaly Maps of the Geological Survey of Canada; Compilation Techniques and Interpretation", in W. J. Hinze, The Utility of Regional Gravity and Magnetic Anomaly Maps, (Society of Exploration Geophysicists, Tulsa, OK), 1985
- Doering, J. A., "Quaternary Surface Formations of Southern Part of Atlantic Coastal Plain", Journal of Geology, Vol. 68, p. 182-202, 1960

- Fabiano, E. B. and N. W. Peddie, "Grid Values of Total Magnetic Intensity", 1 GRF-1965. U.S. Environmental Science Services Administration Technical Report, C and GS 38, 55 p., 1969
- Gohn, G. S., D. Cottfried, M. A. Lanphere, and B. B. Higgins, "Regional Implications of Triassic or Jurassic Age for Basalt and Sedimentary Red Beds in the South Carolina Coastal Plain", Science, Vol. 202, No. 4370, p. 887-890, 1978
- Hamilton, R. M., J. C. Behrendt, and H. D. Ackermann, "Land Multichannel Seismic-Reflection Evidence for Tectonic Features Near Charleston, South Carolina", in G. S. Gohn, Studies Related to the Charleston, South Carolina, Earthquake of 1886 - Tectonics and Seismicity, U.S. Geological Survey Professional Paper 1313, p. I1-I18, 1983
- Hermance, J. F., "The Asymptotic Response of Three-Dimensional Basin Offsets to Magnetotelluric Fields at Long Periods: the Effect of Current Channeling", Geophysics, Vol. 47, No. 11, p. 1562-1573, 1982
- International Association of Geodesy, "Geodetic Reference System, 1967", Special Publication 3, International Association of Geodesy, 1971
- Klitgord, K. D. and H. Schouten, "Plate Kinematics of the Central Atlantic", in P. R. Vogt, and B. E. Tucholke, The Geology of North America, Volume M, The Western North Atlantic Region, Geological Society of America, 696 p., 1986
- Malde, H.E., "Geology of the Charleston Phosphate Area, South Carolina", U.S. Geological Survey Bulletin, Vol. 1079, 105 p., 1959
- McCartan, L., E. M. Lemon, Jr., and R. E. Weems, "Geologic Map of the Area Between Charleston and Orangeburg, South Carolina", U. S. Geological Survey Miscellaneous Investigation Map I-1472, Scale 1:250,000, 1984
- McCartan, L., R. E. Weems, and E. M. Lemon, Jr., "The Wando Formation (Upper Pleistocene) in the Charleston, South Carolina Area", U.S. Geological Survey Bulletin, Vol. 1502-A, p. 110-116, 1980
- McKee, J. H., "A Geophysical Study of Microearthquake Activity Near Bowman, South Carolina", Master's Thesis, Georgia Institute of Technology, Atlanta, 65 p., 1974
- Morelli, C., "The International Gravity Standardization Net, 1971", Special Publication 4, International Association of Geodesy, 1974

- Phillips, J. D. and W. M. Davis, "Principal Facts for Gravity Stations in Bamberg, Beaufort, Charleston, Colleton, Dorchester, and Orangeburg Counties, South Carolina", U. S. Geological Survey, Open-File Report 85-392, 15 p., 1985
- Sanders, A. E., R. E. Weems, and E. M. Lemon, Jr., "The Chandler Bridge Formation - A New Oligocene Stratigraphic Unit in the Lower Coastal Plain of South Carolina", U.S. Geological Survey Bulletin, Vol. 1529-H, p. 105-124, 1982
- Schilt, F. S., L. D. Brown, J. E. Oliver, and S. Kaufman, "Subsurface Structure Near Charleston, South Carolina; Results of COCORP Reflection Profiling in the Atlantic Coastal Plain", in G. S. Gohn, Studies Related to the Charleston, South Carolina, Earthquake of 1886 - Tectonics and Seismicity, U. S. Geological Survey Professional Paper 1313, p. H1-H19, 1983
- Smith, W. A., P. Talwani, and D. J. Colquhoun, "The Seismotectonics of the Bowman Seismic Zone, South Carolina", submitted to Geological Society of America Bulletin, Dec. 1987
- Tarr, A. C., "Recent Seismicity Near Charleston, South Carolina, and Its Relationship to the August 31, 1886 Earthquake", in D. W. Rankin, Studies Related to the Charleston, South Carolina Earthquake of 1886 - A Preliminary Report, U. S. Geological Survey Professional Paper 1028, p. 43-57, 1977
- Tucholke, B. E. and F. W. McCoy, "Paleogeographic and Paleobathymetric Evolution of the North Atlantic Ocean", in P. R. Vogt, and B. E. Tucholke, The Geology of North America, Volume M., The Western North Atlantic Region, Geological Society of America, 696 p., 1986
- U.S. Geological Survey and Society of Exploration Geophysicists, "Composite Magnetic Anomaly Map of the United States, Part A: Conterminous United States", Map GP 954-A, U.S. Geological Survey, Scale 1:1,250,000, 2 sheets, 1982
- Valentine, P. C., "Upper Cretaceous Subsurface Stratigraphy and Structure of Coastal Georgia and South Carolina", U.S. Geological Survey Professional Paper 1222, p. 32-33, 1982
- Webring, M., "MINC, a Fortran Gridding Program Based on Minimum Curvature", U. S. Geological Survey Open-File Report 81-1223, 1981
- Weems, R. E. and E. M. Lemon, Jr., "Geologic Map of the Mount Holly Quadrangle, Berkeley and Charleston Counties, South Carolina", U.S. Geological Survey Map GQ-1579, 1984a

- Weems, R. E. and E. M. Lemon, Jr., "Geologic Map of the Stallville Quadrangle, Dorchester and Charleston Counties, South Carolina", U.S. Geological Survey Map GQ-1581, 1984b
- Weems, R. E., E. M. Lemon, Jr., L. McCartan, L. M. Bybell, and A. E. Sanders, "Recognition and Formalization of the Pliocene "Goose Creek Phase" in the Charleston, South Carolina Area", U. S. Geological Survey Bulletin, Vol. 1529-H, p. 137-148, 1982
- Williams, H. and R. D. Hatcher, Jr., "Appalachian Suspect Terranes", Geological Society of America Memoir 158, p. 33, 1983
- Woollard, G. P., Bonini, W. E. and Meyer, R. P., "A Seismic Refraction Study of the Subsurface Geology of the Atlantic Coastal Plain and Continental Shelf Between Virginia and Florida", Department of Geology and Geophysics Technical Report, Contract No. 570NR-285121, University of Wisconsin-Madison, 128 p., 1957
- Yantis, B. R., J. K. Costain, and H. D. Ackermann, "A Reflection Seismic Study Near Charleston, South Carolina", in G. S. Gohn, Studies Related to the Charleston, South Carolina, Earthquake of 1886 - Tectonics and Seismicity, U. S. Geological Survey Professional Paper 1313, p. G1-G20, 1983
- Young, C. T., M. R. Kitchen, J. C. Rogers, and J. C. Mareschal, "Magnetotelluric Soundings in the Charleston, South Carolina Area", in J. E. Beavers, Proceedings, Third U.S. National Conference on Earthquake Engineering, (Earthquake Engineering Research Institute, El Cerrito, CA), p. 83-91, 1986

CHAPTER 5

GEOLOGIC MODEL

5.1 Current State of Knowledge

Charleston lies within a region of Mesozoic extensional terrane which is characterized by rift basins filled with sediments of late Triassic to early Jurassic age and mafic intrusions of Paleozoic age. Coastal Plain sediments of Cretaceous to Quaternary age overlie the extensional terrane. The region of extensional terrane has been referred to as the South Georgia Rift (Daniels, et al., 1983) and the Brunswick suspect terrane (Williams and Hatcher, 1983).

In this chapter we develop a geologic model of the Charleston area that, in combination with the results of regional and local stress modeling (Chapters 6 and 7), will allow the evaluation of hypotheses as to the cause of Charleston's seismicity.

Although the bulk of the data that we use existed prior to this project, it had not been formatted and processed to allow analysis to form a single geologic model of the Charleston area at seismogenic depths. This data manipulation and formatting is described in Chapter 4. In this chapter we combine the geophysical and geologic data prepared in Chapter 4 to build the geologic model.

5.2 Modeling Approach

Our approach is to use forward modeling of gravity and magnetic data, constrained by geologic, seismologic, and other available data. To do this we utilize two computer programs, MAGGRAV and PLATES. MAGGRAV is a forward model that generates the magnetic and gravity anomalies for two-dimensional structures which can be approximated by horizontal polygons. For magnetic modeling, induced magnetism, remnant magnetism or both can be computed. The equations for the calculation of the gravity anomalies are from Talwani, et al. (1959). The equations for the computation of the magnetic anomalies are from Talwani and Heirtzler (1964). Our version of MAGGRAV was written at Georgia Tech and then modified by us as part of this project. The program resides on a PC-XT equivalent and allows rapid iteration by the interpreter through screen graphics.

PLATES is a three-dimensional, potential-field forward modeling computer program which we use to compute the gravity field from our description of the distribution of density in the subsurface. It uses the methodology developed by Talwani and Ewing (1960). The model as modified by us for this project uses polygons of anomalous density stacked in thin sheets to fill the 128 km x 128 km study area. The program resides both on the time-shared mainframe Cyber computer at Georgia Tech and on a PC-XT equivalent. Program running time is a logistical

problem, due to the size of the files resulting from the scale of our use of PLATES, i.e. 128 x 128 surface grid points, with the contribution from each plate being calculated for each grid point on each iteration of the modeling process. As dedicated access to a fast mainframe system is not cost effective, time-shared mainframe and PC-XT modes have been used. The program structure and modeling schemes have for this reason been modified to be as efficient as possible.

The output of the program is a contoured, computed gravity anomaly field. The computed anomaly field can be subtracted from the actual Bouguer gravity map leaving a residual gravity field. This feature allows the interpreter to model one feature at a time, subtract that anomaly field from the total field, and then model against the remaining residual field.

As input to our structure modeling, we have also used satellite imagery techniques on our 1 km gravity and magnetic data, as described in Chapter 4. The results of using such techniques can be seen in Figures 5-1 through 5-5 for the gravity data, and Figures 5-6 through 5-10 for the magnetic data. Figure 5-1 is a gray-shade image of the Bouguer gravity field. (Note that more detail is available in the actual screen image than in these reproductions.) Higher values appear brighter and lower values appear darker. Stretching the image, so that highs become brighter and lows darker, and masking the image, in order to examine a selected range of values, are readily accomplished, and quickly help delineate areas of interest. Figure 5-2 shows the vertical second derivative of the gravity field. Certain linear trends can be seen, as well as areas where data quality is poor, such as the St. Helena Sound area.

Figure 5-3 shows one of the real strengths of the image processing technique, the combination of images. This figure was produced by using the red band for gravity data, while the green and blue bands were used for the vertical second derivative. The characterization of boundaries between gravity highs and lows as shallow, sharp boundaries, or deeper, more gradual ones becomes immediately apparent. This was used to help delimit the edges of the shallow features.

Another way of using image-processing techniques is to consider the gravity or magnetic data as topography, lit from a given angle. When examined at different angles, subtle trends can be revealed which are usually masked by the major trends in the data. For example, Figure 5-4 shows the gravity data with the source of illumination to the north of the figure. This highlights the obvious east-west structural trends in the gravity data (Figure 5-1). However, in Figure 5-5, the source of illumination is to the east, and the major structural trends have been masked, allowing more subtle cross-features to be observed.

The magnetic data has also been examined in the same way as the gravity data. Figure 5-6 shows the magnetic intensity data,

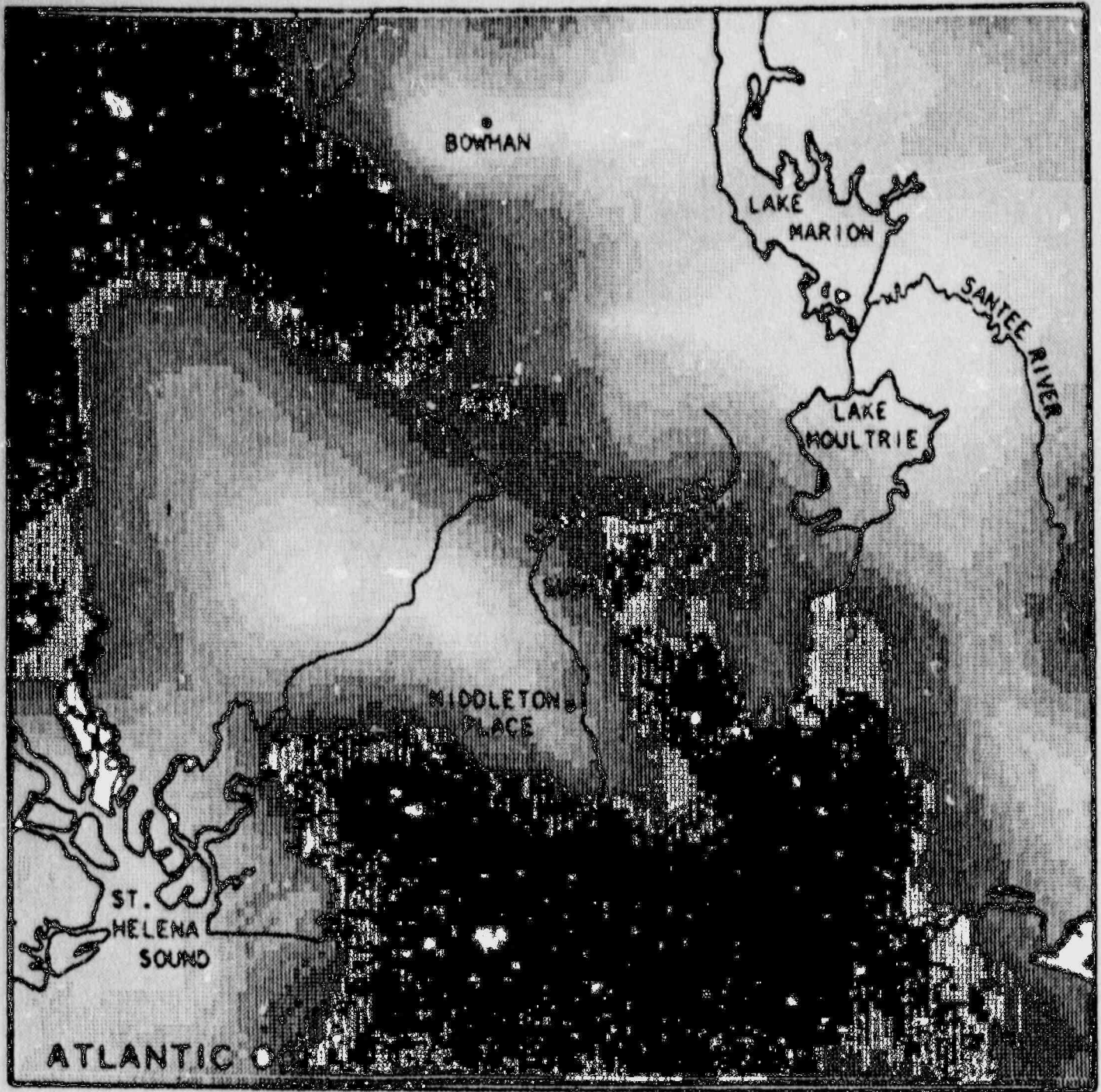


Figure 5-1. Image of Bouguer gravity anomaly field, 1 km grid. Higher values appear lighter, lower values appear darker.



Figure 5-2. Image of vertical second derivative of Bouguer gravity data.

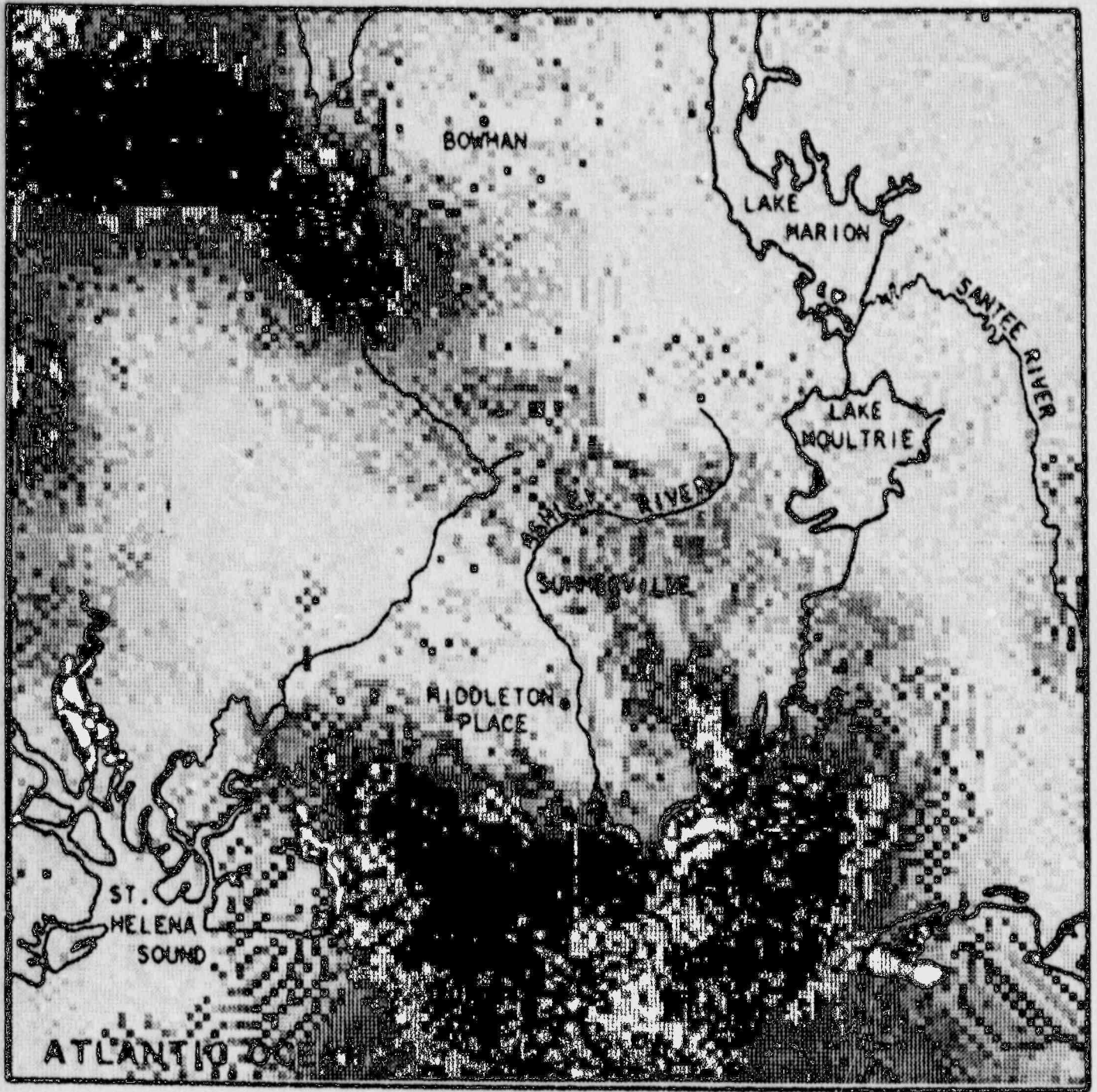


Figure 5-3. Image combining Bouguer gravity field and vertical second derivative (Figures 5-1 and 5-2).

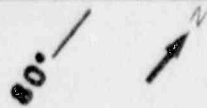
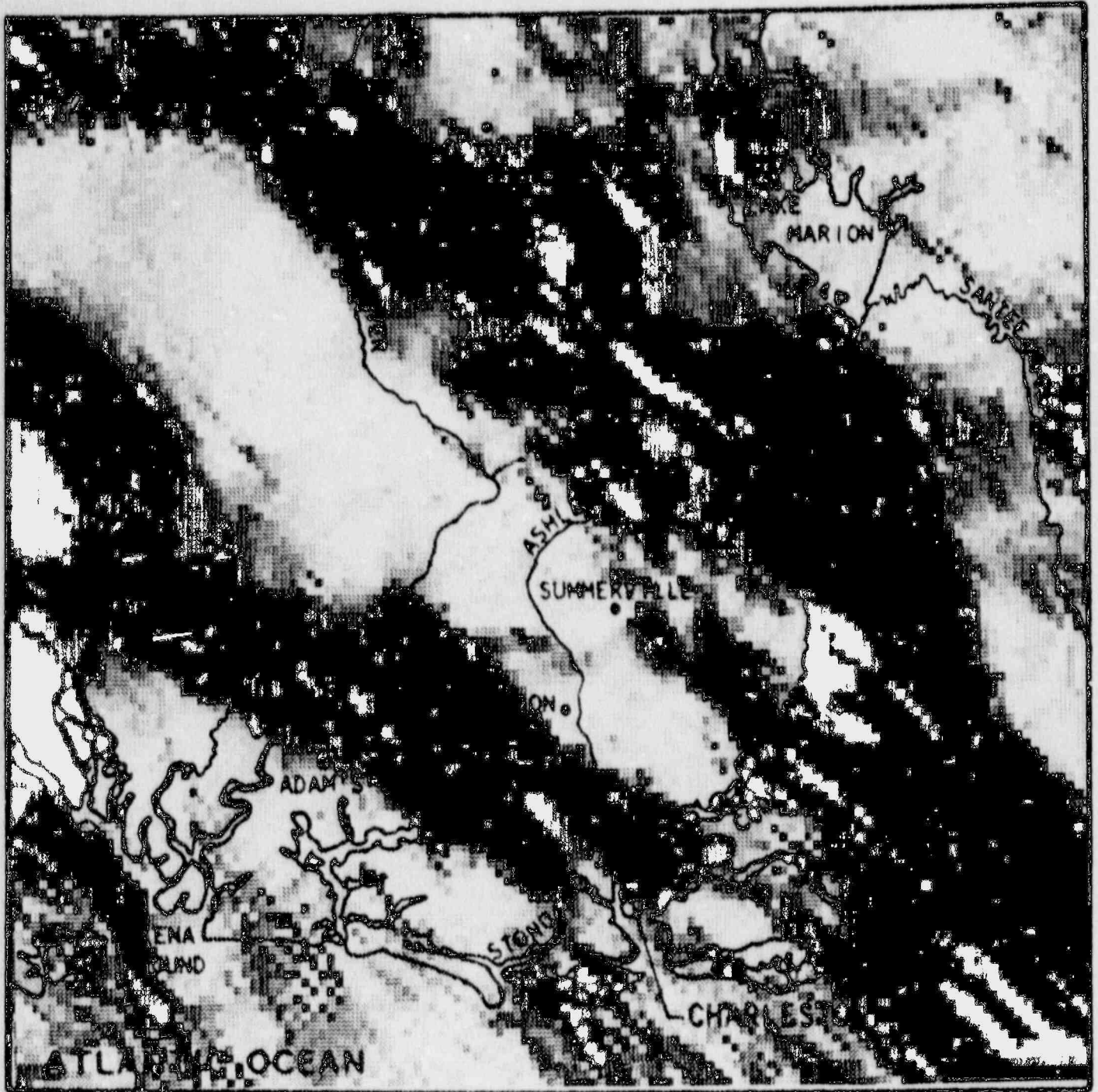


Figure 5-4. Shaded-relief image of Bouguer gravity data. Source of illumination is to north.



Figure 5-5. Shaded relief image of Bouguer gravity data. Source of illumination is to east.

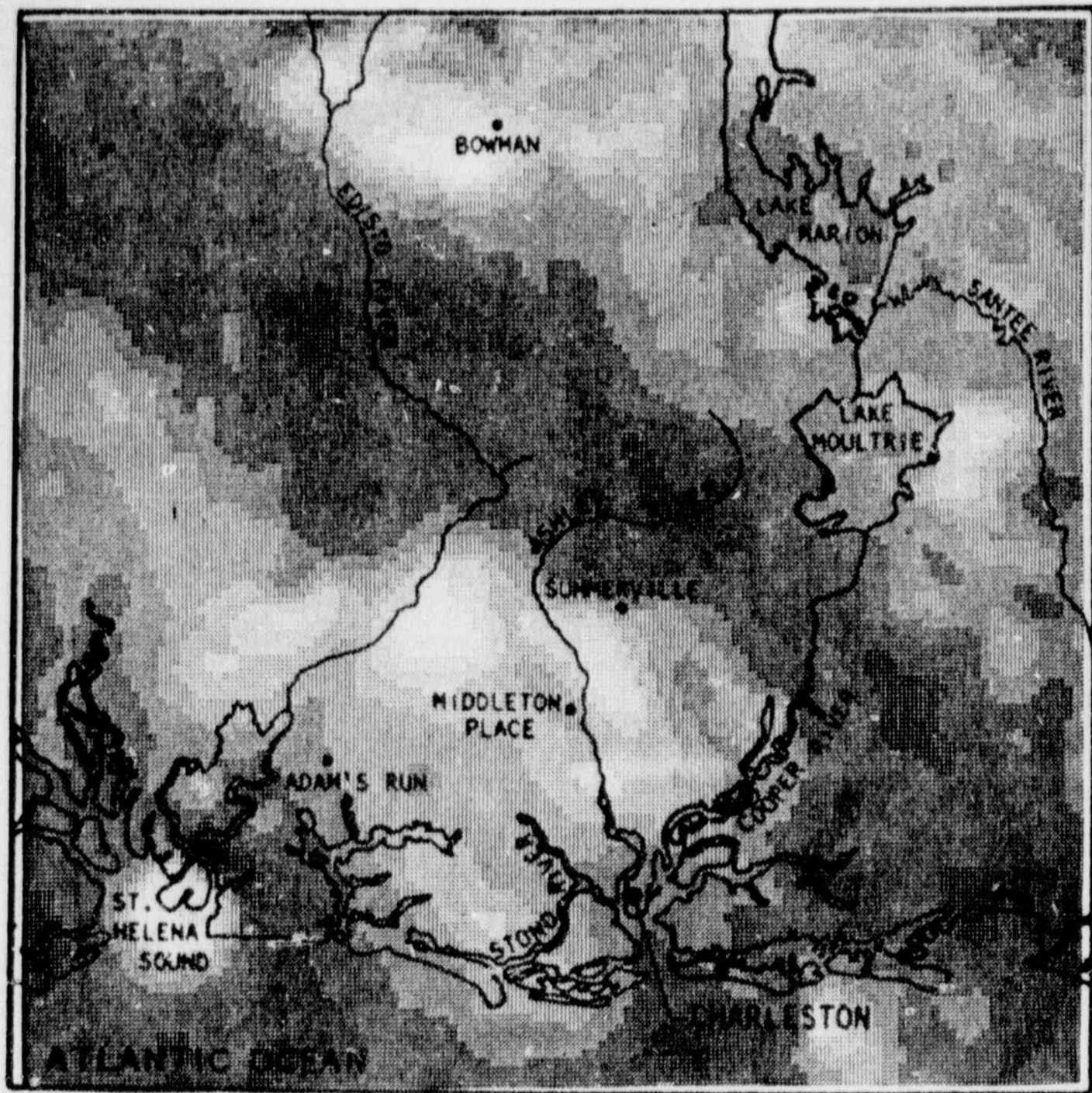


Figure 5-6. Image of magnetic-anomaly data, 1 km grid. Higher values appear lighter, lower values appear darker.

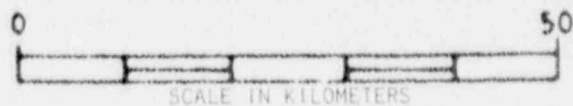
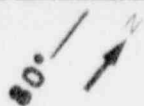
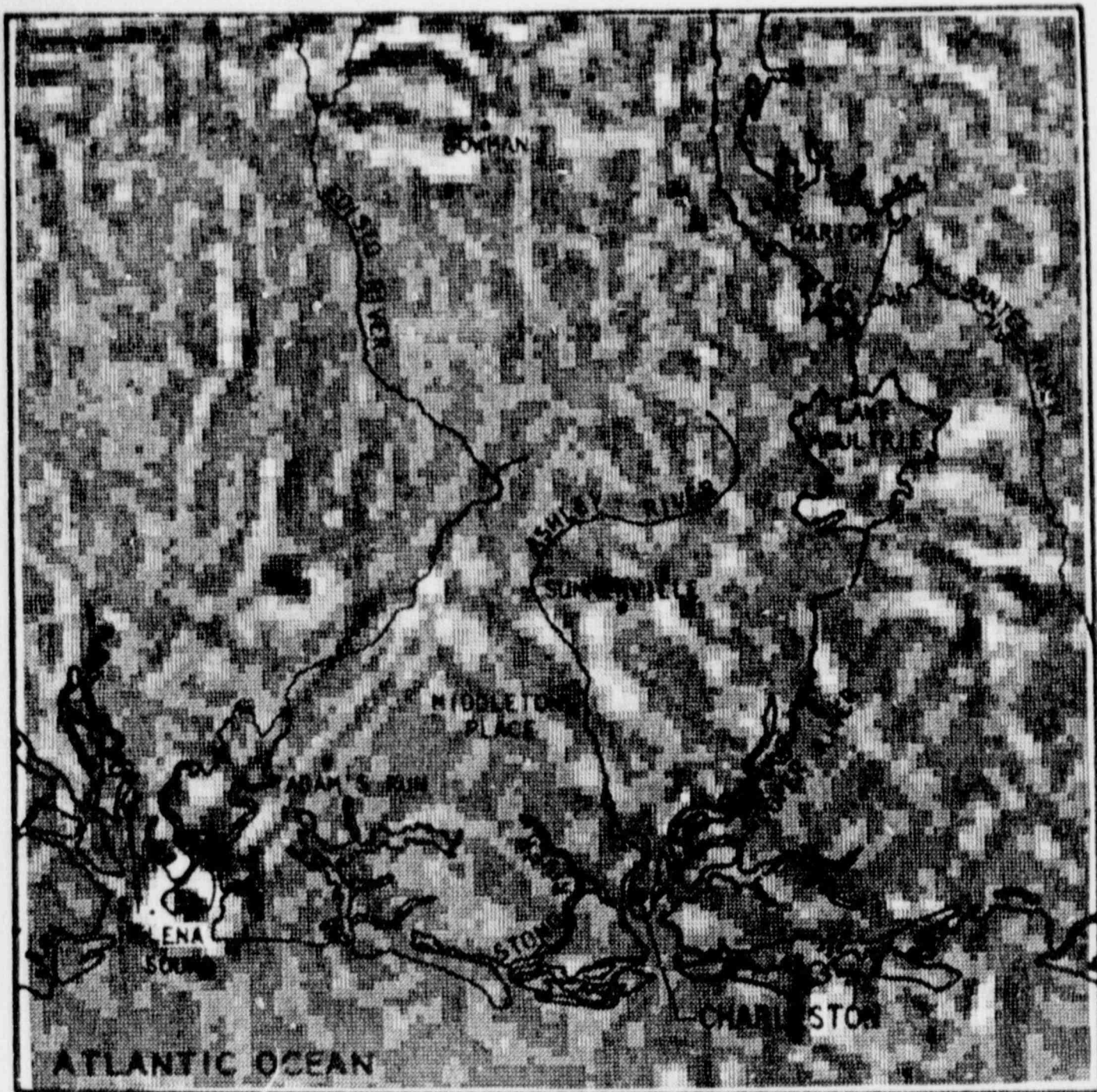


Figure 5-7. Image of vertical second derivative of magnetic-anomaly data.

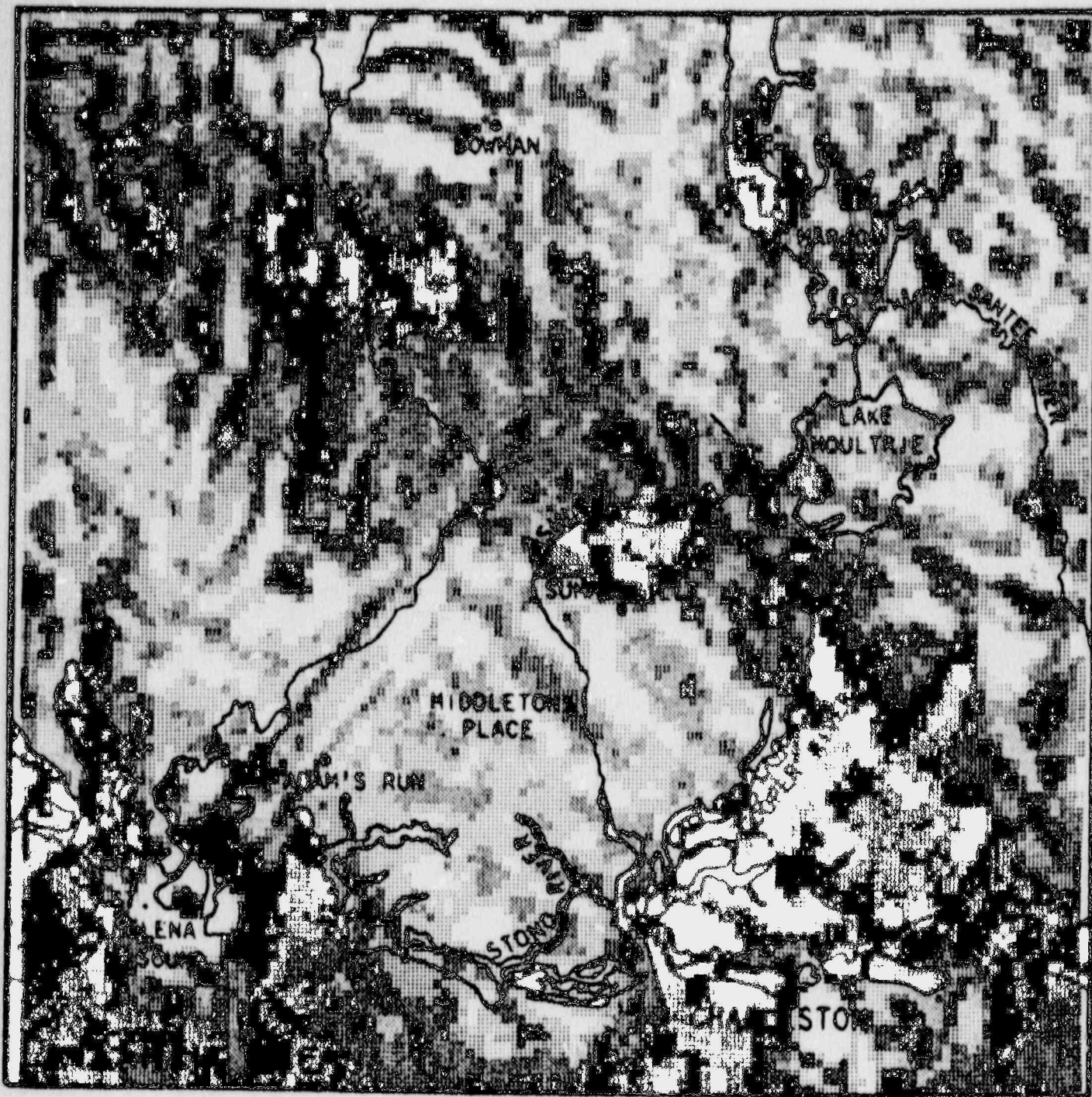


Figure 5-8. Image combining magnetic anomaly data and vertical second derivative (Figures 5-6 and 5-7).

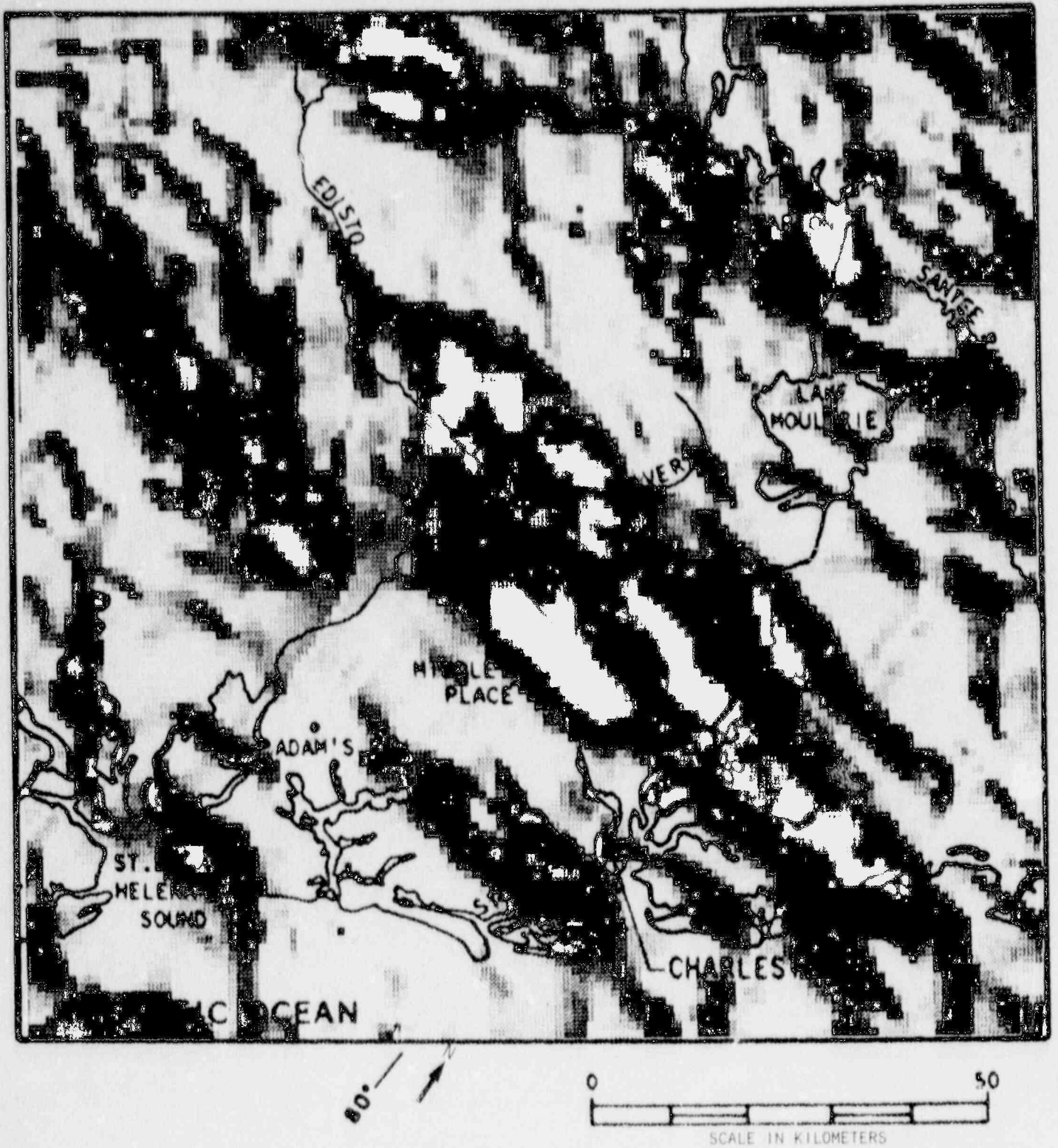


Figure 5-9. Shaded-relief image of magnetic-anomaly data. Source of illumination is to south.

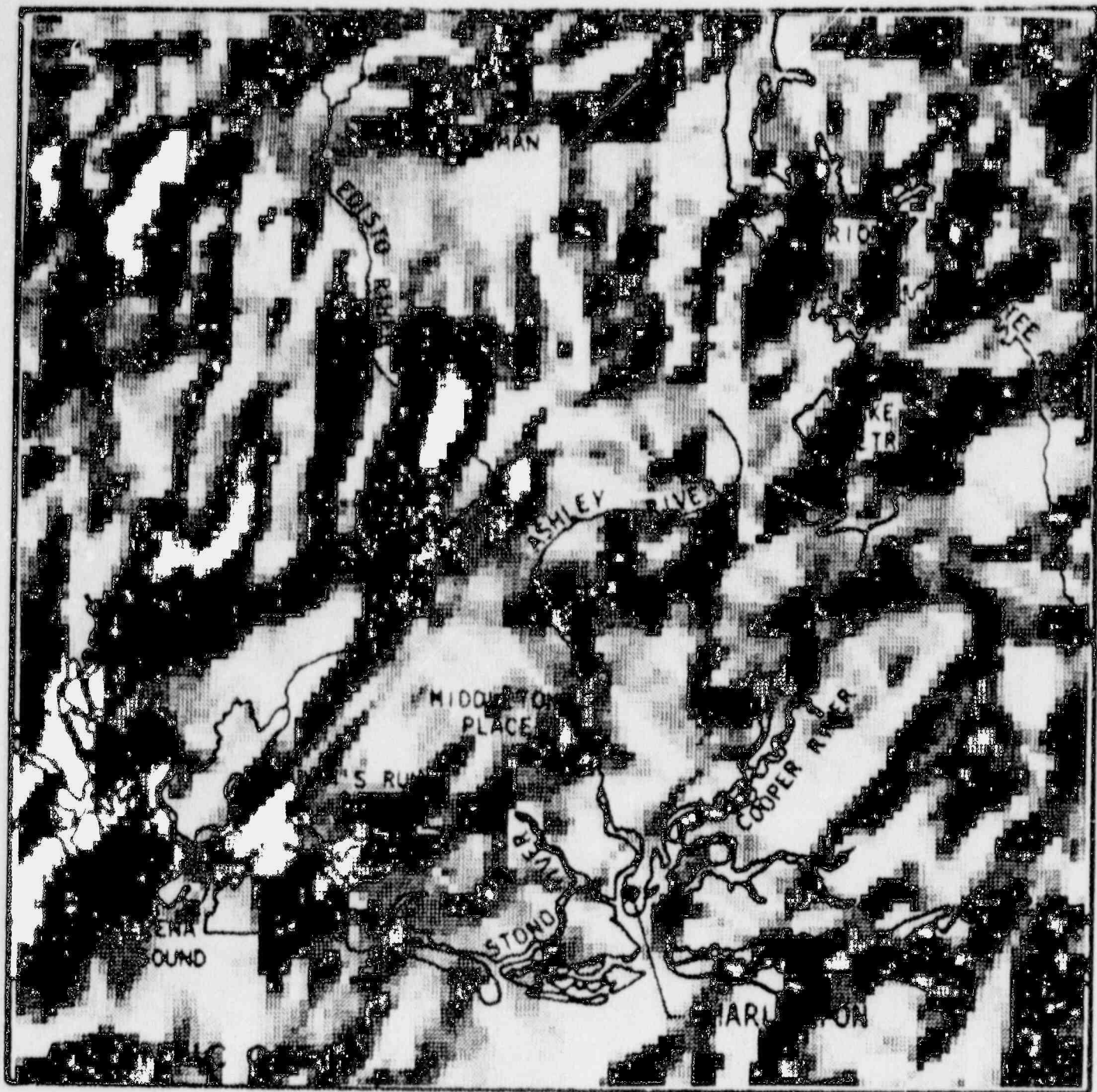


Figure 5-10. Shaded relief image of magnetic anomaly data. Source of illumination is to east.

Figure 5-7 is the vertical second derivative of the magnetic data, and Figure 5-8 is the multi-image combination of both the field and derivative data. Note that the north-south trending lineaments obvious on the vertical second derivative are an artifact of rotating the USGS magnetic data grid to conform with our grid orientation. Figure 5-9, a shaded-relief image lit from the south, shows the obvious structural trends in the data, while Figure 5-10, lit from the east, shows more subtle cross trends.

These images, then, were used as input to the various phases of structure modeling, with regards to both defining the shape of the "B" horizon, and in placement of the plutons.

5.3 Modeling Process

In this section the modeling process is described sequentially, and following that the resulting product will be described as an interpretation of the geology at seismogenic depths.

A generalized interpretation of the area geology was developed from previous work by others and from data obtained in this study. Figure 5-11 shows the interpretation along a NW-SE striking profile through the study area. A wedge of Coastal Plain sediments (Quaternary through Cretaceous) thickens toward the coast and is underlain by a thin Jurassic basalt (called the "J" horizon by Schilt *et al.*, 1983). The "J" horizon is a series of flows covering all but the northwest corner of the study area. Triassic to early Jurassic sediment-filled basins are immediately below the Jurassic basalt. The lithology of the Triassic/Jurassic rocks is not well known locally but using other similar nearby basins and Clubhouse Crossroads Test Hole #3 as a guide, we arrive at a mix of clastic sediments (sandstones, siltstones, shales, argillites, etc.) and perhaps basalt flows.

Crystalline rock underlies the Triassic/Jurassic rock. The crystalline rock may consist of quartz-rich metamorphic rock intruded by mafic or ultramafic plutons. The igneous rocks are thought to be gabbroic in composition and Paleozoic in age, thus predating the basin development.

The top of the crystalline rock has been called the "B" horizon (Schilt *et al.*, 1983). To the northwest the crystalline rock directly underlies the Coastal Plain sediments, i.e. there is no Triassic/Jurassic sediment or Jurassic basalt.

The crystalline rock appears to continue with uniform character to depths of between 10 and 23 kilometers. This depth range corresponds to the maximum hypocentral depths for seismicity. Below 10 to 23 km the physical properties as observed on COCORP reflection profiles appear to change. In the lower crust the COCORP reflection images of the crust change from being seismically transparent to displaying numerous short reflectors

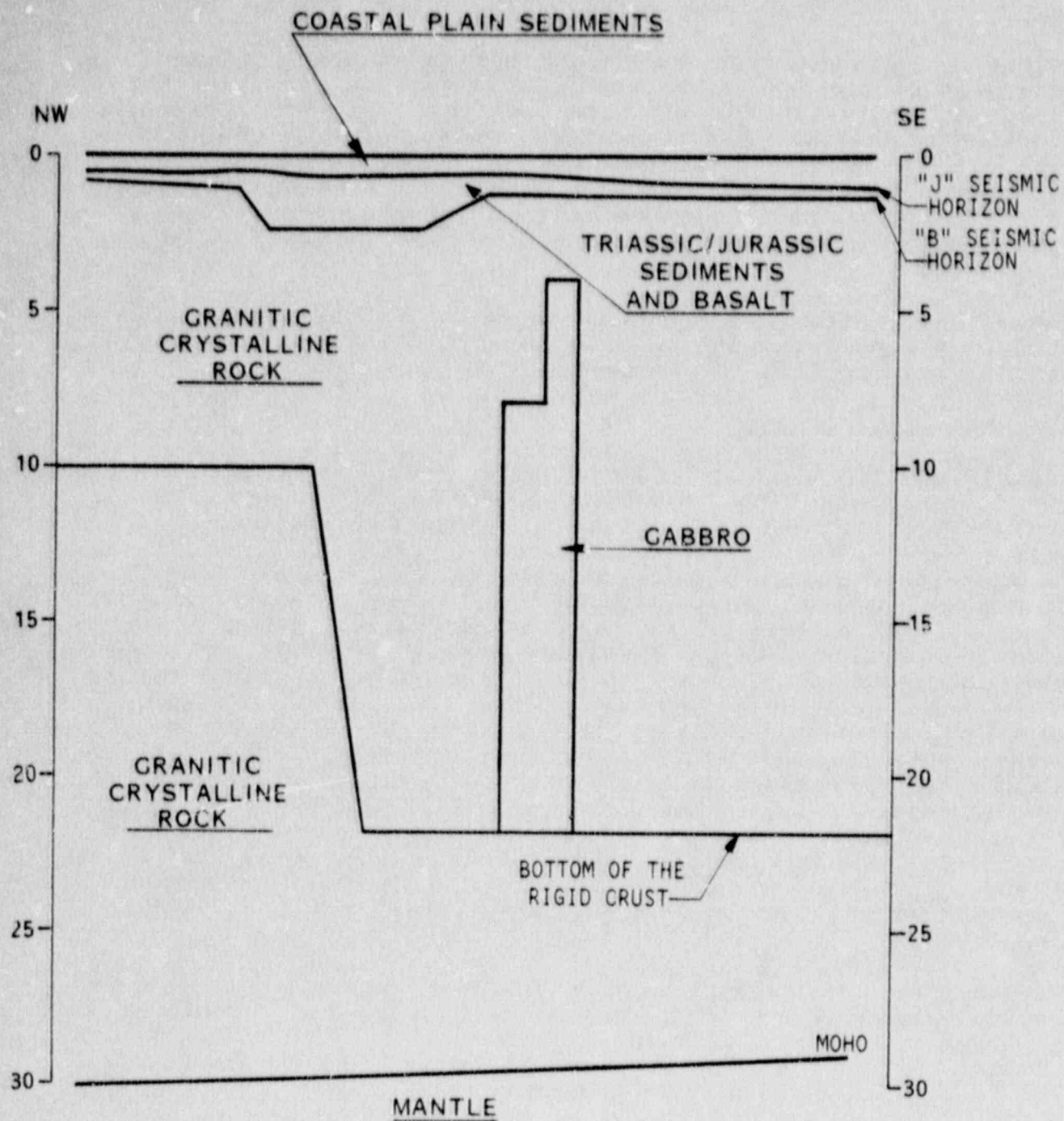


Figure 5-11. Sample cross section of geologic model.

(Schilt et al., 1983). Also the rock of the lower crust becomes more conductive.

The crust/mantle boundary is located at a depth of about 28 to 30 km and is interpreted to become more shallow toward the coast.

Figure 5-12 is a flow chart of the modeling process. We began our modeling with Bouguer gravity and magnetic data at 1 km-spaced grid points over a 128 x 128 km area centered on Charleston. Figures 5-13 and 5-14 are the contoured gravity and magnetic fields, respectively. Chapter 4 describes the development of these data sets in detail. We also began with a considerable amount of other data with which to develop our model. Some of the data was used to constrain the potential field modeling, and other data was used to add features which could not result directly from a potential field model.

The first step in our modeling process was to determine the geometry and bulk density of the sedimentary wedge covering the study area, and then to remove the effect of that wedge from the gravity field. In order to do this, we noted that the sedimentary wedge is immediately underlain by a regional series of basalt flows which are a prominent feature on seismic reflection and refraction lines, both onshore and offshore, and are known as the "J" horizon. We developed an interpretation of the elevation of the "J" horizon primarily from refraction and reflection data and from drilling records (Chapter 4). Figure 5-15 is our structural contour map of the "J" horizon. In general, reflection data contributed to offshore and some onshore control. Refraction data were mainly available onshore in the central study area and drilling records were available to the northwest, where the Coastal Plain sediments are thinner. We used 2.2 g/cm^3 for the density of the material above the "J" horizon, which is based on previous work by us and others (Long and Champion, 1977, Talwani, 1977). The effect of the Coastal Plain sediments was removed from the Bouguer gravity field, yielding the first residual gravity field.

Our next step was to determine the distribution and density of the Triassic/Jurassic sediments, the base of which is the "B" horizon. Control on the "B" horizon is from seismic reflection and refraction in the center of the study area, and from drilling to the northwest where Coastal Plain sediments thin (Chapter 4). In areas where seismic and drilling control was lacking, depths to the top of crystalline rock were initially extrapolated using the first residual gravity field as a guide. These areas were modified later as part of the gravity modeling process. The modeling of the effects of the Triassic/Jurassic sediments and basalt was repeated three times during the overall effort, changing both the interpreted contours of the "B" horizon and the estimated rock density. Our initial estimate for the density of the Triassic/Jurassic materials was 2.57 g/cm^3 , based on recent work by Long in buried

MODELING SEQUENCE

FIGURES ASSOCIATED WITH EACH STEP

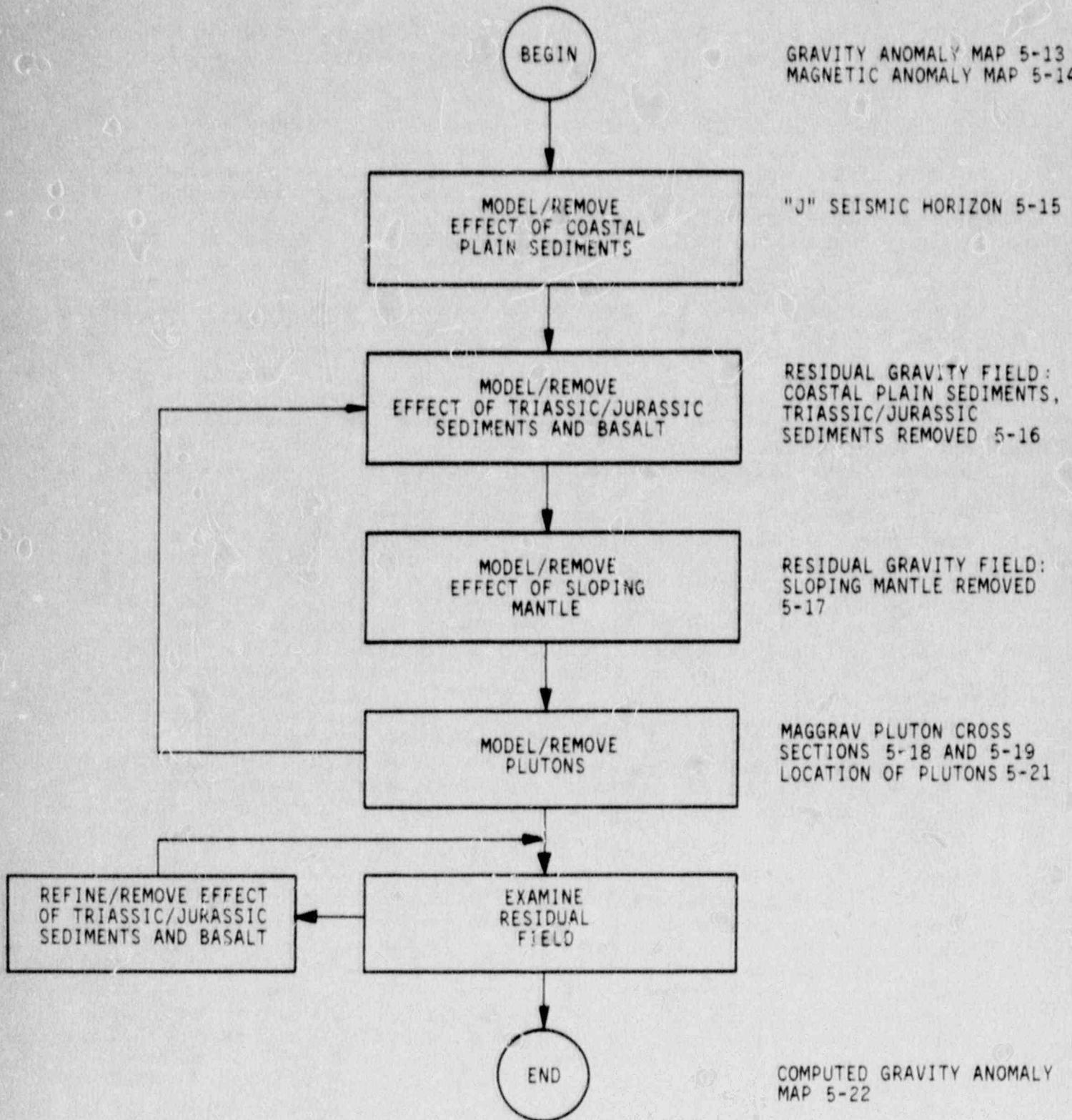


Figure 5-12. Modeling sequence diagram. This figure shows the sequence of modeling and the appropriate figures depicting a particular modeling stage.

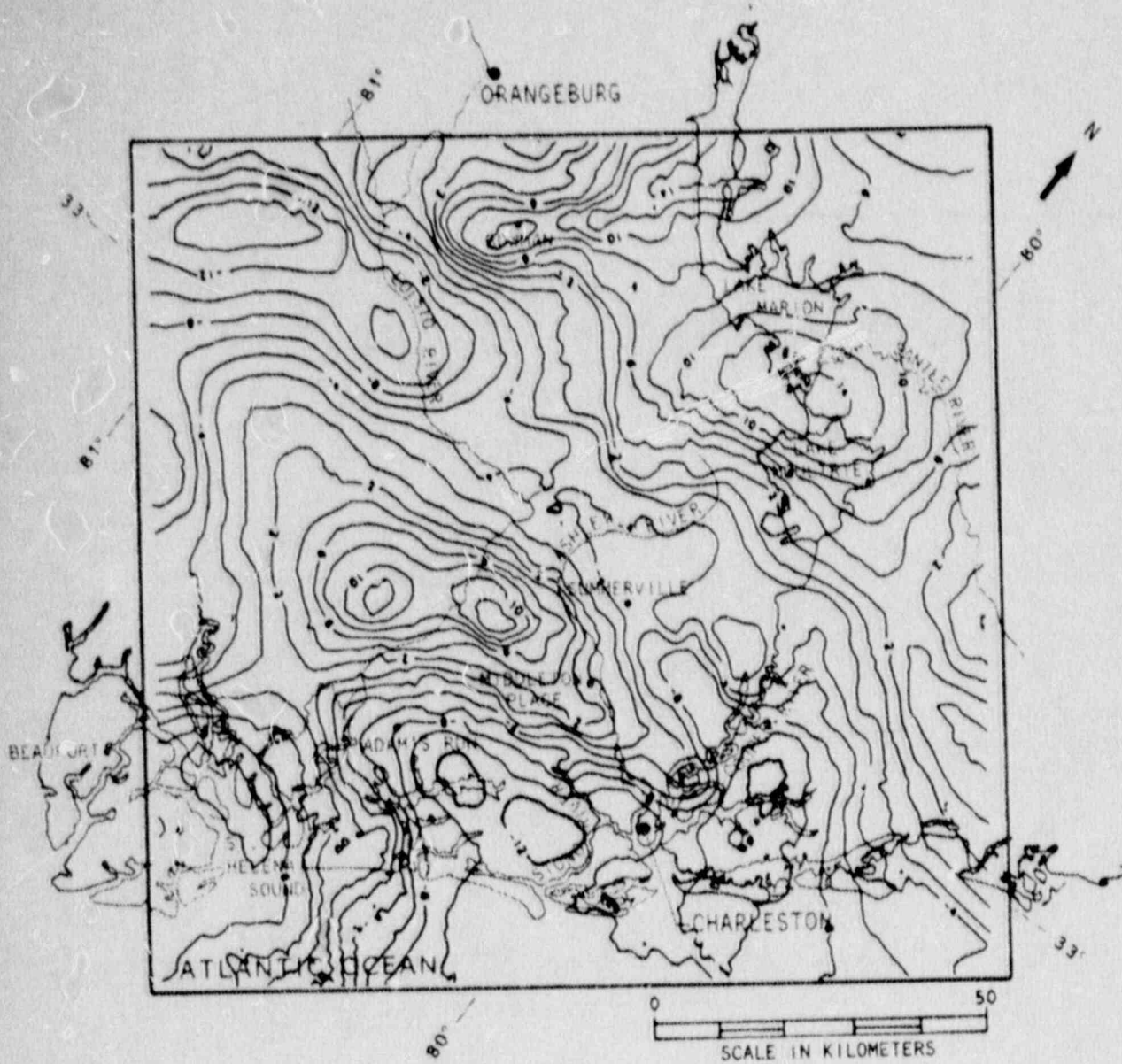


Figure 5-13. Bouguer gravity anomaly map of the Charleston, S.C. area. Contour interval is 2 milligals.

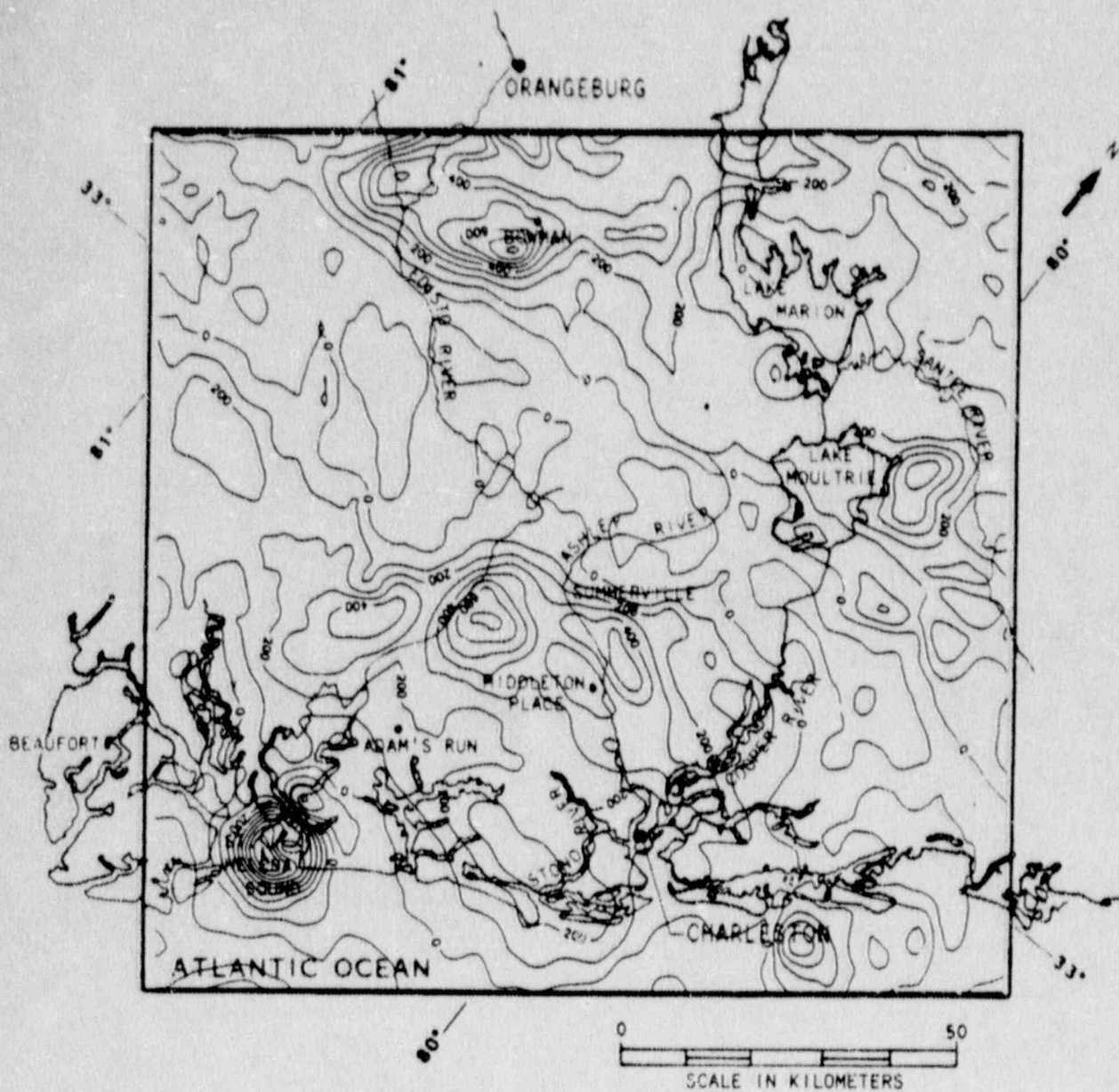


Figure 5-14. Magnetic anomaly map for Charleston area. Contour interval is 100 gammas.

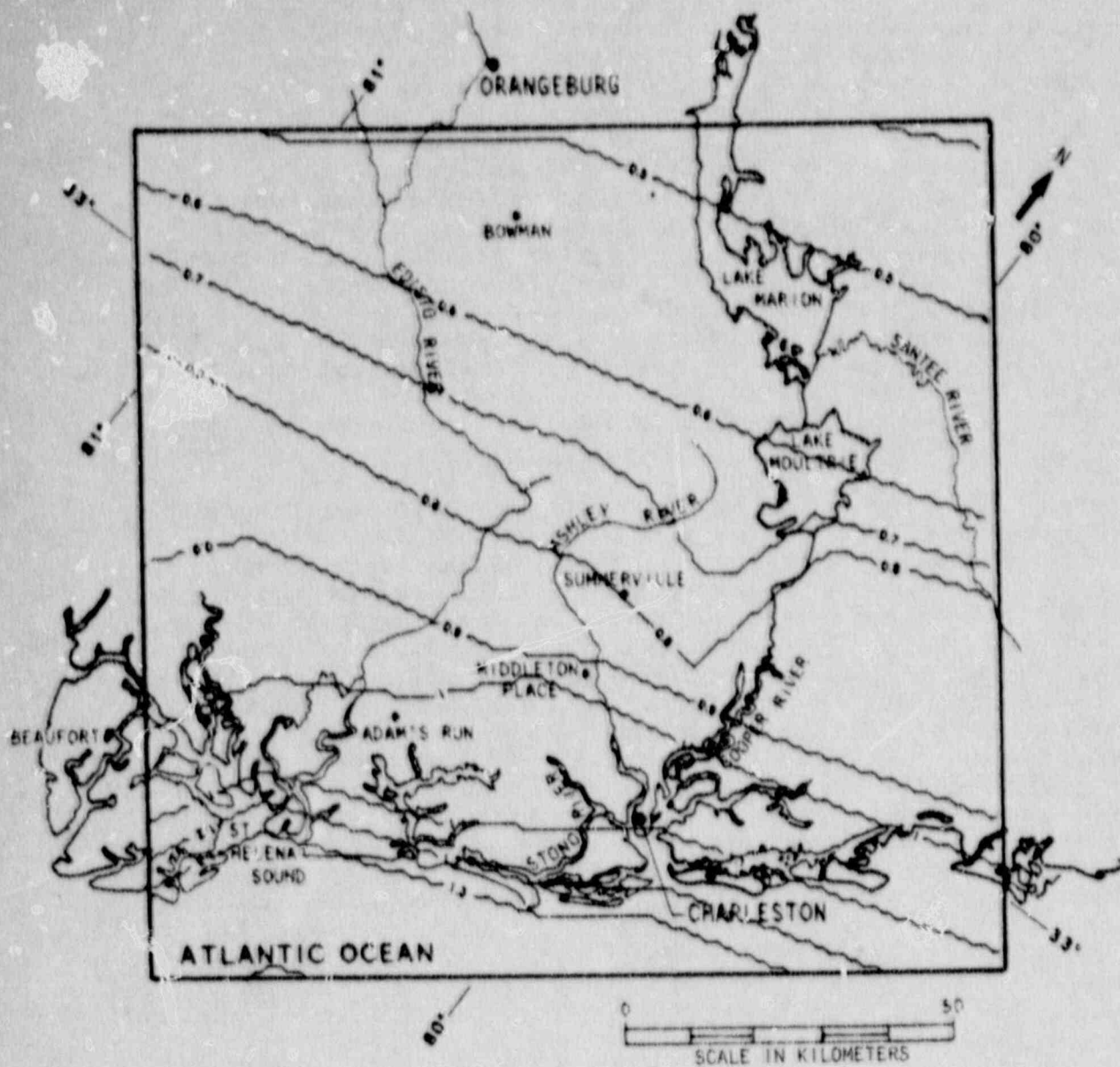


Figure 5-15. Structural contour map of the "J" seismic horizon as used in the geologic model. Contours are depth in kilometers.

Triassic/Jurassic basins in Georgia, since there is no site-specific lithologic data from which to infer densities. As indicated by Figure 5-12, modeling the mafic plutons (whose density we had a closer control on) required a more positive residual field than was left, thus requiring us to return to the Triassic/Jurassic rocks and reduce this density. A value of 2.47 g/cm^3 left sufficient residual anomaly to allow the mafic intrusions to be accommodated. Later, after the plutons were modeled and their positive gravity effect removed, the remaining residual gravity field indicated that alterations in the interpreted structural contours of the "B" horizon needed to be made, and that an average density of 2.52 g/cm^3 was the best choice. The final structural map of the top of crystalline rock ("B" horizon) consists of seismic interpretation, drilling results and gravity modeling (Figure 5-23).

Following modeling of the Triassic/Jurassic sediments, we considered the effect of the mantle/crust boundary (Moho). The need for including the Moho at this point in the modeling process became clear when we removed the effects of the Coastal Plain and Triassic/Jurassic rocks. At this point, we assumed that the resulting residual gravity field should be influenced only by the mafic plutons, and should approach zero at distance from the mafic plutons. However, Figure 5-16 is this second residual gravity field, and a progressive increase in gravity values from west to east can be seen. We therefore decided to examine the effects of a sloping Moho on the gravity field. Using a crust/mantle density contrast of 0.4 g/cm^3 ($2.67/3.07$) and a 1% slope away from the coast, the effect of the gradient in the field from the mantle was calculated and removed from the second residual field of Figure 5-16. The resultant third residual field is shown on Figure 5-17; comparison of the two figures indicates that the assumption of a sloping crust/mantle boundary is appropriate because away from the large positive anomalies belonging to the mafic plutons the residual gravity field now tends toward zero.

As the next step in our modeling process, we consider the mafic plutons. We used MAGGRAV to model each pluton separately using a two-dimensional cross section. The magnetic field to be matched strongly constrained the shapes of the density anomalies we used to model the plutons. Figures 5-18 and 5-19 are examples of MAGGRAV model cross sections through mafic plutons. Figure 5-20 shows the locations of the MAGGRAV cross sections. We assumed that remanent magnetism was not significant and used only induced magnetism. The magnetic susceptibilities used resulted from making the computed magnetic anomalies match the field data. The pluton density used (2.87 g/cm^3) was also required to fit the residual gravity field. It should be pointed out that since two-dimensional models can be inadequate when dealing with finite length bodies, each MAGGRAV solution was checked with PLATES (for example, in this case the pluton density had to be adjusted to 2.97 g/cm^3 for the 3-D model). The computed positive gravity

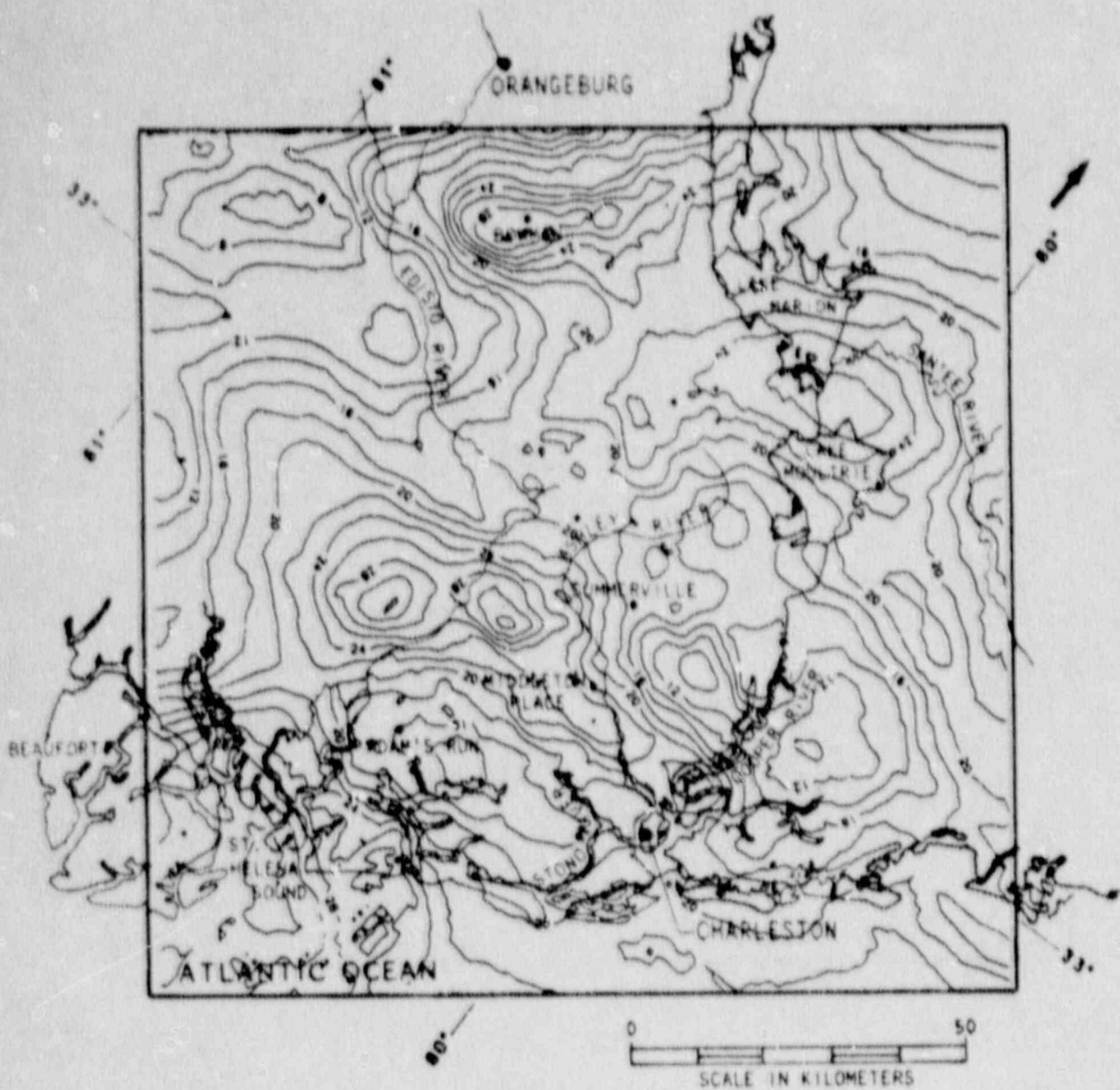


Figure 5-16. Gravity field after removal of the effects of the material above the "B" seismic horizon (including the "J" seismic horizon). Contour interval is 2 milligals.

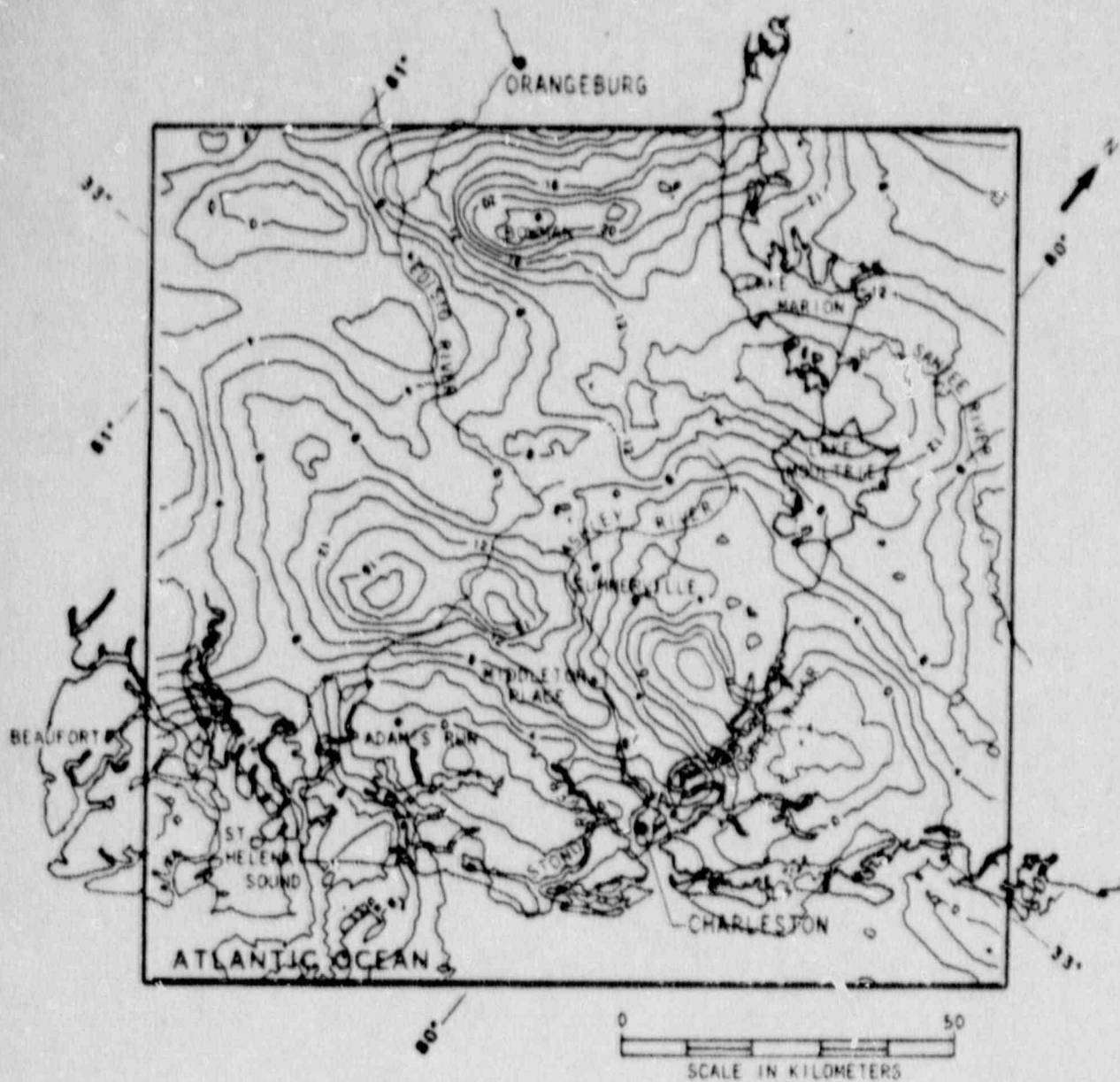


Figure 5-17. Gravity field after removal of the effect of material above the "B" seismic horizon (including the "J" horizon) and removal of the effect of a tilt of the mantle. Contour interval is 2 milligals.

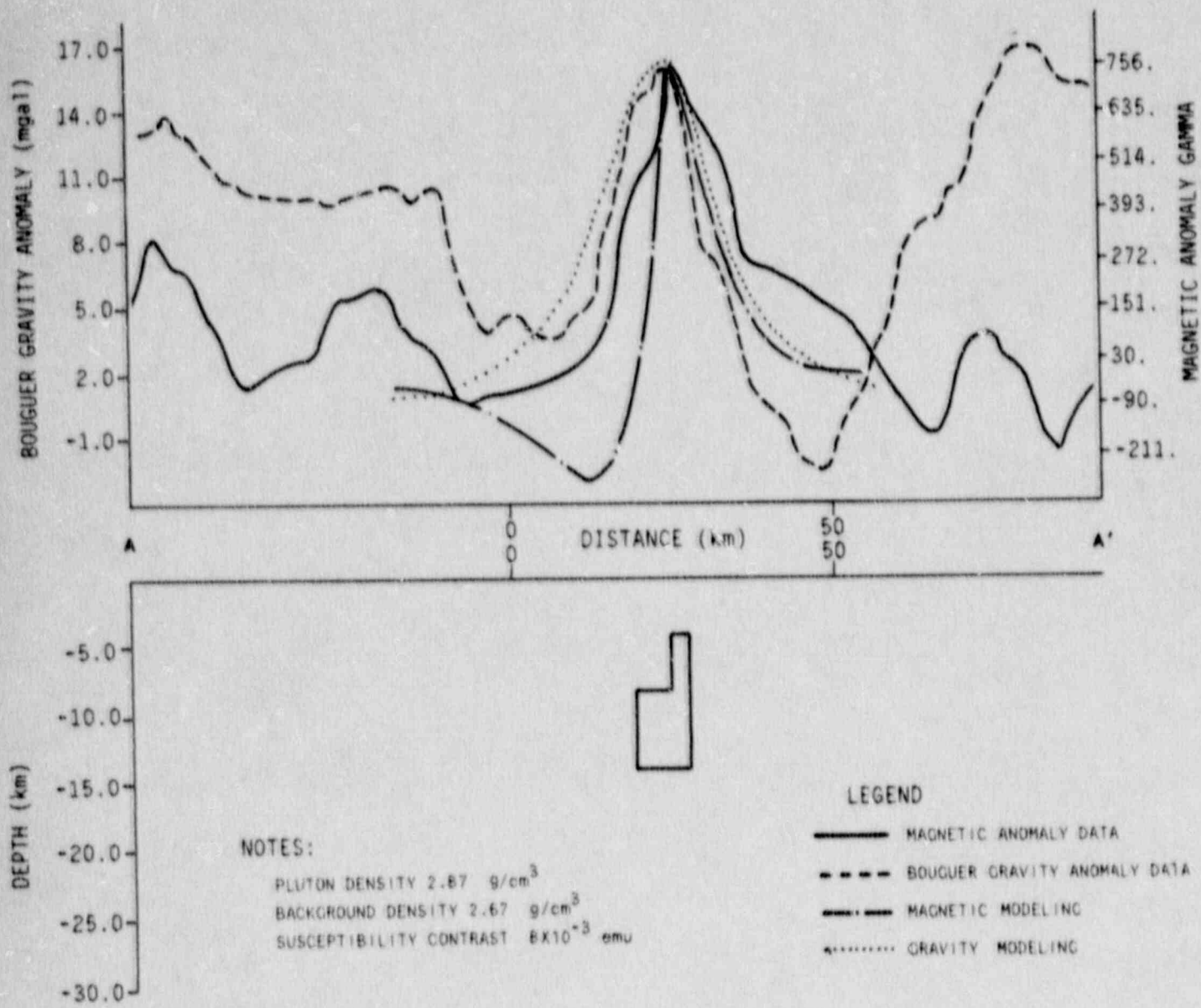


Figure 5-18. Gravity/magnetic forward model of a pluton as modeled by the MAGGRAV computer program (Figure 5-20 for location).

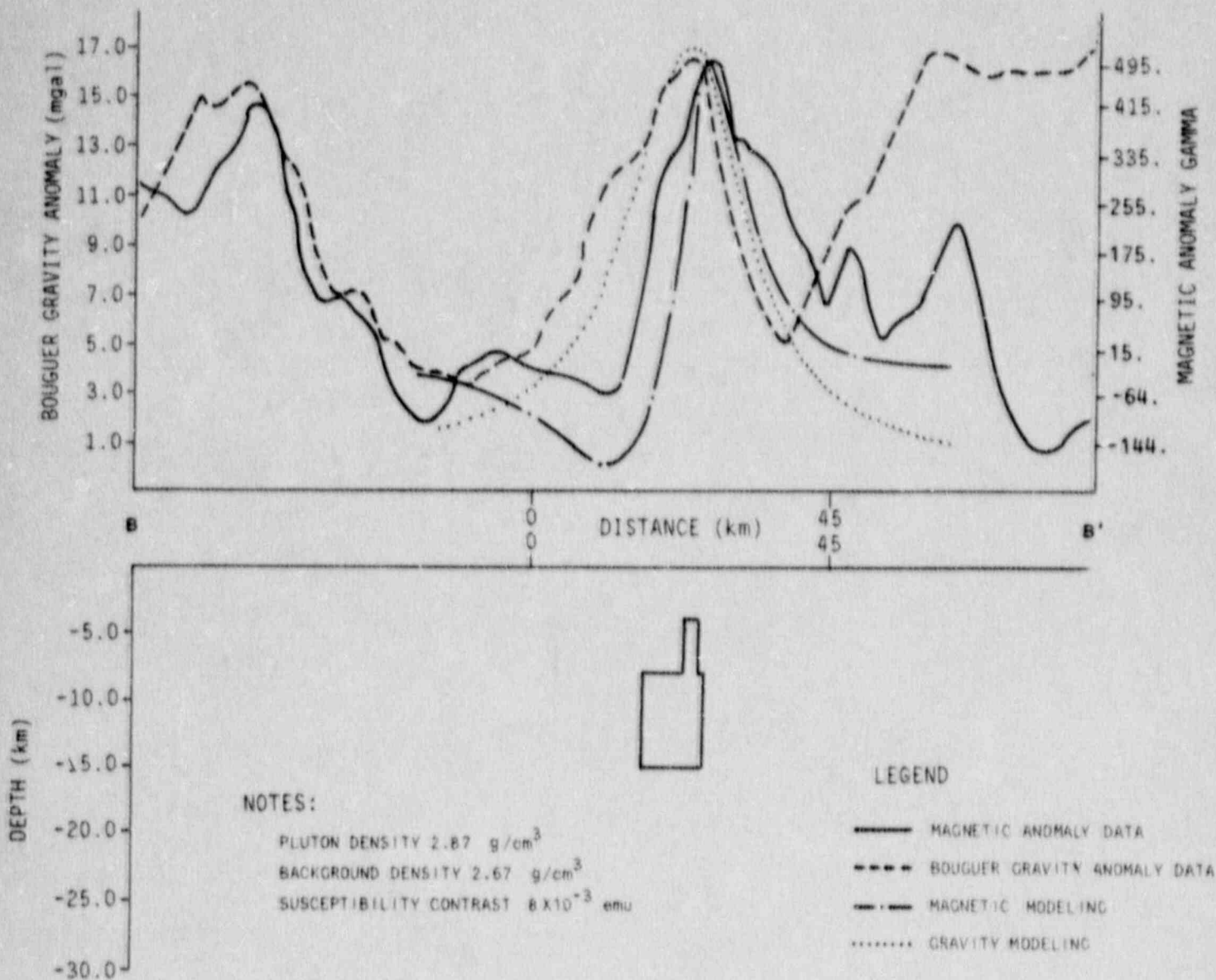


Figure 5-19. Gravity/magnetic forward model of a pluton as modeled by the MAGGRAV computer program (Figure 5-20 for location).

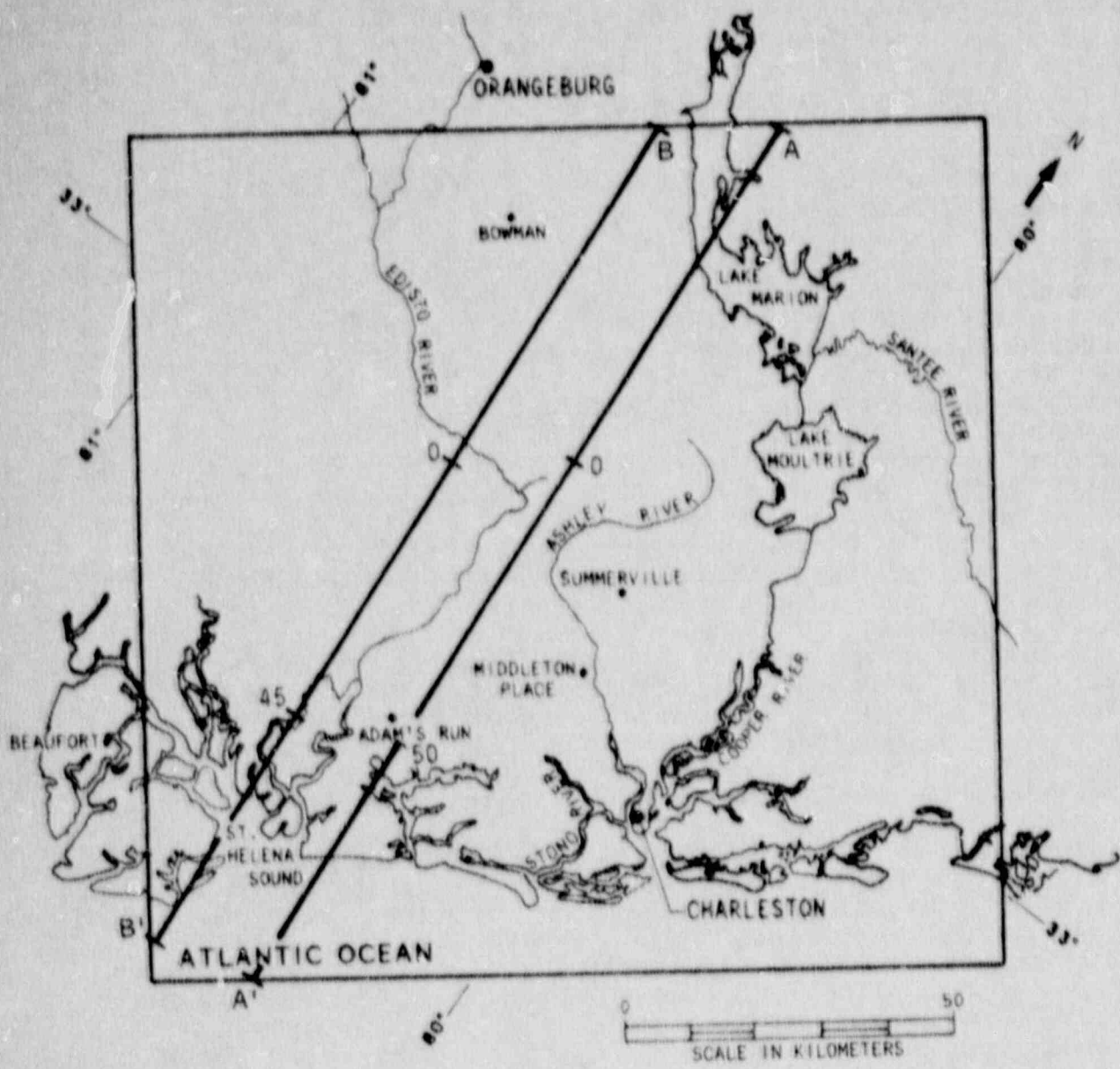


Figure 5-20. Location of MAGGRAV cross sections (Figures 5-18 and 5-19).

anomalies from the plutons were then removed from the gravity field. As described above and indicated on Figure 5-12 the result of removing the pluton-related gravity anomalies caused us to adjust the Triassic/Jurassic rock density value and the structural contour of the "B" horizon.

The modeled location of the plutons and their densities are shown on Figure 5-21.

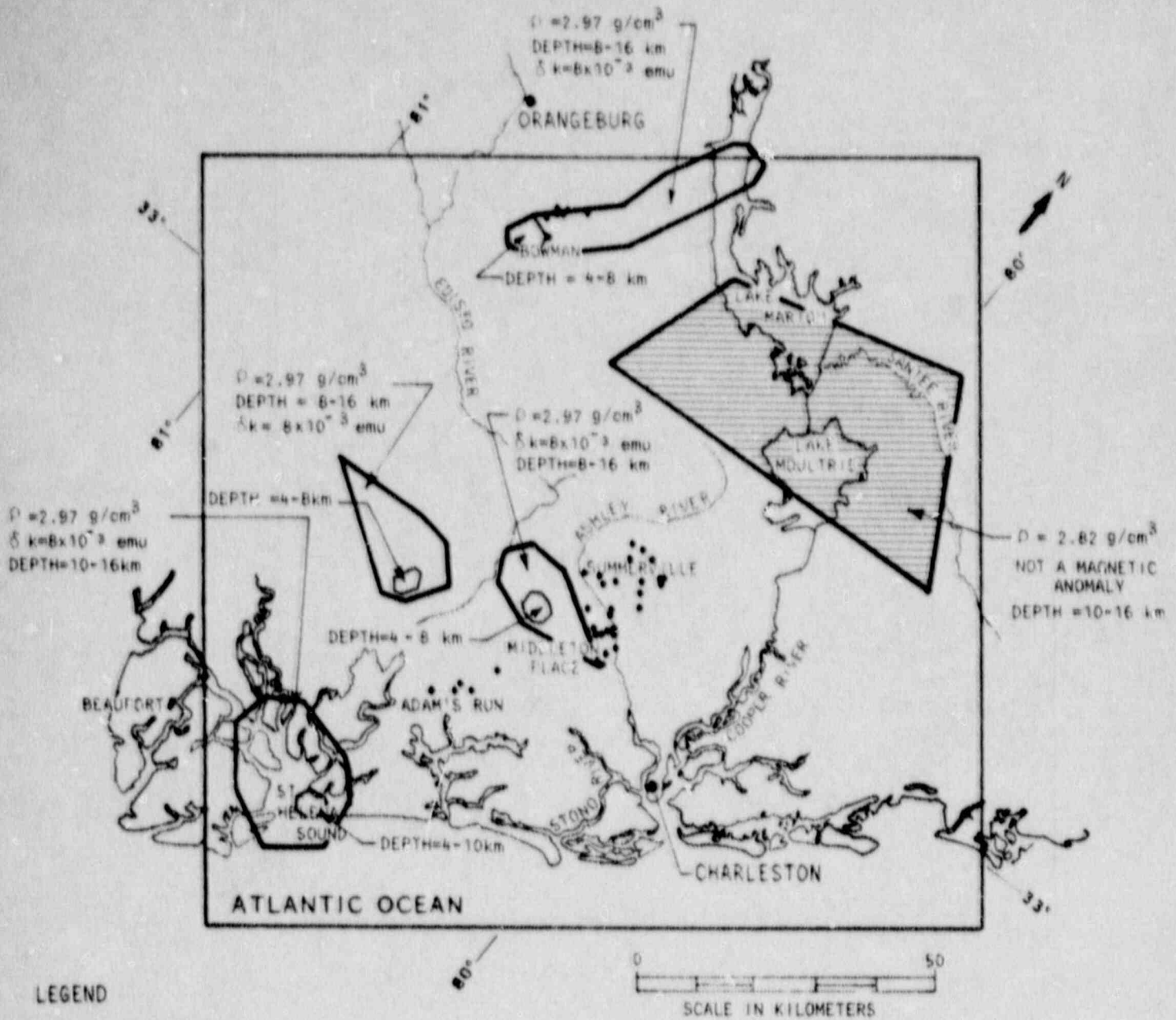
Figure 5-22 shows the computed gravity field from the modeling process. It compares well with Figure 5-13, the measured gravity field. The eastern corner of the study area shows a difference due to the lack of gravity data offshore. Figure 5-14, the magnetic field, shows that the St. Helena Sound mafic pluton's shape is as shown in Figure 5-21.

The final element of the model is a determination of the bottom of the rigid crust (Figure 5-11). Its existence, properties, and geometry were developed as follows. The bottom of the rigid crust is defined as the depth below which the rock responds to crustal stresses in a viscoelastic manner and, therefore, will not accumulate sufficient stress to cause elastic failure. Instead, stress is released through viscoelastic deformation. This condition is caused by mineral alteration at elevated temperature and pressure. Serpentine, which is probably a mineral constituent of the mafic intrusives, dehydrates at about 500°C and would contribute to gabbro becoming viscoelastic. Other minerals undergo alterations near this temperature with the same result.

Our evidence for the location of this boundary between 10 and 23 kilometers depth in the Charleston area is based on maximum depths of seismicity, seismic reflection sections, and magnetotelluric soundings. The magnetotelluric soundings gave as a solution a low resistivity zone beginning at depths between 10 and 23 km. Figures 4-12 and 4-13 show 200 ohm-meter material at that depth. Figures 4-17 through 4-19, crustal seismic reflection sections, show that this depth is where discontinuous reflections begin and above which the rock is seismically transparent. The maximum depth of earthquakes follow the same general pattern. In the Charleston-Summerville area, they are in the 10-20 km range while to the northwest they remain shallow (above 10 km). No single line of evidence alone is convincing on defining this boundary. The magnetotelluric sounding solutions are not unique, the seismic reflections at that depth may have other interpretations, and earthquake depths are not well constrained. We feel however, that the combination of evidence strongly supports the existence of this boundary and its general location.

5.4 Results

In this section we describe the results of our work in Chapter 5; namely, the geologic model of the crust at seismogenic depths in the Charleston area. Figure 5-11 shows the elements



LEGEND

- EARTHQUAKE EPICENTER [SOURCE: TARR AND RHEA (1983)]
- ρ DENSITY
- Δk MAGNETIC SUSCEPTIBILITY DIFFERENCE
- DEPTH = RANGE OF TOP TO BOTTOM OF PLUTON SEGMENT

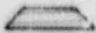

-  HIGHER DENSITY BASEMENT
-  MODELED PLUTONS WITH DEPTH RANGES

Figure 5-21. Location of interpreted mafic plutons used for the geologic model. Also shown is recent seismic activity.

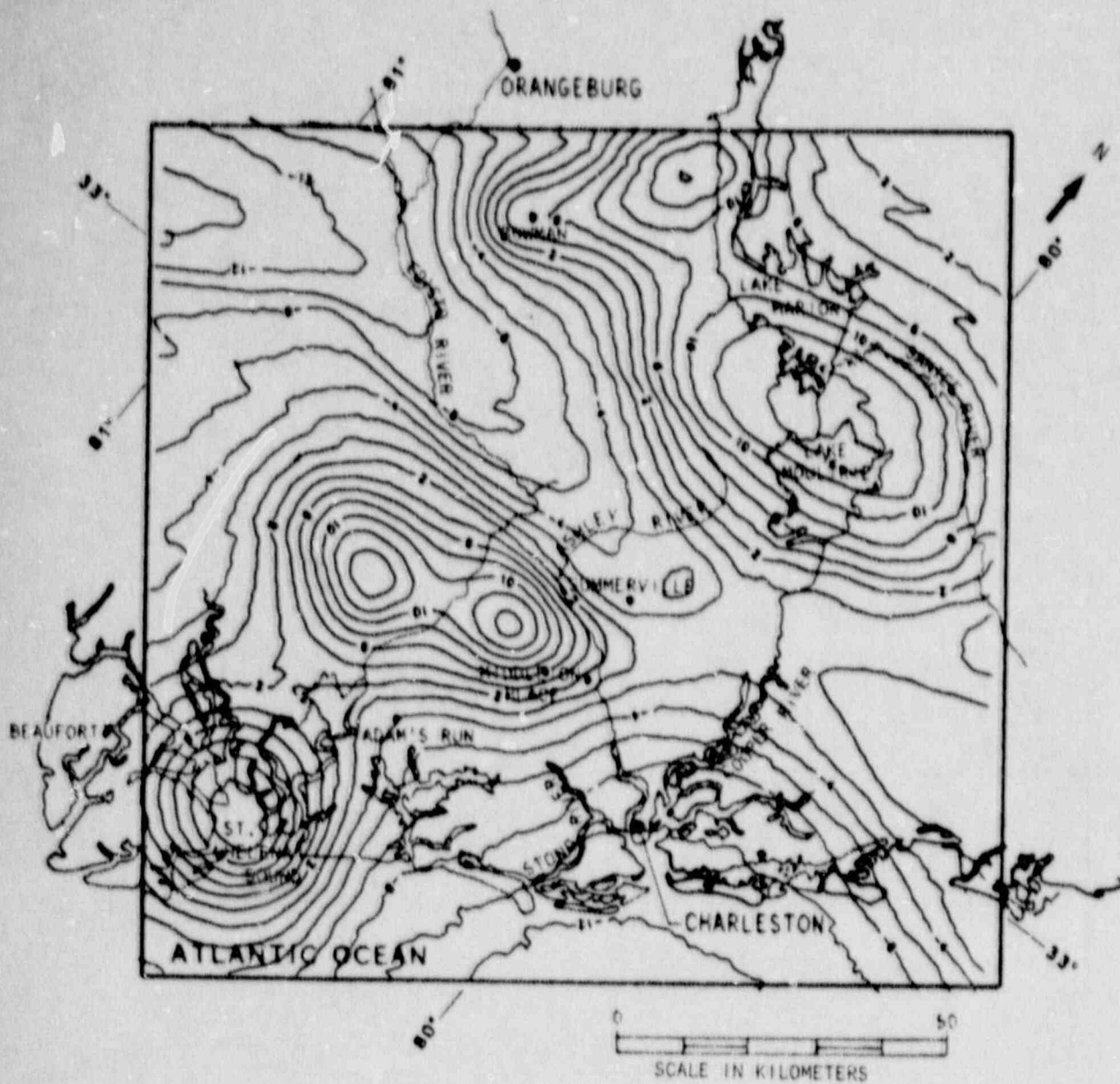


Figure 5-22. Gravity field computed from model. Compare this figure with Figure 5-13 which is the measured gravity field. Contour interval is 2 milligals.

of our geologic interpretation in the form of generalized cross section northwest to southeast through the study area. Figures 5-15, 5-23 and 5-25 are structural maps of key horizons; namely, the "J" seismic horizon, the "B" seismic horizon, and the bottom of the rigid crust. Figure 5-24 is an isopach map of Triassic/Jurassic rock and Figure 5-21 locates the plutons.

Figures 5-26 through 5-28 are cross sections through the study area. Figure 5-29 shows the location of the cross sections.

Geologic History: The crystalline crustal rocks in the Charleston area, those below the "B" seismic horizon, represent the subsurface extension of rocks belonging to the Appalachian orogenic belt. Williams and Hatcher (1983) divided the Appalachian orogen into geologically and/or geophysically distinct terranes. The terranes include segments of the North American craton and crustal blocks that were accreted to North America during the Paleozoic. The Charleston area is in the Brunswick terrane, a subsurface Appalachian crustal block recognized by its distinctive signature on magnetic maps (Figure 2-3). Little is known of the lithology of the Brunswick terrane, but it is probably composed of deformed and metamorphosed sedimentary and volcanic rocks intruded by plutons of granite and gabbro based on a comparison with better-known terranes. Our study area is interpreted by us to contain plutons of gabbro within a crust of granitic composition (Figure 5-11). Near the end of the Appalachian orogenies in the late Paleozoic, collision of North America with Africa caused the formation of major thrust faults that underlie much of the Blue Ridge and Piedmont of the southern Appalachians (Cook *et al.*, 1981). There is no clear evidence that major thrust faults exist in the Charleston region, so their existence in the Brunswick terrane is controversial.

After assembly of crustal blocks into a supercontinent in the late Paleozoic, the next major event was the formation of rift basins as the supercontinent began to break up in the late Triassic and early Jurassic. Subaerial clastic sediments and some lacustrine deposits accumulated in rift basins about 210 to 180 Myr ago (Tucholke and McCoy, 1986). Triassic/Jurassic sediments are interpreted to reach a thickness of 2 km in basins in the Charleston area (Figure 5-24).

The drifting apart of North America and Africa began about 180 Myr ago, with the formation of a seaway and oceanic crust to the east of the Charleston area (Klitgord and Schouten, 1986; Tucholke and McCoy, 1986). This episode is marked by extensive basalt flows that lie above the rift sediments in the Charleston area, constituting seismic horizon "J" of this report. The most reliable date for these basalts is 184 +/- 3.3 Myr (Lanphere, 1983).

As the drifting stage progressed, the Charleston area became part of the passive margin of the North American continent, and Coastal Plain sediments of Cretaceous and Cenozoic age

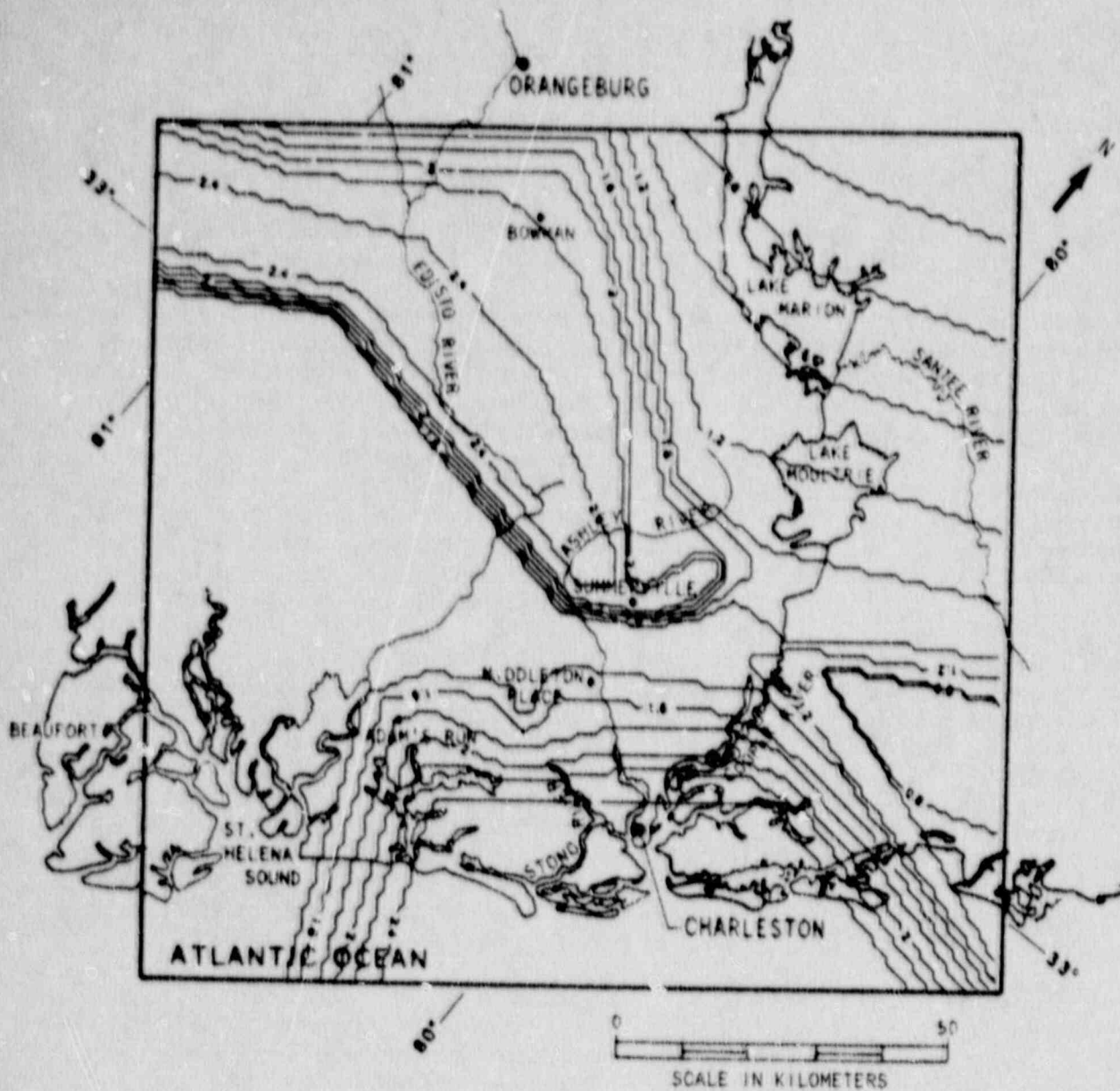


Figure 5-23. Structural contour map of the "B" seismic horizon. Contours are depth in kilometers.

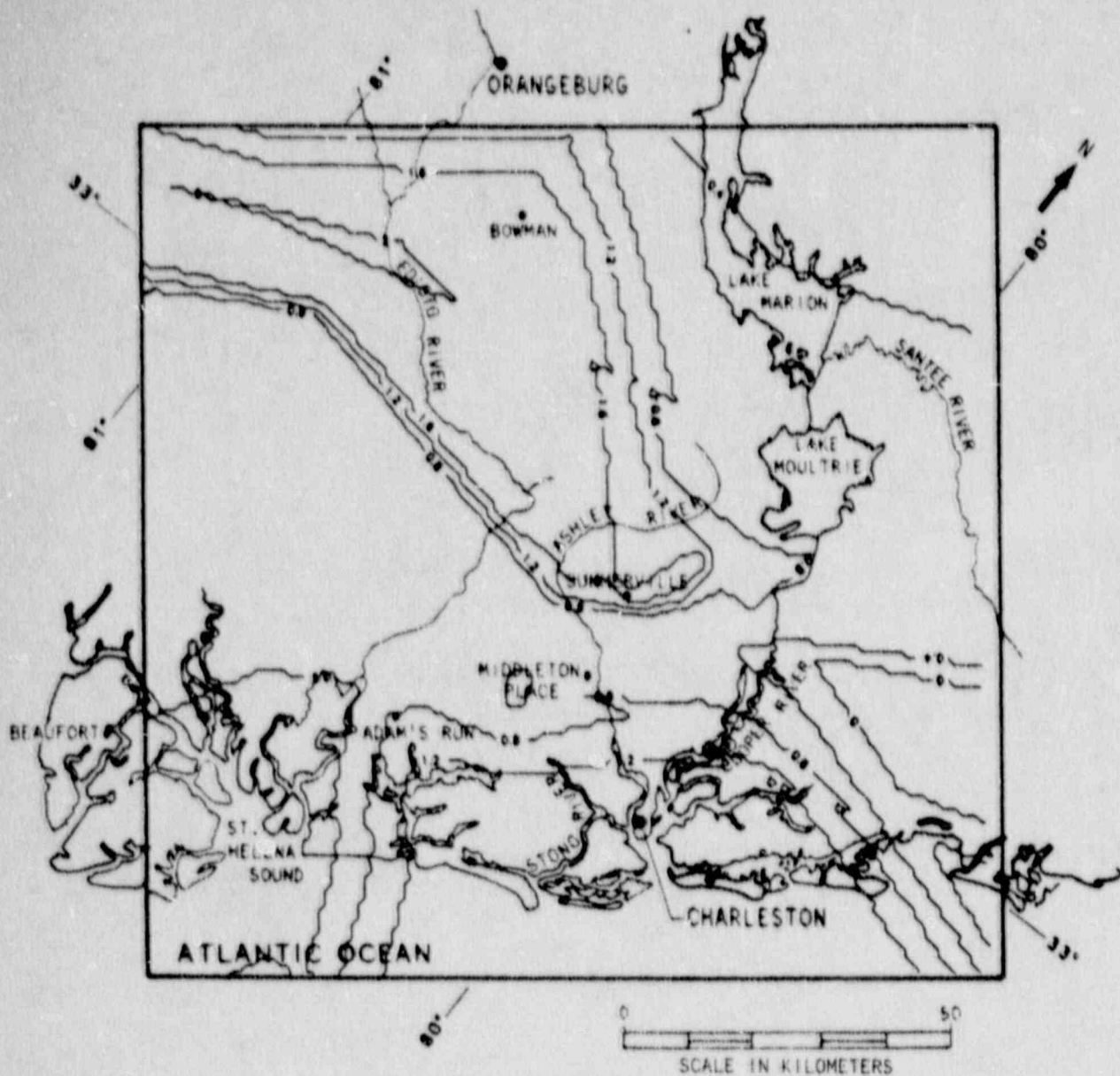


Figure 5-24. This is an isopach map of the Triassic/Jurassic rocks which are interpreted as being all rock between the "J" and "B" seismic horizons. Contours are thickness in kilometers.

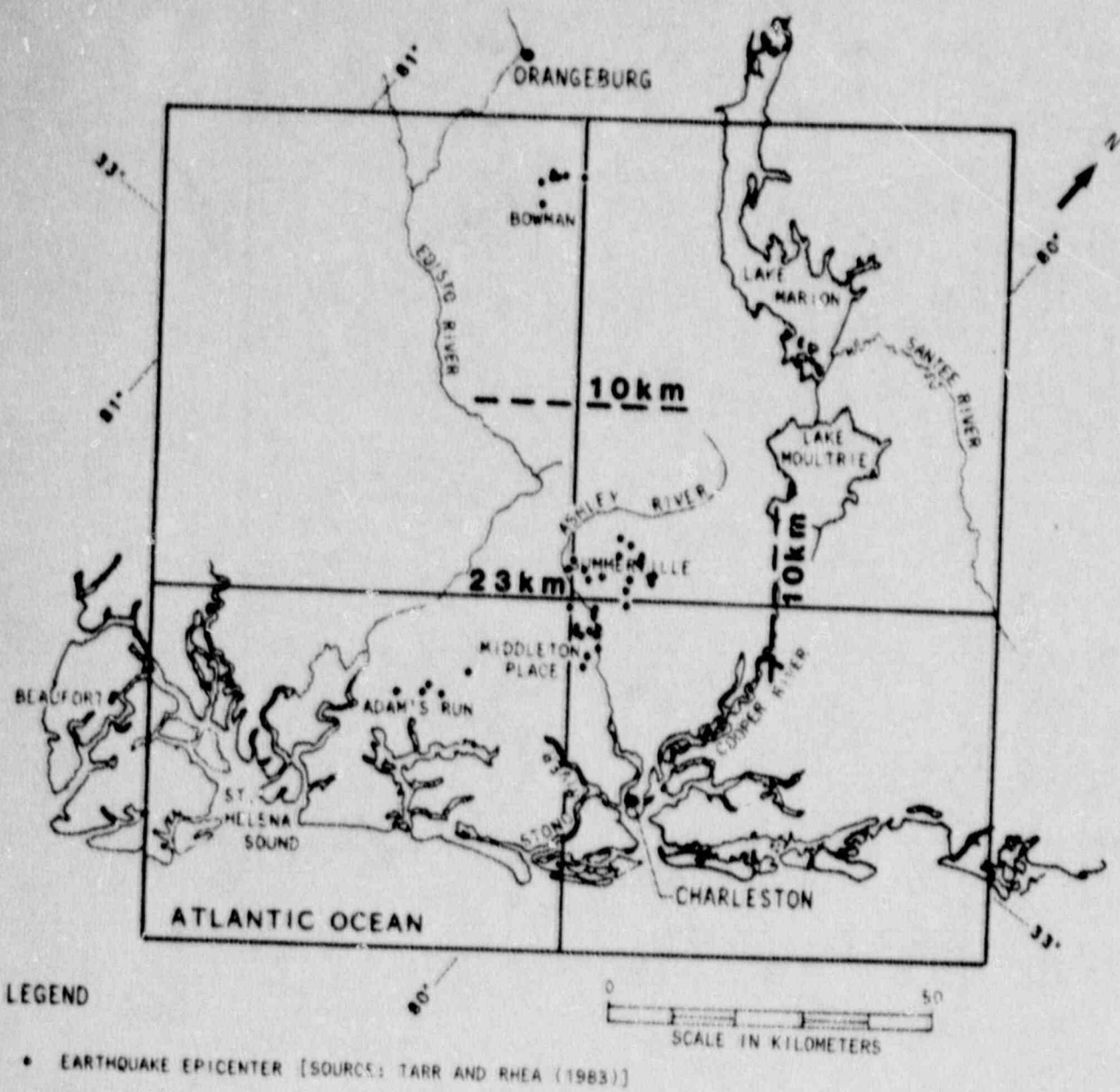


Figure 5-25. Map indicating depth to the base of the rigid crust.

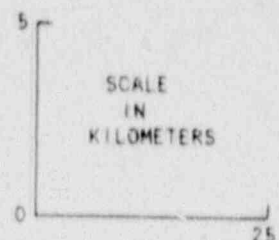
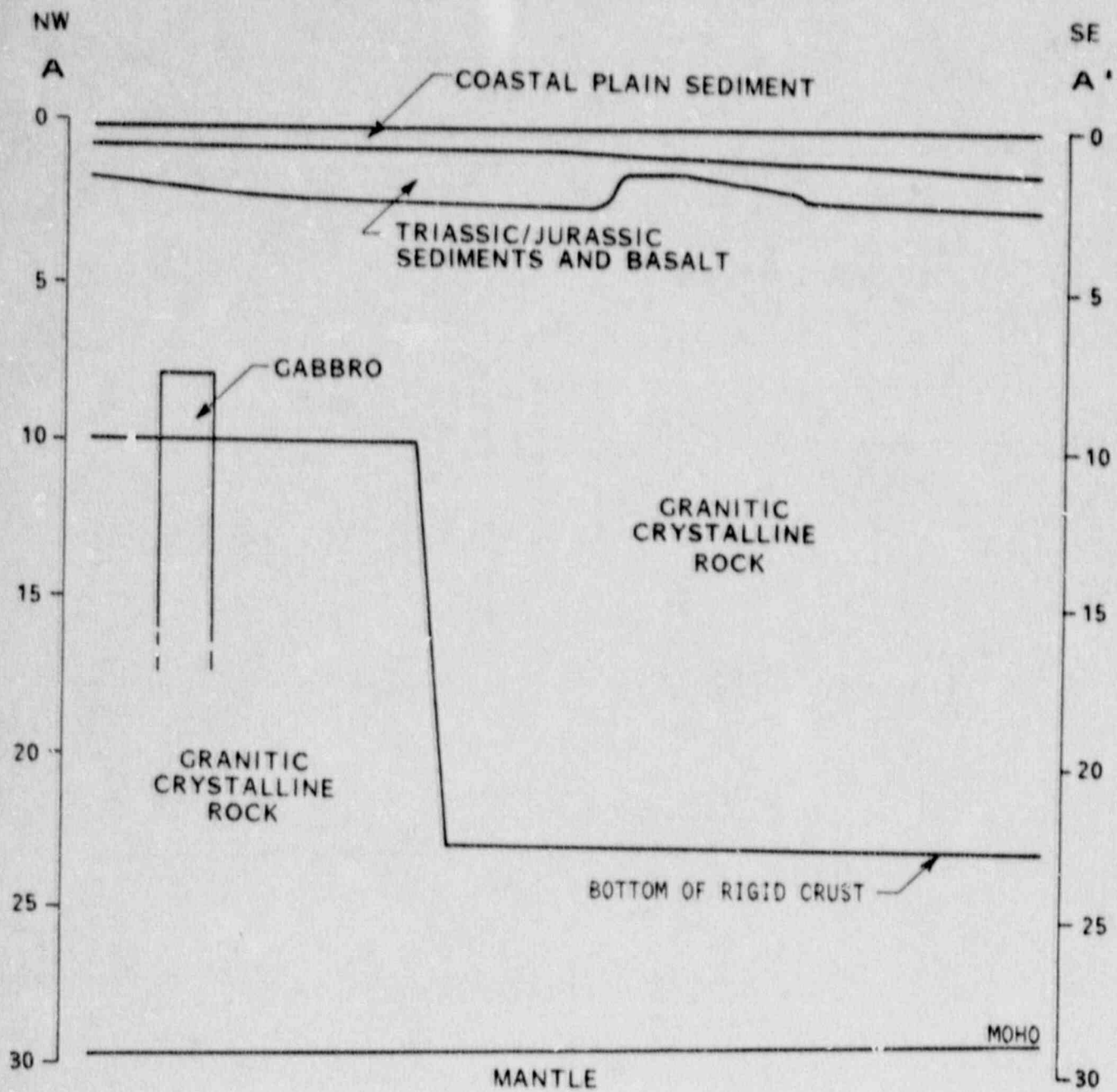


Figure 5-26. Cross section through A-A' (Figure 5-29) showing the geologic model.

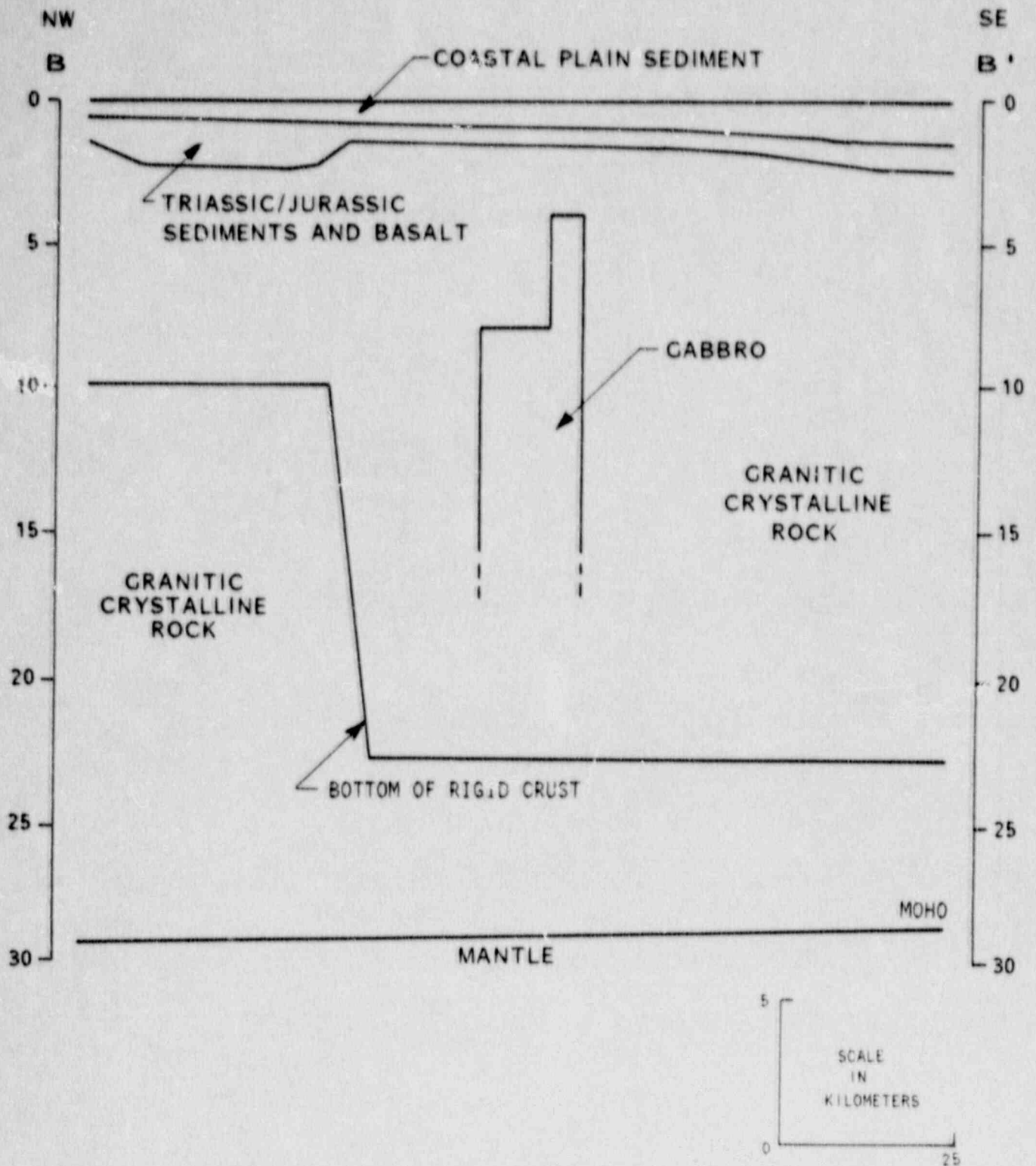


Figure 5-27. Cross section through B-B' (Figure 5-29) showing the geologic model.

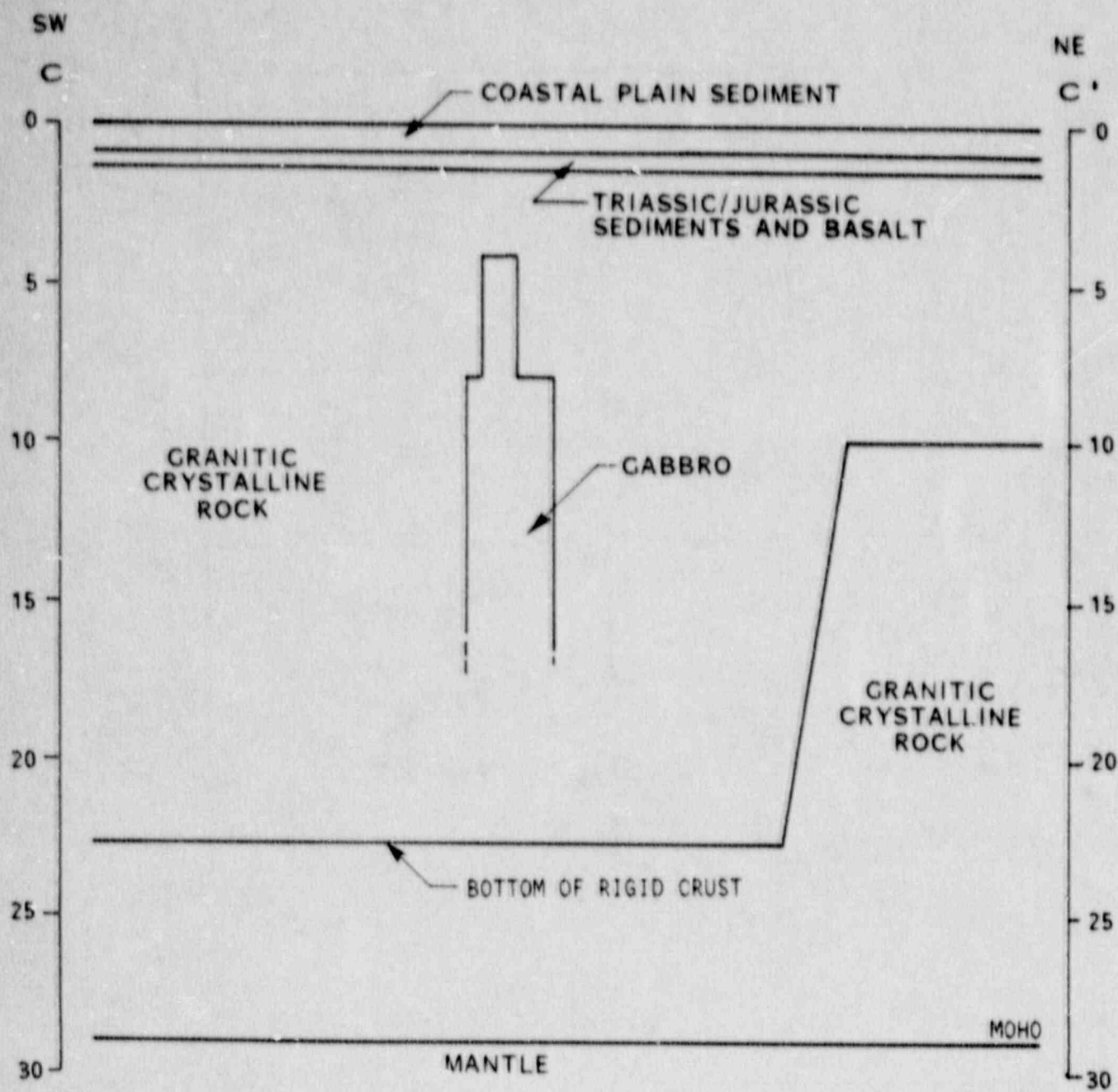


Figure 5-28. Cross section through C-C' (Figure 5-29) showing the geologic model.

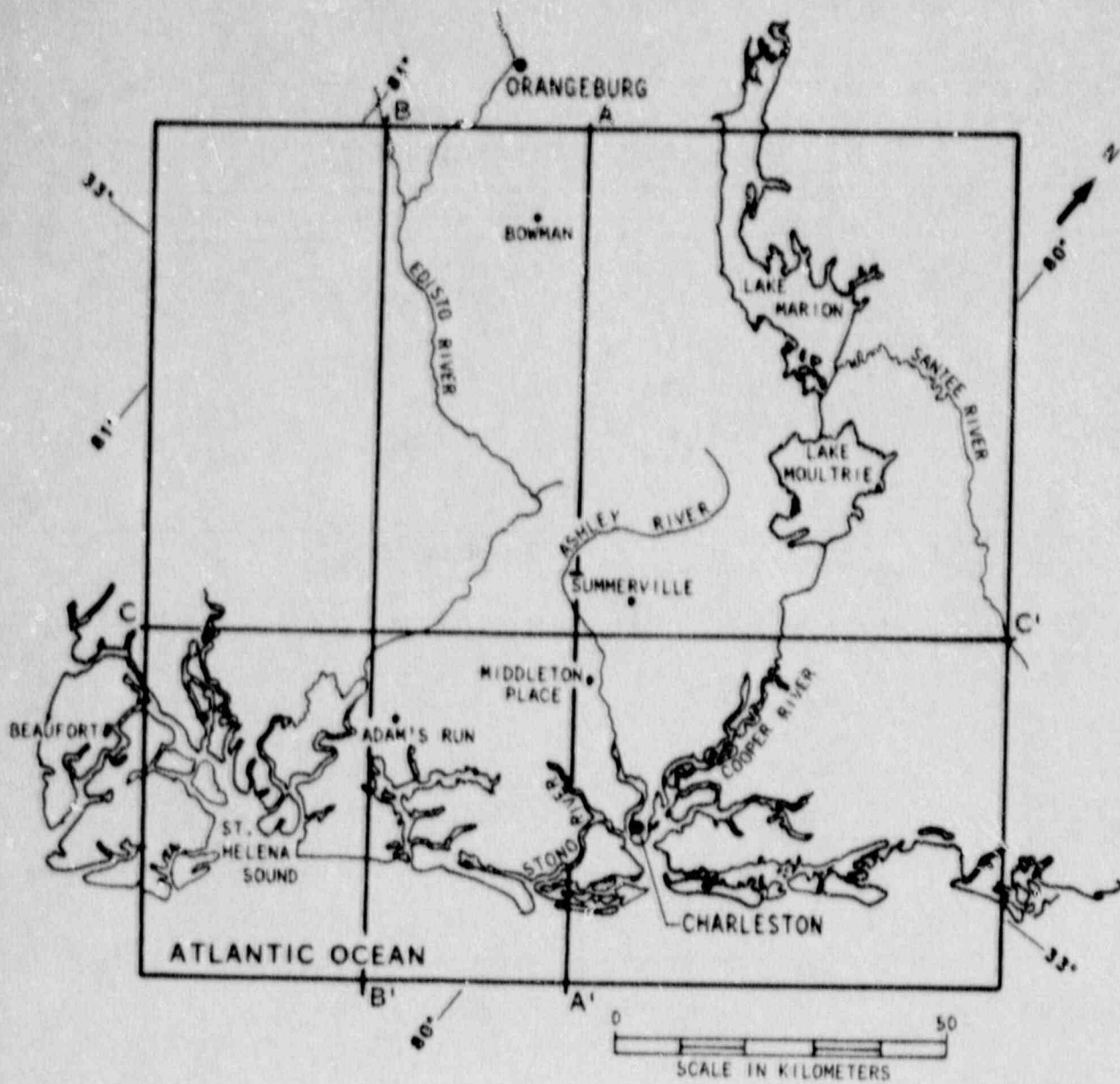


Figure 5-29. Location of cross sections shown in Figures 5-26 through 5-28.

accumulated above the Jurassic basalts (Dillon et al., 1983).

In the area of our study, Coastal Plain sediments vary in thickness from about 300 meters to 1500 meters. This depositional phase continues to the present time. The near-surface stratigraphy of the Charleston area has been interpreted in terms of cycles of submergence and emergence (Colquhoun et al., 1983).

Beneath the present surface, there is an overburden of unconsolidated to weakly consolidated sand and clay with thicknesses of generally 5 to 20 m; these sediments range in age from Holocene to Miocene and possibly to late Oligocene (Force, 1978a and 1978b). Over much of the area, the overburden is underlain by Cooper Formation and Santee Limestone (early Miocene to Eocene age).

Landforms in the area are mainly low scarps and terraces formed by erosion and deposition along the shoreline as the ocean retreated to its present position. These features are modified by fluvial processes along the major streams.

Our geologic model concentrates on the major elements of the crust in the Charleston area. As we are the first to integrate the bulk of the existing geologic and geophysical data, we have rectified divergent crustal interpretations based on different portions of the available data and have provided a sound basis to approach the question of the cause of Charleston seismicity.

- Colquhoun, D. J., I. D. Woollen, D. S. Van Nieuwenhuise, G. G. Padgett, R. W. Oldham, D. C. Boylan, P. D. Howell, and J. W. Bishop, "Surface and Subsurface Stratigraphy, Structure, and Aquifers of the South Carolina Coastal Plain", Report for Department of Health and Environmental Control, Ground Water Protection Division, published through the Office of the Governor, State of South Carolina, Columbia, South Carolina, 78 p., 1983
- Cook, F. A., L. D. Brown, S. Kaufman, J. E. Oliver, and T. A. Petersen, "COCORP Seismic Profiling of the Appalachian Orogen Beneath the Coastal Plain of Georgia", Geological Society of America Bulletin, Part I, Vol. 92, p. 738-748, 1981
- Daniels, D. L., I. Zietz, and P. Popenoe, "Distribution of Subsurface Lower Mesozoic Rocks in the Southeastern United States, as Interpreted From Regional Aeromagnetic and Gravity Maps", in G. S. Gohn, Studies Related to the Charleston, South Carolina Earthquake of 1886 - Tectonics and Seismicity, U. S. Geological Survey Professional Paper 1313, p. K1-K24, 1983
- Dillon, W. P., K. D. Klitgord, and C. K. Paull, "Mesozoic Development and Structure of the Continental Margin off South Carolina", in G. S. Gohn, Studies Related to the Charleston, South Carolina Earthquake of 1886 - Tectonics and Seismicity, U. S. Geological Survey Professional Paper 1313, p. N1-N16, 1983
- Force, L. M., "Geological Studies of the Charleston, South Carolina Area-Thickness of Overburden", U.S. Geological Survey Miscellaneous Field Studies Map, MF-1021B, Scale 1:250,000, 1978
- Force, L. M., "Geological Studies of the Charleston, South Carolina Area-Elevation Contours on the Top of the Cooper Formation", U.S. Geological Survey Miscellaneous Field Studies Map, MF-1021A, Scale 1:250,000, 1978a
- Klitgord, K. D. and H. Schouten, "Plate Kinematics of the Central Atlantic", in P. R. Vogt and B. E. Tucholke, The Geology of North America, Volume M., The Western North Atlantic Region, Geological Society of America, 696 p., 1986
- Lanphere, M. A., "Argon-40/Argon-39 Ages of Basalt From Clubhouse Crossroads Test Hole PS2 Near Charleston, South Carolina", in G. S. Gohn, Studies Related to the Charleston, South Carolina Earthquake of 1886 - Tectonics and Seismicity, U. S. Geological Survey Professional Paper 1313, p. B1-B8, 1983

- Long, L. T. and J. W. Champion, Jr., "Bouguer Gravity Map of the Summerville-Charleston, South Carolina Epicentral Zone and Tectonic Implications", in D. W. Rankin Studies Related to the Charleston, South Carolina Earthquake of 1886 - A Preliminary Report, U. S. Geological Survey Professional Paper 1028, p. 151-166, 1977
- Schilt, F. S., L. D. Brown, J. E. Oliver, and S. Kaufman, "Subsurface Structure Near Charleston, South Carolina; Results of COCORP Reflection Profiling in the Atlantic Coastal Plain", in G. S. Gohn, Studies Related to the Charleston, South Carolina Earthquake of 1886 - Tectonics and Seismicity, U. S. Geological Survey Professional Paper 1313, p. H1-H19, 1983
- Talwani, P., "A Preliminary Shallow Crustal Model Between Columbia and Charleston, South Carolina Determined From Quarry Blast Monitoring and Other Geophysical Data", in D. W. Rankin, Studies Related to the Charleston, South Carolina Earthquake of 1886 - A Preliminary Report, U. S. Geological Survey Professional Paper 1028, p. 177-187, 1977
- Taiwani, M. and J. R. Heirtzler, "Computation of Magnetic Anomalies Caused by Two-Dimensional Bodies of Arbitrary Shape", in G. A. Parks, Computers in the Mineral Industries, Part 1, (Stanford University Publications, Geological Sciences), Vol. 9, p. 464-480, 1964
- Talwani, M. J., L. Worzel, and M. Landisman, "Rapid Gravity Computations for Two-Dimensional Bodies With Application the Mendicino Submarine Fracture Zone", Journal of Geophysical Research, Vol. 64, p. 49-59, 1959
- Tarr, A. C. and S. Rhea, "Seismicity Near Charleston, South Carolina, March 1973 to December 1979", in G. S. Gohn, Studies Related to the Charleston, South Carolina Earthquake of 1886 - Tectonics and Seismicity, U. S. Geological Survey Professional Paper 1313, p. R1-R17, 1983
- Tucholke, B. E. and F. W. McCoy, "Paleogeographic and Paleobathymetric Evolution of the North Atlantic Ocean", in P. R. Vogt and B. E. Tucholke, The Geology of North America, Volume M, The Western North Atlantic Region, Geological Society of America, 696 p., 1986
- Williams, H. and R. D. Hatcher, Jr., "Appalachian Suspect Terranes", Geological Society of America, Memoir 158, p. 33, 1983

CHAPTER 6

REGIONAL CRUSTAL STRESS

6.1 Introduction

Because an earthquake occurs only when a sufficient accumulation (or concentration) of stress has occurred, knowledge of the crustal stress field can give significant insight into which hypotheses for the cause of the 1886 Charleston earthquake are appropriate. An earthquake can be initiated with a decrease in rock strength or an increase in deviatoric stress when it is properly aligned with zones of weakness.

Topography and crustal density heterogeneities can induce large stresses in the lithosphere. In addition, the continental crust is subjected to regional horizontal stresses generated by tectonics of the plate boundaries.

6.2 Current State of Crustal Stress Knowledge

In the current tectonic stress environment, the Charleston area is located in the interior of a tectonic plate. Historically, large earthquakes can occur in plate interiors. However, the nature and cause of the stress fields which can produce these large earthquakes have been the subject of much study and debate. This is due to the scarcity of stress data available, as well as to the variety of mechanisms, both renewable and non-renewable, available to explain the state of stress. Development of a three-dimensional model, therefore, calls for consideration of these various stress sources as well as use of the available stress data.

6.2.1 Regional Stress Data

Actual measurements of the stress field in the southeastern U. S. are sparse. They consist of both in-situ borehole measurements and earthquake focal mechanisms. The borehole information is obtained from hydraulic fracture, drill elongation and overcoring data. Because the data are extremely sparse, they cannot be used alone to develop hypotheses concerning sources of earthquakes. Some of the basis for our interpretation of the regional stress field is discussed here. Although the regional stress direction seems uniform in this area, the local stress directions can vary greatly as can be seen from the stress models described later.

6.2.1.1 In Situ Stress Measurements

The data set of in-situ stress measurements is very sparse in the southeastern United States. A preliminary list is given by Zoback and Zoback (1980). This list has been updated with additional data from South Carolina and Georgia (Zoback, 1983). Other studies in South and North Carolina (Hooker and Johnson,

1969; Law Engineering Testing Co., 1974, Dames and Moore, 1974; Schaeffer et al., 1979) are also available.

6.2.1.2 Earthquake Focal Mechanisms

Some of the best indicators of anomalous stress are well constrained earthquake focal mechanisms. They are the only source of stress data at depth. Unfortunately, there are very few focal mechanisms available because of the low seismicity of the southeastern United States. The quality of those data that do exist is fair to poor for most of the earthquakes.

In the immediate vicinity of the source zone of the 1886 earthquake, there are two clusters of microearthquakes which have had focal mechanism studies: Bowman, and Middleton Place-Summerville. The Bowman events have been described as having NE-SW maximum principal stress with dip-slip faulting (Guinn, 1980). Herrmann (1986) describes a similar maximum principal stress but with strike-slip faulting. The Middleton Place-Summerville events have been described as bearing NE-SW or NW-SE maximum principal stress (Tarr, 1977; Tarr and Rhea, 1983; Guinn, 1980; Herrmann, 1986).

Focal mechanisms for areas beyond the immediate Charleston area are discussed in terms of the interpreted regional stress field in Section 6.2.4.

6.2.2 Sources of Crustal Stress

Hypotheses on the origins of crustal stress have been related to processes at the boundaries of a lithospheric plate or to local sources in the interior of a plate. Processes at the plate boundary can generate homogeneous regional stresses. In contrast, stresses from local sources in the interior of a plate will be inhomogeneous. The magnitudes of plate boundary and internally-derived stresses can be similar. Much of this discussion comes from Law Engineering Testing Company (1986). Only those possible sources of stress needed for stress modeling will be discussed here.

6.2.2.1 Renewable Crustal Stresses

Plate Boundary Stresses: Currently, the leading explanation for plate boundary stresses in eastern North America is gravitational sliding or push from ocean ridges (Forsyth and Uyeda, 1975; Lister, 1975; Richardson, et al., 1979). The base of the lithosphere can experience a drag or push depending on the coupling of mantle convection (Zoback and Zoback, 1980). The gravitational pull in trenches may also contribute to stresses in the plate interior (Hager, 1978). However, subduction zones are only indirectly coupled to eastern North America and are not likely to be a significant factor in determining stresses in eastern North America. All of these plate boundary mechanisms hypothetically generate horizontal stresses. The depth dependence of these stresses are

determined by the properties of a mid-crust strength channel.

Stresses resulting from plate boundary mechanisms which are dominated by ridge push are expected to extend uniformly across the plate. Such stresses may explain the dominance of east-northeast principal stress directions observed in earthquake focal mechanisms and near-surface stress measurements.

Sediment Loading Stress: Bending stresses can be induced in the continental plate by sediment loads at continental margins (Turcotte, *et al.*, 1977; Bott, 1978). The direction of stresses from continental margin loading would be determined by the distribution of the load. With depth, the stresses would change direction. The observed stress data do not provide strong evidence that these bending stresses significantly alter the regional stress in the eastern United States. These bending stresses can be expressed as differential vertical motion of the earth's surface.

Because of the slow rate of erosion, unloading in the Appalachians is less important than loading in the coastal plain. The effect of bending stress is taken into account in the stress modeling through use of the gravity anomalies in the model.

6.2.2.2 Non-Renewable Crustal Stresses

Gravitational Instabilities (Isostasy): Materials of anomalous density must be supported by stress in the crust, and the principle of isostatic equilibrium requires that the response of the crust must be to move in a direction to reduce these stresses (Artyushkov, 1973). Density anomalies, such as those which occur in salt domes, granitic intrusives, mafic bodies of various types, and sedimentary basins, must be supported; hence, they are surrounded by a locally inhomogeneous stress field.

Topographic Stress: Topographic loads on the surface must be maintained by stresses in an elastic crust (Fleitout and Froidevaux, 1982, 1983). Likewise, isostatic compensation at the base of the crust or at other depths will be supported by stresses in the crust. A topographic load and its isostatic compensation will generate horizontal compression, and the largest deviatoric stresses generated will be at mid-crustal depths near the edges of the topography and can be comparable in magnitude to the regional stresses. Topography is an important starting point for the stress model.

Mantle-Induced Crustal Deformation Stress: Viscous deformation of the upper mantle could couple stress to elastic crustal material. Stress levels obey the equations for viscosity where the rate of movement determines the magnitude of stress. However, mantle convective motions reportedly disagree with stress measurements and plate movement (McKenzie, *et al.*, 1980; Zoback and Zoback, 1980). The recent movement of eastern North

America is to the northwest, approximately normal to the direction of maximum stress.

6.2.3 Rheological Properties of Continental Crust

At crustal depths of less than 20 to 30 km, failure occurs as brittle failure or by frictional sliding (Meissner and Strehlau, 1982). Stresses at these depths are limited by the elastic strength of the rock or by the shear strength on existing planes of weakness. Pore pressure on existing planes of weakness can reduce the shear strength to a few tens of MPa in contrast to a rock strength of typically 1000 MPa (Kanamori, 1980).

In the lower crust and upper mantle, geologic materials can deform by viscous or plastic mechanisms. In viscous materials, the maximum allowable stress is determined by the strain rate. Increased water content and temperature can decrease the viscosity and decrease the maximum possible stress for a given strain rate. As the temperature increases with depth, the viscosity and maximum stress decrease with depth. Areas in the crust with high heat flow and higher temperatures would have reduced capability to retain applied stresses in the lower crust.

The combination of failure by frictional sliding at shallow depths and viscous relaxation in the lower continental crust results in a high-strength channel of high deviatoric stress at depths typically of 5 to 25 km in the middle crust (Meissner and Strehlau, 1982). The thickness of the channel as indicated by heat flow data and the implied crustal temperature is consistent with the observed distributions of midplate earthquakes.

Based on a combination of rheological arguments and estimates from earthquake stress drops, the strength of the crust ranges from 10 to 150 MPa (Kanamori, 1980). However, the local strength can be modified significantly by small scale geologic inhomogeneities which can vary widely in strength and deformation properties, even at shallow depths.

6.2.4 Interpreted Regional Stress

In order to assess the quantity and coherence of the stress data, and to try to determine regional differences in the general ridge-push stress field, stress data were used to produce an average stress orientation map for the eastern United States (Figure 6-1) (Law Engineering Testing Company, 1986). The map was made by dividing a data base stress map into $2^{\circ} \times 2^{\circ}$ squares and averaging the stress orientations in each square in such a way that the majority of the orientations fell within $\pm 45^{\circ}$ of the average. Shown in the center of each square is the average stress orientation, along with the individual data points for that square. It can be seen that in many areas, the "average" stress orientation is that of the

single data point available. In some cases, the average seems representative of the actual stress measurements, but in many cases the data would be able to support an orientation very different from that of the numerical average.

Due to the low density of data, our gridded average stress map has a large number of cells lacking data. One area of interest for which this is true is the southeastern Atlantic coast. There has been some question over whether a northeasterly or northwesterly stress regime exists in this area, for which the data seem to provide no solid answer.

The map of average stress orientation (Figure 6-1) was used together with information gained from preliminary stress modeling to produce a stress regime map of the central and eastern United States (Figure 6-2) (Law Engineering Testing Company, 1986). As indicated, two different line types were used to indicate whether or not data were available for the given 2° square. For those areas where data were not available, or where data were ambiguous, we assumed that:

1. The stress orientation of areas in question should provide continuity between surrounding areas of known orientation.
2. From the results of our modeling, there is a deflection of the background compressive stress field of no more than 20° counterclockwise along the southern Atlantic Coast, and clockwise along the Gulf Coast.

The interpreted NE-SW orientation of the maximum principal compressive stress is the basis for the beginning of stress modeling.

6.3 Theory of Three-Dimensional Stress Modeling

The objective of the three dimensional modeling is to examine the hypothesis that the seismicity near Charleston, South Carolina, is associated with areas of concentrated stresses caused by local features and regional structures. The major regional structures that contribute to the crustal stress are the Southern Appalachian Mountains and the shelf edge. The smaller scale crustal features that could affect the stress field near Charleston are exhibited primarily in the gravity anomaly field. The effects of these features will be examined for comparison with focal mechanisms and the distribution of earthquakes. The regional stress fields will be superimposed onto the stresses from local structures in order to examine their effects.

The calculations of the local stress field induced by variations in topography and density are based on a forward method which assumes a lithospheric rheology and computes the stress for a given load. The method used in this study was developed by Mareschal and Kuang (1986) of Georgia Institute of Technology and consists of a two-dimensional Fourier transform

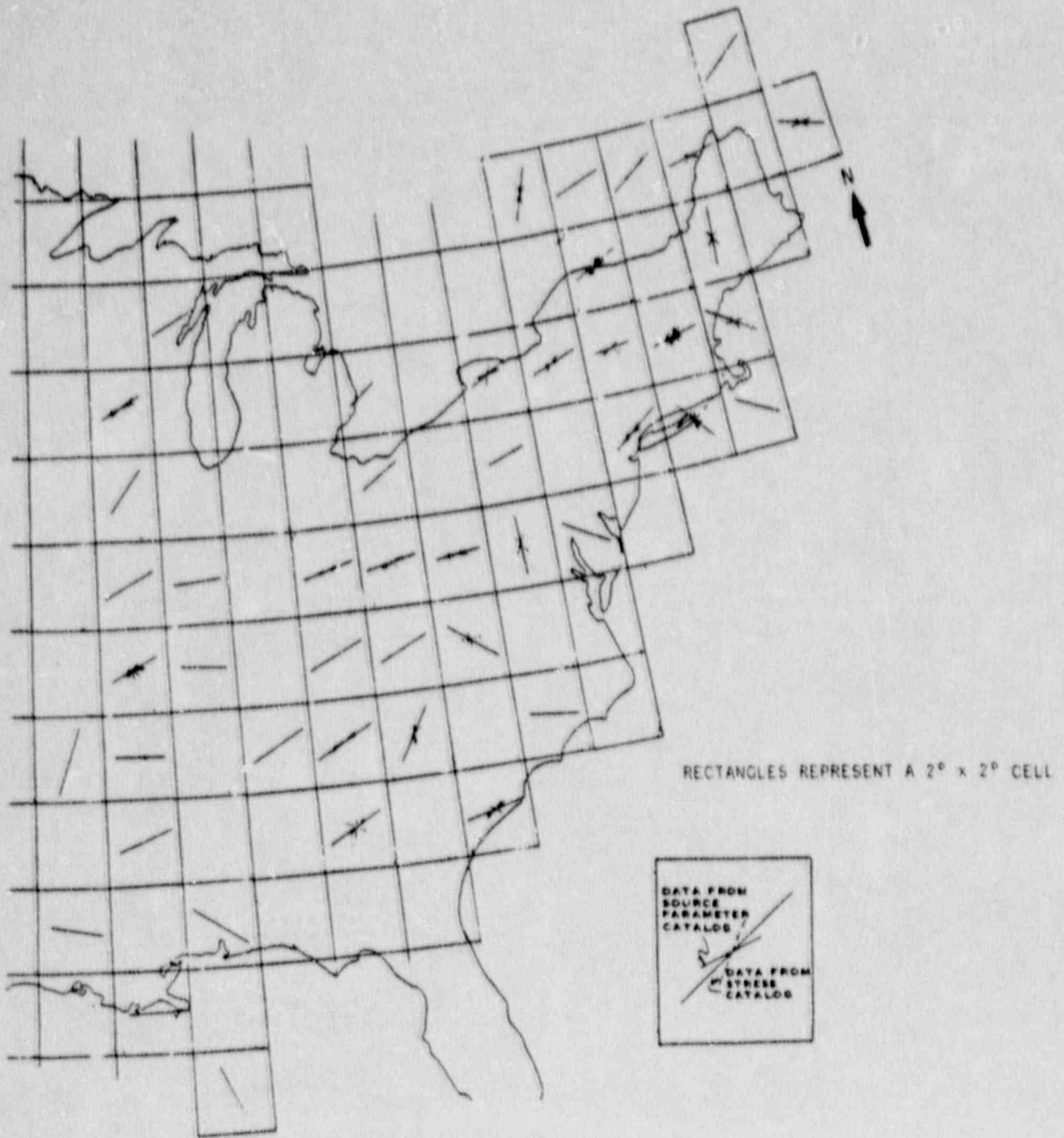


Figure 6-1. Average stress orientations for the eastern United States from source parameter and stress measurements. (From Law Engineering Testing Co., 1986).

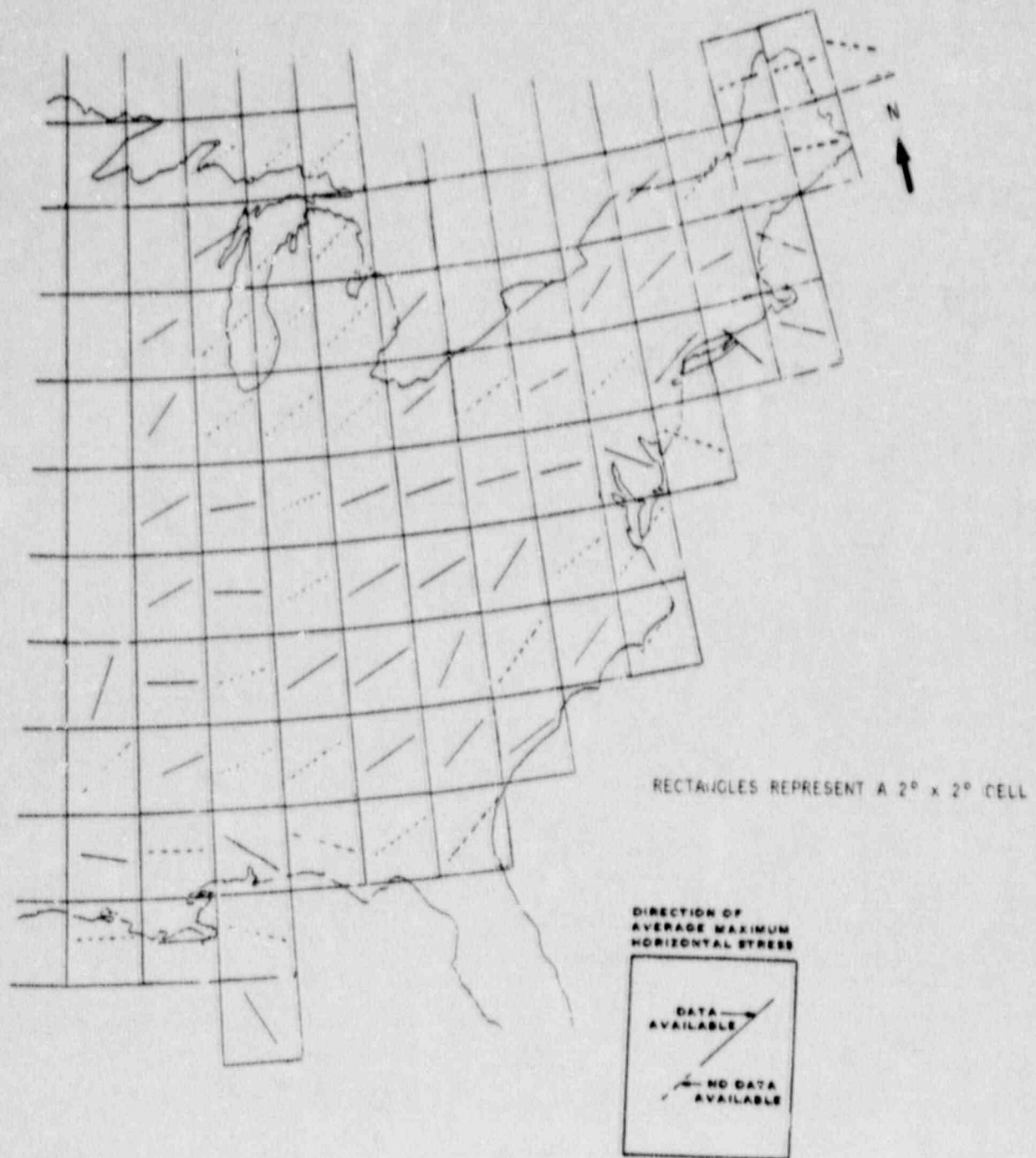


Figure 6-2. Interpreted stress regime for the eastern United States. (From Law Engineering Testing Co., 1986).

solution for a layered elastic slab over an inviscid fluid. The Georgia Institute of Technology authors have applied this approach to the southeastern United States as part of this project. An inviscid fluid has zero viscosity. Topography is used for the load at the surface and internal loads are developed from the downward continuation of gravity data. In the Charleston area, special consideration is given to the surface sediments and water depth offshore. The loads were also modified to conform with models of the crust based on a combination of gravity, magnetic and seismic data.

The lithosphere has a much higher viscosity than the asthenosphere; even on a geologic time scale the viscous deformation of the earth's crust is not perceivable. Stresses can be maintained in the crust for a long time without being dissipated by non-elastic deformations. On the other hand, the post-glacial rebound data indicate that the relaxation time of the asthenosphere is on the order of 10,000 years (Walcott, 1972). Compared with the duration of mountain building, this relaxation time is very short. Therefore, a basic assumption of the physical model is that the earth's lithosphere is an elastic slab floating over the inviscid fluid asthenosphere. The elastic slab may be divided into horizontal layers which differ in density and elastic properties. The viscous shear applied to the base of the lithospheric plate will be on the order of a few megapascals (MPa) and will have little effect on the stress field near the bottom, and almost no effect in the crust since the local stress is on the order of 10 MPa. The topography (or bathymetry) has been treated as a surface load acting at the zero level of the model; the density anomaly inside the lithosphere is condensed to an internal load acting at the interface of the different density layers.

In three-dimensional space, there is no analytic solution for the stress field induced by a surface load in the elastic slab over an inviscid fluid. However, a disk load at the surface can be used to test the reasonableness and quantitative reliability of the solutions. Under such a load, the elastic slab is bent downward at the center as shown by the surface displacement contour (Figure 6-3). The slab under the disk experiences horizontal compression above the mid plane and extension below the mid plane. In general, the displacements and stresses conform to expected results for a point load.

6.4 Application of the Regional Stress Model to the Charleston Area

Figure 6-4 shows the region chosen (grid 3) for the stress analysis of the Charleston area. The region is a 1028 x 1028 km square which extends from central Florida to Maryland and from west in Alabama to the shelf edge. The Charleston epicentral area is near the center of the region. The large region is needed to include the two features that may be responsible for the most significant local stresses, the Appalachian mountains and the shelf edge. The region covers

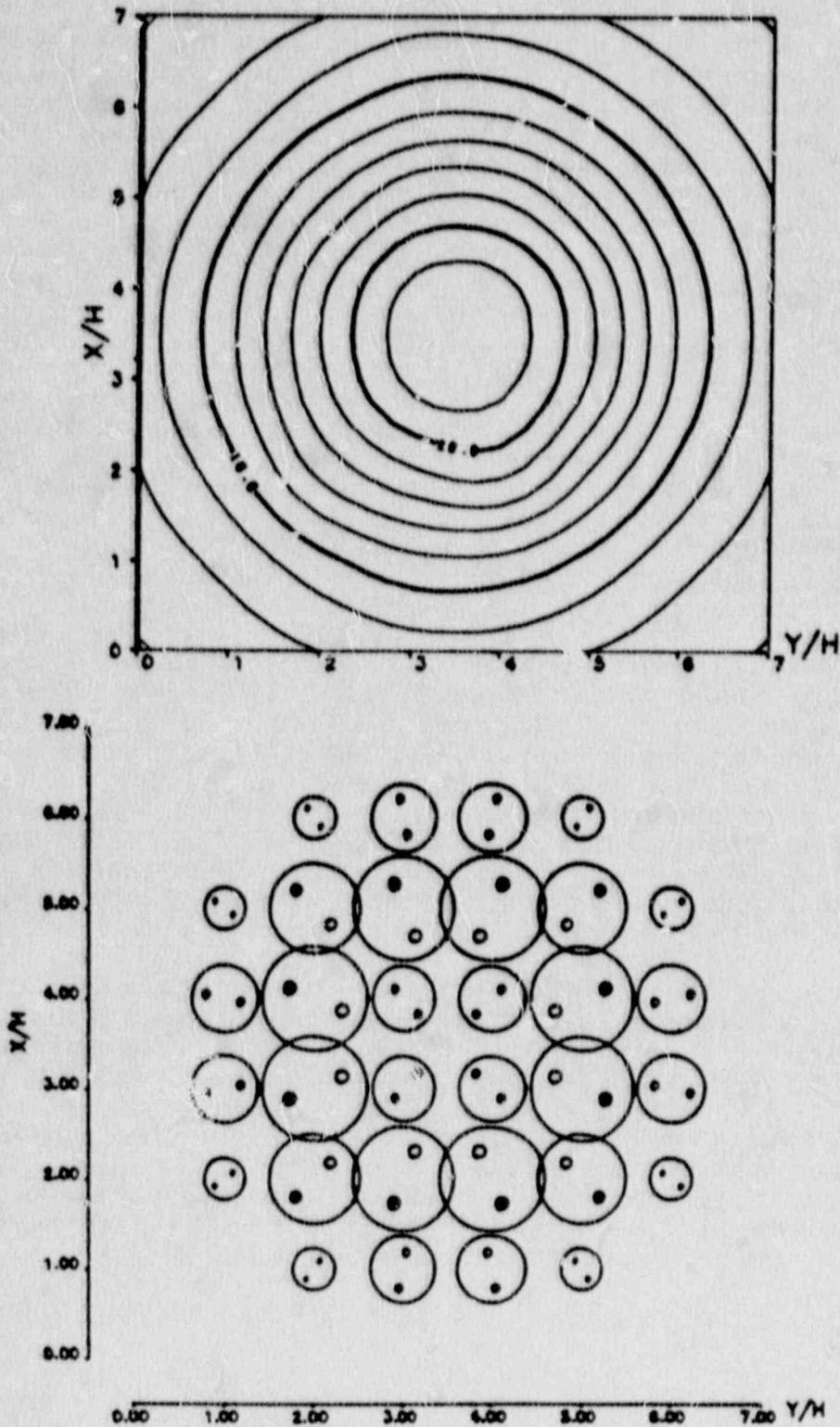


Figure 6-3. Vertical displacements and principal axes for the stress ellipsoid in a plate with a flat cylinder surface load in the center of the computation grid. The open circles are tension axes and the solid dots are pressure axes.

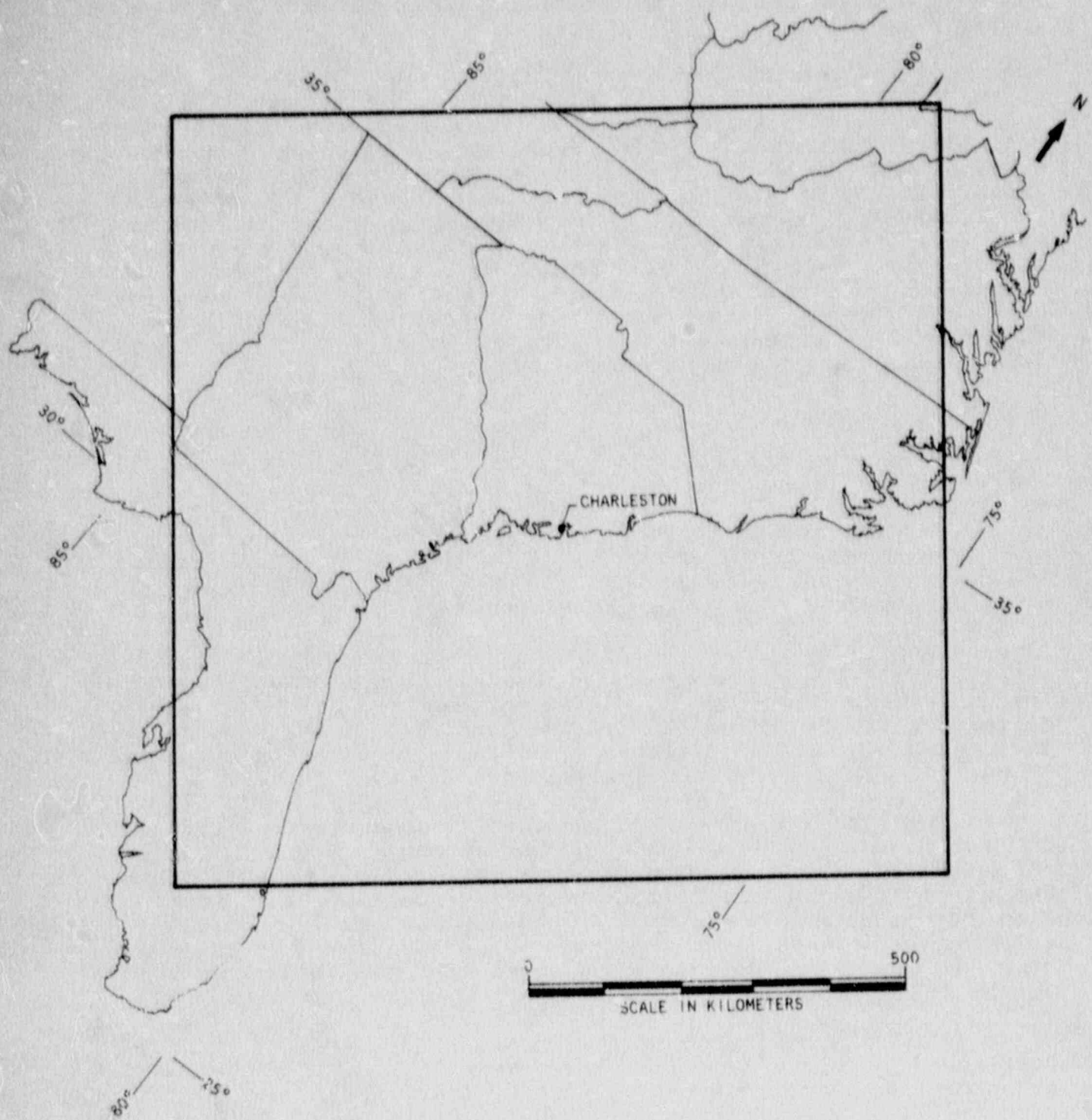


Figure 6-4. Location of 1028 km x 1028 km grid used for regional stress modeling.

all of the southeastern continental margin from North Carolina to northern Florida.

The Bouguer gravity anomaly is illustrated in Figure 6-5, corrected for the effects of bathymetry. The surface Bouguer anomaly has been transformed into the frequency domain and decomposed according to the wavelength. Assuming that the average Moho depth is 30 km, the components with wavelength larger than 30 km are downward continued to the depth of 30 km and considered as the load of the density. Those components with wavelengths less than 30 km are considered as surface mass effects and left as the surface load. For purposes of computing the load at the depth of the Moho, the downward continued Bouguer anomalies were converted to equivalent topography on the Moho and a density contrast of 0.35 g/cm³ was used to compute the density load.

6.5 Modeling Results

We have computed the resulting stress difference ($S_1 - S_3$) fields and principal stress axes orientations for two cases: the stress condition resulting from topographic and density anomalies alone, and the stress condition resulting from the addition of a 30 MPa horizontal plate force from the mid-Atlantic ridge incident upon the site at N80°E. We chose N80°E based on previous studies by us (Figures 6-1 and 6-2).

Figures 6-6 and 6-7 show the first case. It can be seen that the extreme topography of the edge of the continental shelf and to a lesser degree the Appalachian mountains cause high stress difference fields in regions somewhat eastward of the topography. The rest of the stress difference field can be seen to be related to the Bouguer gravity anomaly field (Figure 6-5).

Figures 6-8 and 6-9 show the case where the compressive stress due to the mid-Atlantic ridge spreading force is added. The stress difference magnitudes have about doubled showing that the effects of topography and density variability are of the same magnitude as the effect of the mid-Atlantic horizontal compressive stress field. Figure 6-9 shows that the maximum compressive stress horizontal directions tend to be in the northeast quadrant.

The distribution of stress differences at 10 km depth does not correspond to known seismicity nor does it show the Charleston area to be at either extreme of stress difference values.



Figure 6-5. Contour plot of Bouguer Gravity Anomalies. Contour interval is 10 milligals.

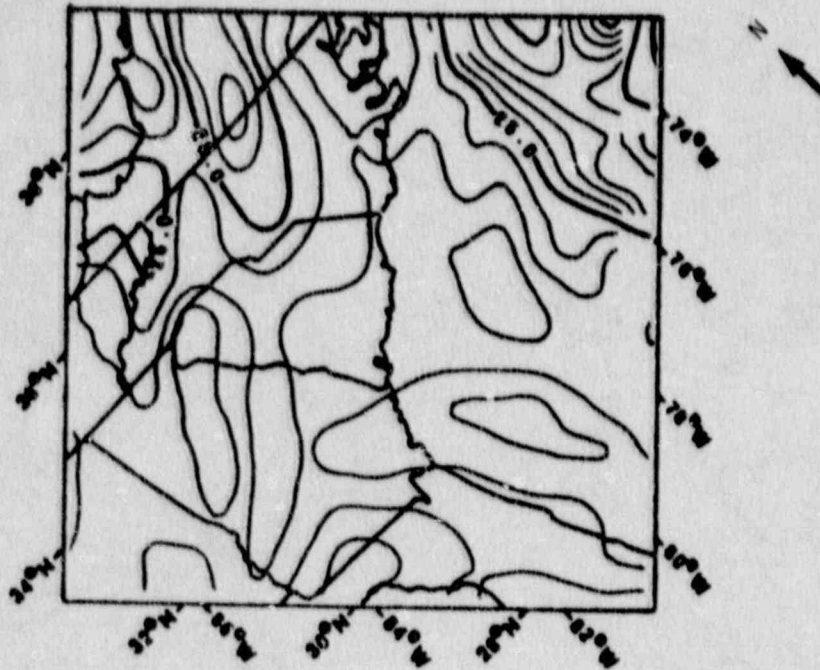


Figure 6-6. Local stress field of the Coastal Plain and the eastern continental margins centered at Charleston, South Carolina at 10 km depth. The stress difference is shown in units of MPa (from Kuang, 1987).

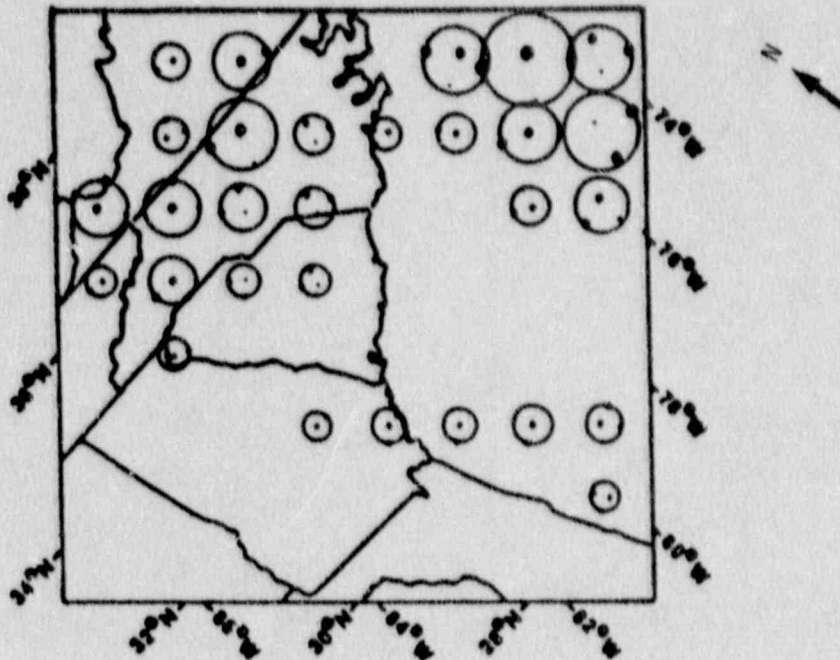


Figure 6-7. The corresponding SNPPSA plots (the Schmidt Net Projection of Principal Stress Axis). The open circle stands for the maximum extensional (S_1 or T) axis, the solid circle represents the maximum compressive (S_3 or P) axis and the dot is the intermediate axis (S_2 or B) axis (from Kuang, 1987).

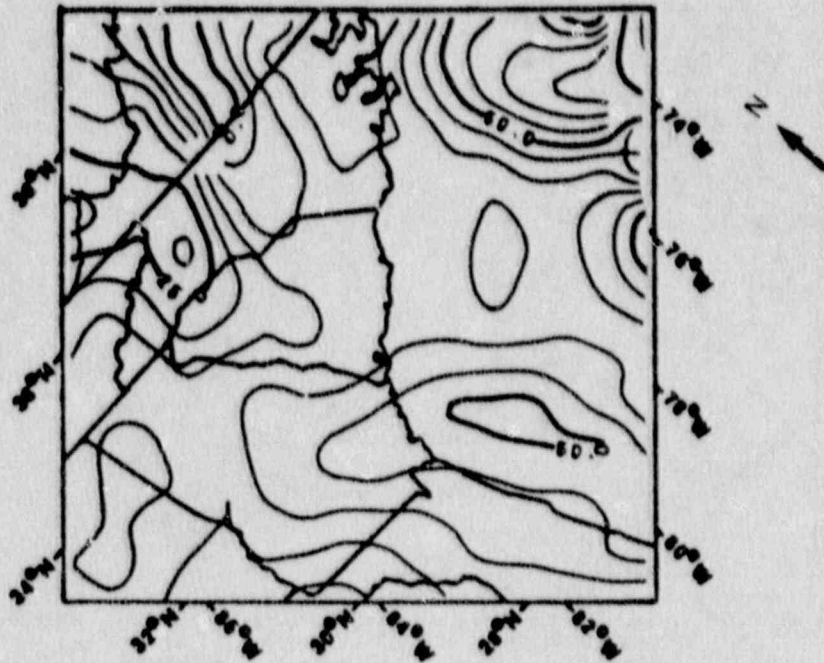


Figure 6-8. The total stress field which combines the local field (Figure 6-6) with a 30 MPa N80°E regional horizontal compression (from Kuang, 1987).

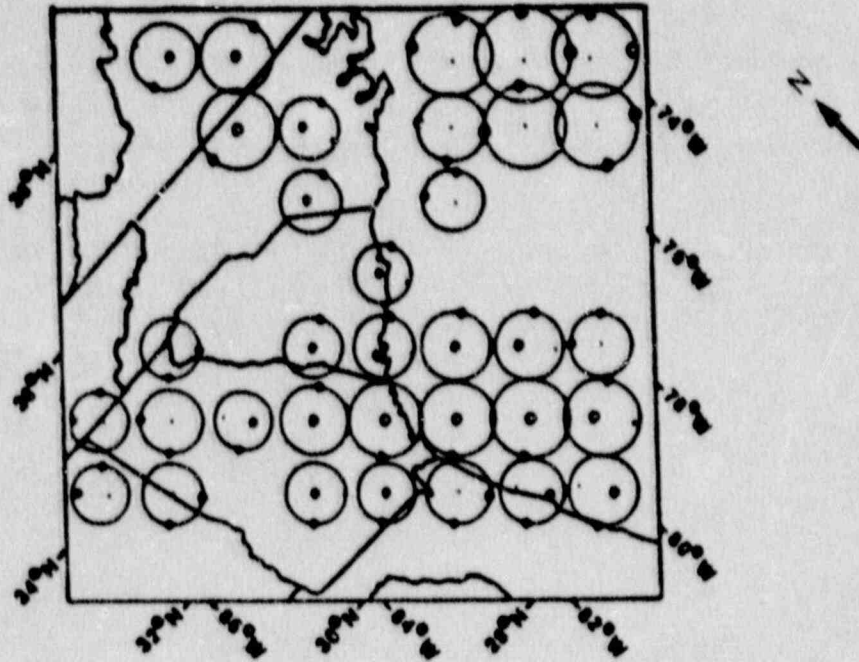


Figure 6-9. The corresponding SNPPSA plots (the Schmidt Net Projection of Principal Stress Axis). The open circle stands for the maximum extensional (S_1 or T) axis, the solid circle represents the maximum compressive (S_3 or P) axis and the dot is the intermediate axis (S_2 or B) axis (from Kuang, 1987).

- Artyushkov, E. V., "Stresses in the Lithosphere Caused by Crustal Thickness Inhomogeneities", Journal of Geophysical Research, Vol. 78, p. 7675-7708, 1973
- Dames and Moore, "In-Situ Stress Measurements by the Overcoring Technique", Virgil C. Summer Nuclear Station: Appendix 2D, Virgil C. Summer Nuclear Station Final Stress Analysis Report, South Carolina Electric and Gas Company, 1974
- Fleitout, L. and C. Froidevaux, "Tectonics and Topography for a Lithosphere Containing Density Heterogeneities", Tectonics, Vol. 1, p. 21-56, 1982
- Fleitout, L. and C. Froidevaux, "Tectonic Stresses in the Lithosphere", Tectonics, Vol. 2, p. 315-324, 1983
- Forsyth, D. W. and S. Uyeda, "On the Relative Importance of the Driving Forces of Plate Motions", Geophysical Journal of the Royal Astronomical Society, Vol. 43, p. 163-200, 1975
- Guinn, S. A., "Earthquake Focal Mechanisms in the Northeastern United States", USNRC Report NUREG/CR-1503, 150 p., 1980
- Hager, B. H., "Oceanic Plate Motions Driven by Lithosphere Thickening and Subducted Slabs", Nature, Vol. 276, p. 156-159, 1978
- Herrmann, R. B., "Surface-Wave Studies of Some South Carolina Earthquakes", Bulletin of the Seismological Society of America, Vol. 76, p. 111-121, 1986
- Hooker, V. E. and C. F. Johnson, "Near Surface Horizontal Stresses Including the Effects of Rock Anisotropy", U. S. Bureau of Mines, Report of Investigations 7224, 29 p., 1969
- Kanamori, H., "The State of Stress in the Earth's Lithosphere", in A. M. Dziewonski and E. Boschi, Physics of the Earth's Interior, Proceedings of the International School of Physics "Enrico Fermi" Course, (North-Holland Pub. Co., New York), p. 531-554, 1980
- Kuang, J., "Intraplate Stress and Seismicity in the Southeastern United States", Doctoral Thesis, Georgia Institute of Technology, Atlanta, 1987
- Law Engineering Testing Company, "Determination of In-Situ Stresses by Overcoring Procedures", Cherokee Nuclear Station, Gaffney, South Carolina: Attachment IX, Appendix 2C, Cherokee Nuclear Station Preliminary Stress Analysis Report, Duke Power Company, 9 p., 1974
- Law Engineering Testing Company, "Seismic Hazard Methodology for the Central and Eastern United States", EPRI NP-4726, Vol. 7, 1986

- Lister, C. R. B., "Gravitational Drive on Oceanic Plates Caused by Thermal Contraction", Nature, Vol. 257, p. 663-665, 1975
- McKenzie, D., A. Watts, B. Parsons, and M. Roufousse, "Plan Form of Mantle Convection Beneath the Pacific Ocean", Nature, Vol. 288, p. 442-446, 1980
- Meissner, R., and J. Strehlau, "Limits of Stress in Continental Crusts and the Relation to the Depth-Frequency Distribution of Shallow Earthquakes", Tectonics, Vol. 1, p. 73-89, 1982
- Richardson, R. M., S. C. Solomon, and N. H. Sleep, "Tectonic Stress in the Plates", Reviews of Geophysics and Space Physics, Vol. 17, p. 981-1020, 1979
- Schaeffer, M. F., R. E. Steffens, and R. D. Hatcher, Jr., "In-Situ Stress and its Relationship to Joint Formation in the Toxaway Gneiss, Northwestern South Carolina", Southeastern Geology, Vol. 20, No. 3, p. 129-143, 1979
- Tarr, A. C., "Recent Seismicity Near Charleston, South Carolina, and Its Relationship to the August 31, 1886 Earthquake", in D. W. Rankin, Studies Related to the Charleston, South Carolina Earthquake of 1886 - A Preliminary Report, U. S. Geological Survey Professional Paper 1028, p. 43-57, 1977
- Tarr, A. C. and S. Rhea, "Seismicity Near Charleston, South Carolina, March 1973 to December 1979", in G. S. Gohn, Studies Related to the Charleston, South Carolina Earthquake of 1886 - Tectonics and Seismicity, U. S. Geological Survey Professional Paper 1313, p. R1-R17, 1983
- Turcotte, D. L., J. L. Ahern, and J. M. Bird, "The State of Stress at Continental Margins", Tectonophysics, Vol. 42, p. 1-28, 1977
- Walcott, R., "Late Quaternary Vertical Measurements in Eastern North America: Quantitative Evidence of Glacio-Isostatic Rebound", Review of Geophysics and Space Physics, Vol. 10, p. 894, 1972
- Zoback, M. L., and M. D. Zoback, "State of Stress in the Conterminous United States", Journal of Geophysical Research, Vol. 85, p. 6113-6156, 1980
- Zoback, M., "Intraplate Earthquakes, Crustal Deformation, and In-Situ Stress", in W. W. Hayes and P. L. Gori, Proceedings of Conference XX, A Workshop on "The Charleston Earthquake and its Implications for Today", U. S. Geological Survey Open-File Report 83-843, p. 169-178, 1983

CHAPTER 7

LOCAL STRESS MODELING

The final geological model for the Charleston area was used as a basis for computing crustal stress in an inhomogeneous crust. The purpose of computing crustal stress was to examine the potential effects of stress amplification and concentration in a geologic model appropriate for the Charleston area. A second objective was to obtain numerical values for stress that can be used in testing hypotheses on the cause of the Charleston seismicity.

7.1 Theory of Two-Dimensional Stress Modeling

The primary considerations for modeling stress in the crust of the Coastal Plain are the larger structures within the crust. The smaller features, those with dimensions less than 5 km, would not contribute significantly to a major earthquake, which would have a fault rupture area with a diameter in excess of 25 km. Hence, the mafic intrusions, Triassic basins, and topography of the base of the rigid crust from the geologic model are the major components of the stress analysis. The stress model was designed to consider a rigid upper crust underlain by a viscoelastic lower crust and a shallowing of this viscoelastic zone suggested by the magnetotelluric data.

The stress model was computed by using a conventional two-dimensional finite-element program for elastic media. We consider this model useful for discussing relative values of stress and strength differences in the crust. A twenty-five kilometer thick portion of the crust was modeled for a distance of 128 kilometers. Within the 128 kilometers two mafic intrusives and two Triassic basins were included. For this model, we varied the depth to the base of the rigid crust from 10 to 23 km, as indicated from our MT study. The elastic constants and the general configuration are given in Figure 7-1. The viscoelastic lower crust was simulated by introducing a medium with a higher Poisson's ratio and lower Young's modulus, to compensate for the viscous dissipation of stress with time.

The boundary conditions constrained the horizontal displacement on the northwest end of the profile and applied a constant horizontal stress on the southeast end. The constant horizontal stress represents the regional plate stress. All other boundaries were free to move in response to the applied stress. Vertical forces, such as might be obtained from topography, were not considered significant for the immediate Charleston area.

The geometry of the model was taken from a profile of the geologic model presented in Chapter 5 (Section AA', Figure 5-29). This profile extends toward the northwest and passes

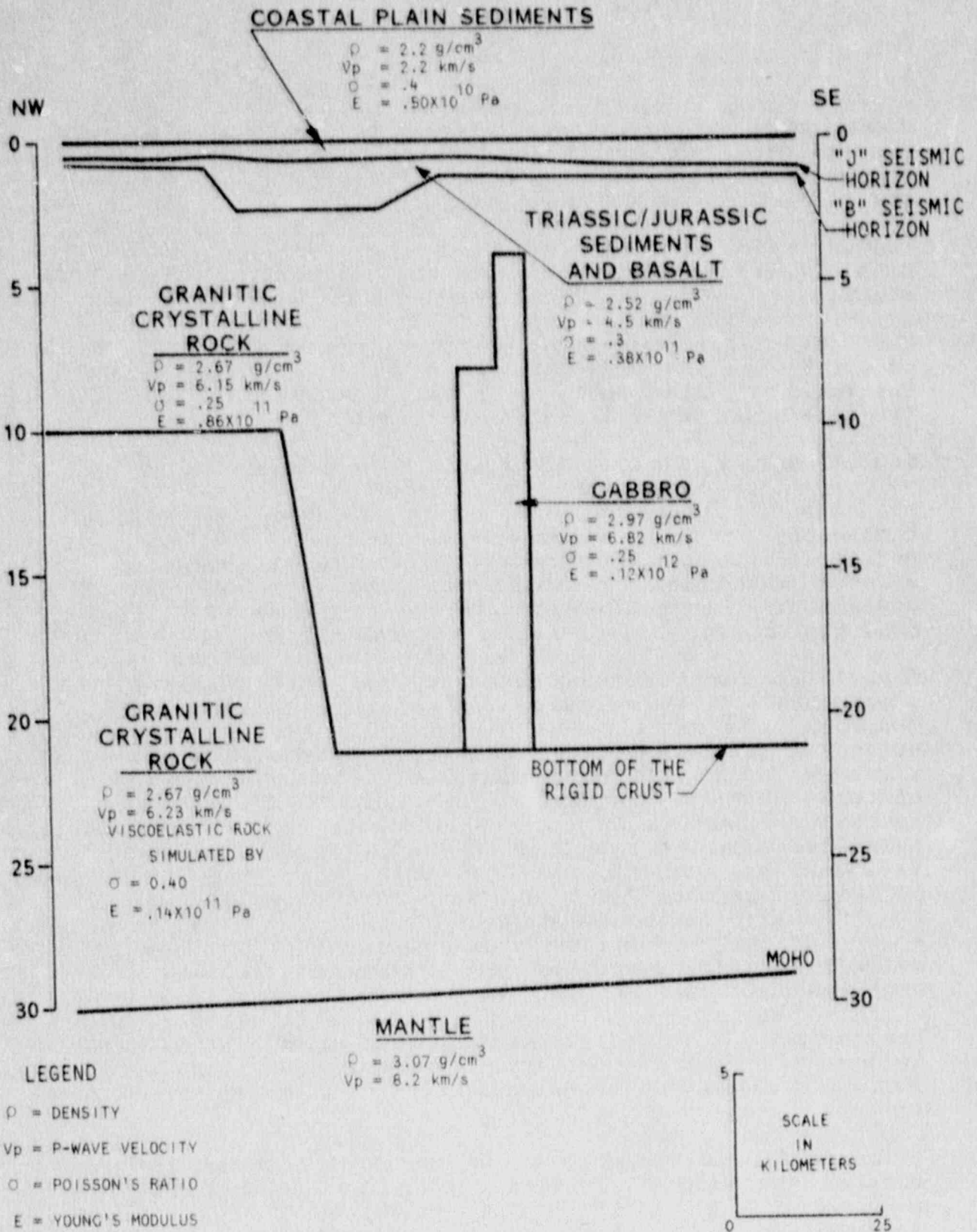


Figure 7-1. Schematic cross section of typical crust in the Charleston area showing elastic constants used in two-dimensional stress modeling.

through a point approximately 10 km southwest of the Charleston epicentral zone. Because cross sections at a number of angles through our geologic model resemble the one chosen, a different compressive regional stress orientation can still be considered as applicable to our model. This would produce a different magnitude of the applied compressive stress but the relative stress differences would be similar.

The finite element mesh is shown in Figures 7-2 through 7-4. Figures 7-5 through 7-7 indicate the magnitude of the principal stress axis. Figures 7-8 through 7-10 indicate the magnitude of the maximum shear stress. The results in Figures 7-5 through 7-10 are two-dimensional and thus apply to a vertical profile in which only normal or reverse faulting could be predicted. The model in the vertical plane precludes interpretation of strike-slip faulting.

7.2 Elastic Properties of Crustal Rock

The elastic properties of rock at seismogenic depths in the Charleston area are necessary to model the response of the subsurface to applied stress. To arrive at estimates of the elastic properties, we began with the interpretation of the distribution of different rock types in the subsurface from our geologic model. Figure 7-1, a generalized section through the study area, shows the model and the elastic properties of each material. The following describes the basis for the initial parameters used in the stress model.

Coastal Plain Sediments: The gravity modeling indicated that 2.2 g/cm^3 is a reasonable estimate of the average density of the Coastal Plain sediments. This implies a density porosity of 25-30 percent which we find reasonable for the Coastal Plain sediments. The average compressional wave velocity of 2.2 km/s was based on refraction results, velocity logging, and seismic reflection results (Ackerman, 1983; Yantis *et al.*, 1983). The Coastal Plain sediments are considered to be everything above the "J" seismic horizon. Comparison of compression wave velocities and densities for sediments indicate that a compressional wave velocity of 2.2 km/s is commonly associated with a density of 2.2 g/cm^3 (Gardner *et al.*, 1974). A Poisson's ratio of 0.4 was based on our experience with similar sediments. Given the density, compressional wave velocity, and Poisson's ratio, a Young's Modulus is computed to be 0.5×10^{10} Pa.

Triassic/Jurassic Sediments and Basalts: For our purposes we treated the Triassic/Jurassic sediments and included basalts (including the capping "J" horizon basalt) as one unit. Gravity modeling constrained by seismic data indicated an average density of 2.52 g/cm^3 . This density would imply a compressional wave velocity of 4.5 km/s (Gardner *et al.*, 1974). We assumed a Poisson's ratio of 0.3. These allowed Young's Modulus to be computed at 0.38×10^{11} Pa. This material is found between the "B" and "J" seismic horizons in Figure 7-1.

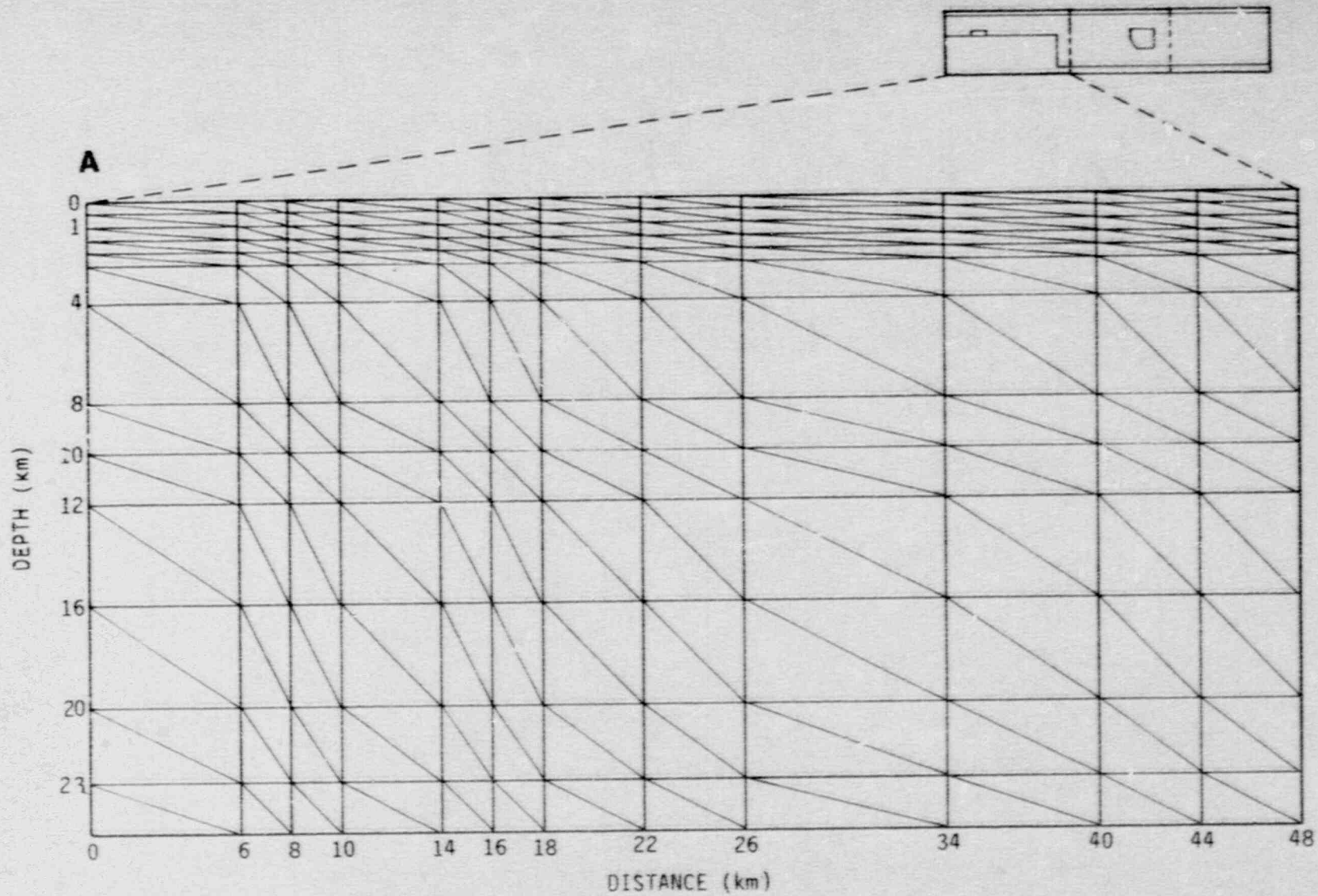


Figure 7-2. Node map used for the two-dimensional stress model (1 of 3).

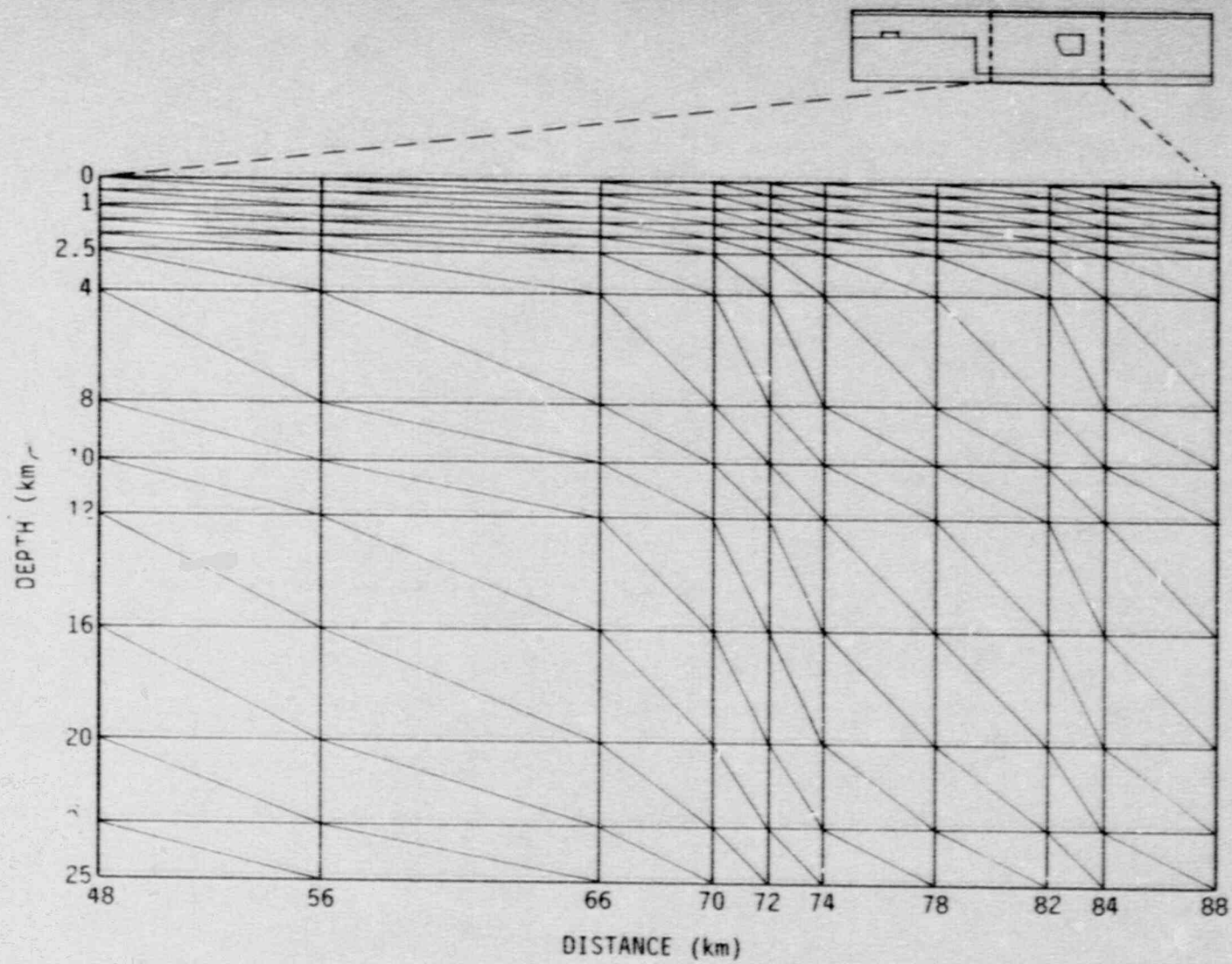


Figure 7-3. Node map used for the two-dimensional stress model (2 of 3).

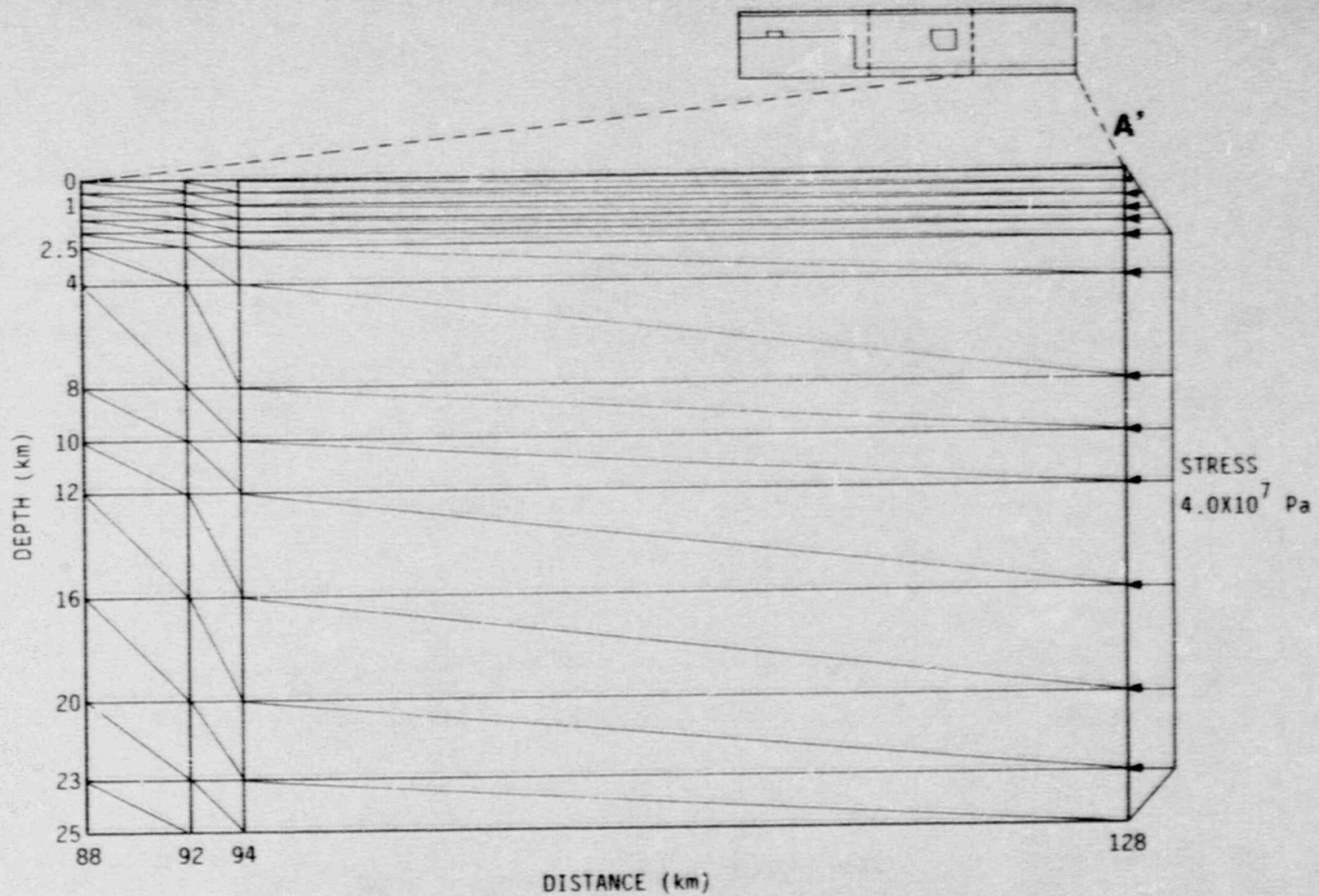


Figure 7-4. Node map used for the two-dimensional stress model (3 of 3).

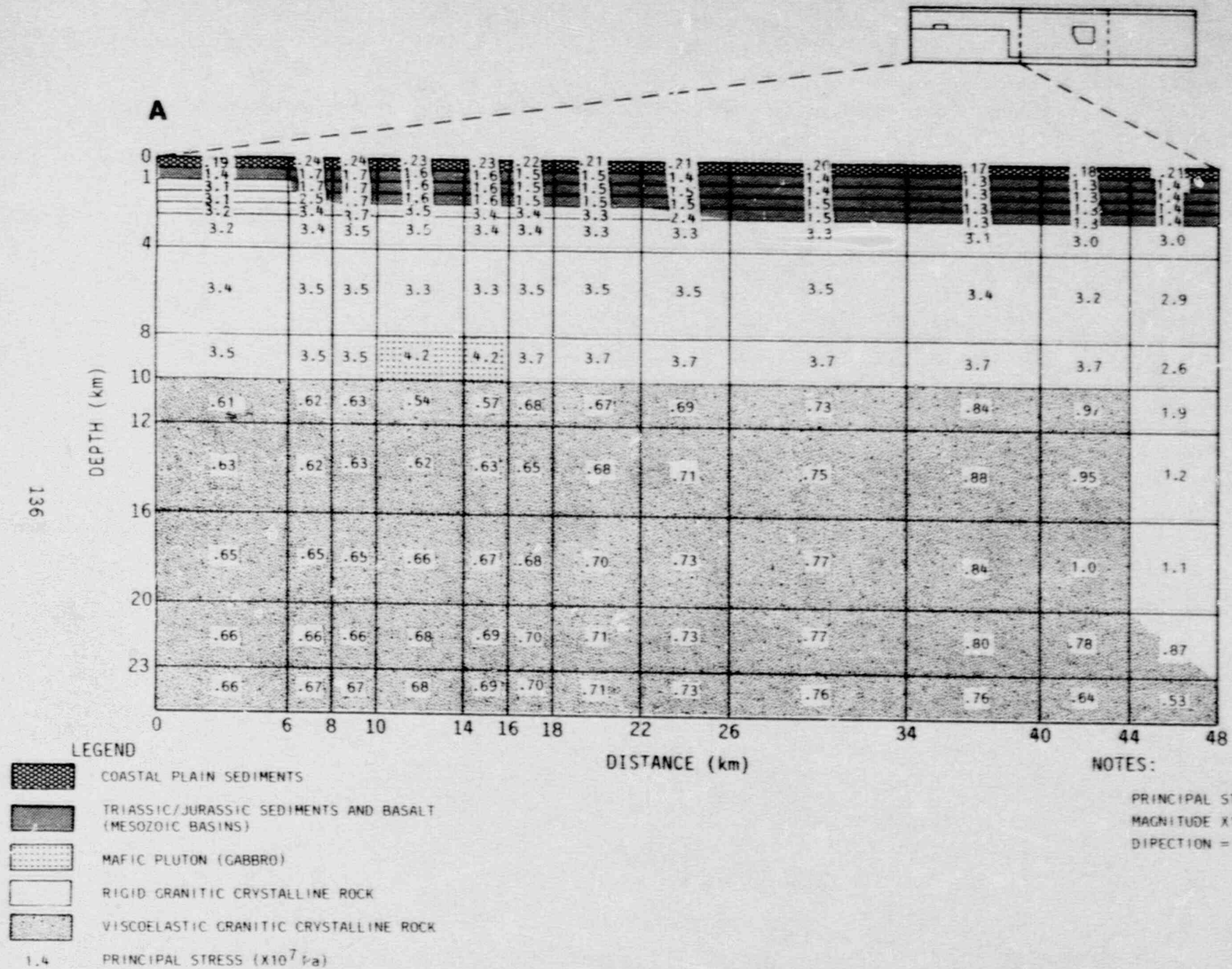
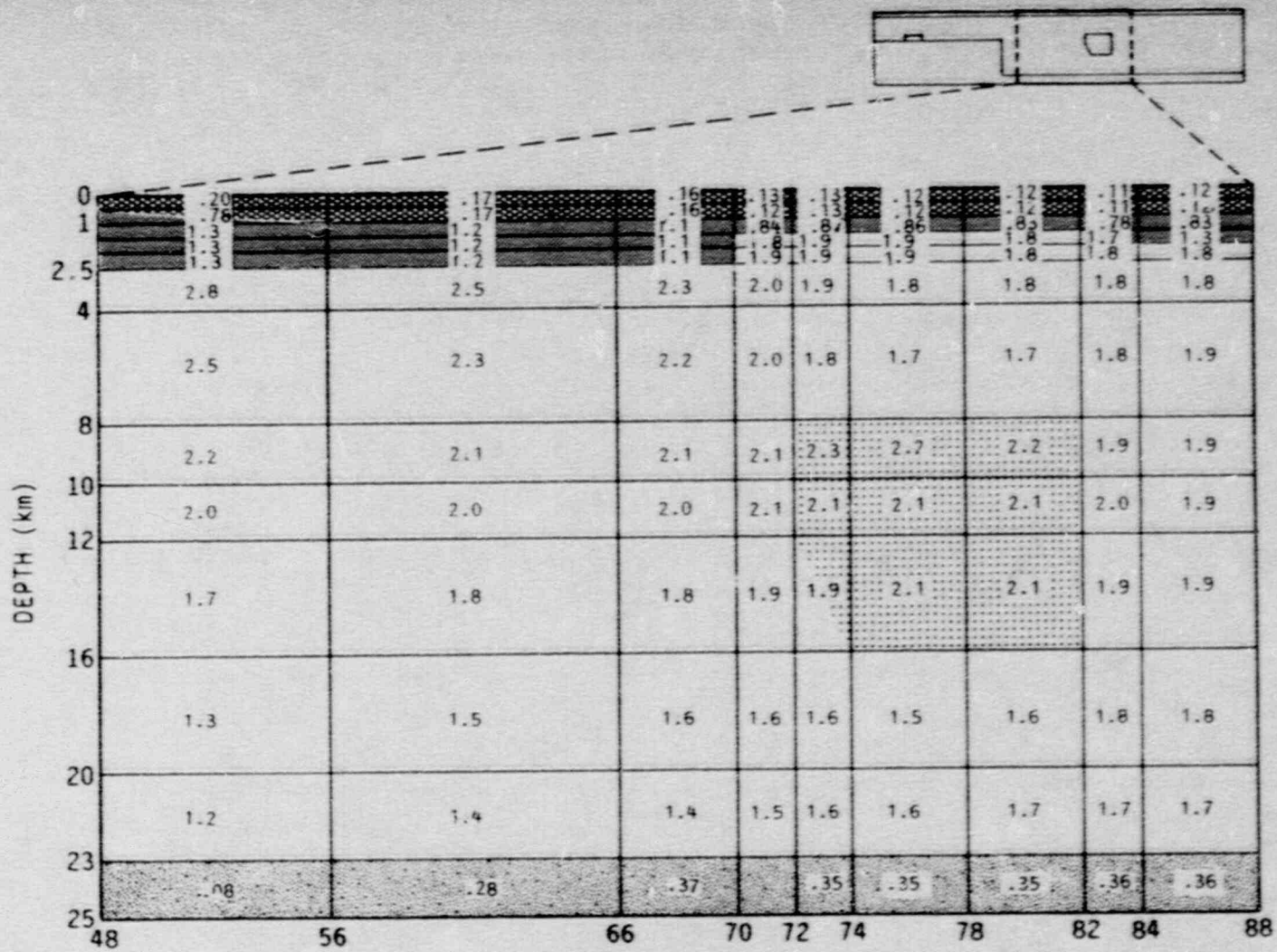



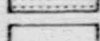
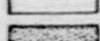


Figure 7-5. Relative principal stress magnitude from the two-dimensional stress model (1 of 3).



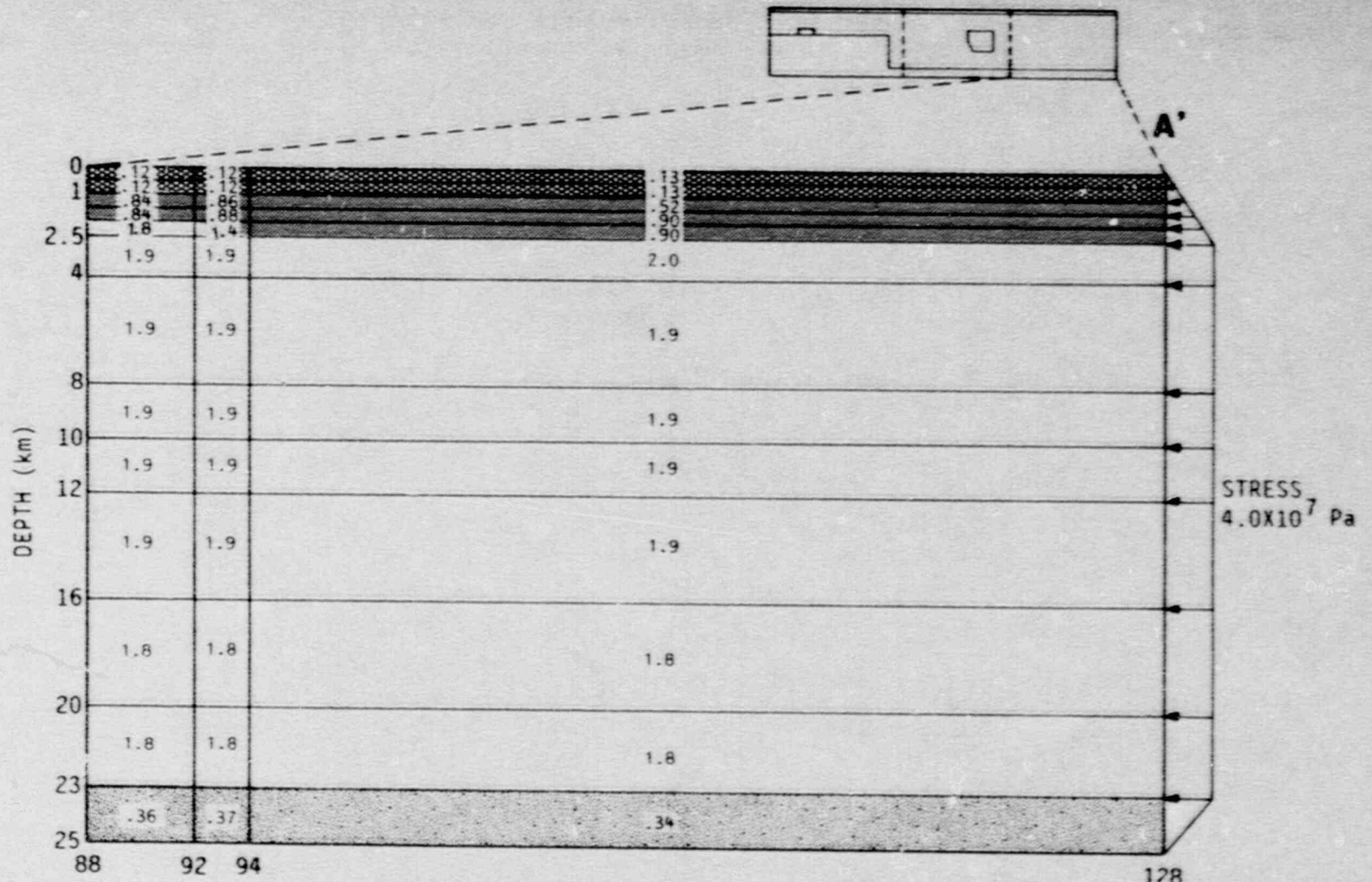
LEGEND

-  COASTAL PLAIN SEDIMENTS
-  TRIASSIC/JURASSIC SEDIMENTS AND BASALT (MESOZOIC BASINS)
-  MAFIC PLUTON (GABBRO)
-  RIGID GRANITIC CRYSTALLINE ROCK
-  VISCOELASTIC GRANITIC CRYSTALLINE ROCK
- 1.2 PRINCIPAL STRESS ($\times 10^7$ Pa)

NOTES:

PRINCIPAL STRESS AXIS:
 MAGNITUDE $\times 10^7$ Pa
 DIRECTION = $90^\circ \pm 12^\circ$

Figure 7-6. Relative principal stress magnitude from the two-dimensional stress model (2 of 3).



- LEGEND
- COASTAL PLAIN SEDIMENTS
 - TRIASSIC/JURASSIC SEDIMENTS AND BASALT (MESOZOIC BASINS)
 - MAFIC PLUTON (GABBRO)
 - RIGID GRANITIC CRYSTALLINE ROCK
 - VISCOELASTIC GRANITIC CRYSTALLINE ROCK
- 1.0 PRINCIPAL STRESS (X10⁷ Pa)

NOTES:

PRINCIPAL STRESS AXIS:
MAGNITUDE X10⁷ Pa
DIRECTION = 90° ± 12°

Figure 7-7. Relative principal stress magnitude from the two-dimensional stress model (3 of 3).

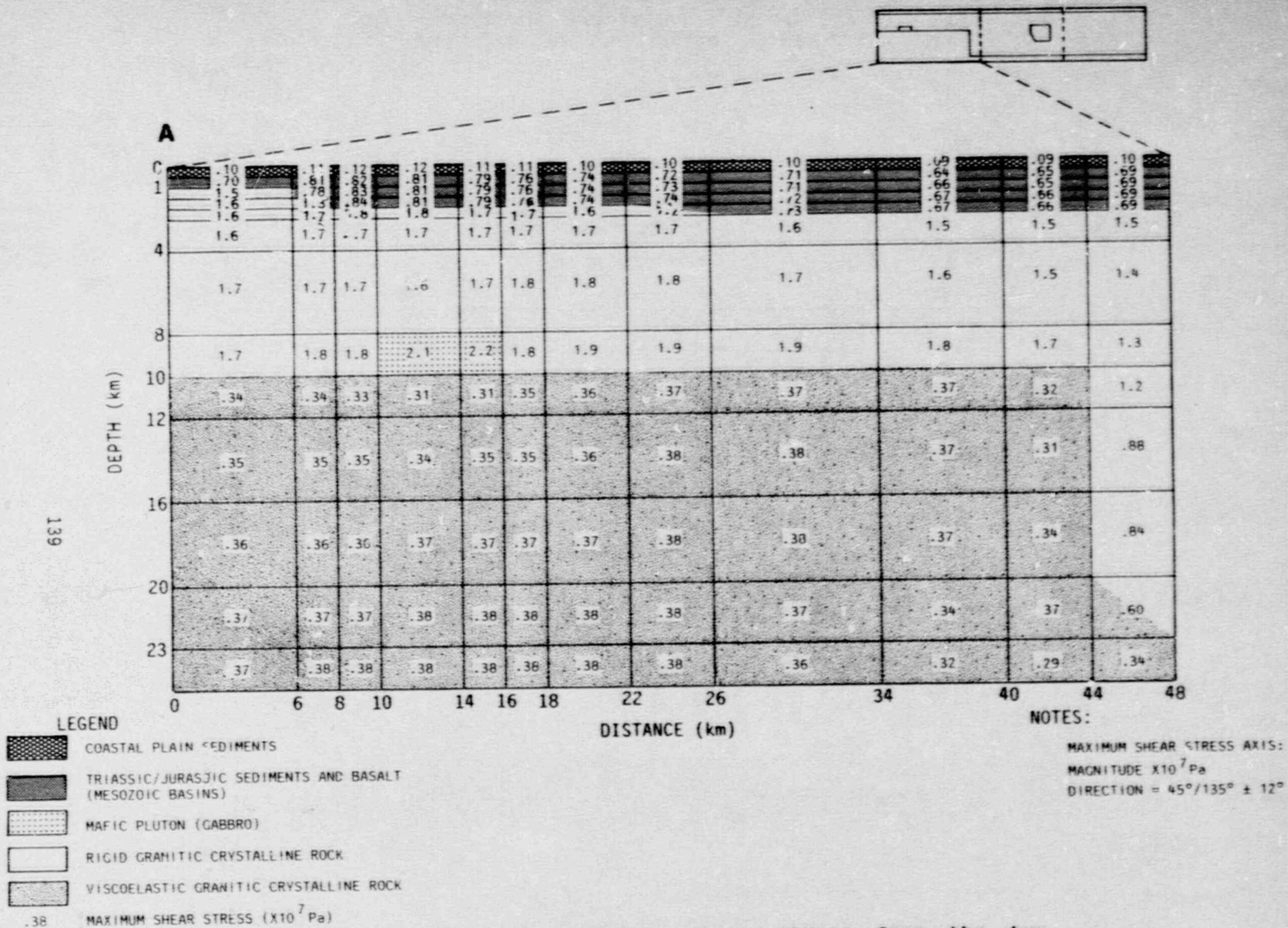
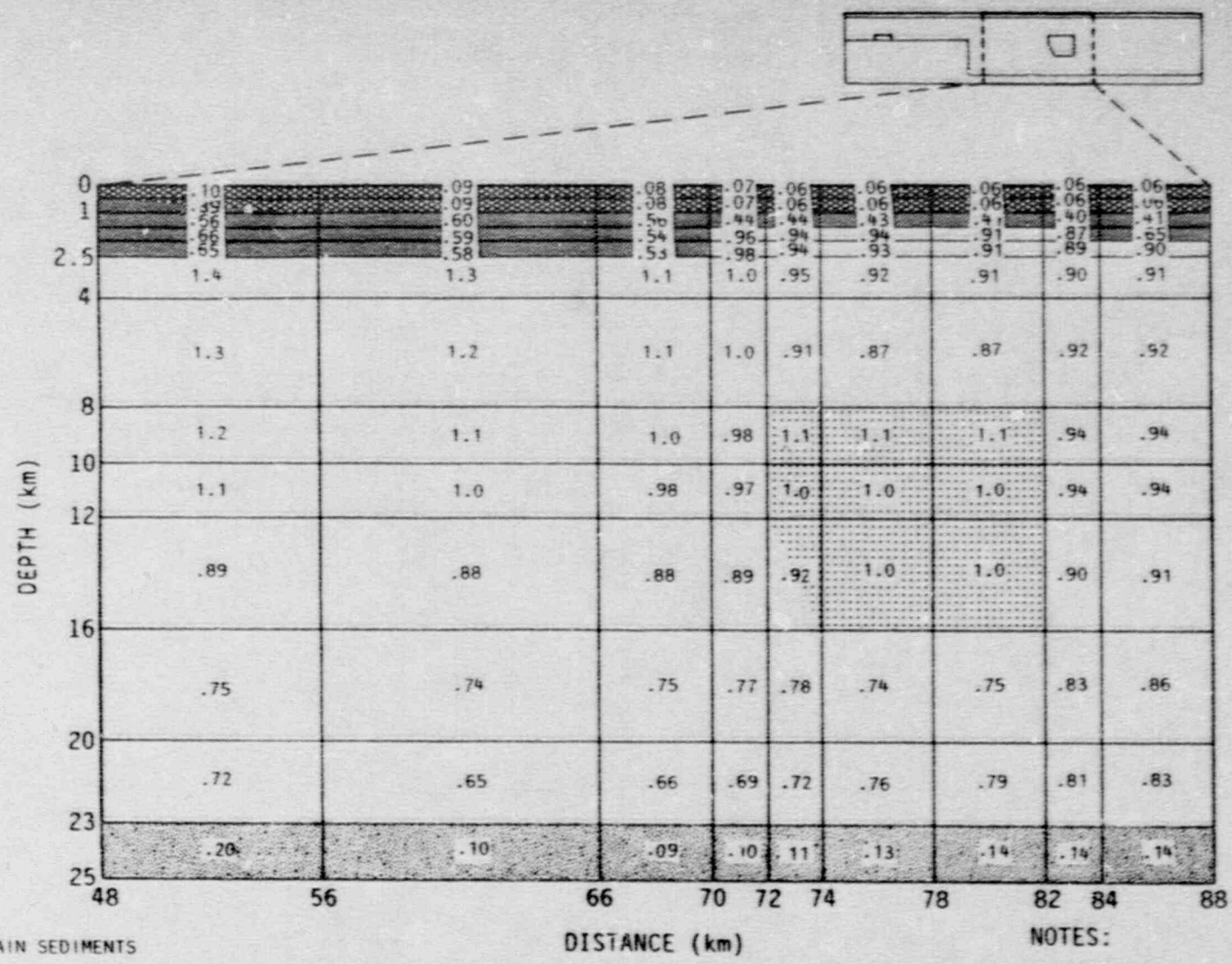


Figure 7-8. Relative maximum shear stress from the two-dimensional stress model (1 of 3).

140



NOTES:
 MAXIMUM SHEAR STRESS AXIS:
 MAGNITUDE X10⁷ Pa
 DIRECTION = 45°/135° ± 12°

- LEGEND
- COASTAL PLAIN SEDIMENTS
 - TRIASSIC/JURASSIC SEDIMENTS AND BASALT (MESOZOIC BASINS)
 - MAFIC PLUTON (GABBRG)
 - RIGID CRANITIC CRYSTALLINE ROCK
 - VISCOELASTIC GRANITIC CRYSTALLINE ROCK
 - MAXIMUM SHEAR STRESS (X10⁷ Pa)

Figure 7-9. Relative maximum shear stress from the two-dimensional stress model (2 of 3).

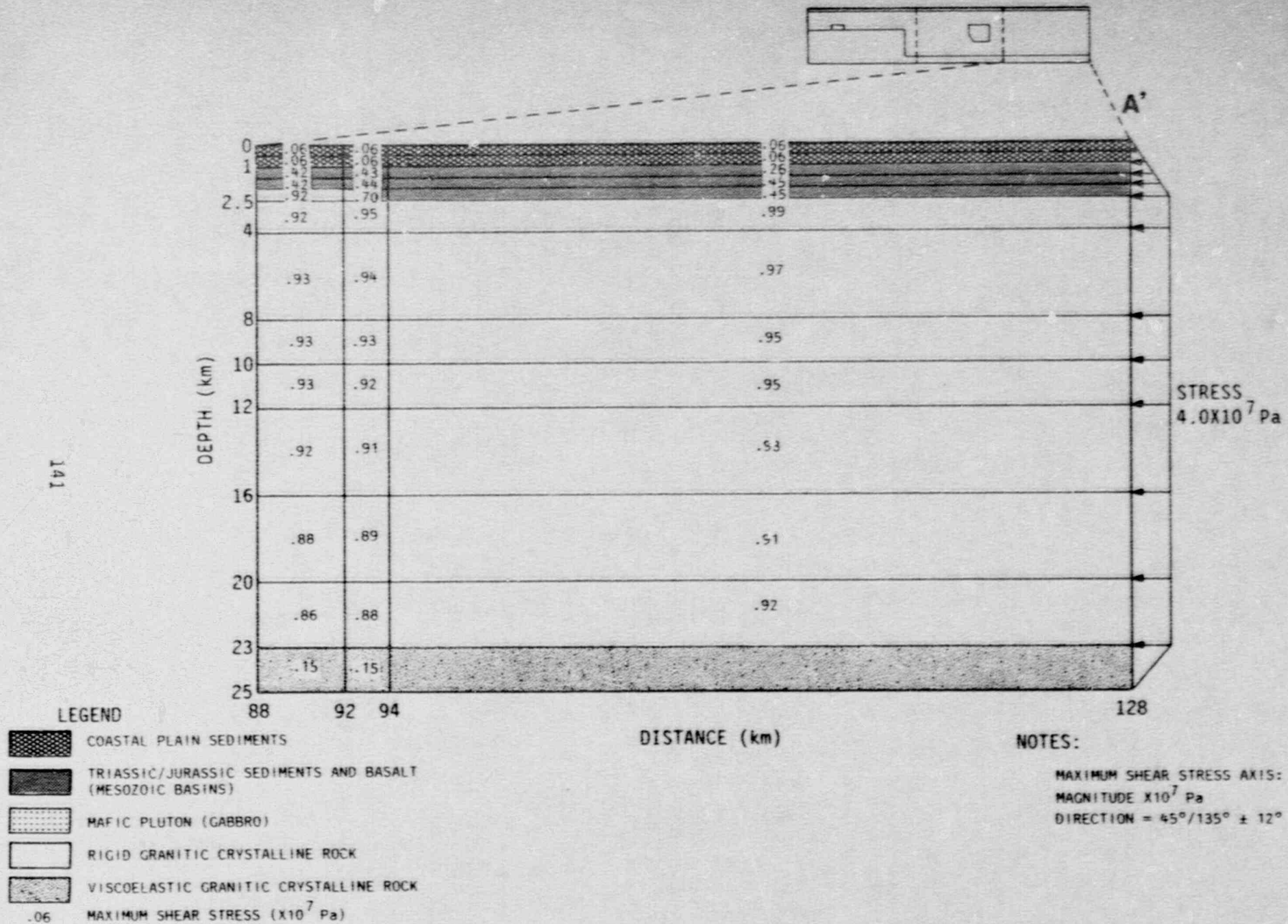


Figure 7-10. Relative maximum shear stress from the two-dimensional stress model (3 of 3).

Granitic Crystalline Rock: Below the "B" horizon we assume crystalline rock of granitic composition. Mafic intrusives and other rock types exist within the granitic rock. For modeling purposes we assume the crystalline rock to be either of granitic or mafic composition. The granitic composition rock was assigned a density of 2.67. The major mafic intrusives were considered to have a composition similar to gabbro and gravity modeling confirmed the use of a density of 2.97 g/cm³ for them. The compressional wave velocities of the rocks and the elastic properties are a function of temperature and pressure. Figure 7-11 shows temperature-pressure relation for granite and gabbro. We do not know the temperature versus depth relationship appropriate for the Charleston area at seismogenic depths, but we consider the use of the curve on Figure 7-11 to be acceptable because at the depths of interest the velocity is relatively insensitive to the temperature. We have chosen compressional wave velocities of 6.15 and 6.82 km/s, respectively for granitic and gabbroic rock within the rigid crust. In both granitic and gabbroic rock, we assume a Poisson's ratio of 0.25 and compute a Young's Modulus of 0.68×10^{11} and 0.12×10^{12} Pa for the granitic and gabbroic rock, respectively. The very flat velocity curves between 5 and 20 km on Figure 7-11 allow us to use single modulus values for the entire thickness of the rigid crust.

Viscoelastic Crustal Rock: The base of the rigid crust varies from 10 to 23 km in depth. The crustal rock in the lower crust below the base of the rigid crust is considered to behave like a viscoelastic medium and to be granitic in composition. A density of 2.67 g/cm³ and a compressional wave velocity of 6.23 km/s were assumed on the basis of the temperature-pressure relation shown on Figure 7-11; however, in order to approximate the effects of the viscoelastic medium we assigned a lower Young's Modulus and Poisson's ratio in the finite-element code.

Mantle: Mantle material is assumed to have a density of 3.07 g/cm³ and a compressional wave velocity of 8.2 km/s. These values were not used in the finite element model because the target of the analysis was the rigid stress channel at mid-crustal depths which is isolated from the mantle by a viscoelastic lower crust.

7.3 Modeling Results

The results of the modeling, using the above described parameters, are indicated in Figures 7-5 through 7-10. The magnitude of the maximum principal stress axis is plotted in Figures 7-5 through 7-7. The direction of the principal stress axis is within 10 degrees of horizontal as would be expected from the application of a horizontal plate stress. The magnitude of the stress in the plate is approximately half the applied stress because the regional stress was applied to only a portion of the end of the plate and because the top of the model was not constrained. The maximum shear stress is shown in Figures 7-8 through 7-10. The maximum shear stress is

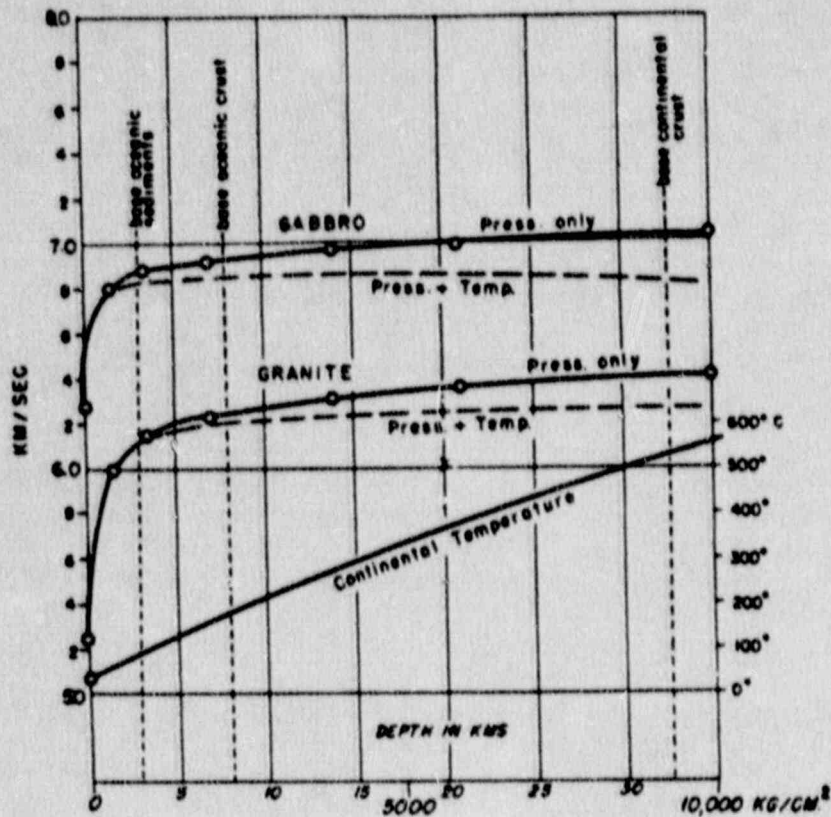


Figure 7-11. Effect of pressure and temperature on compressional velocity. (From Steinhart and Meyer, 1961; modified after Birch, 1960).

strongly controlled by the horizontal plate stress and its magnitude is thus approximately half the magnitude of the maximum principal axis. The direction of the plane of maximum shear stress will be within 12 degrees of 45 and 135 degrees from vertical.

Regional plate stresses in the crust (or horizontal ridge push stresses assumed to be applied uniformly at the southeastern boundary of the model) generate stresses within the Triassic/Jurassic basins that are half the magnitude of the stress in the granitic crystalline rock below them. The greater contrast in Young's modulus between Coastal Plain sediments and the Triassic/Jurassic basin sediments likewise induces lower stress in the Coastal Plain sediments. The fact that Coastal Plain sediments are unconfined at the surface adds to this effect. These results suggest that Coastal Plain and Triassic sediments are effectively insulated from crustal stress.

The maximum shear stress is increased at the interface of Triassic/Jurassic rocks with the crystalline crust. The values at the top of the crystalline rock are as much as 50 percent greater than in the center of the rigid crust. This stress increase is attributed to the difference in rigidity between the two materials.

The thinning of the rigid crust to the northwest increases the maximum shear stress by as much as a factor of two above and to the southeast of the rise in the base of the rigid crust.

Two mafic plutons are included in the model of the crust. The first is 8 km wide at its base and 4 km wide at its top at a depth of 4 km. The stress in the crust above the mafic pluton is decreased in the less rigid rock above and below up to approximately 20 percent. The second pluton rests directly above the viscoelastic lower crust and is 6 km wide and has its top at a depth of 8 km with a bottom at 10 km. The pluton actually extends deeper but is also modeled as viscoelastic below 10 km. Horizontal principal stresses in the pluton are about 20 percent higher than material just above it. The highest stresses in the model are found in this pluton. This pluton is located near the Bowman seismic zone (Figure 8-2). This decrease in the magnitude of the principal stress and maximum shear stress above and below a rigid body may be explained by the bearing of the stress by the rigid body. More extreme variations in strength or geometry will cause proportionally larger stress concentrations.

In summary, our two-dimensional stress model, based on our geologic model for the Charleston epicentral area (Figure 8-2), indicates that perturbations in crustal stress due to stress amplification or concentration can be in the order of 10 to 100 percent. The regional plate stresses are borne mainly by the rigid crystalline portion of the crust. The Triassic-Jurassic basins and Coastal Plain sediments are effectively insulated

from the crustal stress; as a result, there is an amplification of stress in the upper portion of the rigid crystalline crust. There is also a stress amplification of about 20% within the mafic plutons, and a corresponding decrease in stress in the crystalline crust above and below them. Finally, the thinning of the crystalline rigid crust to the northwest of Charleston greatly increases the crustal stress, but also limits the thickness of rigid crust available for faulting, hence limiting the size of the maximum possible earthquakes.

- Ackermann, H. D., "Seismic-Refraction Study in the Area of the Charleston, South Carolina, 1886 Earthquake", in G. S. Gohn, Studies Related to the Charleston, South Carolina Earthquake of 1886 - Tectonics and Seismicity, U. S. Geological Survey Professional Paper 1313, p. F1-F20, 1983
- Birch, F., "The Velocity of Compressional Waves in Rocks to 10 Kilobars, Part I", Journal of Geophysical Research, Vol. 65, p. 1083-1102, 1960
- Gardner, G. H. F., L. W. Gardner, and A. R. Gregory, "Formation Velocity and Density: The Diagnostic Basis for Stratigraphic Traps", Geophysics, Vol. 39, p. 770-780, 1974
- Steinhart, J. S. and R. P. Meyer, Explosion Studies of Continental Structure, Carnegie Institute of Washington Publication 622, Washington, D. C., 1961
- Yantis, B. R., J. K. Costain and H. D. Ackermann, "A Reflection Seismic Study Near Charleston, South Carolina", in G. S. Gohn, Studies Related to the Charleston, South Carolina Earthquake of 1886 - Tectonics and Seismicity, U. S. Geological Survey Professional Paper 1313, p. G1-G20, 1983

CHAPTER 8

HYPOTHESIS TESTING

8.1 Considerations in Hypothesis Testing

Several important results of this study were considered when evaluating the viability of each hypothesis for the cause of the 1886 Charleston earthquake. The results of the regional stress model, two-dimensional stress model, and geologic model were used to evaluate each hypothesis. Previous discussions of hypotheses by others were consulted (Dewey, 1985; Talwani, 1985).

Chapter 2 presents each hypothesis as it has been developed in current literature. This chapter considers the validity of each hypothesis based on the knowledge available to this project.

8.2 Testing Hypotheses for Causes of the 1886 Charleston, S.C. Earthquake

8.2.1 Reactivation of Horizontal (or Decollement) Faults

It has been suggested that the 1886 earthquake has resulted from normal displacement on a low-angle decollement fault underlying much of the southeastern seaboard near Charleston (Seeber and Armbruster, 1981a, 1981b). More generally, aseismic slippage on a mid-crustal detachment surface could produce seismogenic stresses in the upper crust (Seeber, 1983). Stresses caused by this slippage might cause earthquakes on moderately or steeply-dipping faults. The decollement surface could be reactivated by gravity sliding or by compressional forces of unspecified origin (Seeber and Armbruster, 1981b; Armbruster and Seeber, 1981). (from Section 2.3.1.1).

For: The primary evidence in support of this hypothesis is the widespread distribution of aftershocks of the 1886 earthquake and the unusual pattern of high intensities from this event (Seeber and Armbruster, 1987).

Against: One of the strongest points against the hypothesis is that recent epicenters give no evidence of lying along a low angle or horizontal plane (Tarr and Rhea, 1983). There is no evidence for a continuous detachment surface at seismogenic depths in the vicinity of Charleston, nor is there evidence that identifiable near-vertical faults become listric to a detachment surface (Schilt et al., 1983). The direction of ridge-push stress is opposite in direction to the stress due to gravity-sliding and, consequently, gravity sliding stress would tend to be canceled. Finally, there is no evidence of major normal faulting in the Appalachians that would result from repeated slippage along the detachment.

Conclusion: We find that there is little evidence supporting a decollement fault as the cause of the 1886 Charleston earthquake.

8.2.2 Reactivation of Mesozoic Basin Border Faults

This hypothesis suggests that the 1886 earthquake occurred on either northeast or northwest-striking faults on the borders of buried Mesozoic basins. Illies (1982) proposed that large earthquakes could occur on northwest-striking strike-slip shear zones resulting from stress concentrations associated with northeast-trending buried Mesozoic basins. (from Sections 2.3.1.2, 2.3.1.3 and 2.3.1.4).

For: The hypothesis of near-vertical faults surrounding Mesozoic basins being the source of the 1886 Charleston earthquake is supported by several lines of evidence.

First, the Mesozoic basins were formed as grabens during crustal extension. This mechanism requires that the normal faults break the rigid crust beneath the basins and therefore exist at seismogenic depths.

Second, the regional east-west to northeast-southwest stress field supports both northeast-striking and northwest-striking faults as being potentially seismogenic (Figure 6-2).

Lastly, there is spatial association of seismicity with these faults: Figure 8-1 shows the top of crystalline rock ("B" seismic horizon) and recent seismicity. The three zones of recent seismicity are each found near the intersection of northeast- and northwest-trending Mesozoic basin boundaries. These boundaries can be construed to be fault zones which transect the rigid crust which were formed in a period of extensional rifting and are now reactivated in the current compressive stress field.

Against: Focal mechanism data currently available are insufficient to support any single fault orientation. Also, the catalog of recent events does not delineate any fault or set of faults.

Conclusion: This hypothesis is viable. The results of this study strengthen this hypothesis.

8.2.3 High Angle Faults not Associated with Mesozoic Basins

This class of faults consists of high angle faults typically striking northeast or northwest which are thought to be normal faults reactivated as reverse faults. Those faults hypothesized to be the cause of the 1886 Charleston earthquake are hypothesized by their authors to exist at seismogenic depths. We separated these faults from similar ones associated with Mesozoic Basins. (from Sections 2.3.1.2 and 2.3.1.4).

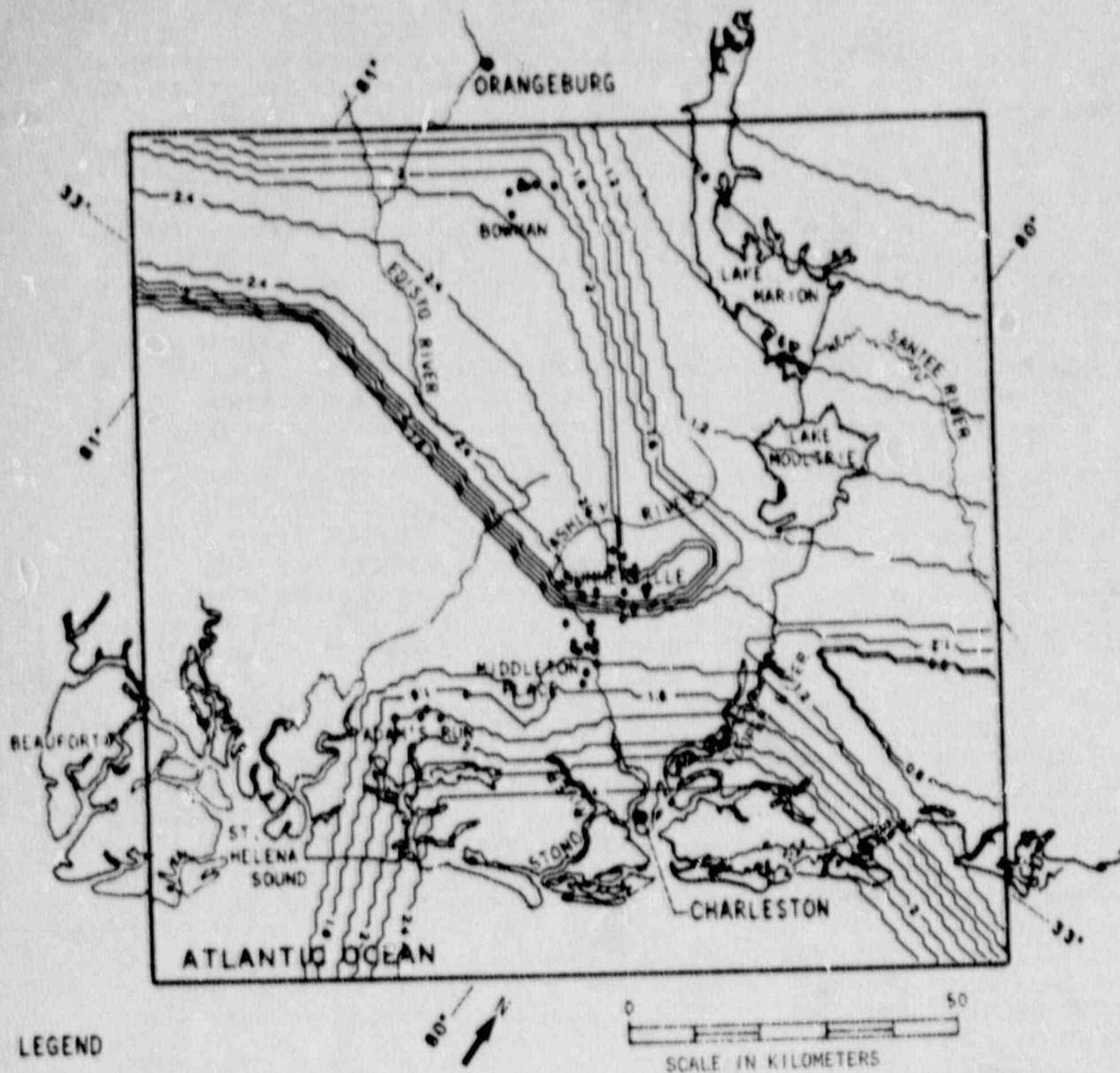


Figure 8-1. Contour map of the top of crystalline rock (the "B" seismic horizon) and recent seismicity. Contours are in kilometers.

For: The regional east-west to northeast-southwest stress field supports many orientations of faults. Some of these faults are spatially associated with earthquakes.

Against: Those faults defined by epicenters are poorly constrained by geologic evidence. Conversely, spatial association of earthquakes with those faults known geologically is not supported by seismicity data. There is a lack of geologic evidence that these faults would penetrate the existing crust.

Conclusion: We have taken these various high-angle faults and have somewhat arbitrarily grouped them. The hypotheses that these faults are seismogenic show various degrees of viability.

8.2.4 Intersecting Structural Trends

Talwani et al. (1979) suggested that the seismicity in the South Carolina Coastal Plain and in the Central Virginia seismic zone occurs at localized zones of weakness formed at the intersection of an older pre-existing zone of weakness; in particular, in the case of the Charleston area, the Blake Spur Fracture Zone intersects the boundary faults of Triassic basins. (From Section 2.3.1.7).

For: The proximity of the Charleston earthquake of 1886 to an area of widespread Mesozoic rifting and to a possible landward extension of Blake Spur Fracture Zone suggest that earthquake activity along the southern Atlantic Coastal Plain may be related to old zones of weakness that were reactivated during the Mesozoic opening of the Atlantic Ocean.

Against: Except for the basement features controlling Mesozoic faulting, no evidence of deep-seated structural trends, such as the landward extension of the Blake Spur Fracture Zone, has been found.

Conclusion: This hypothesis is not supported by available data.

8.2.5 Faults Associated with Basement Province Boundaries

Faults associated with basement province boundaries have been proposed by Talwani (1983) as providing a northwest-trending zone of crustal weakness extending northwest from Charleston. (From Section 2.3.1.5).

For: Northwest-trending offsets in gravity and magnetic anomalies have been interpreted by some as defining crustal blocks 60-70 km wide with apparent displacements. These blocks are oriented in the same sense as fracture zones that exist offshore.

Against: There is a lack of strong indirect evidence and no direct evidence in support of active faults associated with the

block boundaries. Focal mechanism data are no longer considered to support high-angle northwest-striking faults in the Charleston area (Shedlock, 1987).

Conclusion: The evidence does not strongly support this hypothesis.

8.2.6 Ductile Shear Zones in the Lower Crust

Zoback (1983) suggested that there are pre-existing ductile shear zones in the lower crust which concentrate deformation and thus concentrate stresses in the upper crust. Laboratory rock deformation evidence suggest that such zones could exist in the lower crust. Earthquakes caused by such a mechanism would concentrate in areas of weakness in shallow brittle crust in the vicinity of these ductile zones. (from Section 2.3.1.6).

For: This hypothesis is supported by the uneven base in the rigid crust as developed in our geologic model. These shear zones would have their origin beneath extensional Mesozoic rift basins.

Conclusion: Evidence for ductile shear zones in the lower crust exists, but our study has not evaluated the mechanism proposed by Zoback (1983).

8.2.7 Brunswick Suspect Terrane

Brunswick Suspect Terrane is not a hypothesis per se but an area where structural elements that make up viable hypotheses exist. The existence of seismic zones that are spatially and temporally stationary suggest that there is some type of spatial selectivity in the accumulation and release of strain energy in the southeast. Wheeler and Bollinger (1984) suggested that the Charleston area lies in the Brunswick suspect terrane of Williams and Hatcher (1982) and this terrane is more conducive to seismic activity. (from Section 2.3.2.2).

Brunswick Terrane was considered an area of uniform earthquake potential because it is interpreted to have uniform geology at seismogenic depths. Regional stress modeling and geologic data indicate that there is nothing unique about the Brunswick Suspect Terrane in the Charleston area that would limit the earthquakes to that area. Within the Brunswick Terrane, areas with Mesozoic Basin boundary intersections and associated plutons may indicate higher seismogenic potential.

Conclusion: The hypothesis of the Brunswick Suspect Terrane as an area containing conditions associated with a Charleston-type event is still viable.

8.2.8 Topographic and Density Anomaly Loads

Barosh (1983) suggested that adjustments on shallow local

structures due to vertical movements brought about by continued opening of the North Atlantic basin appear to be the cause of the seismicity of the southeastern United States. The main activity seems related to the relative subsidence at the inner edge of embayments within the Coastal Plain. The embayments overlie older grabens that have apparently played a significant role in controlling their location. (from Section 2.3.2.1).

For: Regional stress modeling shows these loads may contribute a significant portion to the total stress field (Chapter 6). However, our regional stress modeling does not indicate such an effect in the Charleston area (Figure 6-6).

Against: It is unlikely that extensional tectonic activity can be continuing to occur given the currently compressional regional stress field.

Conclusion: We believe that the surface loading contribution to anomalous stress is not a sufficient hypothesis in itself for a cause of the 1886 earthquake.

8.2.9 Stress Amplifications Near Plutons

There is evidence from many sources (Long and Champion (1977), Kane (1977), McKeown (1978), and Barstow et al. (1981)) that there is a spatial association between mafic (and ultramafic) plutons and local seismicity. It is hypothesized that mafic intrusions tend to concentrate stress along their margins because of property contrasts between the pluton, surrounding altered country rock, and unaltered country rock. Ravat et al. (1987) found that some mafic intrusives strengthen surrounding rock by alteration, thereby concentrating local stresses. They also found that these mafic plutons dislocate rather than amplify local stress fields.

Kane (1977) and Campbell (1978) proposed that stress amplification is caused by serpentinization of ultramafic plutons. The amount of stress which could be concentrated is a function of the effective rigidity moduli of the contrasting materials. The serpentinized mafic body is substantially less rigid than the surrounding material. This yields the "hole in a plate" model where stresses are concentrated at the edges of the zone of weakness. In contrast, Yang and Aggarwal (1981) have hypothesized that the presence of unfaulted plutons inhibits earthquake activity. (from Section 2.3.2.3).

For: By examining Figure 8-2, which shows recent seismicity and the location of plutons used in the geologic model, it can be seen that there is a spatial association between the edges of mafic plutons and recent seismic activity. Also, these plutons are located near the intersection of Mesozoic basin boundaries. It is possible that these older plutons may have influenced the development and location of the later Mesozoic faulting. It is our interpretation that the mafic plutons remain strong and do not undergo substantial weakening by

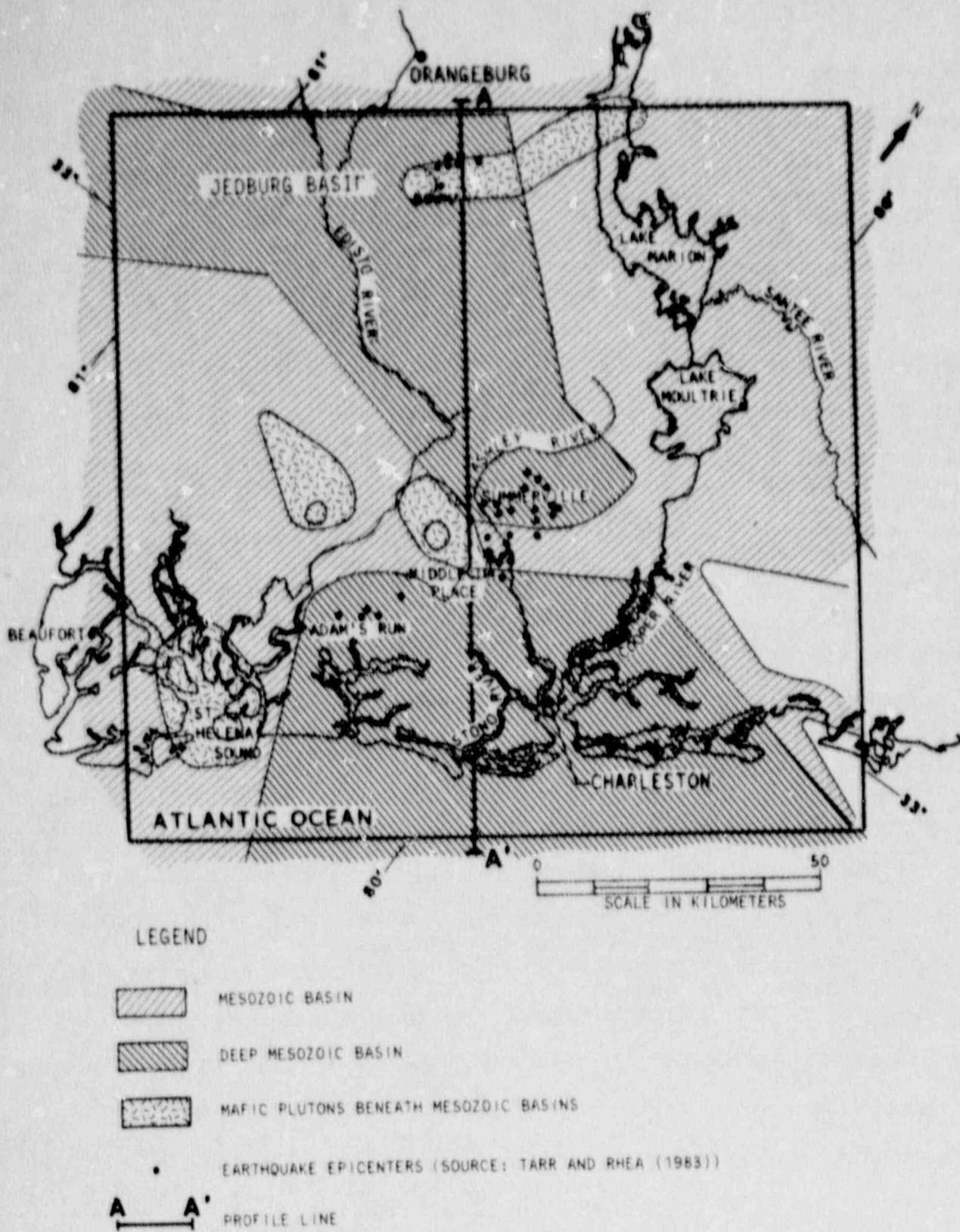


Figure 8-2. This figure shows the location of plutons used in the geologic model and recent seismicity.

serpentinization at depths in the upper rigid crust in this region. Our stress modeling shows that increases in local stress can be induced in areas surrounding plutons (Chapter 7).

Against: The results of the two-dimensional stress modeling imply that the stress amplification exists but the magnitude of the increase in stress (up to about 20%) is not great. Also, the spatial association of earthquakes with plutons in the Charleston area may also be explained by the plutons being at the intersection of Mesozoic border faults as described above.

Conclusion: We believe that this hypothesis is viable based on the information currently available to us. However we consider that the spatial location of earthquake hypocenters with the edges of mafic plutons may be explained by noting that the older plutons have controlled the location of Mesozoic border faults and the intersection of northeast and northwest structures. Mesozoic Basin border faults occur at the pluton as a consequence. The spatial association of earthquakes with plutons may be related to a causal relationship between these fault interpretations and not related to stress amplification at the plutons.

8.3 Conclusion

In summary, the following hypotheses were considered viable:

- o Reactivation of Mesozoic Basin Border Faults
- o Stress Amplification Near Plutons
- o Brunswick Suspect Terranes
- o High Angle Faults not Associated with Mesozoic Basins.

The following hypotheses are not considered viable:

- o Reactivation of Horizontal (or Decollement) Faults
- o Landward Extension of Blake Spur Fracture Zone
- o Topographic and Density Anomaly Loading (Barosh's hypothesis of extensional tectonics)
- o Faults Associated with Basement Province Boundaries.

The following hypothesis remains unevaluated or undecided:

- o Ductile Shear Zones in Lower Crust.

The results of this study indicate that the hypothesis of reactivation of Mesozoic Basin border faults is strongly supported, specifically at the intersections of Mesozoic Basin border faults near buried mafic plutons. These areas are not necessarily restricted to the Charleston area or the area of this study. This hypothesis implies locations for the occurrence of a Charleston-type event in other areas of the eastern U.S.

There appear to be strong differences in the thickness of the

rigid crust which also may limit the location of Charleston-type earthquakes to areas of thicker crust. This would limit the maximum magnitude in areas of thinner crust such as the Bowman seismic zone, thus excluding a Charleston-type event.

- Armbruster, J. C. and L. Seeber, "Seismicity and Back-Slip on the Detachment of the Southern Appalachians", Abstract, Eos Transactions, American Geophysical Union, Vol. 62, p. 403, 1981
- Barosh, P. J., "Use of Seismicity and Tectonic Framework to Define the Seismic Hazard in the Region Encompassing Charleston, South Carolina", in W. W. Hays and P. L. Gori, Proceedings of Conference XX, A Workshop on "The 1886 Charleston, South Carolina Earthquake and Its Implications for Today", U. S. Geological Survey Open-File Report 83-0843, p. 380-390, 1983
- Barstow, N. L., K. G. Brill, Jr., O. W. Nuttli, and P. W. Pomeroy, "An Approach to Seismic Zonation for Siting Nuclear Electric Power Generating Facilities in the Eastern United States", USNRC Report NUREG/CR-1577, U. S. Nuclear Regulatory Commission, 1981
- Campbell, D. L., "Investigation of the Stress-Concentration Mechanism for Intraplate Earthquakes", Geophysical Research Letters, Vol. 5, No. 6, p. 477-479, 1978
- Dewey, J. W., "A Review of Recent Research on the Seismotectonic of the Southeastern Seaboard and an Evaluation of Hypotheses on the Source of the 1886 Charleston, South Carolina, Earthquake", USNRC Report NUREG/CR-4339, 1985
- Illies, J. H., "Der Hohenzollergraben and Intraplatten-Seismizität Infolge Vergitterung Lamellarer Scherung mit Einer Riftstruktur", Oberrhein, Geol. Abh., Vol. 31, p. 47-78, 1982
- Kane, M. F., "Correlation of Major Eastern Earthquake Centers With Mafic/Ultramafic Masses", in D. W. Rankin, Studies Related to the Charleston, South Carolina Earthquake of 1886 - A Preliminary Report, U. S. Geological Survey Professional Paper 1028, p. 199-204, 1977
- Long, L. T. and J. W. Champion, Jr., "Bouguer Gravity Map of the Summerville-Charleston, South Carolina Epicentral Zone and Tectonic Implications", in D. W. Rankin, Studies Related to the Charleston, South Carolina Earthquake of 1886 - A Preliminary Report, U. S. Geological Survey Professional Paper 1028, p. 151-166, 1977
- McKeown, F. A., "Hypothesis: Many Earthquakes in the Central and Southeastern United States are Causally Related to Mafic Intrusive Bodies", U. S. Geological Survey Journal of Research, Vol. 6, p. 41-50, 1978
- Ravat, D. N., L. W. Bralies, and W. J. Hinze, "Earthquakes and Plutons in the Midcontinent-Evidence From the Bloomfield Pluton, New Madrid Rift Complex", Seismological Research Letters, Vol. 58, No. 2, p. 4-52, 1987

- Schilt, F. S., L. D. Brown, J. E. Oliver, and S. Kaufman, "Subsurface Structure Near Charleston, South Carolina; Results of COCORP Reflection Profiling in the Atlantic Coastal Plain", in G. S. Gohn, Studies Related to the Charleston, South Carolina Earthquake of 1886 - Tectonics and Seismicity, U. S. Geologic Survey Professional Paper 1313, p. H1-H19, 1983
- Seeber, L., "Earthquake Hazard and Risk in the Eastern U.S. vs. the Western U.S.", Abstract, Earthquake Notes, Vol. 54, p. 31, 1983
- Seeber, L. and J. G. Armbruster, "The 1886 Earthquake and Intraplate Detachments", Geological Society of America Abstracts With Programs, Vol. 13, No. 7, p. 550, 1981a
- Seeber, L. and J. G. Armbruster, "The 1886 Charleston, South Carolina Earthquake and the Appalachian Detachment", Journal of Geophysical Research, Vol. 86, No. 9, p. 7874-7894, 1981b
- Seeber, L. and J. G. Armbruster, "The 1886-1889 Aftershocks of the Charleston, South Carolina, Earthquakes, A widespread Burst of Seismicity", Journal of Geophysical Research, Vol. 92, p. 2663-2696, 1987
- Shedlock, K. M., "Seismicity Near Charleston, South Carolina - 1974 to Present", Abstract, Eos, Transactions, American Geophysical Union, Vol. 68, No. 16, p. 363, 1987
- Talwani, P., "Intraplate Earthquakes, Block Tectonics, Aeromagnetic and Gravity Anomalies; or Why We Have Earthquakes at Charleston, S.C.", Geological Society of America Abstracts With Programs, Vol. 15, No. 2, p. 64, 1983
- Talwani, P., "Current Thoughts on the Cause of the Charleston, South Carolina Earthquakes", South Carolina Geology, Vol. 29 No. 2, p. 19-38, 1985
- Talwani, P., D. C. Amick, and R. Logan, "A Model to Explain the Intraplate Seismicity in the South Carolina Coastal Plain", Abstract, Eos, Transactions, American Geophysical Union, Vol. 60, p. 311, 1979
- Tarr, A. C. and S. Rhea, "Seismicity Near Charleston, South Carolina, March 1973 to December 1979", in G. S. Gohn, Studies Related to the Charleston, South Carolina Earthquake of 1886 - Tectonics and Seismicity, U. S. Geological Survey Professional Paper 1313, p. R1-R17, 1983
- Wheeler, R. L. and G. A. Bollinger, "Seismicity and Suspect Terranes in the Southeastern U.S.", Geology, Vol. 12, p. 323-326, 1984

Williams, H. and R. D. Hatcher, Jr., "Suspect Terranes and Accretionary History of the Appalachian Orogen", Geology, Vol. 10, p. 530-536, 1982

Yang, J. P. and Y. P. Aggarwal, "Seismotectonics of Northeastern United States and Adjacent Canada", Journal of Geophysical Research, Vol. 86, p. 4981-4998, 1981

Zoback, M. D., "Intraplate Earthquakes, Crustal Deformation, and In-situ Stress", in W. W. Hays and P. L. Gori, Proceedings of Conference XX, A Workshop on "The 1886 Charleston, South Carolina Earthquake and its Implications for Today", U. S. Geological Survey Open-File Report 83-0843, p. 169-178, 1983

BIBLIOGRAPHY

1859

Gibbes, L. R., "Notice of the Phenomena Attending the Shock of the Earthquake of December 19, 1857 (Charleston, South Carolina)", Elliott Society of Natural History Proceedings, No. 1, p. 288-289, 1859

1886

Cope, E. D., "The Recent Earthquake in the United States (Charleston, South Carolina)", American Naturalist, Vol. 20, p. 869-870, 883-884, 1886

Hayden, E., "The Earthquake of August 31, 1886 (Charleston Earthquake)", Science, Vol. 8, p. 224-226, 1886

Hayden, E., "The Charleston Earthquake; Some Further Observations", Science, Vol. 8, p. 246-248, 1886

McGee, W. J., "Some Features of the Recent Earthquake (Charleston)", Science, Vol. 8, p. 271-275, 1886

Meiss, M. C., "The Charleston Earthquake", Science, Vol. 8, p. 390-391, 1886

Mendenhall, T. C., "Report on the Charleston Earthquake", Monthly Weather Review, Vol. 14, p. 233-235, 1886

O'Reilly, J. P., "The Late American Earthquake (Charleston) and its Limits", Nature, Vol. 34, p. 570-571, 1886

Storek, "Line of Origin of the Charleston Earthquake", Columbia University School of Mines Quarterly, Vol. 8, p. 64-73, 1886

1887

Dutton, C. E., "The Charleston Earthquake", Science, Vol. 10, p. 10-11, 35-36, 1887

Dutton, C. E. and E. Hayden, "Abstract of the Results of the Investigation of the Charleston Earthquake", Abstract, Science, Vol. 9, p. 489-501, 1887

Mendenhall, T. C., "The Charleston Earthquake", Science, Vol. 9, p. 584-587, 1887

Rockwood, C. G., "The Charleston Earthquake", American Journal of Science, Vol. 33, p. 71-73, 1887

Toplay, "Notes on Recent Earthquakes in the U.S.", British Association for the Advancement of Science Report 46, p. 656-657, 1887

1888

Claypole, F. W., "Earthquake Shocks at Charleston, South Carolina", American Geology, Vol. 2, p. 135-136, 1888

Dutton, C. E. and S. Newcomb, "The Speed of Propagation of the Charleston Earthquake", American Journal of Science, Vol. 3, No. 35, p. 1-15, 1888

1889

Dutton, C. E., "The Charleston Earthquake of August 31, 1886", U.S. Geological Survey Annual Report, No. 9, p. 203-528, 1889

1890

Dutton, C. E., "The Charleston Earthquake of August 31, 1886", U. S. Geological Survey, 528 p., 1890, c 1979

1905

Davison, "A Study of Recent Earthquakes", Lake Superior Mining Institute, Vol. XII, 355 p., 1905

1906

Fuller, M. L., "Comparative Intensities of the New Madrid, Charleston, and San Francisco Earthquakes", Abstract, Science, Vol. 23, p. 917-918, 1906

1907

Harboe, E. G., "The Charleston Earthquake of August 31, 1886" (Das Erdbeben von Charleston am 31, August 1886), Bertrage zur Geophysik, Vol. 9, p. 105-110, 1907

Hobbs, W. H., "The Charleston Earthquake of August 31st, 1886, in a New Light", Geology Magazine, Vol. 5, No. 4, p. 197-202, 1907

1909

Hovey, "Earthquakes, Their Causes and Effects", Abstract, American Philosophical Society Proceedings, No. 48, p. 235-258, p. 833, 1909

1914

Stephenson, L. W., "A Deep Well at Charleston, South Carolina", U.S. Geological Survey Professional Paper 90-H, p. 69-94, 1914

Taber, S., "Seismic Activity in the Atlantic Coastal Plain Near Charleston, South Carolina", Seismological Society of America Bulletin, No. 4, p. 108-160, 1914

1936

Cooke, C. W., "Geology of the Coastal Plain of South Carolina", U. S. Geological Survey Bulletin 867, 196 p., 1936

1944

Louderback, G. D., "The Personal Record of Ada M. Trotter of Certain After-Shocks of the Charleston (S.C.) Earthquake of 1886", Seismological Society of America Bulletin, Vol. 34, No. 4, p. 199-206, 1944

Stockins, H. E., "The Charleston Earthquake (Aug. 31, 1886)", Nature, Vol. 37, No. 1, p. 16-19, 1944

1945

Wood, H. O., "A Note on the Charleston Earthquake (S.C., 8/31/86)", Seismological Society of America Bulletin, Vol. 35, No. 2, p. 49-56, 1945

1949

Holmes, F. F., "Notes on the Geology of Charleston, S.C.", American Journal of Sciences, Vol. 7, p. 187-201, 1949

1957

Woollard, G. P., W. E. Bonini, and R. P. Meyer, "A Seismic Refraction Study of the Subsurface Geology of the Atlantic Coastal Plain and Continental Shelf Between Virginia and Florida", Department of Geology and Geophysics Technical Report, Contract No. 57ONR-28512, University of Wisconsin-Madison, 128 p., 1957

1959

Malde, H.E., "Geology of the Charleston Phosphate Area, South Carolina", U.S. Geological Survey Bulletin 1079, 105 p., 1959

Pooley, R. N., "Basement Configuration of Subsurface Geology of Eastern Georgia and Southern South Carolina as Determined by Seismic Refraction Measurements", Master's Thesis, University of Wisconsin-Madison, 47 p., 1959

1960

Bonini, W. E. and G. P. Woollard, "Subsurface Geology of North Carolina-South Carolina Coastal Plain from Seismic Data", American Association of Petroleum Geologists Bulletin, Vol. 44, p. 298-315, 1960

Doering, J. A., "Quaternary Surface Formations of Southern Part of Atlantic Coastal Plain", Journal of Geology, Vol. 68, p. 182-202, 1960

Pooley, R. N., R. P. Meyer, and G. P. Woollard, "Yamacraw Ridge, Pre-Cretaceous Structure Beneath South Carolina-Georgia Coastal Plain", Abstract, American Association of Petroleum Geologists Bulletin, Vol. 44, p. 1254-1255, 1960

1965

Colquhoun, D. J., "Terrace Sediment Complexes in Central South Carolina", in Guidebook, Atlantic Coastal Plain Geological Association, Field Conference 1965, (University of South Carolina, Columbia), 62 p., 1965

Overstreet, W. C. and H. Bell, "The Crystalline Rocks of South Carolina", U.S. Geological Survey Bulletin, Vol. 1183, 126 p., 1965

Overstreet, W. C. and H. Bell, "Geologic Map of the Crystalline Rocks of South Carolina", U.S. Geological Survey Miscellaneous Investigations Map MI-413, Scale 1:250,000, 1965

Petty, A. J., F. A. Petrafeso, and F. C. Moore, Jr., "Aeromagnetic Map of the Savannah River Plant Area, South Carolina and Georgia", U.S. Geological Survey Geophysical Investigations Map GP-489, Scale 1:250,000, 1965

1968

Colquhoun, D. J. and H. S. Johnson, Jr., "Tertiary Sea-level Fluctuation in South Carolina", Palaeogeography, Palaeoclimatology, Palaeoecology, Vol. 5, p. 105-126, 1968

Taylor, P. T., I. Zietz, and L. S. Dennis, "Geologic Implications of Aeromagnetic Data for the Eastern Continental Margin of the United States", Geophysics, Vol. 33, p. 755-780, 1968

1969

Colquhoun, D. J., "Geomorphology of the Lower Coastal Plain of South Carolina", Division of Geology, South Carolina State Development Board Manuscript 15, 36 p., 1969

Swift, D. J. P. and S. D. Heron, Jr., "Stratigraphy of the Carolina Cretaceous", Southeastern Geology, Vol. 10, p. 201-245, 1969

1970

Dewey, J. F. and J. M. Bird, "Mountain Belts and the New Global Tectonics", Journal of Geophysical Research, Vol. 75, p. 2625-2647, 1970

U.S. Geological Survey, "Aeromagnetic Map of the Camden-Kershaw Area, North-Central South Carolina", U.S. Geological Survey Open-File Report, 4 sheets, Scale 1:24,000, 1970

1972

Bollinger, G. A., "Historical and Recent Seismic Activity in South Carolina", Seismological Society of America Bulletin, Vol. 62, p. 851-864, 1972

Colquhoun, D. J., T. A. Bond, and D. Chappel, "Santee Submergence, Example of Cyclic Submerged and Emerged Sequences", in B. W. Nelson, Environmental Framework of Coastal Plain Estuaries, Geological Society of America Memoir 133, p. 475-496, 1972

Walters, C. P., "The Charleston Earthquake Considered as a Possible Cryptovolcanic Occurrence and Source of Tektites", Geological Society of America, Abstracts with Programs, Vol. 4, No. 4, p. 298, 1972

1973

Artyushkov, E. V., "Stresses in the Lithosphere Caused by Crustal Thickness Inhomogeneities", Journal of Geophysical Research, Vol. 78, p. 7675-7708, 1973

Bollinger, G. A., "Seismicity and Crustal Uplift in the Southeastern United States", American Journal of Science, Vol. 273A, p. 396-408, 1973

Bollinger, G. A., "Seismicity of the Southeastern United States", Seismological Society of America Bulletin, Vol. 63, p. 1785-1808, 1973; Also Errata, Vol. 64, p. 733-734, 1974

Colquhoun, D. J. and C. D. Comer, "The Stono Arch, a Newly Discovered Breeched Anticline Near Charleston, South Carolina", Geologic Notes, Division of Geology, South Carolina State Board of Development, Vol. 17, p. 97-105, 1973

Long, L. T. and R. P. Lowell, "Thermal Model for Some Continental Margin Sedimentary Basins and Uplift Zones", Geology, Vol. 1, p. 87-88, 1973

McKee, J. H., "A Geophysical Study of Microearthquake Activity Near Bowman, South Carolina", Master's Thesis, Georgia Institute of Technology, Atlanta, 75 p., 1973

Sbar, M. L. and L. R. Sykes, "Contemporary Compressive Stress and Seismicity in Eastern North America: An Example of Intraplate Tectonics", Geological Society of America Bulletin, Vol. 84, p. 1861-1881, 1973

1974

Balaza, E. I., "Vertical Crustal Movements on the Middle Atlantic Coastal Plain as Indicated by Precise Leveling", Geological Society of America, Abstracts with Programs, Vol. 6, No. 1, p. 3, 1974

Colquhoun, D. J., "Cyclic Surficial Stratigraphic Units of the Middle and Lower Coastal Plains, Central South Carolina", in R. W. Oaks and J. R. DuBar, "Post-Miocene Stratigraphy, Central and Southern Atlantic Coastal Plain", (Utah State University Press, 275 p.), p. 179-190, 1974

DuBar, J. R., H. S. Johnson, Jr., B. Thom, and W. O. Hatchell, "Neogene Stratigraphy and Morphology, South Flank of the Cape Fear Arch, North and South Carolina", in R. W. Oaks and J. R. DuBar, "Post-Miocene Stratigraphy, Central and Southern Atlantic Coastal Plain" (Utah State University Press, 275 p.) p. 139-173, 1974

Ferguson, J. F. and D. M. Stewart, "Macroseismic Effects in North Carolina From the 1886 Charleston, S. C. Earthquake", Geological Society of America, Abstracts with Programs, Vol. 6, No. 4, p. 354, 1974

Fletcher, J. P., M. L. Sbar, and L. R. Sykes, "Seismic Zones and Travel Time Anomalies in Eastern North America Related to Fracture Zones Active in the Early Opening of the Atlantic", Abstract, Eos, Transactions, American Geophysical Union, Vol. 55, No. 4, p. 447, 1974

Hadley, J. B. and J. F. Devine, "Seismotectonic Map of the Eastern United States", U. S. Geological Survey Miscellaneous Field Studies Map MF-620, 1974

Higgins, B. B. and P. Popenoe, "A Geologic and Geophysical Study of the Charleston, South Carolina, Earthquake Zone", Earthquake Information Bulletin, Vol. 6, No. 6, p. 16-23, 1974

Marine, J. W. and G. E. Siple, "Buried Triassic Basin in Central Savannah River Area, South Carolina and Georgia", Geological Society of America Bulletin, Vol. 85, p. 311-320, 1974

McKee, J. H., "A Geophysical Study of Microearthquake Activity Near Bowman, South Carolina", Master's Thesis, Georgia Institute of Technology, Atlanta, 65 pp., 1974

Tarr, A. C. and K. W. King, "Preliminary Results From an Earthquake-Monitoring Survey of the Charleston-Summerville Area of South Carolina", Geological Society of America, Abstracts with Programs, Vol. 6, No. 4, p. 407, 1974

Tarr, A. C. and K. W. King, "South Carolina Seismic Program", U. S. Geological Survey Open-File Report 74-58, 15 p., 1974

1975

Ayers, R. L. and G. A. Bollinger, "A Study of Macroseismic and Microseismic Ground Motions in Virginia", Geological Society of America, Abstracts with Programs, Vol. 7, No. 4, p. 466, 1975

Bollinger, G. A., "A Catalog of Southeastern United States Earthquakes, 1754 Through 1974", Research Division Bulletin Vol. 101, Virginia Polytechnic Institute and State University, 68 p., 1975

Champion, J. W., Jr., "A Detailed Gravity Study of the Charleston, South Carolina, Epicentral Zone", Master's Thesis, Georgia Institute of Technology, Atlanta, 1975

Champion, J. W. and L. T. Long, "Bouguer Gravity Anomaly Map of the Charleston, South Carolina Vicinity", Geological Society of America, Abstracts with Programs, Vol. 7, No. 4, p. 477, 1975

Evernden, J. F., "Seismic Intensities, Size of Earthquakes and Related Parameters", Seismological Society of America Bulletin, Vol. 65, No. 5, p. 1287-1313, 1975

Forsyth, D. W. and S. Uyeda, "On the Relative Importance of the Driving Forces of Plate Motions", Geophysical Journal of the Royal Astronomical Society, Vol. 43, p.163-200, 1975

Kanamori, H. and D. L. Anderson, "Theoretical Basis of Some Empirical Relations in Seismology", Seismological Society of America Bulletin, Vol. 65, p. 1073-1095, 1975

Ketterer, W. P., "Aeromagnetic Map of Charleston and Vicinity, South Carolina", U. S. Geological Survey, Open-File Report, Scale: 1:250,000, 1975

Lister, C. R. B., "Gravitational Drive on Oceanic Plates Caused by Thermal Contraction", Nature, Vol. 257, p. 663-665, 1975

Popenoe, P., "The Charleston Earthquake; the Search for a Geologic Cause; New Magnetic and Gravity Data", Geological Society of America, Abstracts with Programs, Vol. 7, No. 4, p. 524, 1975

Rhodehamel, E. C., "Geophysical Logs From a Geologic Test Hole Near Charleston, S. C.", U. S. Geological Survey Open-File Report 75-247, 1 p., 1975

Talwani, P., D. T. Secor, and P. Scheffler, "Preliminary Results of Aftershock Studies Following the 2 August 1974 South Carolina Earthquake", Earthquake Notes, Vol. 46, p. 21-28, 1975

U. S. Geological Survey, "Aeromagnetic Map of Charleston and Vicinity, South Carolina", U. S. Geological Survey, Open-File Report, No. 75-590, Scale: 1:250,000, 1975

1976

Ackermann, H. D., "Exploring the Charleston, South Carolina Earthquake Area by Seismic Refraction", Geological Society of America, Abstracts with Programs, Vol. 8, No. 2, p. 121-122, 1976

Bollinger, G. A., "Reinterpretation of the Intensity Effects of the 1886 Charleston, South Carolina, Earthquake", Geological Society of America, Abstracts with Programs, Vol. 8, No. 2, p. 139-140, 1976

Bollinger, G. A. and C. W. Stover, "List of Intensities for the 1886 Charleston, South Carolina Earthquake", U. S. Geological Survey, Open-File Report, No. 76-66, 31 p., 1976

Brown, L. D. and J. E. Oliver, "Vertical Crustal Movements from Leveling Data and Their Relation to Geologic Structure in the Eastern United States", Review of Geophysics and Space Physics, Vol. 14, p. 13-35, 1976

Campbell, D., "Electric and Electromagnetic Soundings Near Charleston, South Carolina", Geological Society of America, Abstracts with Programs, Vol. 8, No. 2, p. 146, 1976

Higgins, B. B., J. P. Owens, P. Popenoe, and G. S. Gohn, "Structures in the Coastal Plain of South Carolina", Geological Society of America, Abstracts with Programs, Vol. 8, p. 195-196, 1976

LeGrand, H., "Hydrologic Implications of the 1886 Charleston Earthquake", Geological Society of America, Abstracts with Programs, Vol. 8, No. 2, p. 216, 1976

Long, L. T., "Speculations Concerning Southeastern Earthquakes, Mafic Intrusions, Gravity Anomalies and Stress Amplification", Earthquake Notes, Vol. 47, p. 29-35, 1976

- Long, L. T., P. Talwani, and S. R. Bridges, "Simple Bouguer Gravity Map of South Carolina", South Carolina Development Board, Division of Geology, Scale 1:500,000, 1976
- Phillips, J. D., "Magnetic Basement Near Charleston, South Carolina", Geological Society of America, Abstracts with Programs, Vol. 8, No. 2, p. 245, 1976
- Popenoe, P., J. D. Phillips, and B. B. Higgins, "Lithology and Structure of the Basement in the Charleston, South Carolina Area From Interpretation of Gravity and Magnetic Data", Geological Society of America, Abstracts with Programs, Vol. 8, No. 2, p. 248, 1976
- Rankin, D. W., "Appalachian Salients and Recesses: Late Precambrian Continental Breakup and the Opening of the Iapetus Ocean", Journal of Geophysical Research, Vol. 81, No. 32, p. 5605-5619, 1976
- Talwani, P. and D. Howell, "Crustal Structure of South Carolina - Some Speculations at Symposium of the Atlantic Continental Margin", Geological Society of America, Abstracts with Programs, Vol. 8, p. 284, 1976
- Tarr, A. C. and D. L. Carver, "Recent Seismicity in the Source Area of the 1886 Charleston, South Carolina Earthquake", Geological Society of America, Abstracts with Programs, Vol. 8, No. 2, p. 284-285, 1976
- U. S. Geological Survey, "Seismic Refraction in Charleston, South Carolina, Earthquake Area", Abstract, U. S. Geological Survey Professional Paper 1000, p. 64, 1976
- U.S. Geological Survey, "Aeromagnetic Maps of Parts of Georgia, South Carolina, and North Carolina", U.S. Geological Survey Open-File Report 76-181, 13 sheets, Scale 1:250,000, 1976
- U.S. Geological Survey, "Aeromagnetic Map of Parts of the Brunswick and Savannah 1° by 2° Quadrangles, Georgia and South Carolina", U.S. Geological Survey Open-File Report 76-155, Scale 1:250,000, 1976
- Visvanathan, T. R., "Periodicity of Historic Earthquakes in Charleston-Summerville Area", Geological Society of America, Abstracts with Programs, Vol. 8, No. 2, p. 292, 1976
- York, J. E. and J. E. Oliver, "Cretaceous and Cenozoic Faulting in Eastern North America", Geological Society of America Bulletin, Vol. 87, p. 1105-1114, 1976
- Ziagos, J. P., J. H. Sass, and R. J. Munroe, "Heat Flow Near Charleston, South Carolina", U. S. Geological Survey Open-File Report 76-148, 21 p., 1976

Zietz, I., P. Popenoe, and B. B. Higgins, "Regional Structure of the Southeastern United States as Interpreted From New Aeromagnetic Maps of Part of the Coastal Plain of North Carolina, South Carolina, Georgia and Alabama", Geological Society of America, Abstracts with Programs, Vol. 8, p. 307, 1976

1977

Ackermann, H. D., "Exploring the Charleston, South Carolina Earthquake Area With Seismic Refraction - A Preliminary Study", in D. W. Rankin, Studies Related to the Charleston, South Carolina Earthquake of 1886 - A Preliminary Report, U. S. Geological Survey Professional Paper 1028, p. 167-175, 1977

Bollinger, G. A., "Reinterpretation of the Intensity Data for the 1886 Charleston, South Carolina Earthquake", in D. W. Rankin, Studies Related to the Charleston, South Carolina Earthquake of 1886 - A Preliminary Report, U. S. Geological Survey Professional Paper 1028, p. 17-32, 1977

Bollinger, G. A. and T. R. Visvanathan, "The Seismicity of South Carolina Prior to 1886", in D. W. Rankin, Studies Related to the Charleston, South Carolina Earthquake of 1886 - A Preliminary Report, U. S. Geological Survey Professional Paper 1028, p. 33-42, 1977

Campbell, D. L., "Schlumberger Electric Soundings in the Charleston, South Carolina, Earthquake Area", U. S. Geological Survey Open-File Report 77-617, 30 p., 1977

Campbell, D. L., "Electric and Electromagnetic Soundings Near Charleston, South Carolina - A Preliminary Report", in D. W. Rankin, Studies Related to the Charleston, South Carolina Earthquake of 1886 - A Preliminary Report, U. S. Geological Survey Professional Paper 1028, p. 189-198, 1977

Carver, D., L. Turner, and A. C. Tarr, "South Carolina Seismological Data Report May 1974 - June 1975", U. S. Geological Survey Open-File Report 77-429, 66 p., 1977

Fletcher, J. B. and L. R. Sykes, "Earthquakes Related to Hydraulic Mining and Natural Seismic Activity in Western New York", Journal of Geophysical Research, Vol. 82, No. 26, p. 3767-3780, 1977

Gohn, G. S., B. B. Higgins, C. C. Smith, and J. P. Owens, "Lithostratigraphy of the Deep Corehole (Clubhouse Crossroads Corehole 1) Near Charleston, South Carolina", in D. W. Rankin, Studies Related to the Charleston, South Carolina Earthquake of 1886 - A Preliminary Report, U. S. Geological Survey Professional Paper 1028, p. 43-57, 1977

- Gottfried, D., C. S. Ansell, and L. J. Schwarz, "Geochemistry of Subsurface Basalt From the Deep Corehole (Clubhouse Crossroads Corehole 1) Near Charleston, South Carolina - Magma Type and Tectonic Implications", U. S. Geological Survey Professional Paper 1028, p. 91-113, 1977
- Hatcher, R. D., Jr., D. E. Howell, and P. Talwani, "Eastern Piedmont Fault System: Speculation on its Extent", Geology, Vol. 5, p. 636-640, 1977
- Hazel, J. E., L. M. Bybell, R. A. Christopher, N. O. Frederiksen, F. E. May, D. M. McLean, R. Z. Poore, C. C. Smith, N. F. Sohl, P. C. Valentine and R. J. Witmer, "Biostratigraphy of the Deep Corehole (Clubhouse Crossroads Corehole 1) Near Charleston, South Carolina", in D. W. Rankin, Studies Related to the Charleston, South Carolina Earthquake of 1886 - A Preliminary Report, U. S. Geological Survey Professional Paper 1028, p. 71-89, 1977
- Kane, M. F., "Correlation of Major Eastern Earthquake Centers With Mafic/Ultramafic Masses", in D. W. Rankin, Studies Related to the Charleston, South Carolina Earthquake of 1886 - A Preliminary Report, U. S. Geological Survey Professional Paper 1028, p. 199-204, 1977
- Lessing, P. and R. B. Erwin, "Landslides in West Virginia", Reviews of Engineering Geology, Vol. 3, p. 245-254, 1977
- Long, L. T. and J. W. Champion, Jr., "Bouguer Gravity Map of the Summerville-Charleston, South Carolina Epicentral Zone and Tectonic Implications", in D. W. Rankin, Studies Related to the Charleston, South Carolina Earthquake of 1886 - A Preliminary Report, U. S. Geological Survey Professional Paper 1028, p. 151-166, 1977
- Phillips, J. D., "Magnetic Basement Near Charleston, South Carolina - A Preliminary Report", in D. W. Rankin, Studies Related to the Charleston, South Carolina Earthquake of 1886 - A Preliminary Report, U. S. Geological Survey Professional Paper 1028, p. 139-149, 1977
- Popenoe, P. and I. Zietz, "The Nature of the Geophysical Basement Beneath the Coastal Plain of South Carolina and Northeastern Georgia", in D. W. Rankin, Studies Related to the Charleston, South Carolina Earthquake of 1886 - A Preliminary Report, U. S. Geological Survey Professional Paper 1028, p. 119-137, 1977
- Rankin, D. W., "Studies Related to the Charleston, South Carolina Earthquake of 1886 - Introduction and Discussion", in D. W. Rankin, Studies Related to the Charleston, South Carolina Earthquake of 1886 - A Preliminary Report, U. S. Geological Survey Professional Paper 1028, p. 1-15, 1977

- Sass, J. H. and J. P. Ziasos, "Heat Flow From a Corehole Near Charleston, South Carolina", in D. W. Rankin, Studies Related to the Charleston, South Carolina Earthquake of 1886 - A Preliminary Report, U. S. Geological Survey Professional Paper 1028, p. 115-117, 1977
- Talwani, P., "An Intensity Survey of the April 28, 1975, Summerville, South Carolina Earthquake", Bulletin of the Seismological Society of America, Vol. 67, p. 547-549, 1977
- Talwani, P., "A Preliminary Shallow Crustal Model Between Columbia and Charleston, South Carolina Determined From Quarry Blast Monitoring and Other Geophysical Data", in D. W. Rankin, Studies Related to the Charleston, South Carolina Earthquake of 1886 - A Preliminary Report, U. S. Geological Survey Professional Paper 1028, p. 177-187, 1977
- Tarr, A. C., "Recent Seismicity Near Charleston, South Carolina, and Its Relationship to the August 31, 1886 Earthquake", in D. W. Rankin, Studies Related to the Charleston, South Carolina Earthquake of 1886 - A Preliminary Report, U. S. Geological Survey Professional Paper 1028, p. 43-57, 1977
- Turcott, D. L., J. L. Ahern, and J. M. Bird, "The State of Stress at Continental Margins", Tectonophysics, Vol. 42, p. 1-28, 1977
- Winker, C. D. and J. D. Howard, "Correlation of Tectonically Deformed Shorelines on the Southern Atlantic Coastal Plain", Geology, Vol. 5, p. 123-127, 1977
- Zoback, M. D. and J. H. Healy, "In-Situ Stress Measurements Near Charleston, South Carolina", Abstract, Eos, Transactions, American Geophysical Union, Vol. 58, No. 6, p. 493, 1977
- 1978
- Ackermann, H. D., D. L. Campbell and J. D. Phillips, "Upper-Crustal Structures Near Charleston, South Carolina", Abstract, U. S. Geological Survey Professional Paper 1100, p. 171, 1978
- Ackermann, H. D., D. L. Campbell, and J. D. Phillips, "Geophysical Model of Upper-crustal Structures Near Charleston, South Carolina", Geological Society of America Abstracts With Programs, Vol. 10, No. 4, p. 161, 1978
- Amick, D., D. Stevenson, and P. Talwani, "Seismic Refraction Studies Near Summerville, South Carolina", Abstract, Eos, Transactions American Geophysical Union, Vol. 59, No. 4, p. 390, 1978
- Campbell, D. L., "Investigation of the Stress-concentration Mechanism for Intraplate Earthquakes", Geophysical Research Letters, Vol. 5, No. 6, p. 477-479, 1978

- Campbell, D. L., "Stress-concentration Mechanism for Earthquakes in the Charleston, South Carolina, Area", Geological Society of America Abstracts With Programs, Vol. 10, No. 4, p. 161, 1978
- Fletcher, J. B., M. L. Sbar, and L. R. Sykes, "Seismic Trends and Travel Time Residuals in Eastern North America and Their Tectonic Implications", Geological Society of America Bulletin, Vol. 89, p. 1656-1676, 1978
- Force, L. M., "Geological Studies of the Charleston, South Carolina Area - Elevation Contours on the Top of the Cooper Formation", U. S. Geological Survey Miscellaneous Field Studies Map, MF-1021A, Scale 1:250,000, 1978
- Force, L. M., "Geological Studies of the Charleston, South Carolina Area - Thickness of Overburden", U. S. Geological Survey Miscellaneous Field Studies Map, MF-1021B, Scale 1:250,000, 1978
- Force, L. M., "Pleistocene and Holocene Sedimentary Deposits in the Charleston, South Carolina, Area; Paleoenvironments and Genetic Associations", Geological Society of America Abstracts With Programs, Vol. 10, No. 4, p. 169, 1978
- Gohn, G. S., L. M. Bybell, C. C. Smith, and J. P. Owens, "Preliminary Stratigraphic Cross Sections of Atlantic Coastal Plain Sediments of the Southeastern United States - Cenozoic Sediments Along the South Carolina Coastal Margin", U. S. Geological Survey Map MF-1015-B, 1978
- Gohn, G. S., R. A. Christopher, C. C. Smith, and J. P. Owens, "Preliminary Stratigraphic Cross Sections of Atlantic Coastal Plain Sediments of the Southeastern United States - Cretaceous Sediments Along the South Carolina Coastal Margin", U. S. Geological Survey Map 1015-A, 1978
- Gohn, G. S., D. Gottfried, M. A. Lanphere, and B. B. Higgins, "Regional Implications of Triassic or Jurassic Age for Basalt and Sedimentary Red Beds in the South Carolina Coastal Plain", Science, Vol. 202, No. 4370, p. 887-890, 1978
- Gregory, R. G., "A Geothermal Study of Alabama, Georgia and South Carolina", Master's Thesis, University of Florida, Gainesville, 1978
- Hager, H., "Oceanic Plate Motions Driven by Lithosphere Thickening and Subducted Slabs", Nature, Vol. 276, p. 156-159, 1978
- Higgins, B. B., G. S. Cohn, and L. M. Bybell, "Subsurface Geologic Evidence for Normal Faults in the South Carolina Coast Plain Near Charleston", Geological Society of America Abstracts With Programs, Vol. 10, No. 4, p. 171, 1978

- Langer, C. J., "Charleston, South Carolina", Abstract, U. S. Geological Survey Professional Paper 1100, p. 261, 1978
- McKeown, F. A., "Hypothesis: Many Earthquakes in the Central and Southeastern United States are Causally Related to Mafic Intrusive Bodies", U. S. Geological Survey Journal of Research, Vol. 6, p. 41-50, 1978
- Phillips, J. D., D. L. Daniels, I. Zietz, and P. Popenoe, "Geophysical Studies of the Charleston South Carolina, Area; Onshore Aeromagnetic Map", U. S. Geological Survey, Miscellaneous Field Study Map No. MF-1022-A, Scale 1:250,000, 1978
- Rankin, D. W., "The Charleston, South Carolina, Earthquake of 1886 and the Blake Spur Fracture Zone", Geological Society of America Abstracts With Programs, Vol. 10, No. 7, p. 475-476, 1978
- Rankin, D. W., P. Popenoe, and K. Klitgord, "The Tectonic Setting of Charleston, South Carolina", Geological Society of America Abstracts With Programs, Vol. 10, No. 4, p. 195, 1978
- Sykes, L. R., "Intraplate Seismicity, Reactivation of Preexisting Zones of Weakness, Alkaline Magmatism, and Other Tectonism Postdating Continental Fragmentation", Reviews of Geophysics and Space Physics, Vol. 16, p. 621-687, 1978
- Visvanathan, T. R., "Earthquake Prediction For the Charleston-Summerville Area of South Carolina", Eos, Transactions, American Geophysical Union, Vol. 59, No. 4, p. 331, 1978
- Zoback M. D., J. H. Healy, G. S. Gohn, and B. B. Higgins, "In-Situ Stress in the South Carolina Coastal Plain Near Charleston", Geological Society of America Abstracts With Programs, Vol. 10, No. 4, p. 204, 1978
- Zoback, M. D., J. H. Healy, J. C. Roller, G. S. Gohn, and B. B. Higgins, "Normal Faulting and In-Situ Stress in the South Carolina Coastal Plain Near Charleston", Geology, Vol. 6, No. 3, p. 147-152, 1978
- Zoback, M., J. Roller, and J. Healy, "In-situ Measurement of the Earth's Stress Field", Earthquake Information Bulletin, Vol. 10, No. 6, p. 214-219, 1978

1979

- Amick, D. C., "Crustal Structure Studies in the South Carolina Coastal Plain", Master's Thesis, University of South Carolina, Columbia, 1979

- Bagwell, J. B. and D. Amick, "Isoseismal Intensity Studies of 1977-1978 Charleston-Summerville Earthquakes", Abstract, Earthquake Notes, Vol. 50, No. 3, p. 12, 1979
- Behrendt, J. C., R. M. Hamilton, and H. D. Ackermann, "Multichannel Seismic Reflection Profiles in the Charleston, South Carolina, Area", Abstract, Eos, Transactions, American Geophysical Union, Vol. 60, No. 46, p. 885, 1979
- Brown, L., D. Albaugh, J. Brewer, F. Cook, L. Jensen, S. Kaufman, G. Long, J. Oliver, S. Schilt, and D. Steiner, "Structure of the Continental Crust: New Results From COCORP Seismic Reflection Profiling", Abstract, Eos, Transactions, American Geophysical Union, Vol. 60, No. 18, p. 313, 1979
- Cook, F. A., D. S. Albaugh, L. D. Brown, S. Kaufman, and J. E. Oliver, "Thin-skinned Tectonics in the Crystalline Southern Appalachians: COCORP Seismic Reflection Profiling of the Blue Ridge and Piedmont", Geology, Vol. 5, p. 563-567, 1979
- Force, L. M., "Investigation of Stream Morphology in the Seismically Active Charleston, South Carolina, Area; A Progress Report", Geological Society of America Abstracts With Programs, Vol. 11, No. 4, p. 179, 1979
- Harris, L. D., and K. C. Bayer, "Sequential Development of the Appalachian Orogen Above a Master Decollement - A Hypothesis", Geology, Vol. 7, p. 568-572, 1979
- Logan, W. R., D. C. Amick, and P. Talwani, "Seismic Refraction Survey in Bowman Area, South Carolina", Abstract, Earthquake Notes, Vol. 50, No. 3, p. 30, 1979
- Long, L. T., "The Carolina Slate Belt - Evidence of a Continental Rift Zone", Geology, Vol. 7, p. 180-184, 1979
- Lyttle, P. T., G. S. Gohn, B. B. Higgins, and D. S. Wright, "Vertical Crustal Movements in the Charleston, South Carolina - Savannah, Georgia Area", Tectonophysics, Vol. 52, No. 1-4, p. 183-189, 1979
- Nishenko, S. P. and L. R. Sykes, "Fracture Zones, Mesozoic Rifts and the Tectonic Setting of the Charleston, South Carolina Earthquake of 1886", Abstract, Eos, Transactions, American Geophysical Union, Vol. 60, No. 18, p. 310, 1979
- Richardson, R. M., S. C. Solomon, and N. H. Sleep, "Tectonic Stress in the Plates", Reviews of Geophysics and Space Physics, Vol. 17, p. 981-1020, 1979
- Schilt, S., L. Brown, S. Kaufman, and J. Oliver, "Results of Deep Crustal Seismic Reflection Profiling in the Atlantic Coastal Plain Near Charleston, South Carolina", Abstract, Eos, Transactions, American Geophysical Union, Vol. 60, No. 18, p. 313, 1979

Talwani, P., D. C. Amick, and R. Logan, "A Model to Explain the Intraplate Seismicity in the South Carolina Coastal Plain", Abstract, Eos, Transactions, American Geophysical Union, Vol. 60, p. 311, 1979

Ward, L. W., B. W. Blackwelder, G. S. Gohn, and R. Z. Poore, "Stratigraphic Revision of Eocene, Oligocene and Lower Miocene Formations of South Carolina", South Carolina Geological Survey Geologic Notes, Vol. 23, No. 1, p. 2-32, 1979

1980

Ackermann, H. D., J. C. Behrendt, and R. M. Hamilton, "Seismic Reflection Evidence, Seismicity, and Geologic Structure at Charleston, South Carolina", Abstract, U. S. Geological Survey Professional Paper 1175, p. 262, 1980

Amick, D. C., "A Reinterpretation of the Meizoseismal Area of the 1886 Charleston Earthquake", Abstract, Eos, Transactions, American Geophysical Union, Vol. 61, No. 17, p. 289, 1980

Behrendt, J. C., R. M. Hamilton, H. D. Ackermann, V. J. Henry, and K. C. Bayer, "Seismic Reflection Evidence for Cenozoic Reactivation of Older Faults on Land and Offshore in the Area of the Charleston, South Carolina, 1886 Earthquake", Geological Society of America Abstracts With Programs, Vol. 12, No. 7, p. 385-386, 1980

Kanamori, h., "The State of Stress in the Earth's Lithosphere", in A. M. Dziewonski and E. Bosch, Physics of the Earth's Interior, Proceedings of the International School of Physics "Enrico Fermi" Course, (North-Holland Publishing Co., New York), p. 531-554, 1980

Kron, A., and G. Heiker, "Geothermal Map of the Conterminous United States", Los Alamos Scientific Laboratory, Los Alamos, New Mexico, 1980

McCartan, L., R. E. Weems, and E. M. Lemon, "The Wando Formation (Upper Pleistocene) in the Charleston, South Carolina Area", U. S. Geological Survey Bulletin, Vol. 1502-A, p. 110-116, 1980

McKenzie, D., A. Watts, B. Parsons, and M. Roufousse, "Plan Form of Mantle Convection Beneath the Pacific Ocean", Nature, Vol. 288, p. 442-446, 1980

Ormsby, M. R., "Probability That Another Intensity X⁺ Event Could Occur in the Southeast During a 200 Year Period", Master's Thesis, Georgia Institute of Technology, Atlanta, 1980

Rhea, B. S., "Charleston, South Carolina", U. S. Geological Survey Professional Paper 1175, p. 264, 1980

Tyson, N. S., F. E. Riggle, I. Zietz, and D. L. Daniels, "Aeromagnetic Map of Northeast South Carolina", U. S. Geological Survey Open-File Report 80-2020, Scale 1:250,000, 1980

Visvanathan, T. R., "Earthquakes in South Carolina, 1698-1975", South Carolina Geological Survey Bulletin Vol. 40, 61 p., 1980

Wentworth, C. M. and M. Mergner-Keefer, "Atlantic-Coast Reverse-Fault Domain; Probable Source of East Coast Seismicity", Geological Society of America Abstracts With Programs, Vol. 12, No. 7, p. 547, 1980

Zietz, I. and M. W. Higgins, "Interpretation of a New Aeromagnetic Map of the Southeastern Coastal Plain, U.S.A.", Geological Society of America Abstracts With Programs, Vol. 12, No. 7, p. 554, 1980

Zoback, M. L. and M. D. Zoback, "State of Stress in the Conterminous United States", Journal of Geophysical Research, Vol. 85, p. 6113-6156, 1980

1981

Armbruster, J. G. and L. Seeber, "Seismicity and Back-Slip on the Detachment of the Southern Appalachians", Abstract, Eos, Transactions, American Geophysical Union, Vol. 62, p. 403, 1981

Baldelli, J. A. and L. A. Lee, "Correction of Seismic Deficiencies for the Veterans Administration Medical Center, Charleston, South Carolina", in J.E. Beavers Proceedings of Earthquakes and Earthquake Engineering: The Eastern United States, (Ann Arbor Science Publishers, Inc., Ann Arbor, M^l), p. 817-835, 1981

Barstow, N. L., K. G. Brill, O. W. Nuttli, and P. W. Pomeroy, "An Approach to Seismic Zonation for Siting Nuclear Electric Power Generating Facilities in the Eastern United States", NUREG/CR-1577, U. S. Nuclear Regulatory Commission, 1981

Behrendt, J. C. and R. M. Hamilton, "New Multichannel Seismic Reflection Profiles in South Carolina and Implications Concerning the Origin of the Charleston 1886 Earthquake", Abstract, Earthquake Notes, Vol. 52, No. 3, p. 9, 1981

Behrendt, J. C. and R. M. Hamilton, "Could a Charleston-Type Earthquake Occur Elsewhere Along the East Coast of North America?", Geological Society of America Abstracts With Programs, Vol. 13, No. 7, p. 406, 1981

- Behrendt, J. C., R. M. Hamilton, and Anonymous, "Preliminary Interpretation of a Seismic Reflection Profile Crossing the South Carolina Coastal Plain and Piedmont, and Implications Concerning the Origin of the Charleston, 1886, Earthquake", Abstract, Eos, Transactions, American Geophysical Union, Vol. 62, No. 45, p. 984, 1981
- Behrendt, J. C., R. M. Hamilton, H. D. Ackermann, and V. J. Henry, "Cenozoic Faulting in the Vicinity of the Charleston, South Carolina, 1886 Earthquake", Geology, Vol. 9, No. 3, p. 117-122, 1981
- Cook, F. A., L. D. Brown, S. Kaufman, J. E. Oliver, and T. A. Petersen, "COCORP Seismic Profiling of the Appalachian Orogen Beneath the Coastal Plain of Georgia", Geological Society of America Bulletin, Part I, Vol. 92, p. 738-748, 1981
- Coruh, C., J. K. Costain, J. C. Behrendt, R. M. Hamilton, and Anonymous, "New Reflection Seismic Evidence for Deformation of Mesozoic Sediments Near Charleston, South Carolina", Geological Society of America Abstracts With Programs, Vol. 13, No. 7, p. 431, 1981
- Cronin, T. M., "Rates and Possible Causes of Neotectonic Vertical Crustal Movements of the Emerged Southeastern United States Atlantic Coastal Plain", Geological Society of America Bulletin, Vol. 92, No. 11, p. 812-833, 1981
- Earthquake Information Bulletin, "Assessing the Risk of Earthquakes in the Eastern United States", Vol. 13, No. 5, p. 175-178, 1981
- Hamilton, R. M., "Geologic Origin of Eastern United States Seismicity", in J. E. Beavers, Proceedings of Earthquakes and Earthquake Engineering: the Eastern United States, (Ann Arbor Science Publishers, Inc., Ann Arbor, MI), p. 3-23, 1981
- Ormsby, M. R. and Anonymous, "Probability That Another Intensity X Event Could Occur in the Southeast During a 200 Year Period", Abstract, Earthquake Notes, Vol. 52, No. 1, p. 74, 1981
- Schilt, F. S., "Studies of Continental and Oceanic Crust From Seismic Geodetic, and Magnetic Observations", Doctoral Thesis, Cornell University, Ithaca, 206 p., 1981
- Seeber, L. and J. G. Armbruster, "The 1886 Earthquake and Intraplate Detachments", Geological Society of America Abstracts With Programs, Vol. 13, No. 7, p. 550, 1981

- Seeber, L. and J. G. Armbruster, "The 1886 Charleston, South Carolina Earthquake and the Appalachian Detachment", Journal of Geophysical Research, Vol. 86, No. 9, p. 7874-7894, 1981
- Simon, C., "Quakes in the East", Science News, Vol. 120, No. 15, p. 232-234, 1981
- Tarr, A. C., P. Talwani, S. Rhea, D. Carver and D. Amick, "Results of Recent South Carolina Seismological Studies", Bulletin of Seismological Society of America, Vol. 71, p. 1883-1902, 1981
- Visvanathan, T. R. and Anonymous, "Earthquake Activity in the Charleston-Summerville Area", Abstract, Bulletin of the South Carolina Academy of Science, 1981
- Wentworth, C. M. and M. Mergner-Keefer, "Reverse Faulting Along the Eastern Seaboard and the Potential for Large Earthquakes", in J.E. Beavers Proceedings of Earthquakes and Earthquake Engineering: the Eastern United States, (Ann Arbor Science Publishers, Inc., Ann Arbor, MI), p. 109-128, 1981
- Wentworth, C. M. and M. Mergner-Keefer, "Regenerate Faults of Small Cenozoic Offset; Probable Earthquake Sources in the Southeastern United States", U. S. Geological Survey Open-File Report 81-0356, 37 p., 1981
- Yang, J. P. and Y. P. Aggarwal, "Seismotectonics of Northeastern United States and Adjacent Canada", Journal of Geophysical Research, Vol. 86, p. 4981-4998, 1981

1982

- Ackermann, H. D., "Seismic Refraction Study in the Area of the Charleston, South Carolina, 1886 Earthquake", Abstract, U. S. Geological Survey Open-File Report 82-0134, p. 11-12, 1982
- Behrendt, J. C. and R. M. Hamilton, "Record Sections For Multichannel Seismic Reflection Data in the Areas of the Charleston, South Carolina, 1886 Earthquake", U. S. Geological Survey Open-File Report 82-0311, 5 p., 1982
- Behrendt, J. C., R. M. Hamilton, H. D. Ackermann, V. J. Henry and K. C. Bayer, "Marine Multichannel Seismic Reflection Evidence of Cenozoic Faulting and Deep Crustal Structure Near Charleston, South Carolina", Abstract, U. S. Geological Survey Open-File Report 82-0134, p. 19-20, 1982

- Bollinger, G. A., "Speculations on the Nature of Charleston, South Carolina, Seismicity", Abstract, U. S. Geological Survey Open-File Report 82-0134, p. 36-37, 1982
- Bollinger, G. A., "Southeastern United States Seismicity; Results From Recent Network Monitoring", in M. Sherif, Proceedings Third International Earthquake Microzonation Conference, Vol. I, (U. S. National Science Foundation, Washington, DC), p. 39-52, 1982
- Chowns, T. M. and C. T. Williams, "Pre-Cretaceous Rocks Beneath the Georgia Coastal Plain; Regional Implications", in G. S. Gohn, Studies Related to the Charleston, South Carolina Earthquake of 1886; Tectonics and Seismicity, Collected Abstracts, U. S. Geological Survey Open-File Report 82-0134, p. 23-24, 1982
- Colquhoun, D. D., I. D. Woollen, D. D. Van Nieuwenhuise, G. G. Padgett, R. W. Oldham, P. O. Howell, J. W. Bishop, and D. C. Boyland, "Tectonic Framework Development and Initial Glacio-Eustatic Sea Level Change, East Georgia Embayment, U.S.A.", Geological Society of America Abstracts With Programs, Vol. 14, No. 7, p. 466, 1982
- Coruh, C., J. K. Costain, J. H. Behrendt, and R. A. Hamilton, "Mesozoic Faulting in the Charleston, South Carolina Region: New Evidence From Seismic Reflection Data", unpublished, 1982
- Daniels, D. L., I. Zietz, and P. Popenoe, "Distribution of Subsurface Lower Mesozoic Rocks in the Southeastern United States, as Interpreted From Regional Aeromagnetic and Gravity Maps", in G. S. Gohn, Studies Related to the Charleston, South Carolina Earthquake of 1886; Tectonics and Seismicity, Collected Abstracts, U. S. Geological Survey Open-File Report 82-0134, p. 21-22, 1982
- Dewey, J. W., "Relocation of Instrumentally Recorded Pre-1974 Earthquakes in the South Carolina Region", in G. S. Gohn, Studies Related to the Charleston, South Carolina Earthquake of 1886; Tectonics and Seismicity, Collected Abstracts, U. S. Geological Survey Open-File Report 82-0134, p. 31, 1982
- Dillon, W. P., K. D. Klitgord, and C. K. Paull, "Mesozoic Development and Structure of the Continental Margin off South Carolina", in G. S. Gohn, Studies Related to the Charleston, South Carolina Earthquake of 1886; Tectonics and Seismicity, Collected Abstracts, U. S. Geological Survey Open-File Report 82-0134, p. 27, 1982

- Dillon, W. P. and L. D. McGinnis, "Basement Structure Indicated by Seismic Refraction Measurements, Offshore South Carolina and Adjacent Areas", in G. S. Gohn, Studies Related to the Charleston, South Carolina Earthquake of 1886; Tectonics and Seismicity, Collected Abstracts, U. S. Geological Survey Open-File Report 82-0134 p. 28, 1982
- Dooley, R. E. and J. M. Wampler, "Potassium-Argon Relations in Diabase Dikes of Georgia; the Influence of Excess Argon-40 on the Geochronology of Early Mesozoic Igneous and Tectonic Events", in G. S. Gohn, Studies Related to the Charleston, South Carolina Earthquake of 1886; Tectonics and Seismicity, Collected Abstracts, U. S. Geological Survey Open-File Report 82-0134, p. 25-26, 1982
- Fleitout, L. and C. Froidevaux, "Tectonics and Topography for a Lithosphere Containing Density Heterogeneities", Tectonics, Vol. 1, p. 21-56, 1982
- Force, E. R., A. E. Grosz, P. J. Loferski, and A. H. Maybin, "Aeroradioactivity Maps in Heavy-Mineral Exploration - Charleston, South Carolina Area", U. S. Geological Survey Professional Paper 1218, 19 p., 1982
- Gohn, G. S., "Geology of the Basement Rocks Near Charleston, South Carolina; Data From Detrital Rock Fragments in Lower Mesozoic (?) Rocks in Clubhouse Crossroads Test Hole 3", in G. S. Gohn, Studies Related to the Charleston, South Carolina Earthquake of 1886; Tectonics and Seismicity, Collected Abstracts, U. S. Geological Survey Open-File Report 82-0134, p. 9-10, 1982
- Gohn, G. S., B. B. Houser and R. R. Schneider, "Geology of the Lower Mesozoic(?) Sedimentary Rocks in Clubhouse Crossroads Test Hole 3, Near Charleston, South Carolina", in G. S. Gohn, Studies Related to the Charleston, South Carolina Earthquake of 1886; Tectonics and Seismicity, Collected Abstracts, U. S. Geological Survey Open-File Report 82-0134, p. 7-8, 1982
- Gottfried, D., C. S. Ansell, and G. R. Byerly, "Geochemistry and Tectonic Significance of Subsurface Basalts Near Charleston, South Carolina; Clubhouse Crossroads Test Holes 2 and 3", in G. S. Gohn, Studies Related to the Charleston, South Carolina Earthquake of 1886; Tectonics and Seismicity, Collected Abstracts, U. S. Geological Survey Open-File Report 82-0134, p. 3-4, 1982
- Greene, M. R. and P. L. Gori, "Earthquake Hazards Information Dissemination; A Study of Charleston, South Carolina", U. S. Geological Survey Open-File Report 82-0233, 61 p., 1982

- Hamilton, R. M., "Geologic Setting of Seismicity in Eastern North America", Geological Society of America Abstracts With Programs, Vol. 14, No. 1-2, p. 22-23, 1982
- Hamilton, R. M., J. C. Behrendt, and H. D. Ackermann, "Land Multichannel Seismic Reflection Evidence For Tectonic Features Near Charleston, South Carolina", in G. S. Gohn, Studies Related to the Charleston, South Carolina Earthquake of 1886; Tectonics and Seismicity, Collected Abstracts, U. S. Geological Survey Open-File Report 82-0134, p. 17-18, 1982
- Hazel, J. E., L. E. Edwards, G. S. Gohn and E. M. Lemon, "Geology of Tertiary Sediments Near the Cooke Fault, Charleston, South Carolina", U. S. Geological Survey Professional Paper 1375, p. 53, 1982
- Illies, J. H., "Der Hohenzollerngraben und Intraplatten-Seismizität Infolge Vergitterung Lamellarer Scherung mit Einer Riftstruktur", Oberrhein. Geol. Abh., Vol. 31, p. 47-78, 1982
- Iverson, W. P. and S. B. Smithson, "Master Decollement Root Zone Beneath the Southern Appalachians and Crustal Balance", Geology, Vol. 10, No. 5, p. 241-245, 1982
- Klitgord, K. D., W. P. Dillon, and P. Popenoe, "Mesozoic Tectonics of the Southeastern United States Coastal Plain and Continental Margin", in G. S. Gohn, Studies Related to the Charleston, South Carolina Earthquake of 1886; Tectonics and Seismicity, Collected Abstracts, U. S. Geological Survey Open-File Report 82-0134, p. 29-30, 1982
- Lanphere, M. A., "Argon-40/Argon-39 Ages of Basalt From Clubhouse Crossroads Test Hole 2 Near Charleston, South Carolina", in G. S. Gohn, Studies Related to the Charleston, South Carolina Earthquake of 1886; Tectonics and Seismicity, Collected Abstracts, U. S. Geological Survey Open-File Report 82-0134, p. 5, 1982
- Meissner, R. and J. Strehlau, "Limits of Stress in Continental Crusts and the Relation to the Depth-Frequency Distribution of Shallow Earthquakes", Tectonics, Vol. 1, p. 73-89, 1982
- Phillips, J. D., "Paleomagnetic Investigations of the Clubhouse Crossroads Basalt", in G. S. Gohn, Studies Related to the Charleston, South Carolina Earthquake of 1886; Tectonics and Seismicity, Collected Abstracts, U. S. Geological Survey Open-File Report 82-0134, p. 6, 1982
- Sanders, A. E., R. E. Weems, and E. M. Lemon, "The Chandler Bridge Formation - A New Oligocene Stratigraphic Unit in the Lower Coastal Plain of South Carolina", U. S. Geological Survey Bulletin, Vol. 1529-H, p. 105-124, 1982

- Schilt, F. S., L. D. Brown, J. E. Oliver, and S. Kaufman, "Subsurface Structure Near Charleston, South Carolina; Results of COCORP Reflection Profiling in the Atlantic Coastal Plain", in G. S. Gohn, Studies Related to the Charleston, South Carolina Earthquake of 1886; Tectonics and Seismicity, Collected Abstracts, U. S. Geological Survey Open-File Report 82-0134, p. 15-16, 1982
- Seeber, L., J. G. Armbruster, and G. A. Bollinger, "Large-Scale Patterns of Seismicity Before and After the 1886 South Carolina Earthquake", Geology, Vol. 10, No. 7, p. 382-386, 1982
- Talwani, P., "Internally Consistent Pattern of Seismicity Near Charleston, South Carolina", Geology, Vol. 10, No. 12, p. 654-658, 1982
- Talwani, P. and D. J. Colquhoun, "The Ashley River Fault and the Charleston Earthquakes", Abstract, Eos, Transactions, American Geophysical Union, Vol. 63, p. 1025, 1982
- Tarr, A. C. and S. Rhea, "Seismicity Near Charleston, South Carolina, March 1973 to December 1979", in G. S. Gohn, Studies Related to the Charleston, South Carolina Earthquake of 1886; Tectonics and Seismicity, Collected Abstracts, U. S. Geological Survey Open-File Report 82-0134, p. 32-33, 1982
- U. S. Geological Survey and Society of Exploration Geophysicists, "Composite Magnetic Anomaly Map of the United States, Part A: Conterminous United States", Map GP 954-A, U. S. Geological Survey, Scale 1:1,250,000, 2 sheets, 1982
- Valentine, P. C., "Upper Cretaceous Subsurface Stratigraphy and Structure of Coastal Georgia and South Carolina", U. S. Geological Survey Professional Paper 1222, 33 p., 1982
- Weems, R. E., E. M. Lemon, Jr., L. McCartan, L. M. Bybell, and A. E. Sanders, "Recognition and Formalization of the Pliocene "Goose Creek Phase" in the Charleston, South Carolina Area", U. S. Geological Survey Bulletin Vol. 1529-H, p. 137-148, 1982
- Wentworth, C. M. and M. Mergner-Keefer, "Regenerate Faults of Small Cenozoic Offset; Probable Earthquake Sources in the Southeastern United States", in G. S. Gohn, Studies Related to the Charleston, South Carolina Earthquake of 1886; Tectonics and Seismicity, Collected Abstracts, U. S. Geological Survey Open-File Report 82-0134, p. 34-35, 1982
- Williams, H. and R. D. Hatcher, Jr., "Suspect Terranes and Accretionary History of the Appalachian Orogen", Geology, Vol. 10, p. 530-536, 1982

Yantis, B. R., J. K. Costain, and H. D. Ackermann, "A Reflection Seismic Study Near Charleston, South Carolina", in G. S. Gohn, Studies Related to the Charleston, South Carolina Earthquake of 1886; Tectonics and Seismicity, Collected Abstracts, U. S. Geological Survey Open-File Report 82-0134, p. 13-14, 1982

1983

Ackermann, H. D., "Seismic-Refraction Study in the Area of the Charleston, South Carolina, 1886 Earthquake", in G. S. Gohn, Studies Related to the Charleston, South Carolina Earthquake of 1886 - Tectonics and Seismicity, U. S. Geological Survey Professional Paper 1313, p. F1-F20, 1983

Algermissen, S. T., "Probability of Damaging Earthquake Ground Motions in the Eastern United States", in W. W. Hays and P. L. Gori, Proceedings of Conference XX, A Workshop on "The 1886 Charleston, South Carolina, Earthquake and its Implications for Today", U. S. Geological Survey Open-File Report 83-843, p. 51-54, 1983

Armbruster, J. G. and L. Seeber, "A Broad Region of High Seismicity Following the 1886 South Carolina Earthquake", Abstract, Eos, Transactions, American Geophysical Union, Vol. 64, p. 266, 1983

Armbruster, J. G. and L. Seeber, "1886-1889 "Aftershocks" of the Charleston, South Carolina, Earthquake; a Regional Burst of Seismicity", in W. W. Hays and P. L. Gori, Proceedings of Conference XX, A Workshop on "The 1886 Charleston, South Carolina, Earthquake and its Implications for Today", U. S. Geological Survey Open-File Report 83-843, p. 107-116, 1983

Barosh, P. J., "Use of Seismicity and Tectonic Framework to Define the Seismic Hazard in the Region Encompassing Charleston, South Carolina", in W. W. Hays and P. L. Gori, Proceedings of Conference XX, A Workshop on "The 1886 Charleston, South Carolina, Earthquake and its Implications for Today", U. S. Geological Survey Open-File Report 83-843, p. 380-390, 1983

Basham, P. W. and J. Adams, "Earthquakes on the Continental Margin of Eastern Canada; Need Future Large Events Be Confined to the Locations of Large Historical Events?", in W. W. Hays and P. L. Gori, Proceedings of Conference XX, A Workshop on "The 1886 Charleston, South Carolina, Earthquake and its Implications for Today", U. S. Geological Survey Open-File Report 83-843, p. 456-467, 1983

- Baswell, J. B., "The Current State of Earthquake Hazard Awareness in the Southeastern United States", in W. W. Hays and P. L. Gori, Proceedings of Conference XX, A Workshop on "The 1886 Charleston, South Carolina, Earthquake and its Implications for Today", U. S. Geological Survey Open-File Report 83-843, p. 315-322, 1983
- Behrendt, J. C., "Did Movement of a Northeast Trending Listric Fault Near the Southeast Edge of the Jedburg Triassic-Jurassic(?) Basin Cause the Charleston, South Carolina, 1886 Earthquake?", in W. W. Hays and P. L. Gori, Proceedings of Conference XX, A Workshop on "The 1886 Charleston, South Carolina, Earthquake and its Implications for Today", U. S. Geological Survey Open-File Report 83-843, p. 126-131, 1983
- Behrendt, J. C., R. M. Hamilton, H. D. Ackermann, V. J. Henry and K. C. Bayer, "Marine Multichannel Seismic-Reflection Evidence for Cenozoic Faulting and Deep Crustal Structure Near Charleston, South Carolina", in G. S. Gohn, Studies Related to the Charleston, South Carolina Earthquake of 1886 - Tectonics and Seismicity, U. S. Geological Survey Professional Paper 1313, p. J1-J29, 1983
- Bollinger, G. A., "Speculations on the Nature of Seismicity at Charleston, South Carolina", in G. S. Gohn, Studies Related to the Charleston, South Carolina Earthquake of 1886 - Tectonics and Seismicity, U. S. Geological Survey Professional Paper 1313, p. T1-T11, 1983
- Bollinger, G. A. and R. L. Wheeler, "The Charleston, South Carolina, Seismogenic Zone; Terrane Decoupling and Horizontal Versus Vertical Source Geometry", in W. W. Hays and P. L. Gori, Proceedings of Conference XX, A Workshop on "The 1886 Charleston, South Carolina, Earthquake and its Implications for Today", U. S. Geological Survey Open-File Report 83-843, p. 132-136, 1983
- Bollinger, G. A. and R. L. Wheeler, "Seismicity, Tectonics and Seismic Hazards in the Southeastern United States", in W. W. Hays and P. L. Gori, Proceedings of Conference XX, A Workshop on "The 1886 Charleston, South Carolina, Earthquake and its Implications for Today", U. S. Geological Survey Open-File Report 83-843, p. 367-370, 1983
- Brocoum, S., R. B. McMullen, and T. J. Schmitt, "Determining the Cause of the Charleston, South Carolina, Earthquake", in W. W. Hays and P. L. Gori, Proceedings of Conference XX, A Workshop on "The 1886 Charleston, South Carolina, Earthquake and its Implications for Today", U. S. Geological Survey Open-File Report 83-843, p. 164-168, 1983

- Chesnutt, T. W. and F. A. Rossini, "A Preliminary View of the Perception of Seismic Risk in the Southeastern United States", in W. W. Hays and P. L. Gori, Proceedings of Conference XX, A Workshop on "The 1886 Charleston, South Carolina, Earthquake and its Implications for Today", U. S. Geological Survey Open-File Report 83-843, p. 295-301, 1983
- Chowns, T. M. and C. T. Williams, "Pre-Cretaceous Rocks Beneath the Georgia Coastal Plain; Regional Implications", in G. S. Gohn, Studies Related to the Charleston, South Carolina Earthquake of 1886 - Tectonics and Seismicity, U. S. Geological Survey Professional Paper 1313, p. L1-L42, 1983
- Colquhoun, D. J., I. D. Woolen, D. S. Van Nieuwenhuise, G. G. Padgett, R. W. Oldham, P. D. Howell, and J. W. Bishop, "Surface and Subsurface Stratigraphy, Structure and Aquifers of the South Carolina Coastal Plain", Report of the Department of Health and Environmental Control, Ground Water Protection Division, published by Office of the Governor of South Carolina, 78 p., 1983
- Cox, J. H. and P. Talwani, "Discovery of the First Seismically Induced Paleoliquefaction Site Near Charleston, South Carolina", Abstract, Earthquake Notes, Vol. 54, p. 16, 1983
- Daniels, D. L., I. Zietz, and P. Popenoe, "Distribution of Subsurface Lower Mesozoic Rocks in the Southeastern United States, As Interpreted From Regional Aeromagnetic and Gravity Maps", in G. S. Gohn, Studies Related to the Charleston, South Carolina Earthquake of 1886 - Tectonics and Seismicity, U. S. Geological Survey Professional Paper 1313, p. K1-K24, 1983
- Dewey, J. W., "Relocation of Instrumentally Recorded Pre-1974 Earthquakes in the South Carolina Region", in G. S. Gohn, Studies Related to the Charleston, South Carolina Earthquake of 1886 - Tectonics and Seismicity, U. S. Geological Survey Professional Paper 1313, p. Q1-Q9, 1983
- Dewey, J. W., "A Global Search of Continental Midplate Seismic Regions for Scientific Characteristics Bearing on the 1886 Charleston, South Carolina Earthquake", in W. W. Hays and P. L. Gori, Proceedings of Conference XX, A Workshop on "The 1886 Charleston, South Carolina, Earthquake and its Implications for Today", U. S. Geological Survey Open-File Report 83-843, p. 391-426, 1983
- Dillon, W. P., K. D. Klitgord, and C. K. Paull, "Mesozoic Development and Structure of the Continental Margin Off South Carolina", in G. S. Gohn, Studies Related to the Charleston, South Carolina Earthquake of 1886 - Tectonics and Seismicity, U. S. Geological Survey Professional Paper 1313, p. N1-N16, 1983

- Dillon, W. P. and L. D. McGinnis, "Basement Structure Indicated By Seismic-Refraction Measurements Offshore From South Carolina and Adjacent Areas", in G. S. Gohn, Studies Related to the Charleston, South Carolina Earthquake of 1886 - Tectonics and Seismicity, U. S. Geological Survey Professional Paper 1313, p. 01-07, 1983
- Dooley, R. E. and J. M. Wampler, "Potassium-Argon Relations in Diabase Dikes of Georgia; the Influence of Excess Argon-40 on the Geochronology of Early Mesozoic Igneous and Tectonic Events", in G. S. Gohn, Studies Related to the Charleston, South Carolina Earthquake of 1886 - Tectonics and Seismicity, U. S. Geological Survey Professional Paper 1313, p. M1-M24, 1983
- Fleitout, L. and C. Froidevaux, "Tectonic Stresses in the Lithosphere", Tectonics, Vol. 2, p. 315-324, 1983
- Gohn, G. S., "Geology of the Basement Rocks Near Charleston, South Carolina - Data From Detrital Rock Fragments in Lower Mesozoic(?) Rocks in Clubhouse Crossroads Test Hole PS3", in G. S. Gohn, Studies Related to the Charleston, South Carolina Earthquake of 1886 - Tectonics and Seismicity, U. S. Geological Survey Professional Paper 1313, p. E1-E22, 1983
- Gohn, G. S., J. E. Hazel, L. M. Bybell, and L. E. Edwards, "The Fishburn Formation (Lower Eocene), A Newly Defined Subsurface Unit in the South Carolina Coastal Plain", Geological Survey Bulletin, Vol. 1537-C, p.C1-C18, 1983
- Gohn, G. S., B. B. Houser, and R. R. Schneider, "Geology of the Lower Mesozoic(?) Sedimentary Rocks in Clubhouse Crossroads Test Hole PS3, Near Charleston, South Carolina", in G. S. Gohn, Studies Related to the Charleston, South Carolina Earthquake of 1886 - Tectonics and Seismicity, U. S. Geological Survey Professional Paper 1313, p. D1-D17, 1983
- Gori, P. L. and M. R. Greene, "Hazards Information and Warnings", Abstract, U. S. Geological Survey Professional Paper 1375, p. 240-241, 1983
- Gottfried, D., C. S. Ansell, and G. R. Byerly, "Geochemistry and Tectonic Significance of Subsurface Basalts Near Charleston, South Carolina; Clubhouse Crossroads Test Holes PS2 and PS3", in G. S. Gohn, Studies Related to the Charleston, South Carolina Earthquake of 1886 - Tectonics and Seismicity, U. S. Geological Survey Professional Paper 1313, p. A1-A19, 1983

- Hamilton, R. M., J. C. Behrendt, and H. D. Ackermann, "Land Multichannel Seismic-Reflection Evidence for Tectonic Features Near Charleston, South Carolina", in G. S. Gohn, Studies Related to the Charleston, South Carolina Earthquake of 1886 - Tectonics and Seismicity, U. S. Geological Survey Professional Paper 1313, p. 11-118, 1983
- Hays, W. W. and S. T. Algermissen, "Plans and Programs of the U. S. Geological Survey for Studying Eastern Seismicity", in W. W. Hays and P. L. Gori, Proceedings of Conference XX, A Workshop on "The 1886 Charleston, South Carolina, Earthquake and its Implications for Today", U. S. Geological Survey Open-File Report 83-843, p. 471-477, 1983
- Hays, W. W. and P. L. Gori, "Electric Power Research Institute's Program to Address Seismic Hazard Evaluations for Nuclear Electric Generating Plants in the Eastern United States", in W. W. Hays and P. L. Gori, Proceedings of Conference XX, A Workshop on "The 1886 Charleston, South Carolina, Earthquake and its Implications for Today", U. S. Geological Survey Open-File Report 83-843, p. 489-493, 1983
- Higgins, M. W. and I. Zietz, "Geologic Interpretation of Geophysical Maps of the Pre-Cretaceous "Basement" Beneath the Coastal Plain of the Southeastern United States", Geological Society of America Memcir 158, p. 125-130, 1983
- Iverson, W. P. and S. B. Smithson, "Master Decollement Root Zone Beneath the Southern Appalachians and Crustal Balance", Geology, Vol. 10, p. 241-245, 1983
- Kinard, S., "Goals Concerning Earthquake Hazard Awareness", in W. W. Hays and P. L. Gori, Proceedings of Conference XX, A Workshop on "The 1886 Charleston, South Carolina, Earthquake and its Implications for Today", U. S. Geological Survey Open-File Report 83-843, p. 360-363, 1983
- Klitgord, K. D., W. P. Dillon, and P. Popenoe, "Mesozoic Tectonics of the Southeastern United States Coastal Plain and Continental Margin", in G. S. Gohn, Studies Related to the Charleston, South Carolina Earthquake of 1886 - Tectonics and Seismicity, U. S. Geological Survey Professional Paper 1313, p. P1-P15, 1983
- Klitgord, K. D., W. P. Dillon, P. Popenoe, J. S. Schlee, and K. Hine, "Geophysical Studies, U. S. Atlantic Coastal Plain and Continental Margin", Abstract, U. S. Geological Survey Professional Paper 1375, p. 112-113, 1983

- Klitgord, K. D. and P. Popenoe, "Geophysical Tectonic Studies of the U. S. Atlantic Coastal Plain and Continental Margin", in W. W. Hays and P. L. Gori, Proceedings of Conference XX, A Workshop on "The 1886 Charleston, South Carolina, Earthquake and its Implications for Today", U. S. Geological Survey Open-File Report 83-843, p. 185-199, 1983
- Krinitzsky, E. L., "Corps of Engineer Comments on the Potential for a Charleston, South Carolina, Earthquake", in W. W. Hays and P. L. Gori, Proceedings of Conference XX, A Workshop on "The 1886 Charleston, South Carolina, Earthquake and its Implications for Today", U. S. Geological Survey Open-File Report 83-843, p. 484-485, 1983
- Lambright, W. H., "Earthquake Preparedness; the Dynamics of Long Term Policy Innovation", in W. W. Hays and P. L. Gori, Proceedings of Conference XX, A Workshop on "The 1886 Charleston, South Carolina, Earthquake and its Implications for Today", U. S. Geological Survey Open-File Report 83-843, p. 302-314, 1983
- Lanphere, M. A., "Argon-40/Argon-39 Ages of Basalt from Clubhouse Crossroads Test Hole PS2 Near Charleston, South Carolina", in G. S. Gohn, Studies Related to the Charleston, South Carolina Earthquake of 1886 - Tectonics and Seismicity, U. S. Geological Survey Professional Paper 1313, p. B1-B8, 1983
- Leblanc, G., "A Basis for Comparing La Malbaie, Quebec, to Charleston, South Carolina", in W. W. Hays and P. L. Gori, Proceedings of Conference XX, A Workshop on "The 1886 Charleston, South Carolina, Earthquake and its Implications for Today", U. S. Geological Survey Open-File Report 83-843, p. 435-455, 1983
- Leyendecker, E. V., "Seismic Design Requirements in the Southeastern United States", in W. W. Hays and P. L. Gori, Proceedings of Conference XX, A Workshop on "The 1886 Charleston, South Carolina Earthquake and its Implications for Today", U.S. Geological Survey Open-File Report 83-843, p. 251-265, 1983
- Lindbergh, C., "Earthquake Hazard Preparedness in the Southeastern United States; A Patient Revolution", in W. W. Hays and P. L. Gori, Proceedings of Conference XX, A Workshop on "The 1886 Charleston, South Carolina Earthquake and its Implications for Today", U.S. Geological Survey Open-File Report 83-843, p. 339-350, 1983
- Long, L. T., "Role of Geological and Geophysical Data in Evaluation of Critical Hypotheses - The 1886 Charleston, South Carolina, Earthquake", in W. W. Hays and P. L. Gori, Proceedings of Conference XX, A Workshop on "The 1886 Charleston, South Carolina Earthquake and its Implications for Today", U.S. Geological Survey Open-File Report 83-843, p. 200-206, 1983

- McKeown, F. A., "Investigations of the New Madrid Seismic Zone and Their Possible Relevance to the Charleston, South Carolina, Seismic Region", in W. W. Hays and P. L. Gori, Proceedings of Conference XX, A Workshop on "The 1886 Charleston, South Carolina Earthquake and its Implications for Today", U.S. Geological Survey Open-File Report 83-843, p. 427-434, 1983
- McWhorter, J. G., "The Role of Vertical Crustal Movements and Regional Geologic Analysis in Evaluation of the 1886 Charleston, South Carolina, Earthquake", in W. W. Hays and P. L. Gori, Proceedings of Conference XX, A Workshop on "The 1886 Charleston, South Carolina Earthquake and its Implications for Today", U.S. Geological Survey Open-File Report 83-843, p. 231-238, 1983
- Morelli, U., "Federal Emergency Management Agency's Plans for the Charleston, South Carolina, Area", in W. W. Hays and P. L. Gori, Proceedings of Conference XX, A Workshop on "The 1886 Charleston, South Carolina Earthquake and its Implications for Today", U.S. Geological Survey Open-File Report 83-843, p. 479-483, 1983
- Murphy, A. J., "Nuclear Regulatory Commission's Research Plans for the Future", in W. W. Hays and P. L. Gori, Proceedings of Conference XX, A Workshop on "The 1886 Charleston, South Carolina Earthquake and its Implications for Today", U.S. Geological Survey Open-File Report 83-843, p. 468-470, 1983
- Nau, J. M. and A. K. Gupta, "The Earthquake Threat and Its Mitigation in the Southeastern United States", in W. W. Hays and P. L. Gori, Proceedings of Conference XX, A Workshop on "The 1886 Charleston, South Carolina Earthquake and its Implications for Today", U.S. Geological Survey Open-File Report 83-843, p. 239-243, 1983
- Niss, J. M., "Increasing Hazard Awareness in the Southeast; Barriers and Recommendations", in W. W. Hays and P. L. Gori, Proceedings of Conference XX, A Workshop on "The 1886 Charleston, South Carolina Earthquake and its Implications for Today", U.S. Geological Survey Open-File Report 83-843, p. 323-329, 1983
- Palm, R. I., "Improving Hazard Awareness", in W. W. Hays and P. L. Gori, Proceedings of Conference XX, A Workshop on "The 1886 Charleston, South Carolina Earthquake and its Implications for Today", U.S. Geological Survey Open-File Report 83-843, p. 55 - 61, 1983
- Phillips, J. D., "Paleomagnetic Investigations of the Clubhouse Crossroads Basalt", in G. S. Gohn, Studies Related to the Charleston, South Carolina Earthquake of 1886 - Tectonics and Seismicity, U.S. Geological Survey Professional Paper 1313, p. C1-C18, 1983

- Pomeroy, P. W., "Summary Comments on--Eastern Seismicity with Emphasis on the Charleston, South Carolina, Earthquake--Progress, Problems and Competing Hypotheses", in W. W. Hays and P. L. Gori, Proceedings of Conference XX, A Workshop on "The 1886 Charleston, South Carolina Earthquake and its Implications for Today", U.S. Geological Survey Open-File Report 83-843, p. 84-87, 1983
- Prowell, D. C., "Index of Faults of Cretaceous and Cenozoic Age in the Eastern U.S.", U.S. Geological Survey Miscellaneous Field Study Map, M.F. 1269, 2 sheets, 1983
- Ragland, P. C., R. D. Hatcher, Jr., and D. Whittington, "Juxtaposed Mesozoic Diabase Dike Sets from the Carolinas; A Preliminary Assessment", Geology, Vol. 11, No. 7, p. 394-399, 1983
- Ratcliffe, N. M., "Fault Reactivation Models for the Origin of Eastern United States Seismicity; Does the Solution to Charleston Earthquake Reside at Charleston?", in W. W. Hays and P. L. Gori, Proceedings of Conference XX, A Workshop on "The 1886 Charleston, South Carolina Earthquake and its Implications for Today", U.S. Geological Survey Open-File Report 83-843, p. 137-141, 1983
- Reiter, L., "Historic Seismicity Versus Tectonic Hypothesis", in W. W. Hays and P. L. Gori, Proceedings of Conference XX, A Workshop on "The 1886 Charleston, South Carolina Earthquake and its Implications for Today", U.S. Geological Survey Open-File Report 83-843, p. 364-366, 1983
- Robinson, A. and P. Talwani, "Building Damage at Charleston, South Carolina, Associated with the 1886 Earthquake", Bulletin of the Seismological Society of America, Vol. 73, No. 2, p. 633-652, 1983
- Schilt, F. S., L. D. Brown, J. E. Oliver, and S. Kaufman, "Subsurface Structure Near Charleston, South Carolina; Results of COCORP Reflection Profiling in the Atlantic Coastal Plain", in G. S. Gohn, Studies Related to the Charleston, South Carolina Earthquake of 1886 - Tectonics and Seismicity, U.S. Geological Survey Professional Paper, 1313, p. H1-H19, 1983
- Seay, W. M., "Tennessee Valley Authority's Seismic Monitoring Program", in W. W. Hays and P. L. Gori, Proceedings of Conference XX, A Workshop on "The 1886 Charleston, South Carolina Earthquake and its Implications for Today", U.S. Geological Survey Open-File Report 83-843, p. 486-488, 1983
- Seeber, L., "Earthquake Hazard and Risk in the Eastern U.S. vs. the Western U.S.", Abstract, Earthquake Notes Vol. 54, p. 31 1983

- Seeber, L. "Thick vs. Thin-Skin Models for Neotectonics in the Appalachians", in Proceedings of Conference XX, A Workshop on "The 1886 Charleston, South Carolina Earthquake and its Implications for Today", U. S. Geological Survey Open-File Report 83-0843, p. 101-106, 1983
- Seeber, L. and J. G. Armbruster, "Large Strain Effects of the 1886 South Carolina Earthquake", in W. W. Hays and P. L. Gori, Proceedings of Conference XX, A Workshop on "The 1886 Charleston, South Carolina Earthquake and its Implications for Today", U.S. Geological Survey Open-File Report 83-843, p. 142-149, 1983
- Sharpe, R. L., "Earthquake Resistant Design Considerations for Southeastern United States", in W. W. Hays and P. L. Gori, Proceedings of Conference XX, A Workshop on "The 1886 Charleston, South Carolina Earthquake and its Implications for Today", U.S. Geological Survey Open-File Report 83-843, p. 280-287, 1983
- Stewart, R. M. and S. B. Rhea, "Scientific Contributions and Future Uses of Seismic Networks in the Charleston, South Carolina Area", in W. W. Hays and P. L. Gori, Proceedings of Conference XX, A Workshop on "The 1886 Charleston, South Carolina Earthquake and its Implications for Today", U.S. Geological Survey Open-File Report 83-843, p. 221-230, 1983
- Talwani, P., "Intraplate Earthquakes, Block Tectonics, Aeromagnetic and Gravity Anomalies; or, Why We Have Earthquakes at Charleston, S.C.", Geological Society of America Abstracts with Programs, Vol. 15, No. 2, p. 64, 1983
- Talwani, P., "Tectonic Models - Old and New", in W. W. Hays and P. L. Gori, Proceedings of Conference XX, A Workshop on "The 1886 Charleston, South Carolina Earthquake and its Implications for Today", U.S. Geological Survey Open-File Report 83-843, p. 88-100, 1983
- Talwani, P. and D. Amick, "Results and Role of Current Seismicity in Understanding the 1886 Charleston, South Carolina Earthquake", in W. W. Hays and P. L. Gori, Proceedings of Conference XX, A Workshop on "The 1886 Charleston, South Carolina Earthquake and its Implications for Today", U.S. Geological Survey Open-File Report 83-843, p. 24-27, 1983
- Tarr, A. C. and S. Rhea, "Seismicity Near Charleston, South Carolina, March 1973 to December 1979", in G. S. Gohn, Studies Related to the Charleston, South Carolina Earthquake of 1886 - Tectonics and Seismicity, U.S. Geological Survey Professional Paper 1313, p. R1-R17, 1983

- Thiel, C. C., Jr., "The Charleston, South Carolina, Earthquake; A Prospective Assessment", in W. W. Hays and P. L. Gori, Proceedings of Conference XX, A Workshop on "The 1886 Charleston, South Carolina Earthquake and its Implications for Today", U.S. Geological Survey Open-File Report 83-843, p. 62-63, 1983
- Wentworth, C. M., "The Changing Tectonic Basis for Regulatory Treatment of the 1886 Charleston, South Carolina, Earthquake in the Design of Power Reactors", in W. W. Hays and P. L. Gori, Proceedings of Conference XX, A Workshop on "The 1886 Charleston, South Carolina Earthquake and its Implications for Today", U.S. Geological Survey Open-File Report 83-843, p. 266-275, 1983
- Wentworth, C. M., "Reverse Faulting as the Source of Earthquakes Along the Eastern Seaboard of the United States; Problems and Needed Research", in W. W. Hays and P. L. Gori, Proceedings of Conference XX, A Workshop on "The 1886 Charleston, South Carolina Earthquake and its Implications for Today", U.S. Geological Survey Open-File Report 83-843, p. 117-125, 1983
- Wentworth, C. M. and M. Mergner-Keefer, "Regenerated Faults of Small Cenozoic Offset; Probable Earthquake Sources in the Southeastern United States", in G. S. Gohn, Studies Related to the Charleston, South Carolina Earthquake of 1886 - Tectonics and Seismicity, U.S. Geological Survey Professional Paper 1313, p. S1-S20, 1983
- Wheeler, R. L., "Is South Carolina Seismically Active on a Northwestward Projection of the Blake Spur Fracture Zone?", in W. W. Hays and P. L. Gori, Proceedings of Conference XX, A Workshop on "The 1886 Charleston, South Carolina Earthquake and its Implications for Today", U.S. Geological Survey Open-File Report 83-843, p. 150-163, 1983
- Whittington, D. P., C. Ragland, and R. D. Hatcher, "Tectonic Implications of an Apparent Mesozoic Radial Diabase Dike Swarm Centered in the Vicinity of Charleston - Georgetown, South Carolina", Geological Society of America Abstracts With Programs, Vol. 15, p. 92, 1983
- Williams, H. and R. D. Hatcher, Jr., "Appalachian Suspect Terranes", U.S. Geological Society of America Memoir 158, p. 33, 1983
- Yantis, B. R., J. K. Costain, and H. D. Ackermann, "A Reflection Seismic Study Near Charleston, South Carolina", in G. S. Gohn, Studies Related to the Charleston, South Carolina Earthquake of 1886 - Tectonics and Seismicity, U.S. Geological Survey Professional Paper 1313, p. G1-G20, 1983

Zoback, M. D., "Intraplate Earthquakes, Crustal Deformation, and In-situ Stress", in W. W. Hays and P. L. Gori, Proceedings of Conference XX, A Workshop on "The 1886 Charleston, South Carolina Earthquake and its Implications for Today", U.S. Geological Survey Open-File Report 83-843, p. 169-178, 1983

1984

Acharya, H. K., A. S. Lucks, and J. T. Christian, "Seismic Hazard in Northeastern United States", International Journal of Soil Dynamics and Earthquake Engineering, Vol. 3, No. 1, p. 8 -18, 1984

Armbruster, J. G. and L. Seeber, "Low Seismicity in South Carolina Prior to the 1886 Earthquake", Abstract, Eos, Transactions, American Geophysical Union, Vol. 65, p. 241, 1984

Cameron, C. C., E. R. Force, and A. E. Grosz, "Geologic Map of the Hell Hole Bay, Wambaw Swamp, Little Wambaw Swamp, and Wambaw Creek Wildernesses, Berkeley and Charleston Counties, South Carolina", U.S. Geological Survey Map MF-1556-A, 1984

Campbell, K. W., "An Empirical Evaluation of Strong Ground Motion for the Near-Source Region of a Charleston-Size (6.6 m₀) Earthquake in the Eastern U.S.", Abstract, Earthquake Notes, Vol. 55, p. 27, 1984.

Coruh, C. J., K. Costain, G. S. Gohn, J. H. Behrendt, and R. A. Hamilton, "Mesozoic Faulting in the Charleston, South Carolina Region: New Evidence from Seismic Reflection Data", In review, 1984

Cox, J. H., "Paleoseismology Studies in South Carolina", Master's Thesis, University of South Carolina, 75 p., 1984

Cox, J. H. and P. Talwani, "Three-Dimensional Description of an Earthquake Induced Sandblow Near Charleston, S.C.", Abstract Eos, Transactions, American Geophysical Union, Vol. 65, p. 241, 1984

McCartan, L., E. M. Lemon, Jr., and R. E. Weems, "Geologic Map of the Area Between Charleston and Orangeburg, South Carolina", U. S. Geological Survey Miscellaneous Investigation Map I-1472, Scale 1:250,000, 1984

Poley, C. M., "Recent Vertical Crustal Movements in the South Carolina Coastal Plain", Master's Thesis, University of South Carolina, 1984

Poley, C. M. and P. Talwani, "Vertical Tectonics in the South Carolina Coastal Plain", Abstract, Eos, Transactions, American Geophysical Union, Vol. 65, p. 190, 1984

- Rawlins, J. and P. Talwani, "Earthquake Swarms Near Newberry, S.C.", Geological Society of America Abstracts with Programs, Vol. 16, p. 188, 1984
- Talwani, P., "Orientation of Stress in Southeastern United States", Geological Society of America Abstracts with Programs, Vol. 16, p. 202, 1984
- Talwani, P. and C. M. Poley, "Vertical Tectonics in the Charleston, S.C. Area", Abstract, Earthquake Notes, Vol. 55, p. 30, 1984
- Visvanathan, T. R., "Seismic Zones in South Carolina", South Carolina Geological Survey Open-File Report 34A, 21 p., 1984
- Weems, R. E. and E. M. Lemon, Jr., "Geologic Map of the Mount Holly Quadrangle, Berkeley and Charleston Counties, South Carolina", U.S. Geological Survey Map GQ-1579, 1984
- Weems, R. E. and E. M. Lemon, Jr., "Geologic Map of the Stallville Quadrangle, Dorchester and Charleston Counties, South Carolina", U.S. Geological Survey Map GQ-1581, 1984
- Wheeler, R. L. and G. A. Bollinger, "Seismicity and Suspect Terranes in the Southeastern U.S.", Geology, Vol. 12, p. 323 - 326, 1984
- Zoback, M. L., M. D. Zoback, and M. E. Schlitz, "Index of Stress Data for the North American and Parts of the Pacific Plates", U. S. Geological Survey Open-File Report 84-157, 1984
- 1985
- Armbruster, J. G. and L. Seeber, "Spatial Correlation Between the Aftershocks of the 1886 Charleston, S.C. Earthquake and Recent Induced Seismicity in the Southeastern U.S.", Abstract, Earthquake Notes, Vol. 55, p. 25, 1985
- Bagwell, J. B., "Comparison of Seven Recent Isoseismal Maps and Data of the Charleston 1886 Earthquake", Abstract, Earthquake Notes, Vol. 56, p. 69, 1985
- Behrendt, J. C., "Interpretation from Multichannel Seismic-Reflection Profiles of the Deep Crust Crossing South Carolina and Georgia from the Appalachian Mountains to the Atlantic Coast", U. S. Geological Survey Map MF-1656, 1985
- Behrendt, J. C. and A. Yuan, "The Helena Banks Strike-Slip(?) Fault and the Relation to Other Cenozoic Faults Along Reactivated Triassic(?) Basin Boundary Fault Zones in the Charleston, S.C., Earthquake Area---Results from a Marine High-Resolution Multichannel Seismic-Reflection Survey", Geological Society of America Abstracts with Programs, Vol. 17, p. 521, 1985

- Bollinger, G. A. and Others, "Availability of A 6-Year (1977-83) Earthquake Catalog for the Southeastern U.S. Derived from Network Monitoring", Geological Society of America, Abstracts with Programs, Vol. 17, p. 81, 1985
- Costain, J. K. and G. A. Bollinger, "A Hydrologic Model for Intraplate Seismicity in the Southeastern United States", Geological Society of America Abstracts with Programs, Vol. 17, p. 554, 1985
- Dewey, J. W., "A Review of Recent Research on the Seismotectonic, of the Southeastern Seaboard and An Evaluation of Hypotheses on the Source of the 1886 Charleston, South Carolina, Earthquake", U.S. NRC Report NUREG/CR-4339, 1985
- Maley, R. P., R. L. Porcella, and M. Celebi, "The National Strong-Motion Instrumentation Program in the Central and Eastern Regions of the United States", Abstract, Earthquake Notes, Vol. 56, p. 67, 1985
- Obermeier, S. F., G. S. Gohn, R. E. Weems, R. L. Gelinas, and M. Rubin, "Geologic Evidence for Recurrent Moderate to Large Earthquakes Near Charleston, South Carolina", Science, Vol. 227, p. 408-411, 1985
- Obermeier, S. F., R. E. Weems, G. S. Gohn, and M. Rubin, "Distribution and Recurrence of Prehistoric Earthquakes Near Charleston, South Carolina", Abstract, Earthquake Notes, Vol. 55, p. 25, 1985
- Phillips, J. D. and W. M. Davis, "Principal Facts for Gravity Stations in Bamberg, Beaufort, Charleston, Colleton, Dorchester, and Orangeburg Counties, South Carolina", U.S. Geological Survey Open-File Report 85-392, 15 p., 1985
- Prescott, W. H., S. W. Krueger, and M. D. Zoback, "Geodetic Constraints on Strain Rates in the Vicinity of the 1886 Charleston, South Carolina Earthquake", in Proceedings, First International Symposium on Precise Positioning with the Global Positioning System: Positioning with GPS, 1985, U. S. National Oceanic and Atmospheric Administration, p. 887-896, 1985
- Robinson, A. and P. Talwani, "A P-Wave Relative Travel Time Residual Study in the Coastal Plain of South Carolina", Abstract, Earthquake Notes, Vol. 56, p. 71, 1985
- Seeber, L. and J. G. Armbruster, "Spatio-Temporal Distribution of Seismicity Along the Appalachians and the Case for Detachment Reactivation", Abstract, Earthquake Notes, Vol. 56, p. 66, 1985

- Smith, W. A. and P. Talwani, "Preliminary Interpretation of a Detailed Gravity Survey in the Bowman and Charleston, S.C., Seismogenic Zones", Geological Society of America Abstracts with Programs, Vol. 17, p. 137, 1985
- Stewart, R. M., "Laterally Heterogeneous Crustal Model for the Charleston, S. C. Area", Abstract, Earthquake Notes, Vol. 55, p. 27, 1985
- Talwani, P., "Current Thoughts on the Cause of the Charleston, South Carolina Earthquakes", South Carolina Geology, Vol. 29 No. 2, p. 19-38, 1985
- Talwani, P. and D. J. Colquhoun, "Near Surface Evidence for Buried Seismogenic Faults in the Charleston, S.C. Region", Abstract, Eos, Transactions, American Geophysical Union, Vol. 66, p. 970, 1985
- Talwani, P., D. J. Colquhoun, and G. Lennon, "Results of Recent Seismotectonic Studies in the Charleston Area", U.S. Geological Society of America Abstracts with Programs, Vol. 17, p. 732, 1985
- Talwani, P. and J. Cox, "Paleoseismic Evidence for Recurrence of Earthquakes near Charleston, South Carolina", Abstract, Earthquake Notes, Vol. 55, p. 25, 1985
- Weems, R. E., "Possible Subsurface Structures in Coastal Plain Sediments Near Charleston, S.C.", Abstract, Earthquake Notes, Vol. 55, p. 27, 1985
- Weems, R. E. and E. M. Lemon, Jr., "Detailed Sections from Auger Holes and Outcrops in the Cainhoy, Charleston, and Fort Moultrie Quadrangles, South Carolina", U. S. Geological Survey Open-File Report 85-0378, 72 p., 1985
- Weems, R. E., E. M. Lemon, Jr., and E. D. Cron, "Detailed Sections from Auger Holes and Outcrops in the Bethera, Cordsville, Huger, and Kittredge Quadrangles, South Carolina", U. S. Geological Survey Open-File Report 85-0439, 94 p., 1985
- Weems, R. E., E. M. Lemon, Jr., G. S. Gohn, and B. B. Houser, "Detailed Sections from Auger Holes and Outcrops in the Ladson, Moncks Corner, Mount Holly, and Stallville Quadrangles, South Carolina", U. S. Geological Survey Open-File Report 85-0472, 103 p., 1985
- Weems, R. E., E. M. Lemon, Jr., and L. McCartan, "Shallow Subsurface Geology of the North Charleston 7.5-Minute Quadrangle, South Carolina", U. S. Geological Survey, Open-File Report 85-0274, 70 p., 1985

Zoback, M. L., "Reassessment of the State of Stress in the Atlantic Coast Region", Geological Society of America Abstracts with Programs, Vol. 17, p. 759, 1985

Zoback, M. L. and M. D. Zoback, "Uniform NE to ENE Maximum Horizontal Compressive Stress Throughout Mid-Plate North America", Abstract, Eos, Transactions, American Geophysical Union, Vol. 66, p. 1056, 1985

1986

Acharya, H., "Comparison of Parameters for Charleston and Other Seismic Zones in Eastern North America", in Proceedings of the Third U.S. National Conference on Earthquake Engineering, (Earthquake Engineering Research Institute, El Cerrito, California), p. 65-75, 1986

Amick, D. and P. Talwani, "Earthquake Recurrence Rates and Probability Estimates for the Occurrence of Significant Seismic Activity in the Charleston Area: The Next 100 Years", in Proceedings of the Third U.S. National Conference on Earthquake Engineering, (Earthquake Engineering Research Institute, El Cerrito, California), p. 55-64, 1986

Behrendt, J. C., and A. Yuan, "Strike Slip on Reactivated Triassic(?) Basin Boundary Fault Zones as Sources of Earthquakes Near Charleston, S.C.", in Proceedings of the Third U.S. National Conference on Earthquake Engineering, (Earthquake Engineering Research Institute, El Cerrito, California), p. 43-54, 1986

Carr, J. R. and C. E. Glass, "An Evaluation of the Quality of the 1886 Charleston, South Carolina Intensity Data Using Indicator Functions", in Proceedings of the Third U.S. National Conference on Earthquake Engineering, (Earthquake Engineering Research Institute, El Cerrito, California), p. 33-42, 1986

Herrmann, R. B., "Surface-Wave Studies of Some South Carolina Earthquakes", Bulletin of the Seismological Society of America, Vol. 76, p. 111-121, 1986

Klitgord, K. D. and H. Schouten, "Plate Kinematics of the Central Atlantic", in P. R. Vogt and B. E. Tucholke, The Geology of North America, Volume M, The Western North Atlantic Region (Geological Society of America), 696 p., 1986

Law Engineering Testing Company, "Seismic Hazard Methodology for the Central and Eastern United States", EPRI NP-4726, Vol. 7, 1986

- Long, L. T., R. M. White, and J. Dwyer, "The Charleston Earthquake Hypothesis--A Classification by Fundamental Tectonic Processes", in Proceedings of the Third U.S. National Conference on Earthquake Engineering, (Earthquake Engineering Research Institute, El Cerrito, California), p. 25-31, 1986
- Markewich, H. W., M. J. Pavich, M. J. Mausbach, B. N. Stuckey, R. G. Johnson, and V. Gonzalez, "Soil Development and Its Relation to the Ages of Morphostratigraphic Units in Horry County, South Carolina", U. S. Geological Survey Bulletin, Vol. 1589-B, 61 p., 1986
- Nuttli, O. W., G. A. Bollinger, and R. B. Herrmann, "The 1886 Charleston South Carolina, Earthquake - A 1986 Perspective", U. S. Geological Survey Circular 985, 52 p., 1986
- Peters, K. E. and R. B. Herrmann, "First-Hand Observations of the Charleston Earthquake of August 31, 1886, and Other Earthquake Materials", South Carolina Geological Survey Bulletin, Vol. 41, 116 p., 1986
- Poley, C. M. and P. Talwani, "Recent Vertical Crustal Movements Near Charleston, South Carolina", Journal of Geophysical Research, Vol. 91, p. 9056-9066, 1986
- Seeber, L. and J. G. Armbruster, "The 1886-1889 Aftershocks of the Charleston, South Carolina, Earthquake: A Widespread Burst of Seismicity", Journal of Geophysical Research, Vol. 92, No. B3, p. 2663-2696, 1986
- Smith, W. A., P. Talwani, and D. J. Colquhoun, "Tectonics and Seismicity in the Bowman, S. C. Seismogenic Zone", Geological Society of America, Abstracts with Programs, Vol. 18, p. 266, 1986
- Talwani, P., "Current Thoughts on the Cause of the Charleston, South Carolina Earthquakes", South Carolina Geology, Vol. 29, p. 19-38, 1986
- Talwani, P., "Seismotectonics of the Charleston Region", in Proceedings of the Third U.S. National Conference on Earthquake Engineering, (Earthquake Engineering Research Institute, El Cerrito, California), p. 15-24, 1986
- Tucholke, B. E. and F. W. McCoy, "Paleogeographic and Paleobathymetric Evolution of the North Atlantic Ocean", in P. R. Vogt, and B. E. Tucholke, The Geology of North America, Volume M, The Western North Atlantic Region, (Geological Society of America), 696 p., 1986

- Weems, R. E., S. F. Obermeier, M. J. Parich, G. S. Gohn, M. Rubin, R. L. Phipps, and R. B. Jacobson, "Evidence for Three Moderate to Large Prehistoric Holocene Earthquakes Near Charleston, S.C.", in Proceedings of the Third U.S. National Conference on Earthquake Engineering, (Earthquake Engineering Research Institute, El Cerrito, California), p. 3-13, 1986
- Weems, R. E. and A. E. Sanders, "The Chandler Bridge Formation (Upper Oligocene) of the Charleston, South Carolina, Region", U. S. Geological Society of America Centennial Field Guide, Vol. 6, p. 323-326, 1986
- Young, C. T., M. R. Kitchen, J. C. Rogers, and J. C. Mareschal, "Magnetotelluric Soundings in the Charleston, South Carolina Area", in Proceedings of the Third U.S. National Conference on Earthquake Engineering, (Earthquake Engineering Research Institute, El Cerrito, California), p. 83-91, 1986
- Zurflueh, E. G., "NRC Participation in Studies of the Charleston Seismicity", in Proceedings of the Third U.S. National Conference on Earthquake Engineering, (Earthquake Engineering Research Institute, El Cerrito, California), p. 77-81, 1986

1987

- Costain, J. K., G. A. Bollinger, and J. A. Speer, "Hydroseismicity: A Hypothesis for the Role of Water in the Generation of Intraplate Seismicity", Seismological Research Letters, Vol. 58, 1987
- Kuang, J., "Intraplate Stress and Seismicity in the Southeastern United States", Doctoral Thesis, Georgia Institute of Technology, Atlanta, 1987
- Shedlock, K. M., "Seismicity Near Charleston, South Carolina - 1974 to Present", Abstract, Eos, Transactions, American Geophysical Union, Vol. 68, No. 16, p. 363, 1987
- Smith, W. A., P. Talwani, and D. J. Colquhoun, "The Seismotectonics of the Bowman Seismic Zone, South Carolina", submitted to Geological Society of America Bulletin, Dec. 1987

APPENDIX A

APPENDIX A. POTENTIAL DATA ACQUISITION AND ANALYSIS

Report to: Law Engineering Testing Co
Marietta, Georgia

From: School of Geophysical Sciences
Georgia Institute of Technology
Atlanta, Georgia 30332 0340

APPENDIX A

CONTENTS

	<u>Page</u>
Contents.....	i
List of Figures.....	ii
Abstract.....	iii
1. Documentation of Charleston Area Data Sets and Computer Programs.....	A-1-1
Introduction.....	A-1-1
Definition of Grids.....	A-1-1
The Gridding Program.....	A-1-2
Sources of Gravity Data.....	A-1-4
Merging and Compiling of Data.....	A-1-6
Assessment of Precision.....	A-1-7
Presentation of the Data.....	A-1-7
2. Principal Facts for Charleston Area Gravity Data.....	A-2-1
Introduction.....	A-2-1
Sources of Data.....	A-2-1
3. Definition of Data Grids for Charleston Study.....	A-3-1
Introduction.....	A-3-1
Map Projection and Reference Location.....	A-3-1
Grid Definitions.....	A-3-3
4. Details of Magnetic Anomaly Map.....	A-4-1
5. Bibliography.....	A-5-1
6. Program Listings.....	A-6-1
AB, Fills in Areas of Low Data Coverage.....	A-6-2
ALBERS, Albers Equal Area Projection.....	A-6-5
CLEAN, Identify Duplicate Points.....	A-6-7
CLEAR, Identify Inconsistent Data Points.....	A-6-8
SNGGRID, Grid Single Variable Data.....	A-6-14
LLUTM, Geographic Coordinates to UTM.....	A-6-21
UTMILL, UTM to Geographic Coordinates.....	A-6-23

LIST OF FIGURES

<u>Figure</u>	<u>Page</u>
A-1-1. Relation between area of occurrence of values and the grid points affected.	A-1-3
A-1-2. Autocorrelation of gravity data.	A-1-9
A-1-3. Smoothed Bouguer anomalies in GD1SMTG.....	A-1-10
A-1-4. Smoothed elevations in GD1SMTG.....	A-1-11
A-1-5. Smoothed weights in GD1SMTW.....	A-1-12
A-1-6. Smoothed magnetic anomalies in GD1SMTM.....	A-1-13
A-1-7. Bouguer anomalies in GD2RAWG.....	A-1-14
A-1-8. Elevations in GD2RAWE.....	A-1-15
A-1-9. Magnetic anomalies in GD2RAWM.....	A-1-16
A-1-10. Bouguer anomalies in GD3RAWG.....	A-1-17
A-1-11. Elevations in GD3RAWE.....	A-1-18
A-1-12. Magnetic anomalies in GD3RAWM.....	A-1-19
A-2-1. Gravity data coverage prior to the field survey....	A-2-2
A-2-2. Point plot of new gravity data.....	A-2-5
A-2-3a. Gravity data in degree square 33 ^o N, 80 ^o W.....	A-2-6
A-2-3b. Gravity data in degree square 33 ^o N, 81 ^o W.....	A-2-7
A-2-3c. Gravity data in degree square 32 ^o N, 81 ^o W.....	A-2-8
A-2-3d. Gravity data in degree square 32 ^o N, 80 ^o W.....	A-2-9
A-2-3e. Gravity data in degree square 33 ^o N, 79 ^o W.....	A-2-10
A-2-3f. Gravity data in degree square 32 ^o N, 79 ^o W.....	A-2-11
A-2-4. DOD gravity data coding format.....	A-2-12
A-3-1. Relative location of rotated reference axis.....	A-3-2
A-3-2. Location of grid point relative to sample area.....	A-3-2
A-3-3. Relative location of grid points.....	A-3-5

ABSTRACT

The object of this report is to present data relevant to the Charleston Earthquake in a single appropriate format. All data are referenced to equally spaced points on the Universal Transverse Mercator projection, zone 17. Values at each point are weighted averages of surrounding points within a restricted radius of two grid increments. Duplicate or inconsistent data points were removed from the gravity data and the precision was estimated for each grid point.

About 600 new gravity observations were obtained in areas of sparse coverage near the epicenter of the 1886 Charleston earthquake. These new values increased the existing gravity data set by 20 percent from 3150 to 3750 points in a 128 by 128 km rectangular area centered on the epicenter of the Charleston earthquake. Most of the new gravity values were obtained at 0.5 km increments along lines.

The four data grids defined herein are centered about the epicentral zone of the 1886 Charleston earthquake. They are squares in the Universal Transverse Mercator projection and are rotated clockwise 52 degrees about the point $(33.125^{\circ}\text{N}, 81.25^{\circ}\text{W})$, which corresponds to the point (1,1) in the 128x128 point grid with a 1.0 km spacing. The other grids are centered on this grid exactly and have sides of 256 points at 4.0 km spacing, 128 points at 8.0 km spacing and 4096 points at 31.25 m spacing.

1. DOCUMENTATION OF CHARLESTON AREA DATA SETS AND COMPUTER PROGRAMS

Introduction

Most studies, which have analyzed geophysical data covering the epicentral zone of the 1886 Charleston earthquake, have presented the data in a format that is convenient for analysis and provides the best display. But, different data types, such as landsat images, gravity data, magnetic data, and magnetotelluric soundings are best presented and most conveniently analyzed in different and often incompatible formats. Hence, the first objective of this study of data relevant to the Charleston earthquake was to establish a single appropriate format for all data. The format would permit the direct comparison of a variety of data types and the use of analysis techniques for multiple data sets on a common data base. The second objective was to collect the existing data and to adjust the data to be compatible with the common data base. In most cases this requires a change in format and a merging of multiple data sets from different sources. A third objective was to provide a mechanism to update the data when new data become available and to assess the accuracy of the data. The fourth objective was to present the collected data in a format appropriate for distribution.

Definition of Grids

The use of a two-dimensional planar representation of data on an ellipsoidal surface is inherently non-conformable. The distortion of distances, directions and areas will depend on the projection. A variety of projections (including Lambert conic, Universal Transverse Mercator, and Albers equal area) have been used for the data available to this study. A direct comparison of data on different projections can be difficult since equally distant grid points in each projection may not represent the same point on the earth's surface. In order to compare data which were originally in different projections, all the data need to be referenced to a grid in the same projection. The landsat data are conventionally displayed using the Universal Transverse Mercator projection. Because the landsat images contain the greatest number of points, the computational effort required to effect conversion among projections would present the greatest difficulty. For this reason we have chosen the Universal Transverse Mercator projection (zone 17) to map latitude and longitude to a plane surface on which a uniform rectangular grid can be defined. Other projections, for example the Albers Equal Area Conic projection, are more common and more appropriate for large study areas such as the eastern United States. However, the largest area of interest in this study has a longitudinal dimension of about 1500 km and the distortion at this distance related to the Universal Transverse Mercator (UTM) projection is significantly less than the precision necessary for the data presented in the large grid. The area of the largest grid extends beyond zone 17, but for coordinates outside zone 17 the zone is fixed at 17 for consistency. FORTRAN sub

routines UTMLL and LLUTM for converting UTM coordinates to latitude and longitude and back are given in Appendix A-6.

The Gridding Program

The interpolation of data to a rectangular grid was accomplished by a weighted average. The weighted average was limited to a defined small area in order to allow the grid to be easily updated any time new data are available. Also, the computational implementation of the weighted average is efficient and stable.

Values at each grid point were determined by the weighted average of all data points falling within an area defined by a square with four grid points on a side (figure A-1-1). The weights are a function of distance and decrease with increasing distance between the grid point and the data point. The data points are transformed from their original coordinate system to the Universal Transverse Mercator projection. After the grid area surrounding a data point is identified, the surrounding 16 grid points are found. For each grid point the distance to the data point is computed. Then a normalized weight function is calculated by Equation 1.

$$W_i^- = W_i / \sum_{i=1}^{16} W_i \quad (1)$$

where:

W_i = $[1/(1+(r_i/dx)^2)]$, the weight function
 dx = grid point separation
and r_i = distance from data point to grid point

By normalizing the weights, they are equivalent to the number of points contributing to a grid point or the density of data for the area represented by one grid point. With this distance dependent weight, appropriately greater weight is given to the points closer to the grid points. Since data points near the edge of the grid area do not have 16 surrounding grid points, two extra rows (or columns) were added at the four edges of the grid for convenience in programming. These values are preserved for the addition of new data to the grid but are excluded from the grids used in analysis. The FORTRAN program SNGGRID used to generate the grid is given in Appendix A-6.

The gridding technique employed in program SNGGRID works best when the data density is uniform and similar to the density of the grid. In areas where the data are more dense, an averaged and smoothed value is given at the grid point, simulating the average effect of the field surrounding the grid point and not just the value at the grid point. The average is preferable to a point value for modeling since it better

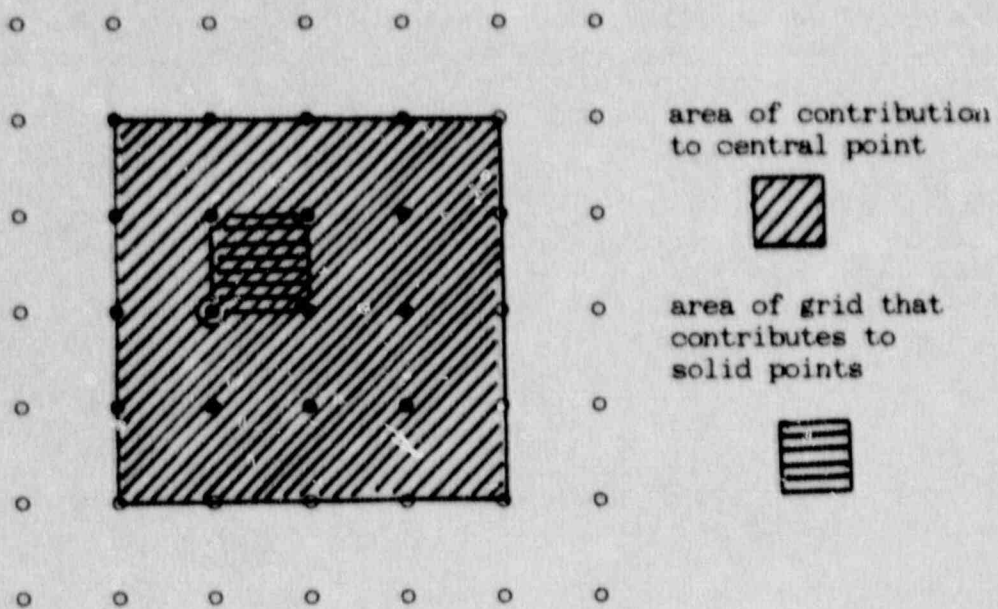


Figure A-1-1. Relation between area of occurrence of values and the grid points affected.

represents the block corresponding to the grid point. In areas of high data density, the gridded data represent a smoothing of the original data within a radius equivalent to the grid spacing. For the more difficult condition of areas which lack data, the gridding technique yields 4 by 4 squares of constant value or grid points with zero value. For these conditions, a program to expand the radius of smoothing was developed. This FORTRAN program, AB, considers each point at which the weight (equivalent number of points) falls below a threshold value determined by the criterion that less than three points contributed to the value. For those points, the area of averaging was expanded until the equivalent of six points contributed to the value and the weighted average was computed. This is equivalent to choosing a larger grid increment and interpolating between grid points. The sparse areas that would be affected the greatest are along the coast or over lakes or swamps outside the Charleston epicenter area. In these areas, the average value is more appropriate than an extrapolated value, because of the extreme values that extrapolated values can obtain when unconstrained on one side.

Sources of Gravity Data

The gravity values on the 1 km 128x128 point grid (see A-3 for definition of grids) were interpolated directly from available gravity observations. The elevation values for the 1 km grid were interpolated from the elevations of the gravity data. Because approximately 600 new gravity observations (described in A-2) were obtained during this project, and additional data have been obtained in the last few years, special care was taken to assure that this data set would be internally consistent. All the data were converted, if necessary, to the IGSN 1971 datum (International Association of Geodesy, 1971b) and anomalies were calculated using the 1967 Geodetic Reference System (International Association of Geodesy, 1971a).

The data from Champion (1975) consist of approximately 2000 observations, 1000 of which are along 11 detailed profiles. The data spacing along the profiles was 0.5 km. The remaining 1000 measurements are regional data having an average station spacing of 1.0 km. LaCosta-Romberg meters were used exclusively and the combined uncertainty in drift and reading precision was 0.15 mGal for the line data. The elevation control limited the precision of the regional data to 0.2 mGal. The Champion (1975) data were obtained in an area defined by the corner locations (32° 37.5' N, 80° W) and (33° 7.5' N, 80° 22.5' W). This area includes a major portion of the epicentral zone of the 1886 earthquake as well as the epicenters of the more recent seismic events.

Gravity data from McKee (1973) cover the region of the February 3, 1972, Bowman, South Carolina, earthquake. Excluding base stations, 344 gravity readings were obtained. The data include one line at 0.5 km spacing and regional data at about 1.0 km spacing in a 400 km² area.

During September, 1981, Georgia Tech was commissioned by the Southeastern Exploration and Production Company to obtain proprietary data in the area of Bamberg, South Carolina. The time limit on the proprietary status expired in 1985. These data consist of 89 observations along two lines. The data spacing was 0.5 km on one line and 1.0 on the other.

The 549 regional gravity measurements obtained from the U. S. Geological Survey (Phillips and Davis, 1985) were collected in July, 1977 and June, 1978, as part of on-going geophysical investigations in the vicinity of epicenter of the 1886 Charleston earthquake. An additional 95 gravity measurements were collected at 500 foot intervals along a southwest trending line crossing the Ashley river.

A data set containing regional data was obtained from the Defense Mapping Agency (DMA). These data are at a spacing of 5 to 15 km. The precision of the older data in this data set is uncertain. The DMA data also contain more recent regional data from Virginia Polytechnic Institute, which are comparable in precision with other recent data.

The Georgia Tech gravity data library also contains gravity data obtained by Woollard during the 1950's. These data predate a national base network and were tied to pendulum data. A bias in the pendulum data introduced a datum shift equivalent of 2 to 4 mGal depending on the location. The Woollard data were not used because most of the stations have subsequently been reoccupied. Also, recent data obtained by the University of South Carolina were not made available, and therefore are not included in the data set. The recent University of South Carolina data cover the northern corner of the 1 km grid.

The marine gravity data available offshore South Carolina are either outside or at the very southeastern edge of the 128 by 128, 1 km grid. Only a few points could contribute to the gravity values. Because there exists a gap of 5 to 10 km between the onshore data and the offshore data and because the contribution of the offshore data would be intermittent and uneven on the edge of the grid, these offshore data were not included in the 128 by 128, 1 km grid.

The magnetic data for the 1.0 km grid were obtained from the US Geological Survey, from a digitization and merging of recent aeromagnetic surveys. (Jeff Phillips, personal communications). The digitized magnetic data from the U. S. Geological Survey were on a Transverse Mercator projection at 0.5 km intervals. These coordinates were converted to the rotated Transverse Mercator projection and gridded at a 1 km interval.

The starting data sets for the 4.0 km and 8.0 km spaced grids were the Electric Power Research Institute (EPRI) magnetic, Bouguer gravity and elevation data grids. These are spaced at 4.0 km increments in the north and east direction using an Albers Equal Area Conic projection with two standard parallels, 29.5° and 45.5°, and origin at the equator and 96° west longitude. The Albers Equal Area Conic projection was converted to our rotated Transverse Mercator projection and gridded at

4.0 and 8.0 km intervals. The data were provided on magnetic tape courtesy of ETKI.

The bathymetry data for areas off-shore were obtained from the National Geophysical Data Center, NOAA, E/GC in the 5 by 5 minute gridded data format. These were used to fill in areas of the EPRI data over the ocean that were lacking in bathymetric data.

Merging and Compiling Data

All the data incorporated in the 1 km grid for gravity data were carefully examined. Duplicate points and points which were inconsistent with neighboring points were removed before generating the grid. The program designed to remove duplicate points "CLEAN" and the program designed to identify inconsistent data "CLERR" are given in Appendix A-6.

Program CLEAN was designed to identify duplicate and virtual duplicate points. Each new point was compared to a sorted listing of the gravity points and those pairs that were closer than a distance of 0.2 km were listed for examination. One of the duplicate points was then removed. The choice of which point to remove was based on the value of the Bouguer Anomaly. Duplicate points were common because the same data were often obtained from multiple sources. This duplicity was easily identified on the basis of identical gravity values and survey designations. In a few cases the same data were reduced using two different international gravity formulae. The standard differences in the absolute value of gravity allowed a choice of the data referenced to the IGSN 71 datum. When the same location was sampled by two different surveys, the choice of which value to use was more difficult. In general, we chose the value most consistent with neighboring points. In some surveys, data were obtained at closely spaced intervals along lines. Such data tend to bias values computed by a weighted average technique by concentrating excessive weight at a few grid points along these lines. In order to minimize this kind of bias and provide a data set with more uniform data distribution, selected data points were removed from these lines. In essence, points closer than 0.2 km were considered duplicates and selectively removed.

Program CLERR was designed to identify values that were anomalous or inconsistent. Each point tested was removed from the data set and the eight nearest points were found. These points were then used to estimate by a weighted average method the value and uncertainty at the point. Any point that exceeded one standard deviation of the uncertainty of the extrapolated value was considered to be a possible error or inconsistent value. These values were examined for a possible correction. If a correction was not possible and the apparent error could not be explained by gradients or uncertainty in the data, the value was considered in error and removed.

Assessment of Precision

The weighted average method used in gridding the gravity data is easily adaptable to computation of precision. The equations in Heiskanen and Moritz (1968, pg 267) were used. The relation requires the autocorrelation function of the gravity data in order to incorporate the variation of gravity data with distance in the estimate of precision of extrapolated data. The equation used to compute m_p^2 , the variance at a point p, was

$$m_p^2 = m^2 + C_0 - \frac{n}{2} \sum_{i=1}^n a_{pi} C_{pi} + \sum_{i=1}^n \sum_{j=1}^n a_{pi} a_{pj} C_{ik} \quad (2)$$

where m^2 is the variance of the data measurement,
 a_{pi} is the normalized weight for the point p to the gravity value at i
 C_{ik} is the covariance function at a distance equal to the separation of the ith and kth points.
 n is the number of data points in the average.

The autocorrelation function for the gravity data in the Charleston 128 by 128, 1 km grid are shown in figure A-1-2. The correlation distance is 15 km and the variance is 80 mGal² (+ 9 mGal standard deviation). Using this autocorrelation function and the distribution of gravity data, the estimated error at any point can be computed.

Presentation of the Data

A summary of the data grids and computer programs which have been generated is given in table I. The Bouguer gravity anomalies, elevations, and their weights for the 128 by 128, 1 km grid are combined in file GRIDRAW. The weights are identical for the elevations and Bouguer gravity anomalies. The elevations were obtained directly from the gravity data and, thus, if desired, the free air anomalies could be computed from the Bouguer anomalies and elevation data. The Bouguer anomalies are in milligals, the elevation in feet and the weights in data points per square kilometers. The smoothed and extrapolated Bouguer anomalies and elevations, obtained by applying program AB to file GRIDRAW are combined with the magnetic data in file GD1SMT. The precision of the file is limited to 0.1 mGal, .1 ft., and 1.0 gamma. GD1SMT has also been separated for convenience and use on microcomputers into separate files for Bouguer anomalies (GD1SMTG), elevations (GD1SMTE) and magnetic anomalies (GD1SMTM). The contoured versions of these data are shown as figures A-1-3,4, and 5, respectively.

The 64 by 64, 4 km grid and the 128 by 128, 8 km grid data were obtained largely from the EPRI 4 km grid data. The Bouguer gravity anomalies, elevations and magnetic anomalies are contained in GD2RAW and GD3RAW for the 4 km and 8 km grids, respectively. As with the 1 km

grid, separate files are available for the Bouguer anomalies, elevations and magnetic anomalies. These are presented as figures A-1-6, 7, and 8, respectively, for the 4 km grid and as figures A-1-9, 10, and 11, respectively, for the 8 km grid. The Bouguer anomalies in figure A-1-6 and 9 have been corrected for bathymetry over the ocean and hence appear negative off the continental shelf in GD3RAWG. However, the areas of coverage of GD2RAWG is on the continental shelf in shallow water and is not affected significantly by the depth of the water. The elevation data from EPRI did not indicate bathymetry data over the oceans. The ocean elevations were all given as zero. In GD3RAWG and GD3RAWG we have supplemented and replaced the EPRI sea surface values with bathymetry. The magnetic data from EPRI contain two areas with no data. At this time these two areas, which are over the ocean and at the edge of the grid, have been left open until compatible data are found.

Table I. Names of Programs and Data Grids for the Charleston Area.

<filename>	Description
GRIDRAW	Unsmoothed gravity anomalies, elevations and weights in Freefield format. Full precision is preserved for addition of new data.
GD1SMT	Smoothed Bouguer anomalies, elevations, and magnetic anomalies with limited precision. Format is 24I5 in groups of 132. The grid is 132 by 132 and includes the buffer.
GD1SMTG	Bouguer Anomalies from GD1SMT. Format is 24I5 in groups of 132. Units are tenths of mGals.
GD1SMT E	Elevations from GD1SMT. Units are tenths of feet. Format is 24I5 in groups of 132.
GD1SMTM	Magnetic anomalies from GD1SMT.
GD2RAW	Bouguer Gravity, elevations and magnetic anomalies in the 4 km grid. Format is 10F8.1 continuous for the remaining grids (i.e. BOUG(I,J),ELEV(I,J),MAG(I,J), I=1,68,J=1,68)
GD2RAWG	Bouguer anomalies in 4 km grid.
GD2RAW E	Elevations in 4 km grid.
GD2RAWM	Magnetic anomalies in 4 km grid.
GD3RAW	Bouguer anomalies, elevations and magnetic anomalies in the 8 km grid. Format is 10F8.1 continuous. (i.e. BOUG(I,J),ELEV(I,J),MAG(I,J), I=1,132, J=1,132)
GD3RAWG	Bouguer anomalies in 8 km grid.
GD3RAW E	Elevations in 8 km grid.
GD3RAWM	Magnetic anomalies in 8 km grid.
ANSERS3	Unsorted and uncleaned gravity data for 1 km grid. DoD gravity data format.
ANSERS4	Sorted and cleaned gravity data for 1 km grid. DoD gravity data format.
SCDATA	Listing of new Charleston area data (1985-86).

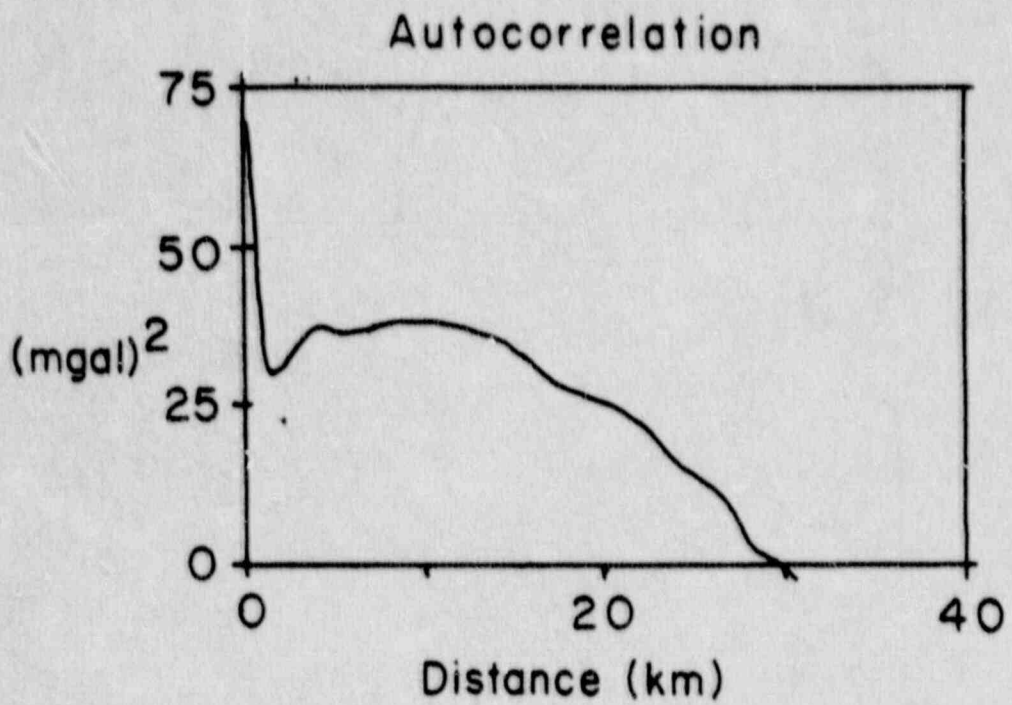


Figure A-1-2. One dimensional approximation for the autocorrelation function of the Charleston area gravity data.

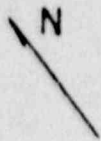
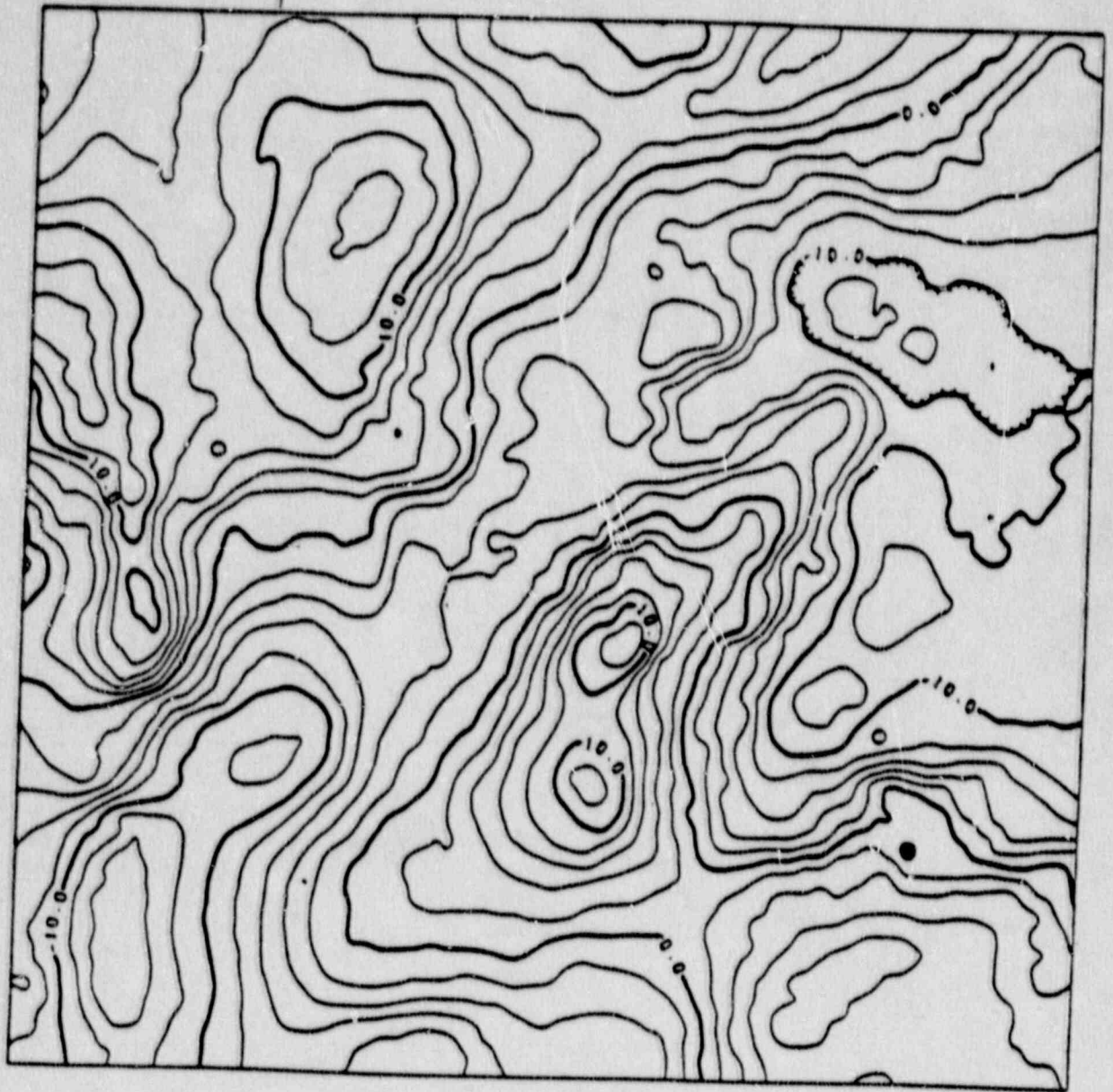


Figure A-1-3. Contour plot of smoothed Bouguer anomalies in GD1SMTG. Data are from the 128 x 128 point grid with a 1.0 km grid interval. Contour interval is 2 mGal.

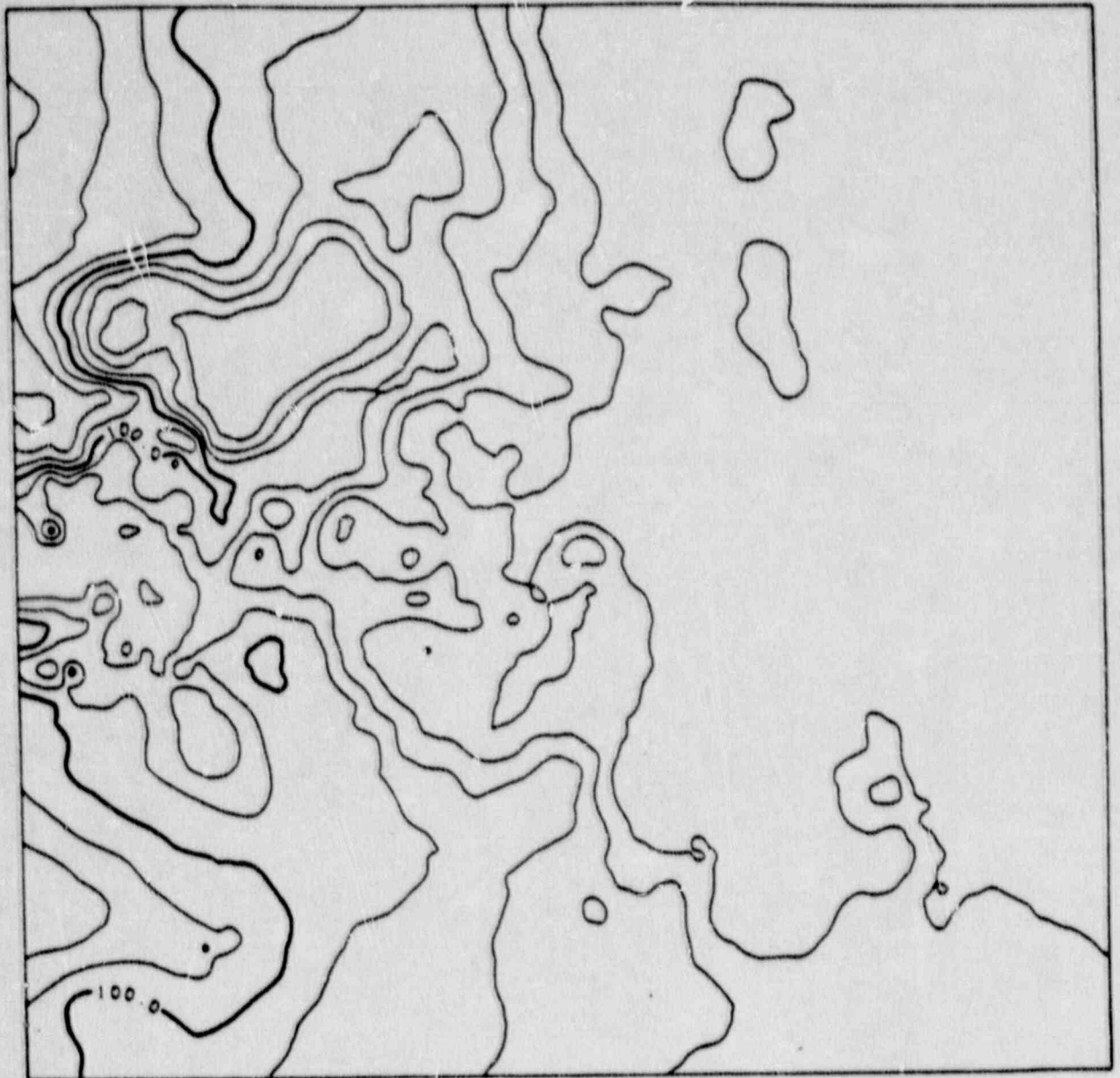


Figure A-1-4. Contour plot of smoothed elevations in GD1SMTE. Data are from the 128 x 128 point grid with a 1.0 km grid interval. Contour interval is 20 feet.

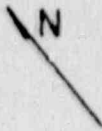
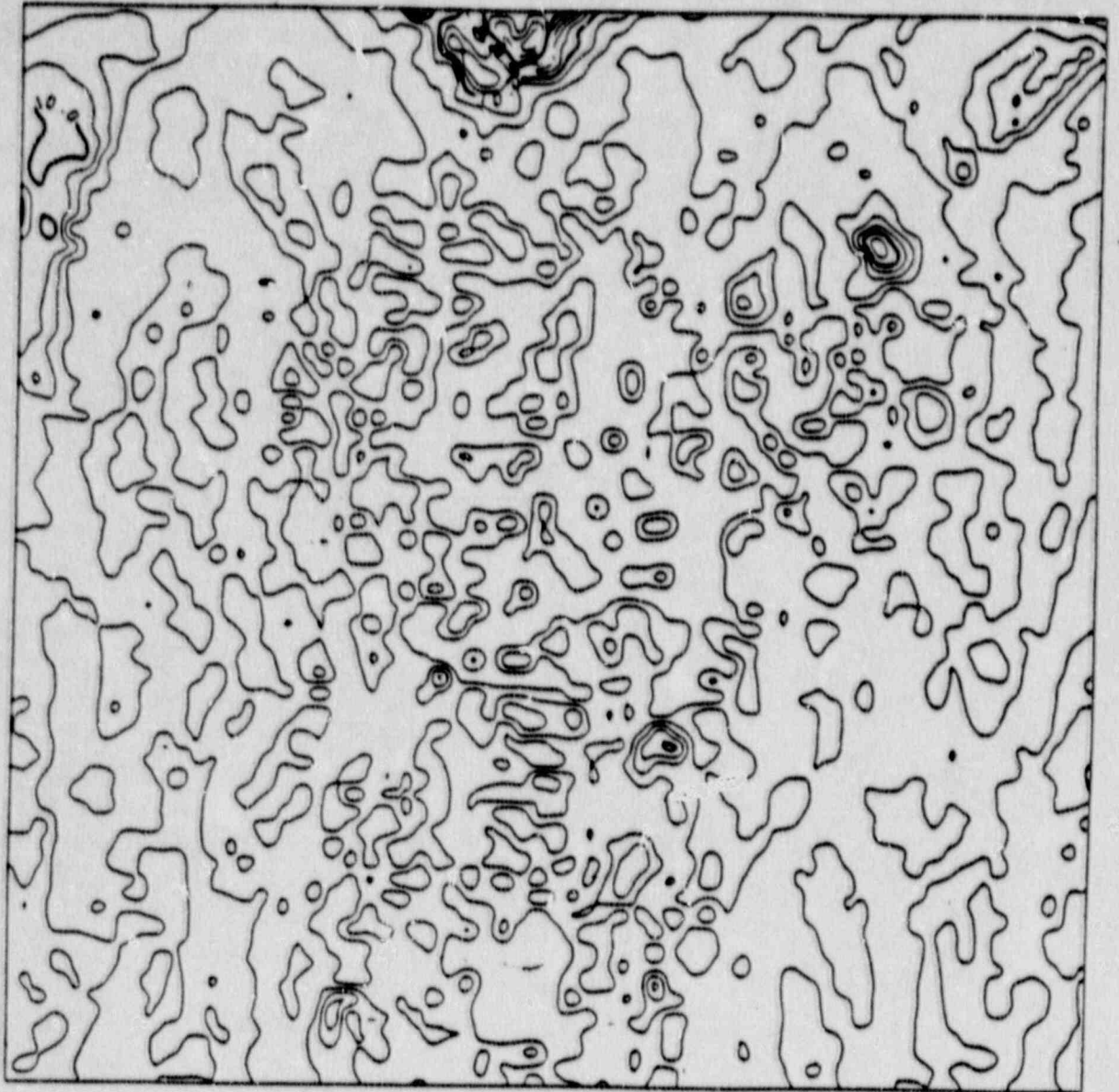


Figure A-1-5. Contour plot of smoothed weights in GD1SMTW. Data are from the 128 x 128 point grid with a 1.0 km grid interval. Contour interval is 1.0 point per square km.

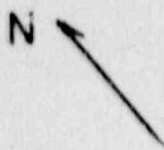
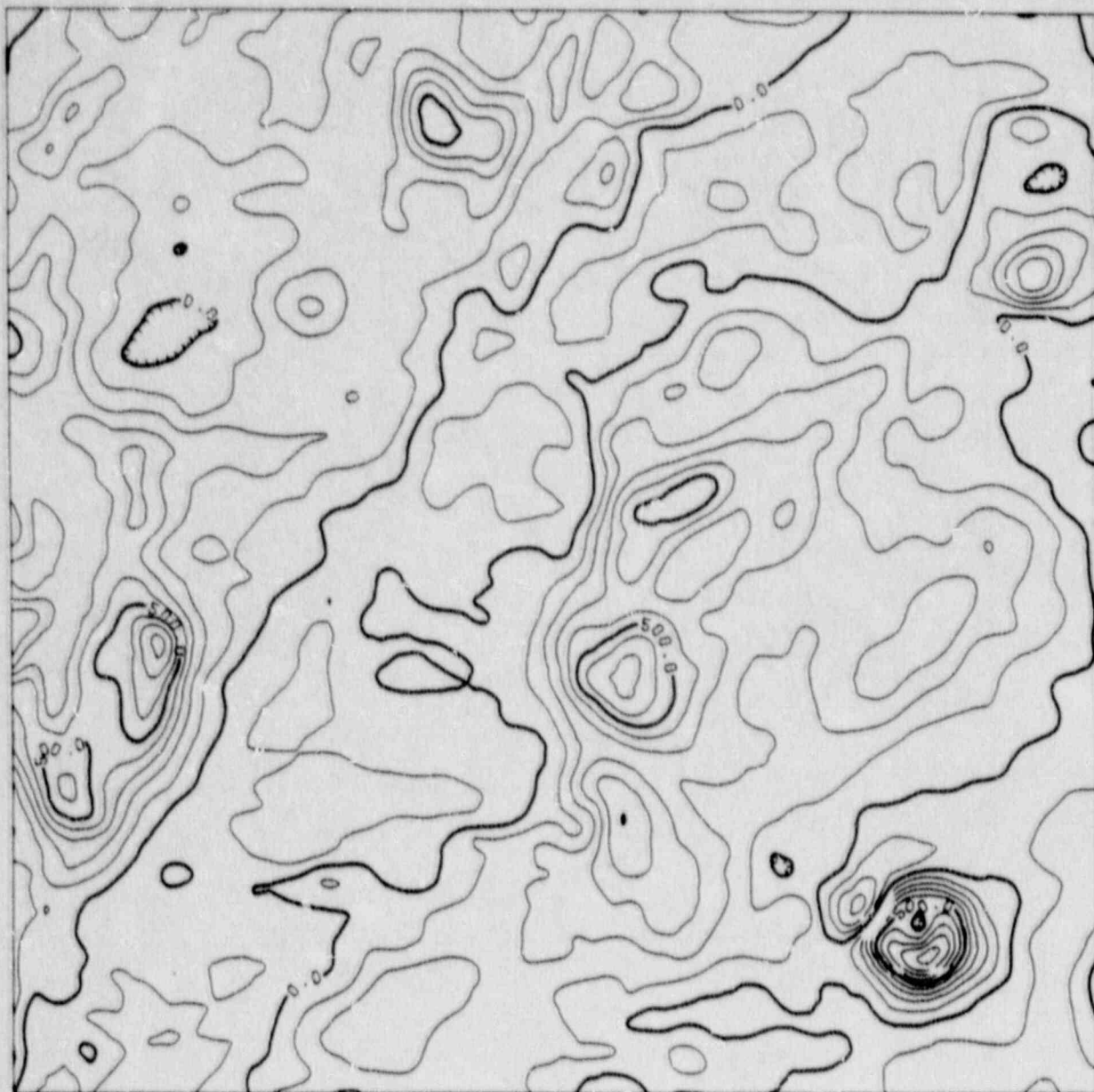


Figure A-1-6. Contour plot of smoothed magnetic anomalies in GD1SM1M. Data are from the 128 x 128 point grid with a 1.0 km grid interval. Contour interval is 100 gammas.

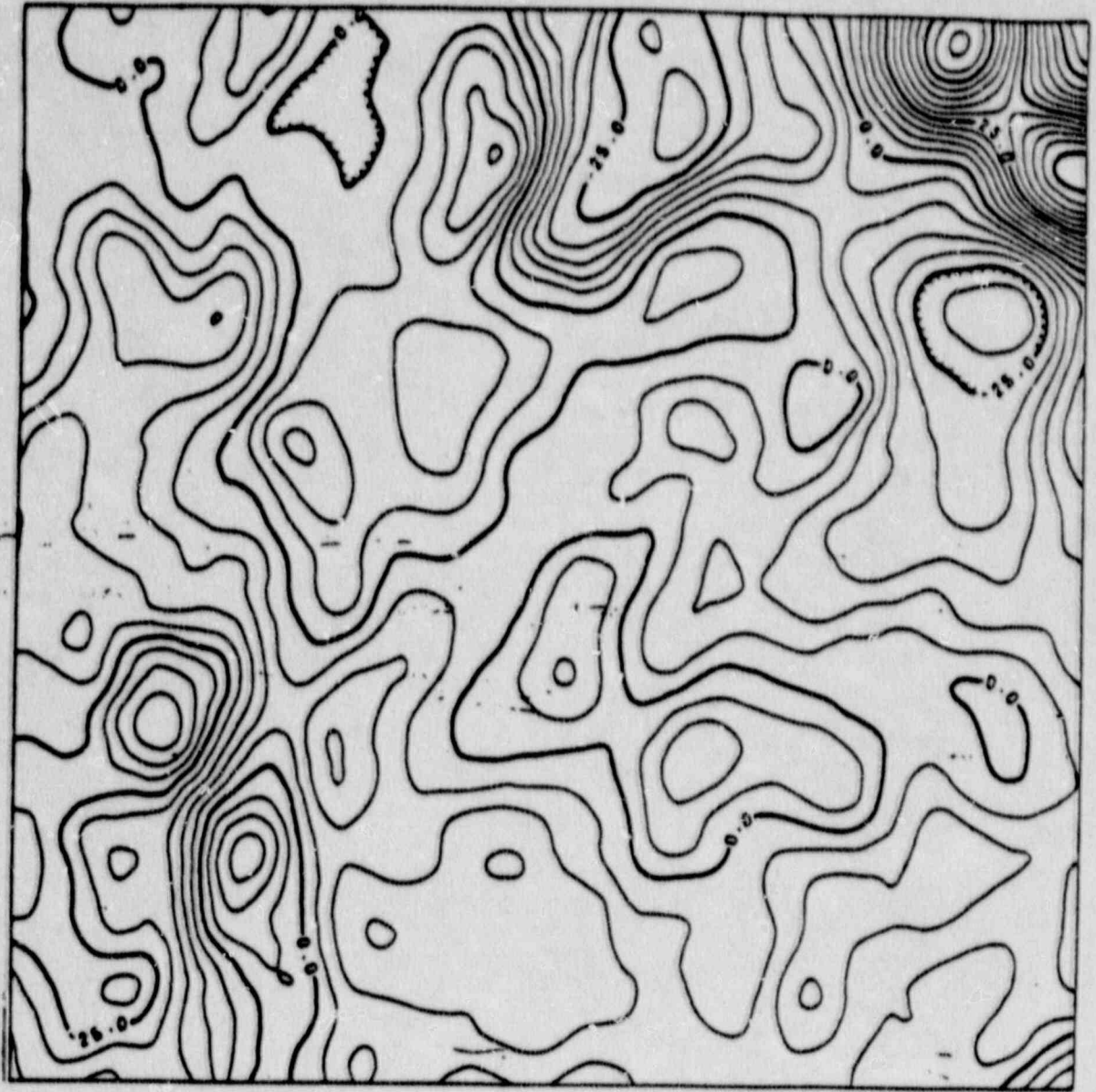


Figure A-1-7. Contour plot of Bouguer anomalies in GD2RAWG. Data are from the 64 x 64 point grid with a 4.0 km grid interval. Contour interval is 5.0 mGal.

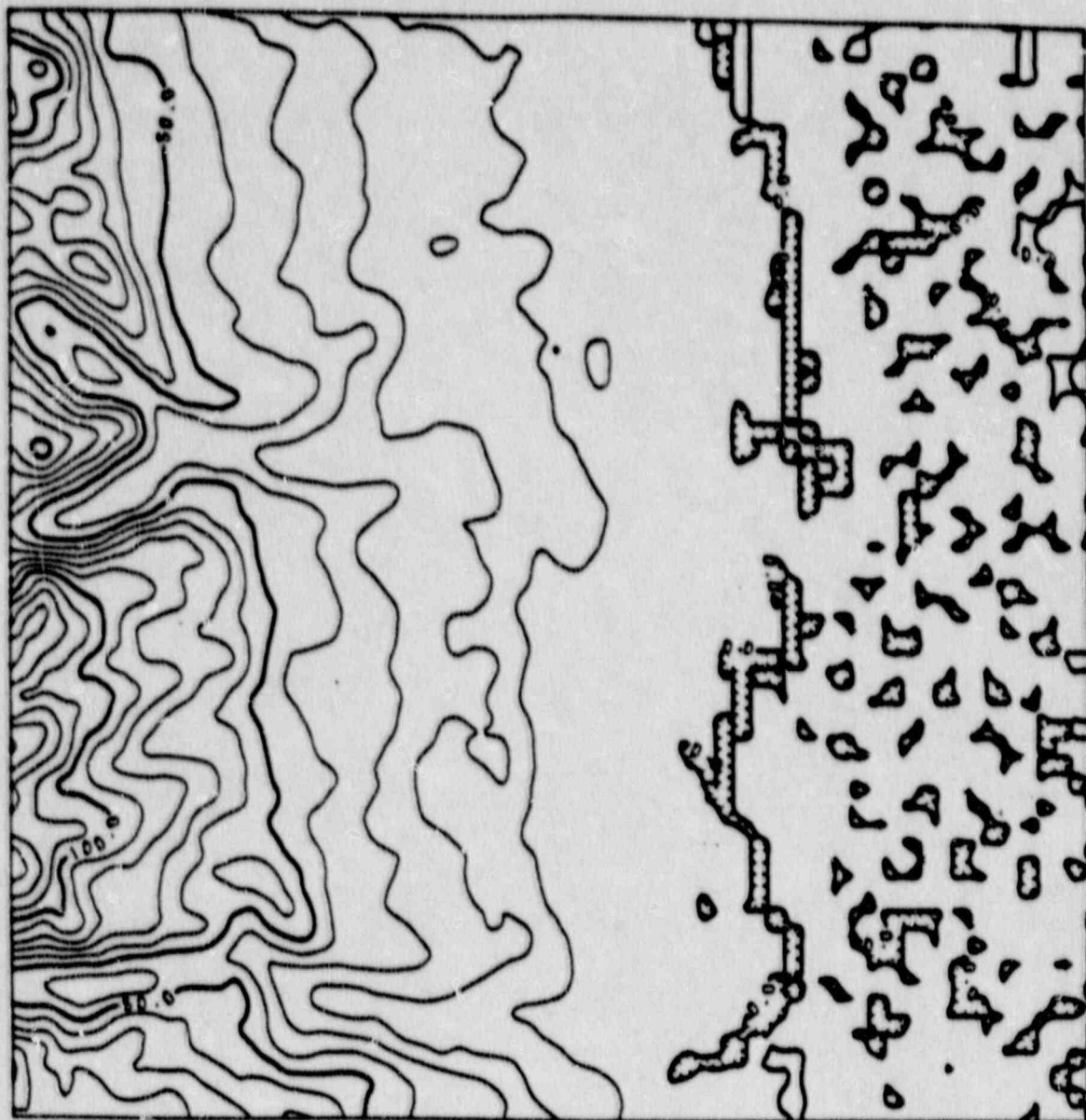


Figure A-1-8. Contour plot of elevations in GD2RAWE. Data are from the 64 x 64 point grid with a 4.0 km grid interval. Contour interval is 10 meters.

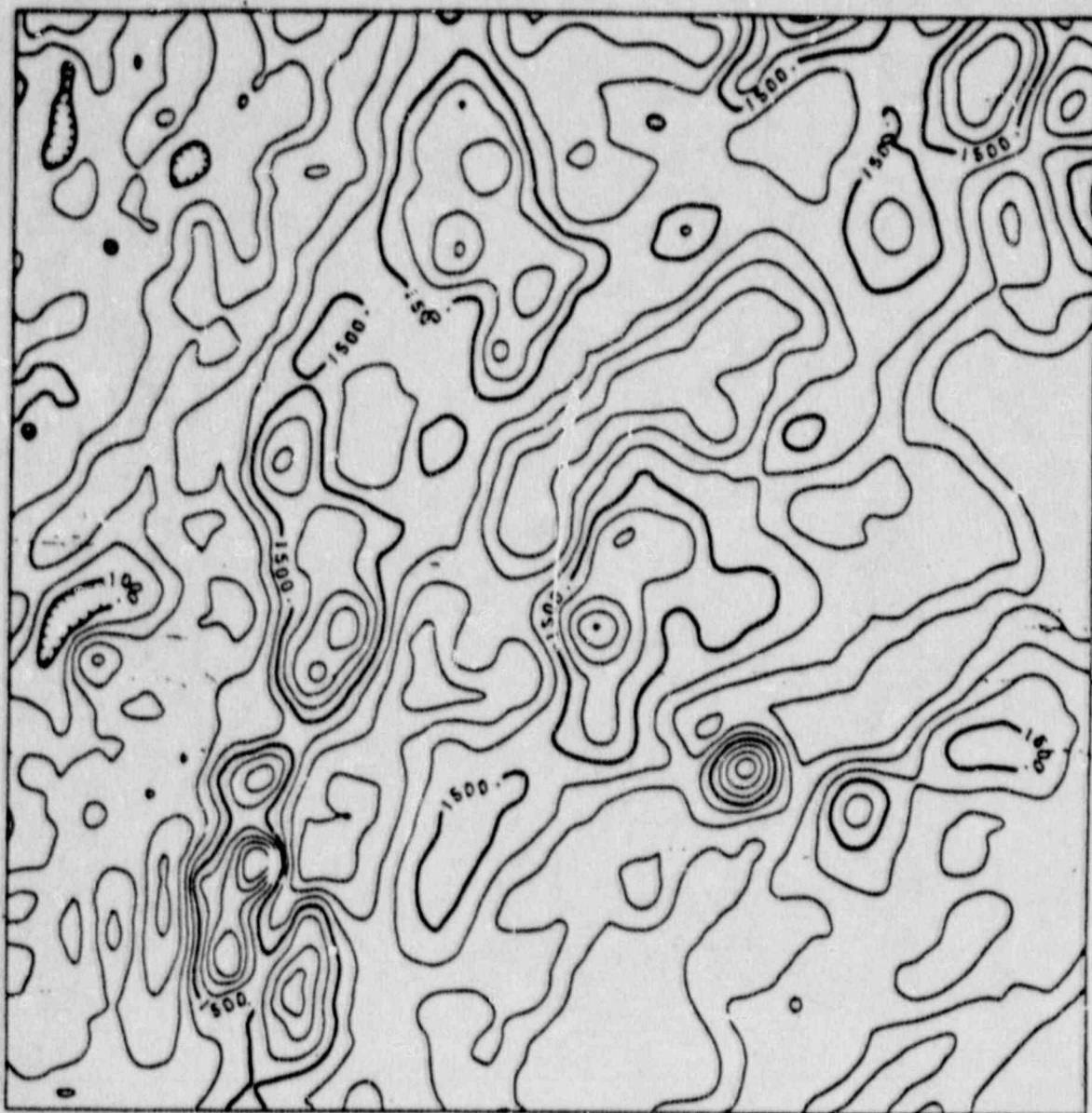


Figure A-1-9. Contour plot of magnetic anomalies in GD2RAWM. Data are from the 64 x 64 point grid with a 4.0 km grid interval. Contour interval is 125 gammas.

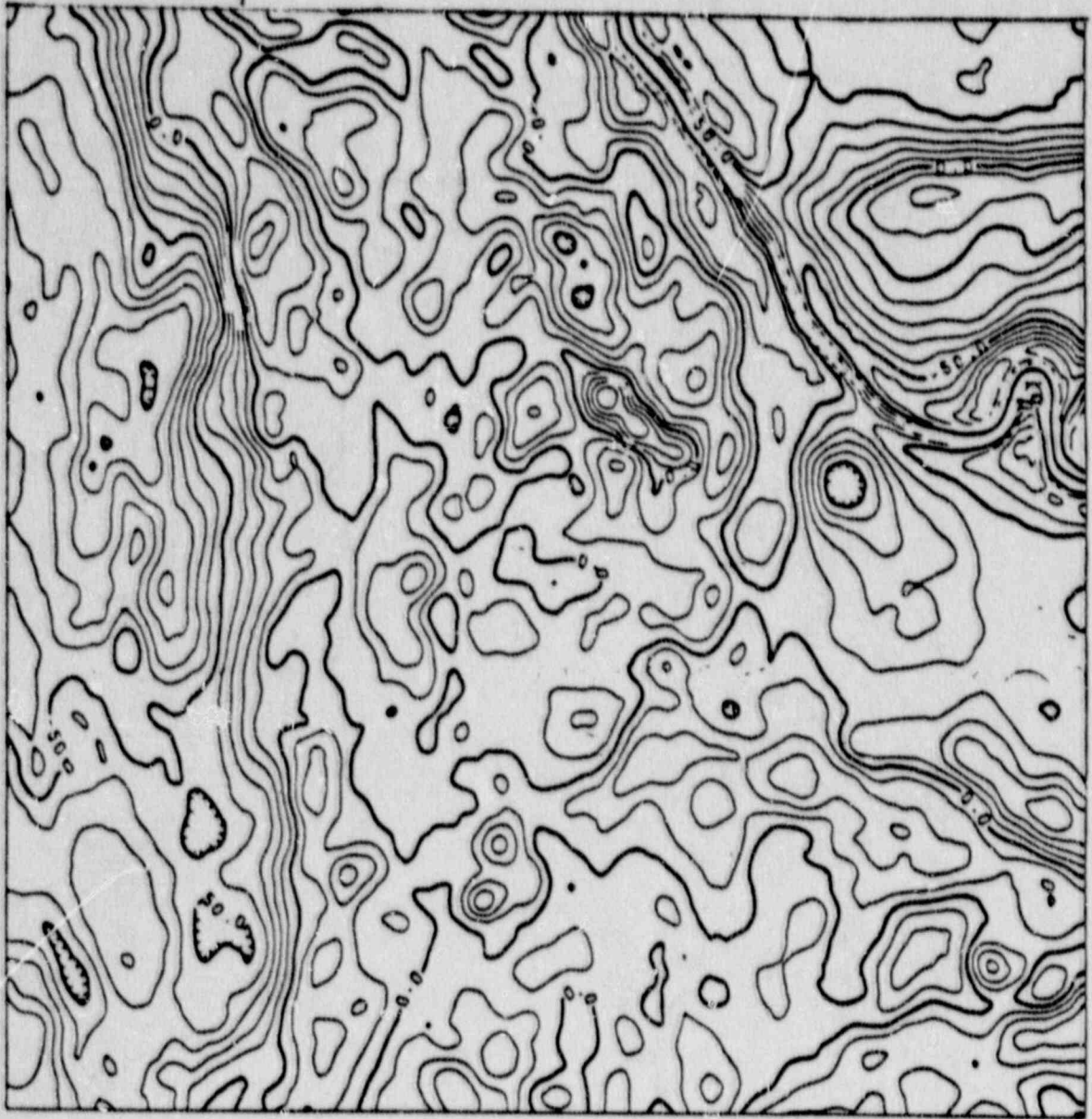


Figure A-1-10. Contour plot of Bouguer gravity anomalies in GD3RAWG. Data are from the 128 x 128 point grid with an 8.0 km grid interval. Contour interval is 10 mGal.

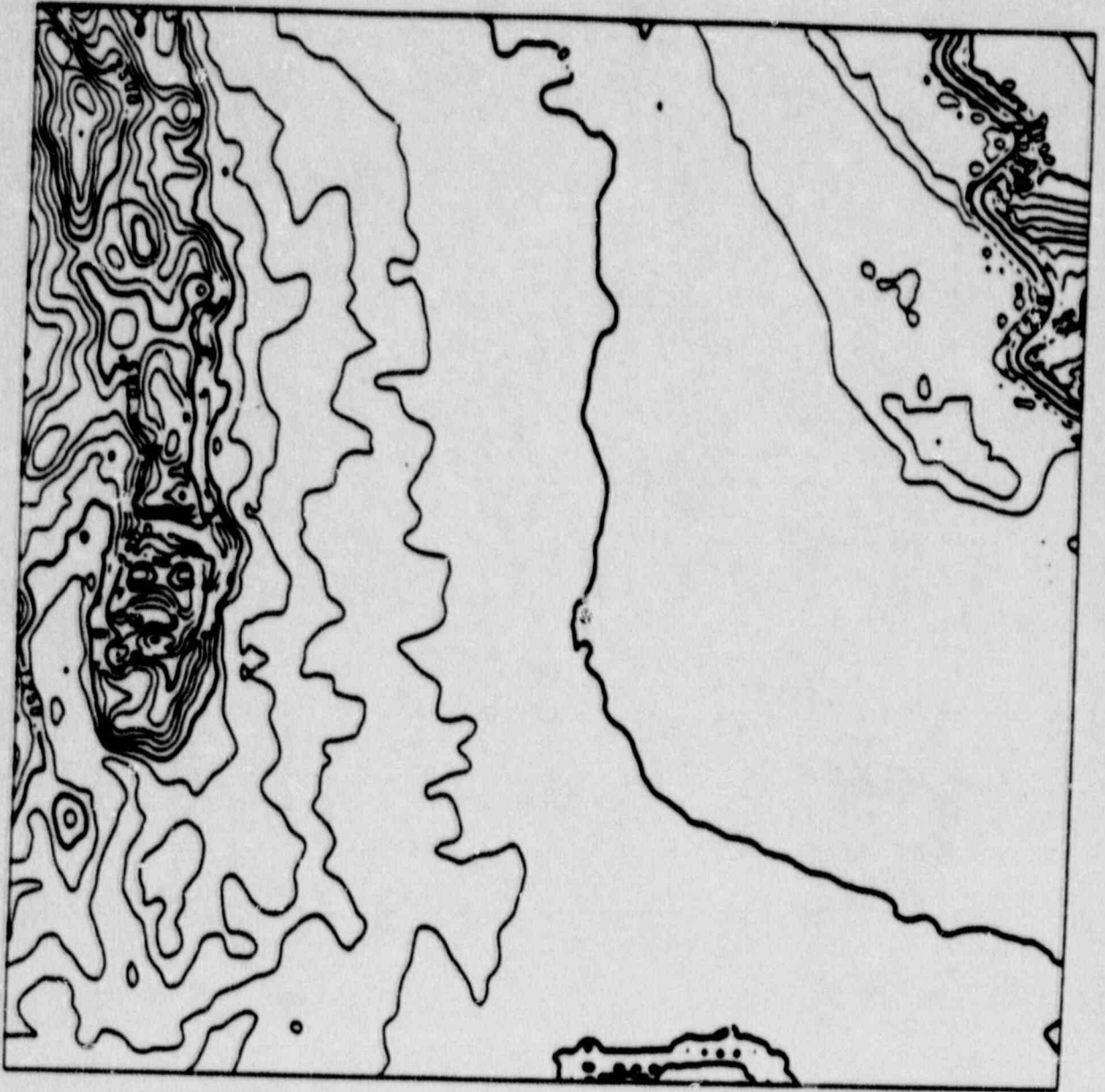


Figure A-1-11. Contour plot of elevation in GD3RAWE. Data are from the 128 x 128 point grid with an 8.0 km grid interval. The contour interval is 250 feet.



Figure A-1-12. Contour plot of magnetic anomalies in GD3RAWE. Data are from the 128 x 128 point grid with an 8.0 km grid interval. The contour interval is 100 gammas.

2. PRINCIPAL FACTS FOR NEW CHARLESTON AREA GRAVITY DATA

Introduction

An investigation and evaluation of the causes of seismicity near Charleston, South Carolina, may be optimized by an examination of available data in a uniform format. The Bouguer gravity anomalies will provide valuable constraints for determination of the structures in the crust. An objective of gravity data acquisition and analysis is to accumulate available gravity data for the Charleston vicinity and to increase the density of coverage, where appropriate, in a 128 by 128 km rectangular area centered on the epicentral zone of the 1886 Charleston earthquake. In this report, the principal facts are documented for new gravity data obtained within the 128 x 128 km area. Other reports will document the design of data grids, and the modeling of the crust using gravity and magnetic data.

The goal in gravity data acquisition was to provide sufficient data to complete a grid with a uniform 1.0 km spacing between points and 128 points on each side. The grid is to be rotated to follow the coastline and maximize the land area. Such a grid would require 16,000 points and only about 3200 points were available prior to this study. Since resources were available for only about 600 new data points, the locations of the 600 points were concentrated in areas of sparse coverage near the epicenter of the 1886 Charleston earthquake. Hence, areas of new data were chosen to expand the areas of existing coverage in the central portion of the grid and to fill in large areas without coverage.

Sources of Data:

The largest single block of data was obtained by Champion (1976). The Champion (1976) data (shaded central block in figure 1) include detailed survey areas near the epicenter of the 1886 earthquake. Gravity data in the area of the 1972 Bowman earthquake were obtained by McKee (1976). Other Georgia Tech data include a selection of detailed line data and existing regional data. U.S. Geological Survey data (Phillips and Davis, 1985) were made available to the study. These data expand the Champion (1976) data to the west, northwest, and north. Data from the Virginia Polytechnic Institute and State University and other data available from the DoD Gravity Services Branch complement the U.S. Geological Survey data. University of South Carolina data (not made available to this study) cover the northern corner of the study area. Consequently, based on this existing coverage, it was decided to obtain additional data east of the Champion (1976) data and to fill in major holes between the U.S. Geological Survey and Bowman area data. The only remaining significant areas of sparse data would be in areas of difficult access near the coast and lake or swamp areas to the north.

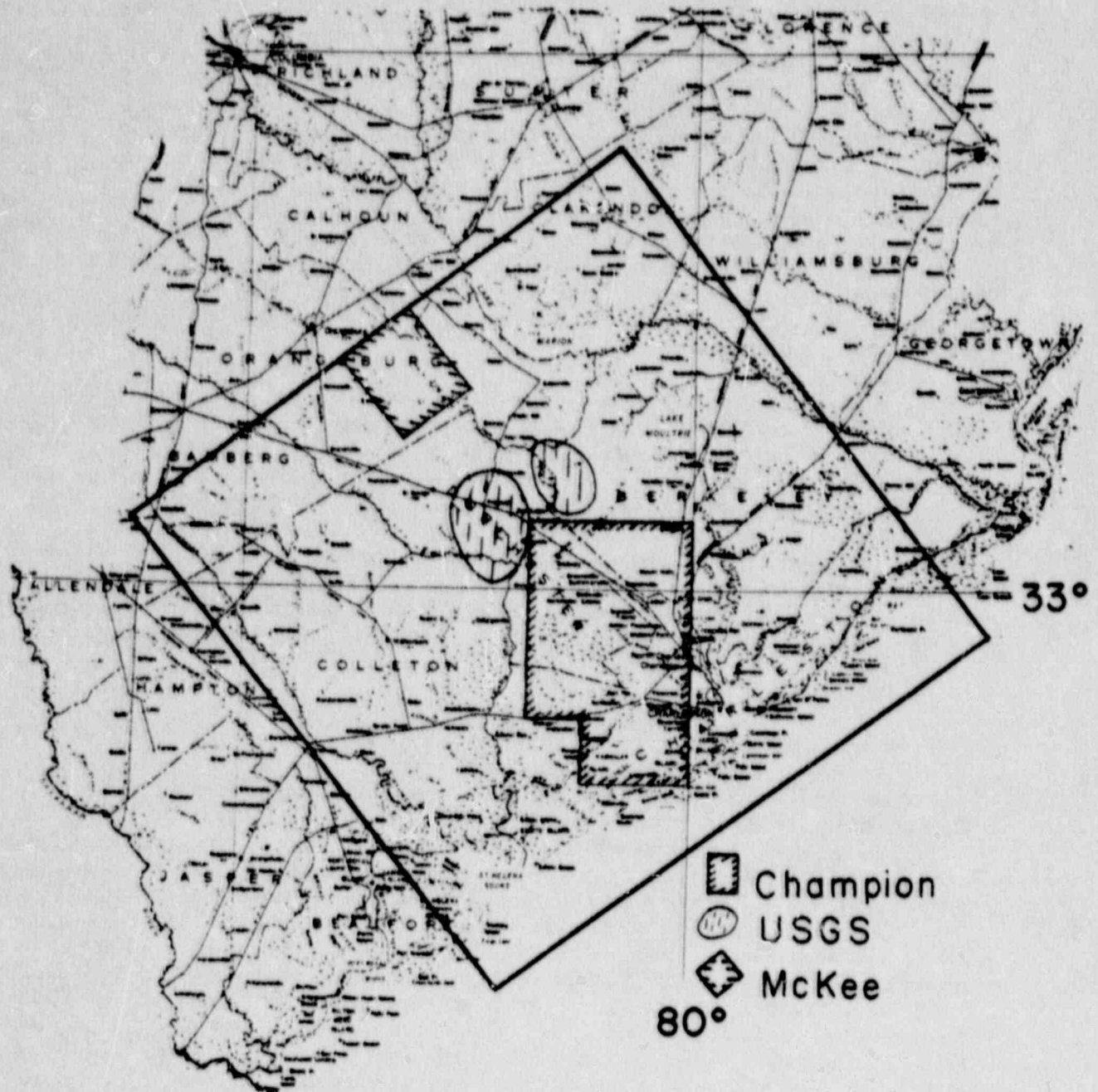


Figure A-2-1. Areas of gravity data coverage prior to the Georgia Tech field survey.

Standard methods of data acquisition and reduction were followed. Data reduction utilized program "GRAVUN" on file at the Georgia Institute of Technology, School of Geophysical Sciences. Corrections were applied for earth tides and drift. Observed gravity values are referenced to the IGSN 1971 datum (International Association of Geodesy, 1971b) and anomalies were calculated using the 1967 Geodetic Reference System (International Association of Geodesy, 1971a). No terrain corrections were applied because of the gentle topography. Data were obtained along lines at a spacing of less than 0.5 km or as regional data at a 1.0 km spacing. These techniques are outlined in Champion, 1976. Table A-2-1 lists the surveys. All surveys were made with LaCoste-Romberg gravity meter number 668. All data are tied to the Branchville state base. Temporary base station values are given in Table A-2-2. Figure 2 is a point plot of the new data obtained and figures 3a-f are point plots of the total composite gravity data coverage, except for the University of South Carolina data which were not made available. Table A-2-3 is a listing of the new gravity data in standard DoD format (figure A-2-4).

Table A-2-1. List of surveys and principal facts.

Survey Number	Data	Time EDST	Quad Sheet(s)	Operator	Type Base	No. Sta.	Drift mGal/hr
909	9/07/85	8:56-12:14 -17:05	Summerville NW	Alexander	Line StJ	41	0.09 0.14
910	9/08/85	9:30-12:56 -15:25	Summerville NW	Alexander	Line EXX	45	0.14 0.05
911	9/09/85	8:50-13:45	Pringletown	Alexander	Line BST	46	0.16
912	9/13/85	10:35-18:28	Kittridge N. Charleston	Alexander	Line Dup	62	0.12
913	9/15/85	12:00-15:57	Kittridge	Alexander	Line TAV	32	-0.01
914	9/16/85	8:29-13:08 -14.03	Maple Cane Sw.	Alexander	Line S18	71	0.13 -0.25
915	9/24/85	12:12-16:34 -18:38	Kittridge Huger	Alexander	Line I41	52	0.09 -0.01
916	9/25/85	11:11-14:14	Huger	Alexander	Line I41	35	0.07
917	9/26/85	10:15-14:16 18:24-19:36	Huger	Alexander	Line 141	54	0.07 0.01
918	9/27/85	11:13-15:07	Maple Cane Sw.	Alexander	Line 161	48	0.09
919	9/23/85	12:22-16:49	Base Stations	Alexander	reg. Wylie	8	0.05
Base station loop "Branchville state base-Wylie-St.J-Tav-EXX-BST-518-Branchville State Base"							
920	6/06/86	11:50-17:54	Base Stations	Alexander	reg. Wylie	5	-0.05
Base station loop "Wylie-Dup-TAV-I41-Wylie"							
922	6/06/86	11:50-17:54 -21:03	St. George SW Maple Cane Sw.	Radford	reg. BSB	28	0.05
923	6/07/86	9:24-13:35 -19:02	Reevesville St. George SW	Radford	reg. BSB	49	-0.01 -0.07

Table A-2-1 (cont.)

<u>Base Station Abbreviations</u>	
BSB	Branchville State Base
TAV	Tavou Church
I41	Highway 41 at S-8-98
Dup	Dupont plant entrance
BST	Beer Store Brick
StJ	Saint James Church
S18	road S 18-30 at 76 station

Table A-2-2. Gravity values at temporary base stations.

Name	Surveys	Latitude	Longitude	Elev.(m)	Value (mgals)
Branchville	922,923	33 .15	80 49.00	38.6	979577.051
Wylie	920,919	33 .97	80 11.67	25.0	979557.292
Dupont	912	33 3.14	79 57.00	3.9	979567.737
TAV	913	33 6.35	79 56.42	9.1	979569.350
I41	915,16,17	33 5.76	79 48.29	7.9	979567.575
StJ	909	33 8.37	80 9.69	20.1	979567.896
EXX	910	33 8.53	80 9.66	20.1	979568.270
BST	911	33 12:50	80 15.43	25.9	979578.955
S18	914	33 1.53	80 23.22	19.2	979561.509
S61	918	33 3.06	80 29.99	18.9	979561.375

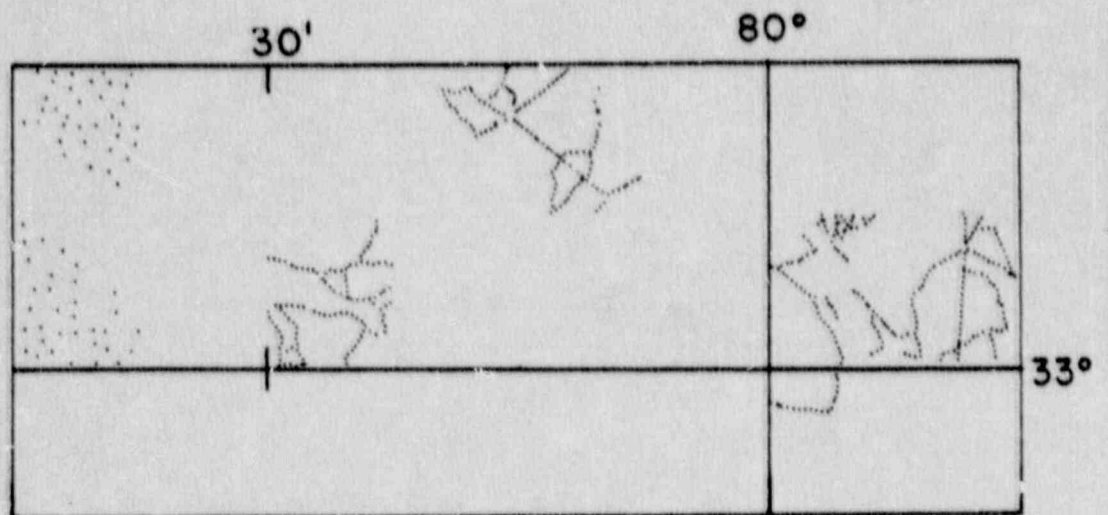


Figure A-2-2. Point plot of new data obtained by Georgia Tech.

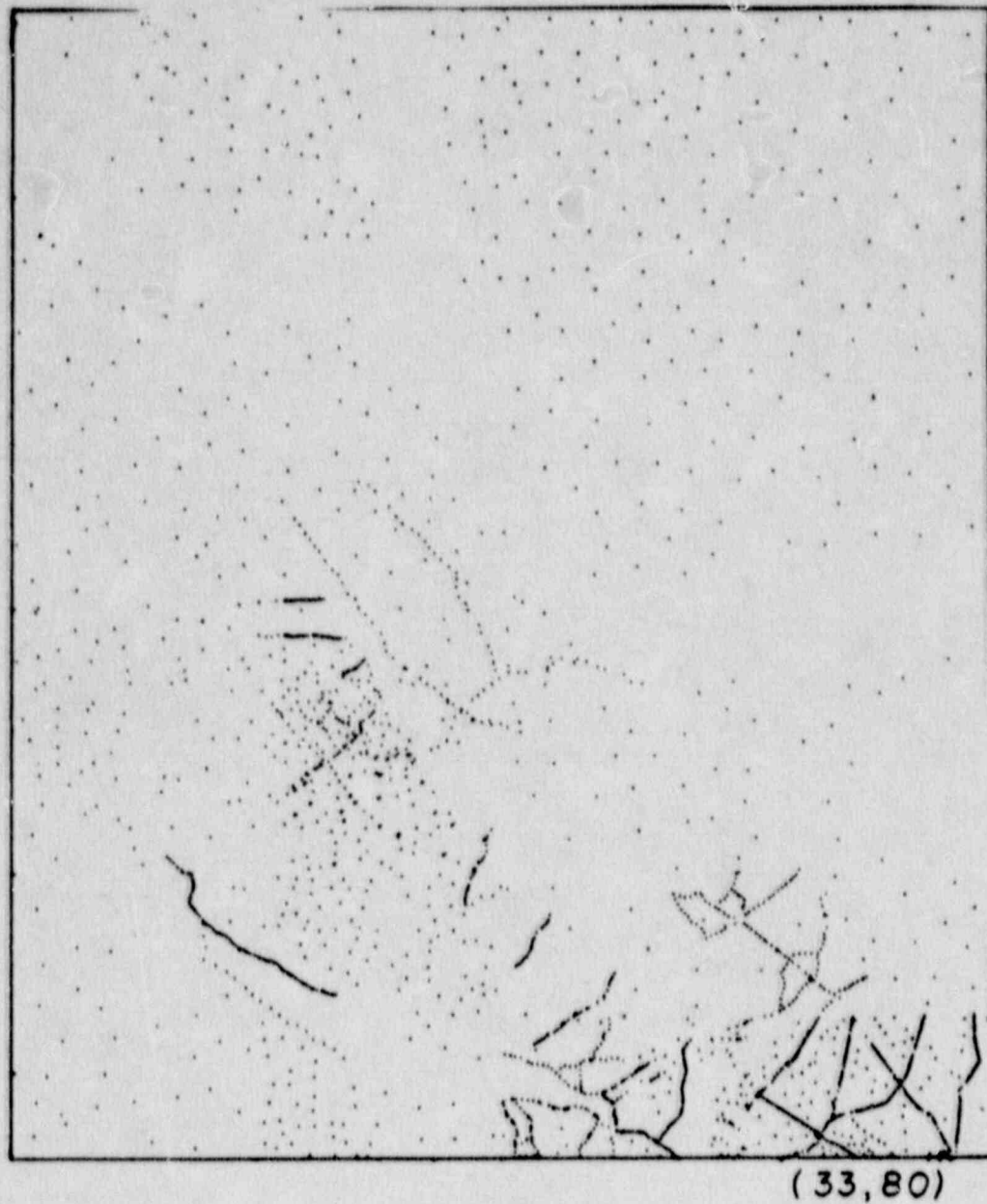
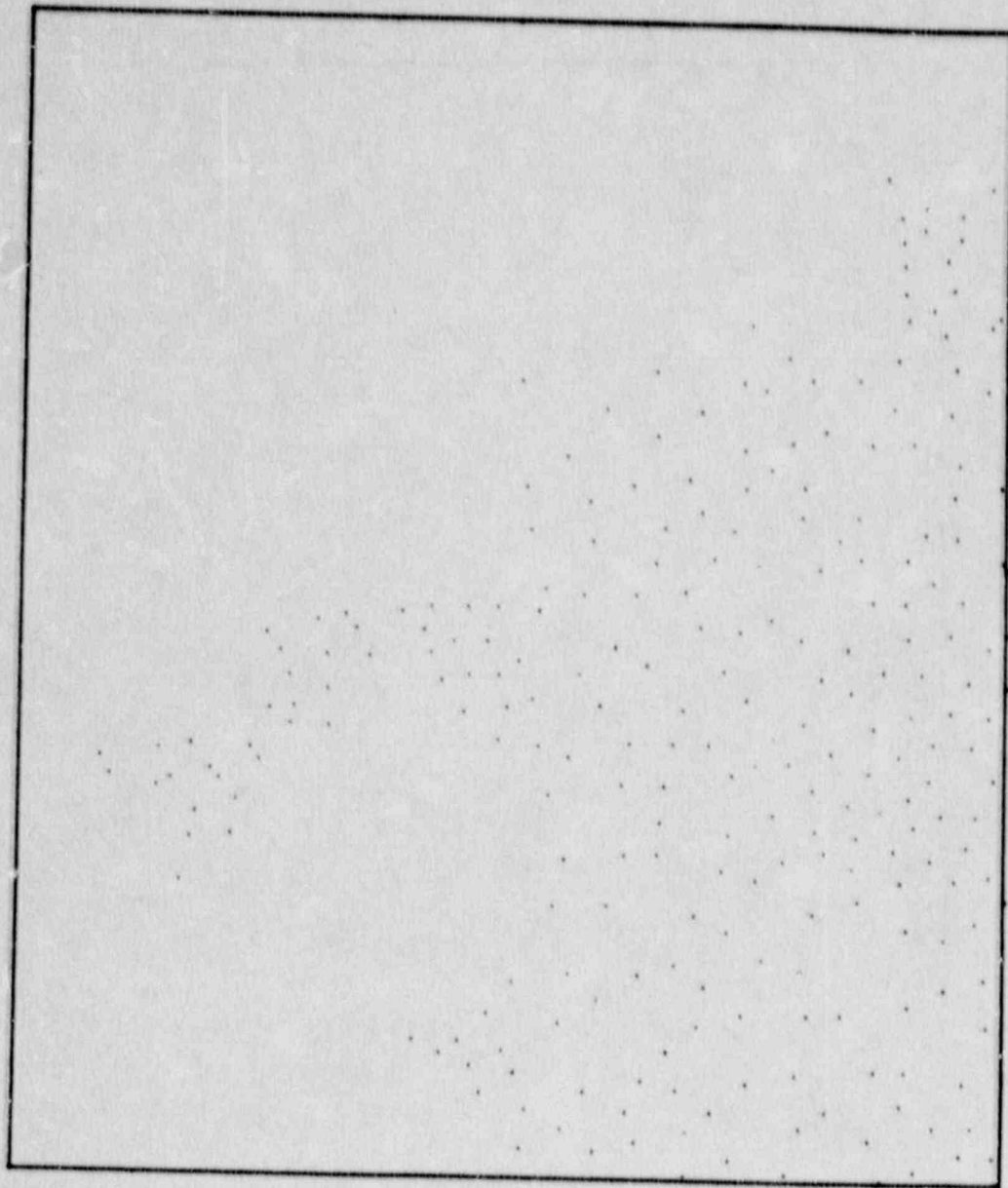


Figure A-2-3a. Point plot of gravity data in the degree square 33°N , 80°W .



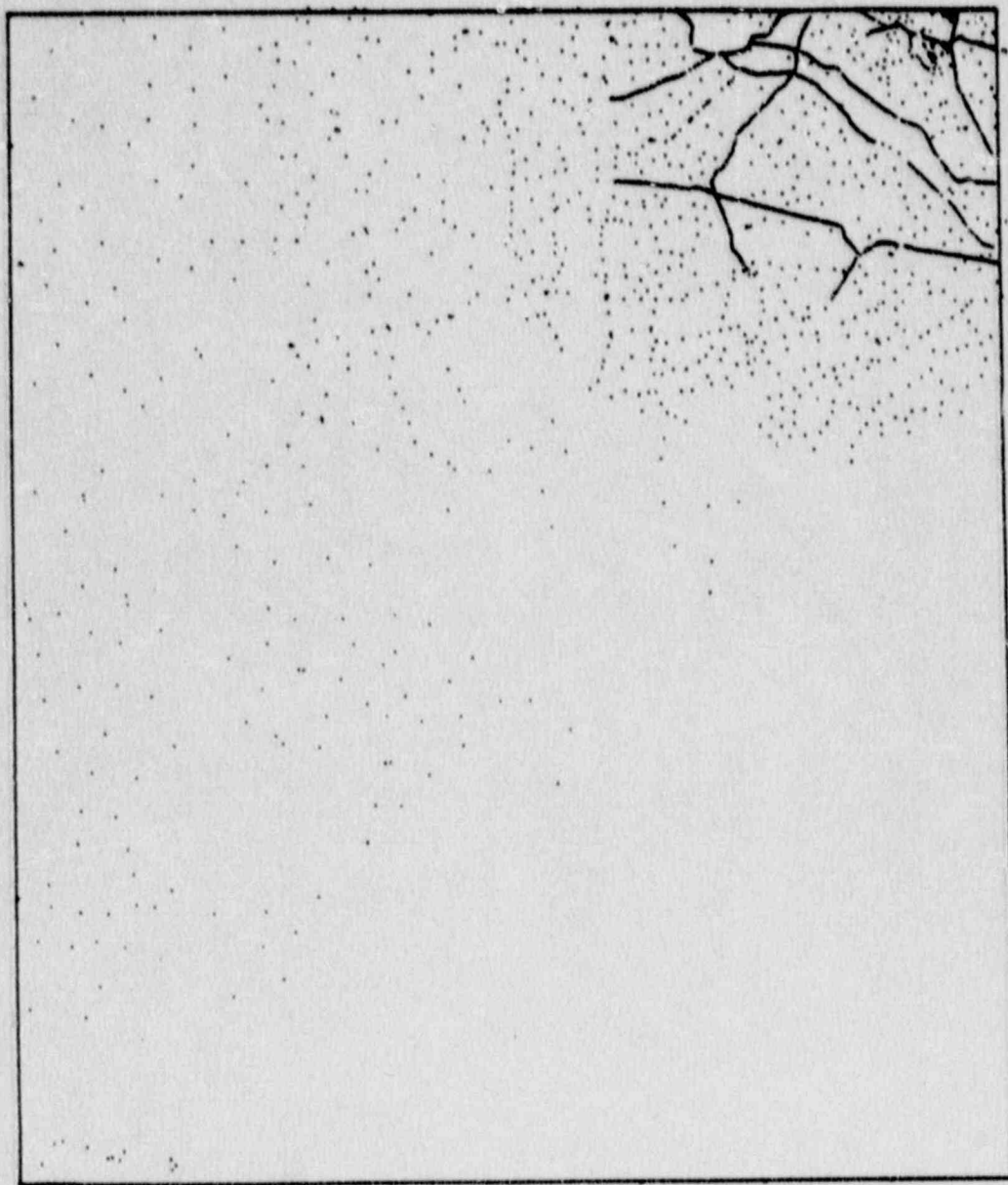
(33, 81)

Figure A-2-3b. Point plot of gravity data in the degree square 33°N , 81°W .



(32, 81)

Figure A-2-3c. Point plot of gravity data in the degree square 32°N . 81°W .



(32, 80)

Figure A-2-3d. Point plot of gravity data in the degree square 32°N , 80°W .

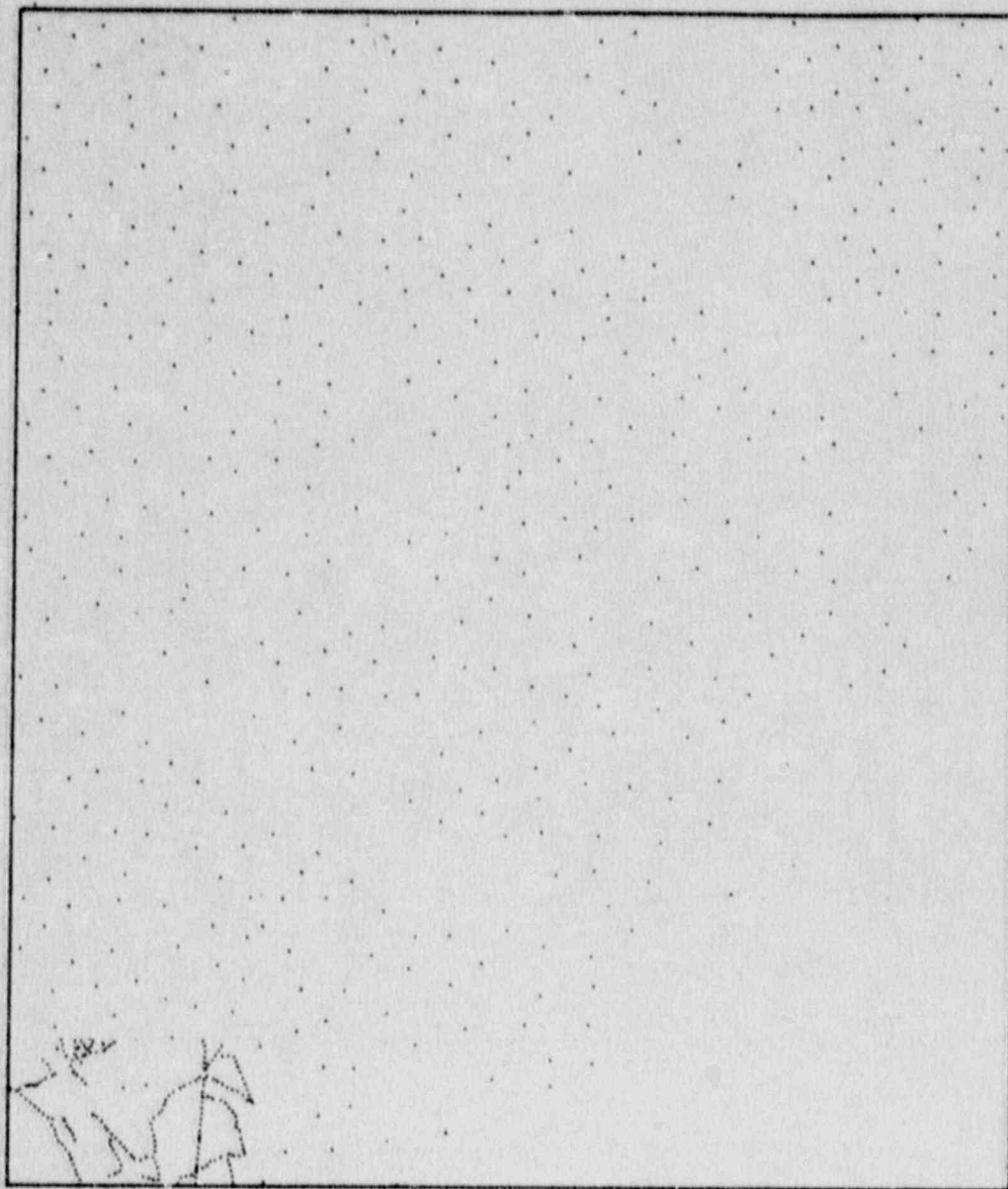
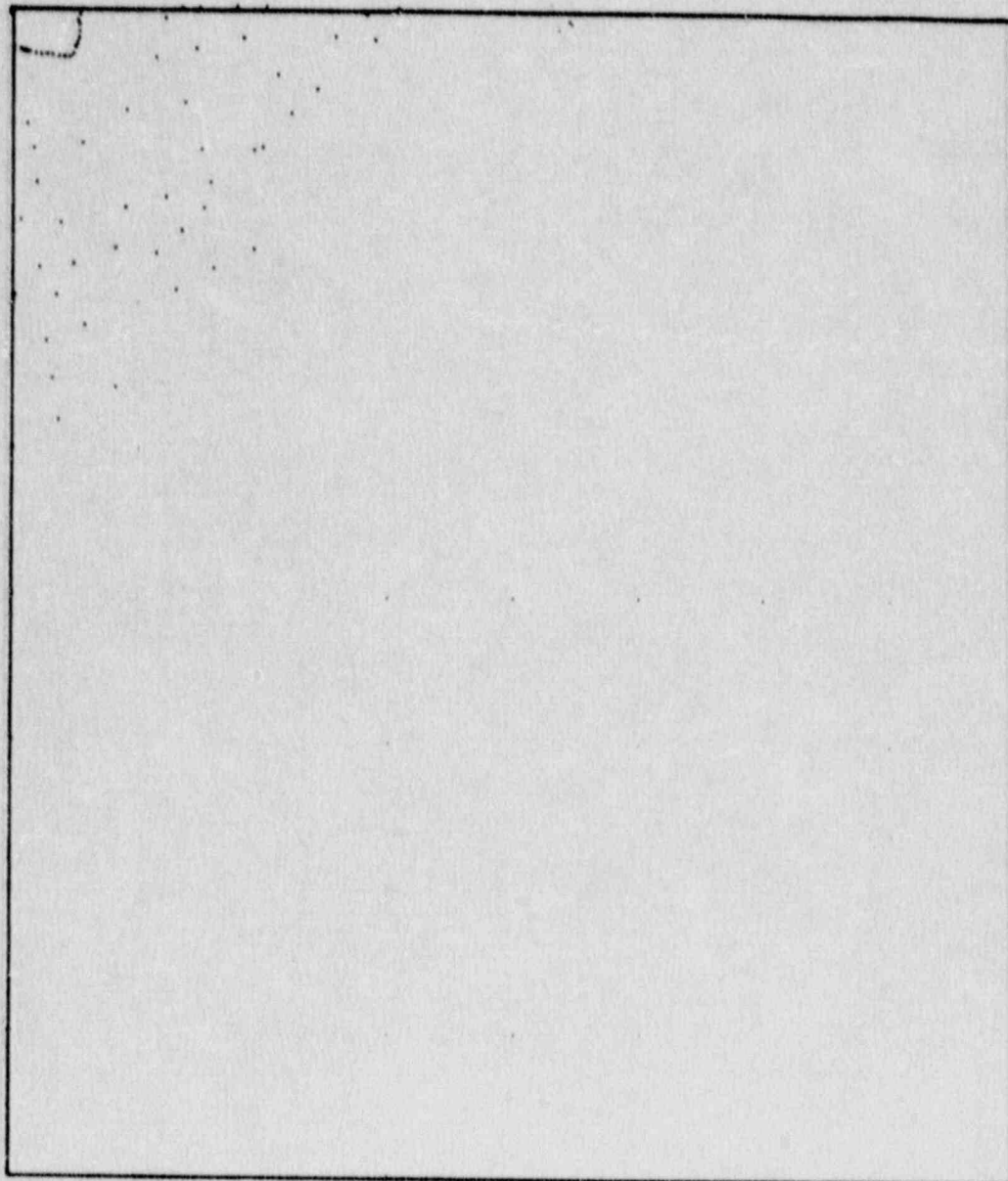


Figure A-2-3e. Point plot of gravity data in the degree square 33°N , 79°W .



(32,79)

Figure A-2-3f. Point plot of gravity data in the degree square 32°N , 79°W .

Figure A-2-4. DoD Gravity data coding format used for the new Charleston Gravity data.

A-2-12

SOURCE NO	TITLE	CODED BY										DATE CODED										SEQUENCE (Col. 69-72)									
SECURITY CLASS (Col. 1)		SECURITY CONTROL (Col. 2)		GEOGRAPHIC UNITS (Col. 3)		TYPE OF ELEVATION (Col. 21)		ELEVATION UNITS (Col. 22)		ELEVATION OF STATION (Col. 23-29)		SUPPLEMENTAL ELEVATION (Col. 31-35)		BOUGUER ANOMALY (Col. 50-54)		ISD OR T.C. CODE (Col. 56)		SOURCE		BASE REFERENCE STATION		SEQUENCE		FILE MAINTENANCE		EST STD DEV		REMARKS			
000000																															
111111																															
222222																															
333333																															
444444																															
555555																															
666666																															
777777																															
888888																															
999999																															

CODES USED IN ABOVE

SECURITY CLASS (Col. 1)
U - UNCLASSIFIED MATERIAL
F - FOR OFFICIAL USE ONLY
C - CONFIDENTIAL
S - SECRET

SECURITY CONTROL (Col. 2)
1 - LIMITED DISSEMINATION, TO FULL-TIME EMPLOYEES OF DEPT OF DEFENSE, CIA AND AEC
2 - NOT RELEASABLE TO FOREIGN NATIONALS
3 - LIMITED DISSEMINATION, NOT RELEASABLE TO FOREIGN NATIONALS
4 - SPECIAL RELEASE FROM ORIGINATING AGENCY REQUIRED FOR DISSEMINATION TO 3RD PARTY
5 - MODIFIED HANDLING AUTHORIZED (INCLUDES FOREIGN "RESTRICTED", NATO, CENTO, SEATO, ETC.)

GEOGRAPHIC UNITS (Col. 3)
BLANK OR D - DEGREES AND MINUTES TO 01 MINUTE
1 - DEGREES, MINUTES AND SECONDS
2 - DEGREES TO .0001 DEGREE

TYPE OF ELEVATION (Col. 21)
1 - LAND
2 - SUBSURFACE
3 - OCEAN SURFACE
4 - OCEAN SUBMERGED
5 - OCEAN BOTTOM
6 - LAKE SURFACE (ABOVE SEA LEVEL)
7 - LAKE BOTTOM (ABOVE SEA LEVEL)
8 - LAKE BOTTOM (BELOW SEA LEVEL)
9 - LAKE SURFACE (ABOVE SEA LEVEL)
WITH LAKE BOTTOM BELOW SEA LEVEL
A - LAKE SURFACE (BELOW SEA LEVEL)
B - LAKE BOTTOM (SURFACE BELOW SEA LEVEL)
C - ICE CAP (BOTTOM BELOW SEA LEVEL)
D - ICE CAP (BOTTOM ABOVE SEA LEVEL)
E - TRANSFER DATA GIVEN

ELEVATION UNITS (Col. 22)
BLANK OR D - METERS
1 - FEET
2 - FATHOMS

ELEVATION OF STATION (Col. 23-29)
NOTE: THIS FIELD WILL CONTAIN DEPTH OF OCEAN (POSITIVE DOWNWARD) IF COL 21 CONTAINS 3, 4, OR 5

SUPPLEMENTAL ELEVATION (Col. 31-35)
DEPTH OF INSTRUMENT, LAKE OR ICE, POSITIVE DOWNWARD FROM SURFACE

BOUGUER ANOMALY (Col. 50-54)
SIMPLE BOUGUER ANOMALY WITH A MEAN DENSITY OF 2.67. NO TERRAIN CORRECTION

ISD OR T.C. CODE (Col. 56)
INDICATES IF ISOSTATIC ANOMALY OR TERRAIN CORRECTION IS GIVEN IN DOCUMENT
0 - NO ISOSTATIC ANOM OR T.C. IN DOCUMENT
1 - TERRAIN CORRECTION GIVEN IN DOCUMENT
2 - ISOSTATIC ANOMALY GIVEN IN DOCUMENT
3 - BOTH ARE GIVEN IN DOCUMENT

Table A-2-3. Listing of new Charleston data in DoD format.

33 853 - 80 966	1	201	3568245-	264-	489	G909	SC	0	2	0
33 870 - 80 998	1	192	3568422-	299-	513	G909	SC	0	3	3
33 886 - 80 028	1	152	3570750-	210-	380	G909	SC	0	4	3
33 904 - 80 1053	1	128	3571073-	278-	421	G909	SC	0	5	2
33 930 - 80 1088	1	207	3570113-	165-	396	G909	SC	0	6	2
33 956 - 80 1076	1	183	3571099-	178-	382	G909	SC	0	7	3
33 985 - 80 1068	1	168	3571325-	242-	429	G909	SC	0	8	3
33 1018 - 80 1061	1	183	3571608-	212-	416	G909	SC	0	9	3
33 1049 - 80 1067	1	192	3571723-	215-	429	G909	SC	0	10	3
33 1071 - 80 1065	1	192	3572290-	189-	403	G909	SC	0	11	2
33 1093 - 80 1046	1	122	3574042-	261-	397	G909	SC	0	12	3
33 1121 - 80 1035	1	189	3573248-	171-	382	G909	SC	0	13	3
33 1148 - 80 1026	1	195	3573890-	127-	344	G909	SC	0	14	2
33 1172 - 80 1027	1	183	3574943-	91-	295	G909	SC	0	15	3
33 1207 - 80 1013	1	192	3575518-	54-	268	G909	SC	0	16	2
33 1385 - 80 1014	1	183	3576578-	222-	426	G909	SC	0	17	3
33 1270 - 80 1013	1	186	3577088-	3-	210	G909	SC	0	18	3
33 1277 - 80 1024	1	168	3578004	23-	164	G909	SC	0	19	3
33 1319 - 80 1037	1	152	3579638	81-	89	G909	SC	0	20	3
33 950 - 80 1114	1	204	3570750-	138-	366	G909	SC	0	22	3
33 968 - 80 1140	1	204	3571356-	103-	331	G909	SC	0	23	3
33 1001 - 80 1185	1	183	3572332-	117-	321	G909	SC	0	24	3
33 1026 - 80 1221	1	192	3573155-	40-	254	G909	SC	0	25	3
33 1042 - 80 1243	1	198	3573993	40-	181	G909	SC	0	26	0
33 1058 - 80 1267	1	201	3574572	85-	139	G909	SC	0	27	2
33 1077 - 80 1293	1	204	3575182	129-	99	G909	SC	0	28	3
33 1095 - 80 1319	1	207	3575528	148-	83	G909	SC	0	29	3
33 1114 - 80 1347	1	207	3575862	156-	75	G909	SC	0	30	3
33 1133 - 80 1375	1	213	3576184	181-	57	G909	SC	0	31	3
33 1144 - 80 1391	1	213	3576726	219-	19	G909	SC	0	32	0
33 1163 - 80 1419	1	213	3577170	238	0	G909	SC	0	33	3
33 1181 - 80 1444	1	219	3577876	303	58	G909	SC	0	34	3
33 1201 - 80 1472	1	226	3578335	340	88	G909	SC	0	35	3
33 1216 - 80 1495	1	232	3578775	382	124	G909	SC	0	36	2
33 1062 - 80 1216	1	189	3574489	33-	178	G909	SC	0	37	3
33 1068 - 80 1181	1	192	3574131	0-	215	G909	SC	0	38	3
33 1069 - 80 1145	1	189	3573644-	61-	272	G909	SC	0	39	3
33 1071 - 80 1107	1	189	3573319-	95-	306	G909	SC	0	40	3
33 871 - 80 937	1	207	3568323-	262-	494	G910	SC	0	2	6
33 880 - 80 903	1	219	3568455-	225-	470	G910	SC	0	3	6
33 892 - 80 872	1	226	3568615-	206-	458	G910	SC	0	4	6
33 905 - 80 853	1	232	3568568-	210-	469	G910	SC	0	5	3
33 920 - 80 822	1	232	3568625-	225-	484	G910	SC	0	6	6
33 933 - 80 791	1	235	3568904-	206-	468	G910	SC	0	7	6
33 943 - 80 768	1	232	3569477-	172-	431	G910	SC	0	8	3
33 1014 - 80 1256	1	183	3573614-	6-	210	G910	SC	0	9	6
33 990 - 80 1272	1	168	3573398-	42-	229	G910	SC	0	10	6
33 968 - 80 1292	1	201	3572569-	9-	215	G910	SC	0	11	3
33 941 - 80 1280	1	192	3571875-	51-	265	G910	SC	0	12	6
33 913 - 80 1269	1	143	3572056-	145-	304	G910	SC	0	13	6
33 886 - 80 1275	1	195	3570400-	114-	332	G910	SC	0	14	6
33 859 - 80 1285	1	213	3570486-	11-	249	G910	SC	0	15	6
33 832 - 80 1294	1	219	3568512-	122-	367	G910	SC	0	16	1
33 800 - 80 1293	1	223	3567925-	157-	406	G910	SC	0	17	6
33 768 - 80 1301	1	226	3567708-	125-	377	G910	SC	0	18	3
33 782 - 80 1272	1	216	3567876-	156-	398	G910	SC	0	19	6
33 800 - 80 1244	1	226	3568080-	132-	384	G910	SC	0	20	6
33 819 - 80 1218	1	207	3568697-	153-	384	G910	SC	0	21	6
33 840 - 80 1197	1	183	3569864-	142-	346	G910	SC	0	22	6
33 865 - 80 1182	1	171	3570219-	178-	368	G910	SC	0	23	6
33 888 - 80 1161	1	158	3570986-	171-	347	G910	SC	0	24	6
33 908 - 80 1136	1	110	3571974-	250-	373	G910	SC	0	25	6
33 931 - 80 1115	1	189	3570248-	210-	420	G910	SC	0	26	6
33 814 - 80 986	1	213	3567363-	261-	499	G910	SC	0	27	6

33 793	- 801011	1	210	3567134-	265-	500	G910	SC	O	28	6
33 773	- 801033	1	207	3567247-	236-	467	G910	SC	O	29	6
331273	- 801508	1	198	3579246	247	26	G910	SC	O	31	6
331288	- 801485	1	253	3579766	448	166	G910	SC	O	32	6
331306	- 801456	1	247	3580245	451	176	G910	SC	O	33	6
331322	- 801425	1	253	3580559	480	198	G910	SC	O	34	6
331341	- 801396	1	256	3580890	495	210	G910	SC	O	35	6
331360	- 801362	1	262	3581165	515	223	G910	SC	O	36	6
331379	- 801336	1	265	3581867	570	274	G910	SC	O	37	6
331399	- 801310	1	274	3582056	589	283	G910	SC	O	38	6
331417	- 801284	1	271	3582934	642	339	G910	SC	O	39	6
331435	- 801257	1	271	3582537	578	276	G910	SC	O	40	6
331453	- 801231	1	271	3582965	596	294	G910	SC	O	41	6
331468	- 801213	1	268	3583342	604	304	G910	SC	O	42	1
331483	- 801194	1	277	3583751	651	342	G910	SC	O	43	6
331499	- 801543	1	259	3578738	71-	218	G910	SC	O	44	6
331231	- 801517	1	235	3578894	382	120	G911	SC	O	2	6
331229	- 801569	1	250	3578919	434	156	G911	SC	O	3	6
331217	- 801629	1	256	3578693	447	161	G911	SC	O	4	6
331204	- 801629	1	253	3578787	465	183	G911	SC	O	5	6
331188	- 801657	1	247	3578849	474	199	G911	SC	O	6	6
331176	- 801688	1	247	3579010	507	232	G911	SC	O	7	6
331154	- 801719	1	244	3579060	519	247	G911	SC	O	8	6
331150	- 801748	1	244	3579184	551	279	G911	SC	O	9	3
331182	- 801759	1	259	3579731	610	321	G911	SC	O	10	6
331205	- 801777	1	290	3579401	638	315	G911	SC	O	11	6
331229	- 801808	1	274	3580654	684	378	G911	SC	O	12	6
331242	- 801839	1	213	3581264	539	301	G911	SC	O	13	6
331268	- 801857	1	183	3583489	631	427	G911	SC	O	14	6
331291	- 801875	1	152	3582029	359	189	G911	SC	O	15	6
331308	- 801902	1	198	3582521	526	305	G911	SC	O	16	6
331333	- 801921	1	287	3583550	867	548	G911	SC	O	17	6
331359	- 801937	1	274	3584404	879	573	G911	SC	O	18	6
331386	- 801948	1	247	3586270	944	669	G911	SC	O	19	3
331377	- 801908	1	268	3585584	953	653	G911	SC	O	20	6
331368	- 801877	1	290	3584603	933	610	G911	SC	O	21	6
331371	- 801845	1	283	3584968	946	630	G911	SC	O	22	6
331389	- 801815	1	274	3585475	945	639	G911	SC	O	23	6
331391	- 801780	1	262	3585374	894	601	G911	SC	O	24	3
331375	- 801769	1	259	3584745	844	555	G911	SC	O	25	6
331351	- 801750	1	265	3583332	755	439	G911	SC	O	26	6
331333	- 801724	1	280	3582572	751	438	G911	SC	O	27	6
331318	- 801694	1	299	3581278	698	365	G911	SC	O	28	1
331344	- 801661	1	290	3581794	686	363	G911	SC	O	29	6
331358	- 801631	1	287	3582186	696	377	G911	SC	O	30	6
331380	- 801615	1	287	3582922	739	419	G911	SC	O	31	3
331412	- 801590	1	293	3583617	783	457	G911	SC	O	32	1
331439	- 801576	1	296	3584413	835	505	G911	SC	O	33	6
331468	- 801566	1	293	3585426	887	561	G911	SC	O	34	6
331493	- 801561	1	302	3586625	1001	664	G911	SC	O	35	3
331398	- 801567	1	290	3582944	726	403	G911	SC	O	36	6
331381	- 801550	1	280	3582077	634	321	G911	SC	O	37	6
331372	- 801527	1	268	3581661	567	268	G911	SC	O	38	6
331354	- 801513	1	259	3581633	562	273	G911	SC	O	39	6
331330	- 801514	1	262	3580638	504	212	G911	SC	O	40	6
331311	- 801522	1	274	3579598	465	179	G911	SC	O	41	6
331304	- 801665	1	280	3580700	604	291	G911	SC	O	42	6
331285	- 801637	1	259	3580551	548	259	G911	SC	O	43	6
331270	- 801609	1	229	3579790	399	144	G911	SC	O	44	6
331260	- 801577	1	277	3579292	513	204	G911	SC	O	45	6
33 232	- 795602	1	21	3565782-	210-	234	G912	SC	O	2	6
33 260	- 795611	1	24	3565357-	283-	310	G912	SC	O	3	6
33 286	- 795629	1	67	3565296-	192-	267	G912	SC	O	4	6
33 305	- 795651	1	70	3565558-	182-	260	G912	SC	O	5	6
33 332	- 795662	1	67	3566105-	175-	250	G912	SC	O	6	6
33 338	- 795733	1	21	3567887-	146-	170	G912	SC	O	7	6

33 346 - 795764 1	18	3568454 -	110-	130	G912 SC O	8	6
33 365 - 795791 1	40	3568928 -	22-	66	G912 SC O	9	6
33 384 - 795816 1	64	3568598 -	7-	78	G912 SC O	10	6
33 404 - 795840 1	76	3566703 -	186-	271	G912 SC O	11	6
33 424 - 795867 1	24	3570062 -	38-	65	G912 SC O	12	6
33 442 - 795894 1	67	3569321 -	4-	79	G912 SC O	13	6
33 461 - 795920 1	73	3569445 -	0-	81	G912 SC O	14	6
33 481 - 795948 1	91	3569589 -	44-	58	G912 SC O	15	6
33 572 - 795721 1	34	3570430 -	177-	214	G912 SC O	16	6
33 641 - 795796 1	34	3570654 -	250-	287	G912 SC O	17	6
33 619 - 795767 1	27	3570657 -	237-	237	G912 SC O	18	6
33 596 - 795750 1	30	3570536 -	209-	243	G912 SC O	19	6
33 561 - 795740 1	30	3570617 -	152-	186	G912 SC O	20	6
33 547 - 795775 1	9	3570748 -	185-	195	G912 SC O	21	6
33 531 - 795804 1	9	3570840 -	153-	164	G912 SC O	22	6
33 517 - 795825 1	15	3571031 -	97-	114	G912 SC O	23	6
33 512 - 795865 1	52	3570294 -	50-	108	G912 SC O	24	6
33 507 - 795895 1	70	3570160 -	0-	78	G912 SC O	25	6
33 494 - 795928 1	55	3570462 -	1-	60	G912 SC O	26	6
33 491 - 795984 1	88	3579697 -	32-	67	G912 SC O	27	3
325805 - 795999 1	88	3551946 -	800-	899	G912 SC O	29	6
325796 - 795959 1	82	3552546 -	746-	838	G912 SC O	30	6
325789 - 795935 1	76	3552707 -	740-	825	G912 SC O	31	6
325783 - 795901 1	101	3552167 -	710-	822	G912 SC O	32	6
325775 - 795866 1	76	3551839 -	807-	892	G912 SC O	33	6
325770 - 795832 1	91	3551463 -	790-	892	G912 SC O	34	6
325770 - 795798 1	76	3552423 -	741-	826	G912 SC O	35	3
325770 - 795764 1	79	3551823 -	792-	880	G912 SC O	36	6
325762 - 795729 1	82	3552234 -	730-	822	G912 SC O	37	6
325761 - 795695 1	91	3551686 -	755-	857	G912 SC O	38	6
325759 - 795660 1	76	3550825 -	886-	971	G912 SC O	39	1
325777 - 795637 1	46	3551815 -	906-	957	G912 SC O	40	6
325810 - 795625 1	30	3552105 -	969-	1003	G912 SC O	41	6
325831 - 795612 1	30	3552141 -	995-	1029	G912 SC O	42	6
325858 - 795603 1	30	3552743 -	972-	1006	G912 SC O	43	6
325888 - 795600 1	37	3552773 -	991-	1032	G912 SC O	44	6
325922 - 735599 1	24	3554161 -	937-	964	G912 SC O	45	6
325946 - 795607 1	15	3554888 -	925-	942	G912 SC O	46	6
325975 - 795595 1	49	3555332 -	817-	871	G912 SC O	47	6
33 2 - 795580 1	37	3556821 -	743-	784	G912 SC O	48	6
33 30 - 795568 1	30	3557773 -	706-	740	G912 SC O	49	6
33 56 - 795584 1	30	3559133 -	605-	639	G912 SC O	50	6
33 80 - 795593 1	30	3560506 -	501-	535	G912 SC O	51	6
33 109 - 795607 1	52	3561697 -	356-	414	G912 SC O	52	6
33 137 - 795618 1	24	3562632 -	385-	412	G912 SC O	53	6
33 162 - 795632 1	21	3563943 -	298-	322	G912 SC O	54	6
33 187 - 795652 1	18	3565795 -	156-	177	G912 SC O	55	6
33 210 - 795674 1	18	3565561 -	211-	232	G912 SC O	56	6
33 231 - 795698 1	24	3566159 -	161-	188	G912 SC O	57	6
33 257 - 795712 1	30	3566735 -	121-	155	G912 SC O	58	6
33 285 - 795720 1	27	3567430 -	99-	130	G912 SC O	59	6
33 309 - 795738 1	15	3568085 -	105-	122	G912 SC O	60	6
33 662 - 795655 1	88	3569715 -	202-	301	G913 SC O	2	6
33 690 - 795668 1	91	3569776 -	226-	328	G913 SC O	3	6
33 700 - 795709 1	91	3569426 -	275-	377	G913 SC O	4	6
33 718 - 795677 1	107	3569250 -	270-	389	G913 SC O	5	3
33 746 - 795686 1	82	3569902 -	318-	410	G913 SC O	6	6
33 612 - 795629 1	88	3569280 -	177-	276	G913 SC O	7	3
33 641 - 795620 1	110	3568692 -	210-	333	G913 SC O	8	6
33 653 - 795589 1	128	3567807 -	258-	401	G913 SC O	9	6
33 629 - 795567 1	113	3568612 -	192-	318	G913 SC O	10	6
33 664 - 795557 1	165	3567112 -	231-	414	G913 SC O	11	6
33 670 - 795543 1	177	3566761 -	236-	433	G913 SC O	12	3
33 696 - 795534 1	155	3567302 -	283-	457	G913 SC O	13	6
33 718 - 795552 1	152	3568309 -	223-	393	G913 SC O	14	6
33 741 - 795568 1	152	3567829 -	303-	473	G913 SC O	15	6

33 706 - 795581	1	152	3567901-	247-	417	G913	SC	O	16	6
33 702 - 795599	1	116	3568606-	284-	413	G913	SC	O	17	6
33 737 - 795603	1	110	3569033-	309-	431	G913	SC	O	18	6
33 673 - 795603	1	137	3568327-	206-	359	G913	SC	O	19	6
33 716 - 795508	1	158	3567295-	302-	479	G913	SC	O	20	6
33 739 - 795496	1	168	3573644	329	142	G913	SC	O	21	6
33 682 - 795511	1	155	3567178-	277-	450	G913	SC	O	22	6
33 682 - 795477	1	140	3567255-	316-	472	G913	SC	O	23	6
33 700 - 795423	1	143	3567472-	311-	470	G913	SC	O	24	6
33 728 - 795438	1	149	3567601-	316-	483	G913	SC	O	25	6
33 719 - 795398	1	131	3567888-	333-	479	G913	SC	O	26	6
33 737 - 795371	1	137	3567904-	337-	490	G913	SC	O	27	6
33 584 - 795612	1	02	3569179-	163-	260	G913	SC	O	28	6
33 566 - 795589	1	73	3568665-	222-	303	G913	SC	O	29	6
33 544 - 795559	1	58	3568683-	236-	301	G913	SC	O	30	3
33 521 - 795529	1	76	3568199-	197-	282	G913	SC	O	31	6
33 176 - 802302	1	195	3561663-	10-	227	G914	SC	O	2	6
33 204 - 802300	1	186	3561710-	71-	278	G914	SC	O	3	6
33 230 - 802314	1	189	3562598-	9-	220	G914	SC	O	4	6
33 259 - 802310	1	189	3562573-	51-	262	G914	SC	O	5	6
33 289 - 802325	1	189	3562678-	83-	293	G914	SC	O	6	3
33 307 - 802297	1	186	3562644-	119-	327	G914	SC	O	7	6
33 322 - 802270	1	192	3562789-	107-	321	G914	SC	O	8	6
33 318 - 802367	1	192	3562627-	117-	332	G914	SC	O	9	3
33 340 - 802390	1	210	3562557-	98-	333	G914	SC	O	10	1
33 351 - 802359	1	210	3562536-	116-	350	G914	SC	O	11	6
33 366 - 802329	1	216	3562030-	168-	409	G914	SC	O	12	6
33 383 - 802304	1	213	3562541-	150-	388	G914	SC	O	13	6
33 397 - 802273	1	229	3562420-	135-	390	G914	SC	O	14	1
33 338 - 802427	1	122	3563922-	231-	367	G914	SC	O	15	6
33 337 - 802462	1	116	3564351-	207-	336	G914	SC	O	16	6
33 341 - 802495	1	116	3564411-	206-	336	G914	SC	O	17	6
33 351 - 802522	1	122	3564559-	187-	323	G914	SC	O	18	3
33 380 - 802522	1	122	3564774-	205-	341	G914	SC	O	19	6
33 406 - 802522	1	119	3565196-	208-	341	G914	SC	O	20	6
33 437 - 802625	1	119	3565713-	199-	332	G914	SC	O	21	6
33 463 - 802529	1	168	3565281-	128-	315	G914	SC	O	22	6
33 494 - 802525	1	228	3564092-	101-	356	G914	SC	O	23	3
33 513 - 802503	1	223	3564159-	139-	387	G914	SC	O	24	6
33 514 - 802466	1	168	3565016-	224-	411	G914	SC	O	25	6
33 530 - 802437	1	195	3564709-	192-	409	G914	SC	O	26	6
33 522 - 802400	1	155	3565309-	243-	417	G914	SC	O	27	6
33 514 - 802366	1	128	3565951-	253-	396	G914	SC	O	28	6
33 525 - 802333	1	128	3566249-	238-	381	G914	SC	O	29	3
33 525 - 802293	1	128	3566027-	260-	403	G914	SC	O	30	6
33 514 - 802259	1	125	3566040-	253-	392	G914	SC	O	31	6
33 556 - 802437	1	238	3564029-	164-	429	G914	SC	O	32	6
33 579 - 802418	1	244	3564107-	168-	440	G914	SC	O	33	6
33 601 - 802396	1	280	3564131-	85-	398	G914	SC	O	34	6
33 626 - 802380	1	283	3564334-	90-	406	G914	SC	O	35	6
33 655 - 802373	1	290	3564687-	55-	378	G914	SC	O	36	6
33 676 - 802347	1	283	3565410-	50-	366	G914	SC	O	37	6
33 702 - 802343	1	241	3567256-	33-	301	G914	SC	O	38	6
33 731 - 802347	1	265	3568788	155-	141	G914	SC	O	39	6
33 483 - 802555	1	213	3564000-	141-	379	G914	SC	O	40	6
33 482 - 802591	1	238	3563691-	96-	362	G914	SC	O	41	3
33 538 - 802620	1	232	3563606-	132-	390	G914	SC	O	42	6
33 470 - 802646	1	219	3563882-	117-	362	G914	SC	O	43	6
33 450 - 802672	1	216	3563802-	107-	348	G914	SC	O	44	3
33 471 - 802697	1	262	3563036-	71-	363	G914	SC	O	45	6
33 488 - 802723	1	290	3562242-	89-	412	G914	SC	O	46	6
33 492 - 802755	1	311	3561677-	86-	433	G914	SC	O	47	6
33 496 - 802789	1	271	3562310-	150-	452	G914	SC	O	48	6
33 500 - 802822	1	277	3561697-	197-	507	G914	SC	O	49	6
33 512 - 802849	1	229	3562255-	309-	564	G914	SC	O	50	6
33 530 - 802891	1	329	3560837-	165-	532	G914	SC	O	51	0

33 537 - 802925 1	326	3560647-	203-	567	G914	SC	O	52	6
33 543 - 802957 1	314	3561159-	198-	548	G914	SC	O	53	6
33 548 - 802991 1	277	3561963-	238-	548	G914	SC	O	54	6
33 429 - 802647 1	149	3565160-	148-	315	G914	SC	O	55	6
33 405 - 802619 1	134	3565391-	139-	289	G914	SC	O	56	6
33 385 - 802597 1	134	3564938-	158-	307	G914	SC	O	57	3
33 368 - 802558 1	122	3564509-	214-	350	G914	SC	O	58	6
33 163 - 802351 1	149	3562144-	84-	250	G914	SC	O	60	0
33 179 - 802389 1	143	3562332-	106-	266	G914	SC	O	61	6
33 207 - 802415 1	128	3562673-	158-	301	G914	SC	O	62	3
33 180 - 802427 1	113	3562820-	153-	279	G914	SC	O	63	6
33 155 - 802439 1	113	3562844-	116-	242	G914	SC	O	64	6
33 130 - 802457 1	113	3562925-	74-	199	G914	SC	O	65	6
33 105 - 802475 1	101	3563129-	57-	169	G914	SC	O	66	6
33 82 - 802492 1	98	3563439-	3-	112	G914	SC	O	67	6
33 65 - 802518 1	107	3563321	37-	82	G914	SC	O	68	6
33 41 - 802533 1	107	3562927	30-	89	G914	SC	O	69	3
33 14 - 802526 1	104	3563078	73-	43	G914	SC	O	70	6
33 561 - 794859 1	15	3568016-	458-	475	G915	SC	O	2	6
33 543 - 794884 1	61	3566201-	474-	542	G915	SC	O	3	6
33 530 - 794916 1	101	3564649-	420-	602	G915	SC	O	4	6
33 516 - 794949 1	94	3564249-	529-	635	G915	SC	O	5	3
33 502 - 794978 1	46	3564899-	596-	647	G915	SC	O	6	6
33 484 - 795016 1	88	3563316-	597-	695	G915	SC	O	7	3
33 465 - 795043 1	98	3562917-	582-	691	G915	SC	O	8	6
33 441 - 795061 1	76	3562789-	629-	714	G915	SC	O	9	6
33 418 - 795073 1	104	3562192-	571-	687	G915	SC	O	10	3
33 389 - 795083 1	37	3563541-	604-	645	G915	SC	O	11	6
33 372 - 795105 1	113	3561909-	509-	635	G915	SC	O	12	1
33 348 - 795135 1	113	3561917-	475-	600	G915	SC	O	13	6
33 320 - 795151 1	119	3561195-	489-	622	G915	SC	O	14	1
33 291 - 795146 1	110	3560839-	513-	636	G915	SC	O	15	6
33 260 - 795134 1	101	3560270-	555-	667	G915	SC	O	16	1
33 233 - 795126 1	88	3559660-	617-	716	G915	SC	O	17	3
33 207 - 795122 1	43	3560094-	679-	727	G915	SC	O	18	6
33 178 - 795123 1	37	3559474-	720-	761	G915	SC	O	19	6
33 365 - 795497 1	61	3564982-	351-	419	G915	SC	O	20	6
33 352 - 795471 1	98	3564556-	291-	390	G915	SC	O	21	3
33 331 - 795444 1	94	3563994-	300-	405	G915	SC	O	22	6
33 303 - 795423 1	88	3563823-	297-	396	G915	SC	O	23	6
33 288 - 795408 1	91	3563257-	323-	425	G915	SC	O	24	6
33 264 - 795382 1	94	3562453-	362-	467	G915	SC	O	25	6
33 243 - 795357 1	94	3562147-	364-	469	G915	SC	O	26	6
33 221 - 795333 1	94	3561081-	440-	546	G915	SC	O	27	6
33 200 - 795313 1	85	3560731-	475-	570	G915	SC	O	28	6
33 180 - 795292 1	82	3559914-	538-	630	G915	SC	O	29	6
33 158 - 795266 1	85	3558709-	618-	714	G915	SC	O	30	6
33 142 - 795249 1	76	3557995-	696-	721	G915	SC	O	31	6
33 133 - 795212 1	61	3557693-	761-	829	G915	SC	O	32	6
33 150 - 795176 1	76	3557572-	749-	834	G915	SC	O	33	6
33 149 - 795133 1	61	3557677-	784-	852	G915	SC	O	34	6
33 123 - 795121 1	91	3556119-	810-	912	G915	SC	O	36	6
33 95 - 795108 1	37	3556327-	921-	962	G915	SC	O	37	6
33 63 - 795102 1	73	3554815-	915-	996	G915	SC	O	38	6
33 35 - 795100 1	82	3553429-	986-	1078	G915	SC	O	39	6
33 31 - 795132 1	88	3553191-	987-	1085	G915	SC	O	40	6
33 42 - 795163 1	101	3553616-	921-	1033	G915	SC	O	41	6
33 50 - 795195 1	113	3553975-	859-	985	G915	SC	O	42	6
33 234 - 795390 1	91	3561643-	411-	513	G915	SC	O	43	6
33 209 - 795390 1	94	3561048-	427-	532	G915	SC	O	44	6
33 184 - 795372 1	67	3560656-	517-	591	G915	SC	O	45	6
33 159 - 795354 1	64	3559492-	607-	678	G915	SC	O	46	6
33 133 - 795341 1	67	3558800-	631-	706	G915	SC	O	47	6
33 106 - 795328 1	94	3557319-	657-	763	G915	SC	O	48	6
33 79 - 795331 1	107	3556196-	696-	815	G915	SC	O	49	6
33 63 - 795360 1	49	3557322-	739-	793	G915	SC	O	50	3

33 49 - 795393	1	18	3557663-	780-	800	G915 SC O	51	6
33 606 - 794827	1	91	3568280-	260-	362	G916 SC O	2	6
33 635 - 794829	1	98	3568917-	216-	325	G916 SC O	3	6
33 664 - 794829	1	94	3569697-	188-	293	G916 SC O	4	6
33 693 - 794825	1	101	3570602-	119-	232	G916 SC O	5	6
33 721 - 794827	1	82	3571582-	116-	208	G916 SC O	6	6
33 747 - 794839	1	91	3572241-	58-	160	G916 SC O	7	3
33 602 - 794818	1	101	3567835-	270-	382	G916 SC O	8	6
33 625 - 794800	1	101	3568848-	201-	313	G916 SC O	9	6
33 648 - 794792	1	91	3569849-	161-	263	G916 SC O	10	6
33 673 - 794763	1	107	3570482-	84-	203	G916 SC O	11	3
33 698 - 794744	1	94	3571529-	51-	157	G916 SC O	12	6
33 724 - 794728	1	94	3572144-	26-	131	G916 SC O	13	6
33 669 - 794724	1	98	3570693-	87-	195	G916 SC O	14	6
33 672 - 794687	1	98	3571005-	59-	168	G916 SC O	15	6
33 666 - 794652	1	98	3571280-	24-	132	G916 SC O	16	6
33 642 - 794640	1	104	3570844-	16-	131	G916 SC O	17	3
33 616 - 794627	1	101	3570346-	39-	151	G916 SC O	18	6
33 589 - 794614	1	101	3569837-	52-	164	G916 SC O	19	6
33 557 - 794599	1	101	3569029-	88-	201	G916 SC O	20	3
33 526 - 794584	1	104	3567957-	143-	259	G916 SC O	21	6
33 499 - 794572	1	107	3567027-	190-	309	G916 SC O	22	6
33 472 - 794558	1	113	3566072-	230-	355	G916 SC O	23	6
33 445 - 794546	1	116	3565178-	273-	402	G916 SC O	24	6
33 432 - 794536	1	119	3564468-	317-	449	G916 SC O	25	6
33 445 - 794568	1	125	3564638-	298-	437	G916 SC O	26	6
33 472 - 794597	1	107	3565938-	262-	381	G916 SC O	27	6
33 489 - 794629	1	110	3566324-	237-	360	G916 SC O	28	6
33 499 - 794661	1	82	3567337-	235-	327	G916 SC O	29	6
33 509 - 794691	1	94	3566846-	260-	366	G916 SC O	30	6
33 527 - 794719	1	79	3567239-	293-	381	G916 SC O	31	6
33 540 - 794749	1	43	3567804-	366-	414	G916 SC O	32	6
33 553 - 794775	1	88	3567392-	285-	384	G916 SC O	33	6
33 567 - 794813	1	94	3567296-	295-	400	G916 SC O	34	6
33 548 - 794831	1	30	3567719-	423-	457	G917 SC O	2	6
33 520 - 794833	1	21	3566938-	491-	515	G917 SC O	3	6
33 484 - 794836	1	85	3564350-	502-	598	G917 SC O	4	3
33 461 - 794807	1	91	3564482-	440-	542	G917 SC O	5	6
33 450 - 794776	1	104	3563745-	460-	576	G917 SC O	6	6
33 444 - 794730	1	104	3564308-	396-	512	G917 SC O	7	6
33 430 - 794699	1	88	3564455-	408-	507	G917 SC O	8	6
33 405 - 794682	1	67	3563783-	507-	582	G917 SC O	9	6
33 385 - 794658	1	94	3562794-	493-	599	G917 SC O	10	6
33 362 - 794638	1	101	3562224-	500-	613	G917 SC O	11	6
33 333 - 794633	1	98	3562078-	485-	594	G917 SC O	12	6
33 307 - 794634	1	58	3561626-	617-	681	G917 SC O	13	6
33 286 - 794612	1	98	3560655-	562-	671	G917 SC O	14	6
33 248 - 794605	1	101	3559849-	581-	694	G917 SC O	15	6
33 216 - 794599	1	98	3559350-	597-	706	G917 SC O	16	6
33 192 - 794591	1	104	3558750-	605-	721	G917 SC O	17	6
33 171 - 794584	1	107	3558283-	614-	733	G917 SC O	18	3
33 159 - 794614	1	104	3557652-	669-	784	G917 SC O	19	6
33 160 - 794646	1	104	3557410-	695-	810	G917 SC O	20	6
33 168 - 794677	1	104	3557492-	697-	813	G917 SC O	21	6
33 138 - 794682	1	98	3556661-	759-	868	G917 SC O	22	6
33 111 - 794671	1	104	3555785-	790-	905	G917 SC O	23	6
33 83 - 794663	1	101	3554911-	848-	960	G917 SC O	24	6
33 55 - 794657	1	104	3554044-	886-	1002	G917 SC O	25	6
33 26 - 794652	1	110	3553329-	900-	1023	G917 SC O	26	6
33 154 - 794724	1	101	3556820-	755-	867	G917 SC O	27	6
33 136 - 794758	1	104	3555748-	828-	943	G917 SC O	28	6
33 131 - 794787	1	110	3555509-	825-	948	G917 SC O	29	3
33 108 - 794807	1	113	3554502-	886-	1012	G917 SC O	30	6
33 93 - 794835	1	119	3553956-	901-	1034	G917 SC O	31	6
33 74 - 794871	1	119	3553148-	956-	1088	G917 SC O	32	3
33 45 - 794874	1	119	3552350-	995-	1128	G917 SC O	33	6

33 16 - 794877 1	119	3551395- 1051- 1183	G917 SC O	34	6
33 62 - 794901 1	122	3552565- 988- 1124	G917 SC O	35	6
33 54 - 794934 1	125	3552305- 993- 1133	G917 SC O	36	6
33 43 - 794966 1	110	3552114- 1044- 1166	G917 SC O	37	6
33 13 - 794981 1	91	3552013- 1073- 1175	G917 SC O	38	6
33 462 - 794838 1	85	3564463- 462- 557	G917 SC O	40	6
33 433 - 794840 1	85	3563568- 512- 607	G917 SC O	41	6
33 404 - 794843 1	85	3563344- 494- 589	G917 SC O	42	6
33 375 - 794845 1	82	3562834- 514- 606	G917 SC O	43	6
33 345 - 794848 1	91	3562384- 490- 592	G917 SC O	44	6
33 317 - 794851 1	91	3561795- 509- 611	G917 SC O	45	6
33 287 - 794853 1	85	3560845- 583- 678	G917 SC O	46	6
33 258 - 794854 1	113	3559862- 557- 682	G917 SC O	47	6
33 230 - 794857 1	125	3558616- 604- 744	G917 SC O	48	6
33 200 - 794860 1	98	3558066- 703- 812	G917 SC O	49	6
33 171 - 794862 1	101	3557979- 662- 774	G917 SC O	50	6
33 143 - 794865 1	104	3556797- 732- 848	G917 SC O	51	6
33 113 - 794868 1	110	3556034- 748- 871	G917 SC O	52	6
33 94 - 794870 1	116	3555265- 781- 910	G917 SC O	53	6
33 278 - 802993 1	192	3561111- 215- 429	G918 SC O	2	6
33 251 - 802983 1	195	3560756- 203- 421	G918 SC O	3	6
33 226 - 802967 1	192	3560656- 188- 402	G918 SC O	4	6
33 203 - 802945 1	189	3560605- 171- 382	G918 SC O	5	6
33 179 - 802924 1	183	3560774- 141- 345	G918 SC O	6	6
33 150 - 802913 1	183	3560723- 105- 309	G918 SC O	7	6
33 122 - 802913 1	177	3560686- 88- 286	G918 SC O	8	6
33 95 - 802924 1	171	3560516- 88- 278	G918 SC O	9	6
33 62 - 802923 1	186	3560382- 9- 216	G918 SC O	10	6
33 33 - 802923 1	192	3560252- 37- 178	G918 SC O	11	6
33 5 - 802930 1	201	3559797- 58- 166	G918 SC O	12	6
33 10 - 802894 1	201	3559770- 49- 175	G918 SC O	13	6
33 13 - 802859 1	192	3560290- 69- 145	G918 SC O	14	6
33 4 - 802828 1	174	3560600- 55- 139	G918 SC O	15	6
33 12 - 802796 1	168	3560942- 60- 127	G918 SC O	16	6
33 12 - 802770 1	162	3561277- 75- 106	G918 SC O	17	3
33 37 - 802787 1	158	3561025- 5- 172	G918 SC O	18	6
33 62 - 802805 1	186	3560825- 36- 171	G918 SC O	19	6
33 87 - 802821 1	177	3560826- 26- 22	G918 SC O	20	6
33 100 - 802852 1	186	3560787- 20- 228	G918 SC O	21	6
33 80 - 802881 1	189	3560427- 19- 230	G918 SC O	22	6
33 115 - 802818 1	177	3560869- 62- 259	G918 SC O	23	6
33 143 - 802829 1	165	3561234- 101- 285	G918 SC O	24	3
33 171 - 802824 1	171	3561361- 108- 299	G918 SC O	25	6
33 201 - 802822 1	162	3561382- 175- 355	G918 SC O	26	6
33 224 - 802845 1	143	3561859- 216- 376	G918 SC O	27	6
33 244 - 802869 1	146	3561858- 234- 398	G918 SC O	28	6
33 267 - 802891 1	152	3561816- 252- 422	G918 SC O	29	6
33 289 - 802916 1	152	3561882- 274- 444	G918 SC O	30	6
33 312 - 802946 1	162	3561924- 274- 454	G918 SC O	31	3
33 229 - 802437 1	125	3562720- 192- 331	G918 SC O	32	6
33 246 - 802464 1	131	3562956- 174- 320	G918 SC O	33	6
33 262 - 802493 1	125	3562984- 212- 352	G918 SC O	34	6
33 273 - 802524 1	119	3563134- 230- 363	G918 SC O	35	3
33 274 - 802558 1	131	3563144- 193- 339	G918 SC O	36	3
33 265 - 802592 1	134	3563182- 168- 317	G918 SC O	37	6
33 258 - 802624 1	134	3562888- 188- 337	G918 SC O	38	6
33 263 - 802657 1	137	3562884- 185- 338	G918 SC O	39	6
33 269 - 802686 1	140	3562445- 178- 334	G918 SC O	40	3
33 280 - 802717 1	137	3562974- 199- 352	G918 SC O	41	6
33 301 - 802781 1	134	3562984- 237- 386	G918 SC O	42	6
33 305 - 802815 1	143	3562815- 232- 392	G918 SC O	43	6
33 309 - 802849 1	149	3562560- 243- 410	G918 SC O	44	6
33 312 - 802884 1	155	3562445- 240- 413	G918 SC O	45	6
33 312 - 802918 1	158	3562338- 242- 419	G918 SC O	46	6
33 1345 - 804315 1	398	3570998- 61- 505	G922 SC O	2	3
33 1289 - 804258 1	346	3570165- 227- 613	G922 SC O	3	3

331227	-	804361	1	394	3567232-	287-	726	G922	SC	O	4	3
331223	-	804451	1	375	3567154-	348-	766	G922	SC	O	5	6
331286	-	804338	1	395	3569351-	153-	594	G922	SC	O	6	6
331211	-	804210	1	368	3567467-	321-	732	G922	SC	O	7	3
331129	-	804234	1	359	3565420-	441-	841	G922	SC	O	8	3
331060	-	804207	1	348	3563671-	554-	943	G922	SC	O	9	3
331200	-	804116	1	369	3566398*	410-	822	G922	SC	O	10	3
331125	-	804085	1	341	3565377-	495-	875	G922	SC	O	11	3
331001	-	804051	1	333	3563247-	562-	933	G922	SC	O	12	3
33 978	-	803942	1	300	3563265-	630-	965	G922	SC	O	13	3
33 916	-	803889	1	310	3562164-	624-	970	G922	SC	O	14	3
331042	-	803827	1	302	3564958-	543-	880	G922	SC	O	15	3
331116	-	803779	1	300	3565789-	468-	803	G922	SC	O	16	3
33 0	-	803000	1	189	35L1302	178-	33	G922	SC	O	17	3
331473	-	804258	1	345	3576972	196-	188	G922	SC	O	19	3
331479	-	804168	1	416	3576898	400-	64	G922	SC	O	20	3
331426	-	804275	1	389	3574048	105-	329	G922	SC	O	21	3
331251	-	804189	1	327	3569256-	324-	689	G922	SC	O	22	3
331465	-	804159	1	381	3574870	108-	317	G922	SC	O	23	6
331392	-	804170	1	390	3571935-	57-	492	G922	SC	O	24	6
331324	-	804116	1	386	3569439-	225-	655	G922	SC	O	25	3
331207	-	804019	1	366	3566597-	409-	817	G922	SC	O	26	3
33 0	-	803000	1	189	3561451	193-	18	G922	SC	O	27	3
331087	-	803933	1	312	3565319-	538-	886	G923	SC	O	2	3
331159	-	803889	1	324	3566496-	483-	844	G923	SC	O	3	3
331254	-	803922	1	349	3568034-	383-	772	G923	SC	O	4	3
331348	-	803990	1	381	3569818-	235-	660	G923	SC	O	5	3
331426	-	804046	1	387	3572255-	80-	512	G923	SC	O	6	3
331419	-	803934	1	352	3572521-	153-	545	G923	SC	O	7	3
331469	-	802973	1	386	3573904-	22-	409	G923	SC	O	8	3
331460	-	803803	1	370	3573146-	91-	504	G923	SC	O	9	3
331408	-	803833	1	353	3571714-	215-	609	G923	SC	O	10	3
331320	-	803854	1	354	3569412-	321-	715	G923	SC	O	11	3
331215	-	803875	1	341	3567498-	407-	788	G923	SC	O	12	3
331198	-	803769	1	280	3568811-	441-	753	G923	SC	O	13	3
33 0	-	803000	1	189	3561237	172-	39	G923	SC	O	14	3
33 182	-	803767	1	263	3559317-	42-	336	G923	SC	O	15	3
33 79	-	803810	1	271	3558606	53-	249	G923	SC	O	16	3
33 20	-	803888	1	251	3558835	95-	185	G923	SC	O	17	3
33 89	-	803956	1	259	3558373-	21-	310	G923	SC	O	18	3
33 181	-	803971	1	268	3557837-	174-	473	G923	SC	O	19	3
33 277	-	803900	1	259	3558707-	246-	535	G923	SC	O	20	3
33 375	-	803909	1	265	3558812-	352-	648	G923	SC	O	21	3
33 513	-	804140	1	295	3555707-	760-	1089	G923	SC	O	23	3
33 432	-	804147	1	291	3555160-	686-	1010	G923	SC	O	24	3
33 328	-	804149	1	283	3555840-	529-	845	G923	SC	O	25	3
33 255	-	804155	1	270	3556629-	390-	691	G923	SC	O	26	6
33 174	-	804146	1	258	3557492-	229-	517	G923	SC	O	27	3
33 188	-	804040	1	251	3558149-	205-	485	G923	SC	O	28	3
33 117	-	804031	1	255	3558367-	73-	357	G923	SC	O	29	6
33 17	-	804022	1	256	3558467	78-	207	G923	SC	O	30	3
33 20	-	804173	1	230	3559785	126-	131	G923	SC	O	31	3
33 82	-	804286	1	247	3558479-	38-	314	G923	SC	O	32	3
33 134	-	804338	1	257	3558108-	116-	402	G923	SC	O	33	3
33 53	-	804274	1	262	3558802	72-	220	G923	SC	O	34	3
33 193	-	804450	1	262	3558007-	192-	484	G923	SC	O	35	3
33 83	-	804442	1	260	3558847	38-	252	G923	SC	O	36	6
33 173	-	804241	1	250	3557689-	233-	512	G923	SC	C	37	6
33 392	-	804300	1	281	3555337-	674-	987	G923	SC	O	38	6
33 288	-	804252	1	268	3556015-	503-	802	G923	SC	C	39	6
33 203	-	804354	1	258	3557374-	281-	569	G923	SC	O	40	6
33 296	-	804419	1	270	3556847-	425-	726	G923	SC	O	41	6
33 393	-	804392	1	285	3555532-	643-	961	G923	SC	O	42	3
33 542	-	804426	1	302	3555173-	832-	1169	G923	SC	O	43	3
33 464	-	804290	1	299	3554941-	757-	1091	G923	SC	O	44	6
33 587	-	804221	1	292	3555647-	878-	1203	G923	SC	O	45	6
33 639	-	804340	1	317	3555579-	879-	1232	G923	SC	O	46	3
33 715	-	804460	1	327	3555844-	926-	1291	G923	SC	O	47	3
33 628	-	804450	1	317	3555266-	895-	1249	G923	SC	O	48	3

3. DEFINITION OF DATA GRIDS FOR CHARLESTON STUDY

Introduction

A major objective of the Nuclear Regulatory Commission Charleston study is to collect and examine sets of data on a common geographic reference base. In this way the various data sets can be uniformly evaluated for completeness and density of information content. The data sets can then be used to assess the hypotheses that have been proposed to explain the Charleston event and to either identify the best hypothesis or to develop a new verifiable explanation. Four grids are chosen to be compatible with available data and the relative resolution of different types of data.

Map Projection and Reference Location

The Universal Transverse Mercator (UTM) Projection (Zone 17) is used to project the latitudes and longitudes to a plane surface on which a uniform rectangular grid can be defined. The choice of the Universal Transverse Mercator Projection is based on the common use of this system for referencing landsat data. FORTRAN subroutines for converting UTM (Zone 17) to latitude and longitude and back are given in Appendix A-6. The reference grid is a 128x128 point grid approximately centered on the aftershock zone of the 1886 Charleston earthquake. The origin and orientation of this grid are chosen to provide the minimum data over the ocean, provide the best Landsat image coverage and to parallel the regional structure. The 1.0 km grid reference point (1,1) is fixed at the point (33.125°N, 81.25°W) and this point is defined as the origin in this study. The reference axis and grid are rotated clockwise about this point 52 degrees. The relationship between the UTM projection and the rotated system is shown in figure A-3-1.

The locations in the rotated system are found by the following steps:

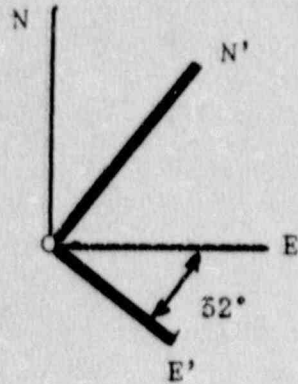
- 1) transform geographic coordinates to UTM zone 17.
- 2) shift origin to grid point (1,1) at (N_0, E_0)
- 3) rotate axes clockwise 52 degrees to primed coordinate system.
- 4) find index of grid point closest to the data point

Computer programs to transform geographic coordinates to UTM zone 17 are included in Appendix I. The equations for step two, the translation, and step three, the rotation, may be combined as follows:

$$\begin{aligned} E' &= (E-E_0)\cos(A) - (N-N_0)\sin(A) \\ N' &= (E-E_0)\sin(A) + (N-N_0)\cos(A) \end{aligned}$$

where A is positive clockwise.

The new primed axes (N', E') represent a clockwise rotation of the old axes (N, E) about (N_0, E_0) .



Origin

Latitude = 33.125
 Longitude = -81.250

$N^{\circ} = 3664980.84$
 $E^{\circ} = 476678.49$

Figure A-3-1. Relative location of rotated reference axis of grid.

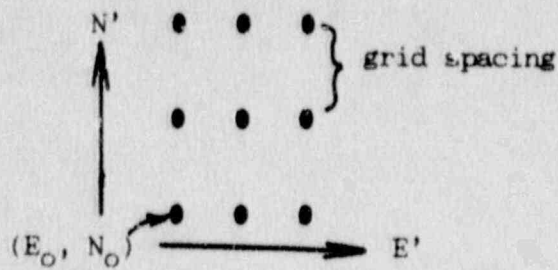


Figure A-3-2. Location of grid point relative to sample area.

Grid Definitions

Within each grid, a grid point represents data in a rectangular area centered over the grid point and with sides equal to the grid spacing. Figure A-3-2 shows the relation of the area to the grid point.

Four grids are defined. Three are located by centering them on the reference grid. Table I gives the dimensions of the grids and the coordinates of the four corner points of each grid. The relative locations of the grid points in each of the four grids are shown in figure A-3-3.

The 64x64 point grid with dimensions of 256 km is centered on the reference grid. In the primed or rotated system, the grid reference point (1,1) for the 64x64 point grid is located at $N' = -62.5$ km and $E' = -62.5$ km.

The 128x128 point grid with 8 km grid interval and dimensions of 1024 km is also centered on the reference grid. In the primed system, the grid reference point (1,1) for the 128x128 point 8 km grid is located at $N' = -444.5$ km and $E' = -444.5$ km.

The landsat data have 4096x4096 points which can be divided into 64-512x512 point units for convenient display. Each unit of 512x512 points will cover an area of side length 16 km or an area of 256 square km. The pixels are rectified to the 128x128 point 1.0 km grid points such that each 1.0 km grid point will be surrounded by four areas of 16x16 pixels. The pixels are 31.25 meters apart and the origin is at the point $N' = -484.375$ m, $E' = -484.375$ m.

The index (IX,IY) of the grid points closest to a specified latitude and longitude coordinate (or UTM coordinate position) can be obtained from the following equations:

$$\begin{aligned} IY &= 1 + \text{Int}[(N' - R(I) + DY(I)/2.0)/DY(I)] \\ IX &= 1 + \text{Int}[(E' - R(I) + DX(I)/2.0)/DX(I)] \\ &(\text{Int}[] \text{ truncates fractional part of number}) \end{aligned}$$

Where $R(I)$ is the origin in the primed system of the Ith grid DX or DY is the grid point spacing of the Ith grid and in this study $DX(I) = DY(I)$.

Table A-3-Ia Size of the four grids.

<u>Grid No.</u>	<u>Pts/side</u>	<u>length(km)</u>	<u>grid interval</u>	<u>data</u>
1	128	128	1.0 km	grav., mag., elev.
2	64	256	4.0 km	grav., mag., elev.
3	128	1024	8.0 km	elev., mag.
4	4096	128	.03125	landsat,

Table A-3-Ib Coordinates of corners of grids.

<u>X</u>	<u>Y</u>	<u>N</u>	<u>E</u>	<u>Latitude</u>	<u>Longitude</u>
Grid 1					
1	1	3,664,980	476,678	33.1250	81.2500
1	128	3,564,903	554,867	32.2211	80.4177
128	1	3,743,170	576,756	33.8277	80.1705
128	128	3,643,092	654,945	32.9168	79.3430
Grid 2					
1	1	3,675,753	388,949	33.2167	82.1916
1	64	3,477,173	544,095	31.4301	80.5360
64	1	3,830,899	587,527	34.6180	80.0453
64	64	3,632,320	742,674	32.8038	78.4084
Grid 3					
1	1	3,741,590	47,254	33.6190	87.9710
1	128	2,940,971	478,258	26.5908	81.2183
128	1	4,367,102	653,365	39.4417	79.2178
128	128	3,566,483	1,278,877	31.9683	72.7695
Grid 4					
1	1	3,665,064	475,999	33.12574	81.25729
1	4096	3,564,224	554,784	32.21497	80.41865
4096	1	3,743,850	576,839	33.83385	80.16958
4096	4096	3,643,009	655,624	32.91597	79.33577

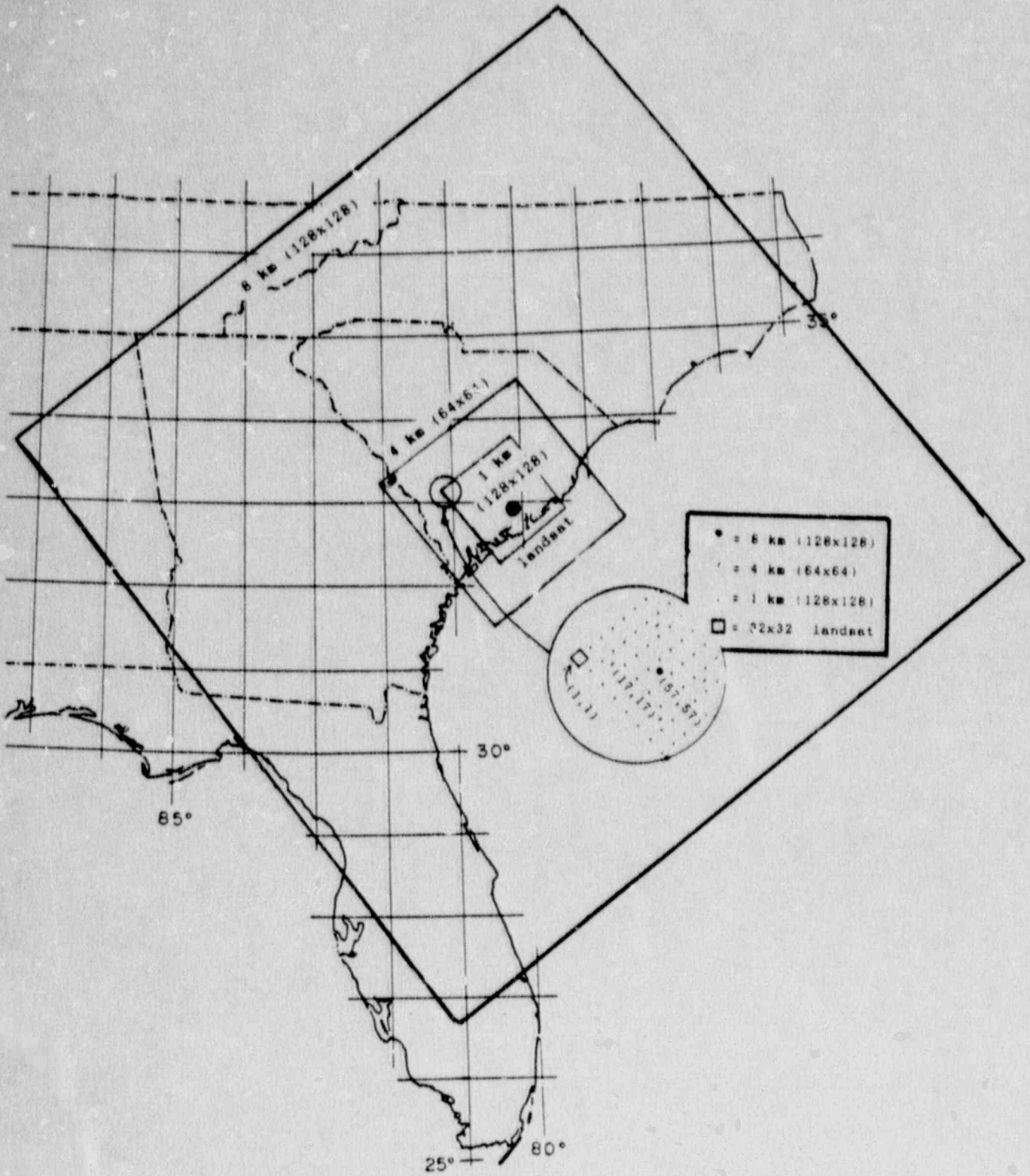


Figure 3 Relative location of grid points

COMPOSITE MAGNETIC ANOMALY MAP OF THE UNITED STATES

PART A. CONTERMINOUS UNITED STATES

Compiled under the direction of

Isidore Zietz

UNITED STATES GEOLOGICAL SURVEY
in cooperation with
THE SOCIETY OF EXPLORATION GEOPHYSICISTS

EDITORIAL COMMITTEE

Isidore Zietz, Chairman

John D. Corbett

Gordon P. Eaton

Michael D. Fuller

Richard H. Godson

William F. Hanna

James R. Hertzler

William J. Hinze

James A. Schwartz

The accompanying magnetic-anomaly map of the conterminous United States and adjacent offshore areas was compiled as a cooperative effort by the U.S. Geological Survey and the Society of Exploration Geophysicists (Hinze, 1976). The map is published in two sheets in color showing magnetic anomaly contours at an interval of 200 gammas (nanoteslas) with supplemental contours at an interval of 100 gammas on an Albers equal-area projection at the scale of 1:2,500,000. The map may be compared directly with the tectonic (U.S. Geol. Survey and Am. Assoc. Petroleum Geologists, 1961), Bouguer gravity anomaly (Am. Geophys. Union, 1964), basement rock (Bayley and Muehlberger, 1968), and geologic (King and Beikman, 1974) maps of the conterminous United States published by the U.S. Geological Survey in cooperation with professional societies.

Hundreds of magnetic-data sources were used in the map compilation. Most of them were total-intensity aeromagnetic-anomaly data; others included total-intensity ground and shipborne magnetic-anomaly data and vertical-intensity ground magnetic-anomaly data. Flight altitudes, directions, and spacings of aeromagnetic surveys varied widely; no attempt was made to analytically continue magnetic-anomaly data to a common altitude. The anomaly data were referenced to numerous magnetic-field datums; however, an attempt was made to adjust most anomaly data to a common magnetic-field datum. On the basis of comparisons with aeromagnetic-anomaly data of the U.S. Naval Oceanographic Office and the National Uranium Resource Evaluation (NURE) program of the Department of Energy, we inferred that the zero level of the compiled map is approximately 1,000 gammas higher than the zero level of data based on the International Geomagnetic Reference Field (IGRF). Because the quality of the map is limited by the diversity of data types, data-acquisition specifications, and the compilation techniques, it is strongly recommended that the map be used only at the 1:2,500,000 publication scale or smaller scales of interest in broad regional investigations. For more detailed work at scales larger than the 1:2,500,000 publication scale, we recommend that original data sources be used.

Compilation involved the following steps: (1) Magnetic anomaly data of a given survey were inspected and, as necessary, were referenced to the IGRF (Fabiano and Peddie, 1969; Barraclough and Fabiano, 1978), adjusted for the

time of the survey, and an arbitrary zero datum; (2) contour lines at an interval of 100 or 200 gammas were selected; (3) the map of the selected contour lines was reduced to the 1:1,000,000 compilation scale; (4) the reduced map was placed on an Albers equal-area projection master base map of the conterminous United States and offshore areas; (5) near the boundaries of adjacent surveys, contour lines were visually joined as smoothly as possible; and (6) where major discontinuities of anomaly values existed, contoured NURE data were used to guide the connecting of contour lines; and (7) the map at the 1:1,000,000 compilation scale was photographically reduced to the 1:2,500,000 publication scale.

The NURE data, acquired during a 7-year period for the conterminous United States and referenced to the IGRF, provided a reliable base net for controlling the compilation of individual surveys. As an independent check on the validity of the compilation, profiles from the map were compared with a series of north-south aeromagnetic traverses of the U.S. Naval Oceanographic Office (NOO). The traverses were flown in 1976 and 1977 and were spaced approximately one degree of longitude apart across the conterminous United States. This comparison shows that the compiled data agree with the NOO data, after adjustment to the IGRF, to within 100 gammas throughout the country. Magnetic profiles for the 83°W, 90°W, and 119°W meridians comparing total-intensity magnetic anomaly data obtained from the NOO survey with those taken from the composite U.S. magnetic anomaly map are shown in Figure 1. The magnetic profiles along each meridian are arbitrarily displaced vertically to effect a better visual comparison.

Individual data sources used in the map compilation are shown on index maps. These index maps are keyed to the "Sources of Data" and "Specifications" (direction, altitude, and spacing of traverses), shown later in this pamphlet. Index maps for the Atlantic Ocean, Gulf of Mexico, and Pacific Ocean are included.

Exceptions: IGRF 1965.0 not updated, was removed from total-intensity data of reference B, Illinois; reference E, Nebraska; reference A, Ohio; and reference 2, Oregon. A field of 9 gammas per mile north and 3.2 gammas per mile east was removed from vertical-intensity data of reference F, South Dakota. Unknown reference fields were removed from vertical-intensity data of reference H, Missouri, and reference 38, New Mexico. It is not known whether a reference field has been removed from the total-intensity or vertical-intensity data of reference 26, New Mexico.

Acknowledgments

The cooperative arrangement between the U.S. Geological Survey and the Society of Exploration Geophysicists, effected in 1975, resulted in formation of the National Magnetic Anomaly Map (NMAM) Committee, which interacted with a group of U.S. Geological Survey personnel. Current members of the NMAM Committee are:

William J. Hinze, Chairman (Purdue University)
Anthony R. Barringer (Barringer Research Inc.)
Sheldon Brenner (Geometrics)
LeRoy Brow (Exxon Production Research Co.)
James E. Case (U.S. Geological Survey)
Howard L. Cobb (Atlantic Richfield Co.)
John D. Corbett (Anaconda Minerals Co.)
Michael D. Fuller (University of California at Santa Barbara)
James R. Hertzler (Woods Hole Oceanographic Inst.)
Charles E. Helsley (University of Hawaii)
Robert H. Higgs (U.S. Naval Oceanographic Office)
Robert A. Langel (U.S. National Aeronautics & Space Admin.)
H. David MacLean (Gulf Mineral Resources Co.)
Emil J. Mateker, Jr. (Aero Service Co.)
Alfred J. Navazio (Carson Helicopters)
George Podolsky (Kidd Creek Mines Ltd.)
Michael S. Reford (Geotemex Ltd.)
James A. Schwartz (Gulf Oil Exploration and Production Co.)
Paul H. Serson (Canada Dept. of Energy, Mines & Resources)
Kendall L. Svendsen (U.S. National Oceanic & Atmospheric Admin.)
Eric E. Wicherts (Amoco International Co.)
Richard J. Wold (U.S. Geological Survey)
Isidore Zietz (Phoenix Corp.)
W. Glen Zinn (Moly Corp. Inc.)

Previous members of the committee and their affiliation during their period of participation are:

Joseph W. Berg, Jr. (National Academy of Sciences)
Bimal K. Bhattacharyya (Deceased) (U.S. Geological Survey)
Ernest J. Juler (U.S. National Aeronautics & Space Admin.)
John J. Landau (Gulf Research & Development Co.)
P. Lawrence (Mobil Oil Corporation)
D. Beadle Moore (Exxon Co., U.S.A.)
Robert F. McMahon (Chevron Oil Co.)
Robert D. Regan (U.S. Geological Survey)

U.S. Geological Survey coordinators of the cooperative effort were Martin F. Kane, William F. Hanna, Gordon P. Eaton, and Charles J. Zablocki. Richard D. Hovey (Chevron Overseas Petroleum Co.) and Val W. Chandler (Minnesota Geological Survey) assisted the Editorial Committee in reviewing selected areas of preliminary versions of the map.

The Amoco Production Company, Chevron Oil Company, Gulf Oil Corporation, and Mobil Exploration and Production Services contributed data to the map. Compilation of the map was performed by Kevin R. Bond, Francis P. Gilbert (Deceased), John R. Kirby, Fredenc E. Riggie, and Stephen L. Snyder, all of the U.S. Geological Survey.

References Cited

- American Geophysical Union. Special Committee for the Geophysical and Geological Study of the Continents. 1964. Bouguer gravity anomaly map of the United States (exclusive of Alaska and Hawaii). Washington, D.C., U.S. Geological Survey, 2 sheets, scale 1:2,500,000.
- Barracough, D. R., and Fabiano, E. B., 1978. Grid values and charts for the International Geomagnetic Reference Field-1975. U.S. Department of Commerce, National Technical Information Service PB-276 630, 139 p.
- Bayley, R. W., and Muehlberger, W. R., compilers, 1968. Basement rock map of the United States (exclusive of Alaska and Hawaii). Washington, D.C., U.S. Geological Survey, 2 sheets, scale 1:2,500,000.
- Fabiano, E. B., and Peddie, N. W., 1969. Grid values of total magnetic intensity, IGRF-1965. U.S. Environmental Science Services Administration Technical Report, C and GS 38, 55 p.
- Hinze, W. J., 1976. Report of the SEG Committee for a National Magnetic Anomaly Map. Geophysics, v. 41, no. 5, p. 1055.
- King, P. B., and Beikman, H. M., compilers 1974. Geologic map of the United States (exclusive of Alaska and Hawaii). Reston, Va., U.S. Geological Survey, 3 sheets, scale 1:2,500,000.
- U.S. Geological Survey and American Association of Petroleum Geologists, 1961. Tectonic map of the United States (exclusive of Alaska and Hawaii). Washington, D.C., U.S. Geological Survey, 2 sheets, scale 1:2,500,000.

5. BIBLIOGRAPHY

Champion, J.W., Jr., 1975. A detailed gravity study of the Charleston, South Carolina, epicentral zone: Master's Thesis, Georgia Institute of Technology, Atlanta, Georgia, 97p.

Heiskanen, Weikko, A. and Moritz, Helmut, 1967. Physical Geodesy, W. H. Freeman and Company, San Francisco 364 pp.

International Association of Geodesy, 1971a. Geodetic reference system 1967: International Association of Geodesy Publication Speciale No. 3, 116 p.

International Association of Geodesy, 1971b. The international gravity standardization net 1971, International Association of Geodesy Publication Speciale No. 4, 49p.

McKee, J.H., 1974. A geophysical study of microearthquake activity near Bowman, South Carolina: Master's Thesis, Georgia Institute of Technology, Atlanta, Georgia, 65p.

Phillips, Jeffrey D. and W. Minor Davis, 1985. Principal facts for Gravity stations in Bamberg, Beaufort, Charleston, Colleton, Dorchester, and Orangeburg Counties, South Carolina, United States Department of the Interior, Geological Survey, Open-File Report 85-392, 15p.

PROGRAM LISTING

- AB Extends grids into areas of limited coverage by increasing the area used to compute the weighted average
- ALBERS Conversion between Albers equal area projection and latitude and longitude.
- CLEAN Identifies duplicate or very similar data points.
- CLERR Identifies inconsistent data points.
- LLUTM Geographic coordinates to UTM.
- SNGGRID Weighted average gridding of single variable.
GRVGRID is a two variable version of SNGGRID.
- UTMEL UTM to geographic coordinates.

```

PROGRAM AB(INPUT,OUTPUT,TAPE3,TAPE7)
  DIMENSION W(132,132),W2(132,132),ELEV(132,132),
+  ELEV2(132,132),BA(132,132),BA2(132,132),IB(8),IEL(8),IWT(8)

```

```

C
C
C *****
C *
C *
C *          PROGRAM "AB"
C *
C * PROGRAM "AB" IN FILE AB(GP310GR) IS A VARIABLE *
C * RADIUS SMOOTHING OPERATOR FOR WEIGHTED POTENTI-*
C * AL DATA. THE RADIUS OF SMOOTHING IS INCREASED *
C * UNTIL IT CONTAINS AT LEAST 6 DATA POINTS WITHIN*
C * THE GRID. USING THAT RADIUS, THE VALUE IS RE- *
C * COMPUTED. THIS PROCESS IS REPEATED FOR EACH *
C * GRID POINT.THE PROGRAM ACCEPTS DATA FROM PROGRAM *
C * "GRVGRID". EFFECTIVELY FILLING IN ANY AREAS OF *
C * NO DATA AND SMOOTHING AREAS OF LIMITED DATA. *
C * AREAS OF HIGH DATA DENSITY REMAIN UNCHANGED. *
C *****
C
C ***
C *** RECOMMENDED COMMANDS TO RUN THIS PROGRAM ON THE
C *** GEORGIA TECH CYBER B SYSTEM:
C *** LGO,,,TAPE3,TAPE7
C *** WHERE
C *** TAPE3=DATA FILE
C *** TAPE7=OUTPUT FILE
C
C *** MM=132
C *** NN=132
C *** INPUT
C
C READ(3,*,END=10001) NPOINT,DX,OLAT,OLONG,M,N,A,SCALE
2 READ(3,*,END=10001) ((BA(I,J),ELEV(I,J),W(I,J),I=1,
+ M),J=1,N)
C PRINT*,NPOINT,DX,OLAT,OLONG,M,N,A,SCALE
10001 PRINT*, 'INPUT PAST END OF FILE'
C WSUM=0.0
C *** CONVERT TO WEIGHTED SUMS
C DO 10 I=1,M
C DO 10 J=1,N
C BA(I,J)=BA(I,J) * W(I,J)
C ELEV(I,J)=ELEV(I,J) * W(I,J)
C WSUM=WSUM+W(I,J)
10 CONTINUE
C *** COMPUTE RADIUS FOR 6 DATA POINTS
C DO 1000 I=1,132
C DO 1000 J=1,132
C IF(W(I,J).GT.0.5) GO TO 901
C SW=W(I,J)
C DO 700 IR=2,30
C SW1=0
C SW2=0
C IEND=IR*2-1
C DO 600 IIR=1,IEND
C INDX=I-IR+IIR

```

```

IF(INDX.LT.1.OR.INDX.GT.132) GO TO 600
JNDX1=J+IR-1
JNDX2=J-IR+1
IF(JNDX1.GT.132) GO TO 599
SW1=W(INDX,JNDX1)+SW1
599 IF(JNDX2.LT.1) GO TO 600
SW2=W(INDX,JNDX2)+SW2
600 CONTINUE
SW=SW1+SW2+SW
SW1=0
SW2=0
IEND=IR*2-3
DO 602 JJR=1,JEND
INDX1=I+IR-1
INDX2=I-IR+1
JNDX=J-IR+JJR+1
IF(JNDX.LT.1.OR.JNDX.GT.132) GO TO 602
IF(INDX1.GT.132) GO TO 601
SW1=SW1+W(INDX1,JNDX)
601 IF(INDX2.LT.1) GO TO 602
SW2=SW2+W(INDX2,JNDX)
602 CONTINUE
SW=SW1+SW2+SW
IF(SW.GT.6)GO TO 701
700 CONTINUE
701 IRAD=IR
C *** COMPUTE NEW WEIGHTED VALUES OF BOUGUER,ELEVATION
C *** AND WEIGHTS
ADIST=FLOAT(IR-1)/2.0
805 IMIN=MAX0(I-IRAD+1,1)
806 IMAX=MIN0(I+IRAD-1,132)
807 JMIN=MAX0(J-IRAD+1,1)
808 JMAX=MIN0(J+IRAD-1,132)
DO 900 IR=IMIN,IMAX
DO 900 JR=JMIN,JMAX
IF(IR.EQ.I.AND.JR.EQ.J) GO TO 875
DIST=(FLOAT((I-IR)*(I-IR)+(J-JR)*(J-JR)))
WT2=1.0/(1+DIST/(ADIST*ADIST))
ELEV2(I,J)=ELEV2(I,J)+ELEV(IR,JR)*WT2
BA2(I,J)=BA2(I,J)+BA(IR,JR)*WT2
W2(I,J)=W2(I,J)+W(IR,JR)*WT2
GO TO 900
875 ELEV2(I,J)=ELEV2(I,J)+ELEV(I,J)
BA2(I,J)=BA2(I,J)+BA(I,J)
W2(I,J)=W2(I,J)+W(I,J)
900 CONTINUE
GO TO 1000
901 CONTINUE
W2(I,J)=W(I,J)
BA2(I,J)=BA(I,J)
ELEV2(I,J)=ELEV(I,J)
1000 CONTINUE

```

```

C *** RECOMPUTE WEIGHTED AVERAGES
      DO 50 I=1,M
      DO 50 J=1,N
      IF(W2(I,J))50,50,40
40     BA2(I,J)=BA2(I,J)/W2(I,J)
      ELEV2(I,J)=ELEV2(I,J)/W2(I,J)
50     CONTINUE

C *** THE FOLOWING WRITES GRIDDED VALUES IN TABLE FORM TO TAPE7
C *** OUTPUT IN INTEGER FORMAT FOR USE IN DISPLAY AND ANALYSIS
      REWIND 3
      WRITE(7,*) NPOINT,DX,OLAT,OLONG,M,N,A,SCALE
      DO 2010 I=1,M
      DO 2010 J=1,N,8
      ISTOP=8
      IF(J.EQ.129) ISTOP=4
      DO 2020 K=1,ISTOP
      IB(K)=INT(BA2(I,J+K-1)*10.)
      IEL(K)=INT(ELEV2(I,J+K-1)*10.)
2020     IWT(K)=INT(W2(I,J+K-1)*1000.)
      WRITE(7,2000) (IB(K),IEL(K),IWT(K),K=1,ISTOP)
2010     CONTINUE
2000     FORMAT(24I5)
      STOP
      END

```

```

C                                     ALBERS
C
C     ALBERS WILL TAKE LATITUDE AND LONGITUDE AS INPUT AND OUTPUT
C     THE X AND Y VALUES FOR AN ALBERS EQUAL AREA PROJECTION
C
C*****
PROGRAM ALBERT (INPUT,OUTPUT,XY,TAPE5=INPUT,TAPE6=OUTPUT,
+ TAPE7=XY)
10 DO 31 I=31,32
  ALAT = I-1
  ALONG = 96.
  CALL ALBERS(X,Y, ALAT,ALONG,1.0)
  WRITE (7,20)ALAT,ALONG,X,Y
20 FORMAT (3X,'LAT = ',1X,F8.2,2X,'LON = ',1X,F8.2,2X,'X = ',
+F11.2,2X,'Y = ',F11.2)
  CALL ALBERS(X,Y,ALAT,ALONG,-1.0)
  WRITE (7,20)ALAT,ALONG,X,Y
31 CONTINUE
99 STOP
END
SUBROUTINE ALBERS(X,Y, ALAT,ALONG,SGN)
C
C     ASSUMES 96 DEGREES WEST AND EQUATOR AS ORIGIN
C
AN = 0.602903500628
RSQ = 1.509957717935E+14
RO = 12288033.68296
RPD = ATAN(1.0)/45.0
EE = 6.768657997291054E-03
ARAD = 6378206.4
REFLONG = 96.
SMALL = 1.0E-12
IF (SGN.LT.0) GO TO 30
C*****
C     FORMULA USED TO COMPUTE CONSTANTS
C     E = FIRST ECCENTRICITY (SQRT(A*A-B*B)/A) FROM CLARKE, 1866
C     EE = E*E ((A*A-B*B)/A)
C     COSPH1 = COS(29.5*RPD)
C     COSPH2 = COS(45.5*RPD)
C     CSQ1 = COSPH1*COSPH1
C     CSQ2 = COSPH2*COSPH2
C     SINPH1 = SIN(29.5*RPD)
C     SINPH2 = SIN(45.5*RPD)
C     SSQ1 = SINPH1*SINPH1
C     SSQ2 = SINPH2*SINPH2
C     AN = CSQ1/(1.0 - EE*SSQ1) - CSQ2/(1.0 - EE*SSQ2)
C     SER1 = SINPH1*(1.0 + EE*SSQ1*(2./3. + EE*SSQ1*(3./5.
C + EE*SSQ1*(4./7. + EE*SSQ1*(5./9. + EE*SSQ1*6./11.))))
C     SER2 = SINPH2*(1.0 + EE*SSQ2*(2./3. + EE*SSQ2*(3./5.
C + EE*SSQ2*(4./7. + EE*SSQ2*(5./9. + EE*SSQ2*6./11.))))
C     AN = AN/(2.0*(1.0-EE)*(SER2 - SER1))
C     RHO1SQ = ARAD*ARAD*CSQ1/(AN*AN*(1.0-EE*SSQ1))
C     RSQ = RHO1SQ + 2.0*ARAD*ARAD*(1.0-EE)*SER1/AN
C     RO = SQRT(ABS(RSQ))
C     C2 = ARAD*ARAD*(1.0-EE)*(1.0+EE*(2./3. +EE*(3./5. +EE*
C + (4./7. +EE*(5./9. +EE*6./11.))))

```



```

200 REFLONG = 96
    SINPHI = SIN(ALAT*RPD)
    SP2 = SINPHI*SINPHI
    SB = SINPHI*(1.0 + EE*SP2*(2./3. + EE*SP2*(3./5. + EE*SP2*
+ (4./7. + EE*SP2*(5./9. + EE*SP2*6./11.))))))
    RHO = 2.0*ARAD*ARAD*(1.0-EE)*SB/AN
    RHO = SQRT(RSQ -RHO)
    THETA = AN*(REFLONG - ALONG)
    X = RHO*SIN(THETA*RPD)
    Y = RO - RHO*COS(THETA*RPD)
    GO TO 100
30  THETA=ATAN(X/(RO-Y))
    ALONG = REFLONG - THETA/(AN*RPD)
    RHO = (Y-RO)/COS(THETA)
    SB = (RSQ-RHO*RHO) * AN/(2.0*ARAD*ARAD*(1.0-EE))
    ALAT = SB-2.0*EE*SB*SB*SB/3.0
        DO 50 I=1,8
            OLDLAT =ALAT
            A2 = EE*ALAT*ALAT
            ALAT = SB/(1.0+A2*(2./3.+A2*(0.6+A2*(4./7.+A2*
+ (5./9. +A2*6./11.))))))
            WRITE(6,*) I,ALAT,OLDLAT
            IF (ABS(ALAT-OLDLAT).LT.SMALL) GO TO 60
50  CONTINUE
60  ALAT = ASIN(ALAT)/RPD
100 RETURN
    END

```

```

PROGRAM CLEAN(INPUT,OUTPUT,TAPE5,TAPE6,TAPE7)
DIMENSION ALAMIN(8000),ALOMIN(8000),ALAT(8000),ALONG(8000),
+EL(8000),BOUG(8000),DDLON(8000),DDLAT(8000)
CHARACTER*14 SURV(8000)
10 READ(5,101,END=20)ALAT(I),ALAMIN(I),ALONG(I),ALOMIN(I),EL(I),
+IBOUG,SURV(I)
101 FORMAT(3X,F3.0,F4.2,2X,F3.0,F4.2,3X,F7.1,20X,I5,A15)
BOUG(I)=FLOAT(IBOUG)/10.
DDLAT(I)=ALAT(I)+ALAMIN(I)/60.
DDLON(I)=ABS(ALONG(I))+ALOMIN(I)/60.
I=I+1
GO TO 10
20 ITOT1=I
30 READ(6,101,END=40)ALAT(I),ALAMIN(I),ALONG(I),ALOMIN(I),
+EL(I),IBOUG,SURV(I)
BOUG(I)=FLOAT(IBOUG)/10.
DDLAT(I)=ALAT(I)+ALAMIN(I)/60.
DDLON(I)=ABS(ALONG(I))+ALOMIN(I)/60.
I=I+1
GO TO 30
40 ITOT2=I-1
WRITE(7,100)
100 FORMAT('-----OUTPUT OF CLEAN-----'///)
WRITE(7,*) ' LAT LONG ELEV BOUGER SURVEY
+J1 OR K ADIF'
DO 60 J=2,ITOT1
J1=J-1
DO 70 K=J,ITOT2
IF(ABS(DDLAT(K)-DDLAT(J1)).GT..0018)GO TO 70
IF(ABS(DDLON(K)-DDLON(J1)).GT..0018)GO TO 70
ADIF=BOUG(J1)-BOUG(K)
WRITE(7,102)ALAT(J1),ALAMIN(J1),ALONG(J1),ALOMIN(J1),
+EL(J1),BOUG(J1),SURV(J1),J1,ADIF
WRITE(7,102)ALAT(K),ALAMIN(K),ALONG(K),ALOMIN(K),EL(K),
+BOUG(K),SURV(K),K,ADIF
70 CONTINUE
60 CONTINUE
102 FORMAT(F3.0,1X,F5.2,3X,F3.0,1X,F5.2,3X,F6.1,3X,F6.2,A14,I5,
+F6.2)
STOP
END

```

```

C*****
C/
C*
C* PROGRAM CLERR
C* -----
C* THIS PROGRAM TESTS A PORTION OF A TOTAL DATA SET AGAINST *
C* ITSELF (OR ANOTHER DATA SET AGAINST THE TOTAL DATA SET) *
C* FOR CONSISTANCY. POINTS NOT CONSISTANT WITH VALUES THAT *
C* ARE DETERMINED BY THE AUTOCORRELATION FUNCTION OF THE *
C* DATA SET AND THE WEIGHTED VALUE OF THE EIGHT NEAREST *
C* NEIGHBORS ARE THE PROGRAM OUTPUTS. *
C*
C*****

```

```

C
C
C PROC W: CLERR ( FILE1,FILE2,FILEOUT,TAPE6=FILE1,TAPE7=FILE2,
+TAPE5=FILEOUT)
C
C FILE1 CONTAINS THE TOTAL DATA SET (USED AS A STANDARD)
C FILE2 CONTAINS THE NEW DATA SET OR A PORTION OF FILE1
C TO TEST FOR CONSISTANCY. FIRST CARD IN (15 FORMAT) 0 OR 1, FOR
C PREDEFINED OR INTERNALLY COMPUTED AUTOCORRELATION RESPECTIVELY
C
C DIMENSION ALAT(8000),ALONG(8000),DAT(8000),AUTO(30),R(10),
+D(10),DLAT(10),DLONG(10),DLON(10),W(10)

```

```

C
C READ IN THE REFERENCE DATA IN DOD FORMAT
C
C RPD = ATAN(1.0) / 45.
C I = 1
10 READ(6,101,END=20) LAT,LATMN,LON,LONMN,IDATA
101 FORMAT (3X,13,14,2X,13,14,3CX,16)
ALAT(I) = FLOAT(LAT) + FLOAT(LATMN) / 6000.
ALONG(I) = FLOAT(LON) + FLOAT(LONMN) / 6000.
DAT(I) = FLOAT(IDATA) / 100.
I = I + 1
GOTO 10
20 IFST = I - 1

```

```

C
C READ IN THE FILE TO BE TESTED
C - OPTAUT = : IF THIS IS GREATER THAN 0 THEN COPUTES AUTOCORRELATION
C FROM DATA ELSE IT USES PREDEFINED AUTOCORRELATION.
C
C READ(7,100,END=30) OPTAUT
100 FORMAT(15)
21 READ(7,101,END=30) LAT,LATMN,LON,LONMN,IDATA
ALAT(I) = FLOAT(LAT) + FLOAT(LATMN) / 6000.
ALONG(I) = FLOAT(LON) + FLOAT(LONMN) / 6000.
DAT(I) = FLOAT(IDATA) / 100.
I = I + 1
GOTO 21

```

```

30  IEND = I-1
C
C  CALCULATE THE MEAN AND VARIANCE OF THE TOTAL DATA SET
C
    SUMX=0.0
    SUMXX=0.0
    AVLAT= 0.0
    AVLONG= 0.0
    DO 35  I= 1,IEND
        AVLAT= AVLAT + ALAT(I)
        AVLONG= AVLONG + ALONG(I)
        SUMX= SUMX + DAT(I)
        SUMXX= SUMXX + DAT(I)*DAT(I)
35  CONTINUE
    AMEAN= SUMX/FLOAT(IEND)
    VAR= (SUMXX/FLOAT(IEND)) - AMEAN*AMEAN
    OLAT= AVLAT/FLOAT(IEND)
    OLON= AVLONG/FLOAT(IEND)
    WRITE(5,77) VAR,OLAT,OLON,AMEAN,IEND
77  FORMAT (6HVAR = ,F8.3/7HOLAT = ,F10.4/7HOLON = ,F10.4/
+8HAMEAN = ,F8.3/7HIEND = ,16)
C
C  CONVERT TO MAP DISTANCES IN KILOMETERS
C
    DO 38  I= 1,IEND
        CALL MAPS (ALAT(I),ALONG(I),OLAT,OLON)
38  CONTINUE
    IF(OPTAUT.GT.0) GO TO 38
    DO 39  I=1,30
        II=I-1
39  AUTO(I)=COS(II*90*RPD/15.)*EXP(II*90*RPD/15.)
    GO TO 89
C
C  FIND THE AUTOCORRELATION FUNCTION OF THE DATA
C
C 88  CALL AUTOCHF (ALAT,ALONG,AUTO,IEND,VAR,AMEAN,DAT)
C
C  SORT IN ORDER OF LATITUDE
C
89  DO 103 I= 2,IEND
    IS= I-1
    DO 90 J= I,IEND
        IF (ALAT(IS) .LE. ALAT(J)) GOTO 90
        IS= J
90  CONTINUE
    ALATS= ALAT(IS)
    ALONGS= ALONG(IS)
    DATS= DAT(IS)
    IM1= I-1
    ALAT(IS)= ALAT(IM1)
    ALONG(IS)= ALONG(IM1)
    DAT(IS)= DAT(IM1)

```

```

        ALAT(IM1)= ALATS
        ALONG(IM1)= ALONGS
        DAT(IM1)= DATS
103  CONTINUE
C
C  COMPUTE THE EXTRAPOLATED VALUE BY THE LISTANCE WEIGHTED
C  SUM OF THE EIGHT NEAREST POINTS
C
C  REWIND FILE2
C
REWIND 7
ISTOP= IEND-IPST
DO 200 II= 1,ISTOP
    READ(7,101,END=201) LAT,LATMN,LON,LONMN,IDATA
    TLAT= FLOAT(LAT) + FLOAT(LATMN)/ 6000.
    TLONG= FLOAT(LON) + FLOAT(LONMN)/ 6000.
    TDAT= FLOAT(IDATA)/ 100.
    CALL MAPS (TLAT,TLONG,OLAT,OLON)
C
C  FIND START INTEGER FOR THE SEARCH
C
DO 220 I= 1,IEND
    IF (TLAT .LF ALAT(I)) GOTO 221
220  CONTINUE
221  ISTART= I-4
    IF (ISTART .LT. 1) ISTART= 1
C
C  COMMENCE SEARCH FOR EIGHT NEAREST POINTS
C
IF (ISTART .GT. (IEND-9)) ISTART= IEND-9
JJ= 1
DO 250 J= 1,9
    J1= J-1+ ISTART
    DLAT(JJ)= ALAT(J1)
    DLON(JJ)= ALONG(J1)
    R(JJ)= (TLAT - ALAT(J1))**2 + (TLONG - ALONG(J1))**2
    D(JJ)= DAT(J1)
    IF (R(JJ) .LT. .01 .AND. J .EQ. JJ) GOTO 250
    JJ= JJ+1
250  CONTINUE
    AMAXRR= 0.0
    DO 260 K= 1,8
        IF (R(K) .GT. AMAXRR) AMAXRR= R(K)
260  CONTINUE
C
KINC= 4
DO 300 K= 1,IEND
    KINC= KINC+1
    K1= I-KINC
    IF (K1 .LT. 1) GOTO 319
    RTEST= (TLAT - ALAT(K1))**2 + (TLONG - ALONG(K1))**2
    IF (RTEST .GE. AMAXRR) GOTO 320

```

```

DO 310 KK= 1,8
  IF (R(KK) .LT. AMAXRR) GOTO 310
  AMAXRR= RTEST
  R(KK)= RTEST
  D(KK)= DAT(K1)
  DLAT(KK)= ALAT(K1)
  DLON(KK)= ALONG(K1)
  GOTO 320
310 CONTINUE
319 K1= K+KINC
320 K2= K+KINC
  IF (K2 .GT. IEND) GOTO 329
  RTEST= (TLAT - ALAT(K2))**2 + (TLONG - ALONG(K2))**2
  IF (RTEST .GE. AMAXRR) GOTO 330
  DO 340 KK= 1,8
    IF (R(KK) .LT. AMAXRR) GOTO 340
    AMAXRR= RTEST
    R(KK)= RTEST
    D(KK)= DAT(K2)
    DLAT(KK)= ALAT(K2)
    DLON(KK)= ALONG(K2)
    GOTO 330
340 CONTINUE
329 K2= K1
330 ATM1= (TLAT - ALAT(K1))**2
  ATM2= (TLAT - ALAT(K2))**2
  IF (AMAXRR .LT. ATM1 .AND. AMAXRR .LT. ATM2) GOTO 400
300 CONTINUE
C
C COMPUTE THE EXTRAPOLATED VALUE (SD)
C
C FIRST COMPUTE WEIGHTS. THEN NORMALIZE
C
400 SWT= 0.0
  DO 410 J= 1,8
    W(J)= 1/(1.0 + R(J)/4.0)
    SWT= SWT + W(J)
410 CONTINUE
  DO 411 J=1,8
    W(J)= W(J)/SWT
411 CONTINUE
C
SD= 0.0
S1= 0.0
S2= 0.0
S3= 0.0
DO 450 KI= 1,8
  SD= SD + W(KI)*D(KI)
  S1 = S1 + W(KI)*W(KI)*.09
  S2= S2 + 2.0*W(KI)*AUT(R(KI),AUTO)
  DO 450 KII= 1,8
    RR= (DLAT(KII) - DLAT(KI))**2 + (DLON(KII) - DLON(KI))**2
    S3= S3 + W(KI)*W(KII)*AUT(RR,AUTO)
450 CONTINUE

```

```

C
S4=AUT(0.,AUTO) - S2 + S3
IF (S4 .LE. 0.) S4 = 0.
ERROR= SQRT(S1 + S4)
IF (ABS(TDAT - SD) .LT. ERROR) GOTO 200

C
C APPROXIMATE LAT. AND LONG. - PRINT OUT BAD POINT.
C
WRITE(5,113) LAT,LATMN,LON,LONMN
113 FORMAT(1H ,6HLAT =,12,1H ,15,8H LON =,13,1H ,15)
WRITE(5,112) TLAT,TLONG,TDAT,ERROR,SD
112 FORMAT(1H ,5HLAT =,F10.4,8H LONG =,F10.4,9H VALUE =,
+ F8.2,4H +/-,F8.2,8H EST = ,F8.2)
200 CONTINUE

C
C
201 STOP
END

C
C
SUBROUTINE AUTOCF (X,Y,AUTO,IEND,VAR,AMEAN,DAT)
DIMENSION X(IEND),Y(IEND),AUTO(30),NUM(30),DAT(IEND),AM(30)

C
C EXPECT 1KM SEPARATION FOR THE DATA AND COMPUTE THE
C AUTOCORRELATION OUT TO 30 KM.
C
DO 100 I= 2,IEND
  ISTOP= MIN0(I+50,IEND)
  DO 100 J= I,ISTOP
    NX= SQRT((X(I-1)-X(J))**2 + (Y(I-1)-Y(J))**2) + 1.5
    IF (NX .GT. 30) NX=30
    AUTO(NX)= AUTO(NX)+ (DAT(I-1)*(DAT(J)))
    NUM(NX)= NUM(NX) + 1
    AM(NX)=AM(NX)+DAT(I-1)+DAT(J)
100 CONTINUE

C
DO 200 I= 1,30
  IF (NUM(I) .EQ. 0) GOTO 200
  AUTO(I) = AUTO(I)/FLOAT(NUM(I)) - (AM(I)/FLOAT(2*NUM(I)))**2
200 CONTINUE
AUTO(1)= VAR

C
WRITE(5,105)
WRITE(5,106) (AUTO(I),NUM(I), I= 1,30)
105 FORMAT (1H1, 'AUTOCORRELATION FUNCTION USED')
106 FORMAT (1X,6HAUTO =,F10.2,5X,8HNUMBER =,I6)
C

```

```

C      SMOOTH THE AUTOCORRELATION FUNCTION
C
      SAUT= AUTO(1)
      DO 300 I= 2,29
        SAUT2= AUTO(I)
        AUTO(I)= (SAUT*NUM(I-1)+2*AUTO(I)*NUM(I)+AUTO(I+1)*NUM(I+1))/
+ (NUM(I-1)+2*NUM(I)+NUM(I+1))
        SAUT= SAUT2
300  CONTINUE
      WRITE(5,97)
      WRITE(5,106) (AUTO(I),NUM(I), I=1,30)
97   FORMAT(///'SMOOTHED AUTOCORRELATION FUNCTION ')
C
      RETURN
      END
C
C
      FUNCTION AJT(R,AUTO)
      DIMENSION AUTO(30)
      IR= SQRT(R) + 1.0
      IF (IR .GT. 30) IR=30
      AJT= AUTO(IR)
      RETURN
      END
C
C
      FUNCTION COLAT(P)
      COLAT= 1.570796327 - P + (0.3393028E-2)*SIN(2.*P)
      COLAT= COLAT - (0.47996E-5)*SIN(4.*P) + (0.8469E-8)*SIN(6.*P)
      RETURN
      END
C
C
      SUBROUTINE MAPS(ALAT,ALONG,OLAT,OLONG)
      CF = 0.0174532925
      PI =3.141592653
      AK =6688.3748
      AL =0.63305171
      ALAT = ALAT*CF
      ALONG = (OLONG - ABS(ALONG))*CF
      R = COLAT(ALAT)/2.
      R = AK*(TAN(R)**AL)
      X = R*SIN(AL*ALONG)
      P30 = OLAT*CF
      Z30 = COLAT(P30)
      R30 = AK*((TAN(Z30/2.))**AL)
      Y = R30 - R*COS(AL*ALONG)
      ALONG = X*0.072960*25.4
      ALAT = Y*0.072960*25.4
      RETURN
      END

```



```

C      (DECIMAL DEGREES)
C      OLONG = LONGITUDE OF ORIGIN OF GRID (SW CORNER WITH NO ROTATION)
C      (DECIMAL DEGREES)
C      M = NUMBER OF COLUMNS (EAST-WEST DIRECTION)
C      N = NUMBER OF ROWS (NORTH-SOUTH DIRECTION)
C      A = ANGLE OF ROTATION ABOUT THE ORIGIN (POSITIVE CLOCKWISE)
C      SCALE = SCALE AT WHICH MAP IS TO BE PLOTTED
C      DATA = M X N DATA POINTS IN FREE FIELD FORMAT
      READ(3,*,END=10000) NPOINT,DX,DY,OLAT,OLONG,M,N,A,SCALE
10000 IF(EOF(3))1,2,1

2      READ(3,665,END=10001) AA
      DO 143 J=1,N
      DO 143 I=1,M,8
      READ(3,666,END=10001) (BA(I+K-1,J),K=1,8)
143    CONTINUE
      READ(3,665,END=10001) AA
      DO 144 J=1,N
      DO 144 I=1,M,8
      READ(3,666,END=10001) (W(I+K-1,J),K=1,8)
144    CONTINUE
10001 CONTINUE
665    FORMAT(A30)
666    FORMAT(8F10.2)
C
C      PRINTS VALUES FROM OLD GRID (OLD BOUG, OLD WTS)
C      FOR REVIEW AND REFERENCE.
C      PRINT*, 'DO YOU WISH A LINE PRINTER INTEGER PLOT? ENTER Y OR N'
C      READ(5,*) IANS
C      IF (IANS.EQ.N) GO TO 3
C
      WRITE(6,102) NPOINT
102    FORMAT(1H1, 'OLD GRID CONTAINS', I6, ' POINTS', /)
103    FORMAT(1H1, 'OLD BOUGUER ANOMALIES * 10', /)
      WRITE(6,103)
      CALL PRGRID(BA,10.,M,N,MM,NN)
105    FORMAT(1H1, 'OLD WEIGHTS * 100', /)
      WRITE(6,105)
      CALL PRGRID(W,100.,M,N,MM,NN)
3      DO 10 I=1,M
      DO 10 J=1,N
      BA(I,J) = BA(I,J) * W(I,J)
10     CONTINUE
1      WRITE(6,106)
106    FORMAT(1H1, 'DATA INSERTED INTO GRID THIS PASS', /)
C

```

```

C THE FOLOWING READS THE FIRST CARD OF THE NEW DATA FILE
C DX = INCREMENT OF GRID IN KILOMETERS IN THE X DIRECTION
C DY = INCREMENT OF GRID IN KILOMETERS IN THE Y DIRECTION
C OLAT =LATITUDE OF ORIGIN OF GRID (SW CORNER WITH NO ROTATION)
C (DECIMAL DEGREES)
C OLONG = LONGITUDE OF ORIGIN OF GRID (SW CORNER WITH NO ROTATION)
C (DECIMAL DEGREES)
C M = NUMBER OF COLUMNS (EAST-WEST DIRECTION)
C N = NUMBER OF ROWS (NORTH-SOUTH DIRECTION)
C A = ANGLE OF ROTATION ABOUT THE ORIGIN (POSITIVE CLOCKWISE)
C SCALE = SCALE AT WHICH MAP IS TO BE PLOTTED
C DATA = M X N DATA POINTS IN STANDARD DOD FORMAT
C
IF (DX.EQ.0)GO TO 132
READ(7,*)TDX,TDY,TOLAT,TOLONG,IM,IN,TA,TSCALE
C TEST FOR CONSISTENCY
IF(TDX.NE.DX)GO TO 131
IF(TOLAT.NE.OLAT)GO TO 131
IF(TOLONG.NE.OLONG)GO TO 131
IF(IM.NE.M)GO TO 131
IF(IN.NE.N)GO TO 131
IF(TA.NE.A)GO TO 131
IF(TSCALE.NE.SCALE)GO TO 131
GO TO 133
131 PRINT*, 'GRID PARAMETERS ARE NOT THE SAME AS ON THE
+ PREVIOUS RUN. DO YOU WISH TO CONTINUE? (Y OR N)'
READ(5,130)IANS
130 FORMAT(A1)
IF(IANS.EQ.N)STOP
GO TO 133
132 READ(7,*) DX,DY,OLAT,OLONG,M,N,A,SCALE
C FIND THE NORTHING AND EASTING (TMOLAT,TMOLONG) OF THE ORIGIN
C LONGITUDE AND ORIGIN LATITUDE (OLONG,OLAT)
133 DOLONG=OLONG
DOLAT=OLAT
C CHARLESTON GRIDS ARE ZONE -17
ZONE=-INT((186-INT(OLONG))/6)
C CHANGE ZONE TO CORRESPONDED TO AREA OF MAP (KEEP NEGATIVE TO
C FIX)
CALL LLUTM(TMOLAT, TMOLONG, DOLAT, DOLONG, -17)
C PRINT*, 'TMOLONG=', TMOLONG, ' TMOLAT=', TMOLAT, 'DOLONG=', DOLONG,
C + 'DOLAT=', DOLAT
C
C
**11 READ(7,107,END=10003)ALAT,ALONG,BOUG

```

```

***** THE FOLLOWING LINES ARE FOR READING DATA
***** FROM SPECIAL TAPES THAT CONTAIN DATA USED IN THE
***** 132 KM LENGTH CHARLESTON, S.C. GRID.
***** TO RUN THE ORIGINAL SNGGRID, COMMENT THESE LINES
***** AND REMOVE THE "***" FROM THE ORIGINAL LINES.
C*
C*
C* READ ERPI DATA (IN ALBERS PROJECTION) AND
C* CONVERT TO A NEW CHARLESTON GRID (IN TRANSVERSE MERCATOR
C* PROJECTION
READ(7,100) NCOLS,NROWS,XMIN,XMAX,YMIN,YMAX,RNULL
100 FORMAT (2I5,5(2X,E12.5))
YMET= YMIN
C THIS ZEROES THE ARRAY OF TEMPORARY VALUES
C
777 DO 390 I= 1,397
      T(I)= 0.0
390 CONTINUE
C SET XMET BACK ONE X INCREMENT
XMET= XMIN - 4000.
C LOOP TO READ IN THE 50 LINES OF A BLOCK.
C THERE ARE EIGHT VALUES PER LINE.
C
DO 400 I= 1,400,8
      READ(7,150,END=10003) T(I),T(I+1),T(I+2),T(I+3),
+ T(I+4),T(I+5),T(I+6),T(I+7)
150 FORMAT(8E10.4)
400 CONTINUE
C
C LOOP OVER EACH BLOCK, TEST IF THE POINT IS IN THE GRID
C
DO 600 K= 1,396
      XMET= XMET + 4000.
      IF(T(K) .EQ. RNULL) GOTO 600
      CALL ALBERS (XMET,YMET,ALAT,ALONG,-1.)
      BOUG= T(K)
C WRITE(6,*)ALAT,ALONG,BOUG
10003 IF (EOF(7))12,4,12
107 FORMAT(26X,2F8.3,6X,F6.2)
CC
C NEXT, COMPUTES X AND Y WHERE + WEST, + NORTH
C
4 DXX = ABS(ALONG)
DYY = ALAT
C WRITE(6,601)DYY
601 FORMAT('DYY=',F12.4)
C

```

```

C
C   NEXT DETERMIN THE DISTANCE IN KILOMETERS BETWEEN (X,Y)
C   +AND (OLONG, OLAT) FOR UTM PROJECTION
C
C   CALL LLUTM(AN1,E1,DYY,DX, -17)
C   WRITE(6,502)AN1,TMOLAT
602  FORMAT('AN1=',F15.4,'TMOLAT=',F15.4)
      Y = (AN1-TMOLAT)
      X = (E1-TMOLONG)
C   WRITE(6,500)X,Y
C500 FORMAT('X=',F10.3,'Y=',E15.6)
C   NEXT, ROTATE GRID BY (A) . THE NEW AXIS IS ROATED (A) DEGREES
C   (B) RADIANS CLOCKWISE FROM OLD AXIS ABOUT THE ORIGIN.
C   IF (A.EQ.0) GO TO 27
      B=A*RAD
      XSAVE=X*COS(B)-Y*SIN(B)
      YSAVE=X*SIN(B)+Y*COS(B)
      X=XSAVE
      Y=YSAVE
C
C
C   THE FOLOWING PUTS OLAT, OLONG AT PT 3,3 OF GRID
C
C   X = X/(DX*1000.) + 3
27   Y = Y/(DY*1000.) + 3
C   NEXT, INTERGERIZES X AND Y TO GIVE GRID COORDINATES
      IX=X
      IY=Y
C   WRITE(6,501)IX,IY
501  FORMAT('IX=',I5,'IY=',I5)
C
C   THE FOLOWING DETERMINES IF A PT IS OUT OF RANGE
C   IF IT IS, SKIP IT.
C
*****   TO RUN THE ORIGINAL SNGGRID, CHANGE 600 TO 11
*****   IN THE NEXT TWO LINES.
      IF(IABS(IX-M/2).GT.M/2-2)GO TO 600
      IF(IABS(IY-N/2).GT.N/2-2)GO TO 600
      NPOINT = NPOINT + 1
C
C   THE FOLOWING WRITES THE OUTPUT, STARTING WITH
C   THE VALUES READ FROM TAPE5
C
C   WRITE(6,108) ALAT,ALONG,BOUG
108  FORMAT(2F8.3,F6.2)
      CALL CALTW(TW,X,Y,DX,DY)
C   WRITE(6,502)TW

```

```

502  FORMAT('TW=',F10.3)
      DO 20 I=1,4
      DO 20 J=1,4
      IXI = IX-2+I
      JYJ = IY-2+J
      W(IXI,JYJ) = W(IXI,JYJ) + TW(I,J)
      BA(IXI,JYJ) = BA(IXI,JYJ) + BOUG*TW(I,J)
20    CONTINUE
**    GO TO 11
*****  TO RUN THE ORIGINAL SNGGRID, REMOVE "***" FROM
*****  PREVIOUS LINE AND COMMENT THE NEXT TWO LINES.
600    CONTINUE
C      INCREMENT YMET FOR THE NEXT BLOCK
C
      YMET= YMET + 4000.
      GOTO 777
12     CONTINUE
      DO 50 I=1,M
      DO 50 J=1,N
      IF(W(I,J))50,50,40
40     BA(I,J) = BA(I,J)/W(I,J)
50     CONTINUE
C
C      NEXT, CONTINUES TO WRITE TO TAPE6.
C      (1) # OF PTS IN NEW GRID
C      (2) NEW BOUGER ANOMALIES TIMES 10
C      (4) NEW WEIGHTS TIMES 100
C
      WRITE(6,109) NPOINT
109    FORMAT(1H1,'NEW GRID CONTAINS',I6,' POINTS',/)
      WRITE(6,110) SCALE
110    FORMAT(1H1,'NEW ANAMOLIES * SCALE',E11.4,/)
      CALL PRGRID(BA,SCALE,IY,K,MM,NN)
      WRITE(6,112) SCALE
112    FORMAT(1H1,'NEW WEIGHTS * SCALE',F8.1,/)
      CALL PRGRID(W,SCALE,M,N,MM,NN)
C
C      THE FOLOWING WRITES GRIDDED VALUES IN TABLE FORM TO TAPE3
C
      REWIND 3
      WRITE(3,*) NPOINT,DX,DY,OLAT,OLONG,M,N,A,SCALE
      WRITE(3,111)
111    FORMAT('NEW ANOMALIES')
      DO 149 J=1,N
      DO 149 I=1,M,8
      WRITE(3,666) (BA(I+K-1,J),K=1,8)
149    CONTINUE
      WRITE(3,113)
113    FORMAT('NEW WEIGHTS')
      DO 190 J=1,N
      DO 190 I=1,M,8
      WRITE(3,666) (W(I+K-1,J),K=1,8)
190    CONTINUE
      STOP
      END

```

```

C
      SUBROUTINE CALTW(TW,X,Y,DX,DY)
C THIS SUBROUTINE ASSUMED THAT THE WEIGHTS ARE COMPUTED AS
C IF IN A SQUARE GRID (DX=DY)
      DIMENSION TW(4,4)
      A = 0.5
      SW = 0.0
      IX = X
      IY = Y
      X = X-IX
      Y = Y-IY
      DO 10 IX=1,4
        DO 10 IY=1,4
          X2=(2.0-IX+X)*(2.0-IX+X)
          Y2=(2.0-IY+Y)*(2.0-IY+Y)
          RR=X2+Y2
          TW(IX,IY)=1.0/(RR/(A*A)+1.0)
10      SW=SW+TW(IX,IY)
      DO 20 IX=1,4
        DO 20 IY=1,4
20      TW(IX,IY) = TW(IX,IY)/SW
      RETURN
      END

```

```

C
      SUBROUTINE PRGRID(A,SCALE,M,N,MN,NN)
      DIMENSION K(32),A(MM,NN)
      DO 20 L=1,M,32
        L1 = L
        L2 = L + 31
        IF (L2.GT.M) L2=M
        DO 30 IJ=1,N
          J = N - IJ + 1
          DO 40 I=L1,L2
40      K(I-L1+1)=SCALE*A(I,J)
          L3=L2-L1+1
30      WRITE(6,101) (K(I),I=1,L3)
20      CONTINUE
101     FORMAT(1X,/,32I4)
      RETURN
      END

```

C
C
C
C
C
C
C

***** PLTX *****

WHEN GIVEN THE LATITUDE AND LONGITUDE OF A POINT AS INPUT,
PROGRAM PLTX WILL OUTPUT THE GRID INDICIES CORRESPONDING
TO THE POINT FOR EACH OF THE FOUR GRIDS DEFINED FOR THE
CHARLESTON STUDY.

```
PROGRAM PLTX (INPUT, OUTPUT, 1, TAPE5=INPUT, TAPE6=OUTPUT,  
+TAPE7=XY)  
  DIMENSION IX(4), IY(4)  
  WRITE (6, 7)  
7  FORMAT ('ENTER POINT IN DECIMAL DEGREES, (LAT, LON)')  
4  READ (5, *, END=99) ALAT, ALONG  
  CALL LATTOX (ALAT, ALONG, AN, AE, IX, IY)  
8  FORMAT ('OUTPUT OF LATTOX')  
  WRITE (7, 9)  
9  FORMAT ('-----')  
  WRITE (7, 10) ALAT, ALONG  
10 FORMAT ('LATITUDE=', F15.6, 8X, 'LONGITUDE=', F15.6)  
  WRITE (7, *) ' '  
  WRITE (7, 30)  
30 FORMAT (1X, 'GRID NO.', 5X, 'X', 8X, 'Y')  
  WRITE (7, 40)  
40 FORMAT ('-----')  
  DO 60 I=1, 4  
  WRITE (7, 61) I, IX(I), IY(I)  
61  FORMAT (5X, I2, 3X, I8, 1X, I8)  
60  CONTINUE  
  GO TO 4  
99  STOP  
  ENI  
C  
  SUBROUTINE LATTOX (ALAT, ALONG, AN, AE, IX, IY)  
  DIMENSION R(4), DX(4), IX(4), IY(4)  
  REAL N, NP  
  IF (OLAT.NE.0.0) GO TO 10  
C*****  
C      DEFINE CONSTANTS OF THE CHARLESTON GRID DEFINITIONS  
C      OLAT= ORIGIN LATITUDE, OLONG= ORIGIN LONGITUDE,  
C      DX= GRID INCREMENT IN METERS, R= DISTANCE FROM ORIGIN IN METERS  
C      ANG= ANGLE OF GRID ROTATION, CLOCKWISE  
C*****  
  OLAT= 33.125  
  OLONG= 81.25  
  DATA DX/1000., 4000., 8000., 31.25/  
  DATA R/0., 62500., 444500., 484.375/  
  RPD=ATAN(1.0)/45.  
  ANG=52*RPD
```



```

        CALL LLUTM(ON,OE,OLAT,OLONG,-17.)
        WRITE(7,60) ON,OE
60      FORMAT(10H ORIGIN N=,F15.2,10H ORIGIN E=,F15.2)
10      CALL LLUTM(N,E,ALAT,ALONG,-17.)
        WRITE(7,61) N,E
61      FORMAT(10H POINT N =,F15.2,10H POINT E =,F15.2)
        N=N-ON
        AN=N
        E=E-OE
        AE=E
        NP=E*SIN(ANG)+N*COS(ANG)
        EP=E*COS(ANG)-N*SIN(ANG)
        DO 50 I=1,4
            IY(I)=IFIX(((NP+R(I))+DX(I)/2)/DX(I))+1
            IX(I)=IFIX(((EP+R(I))+DX(I)/2)/DX(I))+1
50      CONTINUE
        RETURN
        END

```

```

C
      SUBROUTINE LLUTM(ZN,ZE,ZLAT,ZLON,ZONE)
C*****
C      CONVERTS LATITUDE AND LONGITUDE IN DEGREES
C      TO UTM NORTH AND EAST IN METERS
C

```

```

C*****
      IMPLICIT DOUBLE PRECISION (A-Y)
      DIMENSION NCO(8),LCO(10)
C*****

```

```

      LAT=ZLAT
      LON=ZLON
      AZONE=ZONE
      KZERO=.9996D0
      SEMAJ=6378206.4D00
      SEMIN=6356583.8D00
      ECC=8.227185422300300D-02
      ECCSQ=6.760657997291054D-03
      EPSQ=6.814784945915042D-03
      NCO(1)=6.367399689169782D 06
      NCO(2)=-3.250286241790479D 04
      NCO(3)=1.384048366716706D 02
      NCO(4)=-7.535398130601429D-01
      NCO(5)=4.219413411982918D-03
      NCO(6)=-2.529287942342808D-05
      NCO(7)=1.556058285276389D-07
      NCO(8)=-9.738474374730020D-10
      LCO(1)=1.000000000000000D 00
      LCO(2)=-1.353731599458211D-02
      LCO(3)=9.162946216858431D-05
      LCO(4)=-3.095662638412468D-05
      LCO(5)=4.148716543194615D-07
      LCO(6)=-1.268441397827776D-07
      LCO(7)=2.158262546320965D-09
      LCO(8)=-6.173915584213417D-10
      LCO(9)=1.190710620936894D-11
      LCO(10)=-3.157184252484188D-12

```

```

RPD=ATAN(1.)/45.
PI=3.141592653589793DO
FTPERM=3.28083333333333DO
SINSEC=4.8481368110952D-6
IF (AZONE.GE.0) AZONE=(186DO - LON) / 6DO
IF (LAT.EQ.PHI) GO TO 2
PHI=LAT
ARG=LAT*RPD
COSPHI=DCOS(ARG)
COSSQ=COSPHI**2
SINPHI=DSIN(ARG)
SINSQ=SINPHI**2
TANSQ=SINSQ/COSSQ
TANPHI=SINPHI/COSPHI
NUPHIK=KZERO * SEMAJ / DSQRT(1DO-ECCSQ * SINSQ)
FILAT=((((((NCO(8)*COSSQ+NCO(7))*COSSQ+NCC(6))*COSSQ+NCO(5))
+*COSSQ+NCO(4))*COSSQ+NCO(3))*COSSQ+NCO(2))*COSPHI*SINPHI
++NCO(1)*ARG)*KZERO
2 CONTINUE
CENLON=(30-DABS(AZONE))*6DO+3DO
P=(CENLON-LON) * RPD
PSCS=P*P*COSSQ
ESCS=EPSQ*COSSQ
FIIIP=((4DO * ESCS + 9DO) * ESCS + 5DO - TANSQ) * 30DO
A6P=(TANSQ - 58DO) * TANSQ + 60D2 * ESCS - 330DO * EPSQ + 61DO
N=((A6P*PSCS+FIIIP)*PSCS+360DO)*PSCS*TANPHI*NUPHIK/720DO * FILAT
FVP=(1DO - TANSQ + ESCS) * 20DO
B5F=(TANSQ - 18DO) * TANSQ + 72DO * ESCS - 58DO * EPSQ + 5DO
E=((B5F * PSCS + FVP) * PSCS + 120DO) * P * COSPHI * NUPHIK/
+120DO + 500000DO
ZN=SNGL(N)
ZE=SNGL(E)
RETURN
END

```

```

PROGRAM PXTL (LATLON, INPUT, OUTPUT, TAPE7=LATLON, TAPE5=INPUT,
+TAPE6=OUTPUT)

```

```

1 PRINT*, 'ENTER GRID NUMBER (1=128KM, 2=256KM, 3=1028KM,
+4=LANDSAT), INDEX TO SE, INDEX TO NE'
READ(5,*) IGRIDN, X, Y
IX = X
IY = Y
IF (IGRIDN.GT.4..OR.IGRIDN.LT.1.) GO TO 9
CALL XTOLAT (ALA, ALONG, AN, AE, IX, IY, IGRIDN)
WRITE(7,*) '-----'
WRITE(7,45)
45 FORMAT('OUTPUT OF XTOLAT')
WRITE(7,47)
47 FORMAT('-----')
WRITE(7,50) IGRIDN

```

```

50 FORMAT('GRID NUMBER=',I3)
   WRITE (7,52) X,Y
52 FORMAT('X=',F5.2,8X,'Y=',F5.2)
   WRITE (7,54) AN,AE
54 FORMAT('NORTHING=',F15.3,2X,'EASTING=',F15.3)
   WRITE (7,56) ALAT,ALONG
56 FORMAT('LATITUDE=',F15.7,3X,'LONGITUDE=',F15.7)
   GO TO 9
9 STOP
END
SUBROUTINE XTOLAT(ALAT,ALONG,AN,AE,IX,IY,I)
  DIMENSION R(4),DX(4)
  DATA R/0.,62500.,444500.,484.375/
  DATA DX/1000.,4000.,8000.,31.25/
  ON=3664980.84
  OE=476678.49
  RPD=ATAN(1.0)/45.
  A=-52*RPD
  AN=FLOAT(IY-1)*DX(1)-R(1)
  AE=FLOAT(IX-1)*DX(1)-R(1)
  AES=AE*COS(A) - AN*SIN(A)
  AN=AE*SIN(A) + AN*COS(A)
  AE = AES
  AN = AN + ON
  AE = AE + OE
  CALL UTMLL(AN,AE,ALAT,ALONG,17.)
  RETURN
END
SUBROUTINE UTMLL(ZN,ZE,ZLAT,ZLON,ZONE)
C*****
  IMPLICIT DOUBLE PRECISION (A-Y)
  DIMENSION NCO(8),LCO(10)
C*****
  N = ZN
  AZONE = ZONE
  E = ZE
  LAT = ZLAT
  LON = ZLON
  KZERO=.9996D0
  SEMAJ=6378206.4D00
  SEMIN=6356583.8D00
  ECC=8.227105422300300D-02
  ECCSQ=6.768657997291054D-03
  EPSQ=6.814784045915042D-03
  NCO(1)=6.367339689169782D 06
  NCO(2)=-3.250286241790479D 04
  NCO(3) =1.384048366716706D 02
  NCO(4)=-7.325388130601429D-01
  NCO(5) =4.219413411982918D-03
  NCO(6)=-2.529287942342808D-05
  NCO(7) =1.556058285276589D-07
  NCO(8)=-9.738474374730020D-10
  LCO(1) =1.000000000000000D 00

```

```

LCO(2)=-1.353731599458211D-02
LCO(3)=9.162946216858431D-05
LCO(4)=-3.095662638412468D-05
LCO(5)=4.148716543194615D-07
LCO(6)=-1.268441397827776D-07
LCO(7)=2.158262546320965D-09
LCO(8)=-6.173915584213417D-10
LCO(9)=1.190710620936894D-11
LCO(10)=-3.157184252484188D-12
RPD=ATAN(1.)/45.
PI=3.141592653589793D0
FTPERM=3.280833333333333D0
SINSTC=4.8481368110952D-6
IF(N.EQ.FILAT) GO TO 2
FIK=N/KZERO
ARG=FIK/NCO(1)
COSPHI=DCOS(ARG)
COSSQ=COSPHI**2
SINPHI=DSIN(ARG)
1 APPARG=ARG
PART=((((NCO(8)*COSSQ+NCO(7))*COSSQ+NCO(6))*COSSQ+NCO(5))*
+COSSQ+NCO(4))*COSSQ+NCO(3))*COSSQ+NCO(2))*COSPHI*SINPHI
ARG=(FIK-PART)/NCO(1)
COSPHI=DCOS(ARG)
COSSQ=COSPHI**2
SINPHI=DSIN(ARG)
IF(DABS(APPARG-ARG).GT.5D-10) GO TO 1
SINSQ=SINPHI**2
NUPHIK=KZERO*SEMAJ/DSQRT(1D0-ECCSQ*SINSQ)
TANSQ=SINSQ/COSSQ
TANPHI=SINPHI/COSPHI
PHI=ARG/RPD
FILAT=(((((((NCO(8)*COSSQ+NCO(7))*COSSQ+NCO(6))*COSSQ+NCO(5))*
+COSSQ+NCO(4))*COSSQ+NCO(3))*COSSQ+NCO(2))*COSPHI*SINPHI+
+NCO(1)*AGR)*KZERO
2 CONTINUE
Q=0.5D0-E*1D-6
C**** Q IS NEGATIVE EAST OF CENTRAL MERIDIAN ****
QNK=(Q/NUPHIK)**2
ESCS=EPSQ*COSSQ
FV11=(ESCS+1D0)*5D11
FV111=(((ESCS+2D0)*(COSSQ-SINSQ)-ESCS-ESCS)*EPSQ+TANSQ)
+*3D0+5D0)/24D-24
D6=((COSSQ*107D0-SINSQ*162D0)*EPSQ+(2D0+TANSQ-EPSQ+ESCS)
+*45D0*TANSQ+61D0)/72D0-36
LAT=PHI-((D6*QNK-FV111)*QNK+FV11)*QNK*TANPHI/RPD
C FIX=1D6
FX=(1D0+TANSQ+TANSQ+ESCS)/6D-18
E5=((24D0*TANSQ+28D0)*TANSQ-2D0*ESCS+8D0*EPSQ+5D0)/12D0-30
LON=(30-AZONE)*6D0+3D0+((E5*QNK-FX)*QNK+1D6)*Q/
+(COSPHI*RPD*NUPHIK)
ZLAT=LAT
ZLON=LON
PRINT*, 'ZLAT=', ZLAT, ' ZLON=', ZLON, ' ZN=', ZN, ' ZE=', ZE
RETURN
END

```

APPENDIX E

APPENDIX B-1

MAGNETOTELLURIC SOUNDINGS
NEAR CHARLESTON, SOUTH CAROLINA

VOLUME I: PRINCIPLES

**MAGNETOTELLURIC SOUNDINGS
NEAR CHARLESTON,
SOUTH CAROLINA**

VOLUME I: PRINCIPLES

by: C. T. Young & J. C. Rogers
Michigan Technological University

December 1985

MTU Contract No. E26805

TABLE OF CONTENTS

List of Figures	iii
List of Tables	iii
CHAPTER 1. INTRODUCTION	B-1-1
CHAPTER 2. PRINCIPLES OF TENSOR MAGNETOTELLURICS	B-1-3
2.1 Overview	B-1-3
2.2 Signal Source	B-1-7
2.3 Definitions of Quantities Presented	B-1-7
A. Impedance Tensor, Apparent Resistivity and Phase	B-1-7
B. Polarization Modes Over Two-Dimensional Earth	B-1-9
i. Apparent Resistivities Over a Fault	B-1-11
ii. Apparent Resistivities Over a Narrow Conductor	B-1-11
iii. Rotation of Axis to Find Orientation of Structure	B-1-11
C. Skew and Ellipticity	B-1-14
D. Vertical Magnetic Field and Tipper	B-1-15
E. Interpretation of Tipper Data Based on a Simple Fault Model	B-1-15
F. Effect of Conductive Sea Water and Sediments	B-1-16
2.4 Signal Analysis and Remote Reference Processing	B-1-18
A. The Use of Auto and Cross Spectra to Estimate Tensor Elements	B-1-18
B. Magnetic Field and Electric Field Reference Processing	B-1-19
C. Principles of Noise Bias Reduction Using Remote Reference Data	B-1-20
D. Calculation of Standard Deviations	B-1-25
E. Calculation of Fourier Coefficients	B-1-25

CHAPTER 3. INSTRUMENTATION	B-1-28
3.1 System Specifications	B-1-28
3.2 Procedures and Precautions	B-1-29
A. Site Selection, Installation and Operation	B-1-29
CHAPTER 4. CALIBRATION AND VERIFICATION OF PROPER SYSTEM OPERATION	B-1-31
4.1 Calibration Procedure	B-1-31
4.2 Performance Compared to Three Other MT Systems	B-1-34
CHAPTER 5. FINAL PLOTS AND TABLES	B-1-39
5.1 Strip Chart Output	B-1-39
5.2 Header Page and Operator Log	B-1-39
5.3 Apparent Resistivity and Phase of Rho-max and Rho-min	B-1-41
5.4 Bostick One-Dimensional Inversion	B-1-45
5.5 Tipper Magnitude and Phase	B-1-46
5.6 Skew, Ellipticity, Tipper Strike and Impedance Strike	B-1-46
5.7 E, H and Ordinary Coherencies	B-1-49
5.8 Amplitude Spectra, E and H	B-1-49
CHAPTER 6. CHARLESTON, SOUTH CAROLINA FIELD AREA	B-1-52
6.1 General	B-1-52
6.2 Conduct of Survey	B-1-52
6.3 General Appearance of Data	B-1-52
6.4 Summary	B-1-53
Acknowledgements	B-1-54
REFERENCES	B-1-55

List of Figures

1.1	Location map of work area	B-1-2
2.1	Block diagram of MT system	B-1-4
2.2	Flowchart of MT signal analysis	B-1-5
2.3	Field emplacement of MT apparatus	B-1-6
2.4	MT polarization mode definitions	B-1-10
2.5	Apparent resistivities across a contact between blocks of different resistivities	B-1-12
2.6	Apparent resistivities over a narrow conductor	B-1-13
2.7	Magnetic field over a contact between blocks of different resistivities	B-1-17
2.8	Example of remote H reference field processing	B-1-23
2.9	Example of local H references field processing	B-1-24
4.1	Sample transfer function plots for channel 1, Hx	B-1-35
4.2	Normal operating configuration for E channels	B-1-36
4.3	Calibration of E channels	B-1-37
4.4	Comparison of four MT systems measurement results	B-1-38
5.1	Chart recorder output produced by HP9845 graphics	B-1-40
5.2	Header page and operator log	B-1-42
5.3	Apparent resistivity and phase	B-1-43
5.4	Smoothed apparent resistivity and Bostick 1-D inversion	B-1-44
5.5	Tipper, magnitude and phase	B-1-47
5.6	Skew, ellipticity, T strike and Z strike	B-1-48
5.7	E, H, and ordinary coherencies	B-1-50
5.8	Telluric amplitude and magnetic amplitude spectra	B-1-51

List of Tables

4.1	Sample printed output of calibration program	B-1-31 B-1-33
-----	--	------------------

CHAPTER 1. INTRODUCTION

The remote reference tensor magnetotellurics (MT) measurements described here were conducted by Michigan Technological University near Charleston, South Carolina during October and November of 1985. A real-time magnetotellurics apparatus manufactured by Phoenix Geophysics of Willowdale, Ontario, Canada was used to make deep soundings, which are to be used by Law Engineering for investigation of deep crustal structure related to earthquake activity near Charleston. Figure 1.1 indicates the location of the twelve MT sites. Principles of tensor MT and details of signal analysis including remote reference processing are provided in Chapter 2. Information on the instrumentation and details of the operating procedure are given in Chapter 3 while Chapter 4 presents material on system calibration. Results of the survey are presented in a separate data volume in the form of graphs and tables which are discussed in Chapter 5. Details of the work near Charleston and discussion of the data obtained are contained in Chapter 6 along with a summary.

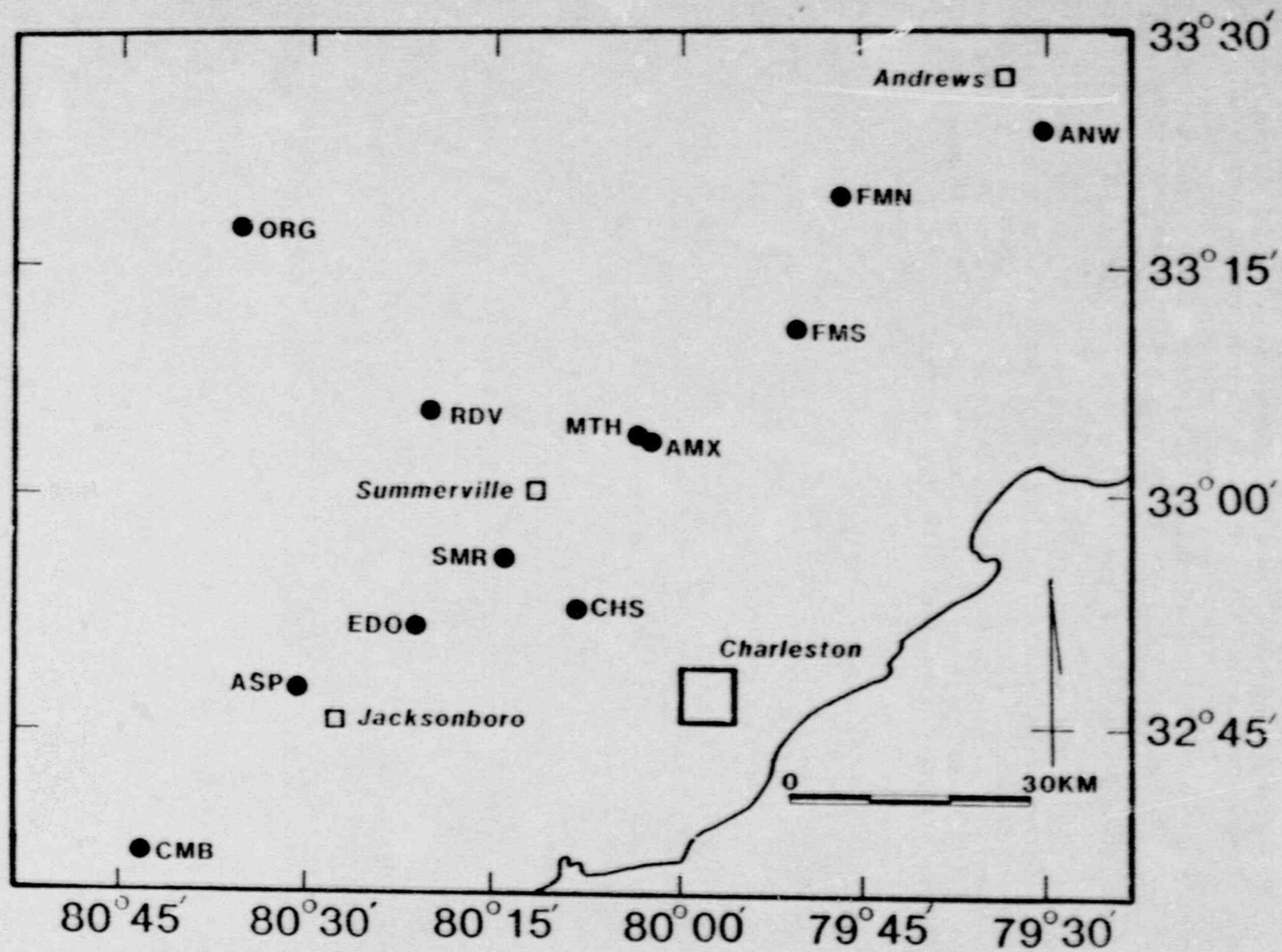


Figure 1.1 Location map of work area.

CHAPTER 2. PRINCIPLES OF TENSOR MAGNETOTELLURICS

2.1 Overview

Tensor magnetotellurics (MT) uses natural time-varying electric and magnetic fields to determine the surface impedance of the earth. From the impedance at one or more sites, a resistivity cross section can be estimated which can reveal geologic structure. Thus, MT can be used for commercial geophysical exploration for petroleum, evaluating geothermal resources, delineating ground water or exploring for minerals. The Michigan Technological University MT system uses a computer to analyze the data in real-time, producing high quality tables and plots at the field site. Thus, early results may be used to modify the survey plan.

The advantages of MT over conventional electrical exploration are:

1. great depth of penetration, up to tens of kilometers,
2. high lateral resolution,
3. no signal source needed.

One disadvantage of MT is that relatively sophisticated apparatus is needed, including a computer.

The Michigan Tech system analyzes seven signals: two orthogonal local electric fields, three orthogonal local magnetic fields and two orthogonal remote magnetic fields. A block diagram is shown in Figure 2.1 and a signal flow chart is shown in Figure 2.2. The signals are digitized with 16 bit accuracy and processed by a Hewlett Packard 9845B computer, which computes auto and cross spectra of signal pairs. Spectral computations from several successive data segments and are used to calculate tensor impedance, apparent resistivities, tipper and other MT response characteristics. The accumulated results may be viewed and plotted as the data are being recorded. Real time analysis and display prevents acquisition of bad data because of mistakes in equipment setup or other possible problems. Figure 2.3 indicates field emplacement of the MT apparatus.

After the signal source is discussed in Section 2.2, the basic equations used in analysis of MT signals are presented and the significance of the results are briefly described in Section 2.3. The basic physical principles of MT are discussed in Keller and Frischknecht (1966), who present equations for

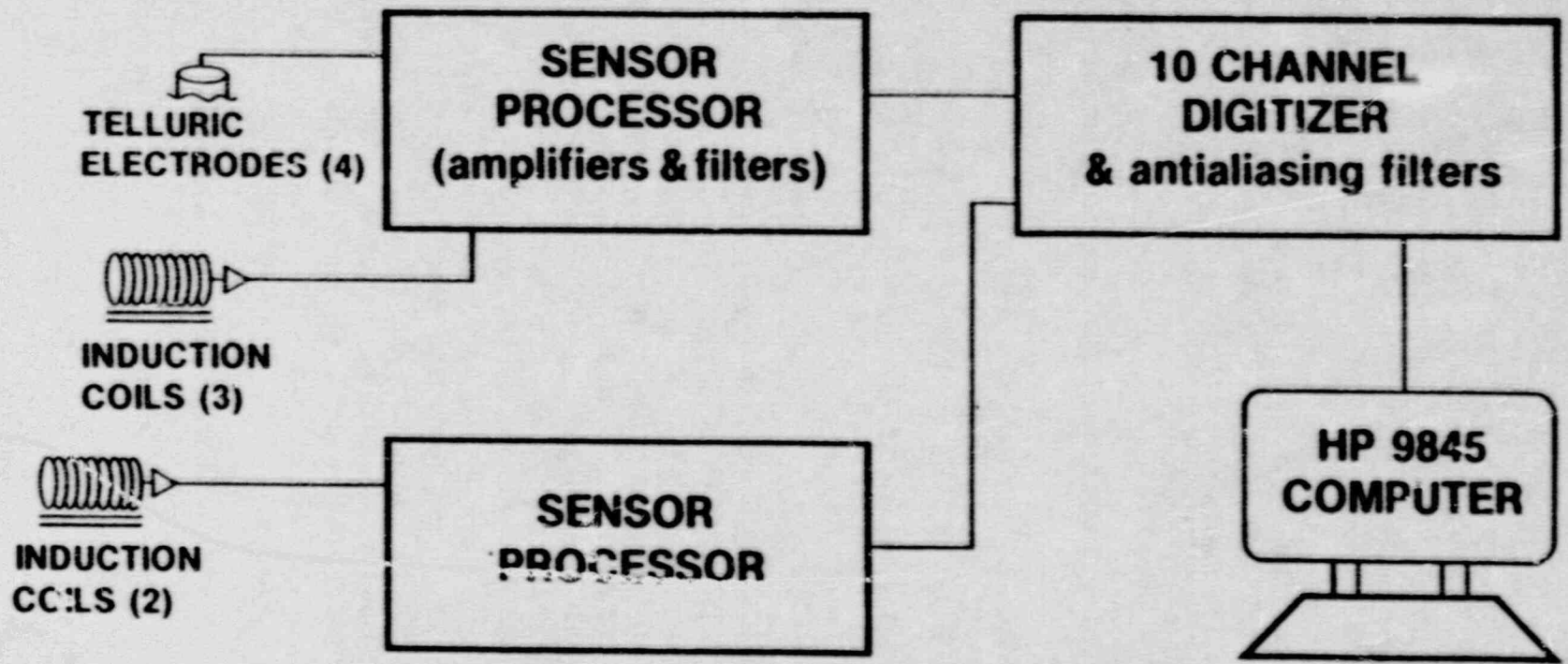
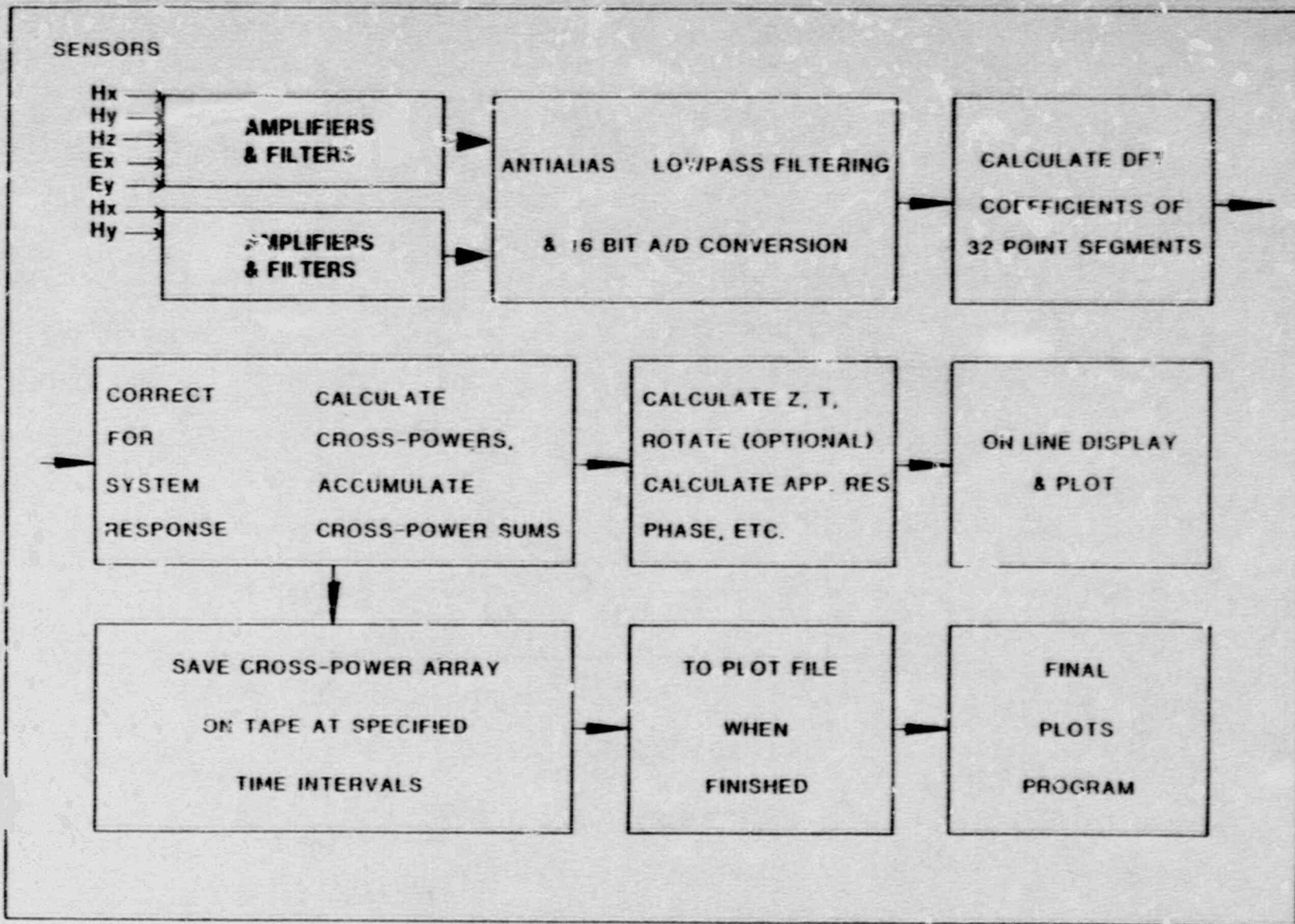


Figure 2.1 Block diagram of MT system.



B-1-5

Flowchart of MT Signals.

Figure 2.2 Flowchart of MT signal analysis.

B-1-6

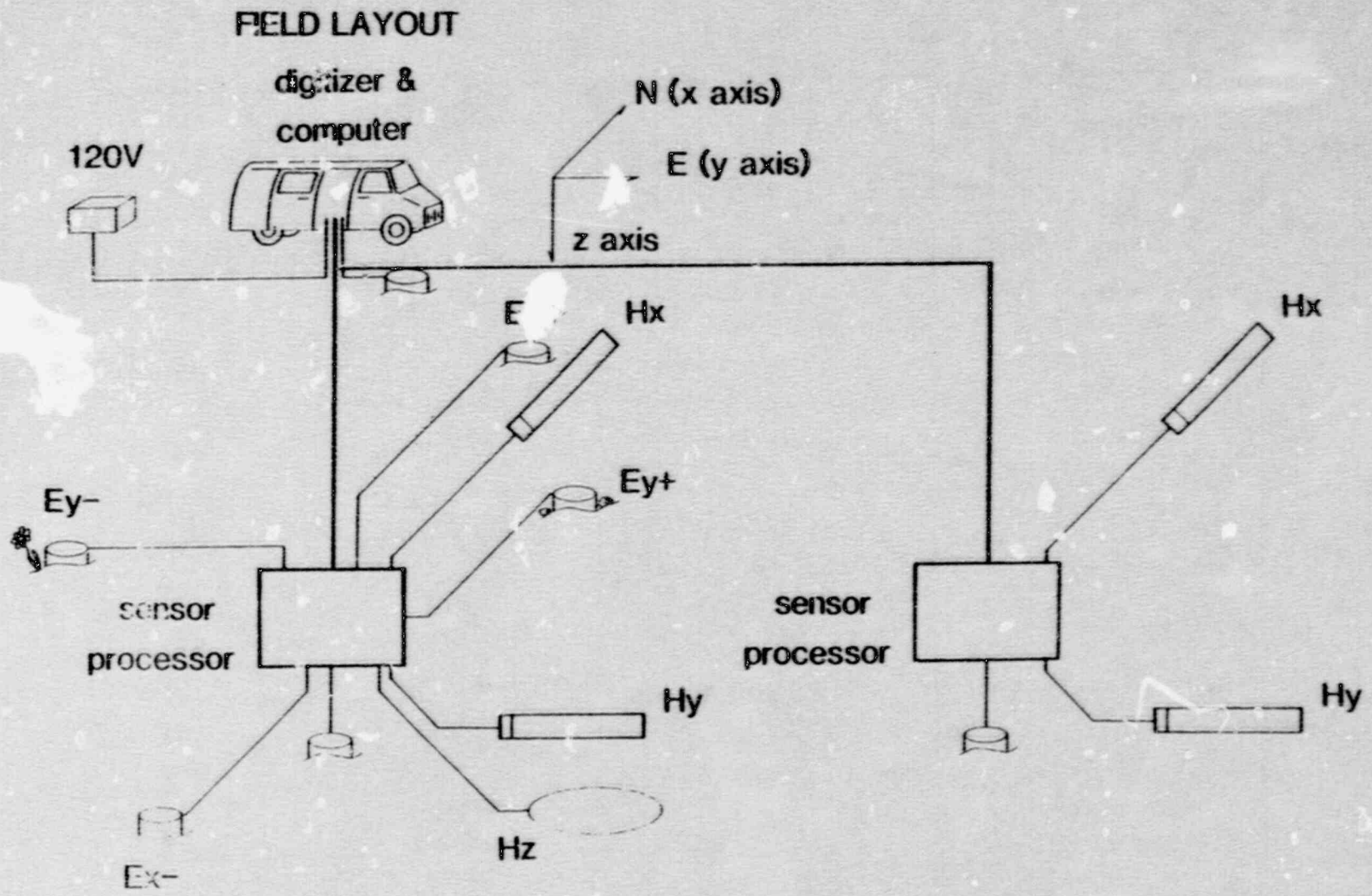


Figure 2.3 Field emplacement of MT apparatus.

the response of a flat layered earth. Interpretations of MT responses over more complicated structures are discussed by Vozoff, 1972 and Ting and Hohman, 1981. Also, Kauffman and Keller (1981) and Berdichevsky and Dmitriev (1976) discuss MT measurements for several different assumed models.

Section 2.4 discusses computation of the Fourier coefficients, the impedance tensor elements, and the process of cascade decimation.

2.2 Signal Source

MT signals below about 1 Hz are due to magnetic micropulsations, which are transient magnetic fields generated by motions of charged particles in the ionosphere. Above 1 Hz, the sources are spherics (atmospheric discharges), i.e., lightning strokes from distant thunderstorms.

The interpretation of magnetotelluric responses assumes vertically incident plane waves. This assumption is valid, since even near-horizontal incidence waves are refracted to vertical within the earth, due to the earth's high effective index of refraction. The electric and magnetic fields should be measured far enough away from the source so that the surface impedance is not dependent on the source distance or source geometry. In general, MT signal sources are distant enough to fulfill this criterion, the only exception being local thunderstorms. The electric and magnetic fields of the incident plane waves are used to determine the earth's surface impedance.

2.3 Definitions of Quantities Presented

A. Impedance Tensor, Apparent Resistivity and Phase Definitions

The surface scalar and tensor impedance and scalar and tensor apparent resistivity are defined below. Knowing these quantities over a wide frequency band, one can interpret the resistivity structure under the measurement site. Section 2.4 contains examples of two theoretical apparent resistivity profiles over two-dimensional structures. The discussion here is based on Word, Smith and Bostick, 1970; Sims, 1969; Vozoff, 1972; and Swift, 1971. The method of determining the impedance tensor from the measured data is discussed in Section 2.4.

The horizontal components of the electric and magnetic fields (E and H) are related by an impedance tensor, Z , with components Z_{XX} , Z_{XY} , Z_{YX} , Z_{YY} .

$$E_x = Z_{XX}H_x + Z_{XY}H_y \quad (2.1)$$

$$E_y = Z_{YX}H_x + Z_{YY}H_y$$

The positive X direction is commonly taken as north, the positive Y direction is east and the positive Z direction is downward.

The MKS units here are: E, volts/meter; H, amps/meter; Z, ohms. For an inhomogeneous earth, the components of Z are functions of frequency and orientation. Z can be thought of as a transfer function between two input channels, H_x and H_y , and two output channels, E_x and E_y . The manner of estimating the elements of Z is a reasonably well-known problem of random signal analysis. The specific method used by the Michigan Tech program is discussed in Section 2.4.

In the case of the homogeneous earth, Z is independent of orientation, Z_{XX} and Z_{YY} are 0, $Z_{XY} = -Z_{YX}$, and Z has the value

$$Z = E_x/H_y = (j\omega\mu\rho)^{1/2} \quad (2.2)$$

ρ = resistivity of homogeneous earth in ohm-meters

μ = permeability of the medium in Henrys/meter. The permeability of most rocks is equal to that of free space, $\mu_r = 4\pi \times 10^{-7}$ H/m.

ω = angular frequency = $2\pi f$, radians per second

$$j = (-1)^{1/2}$$

For a homogeneous earth, H is orthogonal to E and has a phase lag of 45° . The skin depth in the earth is expressed by

$$\delta = \left(\frac{2\rho}{\omega\mu}\right)^{1/2} \approx 500(\rho/f)^{1/2} \text{ meters} \quad (2.3)$$

and represents the depth at which the wave is attenuated to 1/e of its amplitude at the surface.

This homogeneous earth case is used to define apparent resistivity, ρ_a

$$\rho_a = \frac{1}{\omega\mu} \left| \frac{E_x}{H_y} \right| \quad \text{or} \quad \frac{1}{\omega\mu} |Z|^2 \quad (2.4)$$

Customary geophysical electric and magnetic field units are mv/km for electric field and gamma for magnetic field, where 1 gamma = 10^{-9} Tesla. With these units, the apparent

resistivity, Equation 2.4 becomes

$$\rho_a = \frac{1}{5f} |Z|^2 \quad (2.5)$$

where $Z = E_i/H_j$

$i, j = X, Y$ or Y, X

with $f =$ frequency in Hz

The apparent resistivity for a homogeneous earth or flat-layered earth is independent of the orientation of the measurement axis. The variation of apparent resistivity and the phase of E to H with frequency for a layered earth is discussed in Keller and Frischknecht (1966), pages 214 to 227.

Apparent resistivity, defined by Equation 2.4, is usually called the scalar apparent resistivity, with phase equal to the phase difference of E_x and H_y . The tensor apparent resistivity is similarly defined as

$$\rho_{a,ij} = \frac{1}{5f} |Z_{ij}|^2 \quad (2.6)$$

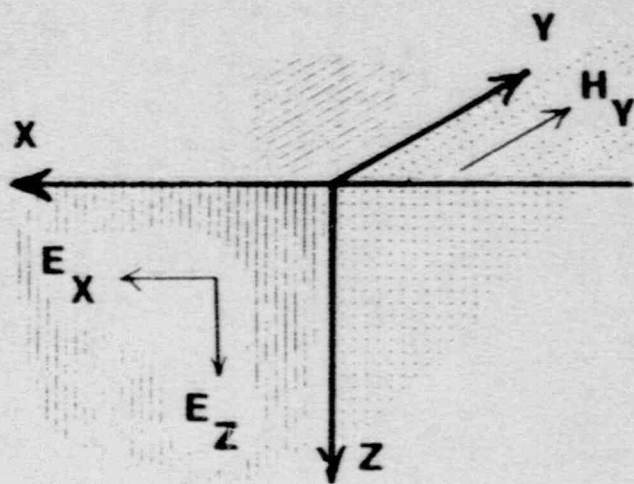
$i, j = X$ or Y

where the Z_{ij} are defined in Equation 2.1. The phase of the tensor resistivity is defined as the phase of the corresponding impedance element. These impedances are used to interpret the resistivity structure under the measurement site. The next section contains examples of two theoretical responses over two-dimensional structures: (1) a fault between two blocks of different resistivity; (2) a narrow vertical conductor with overburden.

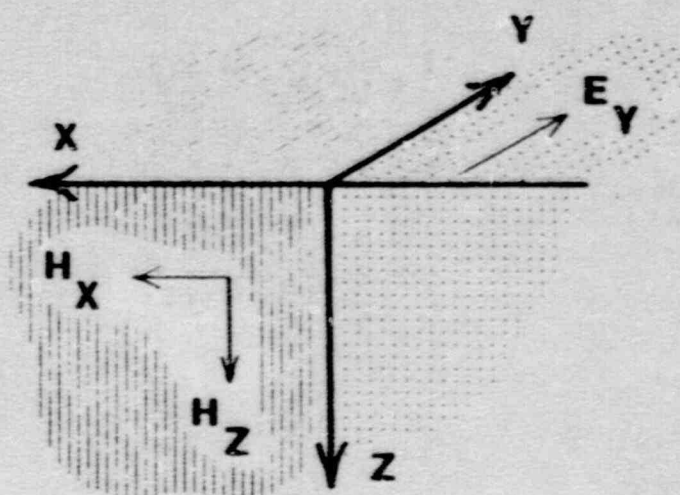
B. Polarization Modes Over a Two-Dimensional Earth

Structures such as faults, dikes or fold belts are frequently the subject of geophysical investigation. In many cases, such structures are approximately two-dimensional, meaning there is little or no variation along one horizontal axis, such as along the strike of a fault or along the axis of a fold belt. Using the tensor magnetotelluric method, it is possible to determine the orientation of such structures by rotating the coordinate system to find minimum and maximum apparent resistivities. If the axes of measurement are aligned with the structures, Z_{XY} and Z_{YX} are the impedance of the E-perpendicular and E-parallel modes of propagation, respectively, as in Figure 2.4. These modes are decoupled from each other. For a perfectly two-dimensional earth, components

STRIKE ALONG Y AXIS



E PERPENDICULAR



E PARALLEL

POLARIZATION MODES

Figure 2.4. H. T. polarization mode definitions

Z_{xx} and Z_{yy} are zero when the measuring axes are aligned with the structure. For geometry which is only approximately two-dimensional, Z_{xx} and Z_{yy} are considerably smaller than Z_{xy} and Z_{yx} . In the event that the measurement axes are not aligned with the structure, the impedances must be mathematically rotated using the formulas given later.

i. Apparent Resistivity Over a Fault

The case of a simple two-dimensional model of a fault or contact consisting of adjacent blocks of different resistivities is shown in Figure 2.5. The E-perpendicular apparent resistivity is discontinuous across the fault while the E-parallel value shows a smooth transition from the true resistivity on one side of the fault to the true resistivity of the other side (Swift, 1971).

ii. Apparent Resistivities Over a Narrow Conductor

Figure 2.6 gives sample theoretical E-perpendicular and E-parallel profiles over a buried narrow vertical conductor.

The narrow conductor might be a reasonable model for a lateral fault filled with circulating fluids. The E-perpendicular anomaly is narrow, approximately the width of the conductor. Other models and field examples show that it is very difficult to locate narrow structures with the E-perpendicular measurement, since the measurement station must be nearly centered on the conductor in order to detect it. Thus, if narrow conductors are near an MT site, E-perpendicular data may be more useful for constructing one-dimensional layered earth models, while E-parallel data may be more useful for locating structural changes.

iii. Rotation of Axes to Find Orientation of Structure

The estimates of Z must be rotated mathematically to find maximum and minimum values for Z_{xy} and Z_{yx} , respectively. For a two-dimensional structure, rotation presents the principal axes. The general rotation rule for the Z tensor is

$$Z'_{xy} = \left(\frac{Z_{xy} - Z_{yx}}{2}\right) \cos(2\phi) + \left(\frac{Z_{xy} + Z_{yx}}{2}\right) \sin(2\phi) - \left(\frac{Z_{xx} - Z_{yy}}{2}\right) \sin(2\phi) \tag{2.7}$$

$$Z'_{yx} = \left(\frac{Z_{xy} - Z_{yx}}{2}\right) \cos(2\phi) - \left(\frac{Z_{xy} + Z_{yx}}{2}\right) \sin(2\phi) + \left(\frac{Z_{xx} - Z_{yy}}{2}\right) \sin(2\phi)$$

where the primes refer to results in the rotated reference frame and ϕ is the angle of rotation. For the correct values

CONDUCTIVITY MODEL

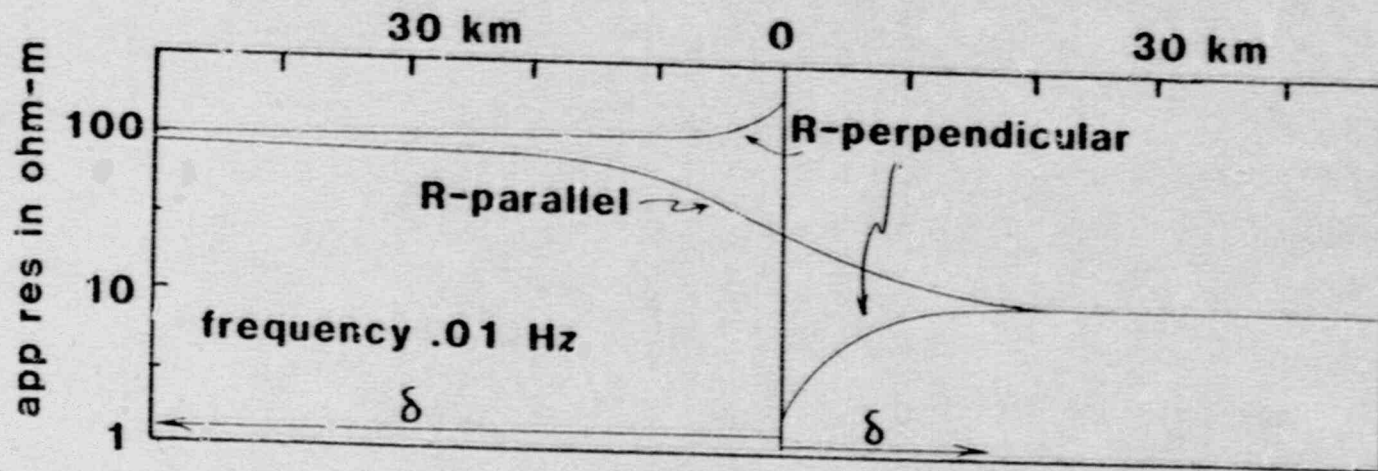
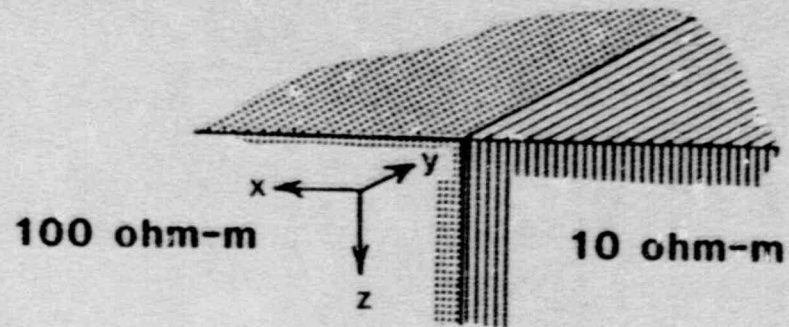


Figure 2.5. Apparent resistivities across a contact between blocks of different resistivities.

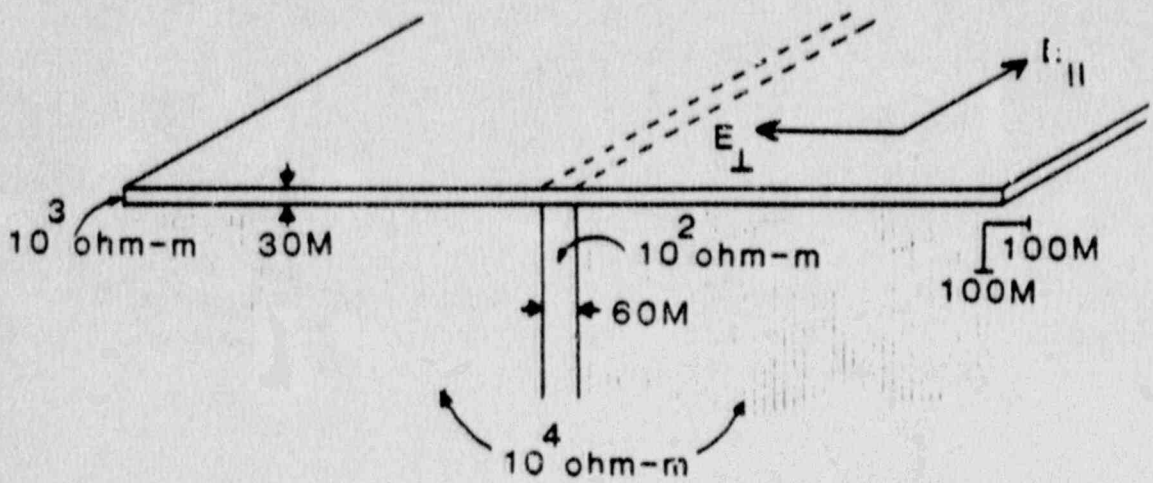
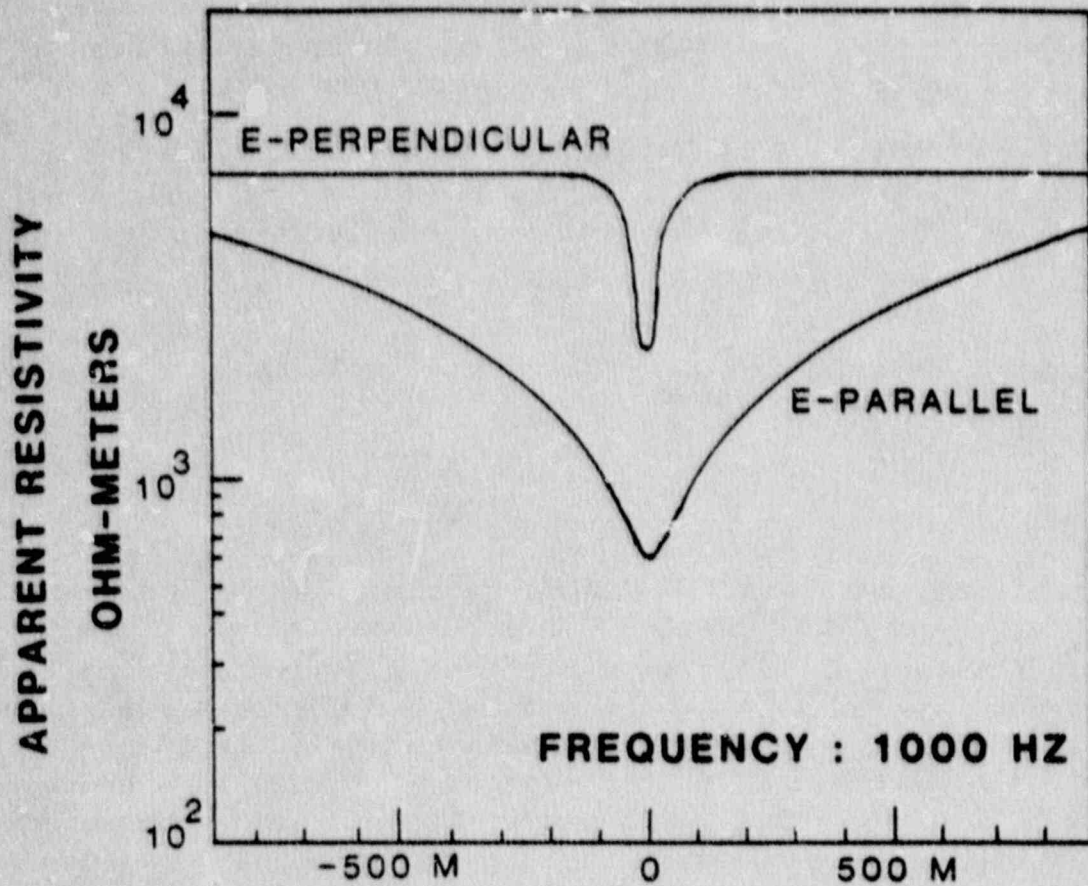


Figure 2.6. Apparent resistivities over a narrow conductor.

of ϕ , Z_{XY} is maximized and Z_{YX} is minimized, or vice versa. The impedances for E-parallel and E-perpendicular modes of propagation will be equal to Z_{XY} and Z_{YX} , or vice versa.

It is not necessary to rotate by increments and check Z_{XY} and Z_{YX} for extrema to find ϕ . The angle of the rotated axes may be found directly by the following relationship (Sims, 1969):

$$4\phi = \tan^{-1} \frac{2(ac+bd)}{(a^2+b^2) - (c^2+d^2)} \quad (2.8)$$

where

$$Z_{XX} + Z_{YY} = a + jb \quad Z_{XY} + Z_{YX} = c + jd$$

Evaluating ϕ in Equation 2.8 yields four angles 90 degrees apart. Comparing the resultant values of Z_{XY} for these rotations, one can identify two directions, 180 degrees apart, as the orientation of Z-max and the other two directions as the orientation of Z-min. However, there is no way to tell whether Z-max or Z-min corresponds to the geological strike at a site. Therefore, the vertical magnetic field is measured simultaneously with the horizontal magnetic field and is used to determine strike.

C. Skew and Ellipticity

These quantities, calculated from Z, are used to describe the degree to which the earth may be three-dimensional, that is, the degree to which there are conductivity variations along all three axes.

Skewness is defined as

$$S = |Z_{XX} + Z_{YY}| / |Z_{XY} - Z_{YX}| \quad (2.9)$$

For noise-free data over a two-dimensional earth, the skewness should be zero since Z_{XX} and Z_{YY} would either be zero or would cancel each other. Skewness is independent of rotation angle (Kaufmann and Keller, 1981). A large skewness signifies that structure at the site must be three dimensional in that frequency range (Vozoff, 1972).

Ellipticity is defined as

$$E = (Z_{XX}(\theta) - Z_{YY}(\theta)) / (Z_{XY}(\theta) - Z_{YX}(\theta)) \quad (2.10)$$

where the primes on the Z's and the dependence on θ signify that the impedance tensor is rotated to angle θ . For rotated noise-free data over a two-dimensional earth, ellipticity should be zero, thus ellipticity is also an indicator of three dimensionality.

D. Vertical Magnetic Field and Tipper

For cases of resistivity structure consisting of anything other than plane layers, the vertical component of the magnetic field will be non-zero. A linear relationship is assumed between the three components of magnetic field:

$$H_z = T_x H_x + T_y H_y \quad (2.11)$$

The constants T_x and T_y are a measure of the departure of the earth from a flat-layered configuration, that is, if they are non-zero, the earth must be represented by a two or three dimensional model near that measurement site. The quantity $(T_x^2 + T_y^2)^{1/2}$ is the tipper magnitude; it represents the ratio of vertical magnetic field total horizontal magnetic field.

If the earth is two-dimensional at a measurement site, there will be no change of fields along the strike of the structure; that is, if the strike direction is along the Y axis, then

$$\frac{\partial E_x}{\partial Y} = \frac{\partial E_y}{\partial Y} = \frac{\partial H_x}{\partial Y} = \frac{\partial H_y}{\partial Y} = \frac{\partial H_z}{\partial Y} = 0 \quad (2.12)$$

For the TE or E-parallel mode, the vertical component of magnetic field will be highly correlated to the associated horizontal component of magnetic field which is perpendicular to the strike of the structure. They are components of the same vector. The vertical component of magnetic field will be uncorrelated with the magnetic field parallel to the structure. The latter is associated with the E-perpendicular mode.

Thus, if MT measurements are made over a two-dimensional structure of unknown strike, it is possible to determine the strike by mathematically rotating the tipper to maximize one component, say T_x and minimize T_y .

E. Interpretation of Tipper Data Based on a Simple Fault Model

The linear relation assumed to exist between H_x , H_y and H_z implies that there is a unique direction of tipper. In the simple fault model discussed below, the tipper points to more

resistive material.

Consider a model consisting of blocks of different resistivity ρ_1 and ρ_2 , shown in Figure 2.7. Let us assume that the telluric current flowing in the model, induced by magnetic micropulsations, is of such low frequency that direct current principles may be applied.

A uniform current density of infinite width would give rise to a magnetic field which is only horizontal. The vertical component of magnetic field over the contact in the model is an edge effect. Its direction can be determined by applying the right hand rule to currents flowing along the edge of the conductor. Suppose this magnetic field is measured and the coordinate system is rotated so that the positive X direction is aligned with the horizontal component of the magnetic field (to the right in the diagram). This direction is normally considered as the direction of tipper. The tipper points to the high resistivity region. For the extremely low frequency case we are considering, tipper phase would be zero, that is, H_z and rotated H_x are in phase. Three-dimensional model calculations by Ting and Hohman, 1981, also show that the tipper points toward resistive material.

Tipper skew and ellipticity may be defined similar to the impedance definition (Jupp and Vozoff, 1976). Tipper skew is

$$\frac{2 |\operatorname{Im}(T_x * T_y)|}{|T_x|^2 + |T_y|^2} \quad (2.13)$$

The imaginary part is used because it is zero for zero phase difference between horizontal and vertical H components.

Tipper ellipticity is

$$\frac{|T'_x(\theta)|}{|T'_y(\theta)|} \quad (2.14)$$

by direct analogy from impedance. The primes again indicate the rotated tipper. For a two-dimensional earth, the ellipticity is also zero for rotated data.

F. Effect of Conductive Seawater and Sediments

The presence of large conductive area is known to affect geomagnetic and magnetotelluric measurements. Electrical currents induced in the ocean by magnetic micropulsations generate a secondary magnetic field which has a vertical component and a component perpendicular to the shoreline.

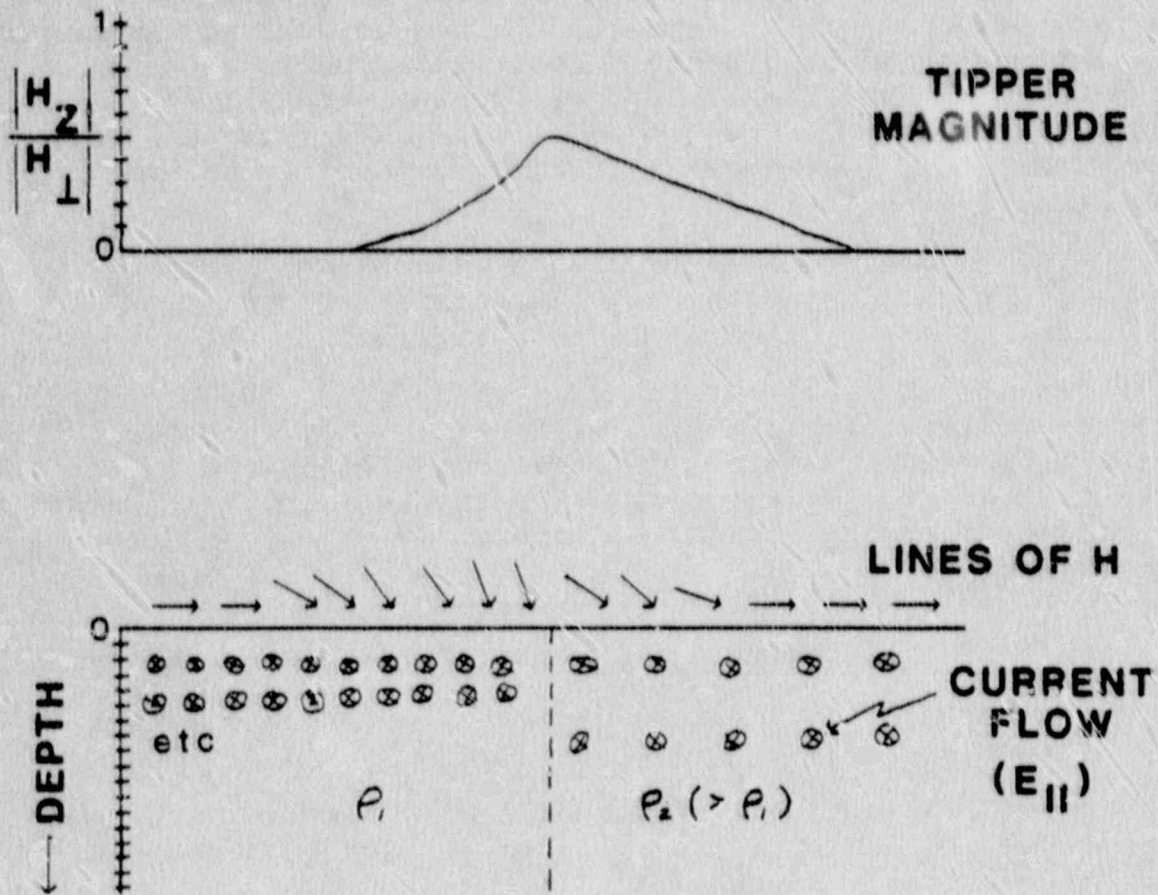


Figure 2.7. Magnetic field over a contact between blocks of different resistivities.

These anomalous fields affect the magnetotelluric tipper and the component of apparent resistivity associated with the magnetic field perpendicular to the coast (ρ - parallel). Boundary conditions at the coast also affect the component of electric field perpendicular to the coast (ρ - perpendicular). Thus, the coast effect perturbs all magnetotelluric quantities.

There are many examples of coast effect computations in the geophysical literature, but most of them emphasize magnetic field effects of interest to those conducting geomagnetic variational studies. Recent computations by P. Wannamaker, at the University of Utah (personal communication, 1984) show that for a realistic geologic model, the coast effect causes a perturbation of at least several percent at least one hundred kilometers from the coast.

Field measurements in Oregon (Neuman and Hernance, 1985) have shown that conductive continental shelf sediments must be included in their model of the coast effect.

In South Carolina, we expect at higher frequencies that magnetotelluric measurements will detect only the locally one-dimension structure of conductive coastal sediments. At lower frequencies the MT response will contain a combination of the northwest trending coastal sediments, seawater, and continental shelf effects.

2.4 Signal Analysis and Remote Reference Processing

A. The Use of Auto and Cross Spectra to Estimate Tensor Elements

This section discusses the estimation of the MT impedance tensor elements. The estimation of tipper elements is mathematically identical.

The components of the impedance tensor, Z , may be estimated from n independent data sets; that is, n successive time series. There is more than one possible way to calculate each component of Z . Four solutions are mathematically correct for Z , two for Z^E and two for Z^H , which minimize noise on the electric and magnetic channels, respectively. These estimates are averaged and the coordinate system is rotated to find maximum and minimum impedances. The results are expressed as rotated tensor apparent resistivities and phases. The following description of the statistical techniques follows Sims, 1969, and the mathematical argument applies to the problem of finding the transfer function of a system with two inputs and one output.

Suppose that there are n consecutive measurements of E_x , H_x , and H_y at a given frequency and one wishes to estimate the elements Z_{xx} and Z_{xy} . The estimates are found by minimizing the sum of the squares of the differences between the observed E_x and the E_x predicted from the values of H_x and H_y ; that is, to minimize the quantity

$$\psi = \sum_{i=1}^n (E_{x_i} - Z_{xx}H_{x_i} - Z_{xy}H_{y_i})(E_{x_i}^* - Z_{xx}^*H_{x_i}^* - Z_{xy}^*H_{y_i}^*) \quad (2.15)$$

where * indicates complex conjugate.

The Z_{xx} which minimizes this quantity is found by setting to zero the derivatives of ψ with respect to the real and imaginary parts of Z_{xx} , then adding the two resulting equations together and dividing by two. This manipulation yields

$$\sum_{i=1}^n H_{x_i}^* E_{x_i} = Z_{xx} \sum_{i=1}^n H_{x_i} H_{x_i}^* + Z_{xy} \sum_{i=1}^n H_{y_i} H_{x_i}^* \quad (2.16)$$

Similarly, setting to zero the derivatives of ψ with respect to the real and imaginary part of Z_{xy} yields

$$\sum_{i=1}^n E_{x_i} H_{y_i}^* = Z_{xx} \sum_{i=1}^n H_{x_i} H_{y_i}^* + Z_{xy} \sum_{i=1}^n H_{y_i} H_{y_i}^* \quad (2.17)$$

Two more equations relating Z_{xx} and Z_{xy} to cross and auto products of field quantities are also given by Sims, 1969

$$\sum_{i=1}^n E_{x_i} E_{x_i}^* = Z_{xx} \sum_{i=1}^n H_{x_i} E_{x_i}^* + Z_{xy} \sum_{i=1}^n H_{y_i} E_{x_i}^* \quad (2.18)$$

$$\sum_{i=1}^n E_{y_i} E_{y_i}^* = Z_{xx} \sum_{i=1}^n H_{x_i} E_{y_i}^* + Z_{xy} \sum_{i=1}^n H_{y_i} E_{y_i}^* \quad (2.19)$$

These auto and cross products such as $\sum_{i=1}^n H_{y_i} E_{y_i}^*$ and $\sum_{i=1}^n H_{x_i} E_{y_i}^*$ are auto and cross power density spectra. The summation over data segments will be abbreviated with the expectation or averaging notation, thus,

$$\sum (H_{y_i} E_{y_i}^*) \equiv \langle H_y E_y^* \rangle \quad (2.20)$$

There are various methods for determining these quantities from a digitized time series. Our analysis program calculates selected discrete Fourier transform coefficients, then computes the above products and sums over many time segments. The Fourier coefficients can be computed for 40 frequencies spaced equally on a logarithmic axis over six decades of frequency. The cross and auto spectra sums at the 40 frequencies are stored in the computer memory and on tape and are updated as new data are acquired. These "crosspower" files are permanently available on tape for updated calculations of impedances, apparent resistivities, phases, tipper, etc., and can be used as a source to reprocess the data in the event that one wants to compare, say, rotated to unrotated data.

B. Magnetic Field and Electric Field Reference Processing

The four equations for Z_{XX} and Z_{XY} above give six possible solutions for each unknown. Sims, 1969, shows that two of the six solutions are unstable on physical grounds, and of the four remaining, two are biased down by noise on the magnetic channel and two are biased up by noise on the electric channel. For example, one form of estimate for Z_{XY} that biases Z_{XY} up due to noise on E_x is

$$Z_{XY}^E = \frac{\langle H_x E_x' \rangle \langle E_y E_y' \rangle - \langle H_x E_y' \rangle \langle E_x E_x' \rangle}{\langle H_x E_x' \rangle \langle H_y E_y' \rangle - \langle H_x E_y' \rangle \langle H_y E_x' \rangle} \quad (2.21)$$

The bias is due to the last term in the numerator, which is the autopower of E_x . One form of Z_{XY} which is biased down by noise in H is

$$Z_{XY}^H = \frac{\langle H_x H_y' \rangle \langle H_x H_x' \rangle - \langle E_x H_y' \rangle \langle H_x H_y' \rangle}{\langle H_x H_x' \rangle \langle H_y H_y' \rangle - \langle H_x H_y' \rangle \langle H_x H_y' \rangle} \quad (2.22)$$

The downward bias is due to the autopower of H_y which appears in the denominator. The second term in each of the brackets of 2.21 and 2.22 is termed the reference field. If Equation 2.21 is used, the impedance is said to be computed with electric field reference. If Equation 2.22 is used, the processing is said to be magnetic field reference processing.

Our programs allow a choice of electric or magnetic field reference and two choices of magnetic field reference are

possible, local or remote. Magnetic field reference is usually used because orthogonal magnetic fields are frequently statistically more independent of one another than the electric fields. The impedances obtained by electric and magnetic field processing can be compared to estimate the noise or bias in the data. Thus, by comparing the impedances computed with different reference fields, one can identify noisy data.

C. Principle of Noise Bias Reduction Using Remote Reference Data

It was seen in the previous section that in one-station MT, noise in a channel causes the estimate to be biased up or down depending on which algebraic solution is used. Remote reference systems use the remote signals in the tensor estimates. Because noise in the remote reference channel is presumed to be uncorrelated with noise in the local channels, the bias in the tensor element estimates should be significantly reduced.

The effect of noise can be demonstrated mathematically. Let the Fourier coefficients included in an auto spectral average be $A_1 \dots A_n$, and let each coefficient be contaminated with noise: $A_i = A_{is} + A_{in}$ where the subscripts s and n refer to signal and noise. Assume that the noise has zero mean, i.e. $\frac{1}{n} \sum_{i=1}^n A_i \equiv \bar{A} = 0$ then, substituting the expression for A_i into $\langle AA^* \rangle$ gives

$$\langle A_{is}A_{is}^* + 2A_{is}A_{in} + A_{in}A_{in}^* \rangle \quad (2.23)$$

In the average, both $A_{is}A_{is}^*$ and $A_{in}A_{in}^*$ will always be positive, and $A_{is}A_{in}$ will be small, since we also assume that A_{in} and A_{is} are uncorrelated. Thus, $\langle AA^* \rangle$ is biased upward by noise and a tensor estimate will be biased up if the auto spectral term appears in the numerator and down if the auto spectral term appears in the denominator.

In remote reference MT, auto spectral terms are replaced with cross spectra of parallel signals, that is AA^* is replaced with $\langle A_1A_2^* \rangle$ where 1 and 2 denote the local and remote stations, respectively. This term can also be expanded as signal plus noise:

$$\langle (A_{1s} + A_{1n})(A_{2s}^* + A_{2n}^*) \rangle = \langle (A_{1s}A_{2s}^* + A_{1s}A_{2n}^* + A_{1n}A_{2s}^* + A_{1n}A_{2n}^*) \rangle \quad (2.24)$$

The base and remote noise are assumed to be uncorrelated

while the base and remote signal are assumed to be identical. thus, all terms but the first become very small, leaving a good estimate of $\langle AA^* \rangle$. The equations for tensor element estimation for remote reference MT are identical to those for single station MT except that the complex conjugate terms are from the remote reference station.

Gamble, 1979, summarizes the equations used to calculate MT impedance with remote reference magnetic fields.

$$\begin{aligned}
 Z_{XX} &= (\langle E_X H_{XR}^* \rangle \langle H_Y H_{YR}^* \rangle - \langle E_X H_{YR}^* \rangle \langle H_Y H_{XR}^* \rangle) / D \\
 Z_{XY} &= (\langle E_X H_{YR}^* \rangle \langle H_X H_{XR}^* \rangle - \langle E_X H_{XR}^* \rangle \langle H_X H_{YR}^* \rangle) / D \\
 Z_{YX} &= (\langle E_Y H_{XR}^* \rangle \langle H_Y H_{YR}^* \rangle - \langle E_Y H_{YR}^* \rangle \langle H_Y H_{XR}^* \rangle) / D \\
 Z_{YY} &= (\langle E_Y H_{YR}^* \rangle \langle H_X H_{XR}^* \rangle - \langle E_Y H_{XR}^* \rangle \langle H_X H_{YR}^* \rangle) / D \\
 D &\equiv \langle H_X H_{XR}^* \rangle \langle H_Y H_{YR}^* \rangle - \langle H_X H_{YR}^* \rangle \langle H_Y H_{XR}^* \rangle
 \end{aligned}
 \tag{2.25}$$

Gamble points out that choosing either remote magnetic field or electric field for the reference field gives mathematically correct results for Z estimates. The remote reference signal appears in both the numerator and the denominator of the Z estimates. Thus one "does not need a precise knowledge of the gains or phase shifts in ... the remote references." Geologic considerations suggest the use of the magnetic channel: magnetic signals are less effected by local changes earth resistivity, thus remote magnetic fields are likely to contain less correlated noise than the remote electric fields. Gamble's paper given examples showing dramatic improvement in data quality which is possible using remote reference magnetic channels. The MTU remote reference system used remote magnetic fields as the reference field.

Figure 2.8 shows a data set containing impedances computed using two different reference fields, local H and remote H. There is good agreement between the two curves which indicates that the remote reference was of limited importance at this site. One other computation, local E, has been made for this

RUN: CHSTON-CHSa/CHsb/
 DATE: DEC 04 1985

Final Crosspowers - MT Reference is 4 = Rem H Reference

F#	Stacks	Wtaug	F#	Stacks	Wtaug	F#	Stacks	Wtaug	F#	Stacks	Wtaug
1	24	.37	11	24	.37	21	288	.23	31	18	.57
2	24	.36	12	24	.29	22	288	.22	32	18	.58
3	36	.33	13	36	.31	23	144	.24	33	9	.69
4	36	.41	14	36	.35	24	144	.24	34	9	.76
5	24	.38	15	24	.47	25	72	.28	35	3	.81
6	24	.57	16	24	.38	26	72	.29	36	3	.49
7	24	.26	17	24	.23	27	18	.69	37	0	0.00
8	24	.31	18	24	.26	28	18	.58	38	0	0.00
9	24	.28	19	532	.28	29	18	.72	39	0	0.00
10	24	.30	20	532	.26	30	18	.58	40	0	0.00

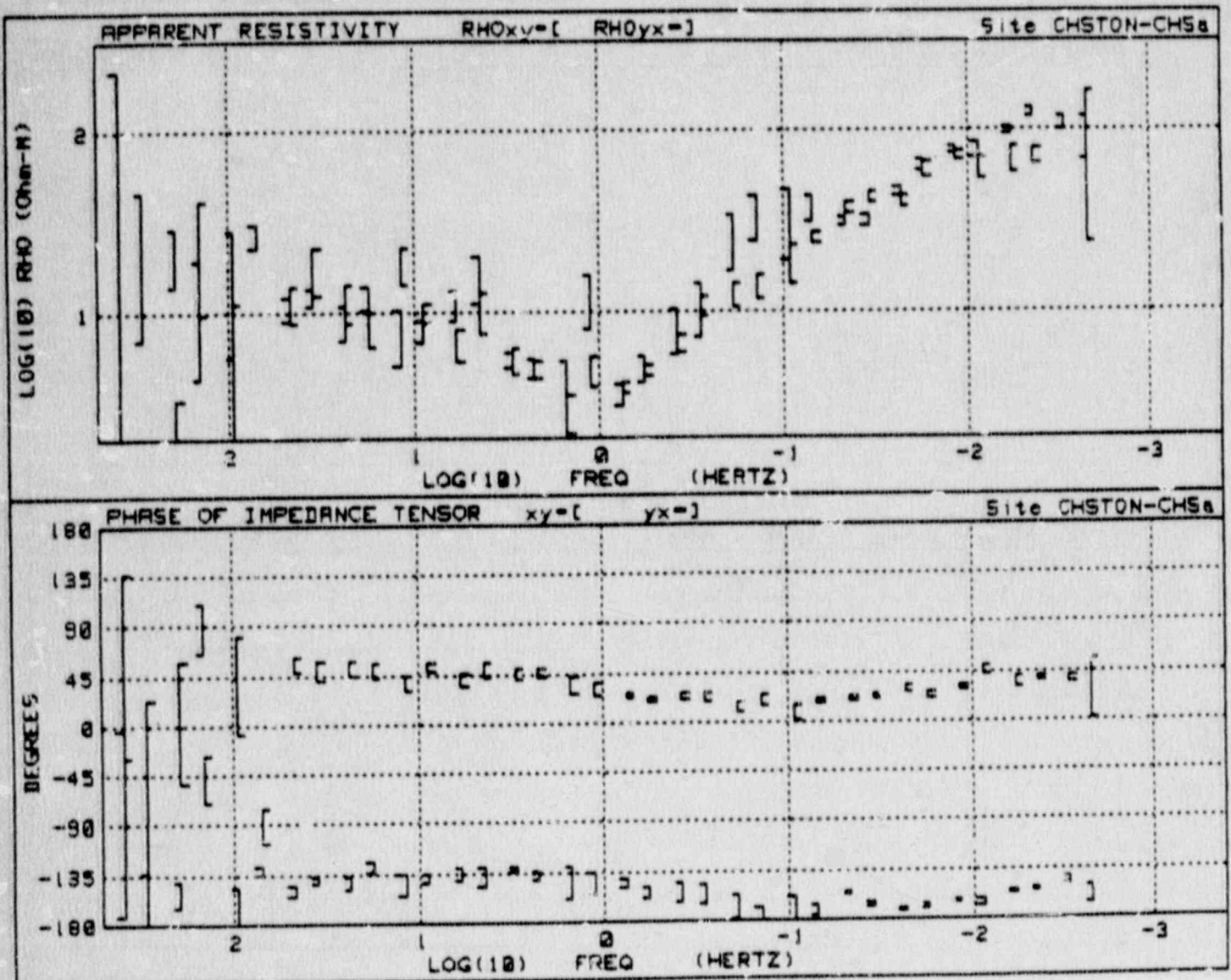


Figure 2.8 Example of remote H reference field processing.

RUN: CHSTON-CHSa/CHSb/
 DATE: DEC 04 1985

Final Crosspowers - MT Reference is 3 = Loc H Reference

F0	Stacks	Wtaug	F0	Stacks	Wtaug	F0	Stacks	Wtaug	F0	Stacks	Wtaug
1	24	.37	11	24	.37	21	200	.23	31	10	.57
2	24	.36	12	24	.29	22	200	.22	32	10	.50
3	36	.33	13	36	.31	23	144	.24	33	9	.69
4	36	.41	14	36	.35	24	144	.24	34	9	.76
5	24	.30	15	24	.47	25	72	.20	35	3	.81
6	24	.57	16	24	.30	26	72	.29	36	3	.49
7	24	.26	17	24	.23	27	18	.59	37	0	0.00
8	24	.31	18	24	.26	28	18	.50	38	0	0.00
9	24	.28	19	532	.20	29	18	.72	39	0	0.00
10	24	.38	20	532	.26	30	18	.50	40	0	0.00

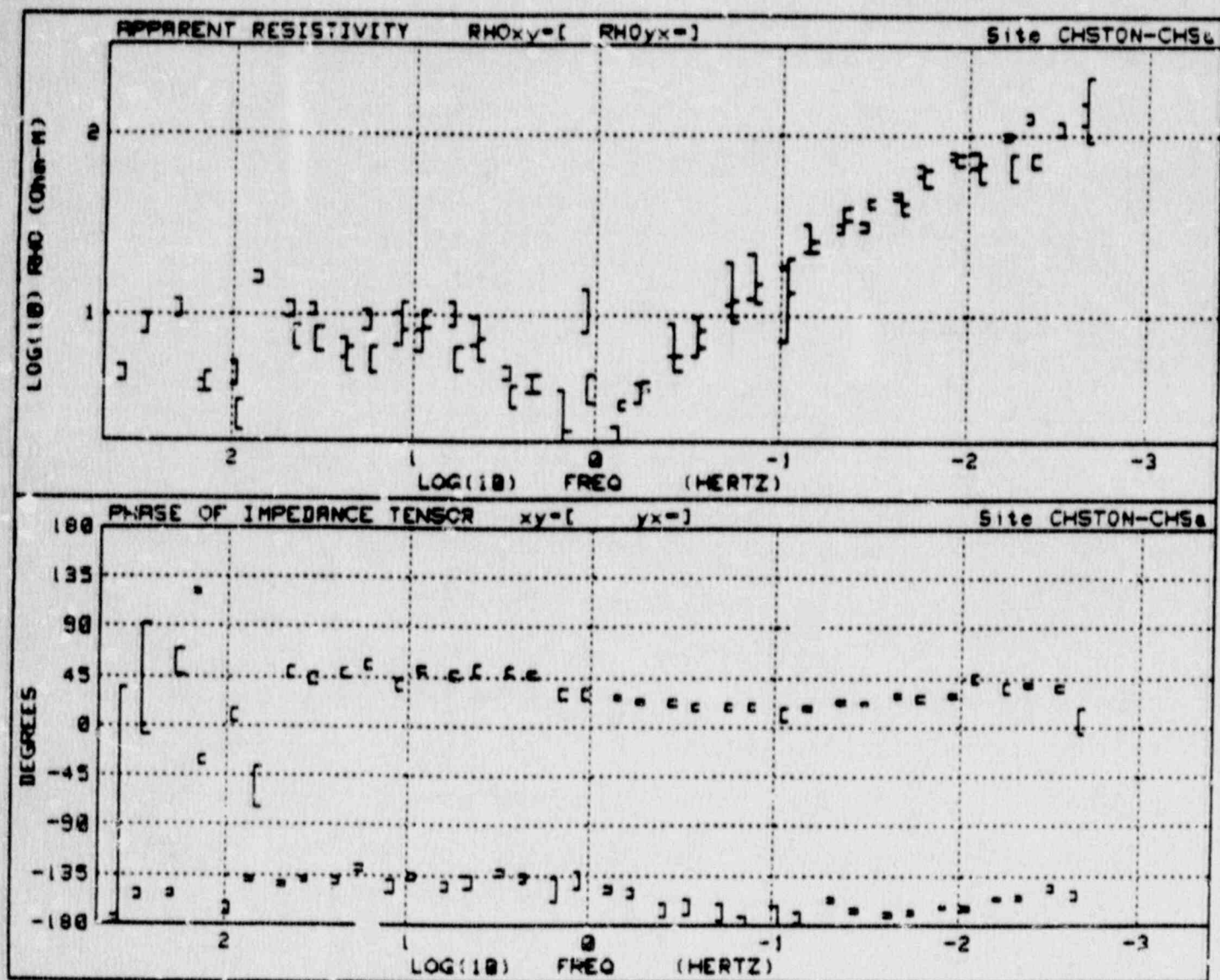


Figure 2.9 Example of local H reference field processing.

site and those results agree closely with the two curves shown although there was more scatter in the computed impedances as might be expected.

D. Calculation of Standard Deviations

The assumptions involved in error analysis of MT data are discussed by Gamble, Goubau and Clark, 1979. They assume that each data segment analysed is statistically independent of other segments and that the noise on each channel is statistically stationary. They show that the variance of a given impedance element Z_{ij} , is given by

$$z \text{ var } (Z_{ij}) = \frac{\langle |\eta|^2 \rangle \langle |A_j|^2 \rangle}{N |D|^2} \quad (2.26)$$

where

η_i = the differences between the measured and predicted values of E for the coordinate I (X or Y). (A different variance could be defined for the differences between H measured and H predicted.

$$A^*_j = A_x \text{ or } A_y \text{ where} \quad 2.27$$

$$A'_x = H_x \langle H_y H'_y \rangle - H_y \langle H_y H'_x \rangle$$

$$A'_y = H_y \langle H_x H'_x \rangle - H_x \langle H_x H'_y \rangle$$

N = Number of independent observations, i.e. the number of data segments

$$|D|^2 = \langle H_x H'_x \rangle \langle H_y H'_y \rangle - \langle H_x H'_y \rangle \langle H_y H'_x \rangle \quad (2.28)$$

The variance of the tipper coefficients is defined in a mathematically similar manner.

The variance of apparent resistivity, phase, etc. are determined from the impedance variances by application of the standard equations for propagation of errors. Sample expressions are given in Gamble et al., 1979.

E. Calculation of Fourier Coefficients

The MTU MT analysis program has a high frequency routine for signals above 1 Hz and a low frequency routine for signals

below 1 Hz. For the high range, signals are low-pass filtered by anti-aliasing circuits in the digitizer, then sixth and eighth harmonic discrete Fourier transform coefficients are calculated for each 32 point time segment, as described below. For the low range, it is desirable to calculate coefficients more or less simultaneously for as many frequencies as possible, so the procedure of cascade decimation which is described later is used.

A time series, $f(T)$, is transformed into complex Fourier frequency coefficients $F(W)$ using the discrete Fourier transform (DFT):

$$F(W) = \sum_{T=0}^{N-1} f(T) e^{-2\pi i W T / N} \quad (2.29)$$

N = number of time series data (numerical time)

T = index of time series data; that is, $f(T) = f(1) \dots f(T) \dots f(N)$

W = index of component (numerical frequency)

$i = (-1)^{1/2}$

Neither the actual times of the digitized data nor the actual frequencies of the Fourier components appear in the computation. They are related to each other by:

Δt = sampling interval (sec)

$N \Delta t$ = total time of signal

$\frac{W}{N \Delta t}$ = frequency of coefficient W

W is allowed to have any value. $F(W=0)$ is the average value. Values of W greater than $N/2$ are repetitions of lower frequencies, and are not needed. Since our analysis programs use only the sixth and eighth harmonics ($W=6$ and 8), it is quite efficient to calculate them directly from the above formula (the more complicated fast Fourier transform routine is not used).

The Fourier coefficients for the 22 output frequencies of the 11 low bands in the low range are calculated as follows:

1. The signals are digitized in contiguous segments 32 points long.
2. Sixth and eighth harmonic DFT coefficients are calculated for one segment.

3. The data are digitally low-pass filtered with a five-point convolution filter and decimated by two (every second point is skipped).
4. 32 data from the next time segment are processed as above. After they have been decimated they are concatenated (added end to end) with the first set of decimated data.
5. This string is analyzed as in setp 2 above.
6. The process proceeds as above with successive cascade decimation and DFT analysis.

The above procedure was designed specifically for MT signal analysis on a small computer by Wight, Bostick and Smith (1977). The advantages of the procedure are:

1. The fractional bandwidth of the sixth and eighth harmonic calculations are appropriate for MT. No averaging over adjacent bands is needed as in other methods which use longer strings of data.
2. Calculation of only even harmonics makes it unnecessary to remove linear trends in the segments.
3. Very little information is lost. After the next stage of decimation, the new sixth and eighth harmonics calculated are the fourth and third harmonics of the original data set.
4. Real-time computation is possible.

CHAPTER 3. INSTRUMENTATION

3.1 System Specifications

The geophysical apparatus used for conducting our magnetotelluric resistivity measurements was manufactured by Phoenix Geophysics. The integrated system includes all apparatus from the electric and magnetic field sensors to the digital computer recording station. Also, calibration and troubleshooting equipment is included. A compact description is given below and detailed calibration information is presented in Chapter 4.

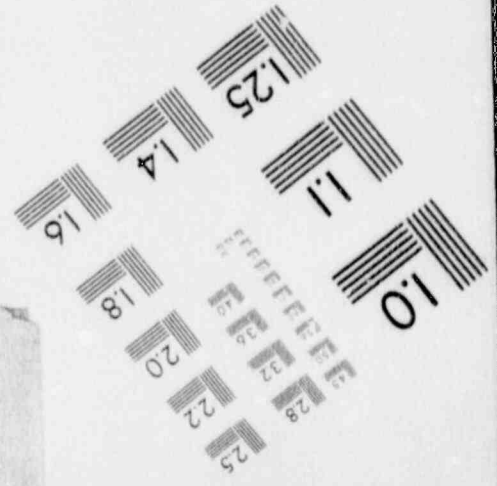
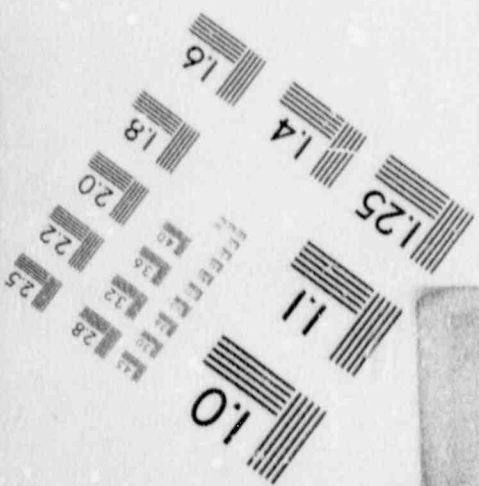
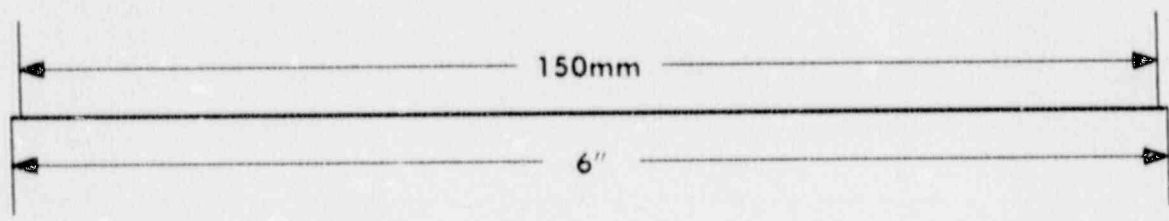
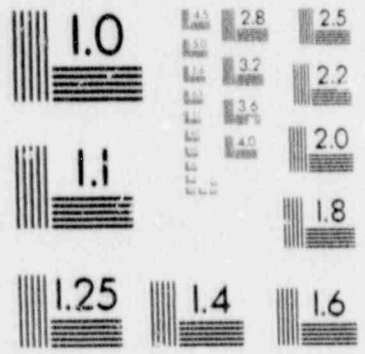
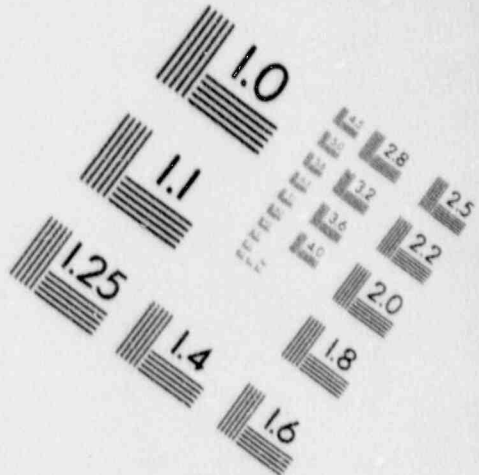
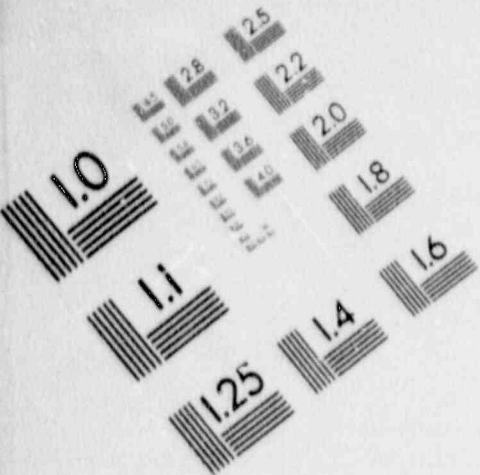
Figure 2.2 showed a detailed signal flow diagram of the magnetotelluric signals and Figure 2.3 indicated field emplacement of the sensors. The north-south and east-west magnetic signals are received via two 1.8 m long mu-metal core coils. The vertical magnetic field is detected by a 200 turn, 10 meter diameter air-core loop. An extremely low noise chopper preamplifier, mounted at the end of each coil, is used to amplify the magnetic signals. The telluric signals are received by non-polarizing electrodes separated by a distance which is typically 100 m. Remote reference signals are provided by a second pair of coils and a second sensor processor.

Amplification and filtering of the input signals is provided by a sensor processor at each location. The input circuits are diodeprotected, and have a gain switch to allow 20 dB extra gain for low signal levels. To combat the effects of high power line interference, cascaded 50 and 180 Hz notch filters are included in each telluric and magnetic amplifier board. Using this scheme, the notches each exhibit an attenuation of at least 40 dB with a Q of 2. The signals are presented to the communications cable by isolated push-pull drivers to prevent unwanted pickup and possible ground loops. The communication cable outputs are then fed through a shielded RF filter to the digitizer.

At the recording station, located at least 100 m away from the sensor array, the signals are passed through anti-aliasing filters. Three two-pole active filters are used, and by programmable parameter adjustment, a six-pole low pass butterworth filter is formed with an appropriate cutoff above the passband. After multiplexing, 16 bit A/D conversion is provided over a ± 10 volt range, and the digital signals are fed into a Hewlett-Packard 9845B computer. The digitizer is controlled by the computer through the input/output (I/O) interface. The digitizer can also be controlled manually for testing with switches on the front panel. All equipment in the recording station is powered from a portable 800 watt gasoline powered generator.

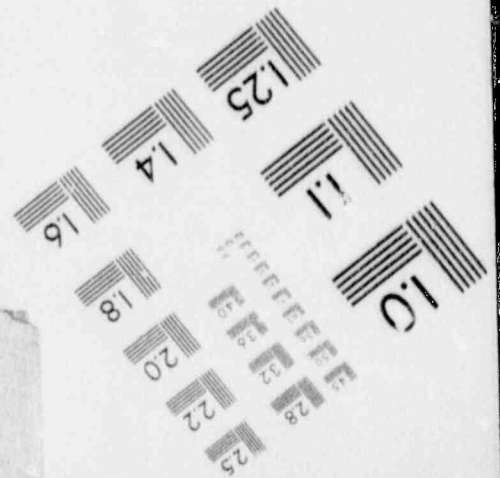
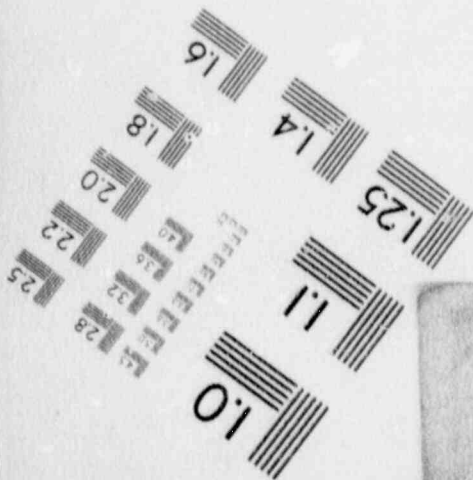
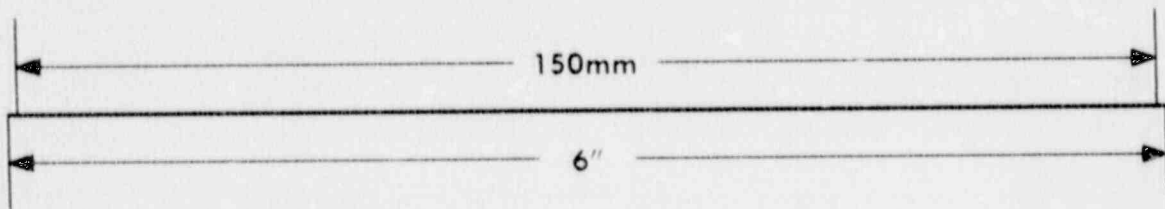
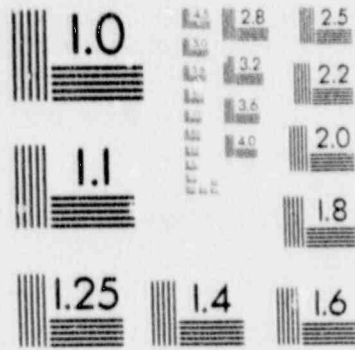
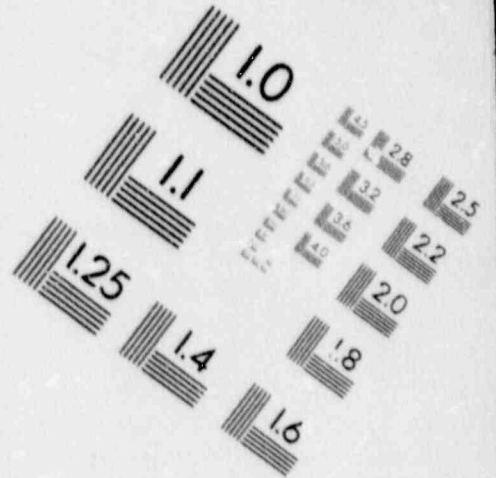
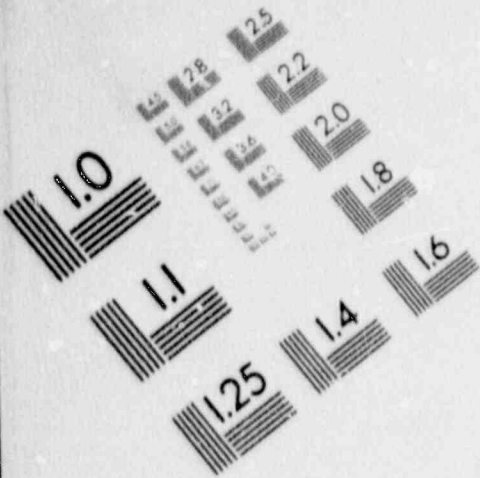
1

IMAGE EVALUATION TEST TARGET (MT-3)



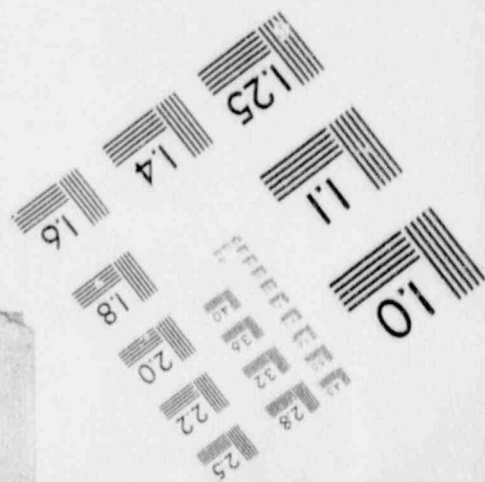
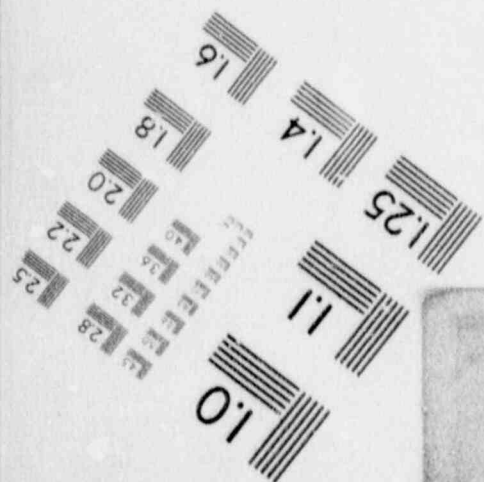
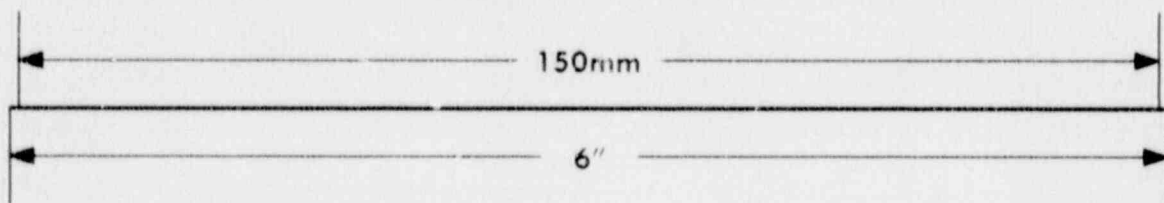
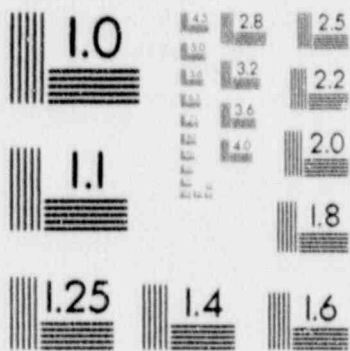
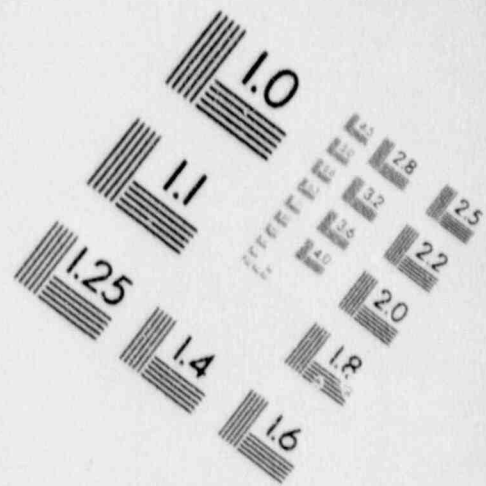
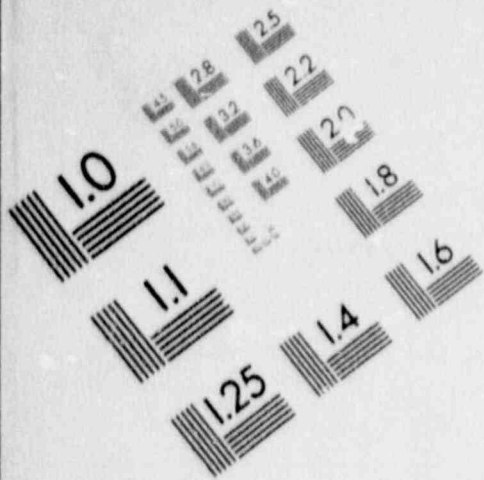
1

IMAGE EVALUATION TEST TARGET (MT-3)



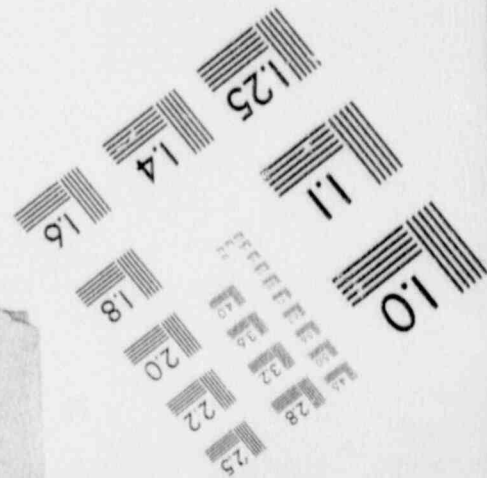
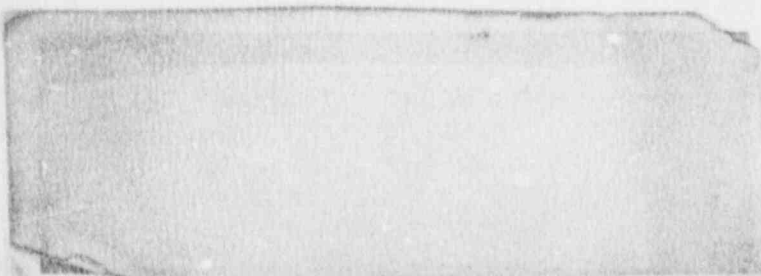
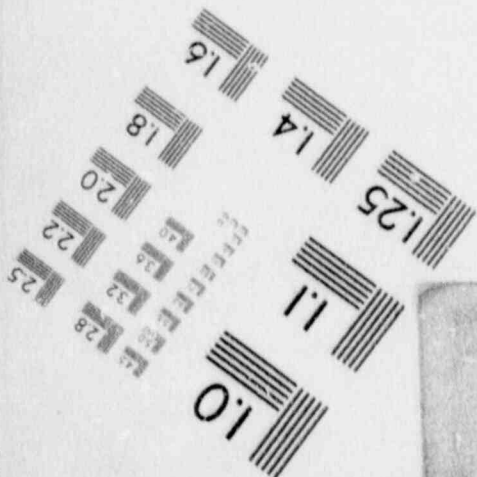
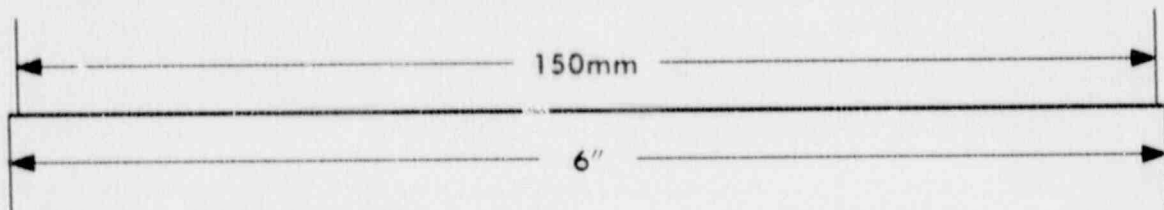
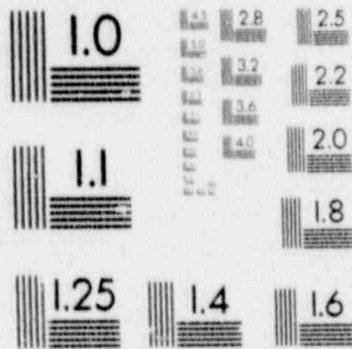
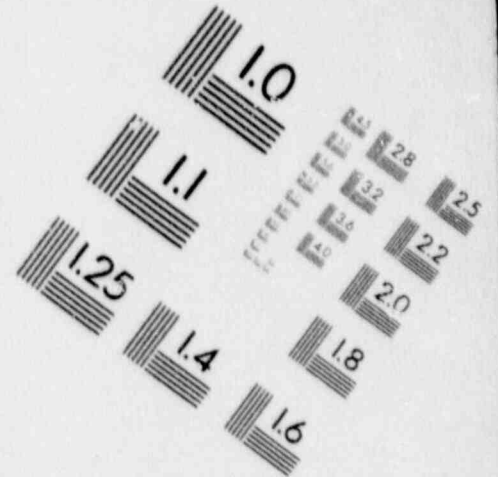
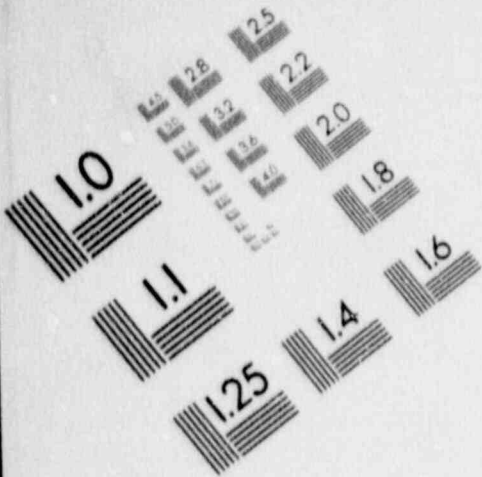
1

IMAGE EVALUATION TEST TARGET (MT-3)



1

IMAGE EVALUATION TEST TARGET (MT-3)



3.2 Procedures and Precautions

A. Site Selection, Installation and Operation

In choosing a site, we wish to have as little cultural noise present as possible, such as power line interference, mining operations, logging, etc. AC digital voltmeter measurements taken from the telluric inputs at each station gave a good indication of the amount of power line interference present. Often anything over 10 mV results in large standard deviations for resistivities by the amplitude of natural signals on any particular day also influences the data quality.

The dc electrode resistance and dc voltage for each station's orientation are also measured at each site. DC resistance readings above 100K ohms can result from poor earth-sensor contact. This is often the case in dry, sandy soil (a situation not too common in the present survey). Also, the contact resistance can be reduced by using a conductive paste in the bottom of each hole. The paste is a saturated solution of potassium chloride in water mixed with microscopic spheres of silica known as Cab-O-Sil. The paste contacts as much of the bottom of the electrode hole as possible, yet the silica granules retain moisture necessary to increase the contact area. Typically electrode resistances on the order of several thousand ohms were encountered in the Charleston area.

After assessing the multimeter measurements, the site is surveyed to place the sensors in the north-south and east-west directions. The vertical magnetic sensor is spread out in a circle.

The recording truck is located some distance away from the electrodes. Typically, one person makes final checks at the site to ensure a proper equipment configuration and verify system operation by monitoring panel meters on the sensor processor. After this check the operation of the main operating program is begun. The operating program is highly interactive: the operator can control or override many of the analysis program functions. The program can simulate an analog stripchart recorder, displaying the signals on the built-in printer. In this mode, the operator can diagnose abnormal signals, or decide to proceed with normal data acquisition. Once the program is analysing data, several data plots can be displayed on the CRT or can be printed. Since the CRT plots are updated continuously as new data are obtained, the results can be viewed immediately. Sites exhibiting high signal levels and low interference are usually completed quickly, whereas noisy sites require more time to gather enough records to improve data quality. In some instances of excessive noise or very weak natural signals the improvement in data quality is limited.

At the noisier sites, an experienced operator can improve the quality of the data by adjusting the acceptance threshold

for data and turning off data acquisition ofr frequency bands where sufficient high quality data have been obtained. By adjusting the threshold, data can be acquired on bands where signals are particularly noisy or weak.

In addition to the above operating procedures, there are other considerations. For example, if the electric field lines vibrate, the earth's magnetic field will generate false electric field signals. Thus, the site installation crew generally anchors the electric field lines with clumps of sod every few feet to reduce movement.

Finally, it is of utmost importance to keep all equipment in good working order. Regular maintenance, such as cleaning the ever-accumulating amount of dust and dirt on the field equipment, changing moisture dessicants, recharging batteries, and maintaining good connections wherever a mechanical electric contact is made, is essential. This assures better data quality, and longer equipment lifetime.

CHAPTER 4. CALIBRATION AND VERIFICATION OF PROPER SYSTEM OPERATION

This chapter presents the procedure for calibrating the magnetotelluric equipment and compares data obtained by our system with those obtained by other MT systems. The equipment is usually calibrated before each field project.

4.1 Calibration Procedure Overview

Before the system can be utilized for recording, it is calibrated using an external reference. The coils are driven by internal calibration windings, while the telluric inputs are driven directly. All calibration signals are generated by an HP 3325 function generator under control of the computer calibration software. After a sufficient number of records have been taken, the calibration data are then transferred to the main operating program. Usually, this is done at a site where MT data will be taken immediately afterwards.

The MT system manufacturer, Phoenix Geophysics, has provided a system calibration program, MTC-A4. The program provides an excellent graphical display of the system transfer function at 40 measurement frequencies.

The program can be operated in several modes. The program segments have the following functions:

1. Operate a programmable signal generator and calculate system transfer functions for
 - a. amplifiers alone.
 - b. amplifiers plus magnetic sensors.
2. Use the results of 1 to calculate transfer functions of each magnetic sensor in units of mv out per gamma in. These results are written to sensor files.
3. Use the results of 1a to create a system amplifier gain file.
4. Plot results and print tables of 2 and 3 above.

Examples of the transfer function plots are shown later.

The program can repeat measurements at each frequency, under operator control, until the standard deviations of the calibration constants obtained meet the operators satisfaction. It is usually possible to obtain standard deviations under one percent.

After the above measurements are complete, the program divides the results of the calibrations with and without magnetic sensors to determine sensor sensitivities. Table 4.1

NT Cal WITHOUT Sensors (x1) Freq 1 (298) Hz							Stacks= 25	
Cal Job: GAINS ON 10,10 By CTY & RLW							Date: JUL 25 1985	
CHAN	REAL		%SD	IMAG		%SD	AMPLITUDE	PHASE
1	-184.927	+	.08%	-101.394	+	.03%	210.689	-151.26
2	-198.210	++	.09%	-91.832	++	.02%	219.450	-155.14
3	-190.507	+++	.09%	-104.498	+++	.05%	217.285	-151.25
4	-5139.997	++++	.75%	-26546.482	++++	1.45%	27137.697	-100.92
5	-3467.725	++++	.20%	-24939.602	++++	.33%	24585.389	-98.11

NT Cal WITHOUT Sensors (x1) Freq 2 (216) Hz							Stacks= 25	
Cal Job: GAINS ON 10,10 By CTY & RLW							Date: JUL 25 1985	
CHAN	REAL		%SD	IMAG		%SD	AMPLITUDE	PHASE
1	-183.703	+	.01%	-26.708	+	.02%	185.635	-171.73
2	-194.220	++	.03%	-21.112	++	.05%	195.364	-173.80
3	-188.062	+++	.02%	-31.595	+++	.04%	190.697	-170.46
4	+1647.229	++++	4.38%	-26547.260	++++	2.60%	26598.315	-85.45
5	+4282.361	++++	.85%	-23482.811	++++	.50%	23869.303	-79.26

NT Cal WITHOUT Sensors (x1) Freq 2 (216) Hz							Stacks= 25	
Cal Job: GAINS ON 10,10 By CTY & RLW							Date: JUL 25 1985	
CHAN	REAL		%SD	IMAG		%SD	AMPLITUDE	PHASE
1	-183.657	+	.01%	-26.657	+	.08%	185.581	-171.74
2	-194.165	++	.01%	-21.029	++	.07%	195.300	-173.82
3	-188.021	+++	.01%	-31.542	+++	.07%	190.648	-170.48
4	+1219.273	++++	5.14%	-24535.642	++++	1.00%	24565.918	-87.16
5	+4161.722	++++	.91%	-23152.740	++++	.20%	23523.803	-79.81

NT Cal WITHOUT Sensors (x1) Freq 3 (144) Hz							Stacks= 25	
Cal Job: GAINS ON 10,10 By CTY & RLW							Date: JUL 25 1985	
CHAN	REAL		%SD	IMAG		%SD	AMPLITUDE	PHASE
1	+15.602	+	.07%	+48.724	+	.06%	51.162	+72.24
2	+21.373	++	.05%	+48.675	++	.09%	53.160	+66.29
3	+15.559	+++	.05%	+48.053	+++	.03%	50.510	+72.06
4	-6496.151	++++	.85%	-1778.509	++++	.39%	6735.212	-164.69
5	-6882.268	++++	1.1%	-2227.814	++++	.07%	7233.863	-162.06

NT Cal WITHOUT Sensors (x1) Freq 4 (108) Hz							Stacks= 25	
Cal Job: GAINS ON 10,10 By CTY & RLW							Date: JUL 25 1985	
CHAN	REAL		%SD	IMAG		%SD	AMPLITUDE	PHASE
1	-273.684	+	.03%	-26.180	+	.05%	274.933	-174.54
2	-286.481	++	.04%	-19.868	++	.05%	286.816	-177.23
3	-275.282	+++	.03%	-27.155	+++	.05%	276.618	-174.37
4	+31932.082	++++	.11%	-18430.138	++++	.44%	36869.064	-29.39
5	+29093.384	++++	.05%	-16778.530	++++	.12%	33584.879	-29.97

Table 4.1 (a). Sample printed output of calibration program.

MT Cal WITHOUT Sensors (x1) Freq 5 (72) Hz							Stacks= 25	
Cal Job: GAINS ON 10,10 By CTY & RLW							Date: JUL 25 1985	
CHAN	REAL		%SD	IMAG		%SD	AMPLITUDE	PHASE
1	-299.985	+	.03%	+7.054	+	.04%	289.471	+178.60
2	-297.287	+	.03%	+33.703	+	.04%	299.191	+173.53
3	-293.609	+	.03%	+10.970	+	.04%	294.014	+177.66
4	+34567.967	+	.66%	-6526.740	+	1.30%	35178.587	-10.69
5	+32426.469	+	.12%	-7180.392	+	.39%	33211.955	-12.49

MT Cal WITHOUT Sensors (x1) Freq 6 (84) Hz							Stacks= 25	
Cal Job: GAINS ON 10,10 By CTY & RLW							Date: JUL 25 1985	
CHAN	REAL		%SD	IMAG		%SD	AMPLITUDE	PHASE
1	+16.993	+	.13%	-120.943	+	.07%	122.131	-82.00
2	+10.487	+	.14%	-125.215	+	.05%	125.653	-85.21
3	+17.018	+	.10%	-122.042	+	.06%	123.222	-82.06
4	-4595.232	+	9.76%	+6710.263	+	6.23%	8132.883	+124.48
5	-4210.020	+	3.46%	+4553.298	+	.75%	6201.360	+132.76

MT Cal WITHOUT Sensors (x1) Freq 7 (96) Hz							Stacks= 25	
Cal Job: GAINS ON 10,10 By CTY & RLW							Date: JUL 25 1985	
CHAN	REAL		%SD	IMAG		%SD	AMPLITUDE	PHASE
1	-162.860	+	.03%	+232.134	+	.08%	283.566	+125.05
2	-157.343	+	.03%	+251.174	+	.07%	296.387	+122.06
3	-165.219	+	.02%	+234.756	+	.07%	287.067	+125.14
4	-3727.181	+	.10%	-37567.667	+	.10%	37752.106	-95.67
5	-96.503	+	.03%	-36808.256	+	.08%	36808.383	-98.15

MT Cal WITHOUT Sensors (x1) Freq 8 (108) Hz							Stacks= 25	
Cal Job: GAINS ON 10,10 By CTY & RLW							Date: JUL 25 1985	
CHAN	REAL		%SD	IMAG		%SD	AMPLITUDE	PHASE
1	-319.257	+	.03%	-103.214	+	.04%	335.526	-162.08
2	-335.389	+	.03%	-99.220	+	.05%	350.717	-163.57
3	-328.259	+	.02%	-105.531	+	.05%	337.198	-161.76
4	+46433.882	+	.23%	-5276.602	+	.02%	46732.728	-6.48
5	+43320.021	+	.04%	-2276.763	+	.05%	43379.810	-3.01

MT Cal WITHOUT Sensors (x1) Freq 9 (126) Hz							Stacks= 25	
Cal Job: GAINS ON 10,10 By CTY & RLW							Date: JUL 25 1985	
CHAN	REAL		%SD	IMAG		%SD	AMPLITUDE	PHASE
1	-329.156	+	.02%	+124.761	+	.08%	352.007	+159.24
2	-333.064	+	.03%	+155.434	+	.07%	357.548	+154.98
3	-331.620	+	.02%	+133.297	+	.07%	357.408	+158.10
4	+43735.702	+	.51%	-27713.291	+	.54%	49268.894	-34.23
5	+37843.613	+	.05%	-25751.588	+	.10%	45778.398	-34.23

Table 4.1 (b). Sample printed output of calibration program.

is a sample of the printed output of this program.

The program then combines the results of the previous operations into a calibration data file that can be read by the main MT analysis program. The channel transfer functions are extrapolated to the lowest frequencies and tables and plots are made of system transfer functions. Figure 4.1 is a sample of the plot output from this program.

All of the magnetic channel gains determined by the above procedure are within a few percent of one another, as are the electric channel gains. This good agreement indicates the precision with which the separate amplifiers are constructed. Figure 4.2 shows the normal operating configuration for the E channels and Figure 4.3 indicates calibration of the E channels. Similar figures apply to the magnetic channels.

Calibration data obtained in the above procedure are on file at MTU and can be supplied on request. Further details and the use of the calibration factors can also be supplied.

4.2 Performance Compared to Three Other MT Systems

Besides absolute calibration performed on our MT systems, it is useful to compare the results with those obtained from other tensor MT systems. Our equipment was compared with others in testing done in August of 1984. As part of a National Science Foundation sponsored study, four MT systems were operated and compared at six sites in various types of terrains. The participating institutions were: Michigan Technological University, University of Utah, University of Oregon and Centro de Investigacion Cientifica y Educacion Superior de Ensenada (CICESE, Baja California, Mexico). Each group occupied each site for a twelve to twenty-four hour period. The results at one of the sites are shown in Figure 4.4. We consider the agreement to be excellent.

It is worth mentioning that all four MT systems were engineered separately and differ significantly in hardware and software details such as electrode lengths, type of magnetic field sensors, and signal processing algorithms, etc. It is also worth mentioning that the MTU system operates at higher frequencies and is more portable than any of the other MT systems.



PHOENIX GEOPHYSICS MT SYSTEM CAL FILE

SYSTEM CALIBRATION FILE

Date Made: AUG 04 1985

H-Chan Hi Pass: .0031 Hz

E-Chan Hi Pass: .035 Hz

NC Cal: SCT 7/24/85 By JCR RLW

NC- File: NC- 1

Cal Program: MTC-R4

Revision: AUG 18 1983

Digitizer: D204

Digitizer Channel	Sensor Box	Sensor
Channel 1 (Hx1)	SE217	none
Channel 2 (Hy1)	SE217	none
Channel 3 (Hz1)	SE217	none
Channel 4 (Ex1)	SE217	none
Channel 5 (Ey1)	SE217	none

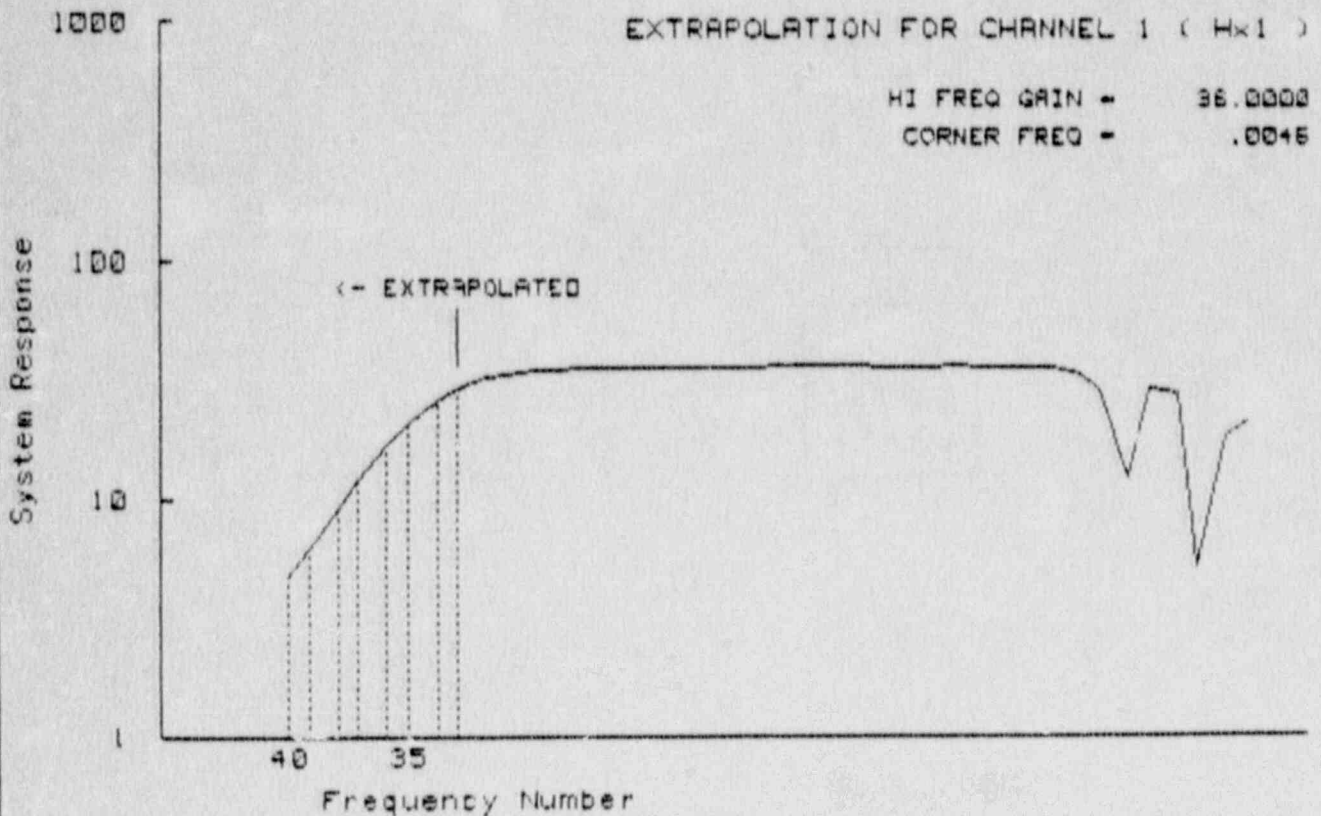
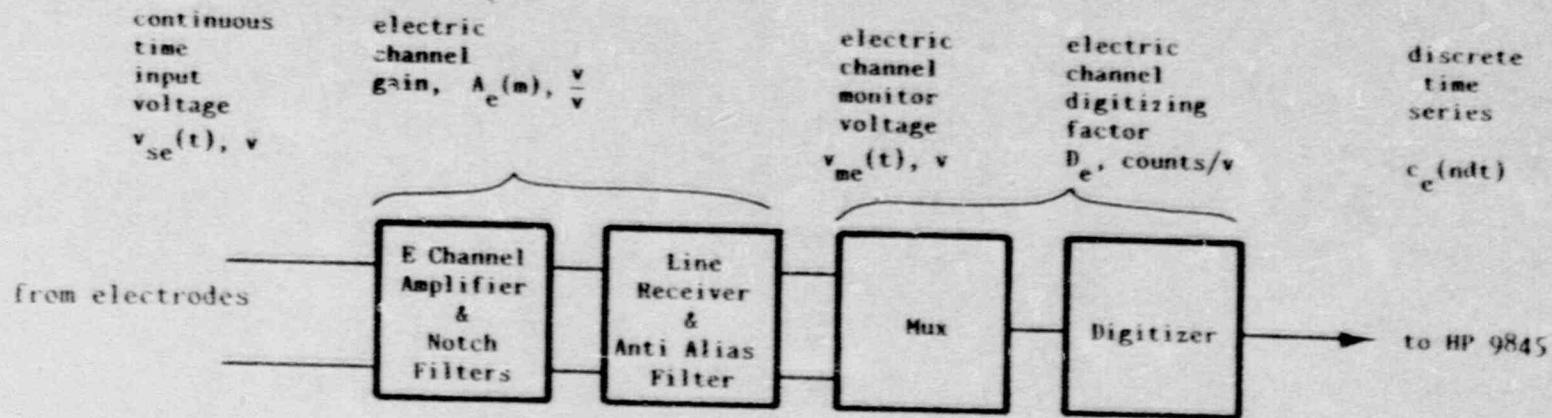


Figure 4.1. Sample transfer function plot for channel 1, H_x



Time Domain:

$$v_{se}(t) * z_e(t) = v_{me}(t)$$

$$v_{me}(t) \delta(ndt) D_e = c_e(ndt)$$

Frequency Domain:

$$V_{se}(m) A_e(m) = V_{me}(m)$$

$$V_{me}(m) D_e = C_e(m)$$

Total System Equation:

$$V_{se}(m) A_e(m) D_e = C_e(m)$$

NOTES: * indicates convolution

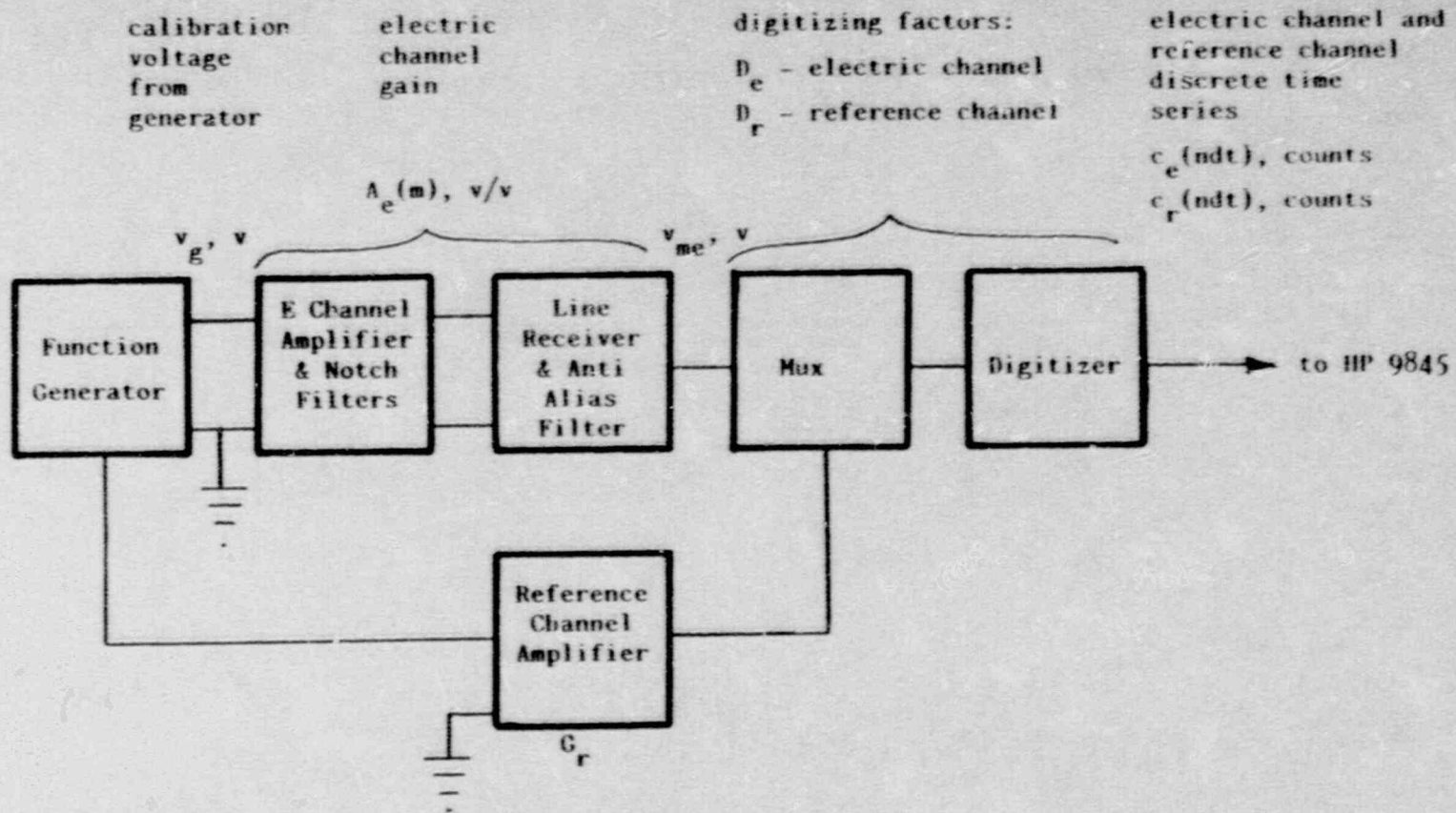
$A_e(t)$ is the impulse response of the electric field channel and $a_e(t) = \text{DFT}^{-1} A_e(m)$.

The discrete Fourier transform (DFT) quantities, $V_{se}(m)$ etc. are understood to represent

$V_{se}(m \omega_0)$ where ω_0 is the fundamental frequency of the transformation.

dt is the time between samples and n is the sample number.

Figure 4.2. Normal operating configuration for E channels.



Time Domain:

$$v_g(t) \approx a_e(t) = v_{me}(t)$$

$$v_{me}(t) \delta(ndt) D_e = c_e(ndt)$$

$$v_g(t) G_r = v_{mr}(t)$$

$$v_{mr}(t) \delta(ndt) D_r = c_r(ndt)$$

Frequency Domain:

$$V_g(m) A_e(m) = V_{me}(m)$$

$$V_{me}(m) D_e = C_e(m)$$

$$V_g(m) G_r = V_{mr}(m)$$

$$V_{mr}(m) D_r = C_r(m)$$

Solution for Gain Factor:

$$V_g(m) A_e(m) D_e = C_e(m)$$

$$\frac{C_e(m)}{C_r(m)} = \frac{A_e(m)}{G_r}, D_e = D_r$$

$$V_g(m) G_r D_r = C_r(m)$$

Figure 4.3. Calibration of E channels.

MINI EMLSLAB SITE 3, R110 YX

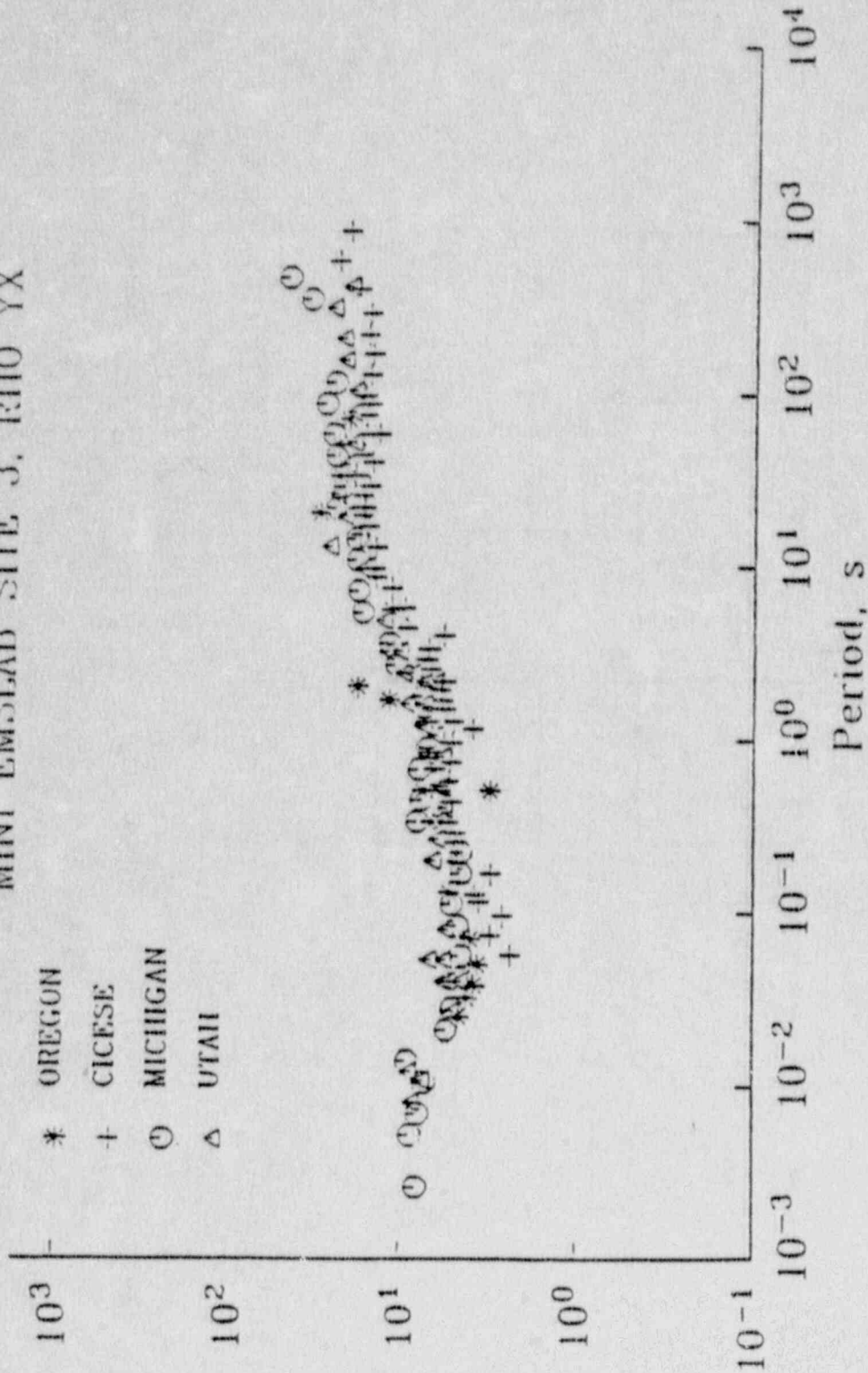


Figure 4-4. Comparison of four MT systems' measurement results.

CHAPTER 5. FINAL PLOTS AND TABLES

While the MT system is accumulating data, a considerable amount of information is available. Any of the quantities discussed in Chapter 2 can be displayed on the computer screen or printed. When the work at a particular site is finished, a complete set of plots and tables can be generated. We discuss here the type of information which is presented in the data volume accompanying this report. The data format used as a sample in this chapter includes high range and low range data, which covers the frequency range 1 to 0.00055 Hz. With the exception of the strip chart discussed in the following section, all of the information discussed below is tabulated for each site and bound in the data volume which accompanies this report.

5.1 Strip Chart Output

The printer of the HP9845 can be programmed to simulate a strip chart recorder. The strip chart mode can be selected in the initial stages of recording, but not while data are being analyzed. Figure 5.1 is a sample of strip chart output showing typical MT signals. The header identifies the individual channels and gives the gain (the top number) and offset of the chart record (the bottom number). The units are in digitizer counts where $\pm 32,768 = \pm 5$ volts. Channels 8 to 10 are not used in our equipment while H_{X2} and H_{Y2} are the remote magnetic reference channels.

The amplitude and range settings are for display purposes only and are not used by the analysis programs. The display also lists the time and the site name at one minute intervals. The plotting is done in bursts from a buffer, so no data are lost during the printing of the headers or the times. The sample traces exhibit characteristics of typical strong MT signals. There is a dominant frequency of about $1 \frac{1}{3}$ cycles per minute present in the plots. The incident magnetic field produces signals on the H_x and H_y channels that are very similar for the local and remote channels. The electric field signals E_x and E_y are very similar indicating a dominant electric field which is about 45 degrees from one of the principal directions (N-S or E-W). The original E_{X1} and H_{Y1} fields have a similar form indicating the Rho X-Y impedance relationship which is computed by the program. Similar statements hold regarding E_{Y1} and H_{X1} .

5.2 Header Page and Operator Log

The first page of the data output gives site-specific information from the operator log record on the field tape as

I+	I	I	E	M	I	I	I	M	M
1071	401	101	101	101	101	101	101	101	101
1071	401	101	101	101	101	101	101	101	101
1071	401	101	101	101	101	101	101	101	101

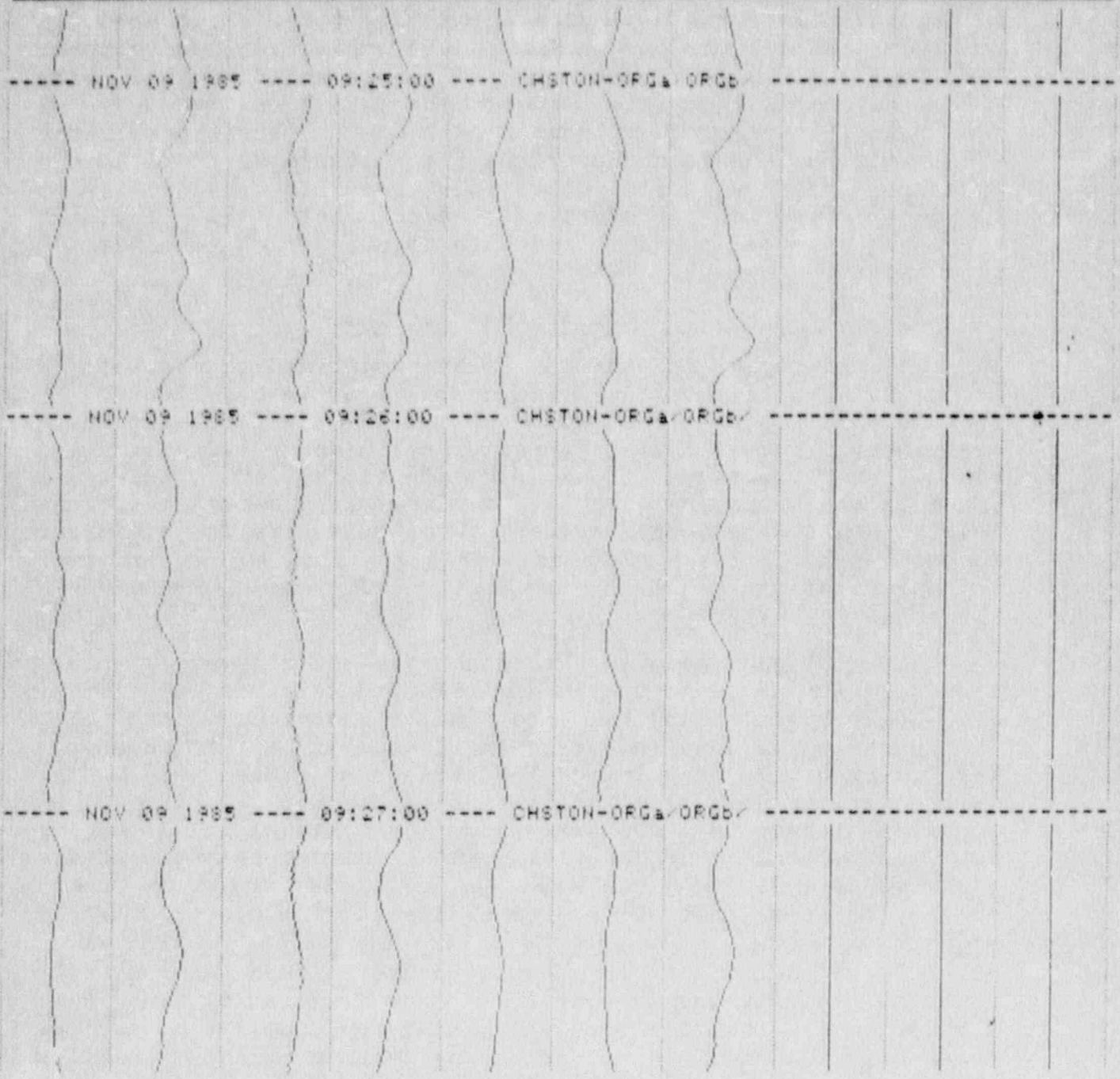


Figure 5.1 Chart recorder output produced by HP 9845 graphics. The first number in each header represents the range of the chart. The record number indicates the offset.

shown in the left-half of Figure 5.2. Most of this information is for site identification and to provide the interpreter with details pertinent to the particular site such as preamplifier gain settings, calibration files used, and the processing used. The third line from the bottom left of the header page indicates mathematical rotation of the data. All the data tabulated in the data volume have been rotated to the principal axis direction. Thus, in all cases Rho-max is plotted, tabulated and labelled as Rho-xy and Rho-min is plotted, tabulated and labelled as Rho-yx.

The middle portion of the header page lists the electrode resistance, dc offset voltages, and broadband ac interference voltages measured at the sensor processor electrodes by the field crew at the site. This information is not used by the program but is printed as a convenience for assessing problems at a site.

5.3 Apparent Resistivity and Phase of Rho-max and Rho-min

These apparent resistivities are calculated from the tensor impedance estimates. They are plotted on the left-half of Figure 5.3 and tabulated on the right-half of Figure 5.3. The error bars plotted are plus and minus one standard deviation. The standard deviations are tabulated as a percent of each resistivity estimate in the right-half of Figure 5.3.

The phases of the rotated resistivities are presented below the resistivity plots. For a uniform earth, all the data for Rho-xy are located at 45 degrees and for Rho-yx at -135 degrees. For a flat layered earth, the first set of phases would be entirely between 0 and 90 degrees and the second set entirely between -90 and -180 degrees. Note that 40 frequencies are tabulated and for each the number of data records stacked to perform the impedance computation is given.

Smoothed apparent resistivities are plotted on the left-half of Figure 5.4 and tabulated on the right-half of that figure. The smoothing routine makes it easier to interpret noisy MT data in terms of flat layers. The routine weighs each apparent resistivity datum according to its error bars, its deviation from a smooth curve and whether or not it lies on a slope of less than plus or minus 45 degrees compared to adjacent points. The smoothing routine is generally very useful in eliminating small fluctuations in the sounding curves due to the random nature of the MT signals. The smoothed resistivity curve presented in Figure 5.4 is based upon remote H reference processing. Often the high frequency points at 72 Hz and 288 Hz are clearly displaced from their proper position by power line interference or can be seen in Figure 5.3. In



MICHIGAN TECH UNIV

MT Site: CHSTON-ORGR

MAGNETOTELLURIC SURVEY REPORT

Run Information

Project: CHIPLESTON 1985
Client: RTU & LHM ENGINEERING
Run: CHSTON-ORGR-ORGR

Operator: JCR
Date: NOV 09 1985
Time: 09:34:12

Program Version: RTS-64
Latest Revision: DEC 03 1982

Reference Field: 4 = Raw H Externals
APR Weighting: 4 = E Coherencies
APR Record Int: 60 Min
Sensor Box Gains: E & - at M's - at
Notch Filters: 60, 160, 360 Hz

System Calibration

NEW SP BOX BY CITY
Date: APR 05 1985
File: C01029

Sensor Calibration

Chan#	Chan	Sensor	Cal Date
1	Hx1	COIL33	APR 05 1985
2	Hx1	COIL34	NOV 01 1985
3	Hx1	LOOP12	NOV 03 1985
6	Hx2	COIL78	NOV 01 1985
7	Hx2	COIL45	NOV 01 1985
8	Hx2	LOOP12	NOV 03 1985



MICHIGAN TECH UNIV

MT Site: CHSTON-ORGR

OPERATOR LOG FOR CHSTON-ORGR-ORGR

Recorded XFR Files:

- X01 - CHSTON-ORGR-ORGR - 09:59:37 NOV 09 1985
- X02 - CHSTON-ORGR-ORGR - 10:48:29 NOV 09 1985
- X03 - CHSTON-ORGR-ORGR - 11:41:06 NOV 09 1985
- X04 - CHSTON-ORGR-ORGR - 12:42:04 NOV 09 1985
- X05 - CHSTON-ORGR-ORGR - 13:44:05 NOV 09 1985
- X06 - CHSTON-ORGR-ORGR - 14:49:46 NOV 09 1985
- X07 - CHSTON-ORGR-ORGR - 15:58:06 NOV 09 1985
- X08 - CHSTON-ORGR-ORGR - 16:03:57 NOV 09 1985
- X09 - CHSTON-ORGR-ORGR - 16:22:35 NOV 09 1985

Operator: JCR

Cultural Factors:

AC INTERFERENCE QUITE HIGH, COILED THE 2 LOOP IN A FIVE TURN LOOP TO PREVENT 60 HZ FROM SATURATING.

Weather Conditions:

CLEAR, LITTLE WIND, 68 F.

Other Factors:

HUBTIPS AND BOGS EVERYWHERE, WE LIVED THROUGH THE SOUTH CAROLINA BEER SEASON.

Station 1

Site Desc: CLEARRING IN MOGDS
Plot File: 1-ORGR

MT Comp	Chan#	Sensor	Azimuth
Hx	1	COIL33	+8 DEG
Hx	2	COIL34	+98 DEG
Hx	3	LOOP12	
Ex	4	77 M	+8 DEG
Ex	5	81 M	+98 DEG
Ex	6	COIL78	+8 DEG
Ex	7	COIL45	+98 DEG

Ex Pot Resistance: 3.4 K Ohms
Ey Pot Resistance: 2.8 K Ohms
Ex Voltage: RC=16.4 mv, DC=31 mv
Ey Voltage: RC=16.1 mv, DC=33 mv

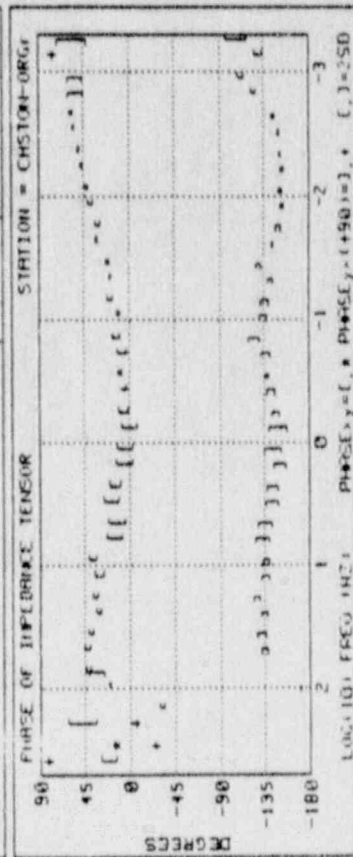
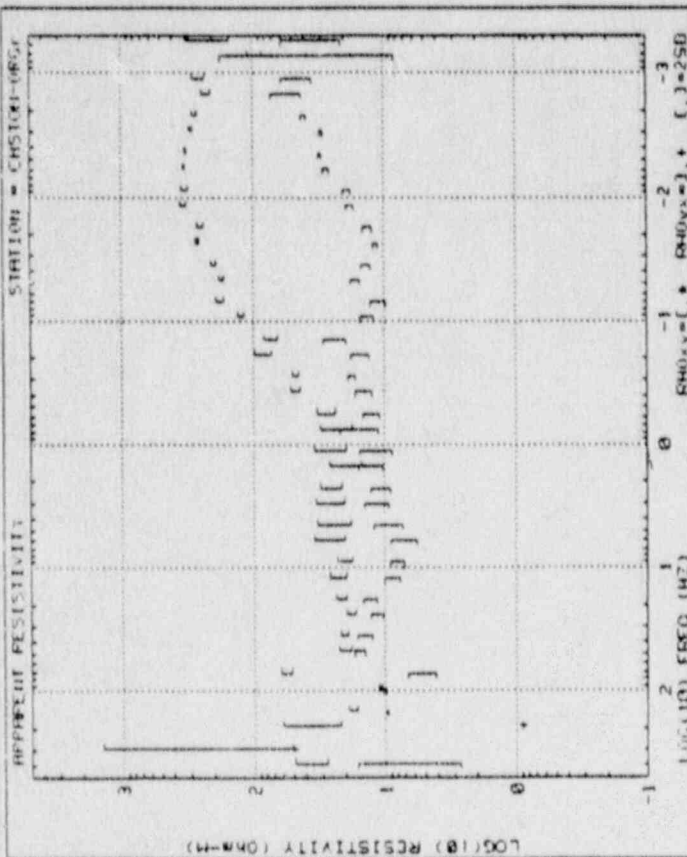
Rotation: Principal N-13

Site Permited by: JAMES WEST
Site Layout by: JCR
Elevation: 200

Figure 5.2 Header page and operator log



MICHIGAN TECH UNIV
MT Site: CHSTON-ORGr



MICHIGAN TECH UNIV
MT Site: CHSTON-ORGr

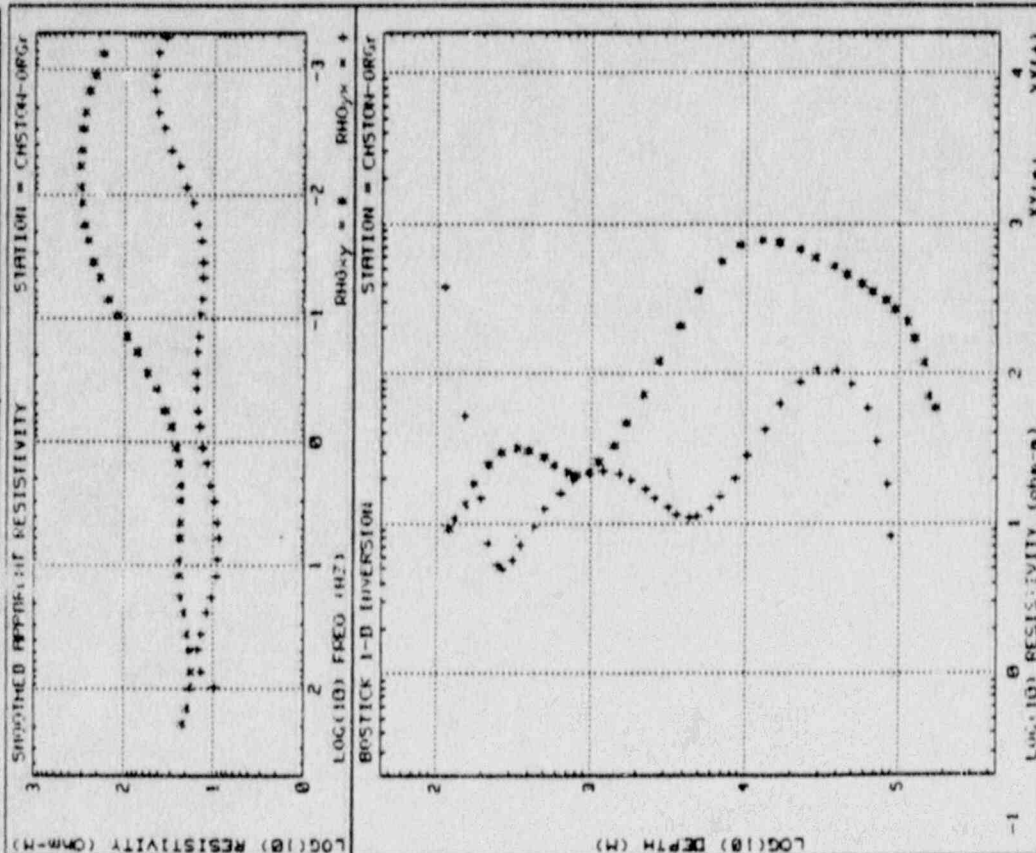
APPARENT RESISTIVITY ESTIMATES

FB	F ₁ -F ₂	STREX ₁	PHO ₁ -y	PHO ₂ -y	PHO ₃ -y	PHO ₄ -y	PHO ₅ -y	PHO ₆ -y	PHO ₇ -y	PHO ₈ -y	PHO ₉ -y	PHO ₁₀ -y	PHO ₁₁ -y	PHO ₁₂ -y	PHO ₁₃ -y	PHO ₁₄ -y	PHO ₁₅ -y	PHO ₁₆ -y	PHO ₁₇ -y	PHO ₁₈ -y	PHO ₁₉ -y	PHO ₂₀ -y	
1	384.00 Hz	68	36.9	32.0	6.6	146.4	21.1	7.9	82.2	25.8													
2	288.00 Hz	68	271.6	428.8	58.6	599.9	18.7	47.7	-24.6	87.1													
3	192.00 Hz	48	36.3	66.7	8.9	861.2	47.9	14.6	-5.3	64.3													
4	144.00 Hz	48	17.6	9.3	9.6	2.2	-31.6	2.5	141.8	-6													
5	96.00 Hz	148	18.8	3.4	18.1	2.5	20.2	-9	-185.6	-7													
6	72.00 Hz	148	56.7	9.3	5.3	27.5	41.9	2.6	33.5	7.0													
7	48.00 Hz	24	28.1	12.1	15.6	16.6	42.3	2.3	-133.8	2.9													
8	36.00 Hz	24	28.4	8.1	14.3	14.7	39.4	2.2	-131.2	3.9													
9	24.00 Hz	24	17.9	6.6	11.5	11.2	38.6	2.4	-133.9	3.1													
10	18.00 Hz	24	21.6	9.6	12.9	11.7	34.5	2.5	-126.4	3.2													
11	12.00 Hz	32	22.6	14.9	8.7	13.8	38.1	8.0	-134.6	3.7													
12	9.60 Hz	32	28.1	15.5	8.1	12.9	37.7	4.1	-135.8	3.5													
13	6.00 Hz	48	28.3	30.1	1.1	26.1	15.4	7.5	-132.4	6.6													
14	4.50 Hz	48	24.2	34.1	9.4	28.5	12.6	6.4	-132.1	7.2													
15	3.00 Hz	70	25.9	29.3	11.4	25.1	16.3	7.4	-142.2	6.4													
16	2.25 Hz	68	25.3	28.5	16.7	19.9	14.6	5.3	-143.2	5.2													
17	1.50 Hz	68	19.8	33.9	12.7	23.6	4.9	6.4	-149.1	6.1													
18	1.12 Hz	68	24.6	32.2	11.6	31.7	4.9	8.0	-142.7	7.9													
19	1.33 S/c	258	23.3	31.1	15.6	38.8	-2.2	7.8	-149.1	9.4													
20	1.78 S/c	258	27.4	17.6	12.6	16.1	5.5	4.6	-145.6	4.3													
21	2.67 S/c	22	46.9	6.7	14.4	16.3	5.7	2.4	-141.1	4.3													
22	3.56 S/c	22	47.3	5.8	17.8	7.3	8.5	1.6	-137.4	2.8													
23	5.33 S/c	12	84.0	15.3	15.2	17.2	7.9	4.1	-135.5	4.6													
24	7.11 S/c	12	73.6	13.4	24.8	21.8	13.3	3.6	-124.1	5.5													
25	16.67 S/c	12	123.4	5.7	13.6	12.5	10.7	1.6	-139.6	3.4													
26	14.22 S/c	14	176.8	7.6	11.1	14.1	16.8	1.9	-134.4	3.8													
27	21.33 S/c	12	172.7	3.7	16.5	8.1	18.4	1.1	-141.1	2.2													
28	28.44 S/c	12	195.8	4.6	13.8	7.7	21.5	1.1	-128.9	2.1													
29	42.67 S/c	12	261.8	3.3	11.7	3.8	33.1	1.9	-142.6	1.1													
30	56.89 S/c	12	251.0	5.8	13.5	7.4	31.2	1.6	-148.7	2.0													
31	65.33 S/c	12	337.8	5.5	18.3	6.7	38.9	1.5	-152.9	1.9													
32	113.78 S/c	12	328.1	5.8	19.1	6.9	42.7	1.4	-158.8	1.9													
33	176.67 S/c	9	331.1	1.4	27.5	5.8	48.2	-4	-150.6	1.5													
34	227.56 S/c	9	322.7	1.6	38.7	2.8	58.7	-4	-148.5	1.9													
35	341.33 S/c	9	294.8	1.9	38.6	3.3	55.6	-5	-148.5	1.9													
36	455.11 S/c	9	273.2	4.2	48.4	4.1	56.4	1.2	-143.8	1.2													
37	682.67 S/c	6	224.8	8.9	55.5	31.8	124.4	2.5	54.8	7.7													
38	918.23 S/c	6	255.5	12.1	45.9	29.8	111.6	3.3	54.8	7.3													
39	1365.34 S/c	3	96.1	13.2	38.3	364.8	128.9	3.6	76.5	44.8													
40	1828.46 S/c	3	218.2	45.1	35.8	67.7	186.3	18.7	57.3	14.8													

Figure 5.3 Apparent resistivity and phase



MICHIGAN TECH UNIV
MT Site: CHSTON-ORGr



MICHIGAN TECH UNIV
MT Site: CHSTON-ORGr

SMOOTHED APPARENT RESISTIVITY AND 1-i INVERSION RESULTS

F#	Freq-Prod	STAGES	RHOxy	RHOyx	TRUE RHOxy	DEPTH	TRUE RHOyx	DEPTH
1	394.00 MZ	60	0.0	0.0	0.0	0.0	0.0	0.0
2	288.00 MZ	60	0.0	0.0	0.0	0.0	0.0	0.0
3	192.00 MZ	48	22.1	0.0	9.2	121.1	0.00	0.0
4	144.00 MZ	48	19.7	0.0	10.0	131.0	0.00	0.0
5	96.00 MZ	140	18.2	9.7	13.4	154.0	376.7	112.9
6	72.00 MZ	140	17.0	13.5	18.4	176.0	51.9	154.0
7	48.00 MZ	24	18.4	14.5	24.6	220.2	14.6	193.7
8	36.00 MZ	24	19.6	13.5	29.0	262.9	7.4	210.1
9	24.00 MZ	24	21.2	11.9	33.4	304.4	5.2	250.1
10	18.00 MZ	24	22.6	10.3	30.6	370.2	5.0	265.7
11	12.00 MZ	33	23.5	9.3	27.1	490.3	5.7	513.1
12	9.00 MZ	33	23.9	6.7	24.3	579.4	7.2	350.0
13	6.00 MZ	48	23.7	6.7	22.0	700.9	9.4	427.7
14	4.50 MZ	48	23.2	9.0	21.1	800.0	12.4	503.2
15	3.00 MZ	60	22.9	9.7	21.1	903.4	16.0	639.4
16	2.25 MZ	60	23.0	16.7	22.6	1137.0	19.4	774.8
17	1.50 MZ	60	23.0	11.0	33.1	1488.7	21.7	999.7
18	1.12 MZ	60	25.0	13.1	46.9	1702.9	22.4	1213.0
19	1.33 SAc	220	29.2	14.2	72.4	2219.1	21.5	1540.4
20	1.70 SAc	220	34.6	15.1	120.2	2790.9	19.5	1640.9
21	2.57 SAc	22	42.0	15.5	205.0	3601.5	17.0	2200.0
22	3.56 SAc	22	54.7	15.5	359.1	4961.5	14.7	2645.5
23	5.33 SAc	12	71.3	15.2	557.0	6937.6	12.7	3200.3
24	7.11 SAc	12	93.4	14.6	721.2	9173.7	11.4	3620.7
25	10.67 SAc	12	121.6	14.0	776.1	12014.0	10.9	4344.1
26	14.22 SAc	12	154.9	13.4	743.4	16703.7	11.1	4915.5
27	21.33 SAc	12	191.4	13.1	673.5	22742.2	12.4	5950.0
28	28.44 SAc	12	227.9	13.2	593.7	28656.2	15.1	6807.1
29	42.67 SAc	12	260.9	13.7	521.9	37544.9	19.9	8614.1
30	56.89 SAc	12	267.2	14.9	455.9	45400.3	20.1	10376.0
31	85.33 SAc	12	305.3	17.0	399.5	57442.5	41.0	15544.7
32	113.70 SAc	12	315.1	20.0	309.3	67500.7	62.7	16900.7
33	170.67 SAc	9	312.2	24.3	207.6	82790.9	80.1	22900.3
34	227.56 SAc	9	300.7	29.7	166.3	94070.3	106.3	29252.2
35	341.33 SAc	9	281.4	35.9	110.0	110000.0	104.7	39373.9
36	455.11 SAc	6	253.0	41.7	170.0	127361.0	65.2	49023.2
37	682.67 SAc	6	210.3	45.6	117.0	148132.0	59.0	62720.0
38	910.23 SAc	6	210.3	45.6	70.0	150000.0	35.1	75000.0
39	1365.34 SAc	3	170.2	41.6	59.3	175544.0	10.2	84793.7
40	1020.46 SAc	3	0.0	34.0	0.0	0.0	0.2	89562.5

Figure 5-4 Smoothed apparent resistivity and Bostick 1-i inversion

severe cases, we have edited out these "flyers" and others since they are clearly in error. The data which have been removed are indicated by zeros in the data table.

5.4 Bostick One-Dimensional Inversion

This commonly used computation converts apparent resistivity data to a continuous resistivity versus depth function. The computation is an approximate method of converting apparent resistivity and phase data to a continuous function of interpreted resistivity versus depth. Bostick, Smith and Boehl (1977) show that data at each frequency may be converted to interpreted true resistivities and depth as follows:

1. Apparent resistivity and frequency are combined to find the depth.

$$D = (\rho_a / \omega \mu)^{1/2} = 319 (\rho_a / f)^{1/2}$$

2. The resistivity at that depth is found from the value and slope of the apparent resistivity curve, according to Bostick's formula

$$\rho = \rho_a \left(\frac{1 - \frac{d \log \rho_a}{d \log \omega}}{1 + \frac{d \log \rho_a}{d \log \omega}} \right)$$

where

ρ = interpreted true resistivity

ρ_a = apparent resistivity

ω = angular frequency

This formula is determined from the two layer model calculations based upon two extreme cases: 1) a perfectly conductive second layer, 2) a perfectly insulating second layer.

Since small random errors in apparent resistivity have a relatively large effect on slope calculation, and since phase data tend to be smoother than apparent resistivity data, Bostick recommends using phase data to compute the derivative in the above equation. It is possible to use phase data because of a theorem which states that if a system transfer function is of the type called minimum phase, then the amplitude and phase of that transfer function are related by a Hilbert transform. The electromagnetic impedance of a layered earth is a minimum phase transfer function. Bostick presents a relation between phase and apparent resistivity which is a

linear first order approximation of the Hilbert transform

$$\frac{d(\log \rho_a)}{d(\log \omega)} = (\theta(\omega)/45^\circ - 1)$$

where θ is the phase in degrees. Thus, a phase which is always 45 degrees gives a zero slope for the apparent resistivity curve. The three equations given above are those used in the Phoenix Bostick 1-D inversion subroutine. It is normal for the phases of Rho-yx to be in the third quadrant, near -135 degrees. These phases must be moved to the first quadrant by adding 180 degrees before being used in the above formula. The Bostick inversion based upon the remote H reference apparent resistivity is shown on the bottom left-half of Figure 5.4, and the values of interpreted resistivity and depth are tabulated on the right. (The reader should substitute the term "interpreted Rho" for "true Rho" in the headings of these tabulations.) In cases where the Rho-xy and Rho-yx values are significantly different the Bostick 1-d interpretations are invalid.

5.5 Tipper Magnitude and Phase

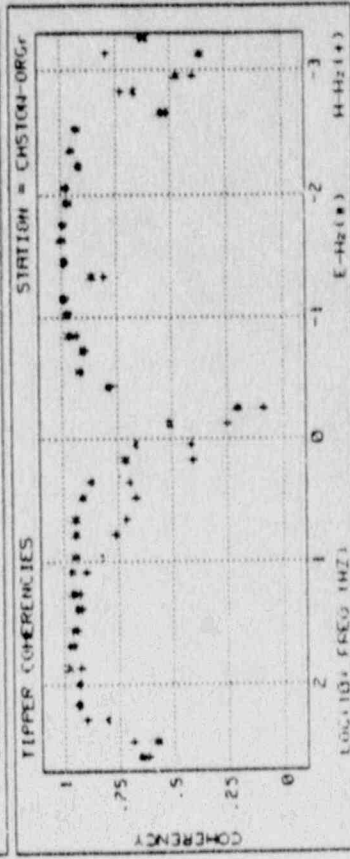
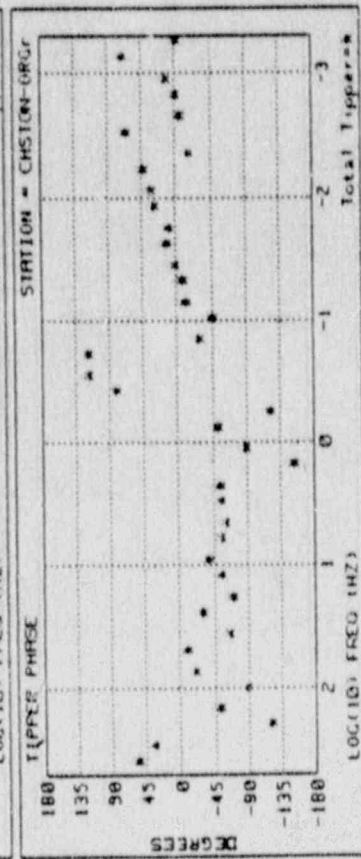
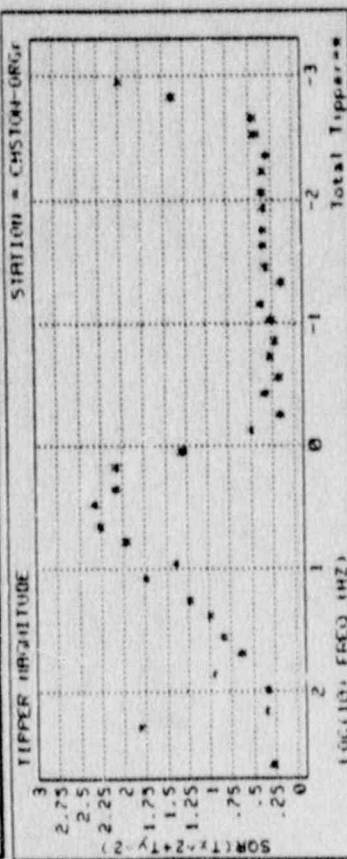
Sample plots and tables of these quantities are found in the left-half of Figure 5.5. Tipper magnitude is defined in Chapter 2. The tipper phase is the phase of the complex number T_x , rotated to its maximum value; it represents the phase of the vertical component of magnetic field with respect to the (maximum) horizontal component of magnetic field. These quantities are tabulated on the right-half of the figure.

5.6 Skew, Ellipticity, Tipper Strike and Impedance Strike

Tipper strike, as used in our analysis program, is defined as the direction of T_y (Equation 2.11) when T_x is rotated to a maximum. Tipper direction is found by subtracting 90 degrees from the tipper strike value. Impedance strike as used in our program should be more correctly termed principal axes or impedance maximum direction. These quantities are plotted on the left-half of Figure 5.6. For a two-dimensional earth, such as that shown in Figure 2.5, R-max is either perpendicular or parallel to the strike of the geologic structure. For the same earth model, the tipper should be at right angles to the strike. Thus, for good data over a two-dimensional earth, R-max and the tipper should be either parallel or orthogonal. If the earth is approximately flat layered or isotropic at a station, the tipper should be weak, and the direction of R-max would be undefined. This effect would give high data scatter in the plot of impedance and tipper orientations. The data in Figure 5.6 show good agreement between T strike and Z strike. The data plotted on the left of Figure 5.6 are tabulated on the right-side of that figure.



MICHIGAN TECH UNIV
MT Site: CHSTON-ORGr



MICHIGAN TECH UNIV
MT Site: CHSTON-ORGr

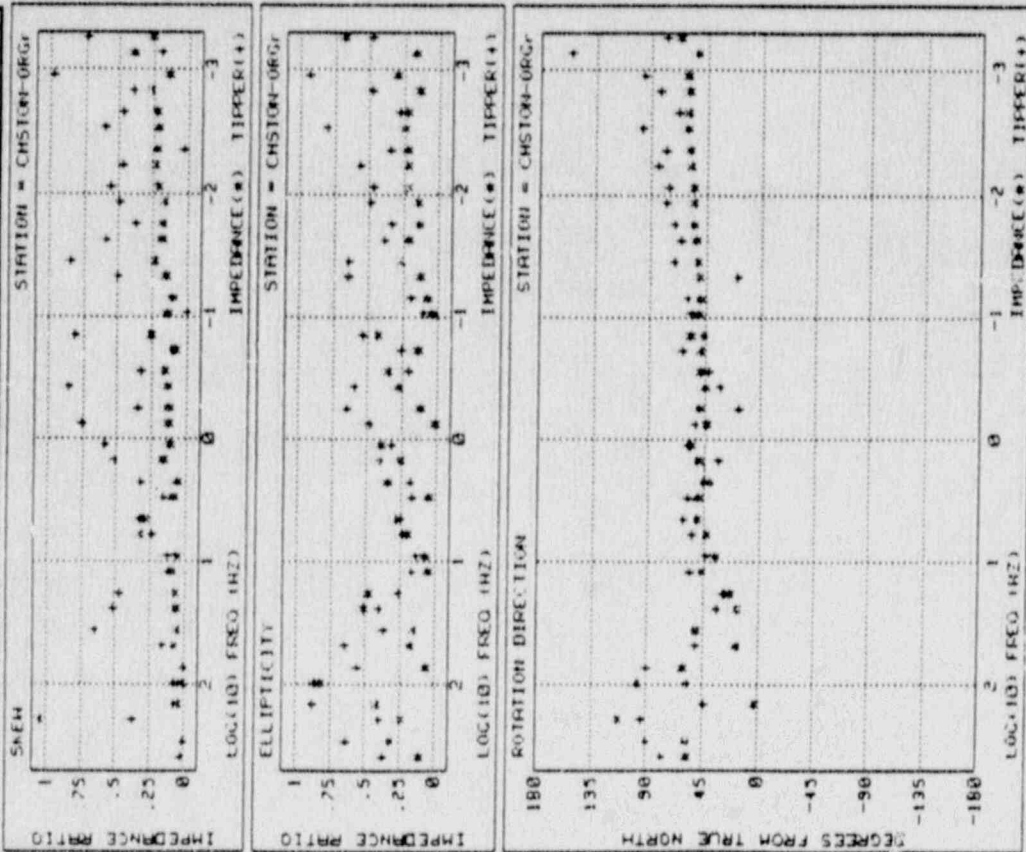
ESTIMATED TIPPER AMPLITUDE, PHASE AND COHERENCIES

F#	Freq/Frd	STREVS	TIP MAG	TIP PHASE	E-MZ	M-MZ
1	384.00 HZ	60	.29	56.22	.65	.62
2	288.00 HZ	60	13.13	34.16	.58	.59
3	192.00 HZ	48	1.62	-121.68	.80	.98
4	144.00 HZ	48	.36	-52.21	.53	.94
5	96.00 HZ	140	.34	-85.12	.93	.93
6	72.00 HZ	140	.96	-26.12	.98	.93
7	48.00 HZ	24	.63	-6.76	.92	.95
8	36.00 HZ	24	.64	-65.38	.96	.94
9	24.00 HZ	24	1.00	-29.68	.94	.91
10	18.00 HZ	24	1.23	-69.97	.96	.93
11	12.00 HZ	33	1.75	-54.93	.96	.98
12	9.00 HZ	33	1.39	-98.56	.94	.82
13	6.00 HZ	48	1.97	-55.28	.95	.76
14	4.50 HZ	48	2.26	-61.31	.94	.71
15	3.00 HZ	68	2.32	-55.12	.91	.66
16	2.25 HZ	68	2.08	-53.68	.87	.78
17	1.50 HZ	68	2.08	-153.22	.71	.41
18	1.12 HZ	68	1.38	-89.24	.67	.42
19	1.33 Sec	228	.58	-52.16	.52	.25
20	1.78 Sec	228	.16	-122.47	.21	.89
21	2.67 Sec	22	.34	61.58	.79	.78
22	3.56 Sec	22	.16	117.51	.92	.92
23	5.33 Sec	12	.28	119.84	.91	.89
24	7.11 Sec	12	.22	-28.27	.96	.93
25	16.67 Sec	12	.27	-45.68	.98	.97
26	14.22 Sec	12	.30	-11.58	.99	.99
27	21.33 Sec	12	.12	-7.11	.86	.81
28	26.44 Sec	12	.33	1.00	.99	.98
29	42.67 Sec	12	.35	12.98	1.00	1.00
30	56.69 Sec	12	.35	5.67	.99	.99
31	85.33 Sec	12	.34	28.73	.97	.97
32	113.78 Sec	12	.36	32.78	.98	.98
33	178.67 Sec	9	.35	43.81	.92	.93
34	227.56 Sec	9	.31	-15.80	.96	.96
35	341.33 Sec	9	.42	65.75	.93	.93
36	453.11 Sec	9	.43	-4.08	.45	.52
37	682.67 Sec	6	1.39	-0.88	.67	.72
38	918.23 Sec	6	2.08	12.27	.48	.48
39	1365.34 Sec	3	12.29	78.95	.37	.79
40	1828.46 Sec	3	6.11	-0.98	.62	.64

Figure 5-5 Tipper, magnitude and phase



MICHIGAN TECH UNIV
MT Site: CHSTON-ORGr



MICHIGAN TECH UNIV
MT Site: CHSTON-ORGr

SKEM, ELLIPTICITY AND STRIKE

F#	Freq/Hz	STROFS	Z-SKEM	Z-ELIP	Z-STRIKE	T-SKEM	T-ELIP	T-STRIKE
1	384.80 Hz	60	1.335	.109	57.373	.625	-.373	77.838
2	288.00 Hz	60	1.727	-.325	57.714	-.067	-.635	90.144
3	192.00 Hz	48	1.849	-.249	113.569	-.376	-.463	94.842
4	144.00 Hz	48	-.846	-.422	2.389	-.073	-.878	43.662
5	96.00 Hz	140	-.015	-.824	98.362	-.671	-.867	57.448
6	72.00 Hz	140	1.576	-.666	51.661	-.607	-.562	96.396
7	48.00 Hz	24	-.084	-.168	17.884	-.168	-.651	58.782
8	36.00 Hz	24	-.058	-.157	58.819	-.651	-.371	51.572
9	24.00 Hz	24	-.066	-.515	17.285	-.516	-.418	34.123
10	18.00 Hz	24	-.071	-.484	23.551	-.471	-.267	28.634
11	12.00 Hz	33	-.058	-.855	46.590	-.119	-.171	55.677
12	9.00 Hz	33	-.620	-.978	35.782	-.129	-.147	43.191
13	6.00 Hz	48	-.323	-.269	42.838	-.242	-.239	54.431
14	4.50 Hz	48	-.292	-.282	58.946	-.331	-.255	61.736
15	3.00 Hz	60	-.086	-.854	49.352	-.161	-.173	58.876
16	2.25 Hz	60	-.667	-.351	45.327	-.327	-.198	40.242
17	1.50 Hz	60	-.165	-.265	58.448	-.528	-.459	33.788
18	1.12 Hz	60	-.122	-.487	53.466	-.569	-.331	58.951
19	1.33 S4C	220	-.138	-.011	43.632	-.761	-.487	52.635
20	1.78 S4C	220	-.131	-.122	49.173	-.354	-.646	17.188
21	2.67 S4C	22	-.138	-.278	44.578	-.853	-.596	32.935
22	3.56 S4C	22	-.159	-.356	48.672	-.327	-.289	41.626
23	5.33 S4C	12	-.085	-.144	49.885	-.184	-.254	63.325
24	7.11 S4C	12	-.258	-.434	57.812	-.689	-.539	46.683
25	10.67 S4C	12	-.148	-.043	51.164	-.884	-.112	57.346
26	14.22 S4C	12	-.186	-.078	43.496	-.189	-.197	68.198
27	21.33 S4C	12	-.133	-.138	58.338	-.592	-.648	19.433
28	28.44 S4C	12	-.188	-.266	51.612	-.847	-.644	71.852
29	42.67 S4C	12	-.188	-.217	53.357	-.596	-.391	65.447
30	56.89 S4C	12	-.178	-.139	55.274	-.373	-.342	71.884
31	85.33 S4C	12	-.168	-.149	55.143	-.457	-.491	77.817
32	113.78 S4C	12	-.214	-.227	55.493	-.568	-.474	75.544
33	178.67 S4C	9	-.234	-.228	57.426	-.473	-.568	84.688
34	227.56 S4C	9	-.238	-.233	58.731	-.635	-.357	78.877
35	341.33 S4C	9	-.228	-.247	68.418	-.687	-.887	97.997
36	455.11 S4C	9	-.232	-.225	68.186	-.467	-.285	68.338
37	682.67 S4C	6	-.268	-.148	55.338	-.359	-.481	82.584
38	918.23 S4C	6	-.144	-.366	68.916	-.974	-.934	96.513
39	1365.34 S4C	3	-.993	-.177	53.853	-.159	-.415	155.407
40	1828.46 S4C	3	-.263	-.681	66.833	-.735	-.482	78.483

Figure 5.6 Skew, ellipticity, T strike and Z strike

5.7 E, H and Ordinary Coherencies

These quantities, plotted in the left-half of Figure 5.7 and tabulated on the right-half of the figure, are the most fundamental indicators of data quality. For example, the first, which should most correctly be termed "E E-predicted coherency", is a test of how well the impedance estimate multiplied by the observed magnetic field predicts the observed electric field. E E-predicted coherency is defined by Swift (1967) as

$$\text{coh}(E_i^P, E_i) \equiv \cdot E_i^P, E_i \cdot / [\cdot E_i^P E_i^{*P} \cdot^{1/2} \cdot E_i E_i^{*} \cdot^{1/2}]$$

$$\text{where } i = X \text{ or } Y, E_i^P = Z_{iX}H_Y + Z_{iY}H_X$$

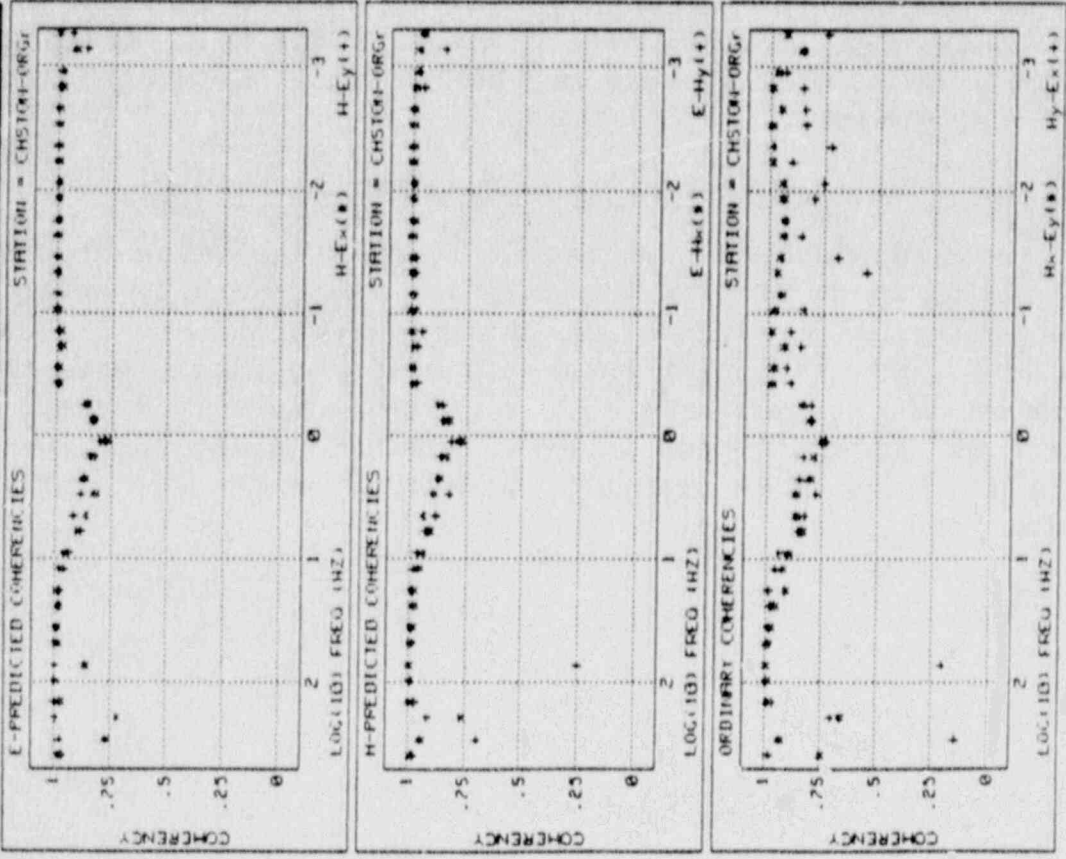
$$\text{and } \cdot E_i^P, E_i^{*} \cdot = Z_{iX} \cdot H_X E_i^{*} \cdot + Z_{iY} \cdot H_Y E_i^{*} \cdot$$

and the Z_{iX} and Z_{iY} are the Z estimates.

The H and tipper predicted coherencies are defined similarly. The predicted coherencies would be almost unity for excellent data. Predicted coherencies below 0.7 are regarded as poor data. The cutoff for data rejection may range from 0.7 to 0.95 depending on accuracy needed, field strength, and time available for a given site. The data for this station were quite good with only those points between 1 Hz and 10 Hz being of lower quality.

5.8 Amplitude Spectra, E and H

Figure 5.8 shows the telluric and magnetic signal amplitude spectra. These quantities are generally omitted from the accompanying data volume but are shown here to indicate the general characteristics of the signals recorded. Note that the weakest signal strength is found in the so-called "dead band" which is typically from 10 Hz to 0.1 Hz. Also, the depression near 100 seconds is probably indicative of two different source mechanisms.



MULTIPLE AND ORDINARY COHERENCIES

FB	Frq-Frd	STAGES	H-E _x	H-E _y	E-H _x	E-H _y	H-E _y	H-E _x
1	384.36 HZ	68	.96	.96	.99	.98	.75	.98
2	266.06 HZ	68	.77	.77	.94	.69	.93	.93
3	192.86 HZ	48	.72	.72	.99	.91	.66	.70
4	144.60 HZ	48	1.00	1.00	1.00	.97	.99	.97
5	96.00 HZ	140	1.00	1.00	.99	.99	.99	.99
6	72.00 HZ	140	.66	.66	1.00	.25	1.00	.21
7	48.00 HZ	24	.98	.98	1.00	.98	.99	.98
8	36.00 HZ	24	.99	.99	.99	.94	.98	.99
9	24.00 HZ	24	.98	.98	.98	.98	.96	.90
10	18.00 HZ	24	.99	.99	.98	.99	.91	.98
11	12.00 HZ	33	.98	.98	.96	.96	.92	.96
12	9.00 HZ	33	.96	.96	.94	.94	.98	.94
13	6.00 HZ	48	.98	.98	.86	.86	.83	.85
14	4.50 HZ	48	.87	.87	.91	.92	.83	.85
15	3.00 HZ	68	.82	.82	.94	.88	.86	.86
16	2.25 HZ	68	.67	.67	.89	.82	.86	.77
17	1.50 HZ	68	.64	.64	.87	.87	.88	.85
18	1.12 HZ	68	.64	.64	.84	.84	.76	.83
19	1.33 S/c	228	.77	.77	.81	.81	.75	.73
20	1.78 S/c	228	.63	.63	.83	.85	.81	.79
21	2.67 S/c	228	.86	.86	.87	.86	.84	.88
22	3.56 S/c	22	.99	.99	.99	.97	.98	.89
23	5.33 S/c	22	.99	.99	1.00	.99	.97	.91
24	7.11 S/c	12	.98	.98	.99	.99	.92	.85
25	10.67 S/c	12	.99	.99	1.00	.95	.98	.89
26	14.22 S/c	12	1.00	1.00	1.00	.98	.97	.84
27	21.33 S/c	12	1.00	1.00	1.00	.99	.94	.94
28	28.44 S/c	12	1.00	1.00	1.00	.99	.95	.95
29	42.67 S/c	12	1.00	1.00	1.00	.99	.96	.89
30	56.69 S/c	12	1.00	1.00	1.00	.99	.95	.85
31	85.33 S/c	12	1.00	1.00	1.00	.99	.93	.93
32	113.76 S/c	12	.99	.99	1.00	.99	.94	.79
33	170.67 S/c	5	.99	.99	1.00	.99	.94	.75
34	227.56 S/c	9	1.00	1.00	1.00	1.00	.99	.98
35	341.33 S/c	9	1.00	1.00	1.00	1.00	.99	.72
36	455.11 S/c	9	1.00	1.00	1.00	1.00	.99	.83
37	682.67 S/c	6	1.00	1.00	1.00	1.00	.95	.84
38	910.23 S/c	6	.99	.99	.99	.95	.99	.85
39	1365.34 S/c	3	.99	.99	.98	.97	.97	.93
40	1826.46 S/c	3	1.00	.94	.92	.87	.86	.85
					.96	.96		.74

Figure 5.7 E, H, and ordinary coherencies



MICHIGAN TECH UNIV
 MT Site: CHSTON-ORGr



MICHIGAN TECH UNIV
 MT Site: CHSTON-ORGr

B-1-51

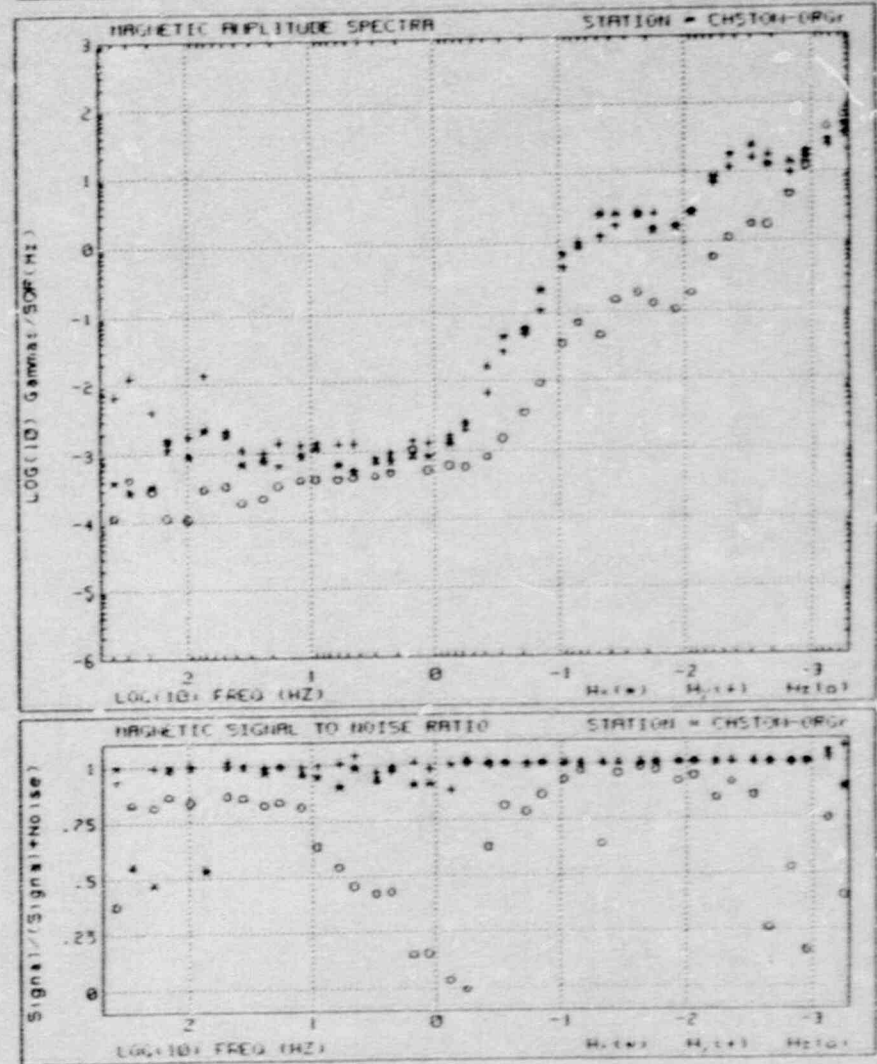
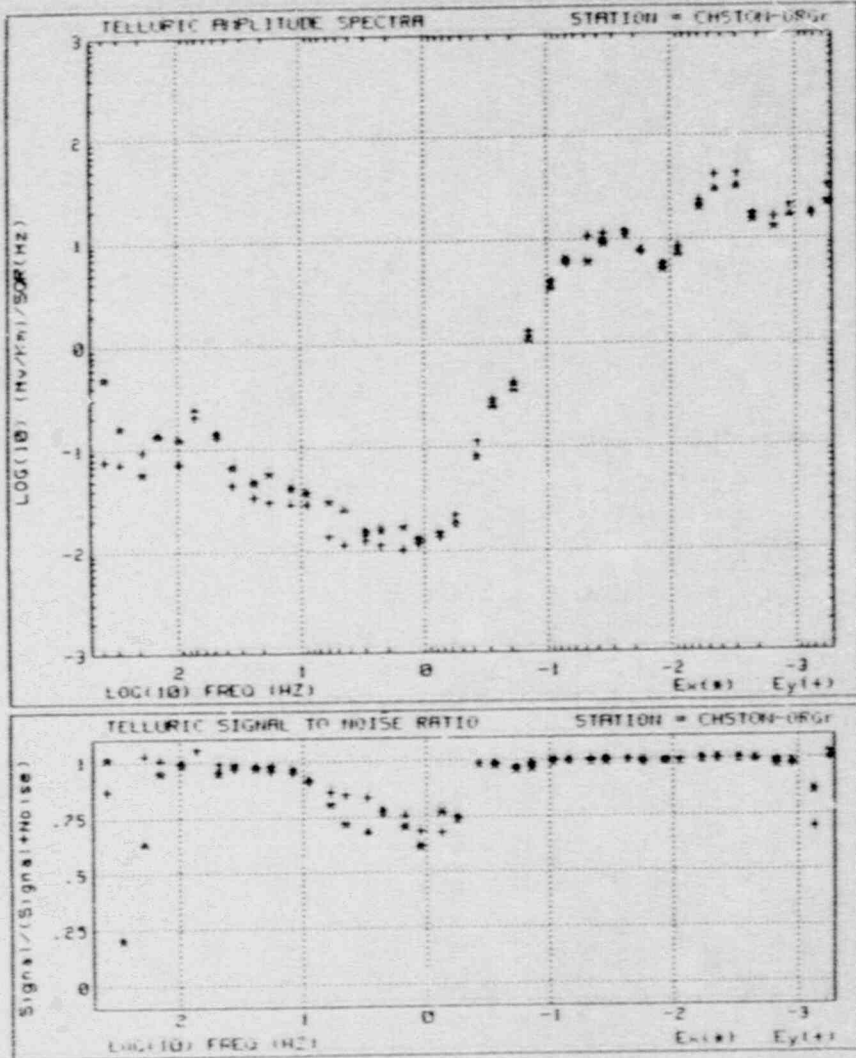


Figure 5.8 Telluric amplitude and magnetic amplitude spectra

CHAPTER 6. CHARLESTON, SOUTH CAROLINA FIELD AREA

6.1 Introduction

The MT measurements were carried out along two perpendicular lines within 100 miles of Charleston, South Carolina. The purpose of the survey was to obtain deep geophysical data that might elucidate the source mechanisms of earthquakes in the Charleston area, the most famous of which occurred in 1886.

The find area has been the subject of a large number of geophysical investigations, summarized in Rankin 1977 and Gohn, 1983. MT was selected as a tool that could compliment these measurements to provide deep coastal data related to the transition from brittle to ductile crust.

6.2 Conduct of Survey

The survey was carried out between October 27 and November 9, 1985. The MTU staff consisted of principal investigators James Rogers and Charles Young and assistants Mark Kitchen and Steve Ruotsala. Sidney Brandwein from Law Engineering was present from October 29 to November 2.

Initial selection of sites was carried out by personnel from Law Engineering. They selected eight sites in a line parallel to the coast and four sites in a line perpendicular to the coast. The lines crossed approximately at Summerville. The sites were assigned a priority and an order in which they were to be occupied. Each was given a name based on a nearby town or geographical feature. The sites and their three letter codes are shown on the map of Figure 1.1. The survey commenced with calibration measurements at the Edisto River Site (EDO). It was discovered that one of the remote reference magnetometers was not functioning. It was necessary to commence data acquisition without remote reference (the local magnetometers were used as signal reference). A replacement magnetometer was obtained from Phoenix Geophysics in Denver. While the magnetometer was in transit, two other soundings were made without remote reference (Frances Marion South and Ridgeville). The remaining soundings were conducted with the remote reference magnetometers.

In order to obtain data at the longest possible period of 1,800 seconds, it was necessary to record for a minimum of six hours.

6.3 General Appearance of Data

The characteristics of the apparent resistivity data described are common to many sites, although considerable variation is present,

1. The high frequency asymptote is approximately 10 ohm-m,

representing near surface sediments. Rho-max and Rho-min are nearly equal in this frequency range.

2. Apparent resistivities from 8 Hz to about 0.2Hz are lower, 2 to 3 ohm-m, representing deeper sediments.

3. Below about 0.2 Hz, the apparent resistivities rise, presumably due to resistive basement, perhaps oceanic coastal material, also Rho-max and Rho-min diverge at these frequencies.

6.4 Summary

The contents of this report and the accompanying data volume constitute the principal items produced on this project. The nonrotated impedance data which have been fully tabulated in the data volume allow interpreters to rotate the data as desired and to thus compare measured results with any two dimensional models of interest. The plotted data shown in the data volume have been rotated frequency by frequency to the principal axis and tabulated so modeling could also be done using these data without the need to rotate to the principal axis. The one dimensional Bostick inversion provided gives guidance for an initial estimate of appropriate two dimensional model.

ACKNOWLEDGEMENTS

The authors of this report wish to acknowledge the assistance of the following: Bob Anderson of Phoenix Geophysics was helpful in supplying replacement equipment. Alan Menzel-Jones of the Canadian Department of Energy, Mines and Resources provided additional equipment for the remote station. Steve Ruotsala and Mark Kitchen from MTU were invaluable during the field work.

REFERENCES

- Berdichevsky, M. N. and Dmitriev, V. I., 1976, Basic principles of interpretation of magnetotelluric sounding curves, in A. Adams, Ed., *Geoelectric and Geothermal Studies*, KAPG Geophysical Monograph, Akademiai Kiado, Budapest, pp. 165-221.
- Bostick, F. X., Smith, H. W., and Boehl, J. E., 1977, Magnetotelluric and dc dipole-dipole soundings in northern Wisconsin: Technical Report, Electrical Geophysics Research Laboratory, University of Texas at Austin.
- Gamble, T. D., Goubau, W. M., and Clarke, J., 1979, Error analysis for remote reference magnetotellurics, *Geophysics*, v. 44, n. 5, pp. 959-968.
- Jupp, D. L. B., and K. Vozoff, 1976, Discussion of "The Magnetotelluric method in the exploration of sedimentary basins," *Geophysics*, v. 41, n. 2, pp. 325-328.
- Gohn, G. S., 1983, Studies Related to the Charleston, South Carolina Earthquake of 1886 - Tectonics and Seismicity, Geological Survey Professional Paper 1313, U.S. Government Printing Office, Washington, D.C.
- Kaufman, A. A. and Keller, G. V., 1981, *The magnetotelluric sounding method*, Elsevier Scientific Publishing Company, New York, 595 p.
- Keller, G. V., and Frischknecht, F. C., 1966, *Electrical Methods in Geophysical Prospecting*, Pergamon Press, New York, 517 pp.
- Newmann, G. A. and Hermance, J. F., 1985, The geomagnetic coast effect in the Pacific Northwest of North America, *Geophy. Res. Letters*, v. 12, n. 8, pp. 502-505.
- Rankin, D. W., Ed., 1977, Studies Related to the Charleston, South Carolina Earthquake of 1886 - A Preliminary Report, Geological Survey Professional Paper 1028. U. S. Government Printing Office Washington, D. C.
- Sims, W. E., 1969, Method of magnetotelluric analysis: Ph.D. Thesis, University of Texas at Austin, 86 pp.
- Swift, C. M., 1967, A magnetotelluric investigation of an electrical conductivity anomaly in the southwestern United States: Ph.D. dissertation, Massachusetts Institute of Technology, 211 pp.
- Swift, C. M., 1971, Theoretical magnetotelluric and turam response from two-dimensional inhomogeneities, *Geophysics*, v. 36, n. 1, pp. 38-52.
- Ting, Sam, C. and Hohman, G. W., 1981, Integral equation

modeling of three-dimensional magnetotelluric response, Geophysics, v. 46, n. 2, Feb., pp. 182-197.

Vozoff, K., 1972, The magnetotelluric method in the exploration and sedimentary basins, Geophysics, v. 37, n. 1, p. 98-141.

Wight, D. E., Bostick, F. X., Jr. and Smith, H. W., 1977, Real time Fourier transformation of magnetotelluric data, Electrical Geophysics Research Laboratory Report, University of Texas at Austin.

Word, D. R., Smith, H. W. and Bostick, F. X., 1970, An investigation of the magnetotelluric tensor impedance method: Technical Report, Electrical Geophysics Research Laboratory, University of Texas at Austin, 264 pp.

APPENDIX B-2

MAGNETOTELLURIC SOUNDINGS
NEAR CHARLESTON, SOUTH CAROLINA

VOLUME II: DATA

(Available on request, see p. 41)

APPENDIX B-3

MAGNETOTELLURIC SOUNDINGS
IN THE CHARLESTON, SOUTH CAROLINA AREA

MAGNETOTELLURIC SOUNDINGS IN THE CHARLESTON, SOUTH CAROLINA AREA

C.T. Young^I, M.R. Kitchen^{II}, J.C. Rogers^{III}, J.C. Mareshal^{IV} and S. Brandwein^V

ABSTRACT

Magnetotelluric soundings in the Charleston, South Carolina area have been interpreted to reveal (a) conductive upper layers corresponding to coastal sediments, (b) a thick resistive layer, (c) a conductive bottom half space. The resistive layer is between 5 and 18 km thick and corresponds to a no-reflection zone in COCORP data. The bottom half space corresponds to deep COCORP reflectors thought to be sediments. A buried thinning of the resistive layer to the north is interpreted as the deep boundary of the South Georgia rift.

Magnetotelluric (MT) profiling was conducted near Charleston, South Carolina to investigate deep crustal structure and to provide parameters for an integrated geophysical model of the area. These soundings were carried out by Michigan Technological University as a subcontract for Law Environmental Services, for the Nuclear Regulatory Commission. This paper presents one dimensional models of the MT soundings and compares them to other geophysical data.

PHYSICAL SETTING

The study area is situated on the emerged part of the Atlantic Coastal Plain near Charleston, South Carolina. The Atlantic Coastal Plain is an eastward-thickening wedge of gently seaward dipping unconsolidated and semiconsolidated sedimentary rocks. These sedimentary rocks taper against the crystalline rocks of the Appalachian Orogenic Belt and thicken to more than one kilometer near the coast in southeast South Carolina [1].

- I. Assistant Professor, Dept. of Geology and Geological Engineering, Michigan Technological University, Houghton, MI 49931
- II. M.S. Candidate, Dept. of Geology and Geological Engineering, Michigan Technological University, Houghton, MI 49931
- III. Professor, Dept. of Electrical Engineering, Michigan Technological University, Houghton, MI 49931
- IV. Professor of Geophysics, University of Quebec at Montreal, Montreal, Quebec, Canada
- V. Senior Geologist, Law Environmental Services, Mariette, GA

Appears in Proceedings, Third U.S. National Conference on Earthquake Engineering, Earthquake Engineering Research Institute, 1986, pp. 83-91.

Test holes (CC#1,CC#2,CC#3) about 25 km southeast of Summerville have penetrated 750-775 meters of Tertiary and Upper Cretaceous sediments and a basalt layer below the sediments [2]. CC#3 passed through 257 meters of the basalt and bottomed at 1031 m in 121 meters of terrestrial red beds. Interpretations of seismic refraction data [3] suggest that CC#3 bottomed within 100 meters of the crystalline basement of pre-Mesozoic age.

The geology below the Atlantic Coastal Plain has been interpreted from rock fragments found in the conglomeritic red beds of CC#3 and from geophysical studies in the area. Three major rock provinces have been identified: the Northern Province, the Central Province, and the Southern Province [4]. The Northern Province is near the Fall Line in Georgia and South Carolina and is an extension of the Appalachian Piedmont below the Coastal Plain rocks. The Southern Province is located in southeast Georgia and Florida, and consists of undeformed Paleozoic sedimentary rocks that are underlain by felsic volcanic rocks and granitic plutonic rocks of Paleozoic or Proterozoic age. The Southern Province is thought to be part of the African Craton that was attached to the North American continent during the closing of the proto-Atlantic. The Northern and Southern Provinces are separated by the Central Province, which is a wide unexposed basin containing lower Mesozoic continental rocks and associated mafic igneous rocks. This basin comprises a large continuous rift system composed of many individual basins known as the South Georgia Rift [5]. This rift trends east-northeast and is a possible extension of the rift associated with the opening of the Gulf of Mexico. The basin and the flanking crystalline rocks are intruded by north-trending and northwest-trending diabase dikes. The area is also intruded by mafic and granitic plutons. The dikes and plutons are visible on gravity and magnetic anomaly maps. The meizoseismal area of the 1886 Charleston earthquake is located within the South Georgia Rift where dikes of different trends overlap. The basement below the Central Province is poorly understood because of the thickness of the overlying basin rocks.

PRINCIPLES OF THE MAGNETOTELLURIC METHOD

A qualitative description of the magnetotelluric method is presented here to illustrate the significance of the survey data. Summaries of principles and examples of MT surveys are given in [6] and [7].

The MT method utilizes natural transient electric and magnetic fields to determine the surface electromagnetic impedance of the earth. These fields are generated by the flow of charged particles in the ionosphere and to distant lightning storms. The electromagnetic impedance expresses an assumed linear relationship between the applied magnetic field and the resulting electric field. The observation depth of a given measurement is dependent upon the frequency of the detected signal and upon the subsurface resistivity. Low frequency electromagnetic waves penetrate more deeply than high frequency waves. Waves of a given frequency penetrate deeper into resistive rocks than into conductive rocks. The impedance is usually expressed as apparent resistivity and plotted as a function period. These plots resemble a highly smoothed electrical log with an axis of frequency rather than depth. The structures giving rise to these curves are determined by comparison of the data with synthetic data computed from models.

For this survey we employed remote reference recording; that is we recorded two horizontal components of electric field and three orthogonal components of magnetic field at the survey station, and simultaneously recorded two components of reference magnetic field at a station a few hundred meters away. The reference field was used to improve the signal to noise ratio. Coincident signals were considered to be correct and non-coincident signals were assumed to be noise. This procedure reduces noise due to circuit noise or local ground vibration.

The horizontal electric and magnetic fields are used to determine the impedance tensor, which is usually mathematically rotated to the principal axis. The direction of principal axis (impedance maximum) and the ratios of the maximum to minimum impedance express the electrical fabric at the measurement site.

The vertical component of the magnetic field is used to define a magnetic field transfer function, which is also used to reveal the electric fabric of the area. If the earth consists only of flat layers, there will be only uniform currents, but if there is a more complicated structure, electric current will concentrate in conductors. The magnetic field of a concentrated current curls around the current, as described by the right hand rule, and thus a horizontal current concentration will have a vertical magnetic field component on either side of it. The ratio of the vertical magnetic field to horizontal magnetic field components, known as the magnetic transfer function, is a tensor consisting of phasors. The axes of this tensor can be mathematically rotated to maximize one component, thus finding the direction perpendicular to the orientation of the current concentration. We will display the direction and magnitude of the maximized rotated transfer function, with the real and imaginary parts rotated separately.

FIELD PROGRAM

Twelve stations were occupied along two lines crossing at Summerville, South Carolina. One line, A-A', on Figure 1 was approximately parallel to the coast running NE-SW and the other, B-B', was approximately perpendicular, running NW-SE. The figure also indicates the epicenters of earthquakes [8] and COCORP lines [9].

The recorded time series were analyzed in the field to obtain impedances, apparent resistivities, magnetic field transfer functions and other related quantities. The impedances were used to compute layered models at each site, which are discussed below.

RESULTS

Figure 2 presents apparent resistivity curves for each site. The data have been rotated at each site to obtain maximum and minimum values. Typically, at a given site, the maximum and minimum resistivities are nearly identical at short periods, indicating a locally flat layered earth.

The apparent resistivities generally drop at intermediate periods, rise at longer periods and drop at the longest periods. This sequence reflects the

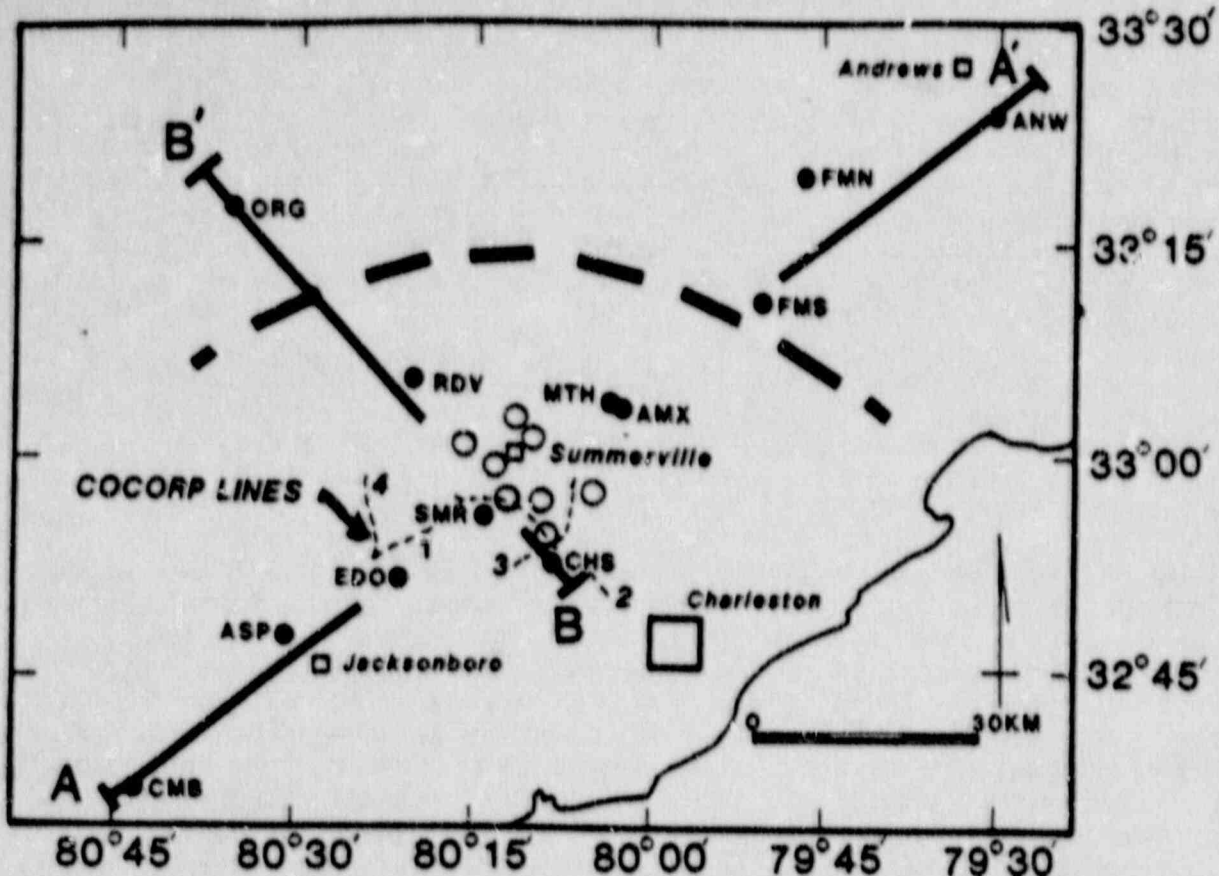


Figure 1. Location of stations (dots) and station identification (three letter codes). A-A' and B-B' are the profiles used for cross-sections in Figure 3. Recent earthquakes [8] are indicated by open circles and COCORP profiles are indicated by dashed lines. The heavy dashed line indicates a boundary determined by the MT survey, and is discussed later.

variation of resistivity with depth. The maximum and minimum apparent resistivity curves diverge with increasing period, indicating that the earth should be modeled in two or three dimensions at these frequencies.

One dimensional modelling assumes that the earth is flat layered at each site. To approximate this condition, the apparent resistivity curves are forced to a single effective apparent resistivity curve at each site by computing the average of the maximum and minimum impedances. Forced one dimensional modelling is used to obtain starting models for two or three dimensional models, and for preliminary interpretation. We found models matching the effective resistivity and effective impedance phase and present them in Figure 3. The cross section also shows the hypocenters of earthquakes [8] and the COCORP lines [9].

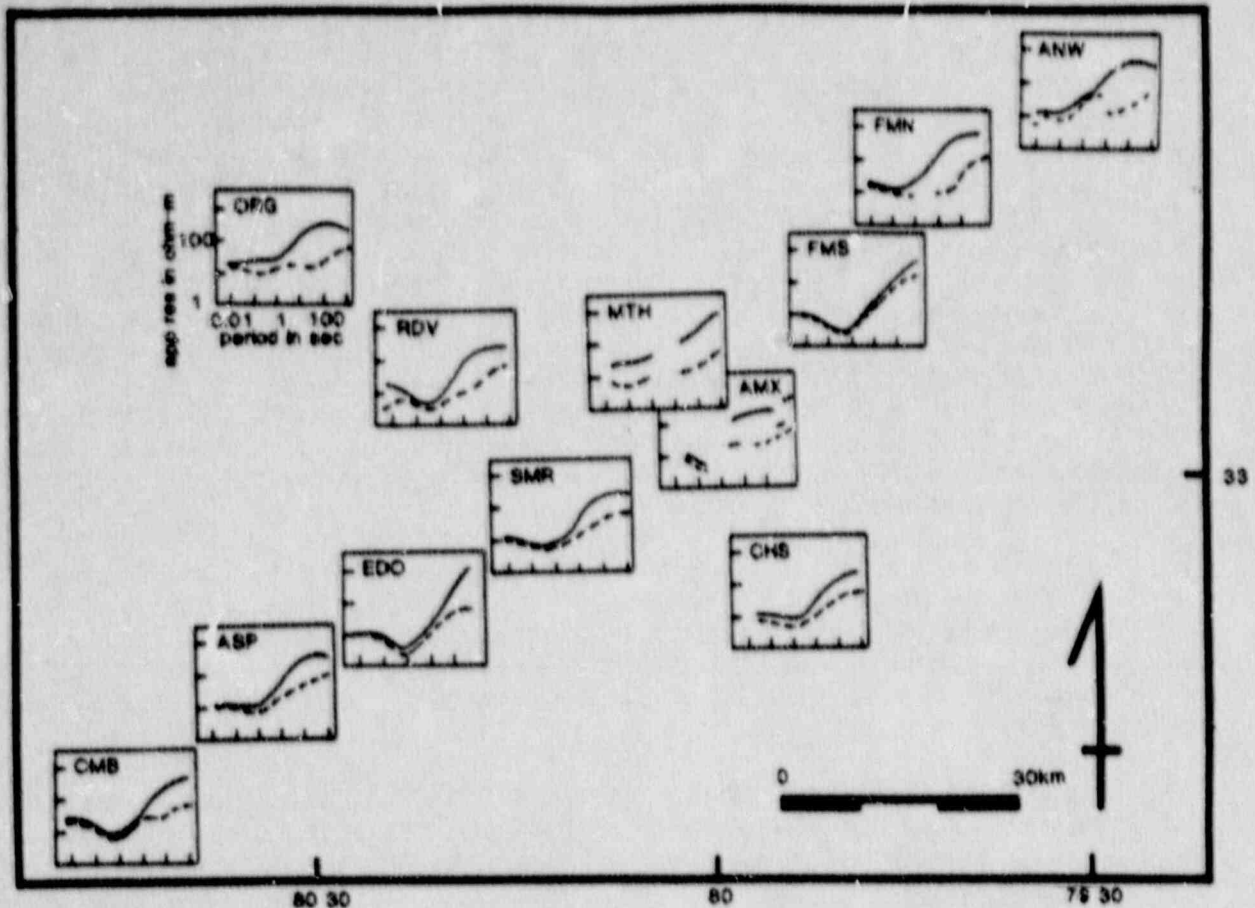


Figure 2. Apparent resistivity curves for all sites. The upper curve at each site is Rho-max (solid line) and the lower curve is Rho-min. Each curve is in its correct geographical position. The scale of all the curves is identical and is presented for the upper left curve only.

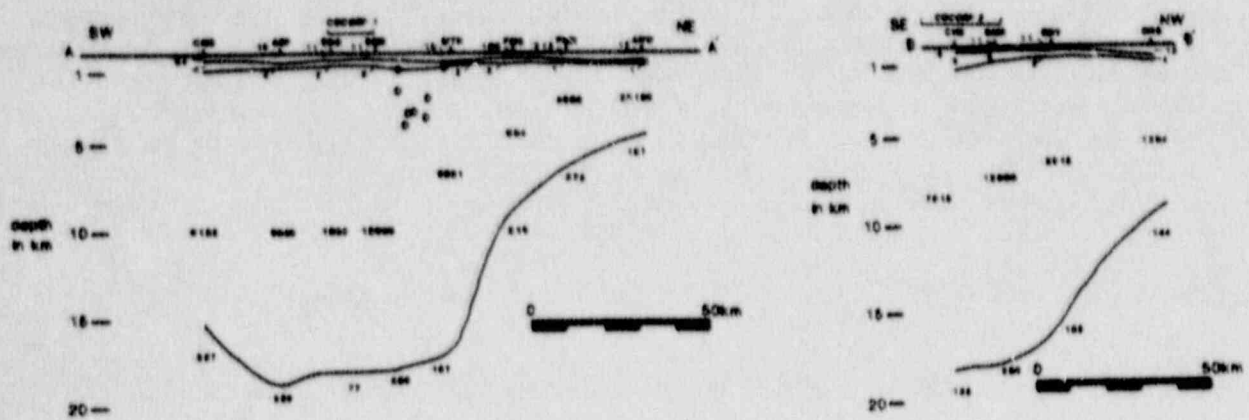


Figure 3. Geophysical cross-sections determined from layered-earth models of effective impedance at each site. The triangles at the top of the sections indicate the sounding locations. Layers are labelled with their interpreted resistivity in ohm-m. COCORP profiles are indicated at the top of each profile. a. NE-SW profile, A-A'. The approximate hypocenters of the earthquakes reported by [7] are indicated by circles on cross section. b. NW-SE profile, B-B'.

The models show four layers. The top layer is moderately conductive (12 to 312 ohm-m) with thickness ranging from 200 to 400 m. The second layer is conductive (1 to 4 ohm-m) with thickness ranging from 200 to 400 m. These two layers correspond to coastal sediments. This is underlain by a high resistivity layer (3000-20000 ohm-m) which is very thick (5 to 18 km). These high resistivities are typical of continental igneous rock, especially dry granite. Below this thick resistive layer, the model consists of an infinitely deep half-space which is moderately conductive (77 to 373 ohm-m). The top of the resistive layer is approximately the same as the depth of magnetic bodies in the area [10]. The bottom of the resistive layer shows a step offset, and is shallower to the northwest and northeast. The offset is indicated by dashed line on the map of Figure 1. The resistive layer corresponds to a region of no seismic reflections on the COCORP profiles. Both the electrical and seismic properties of the resistive layer are consistent with granite or other igneous lithology, where there are no extensive boundaries to reflect energy.

Compared to the COCORP profiles, the deep interface in the MT cross section corresponds to the transition from the reflection-free zone above 5 seconds to a zone of gently dipping discontinuous reflectors below. The presence of reflectors and the moderate resistivities of the bottom half space are consistent with sedimentary lithology. Both COCORP and MT data indicate a general gentle southward dip.

In addition to layered models, MT data can also reveal inhomogeneities and structural grain by anisotropy diagrams and transfer function maps. Figure 4 illustrates polar impedance diagrams to indicate the anisotropy of the impedance tensor. Data from two frequencies are displayed, $T = 85$ sec and 455 sec. These frequencies have a depth of penetration appropriate to regional studies. At each station, two polar diagrams are presented at each frequency. The polar figure drawn with solid lines indicates anisotropy of the diagonal impedance term, Z_{xy} . This quantity represents the electric field in the x direction generated by a magnetic field at right angles to it (the y direction). If the earth is isotropic (no electrical fabric and no nearby inhomogeneities), Z_{xy} should plot as a circle. Similarly, the polar diagram, drawn with a dashed line, represents Z_{xx} , the electric field in the x direction due to a magnetic field in the x direction. For an isotropic earth with no inhomogeneities, Z_{xx} should be zero. The Z_{xy} polar plot makes a peanut shape for a two dimensional earth,

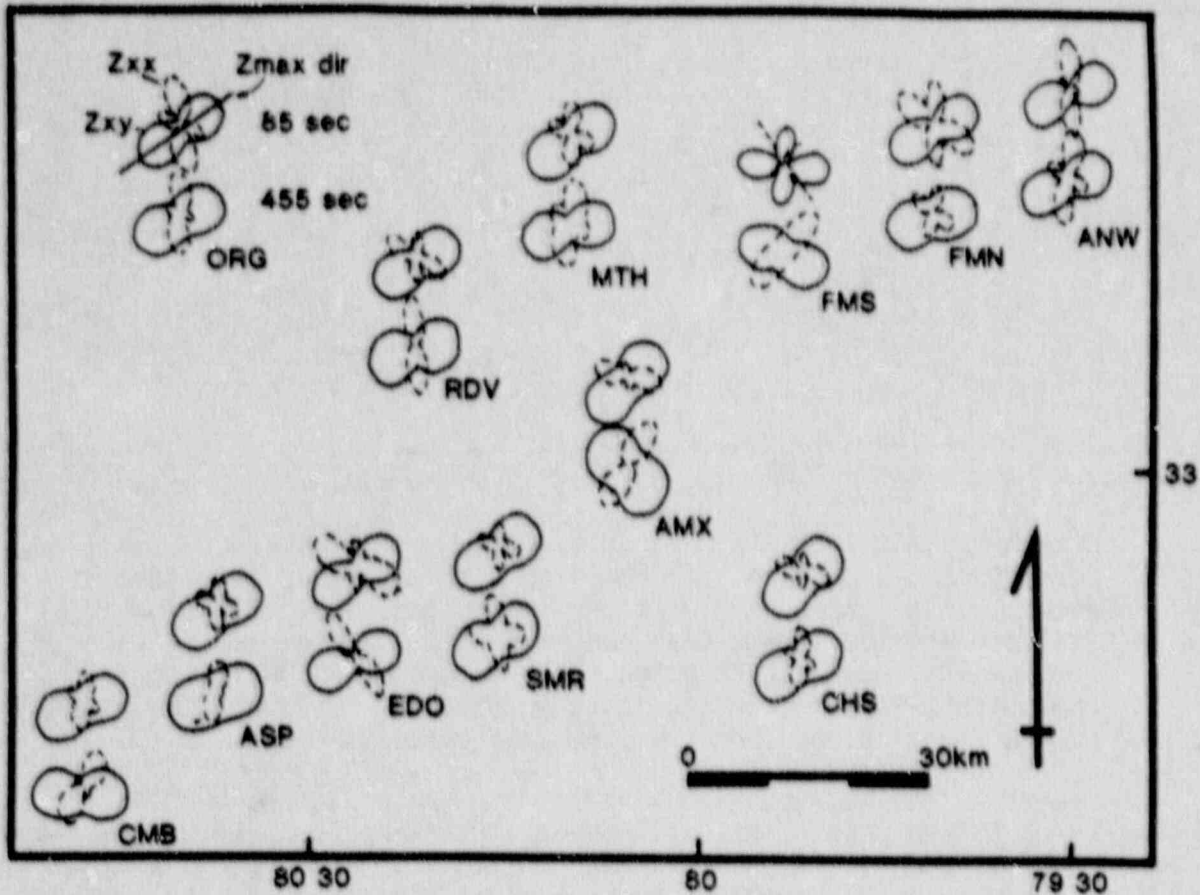


Figure 4. Impedance ellipses at each site. Data from 85 sec and 455 sec are shown at each site, as indicated in the upper left. The solid line indicates the on-diagonal MT impedance tensor, Z_{xy} , as a function of rotation angle and the dashed line indicates the off-diagonal element Z_{xx} .

with its long axis indicating the principal axis of anisotropy, and Z_{xx} should go to zero along the principal axis. Z_{xx} polar diagrams that are not zero along the principal axes indicate a three dimensional earth. The data in Figure 4 indicate that the principal axes at most sites are parallel to the Atlantic sea coast (NE-SW) at both 85 sec and 455 sec, and that the degree of three dimensionality is small. The only exceptions are site AMX, which was near an aluminum refinery that generated significant magnetic field interference, and at site FMS, where the recording was terminated due to an electrical storm.

These impedance orientations are consistent with either large scale electrical anisotropy in the thick resistive layer shown in Figure 3 or with a two-dimensional structure approximately parallel to the sea coast.

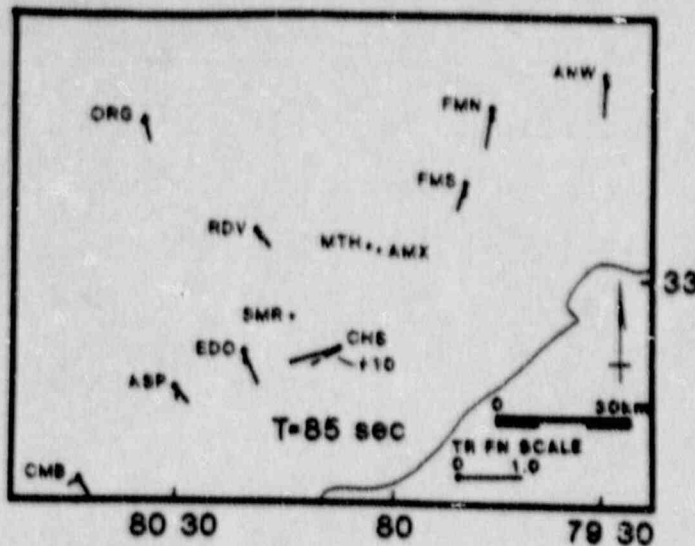


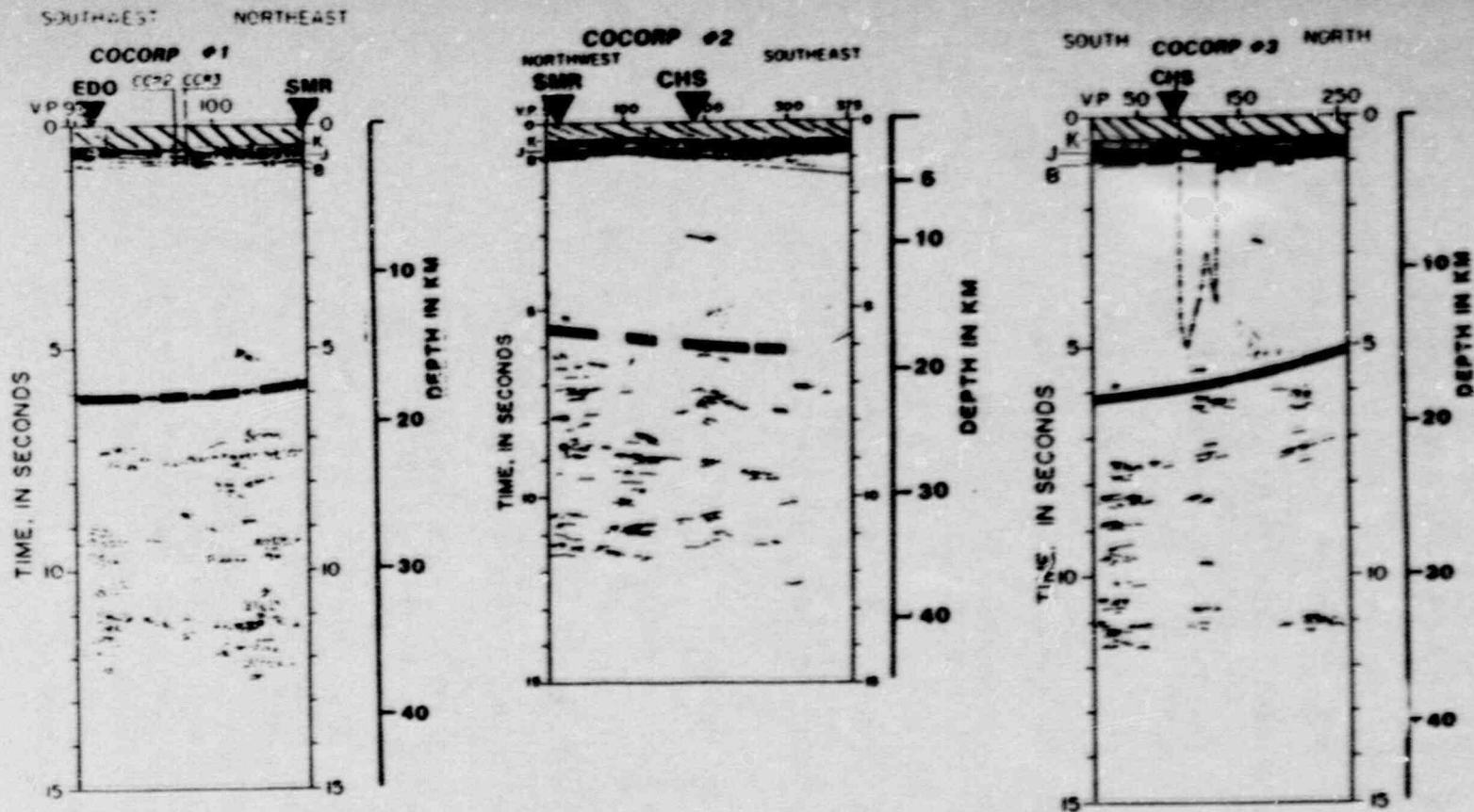
Figure 5. Magnetic field transfer functions for 85 sec. The directions are plotted with the directions reversed according to convention, and thus should point towards conductors. The dots indicate station locations. The solid lines indicates the real component of magnetic transfer function and the dashed line (shorter) indicates the imaginary component. Data for station CHS is ten times larger than the graphical value.

As described earlier, the transfer function relating the vertical magnetic field to the horizontal field reveals concentrations of current in the crust. These transfer functions, also termed induction vectors, are presented in Figure 5 for a period of 85 seconds. The dot indicates the station locations, the solid line indicates the direction and magnitude of the maximum of real part of the transfer functions while the dashed line indicates the maximum of the imaginary part of the transfer function. The directions are plotted reversed, so that the lines point toward the current concentrations. Transfer functions are not reported for stations near population concentrations, because the data quality was poor there, presumably due to interference. The induction vectors shown in Figure 5 generally point toward the coast, except for station CHS which was probably affected by currents induced in power transmission lines or pipelines.

CONCLUSIONS

Magnetotelluric soundings have been interpreted by layered models and interpreted as profiles. The resulting cross-sections indicate a sequence of conductive sediments, overlying a thick resistive layer interpreted as igneous rock. The bottom half space is conductive which is interpreted as sedimentary rock. The MT interpretation is in agreement with COCORP cross sections and magnetic data. The MT data identify the presence of deep sediments under the entire survey area, and indicate a step offset in the depth to the sediments to the northeast and northwest which could be the deep flank of the South Georgia Rift.

Impedance anisotropy and other indicators of two and three dimensionality indicate that higher order models are desired to account for some data characteristics.



Comparison of one-dimensional MT models to COCORP profiles. COCORP profiles 1, 2 and 3 are shown (from Shilt, et al., in Rankin, USGS, 1977) (these profiles are plotted on Figure 1). Four layer one-dimensional MT models from Figure 3 are overlain on the COCORP cross-sections. The four layers represent moderately conductive rock (diagonal lines), conductive rock (solid heavy shading), resistive rock (light shading) and deep moderately conductive rock (no shading, separated by heavy dark line). Notice that the deep boundary from resistive to conductive rock coincides with the seismic transition from a reflection free zone to a zone of gently dipping parallel reflectors. Both the MT and the seismic results are consistent with a transition from granites (high resistivity and reflection free) to sediments (conductive and layered). Note that the dips of the MT boundary and the layered reflectors agree.

ACKNOWLEDGEMENTS

This work was supported by the Charleston Earthquake Research Program of the Nuclear Regulatory Commission, Contract No. NRC-04-85-112 FIN No. B8291 and NRC-04-85-112 FIN No. 138291.

REFERENCES

- [1] Rankin, D.W., Ed., Studies related to the Charleston, South Carolina earthquake of 1885 - a preliminary report: U.S. Geol. Survey Prof. Paper 1028, U.S. Gov't. Pr. Off., Washington, D.C., 1977.
- [2] Gohn, G.S., Higgins, B.B., Smith, C.C., Owens, J.P., Lithostratigraphy of the deep corehole (Club Crossroads Corehole 1) near Charleston, South Carolina, paper E in [1], 59-70, 1977.
- [3] Ackermann, H.D., Seismic-refraction study in the area of the Charleston, South Carolina, 1886 Earthquake, paper F in [1], F1-F20, 1983.
- [4] Gohn, G.S., Geology of the basement rocks near Charleston, South Carolina, Data from detrital rock fragments in Lower Mesozoic(?) rocks from Clubhouse Crossroads test hole #3, paper E in [1], E1-E22, 1983.
- [5] Daniels, D.L., Zeitz, I., and Popenoe, P., Distribution of subsurface lower Mesozoic rocks in the southeastern United States, as interpreted from regional aeromagnetic and gravity maps, paper K in [1], K1-K24, 1983.
- [6] Stanley, W.D., Saad, A.R., and Ohofugi, W., Regional magnetotelluric surveys in hydrocarbon exploration, Panama Basin, Brazil, Am. Assoc. of Pet. Geol. Bull., v. 69, 346-360, 1985.
- [7] Vozoff, K., The magnetotelluric method in the exploration of sedimentary basins, Geophysics, v. 37, 98-141, 1972.
- [8] Tarr, A.C., Recent seismicity near Charleston, South Carolina, and its relation to the August 31, 1886, earthquake, paper D in [1], 43-58, 1977.
- [9] Shilt, F.S., Brown, L.D., Oliver, J.E., and Kaufman, S., Sub-surface structure near Charleston, South Carolina - results of COCORP reflection profiling in the Atlantic Coastal Plain, paper H in [1], 1983.
- [10] Phillips, J.D., Magnetic basement near Charleston, South Carolina, a preliminary report, paper J in [1], 139-149, 1977.
- [11] Gohn, G.S., Studies related to the Charleston, South Carolina earthquake of 1886 - Tectonics and seismicity: U.S. Geol. Survey Prof. Paper 131, U. S. Gov't. Pr. Off., Washington, D.C., 1983.

APPENDIX B-4

TWO DIMENSIONAL MAGNETOTELLURIC MODELS
OF THE CHARLESTON, SOUTH CAROLINA DATA SET

TWO DIMENSIONAL MAGNETOTELLURIC MODELS
OF THE
CHARLESTON, SOUTH CAROLINA DATA SET

by

Charles T. Young, and
Mark R. Kitchen

Dept of Geology and Geological Engineering,
Michigan Technological University, Houghton, MI 49931

March, 1987

This report presents two dimensional models calculated to match magnetotelluric (MT) data obtained along profiles parallel and perpendicular to the seacoast near Charleston, South Carolina. It is assumed that the reader is familiar with the general principles of the MT method, the geologic setting, the general field procedure, and the results of the survey reported by Young and Rogers (1985) and Young et al (1986).

One dimensional modeling of MT data is appropriate in cases where the apparent resistivities of orthogonal apparent resistivity curves are nearly identical. This is the case in the Charleston data set for periods less than one second, representing a penetration depth of about one kilometer. For longer period data, the curves diverge and higher dimensional modeling is desired. For some cases, a two dimensional model may be approximated by a series of side by side one dimensional models, e.g. Young et al (1986). This example utilized the geometric average of the maximum and minimum apparent resistivity at each site, as suggested by Berdichevsky and Dmitriev (1976). Unfortunately, this approach can be misleading, as illustrated in a computational example (Hermance, 1983), which illustrates that for an elongated sedimentary basin with an offset, the maximum resistivity curve at each site provides a more accurate representation of the host structure. The two dimensional models presented here for the Charleston data set agree with Hermance's assertion, and agree with the one dimensional models determined for the maximum resistivity curve at each site. Two dimensional models fitting a given data set are not unique. The non-uniqueness is not as severe as in gravity modeling, because the depth penetration of MT is clearly controlled by the frequency of observation. We present here models which fit the data set as well as possible and are constrained by our knowledge of probable geology. It was not possible within the time constraints of the project to explore other models which fit the data as well as the model presented.

We used the two dimensional MT modeling algorithm described by Ku, Hsieh, and Lim (1973). It uses transmission surface analogy to the MT wave, and solves the resulting matrix by Gaussian elimination. We have tested the program on flat layered models and on simple fault models.

The model represents the earth as a 50 by 30 two dimensional grid. The operator specifies the dimensions of the horizontal and vertical grid elements, the resistivity at the nodes, frequencies to be used in the computation and runs the program for both modes as a batch job. The program computes and prints apparent resistivity and phase above each grid element. The operator compares the output with the field data and changes the program to produce a new output which he expects to be in better agreement with the field data and computes a new model response, and so forth. We computed about 50 models, and present the results of the best fitting one.

Models were created for profiles oriented parallel and perpendicular to the seacoast. For each profile, apparent resistivities were computed for electric field orientations parallel to and perpendicular to the profile line. Computations were carried out at periods of 5.33, 14.22, 42.7, 113.6, 344 and 909 seconds, corresponding to the periods computed by the Phoenix MT system. The profile perpendicular to the seacoast will be discussed first. The model is presented in Figure 1. The main features of the section are:

1. wedges of conductive seawater, sea sediments and older sediments within the upper 5 km, all thickening to the SE, underlain by
2. a 65 km thick resistive layer, underlain by
3. a moderately conductive layer, extending from a depth of 65 km to 190 km, underlain by
4. a conductive bottom half space.

The agreement of model and data is indicated in Figure 2, parts a to c. The match between model and data for the maximum resistivity curve is quite good, often within ten percent. The maximum resistivity curves are oriented parallel to the structure and are termed the E-parallel or TE (transverse electric) mode. This mode is sensitive to regional structure rather than local effects. The match between the model and data for the minimum resistivity curve is not as good. A considerable amount of experimentation yielded a number of slightly different curves and models, none of which produced a better fit. These curves represent an orientation of measurement axis perpendicular to the structure and are termed the E perpendicular or TM (transverse magnetic) mode. This mode is sensitive to local rather than regional structure and the quality of fit is less important to the gross geological interpretation.

The model for the line running parallel to the coast is shown in Figure 3. The comparisons of model to data are shown in Figure 4 parts a, b and c. This model is much simpler, since it runs parallel to the strike of major geological features. Its only structure is a trough in the sediments penetrating into the resistive basement in the center of the model. The deeper layered model is identical to the line perpendicular to the seacoast. The agreement of data and model is not as good for this line. Complete agreement could be achieved only at the longest periods. At some periods, the model and data differ by a factor of three or four. The reader is reminded that the known structure cannot be represented by a cross section along this line, since the structure strikes along the line.

These models agree with inferences from geologic studies which require the ocean and both new and old sediments. The two

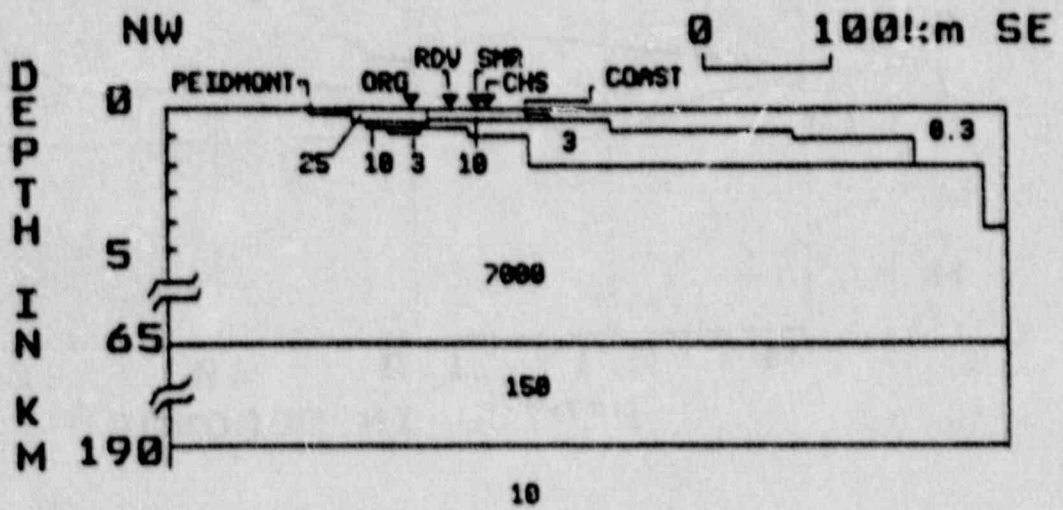


Figure 1. Two dimensional model for cross-section perpendicular to the seacoast, corresponding to line B-B' on Figure 1 of Young et al (1986). The triangles and three letter codes represent the MT sites. The layer resistivities are given in ohm-m.

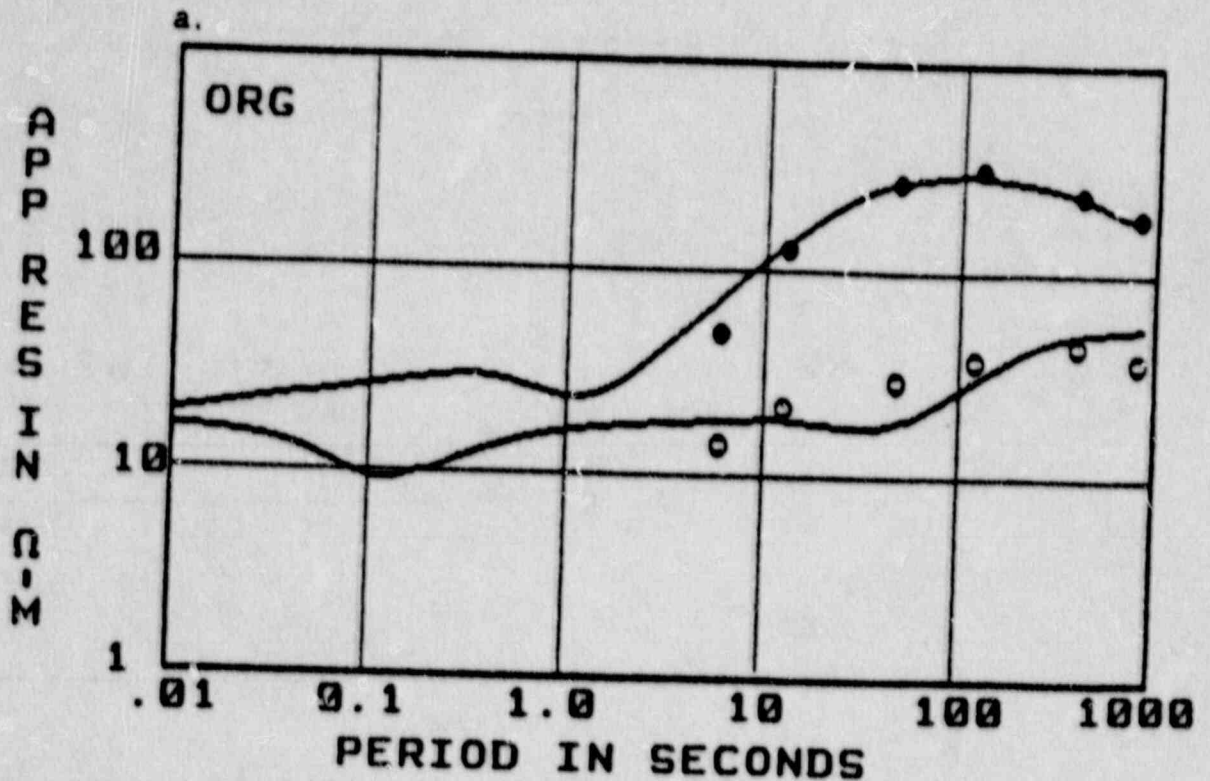
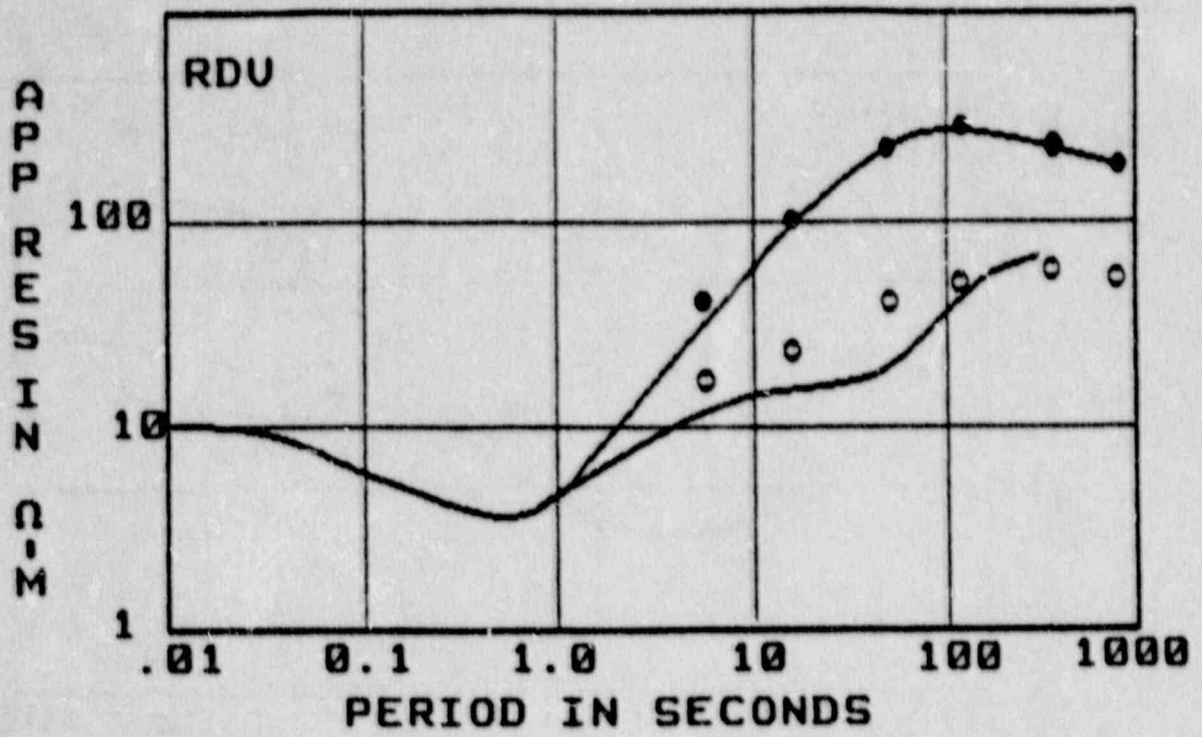


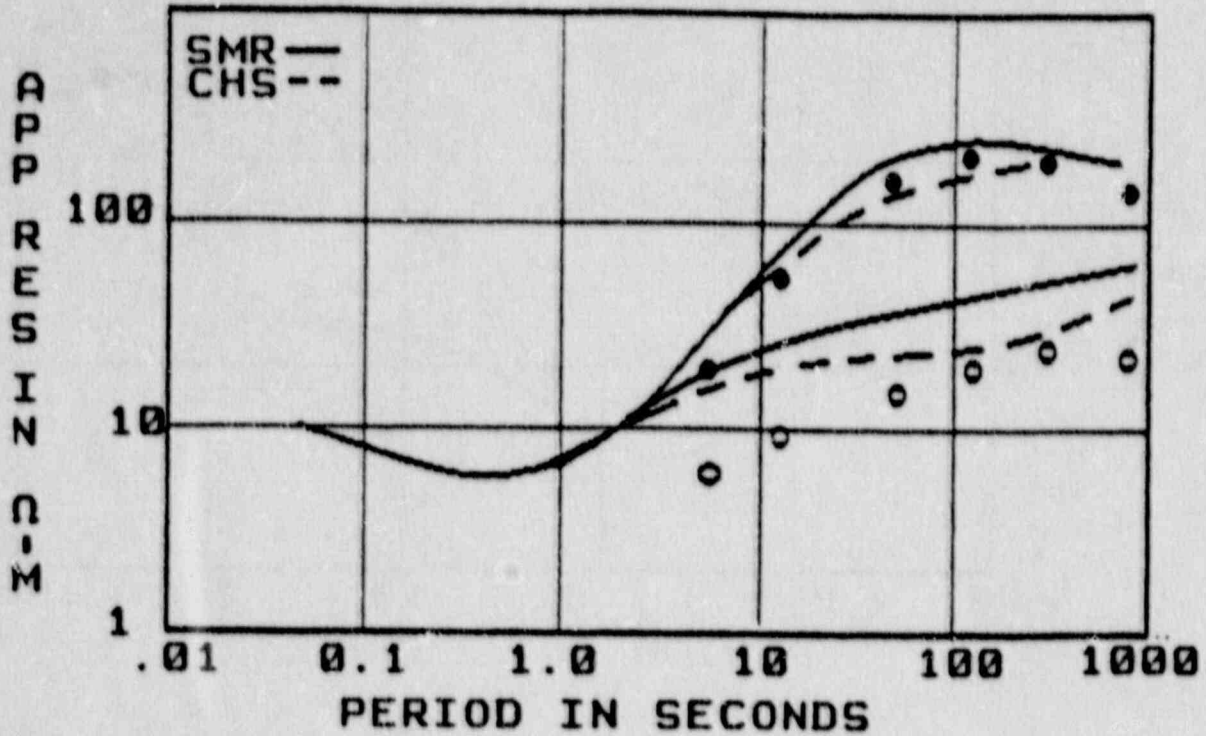
Figure 2. Comparison of field data (continuous lines) and two dimensional model computations (dots) for profile perpendicular to seacoast. The higher values of field data and the solid dots are for electric field parallel to structure (TE mode) and the lower values of field data and the circles are for electric field perpendicular to structure (TM mode).

- a. Site Orangeburg
- b. Site Ridgeville
- c. Sites Summerville and Charleston.

b.



c.



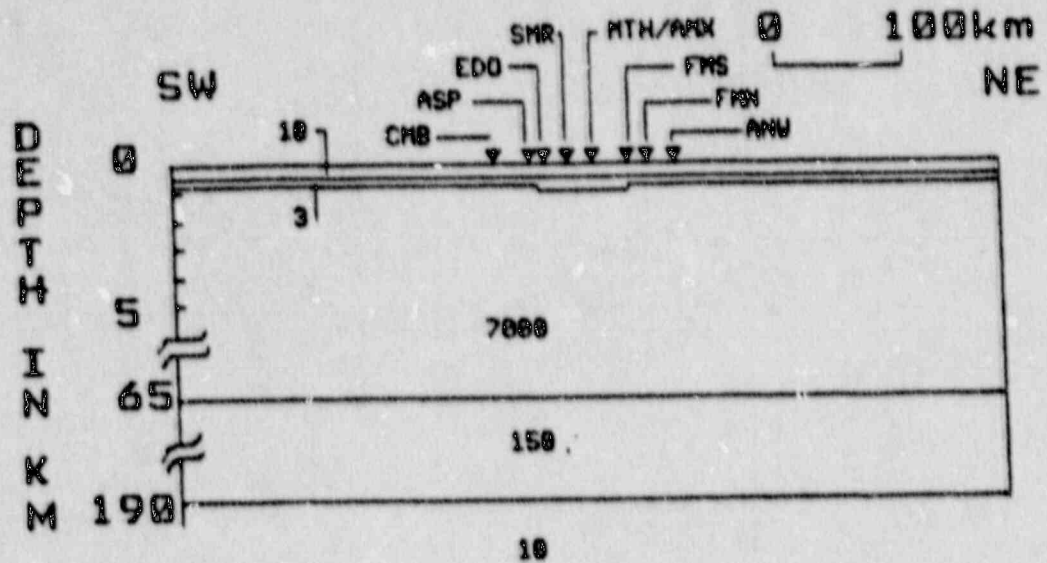


Figure 3. Two dimensional model for cross section parallel to coast, corresponding to line A-A' on Figure 1 of Young et al (1986). The symbols are the same as Figure 1 above.

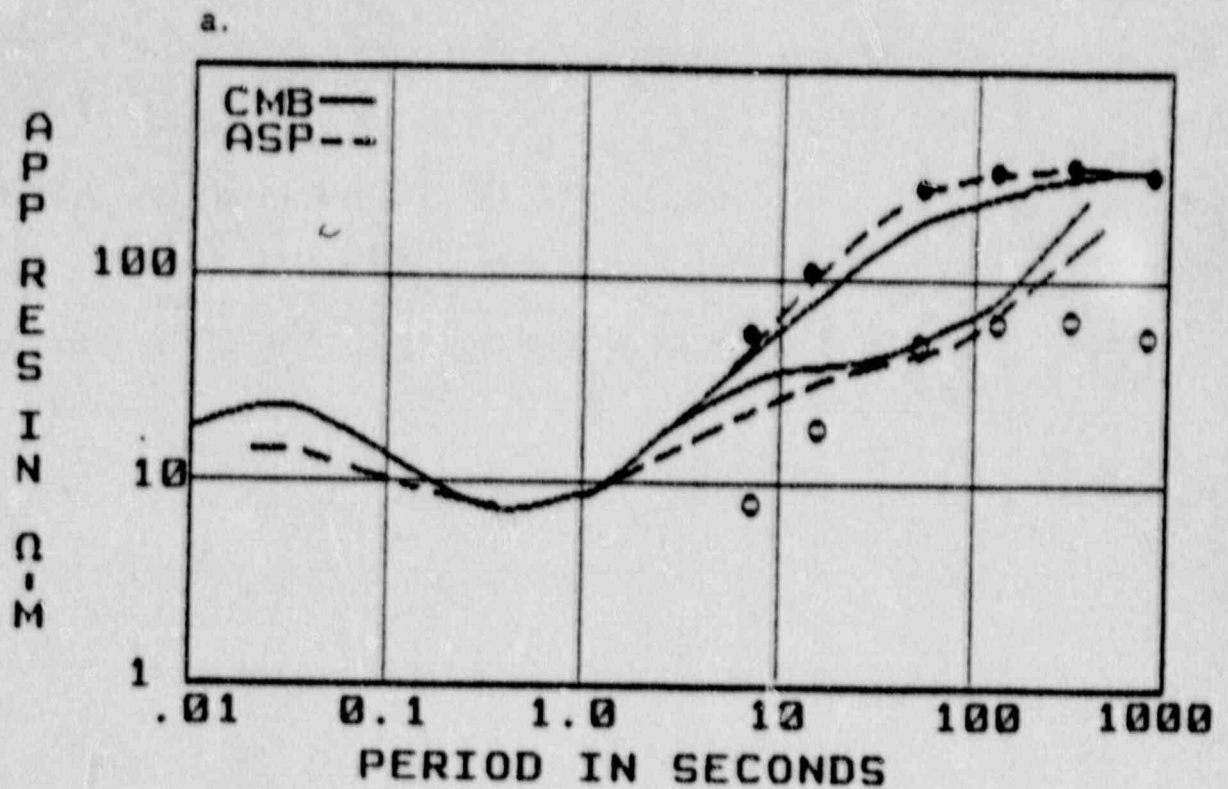
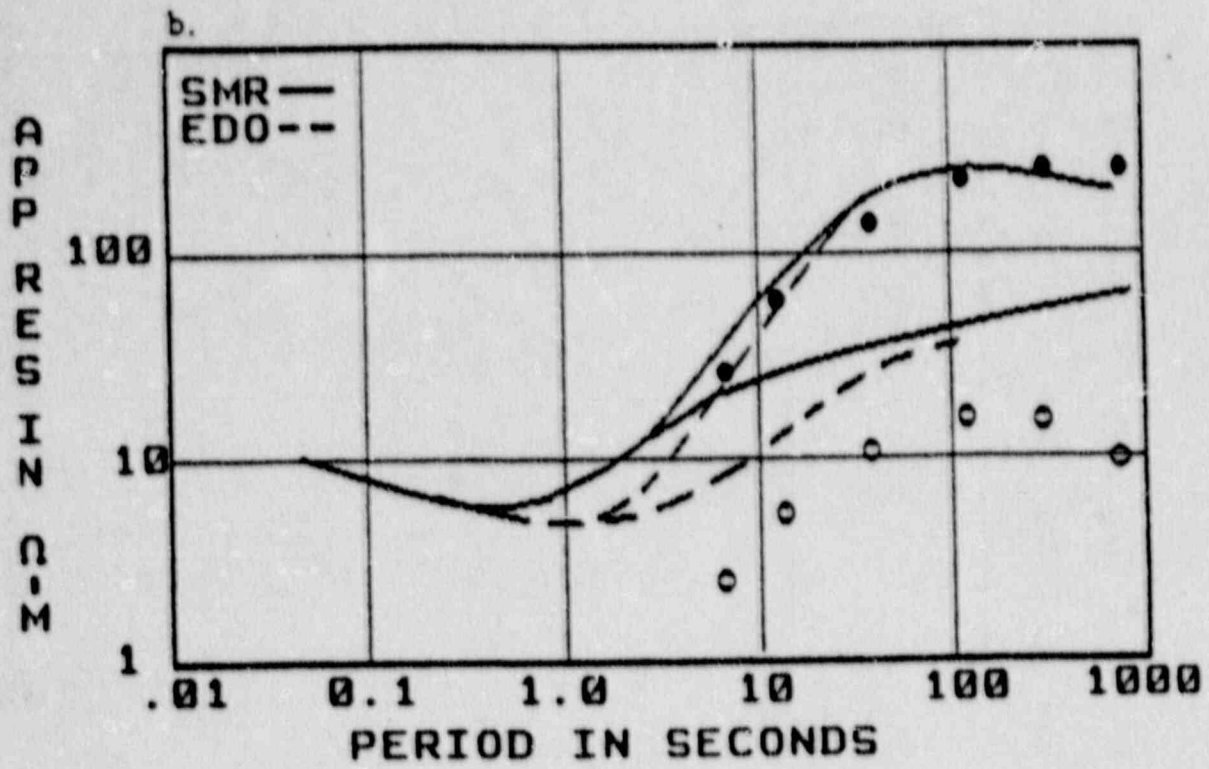
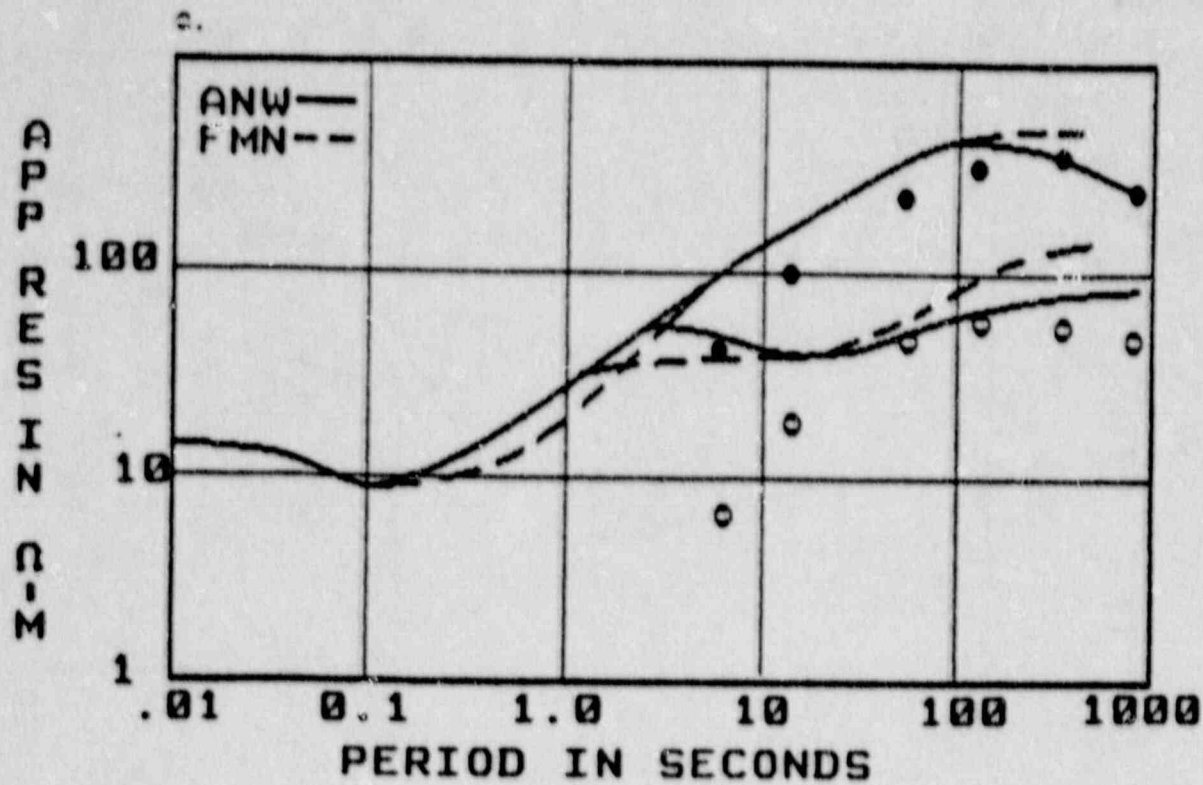


Figure 4. Comparison of field data (continuous data) and two dimensional model computation (dots) for profile parallel to seacoast. Symbols are the same as Figure 2.

- a. Sites Combahee River and Ashepoo.
- b. Sites Edisto River and Summerville.
- c. Sites Frances Marion North and Andrews.





dimensional models indicate that the resistive rocks are about 65 km thick. COCORP data show a reflection-free zone about 15 km thick underlain by reflectors. Magnetic data indicate magnetized bodies in the top of the reflection-free resistive zone. All these properties suggest that igneous rock lies beneath the coastal sediments. The reflectors below 15 km in the COCORP data which are both layered and resistive may be sedimentary rock. If so, they must be unfractured and have low porosity to maintain high resistivity. Examples would be well cemented sandstones, or unfractured limestones.

REFERENCES

Berdichevsky, M. N. and V. I. Dmitriev, 1976, Basic principles of interpretation of magnetotelluric sounding curves, pp 165-221 in Adam, A. ed., Geoelectric and Geothermal Studies, KAPG Geophysical Monograph, Akademiai Kiado, Budapest, 752 p.

Hermance, John F., 1982, The asymptotic response of three-dimensional basin offsets to magnetotelluric fields at long periods: the effect of current channeling, GEOPHYSICS, v. 47, n. 11, pp. 1562-1573.

Ku, C. C., M. S. Hsieh, and S. H. Lim, 1973, The topographic effect in electromagnetic fields, Can. J. Earth Sci., v. 10, pp 645-656.

Young, C. T. and J. C. Rogers, 1985, Magnetotelluric Soundings near Charleston, South Carolina, Project Report to Law Environmental Services.

Young, C. T., M. R. Kitchen, J. C. Rogers, J. C. Mareshal, and S. Brandwein, 1986, Magnetotelluric soundings in the Charleston, South Carolina area, Proc. Third US Natl Conf on Earthquake Engineering, Earthquake Engineering Research Institute, pp 83-91.

APPENDIX C

**INTRAPLATE STRESS AND SEISMICITY
IN THE SOUTHEASTERN UNITED STATES**

A DISSERTATION

presented to

The Faculty of the Division of Graduate Studies

by

Jian Kuang

**In Partial Fulfillment
of the Requirements for the Degree
Doctor of Philosophy
in the School of Geophysical Sciences**

Georgia Institute of Technology

December 1987

ACKNOWLEDGMENTS

The Author wishes to express his deep appreciation to Dr. L.T. Long and Dr. J.C. Mareschal for their guidance and support during the research and writing of this thesis. Thanks are also expressed to Dr. J.M. Wampler, Dr. G. Chimnas, and Dr. T.J. Schmitt for their reading and suggestions concerning this manuscript. Special thanks are due to: Dr. C.S. Kiang for supporting this research and to Ms. Linda Schwanke for her kind help in reading and correcting this manuscript. I wish to thank my classmates and friends who helped to solve various problems encountered during the course of this study. They are (alphabetically) Mr. Mitchell Craig, Mr. Andreas Georgiopoulos, Mr. Jeh-San Liow, Dr. An Tie, Mr. Lowell Whiteside, and Mr. Karl-Heinz Zelt.

This research was supported by the National Science Foundation (grant number EAR 82-18779) and a contract from the Law Engineering Testing Company through a sub-contract from the Nuclear Regulatory Commission.

TABLE OF CONTENTS

	Page
ACKNOWLEDGMENTS	i
LIST OF TABLES	iv
LIST OF ILLUSTRATIONS	v
SUMMARY	xi
CHAPTER	
I. INTRODUCTION	C-1
The Hypotheses of Intraplate Earthquake Mechanisms	C-2
Sources of Stress in the Lithosphere	C-3
Review of Stress Calculations	C-5
II. PHYSICAL MODEL AND MATHEMATICAL EQUATIONS ...	C-8
Assumptions	C-8
Physical Models and Basic Equations	C-9
Simple Testing Models	C-17
Discussions	C-22
III. CRUSTAL STRUCTURES OF THE SOUTHEASTERN UNITED STATES ..?	C-23
Geological Setting	C-23
Geophysical Study of Crustal Structures	C-24
Summary of Crustal Structures	C-26
IV. SEISMICITY AND STRESS OF THE SOUTHEASTERN UNITED STATES	C-28
Seismicity	C-28

	Contemporary Stress Field	C-29
V.	COMPUTED STRESS FIELD	C-33
	Parameters and Loads	C-34
	The Southern Appalachian Region	C-37
	The Charleston Area and Continental Margin	C-39
VI.	CONCLUSIONS AND DISCUSSIONS	C-44
	FIGURES	C-48
	BIBLIOGRAPHY	C-89

LIST OF TABLES

Table		Page
2-1	Comparing Stresses for Different Degrees of Compensation.....	C-21
5-1	Average Values of Laboratory Mechanical Properties of Rocks and A Minerals.....	C-34
5-2	Elastic Parameters.....	C-35
5-3	Coordinates of Corners.....	C-40

LIST OF ILLUSTRATIONS

Figure	Page
1-1	Map of the eastern United States and adjacent Canada showing the seismic frequency for the period 1800-1972 (from Hadley and Devine, 1974). C-48
2-1	The geometry and coordinate system for calculation of stress in a layered elastic slab (lithosphere) floating on an inviscid fluid (asthenosphere). . . C-49
2-2	Stresses and displacements under a surface disk load. The unit of displacement is $1/1000 H$, where H is the thickness of the slab. The unit of distance is H . The unit of stress is in P , where P is the magnitude of the given load.
a.	Horizontal displacement U_x contours at $z=0$ (surface). C-50
b.	Vertical displacement U_z contours at $z=0$ C-50
c.	Horizontal displacement U_x contours at $z=0.5H$ C-51
d.	Horizontal displacement U_x contours at $z=H$ C-51
e.	The SNPPSA at $z=0$. (the Schmidt Net Projection of Principal Stress Axis). The open circle stands for the maximum extensional (S_1 or T) axis, the solid circle represents the maximum compressive (S_3 or P) axis and the dot is the intermediate axis (S_2 or B) axis. C-52
f.	Stress difference (S_1-S_3) contours (SDC) at $z=0$ C-52
g.	SNPPSA at $z=0.5H$ C-53
h.	SDC at $z=0.5H$ C-53
i.	SNPPSA at $z=H$ C-54
j.	SDC at $z=H$ C-54

2-3	Stresses and displacements under a surface dipole load.	
a.	Horizontal displacement contours U_x at $z=0$.	C-55
b.	Vertical displacement contours U_z at $z=0$.	C-55
c.	Horizontal displacement contours U_x at $z=0.5H$.	C-56
d.	Horizontal displacement contours U_x at $z=H$.	C-56
e.	SNPPSA at $z=0$.	C-57
f.	Stress difference (S1-S3) contours (SDC) at $z=0$.	C-57
g.	SNPPSA at $z=0.5H$.	C-58
h.	SDC at $z=0.5H$	C-58
i.	SNPPSA at $z=H$.	C-59
j.	SDC at $z=H$.	C-59
2-4	Stresses for the three-dimensional model with a harmonic load on the surface. Stresses are plotted as a function of the wavelengths of the load and depth. Stresses are divided by the amplitude of the load.	C-60
a.	Shear stress T_{xz} .	
b.	Horizontal normal stress T_{xx} .	
c.	Vertical normal stress T_{zz} .	
2-5	Stresses for the two-dimensional model with a harmonic load on the surface. Stresses are plotted as a function of the wavelengths of the load and depth. Stresses are divided by the amplitude of the load.	C-61
a.	Horizontal normal stress T_{xx} .	
b.	Shear stress T_{xz} .	
2-6	Stresses for the three-dimensional model with a harmonic load on the surface. Stresses are plotted as a function of the wavelengths of the load, depth and the elastic parameters. Lamé's parameter in top layer ($z=0-0.4H$) is 10 GPa which is one quarter of that of second layer. Stresses are divided by the amplitude of the load.	C-62

a.	Horizontal normal stress T_{xx} .	
b.	Shear stress T_{xz} .	
2-7	Stresses for the three-dimensional model with a harmonic load on the surface. Stresses are plotted as a function of the wavelengths of the load, depth and the elastic parameters. Lamé's parameter in top layer ($z=0-0.4H$) is 80 GPa which is two times of that of second layer. Stresses are divided by the amplitude of the load.	C-62
a.	Horizontal normal stress T_{xx} .	
b.	Shear stress T_{xz} .	
3-1	Topographic contours (in meters) of the Southern Appalachians. Contouring interval is 50 meters.	C-63
3-2	Topographic and bathymetric contours (in meters) of the Coastal Plain and eastern continental margin centered at Charleston, South Carolina. Contouring interval is 100 meters.	C-64
3-3	Map of the study area showing the geologic provinces (After Hatcher and Zietz, 1980).	C-65
3-4	The Bouguer gravity anomalies (in mGal) of the Southern Appalachians. Contouring interval is 5 mGal.	C-66
3-5-a.	The original Bouguer gravity anomalies of the Coastal Plain and the eastern continental margin centered at Charleston, South Carolina (before bathymetric correction). Contouring interval is the same in Fig. 3-4.	C-67
3-5-b.	Bouguer anomaly after bathymetric correction.	C-68
3-6	Gravity, magnetic and bathymetric profiles across the southeastern continental margin (From Hutchinson et al., 1983).	C-69
4-1	Historical seismicity (1754-1970) and definition of seismic zones in the southeastern United States (From Bollinger, 1973).	C-70
4-2	Epicenters for recent earthquakes ($M > 0.0$) in the southeastern United	

	States from July 1977 to 1985 (From Sibol and Bollinger, 1986).	C-71
4-3	Seismicity (1961-1975) in the South Carolina-Georgia seismic zone (From Tarr, 1977).	C-72
4-4	Stress map of the eastern United States (from Zoback, 1983).	C-73
5-1	Depth for 58 earthquakes in the Southern Appalachians (from Johnston et al., 1985).	C-74
5-2	Rock strength and depth relations (from Meissner and Strenhlau, 1982). Dry: measurements performed on a great number of dry samples, no pore pressure; wet: pore pressure, assumed to be hydrostatic; V + M: measurement on vermiculite and montmorillonite.	C-75
5-3	Loading for stress calculation in the Southern Appalachians. Contouring interval is 5 MPa.	C-76
	a. Surface load.	
	b. Load at upper-lower crustal boundary, $z=20$ km.	
	c. Load at the Moho, $z=40$ km.	
5-4	Local stress field of the Southern Appalachian area at 10 km depth. The unit of stress is in MPa.	C-77
	a. The coordinates of the study area.	
	b. Deformation shows the direction of local horizontal stress field.	
	c. Stress difference contours (SDC). Contouring interval is 2.5 MPa.	C-78
	d. SNPPSA.	
5-5	The total stress field which combines the local field (Fig.5-4) with a 20 MPa N60°E regional horizontal compression.	C-79
	a. SDC. Contouring interval is 2.5 MPa.	
	b. SNPPSA.	
5-6	The total stress field which combines the local field (Fig.5-4) with a 20 MPa East-West regional horizontal compression.	C-80

- a. SDC. Contouring interval is 2.5 MPa.
- b. SNPPSA.
- 5-7 The total stress field which combines the local field (Fig.5-4) with a 20 MPa S75°E regional horizontal compression. C-81
 - a. SDC. Contouring interval is 2.5 MPa.
 - b. SNPPSA.
- 5-8 Loading for stress calculation in the Coastal Plain-continental margin. Contouring interval is 5 MPa. C-82
 - a. Surface load.
 - b. Load at upper-lower crustal boundary, z = 15 km.
 - c. Load at the Moho, z = 30 km.
- 5-9 Local stress field of the Coastal Plain and continental margin at 10 km depth. The unit of stress is in MPa. C-83
 - a. Coordinates of the study area.
 - b. Deformation shows the direction of local horizontal stress field.
 - c. Stress difference contours (SDC). Contouring interval is 5.0 MPa. C-84
 - d. SNPPSA.
- 5-10 The total stress field which combines the local field (Fig.5-9) with a 30 MPa N60°E regional horizontal compression. C-85
 - a. SDC. Contouring interval is 5.0 MPa.
 - b. SNPPSA.
- 5-11 The total stress field which combines the local field (Fig.5-9) with a 30 MPa East-West regional horizontal compression. C-86
 - a. SDC. Contouring interval is 5.0 MPa.
 - b. SNPPSA.
- 5-12 The total stress field which combines the local field (Fig.5-9) with a 30 MPa S80°E regional horizontal compression. C-87

- a. SDC. Contouring interval is 5.0 MPa.
 - b. SNPPSA.
- 5-13 The total stress field which combines the local field (Fig.5-9) with a 30 MPa S70°E regional horizontal compression. C-88
- a. SDC. Contouring interval is 5.0 MPa.
 - b. SNPPSA.

SUMMARY

The southeastern United States is considered a relatively stable and aseismic region within the North American Plate. Small earthquakes in the southeastern United States are concentrated in a few small areas, such as southeastern Tennessee and the Charleston, South Carolina area. One exception is the 1886 Charleston earthquake which is the largest recorded earthquake in the southeast. The cause of intraplate earthquakes is still an unresolved problem in tectonics. This study tries to find the relationship between the stress induced by topography and density variations within the lithosphere and intraplate seismicity in southeastern Tennessee and the Charleston area.

An elastic lithosphere overlying an inviscid fluid asthenosphere is modeled in three-dimensions and a Fourier transform solution for stresses and displacements induced by surface and internal loads is developed. Several simple surface loads are tested using this model. The derived three-dimensional solution for a surface harmonic load is virtually consistent with the two-dimensional analytic solution (Artem'jev et al., 1972). This three-dimensional Fourier transform technique has been applied to the Southern Appalachians and the Coastal Plain-continental margin centered at Charleston, South Carolina. The magnitude of the local stress, which is induced by topography and lithospheric density variation, is on the order of tens of MPa. The local stresses could be modified and amplified by the superposition of regional tectonic stresses. The calculated local stress field is well correlated with the seismicity in the Southern Appalachians, but not in the Charleston region. We propose that most earthquakes in eastern Tennessee are associated with density inhomogeneity in the crust and changing surface topography. The Coastal Plain area may belong to a different stress regime in which the state of stress may be described by the combination of local and regional stress field.

CHAPTER I

INTRODUCTION

The southeastern United States is a relatively stable tectonic region inside the North American Plate. The present physiographic features were emplaced during the Tertiary when the Atlantic opened. Since then, this area has not experienced major tectonic activity. The region is almost aseismic with few significant earthquakes. Small earthquakes (magnitudes less than 4.0) in the southeastern United States are confined to a few restricted regions, such as the Valley and Ridge and the Blue Ridge provinces of eastern Tennessee, western North Carolina and the Summerville-Charleston, South Carolina area (Bollinger, 1973). However, there was one major earthquake—the 1886 Charleston earthquake of an estimated magnitude of 6.8 to 7.1 (Bollinger et al., 1977), which is the largest recorded event in the southeastern United States. It caused about 60 deaths and extensive damage to the city of Charleston (Rankin, 1977).

Since the advent of plate tectonics theory, plate boundary seismicity has been relatively well understood. Observations indicate that about 90 percent of the seismic activity around the world is plate boundary related. The spatial distribution of earthquakes and their focal mechanisms are controlled by the nature of the plate boundary (Sykes, 1967; Isacks et al., 1968). The remaining 10 percent are intraplate earthquakes, occurring away from plate boundaries within the lithospheric plates, which are thought to be relatively stable. Although intraplate earthquakes are less frequent than plate boundary earthquakes, large-magnitude events in populated areas inside the continental plates present a significant hazard. The most disastrous losses caused by an intraplate earthquake occurred in 1556 in Shensi, China, in which 830,000 people died. China has a high density of intraplate earthquakes. Between 1901 and 1976, 579 earthquakes of magnitude 6 or greater have occurred. Among them, six earthquakes had a magnitude greater than or equal to 8 (Lee et al., 1978).

Intraplate earthquakes have also occurred in South America, Europe, Australia (Lomnitz, 1974; Illies, 1975; Mendiguren and Richter, 1978). In western Australia, there were four recorded intraplate events with magnitudes ≥ 6.0 between 1967 and 1983 (Dewey, 1983). Eastern Australia is also a seismically active region. A recent large event was the 1983 Tasman Sea earthquake ($M_b = 6.0$, Denham, 1985). Several earthquakes of magnitude around 6.0 occurred in the Rhine Graben (West Germany). The 1904 Oslo, Norway earthquake of magnitude 6.0 is the largest recorded event in Fennoscandinavia.

Reports of earthquakes felt in the eastern and central United States could extend back about 300 years. Since the beginning of the last century, two events with magnitudes of about 7.0 have occurred in the St. Lawrence River region and one event with the same magnitude occurred off Cape Ann, Massachusetts. In 1811 and 1812, New Madrid, Missouri had 4 large earthquakes. Their magnitudes were calculated to be 7.1 to 7.4 according to an intensity-based estimation (Nuttli, 1973).

Hadley and Devine (1974) presented a seismic frequency map of the eastern and central United States (Fig. 1-1). There are two major high frequency bands

tending northeast, the Appalachian mountains and New Madrid-Ohio River. And there are other two high frequency bands perpendicular to the Appalachians: the Boston-Ottawa seismic zone and the Charleston, South Carolina seismic zone. The map indicates that in the southeastern United States the area of highest earthquake frequency is Charleston and its vicinity.

1-1 THE HYPOTHESES OF INTRAPLATE EARTHQUAKE MECHANISMS

Understanding of tectonic processes at plate boundaries has improved tremendously during the past 20 years, but advances in understanding intraplate tectonics have been much slower. The causes of the intraplate earthquakes are among the unresolved problems in tectonics.

In-situ stress measurements (Sbar and Sykes, 1973; Zoback and Zoback, 1980) show that, in most places on the continent, horizontal stress is dominant, and horizontal compression is most common. Sbar and Sykes (1973) found that in eastern and central North America and in western Europe (north of the Alps), the greatest principal (compressive) stress from *in-situ* measurements and earthquake focal mechanisms trends generally along the direction of plate motion. They deduced that the plate driving force is the energy source of intraplate seismicity.

Since intraplate earthquakes are concentrated in very restricted areas, the inference that the plate driving forces are the main sources of intraplate seismicity has been questioned, even though the plate boundary stresses may reach up to tens of MPa (Bott and Kusznir, 1984). Sykes (1978), among many others, suggested that the intraplate earthquakes reactivate and follow pre-existing zones of weakness.

Many intraplate earthquakes are correlated with active rift zones, for example, the East African Rift and the Rio Grande rift in North America. Some earthquakes in eastern North America seem to follow inactive rifts. Erving and McGinnis (1975) proposed that the New Madrid seismic zone is associated with a buried Precambrian rift (the Reelfoot rift) which is beneath the Mississippi Embayment. This ancient rift has influenced the geological history as well as the contemporary tectonics of this area. It has controlled sedimentary basin deposits and the location of river systems, and caused localized episodes of reactivation of the old rift structure, which probably resulted in the New Madrid earthquakes (Braile et al., 1982 and 1986).

The Ottawa-Bonnechere Graben is another example of an ancient rift associated seismicity. The southeast-to-east trending fault system is one of the failed arms of a Ridge-Ridge-Ridge type triple junction centered near Montreal (Rankin, 1976), which developed during the Precambrian period and was reactivated since then. The highly active Boston-Ottawa seismic zone is parallel to the graben and past its northeastern edge.

The sutures developed during the closing of oceans may produce another type of zone of weakness for intraplate seismicity (Sykes, 1978). For example, the eastern United States seismicity seems to follow the Appalachian orogenic belt, which was formed during the closing of the Proto Atlantic Ocean. However, one unresolved problem is that the earthquake epicenters are concentrated in a few restricted regions such as southeastern Tennessee and western North Carolina (Bollinger, 1973) and are not distributed uniformly throughout the entire Appalachian mountain belt.

Some seismically active zones, such as the Georgia-South Carolina seismic zone are perpendicular to the trend of the Appalachians.

Kane (1977) found that extensive gravity highs and magnetic anomalies are near the epicenters of some major eastern North American earthquakes such as Charleston, South Carolina, and New Madrid, Missouri, although the immediate surroundings of these anomalies are relatively free of seismicity. He suggested that these anomalies are caused by mafic and ultramafic intrusions, which are serpentinized and have low strength. It has been proposed (Campbell, 1978 among others) that the regional stress may be concentrated locally because of such zones of weakness. The intraplate events near plutons may be explained by the weakness of the plutonic intruded area; stresses are amplified in the vicinity, and earthquakes may be triggered (Long, 1976; Long and Champion, 1977; Sykes, 1978).

Barosh (1986) proposed that many earthquakes in the eastern United States are associated with vertical crustal movement. For example, the Charleston seismic region may be associated with coastal subsidence and the seismicity in the Southern Appalachians may be related to crustal uplift.

The structural framework of the southeastern United States is rather complicated. There may be a diversity of earthquake causes in relation to particular events. A single hypothesis may not explain all these earthquakes.

The objective of this study is to examine the hypothesis that local seismicity in some areas of the Southeast (i.e., southeastern Tennessee and Charleston) is associated with concentration of stress induced by local loading. In some areas, local stress is mainly due to surface topography and density variations in the lithosphere. In the Southeast, the relief may cause a surface load on the order of tens of MPa. The crustal thickness changes laterally. Geophysical data indicate that the depth of the Moho varies from 50 km beneath the high mountains of the Southern Appalachians to less than 20 km at the continental margin. These changes in elevation and crustal thickness could induce stresses on the order of 100 MPa. The purpose of this study is to verify whether locally induced stress concentration correlates with seismicity. The principal stresses will be calculated and compared with the earthquake focal mechanisms and with the principal stress direction determined by *in-situ* measurements. If the computed stress field corresponds in direction to the stress field measured and inferred from earthquake focal mechanism studies, the hypothesis that local stresses trigger the seismicity will be supported.

1-2 SOURCES OF STRESS IN THE LITHOSPHERE

Geological data show that mountain chains have remained as elevated terrain for 10^7 to 10^8 years. The stresses induced by a topographic load can reach up to 100 MPa and these stresses must be balanced by stresses within the lithosphere. The observed stress distribution based on *in-situ* stress measurements, earthquake focal mechanisms and geological studies (Zoback and Zoback, 1980; Sykes, 1978, among others) indicate that the stress state of the plate interior consistently agrees with the direction of plate boundary forces. *In-situ* measurement data show that the horizontal stress level at shallow depth (several hundred meters) is on the order of tens of MPa (Sbar and Sykes, 1973). Various sources have been invoked to explain this level of stress in the lithosphere.

PLATE TECTONIC STRESS

Stress induced at a plate boundary could be transmitted a great distance by the elastic lithosphere which acts as a stress guide. Beneath diverging plate boundaries, where the lithosphere is thin, hot asthenospheric material rises and mid oceanic ridges are elevated because of the lower density of the asthenosphere. A ridge push force is produced by the gravitational sliding of the lithospheric plate away from the crest. The lithospheric plates spread away from the ridge at an average velocity of a few centimeters per year. Extensional stress will dominate in the plate near the crest of the ridge, while compressional stress will dominate the interior of the plate at greater distances from the ocean ridges (McKenzie, 1972; Sbar and Sykes, 1973).

In subduction zones, there are density variations because of the temperature difference between the subducted lithosphere and the surrounding mantle. The subducted plate is colder and denser than the mantle. This results in a slab-pull force on the subducted plate. The compressional ridge-push forces could be on the order of 20 to 30 MPa and the tensional slab-pull forces could reach 50 MPa (Bott and Kuszniir, 1984).

Transform faults offer a resistance to plate motion. The magnitude of forces associated with transform faults is not well determined, but rock strength experiments (Byerlee, 1978, for instance) suggest that the maximum shear acting on the faults is on the order of tens of MPa.

If the lithospheric plates are coupled to the asthenospheric convection flow, the viscous shear exerted at the base of the lithosphere should be approximately proportional to the viscosity of the asthenosphere and to the velocity of the plate relative to the asthenosphere. Several authors have suggested that the lithospheric plates are driven by edge forces rather than by mantle drag, and that the viscous shear on the base of the lithospheric plate will be in opposition to the plate motion (Bott and Kuszniir, 1984; Richardson et al., 1979).

MEMBRANE STRESS

The geoid is approximately an ellipsoid and its curvature varies with latitude. When a lithospheric plate moves in latitude, it deforms in order to adjust to the varying curvature. If a plate migrates away from the equator, as the curvature decreases, the edge of the plate will be in tension and the interior in compression, and vice-versa for motion toward the equator. This so called membrane stress could reach up to 100 MPa (Turcotte, 1974). Turcotte and Oxburgh (1976) suggested that rifting in East Africa was induced by the membrane stress.

THERMAL STRESS

Temperature changes within the lithosphere cause thermal expansion and contraction and thermo-elastic deformation that can lead to stress concentration inside the lithosphere. The main sources of lithospheric heat flow are heat the mantle and from the decay of radioactive material in the crust. Thermal stress due to cooling of oceanic lithosphere could reach up to 100 MPa (Bott and Kuszniir,

1984) but thermal effects may have less effect on the stress field in the continents because the continental crust is much thicker and older than the oceanic crust.

TOPOGRAPHY-INDUCED STRESS

The topography at the earth's surface, density inhomogeneities inside the lithosphere and changes in crustal thickness cause stress in lithospheric plates. The Airy isostatic compensation hypothesis is that the earth's crust is floating on a denser underlying layer (the mantle). The mass excess on the earth's surface must be balanced by a mass deficiency at the crust-mantle boundary, so that the hydrostatic equilibrium is maintained. To maintain the mountains, stresses on the order of tens of MPa are required (Artyushkov, 1973 and 1974).

FLEXURAL STRESS

Isostatic compensation can not be achieved locally because the topography contains short- as well as long-wavelength features. In tectonically active regions, mountain building is faster than isostatic adjustment. The uncompensated loading will cause a flexure in the elastic lithosphere. The extreme variation in crustal thickness occurring at continental margins is also expected to create concentration of bending stress. The flexural stress has been estimated up to 500 MPa (Bott and Kuszniir, 1984).

Bott and Dean (1972) suggested that stresses may be divided into two classes: the renewable stresses, which may restore the strain energy after it has been released by earthquakes; and the non-renewable stresses, which do not restore the strain energy dissipated during earthquakes. The ridge-push, slab-pull and topography-induced stresses are renewable. The lithospheric-flexure, plate-boundary shear, thermal and membrane stresses are non-renewable.

I-3 REVIEW OF STRESS CALCULATIONS

Previous calculations of the local stress field which is induced by topography and density variations have been based mainly on a forward method; assuming the earth's rheology and geological structures, the stress for the given load can be computed.

A frequently cited solution for crustal stress calculation is given by Jeffreys (1929). It is a model of an elastic slab over a heavy fluid with a surface harmonic load. He found that the greatest stress difference in a thin crust will be about three times larger than the given load and will occur at the base of the slab. If the thickness of the slab is much larger than the wavelength of the load, the slab may be modeled as an elastic half space. For this case an analytic solution has been derived.

Based on Jeffreys' work, Artem'jev et al. (1972) assumed that the elastic lithosphere is floating over the asthenosphere, which is treated as an inviscid fluid. They discussed how horizontal normal stress and shear stress vary as a function of the wavelength of surface harmonic loads and showed that horizontal normal stress could be 8 times greater than the given load and that shear stress could be 1.4 times

greater than the magnitude of the load for certain wavelengths. Their results suggest that a 100-mGal isostatic anomaly could induce shear stress great enough to cause an earthquake. They found a correlation between isostatic disturbances and earthquakes in the Crimea and Caucasus areas (USSR).

Isostatic compensation requires only a balance of vertical force while mechanical equilibrium requires not only vertical force but also horizontal force and all moments to be in balance. Artyushkov (1973 and 1974) considered the lithosphere as an elastic slab floating on the asthenosphere and proposed a method to evaluate average deviatoric stresses inside the crust induced by lateral density inhomogeneities and variations in crustal thickness. He estimated that lithospheric stress could be on the order of 100 MPa.

The elastic flexural stress in a thin plate caused by an ice sheet was studied by Walcott (1970). Lambeck and Nakiboglu (1980) and Lago and Cazenave (1981) studied the non-elastic lithospheric flexural stress related to bathymetry and gravity. They found that the flexural stress could be unreasonably large (1000 MPa in some situations). One way to reduce the large stress is to assume a complex rheology of the lithosphere.

Mareschal and Kuang (1986) derived a two-dimensional Fourier transform solution for a layered elastic slab over an inviscid fluid. The loads were derived from the topography and a downward-continued Bouguer anomaly could be applied at the surface or within the lithosphere. The analysis was applied to the Southern Appalachians and the Rio Grande Rift zone. The magnitude of those stresses is comparable to that of regional tectonic stresses. The topography and density heterogeneities within the lithosphere induce stresses that correlate with the seismicity of southeastern Tennessee and with the forces that act on the tectonic provinces near the Rio Grande Rift.

Some authors consider the earth's lithosphere to be a non-elastic material; several viscous and viscoelastic solutions have been derived (Lago and Cazenave, 1981; Turcotte and Oxburgh, 1976). Assuming the lithosphere is a layered, viscous Newtonian fluid, Fleitout and Froidevaux (1982, 1983) applied the Fourier transform technique to the Navier-Stokes equation and the continuity equation. Having calculated velocities and stresses, they found that the mean horizontal stress may be as great as 60 MPa, which is comparable to the ridge push. Their study also indicates that horizontal stress does not depend on the crust being elastic or visco-elastic.

Finite-element methods (e.g., Bott and Dean, 1972), Hankel transform methods (Thomson-Haskell matrix methods) applied for an inclined surface load (Kuo, 1969), conformal mapping methods (e.g., Savage and Swolf, 1986) and other techniques have been used to solve the differential equations of elasticity and to compute the surface-load-induced stress field for different geometries.

Most available solutions for a stress field induced by variations in density are two-dimensional, in which a state of "plane strain" is assumed. This assumption does not correctly represent the physical situation. Two-dimensional solutions may give the general behavior and the magnitude of the stresses but they are inadequate to determine the orientation of three-dimensional principal stresses, which are very important in the cases of the local stress field interaction with the regional field, e.g. in the Southern Appalachians.

In this study, a three-dimensional model of an elastic lithosphere overlying an inviscid fluid asthenosphere will be investigated and a Fourier transform solution of the stress field induced by surface loads and internal loads will be developed.

CHAPTER II

PHYSICAL MODEL AND MATHEMATICAL EQUATIONS

II-1 ASSUMPTIONS

The correlation between the pattern of intraplate stresses and the direction of plate boundary forces suggests that the lithosphere acts as a thin elastic shell in which the stresses could be transmitted over long distances. The lithosphere has a much higher viscosity than the asthenosphere. In many cases the viscous deformation of the upper crust is not detectable even on a geological time scale. Stresses can be maintained in the crust for long periods of times without being dissipated by non-elastic deformations. The existence of many Precambrian or Paleozoic mountain chains suggests that the continental crust can sustain stress levels of 10 to 100 MPa for more than 10^6 years. If the crust behaved viscously, old features such as the Appalachians would have dissipated under application of gravitational body force. Continental lithospheric plates are able to rebound elastically after the removal of an ice sheet from the surface (e.g., Walcott, 1972). The oceanic lithosphere shows its elastic behavior under the load of bathymetry (Lago and Cazenave, 1981). Some calculations suggest that the crust is rigid enough to be considered as an elastic medium. For example, Watts and Cochran's (1974) calculation of flexure in the Hawaiian Emperor seamount chain indicates that the lithosphere is rigid enough to support the surface load for at least 10^7 years.

In this study the basic assumption of the physical model for calculating lithospheric stresses is that for a time scale of less than 10^6 years, which is significantly less than the age of topographic loads, the earth's lithosphere behaves as an elastic slab floating over the asthenosphere. The elastic slab may be divided into many horizontal layers; in each layer the density and elastic parameters are constant.

Secondly, this study assumes that the asthenosphere is an inviscid fluid rather than a viscous fluid. The deformation in the asthenosphere is instantly completed as the loads are applied. After the North American Pleistocene ice sheet melted 10,000 years ago, the lithosphere has been uplifted in response to the removal of the load. The rebound history was recorded in raised beaches and determined by dating the ancient beaches. Those post-glacial rebound data indicate that the relaxation time of the asthenosphere is on the order 10,000 years (Haskell, 1935 and 1936; Walcott, 1972). Compared with the duration of mountain building, this relaxation time is very short. Therefore, it is reasonable to assume that for the computation of stresses in the lithosphere, the response of the asthenosphere to loading is virtually instantaneous.

The viscous shear is affected by the mantle viscosity, the pattern of convection beneath the lithospheric plates and the coupling of the lithosphere to mantle convection cells. Those factors, however, are not well determined. Schubert and Yuen (1978, among others) suggest that viscous shear will be on the order of a few MPa. Such small shear applied at the base of the lithospheric plate may have a small effect on the stress field near the base of the lithosphere, the effect of viscous

shear in the crust is small compared to the magnitude of the local stress, which is on the order of tens of MPa. Because the viscous shear beneath the lithosphere is uncertain, it will be neglected in the computing model. The asthenosphere is usually considered to coincide with the low-velocity zone and is assumed to be slightly lighter than the overlying lithosphere mantle. The thickness of lithosphere varies from 100 to 200 km in continental areas and from 50 to 100 km beneath the oceans. In the southeastern United States, the boundary of the lithosphere and asthenosphere can barely be recognized from seismic data. In this study we assume that the density of the asthenosphere is 3.10 g/cm^3 and that the average thickness of the lithosphere is 100 km in the Southern Appalachians.

The model will include the effects of surface and internal loads. The surface topography or the bathymetry and the shallow, low-density sediments induce a loading P (force per unit area) determined by the equation:

$$P = \Delta\rho gh$$

where $\Delta\rho$ is the density contrast, g is the acceleration of gravity and H is the thickness of the anomaly feature.

Density variations, such as crustal thickening or thinning, within the lithosphere are treated as internal loads. These loads are assumed to be concentrated on a very thin layer of mass excess and to act at the interface between layers. Such an assumption permits the application of linear boundary conditions. It will have no significant effect on the computed stress fields except inside the density anomalies.

II-2 PHYSICAL MODEL AND BASIC EQUATIONS

The elastic lithospheric-slab model consists of $n-1$ horizontal elastic layers above an inviscid fluid which is noted as the n -th layer (see Fig. 2-1). The depth to the top of the i -th layer is h^i ($h^1 = 0$); $h^n = H$ is the thickness of the elastic lithosphere. In the i -th layer the density and the Lamé's parameters are ρ^i , λ^i , and μ^i , respectively.

The governing equation for stress in layered elastic lithosphere is the equation of equilibrium:

$$\nabla \cdot \mathbf{T} = -\bar{g} \rho \quad (2-1)$$

where \bar{g} is the acceleration of gravity, \mathbf{T} is stress tensor and ρ is the density.

In Cartesian coordinates, the stress tensor has six independent components. In each layer, the stress is linearly related to strain by Hooke's law for an isotropic medium:

$$\mathbf{T} = \lambda(\nabla \cdot \bar{\mathbf{U}})I + \mu(\nabla \bar{\mathbf{U}} + \nabla \bar{\mathbf{U}}^T) \quad (2-2)$$

where $\bar{\mathbf{U}}$ is the displacement vector, $\nabla \bar{\mathbf{U}}^T$ is the transpose of the matrix $\nabla \bar{\mathbf{U}}$,

I is the identity tensor, λ and μ are Lamé's parameters.

The boundary conditions corresponding to the proposed model and assumptions are as follows:

At the free surface, $z = h^1 = 0$, the shear stress vanishes and the vertical normal stress is equal to the surface loads P^1 including the effect of displacement:

$$T_{xz}^1 = T_{yz}^1 = 0 \quad (2-3)$$

$$T_{zz}^1 = \rho^1 g U_z^1 - P^1 \quad (2-4)$$

At each interface $z = h^i$, the shear stress and the displacement must be continuous. The change in the normal stress across the interface must be equal to the internal load:

$$\bar{\mathbf{U}}^i = \bar{\mathbf{U}}^{i+1} \quad (2-5)$$

$$T_{xz}^i = T_{xz}^{i+1} \quad (2-6)$$

$$T_{yz}^i = T_{yz}^{i+1} \quad (2-7)$$

$$T_{zz}^{i+1} - T_{zz}^i = (\rho^{i+1} - \rho^i)gU_z^i - P^i \quad (2-8)$$

where P^i is the internal load at the interface $z = h^i$.

At the base of the lithosphere ($z = h^n = H$), shear stresses T_{xz} and T_{yz} vanish and the vertical normal stress T_{zz} equals the load induced by the displacement at the boundary.

$$-T_{zz}^{n-1} = (\rho^n - \rho^{n-1})gU_z^{n-1} \quad (2-9)$$

$$T_{xz}^n = T_{yz}^n = 0 \quad (2-10)$$

Using Eq. 2-2, Eq. 2-1 can be written for a homogeneous medium in terms of displacement:

$$(\lambda + \mu)\nabla(\nabla \cdot \bar{U}) + \mu\nabla^2 \bar{U} = -\bar{g} \rho \quad (2-11)$$

The total stress field may be separated into two parts: the hydrostatic stress and deviatoric stress. The hydrostatic stress is induced by the gravitational force and is a function of depth. Since we calculate the stress differences, only the deviatoric stress is of interest. From now on, only the deviatoric stress is discussed.

The gravitational field is a conservative field.

In order to remove the hydrostatic stress term we take $\nabla \times \nabla \times$ on both sides of Eq. 2-11, the displacement vector must satisfy the biharmonic equation

$$\nabla^4 \bar{U} = 0 \quad (2-12)$$

A convenient way to solve Eq. 2-12 is by the Fourier transform (Sneddon, 1951). The displacement vector can be transformed into the wavenumber domain.

$$\bar{U}(k_x, k_y, z) = \iint \bar{U}(x, y, z) \exp[i(k_x x + k_y y)] dx dy \quad (2-13)$$

where k_x and k_y are the wavenumbers. The inverse transform is:

$$\bar{U}(x, y, z) = \frac{1}{4\pi^2} \iint \bar{U}(k_x, k_y, z) \exp[-i(k_x x + k_y y)] dk_x dk_y \quad (2-14)$$

In the Fourier transform domain, Eq. 2-12 becomes:

$$\left(\frac{\partial^2}{\partial z^2} - k^2 \right)^2 \bar{U} = 0 \quad (2-15)$$

where $k = \sqrt{k_x^2 + k_y^2}$

In each layer the general solution for Eq. 2-15 is:

$$\bar{U} = (\bar{A} + \bar{B} k z) \exp(kz) + (\bar{C} + \bar{D} k z) \exp(-kz) \quad (2-16)$$

where vectors \bar{A} , \bar{B} , \bar{C} and \bar{D} are arbitrary constants to be determined in each layer.

The superscript i was dropped for simplicity.

There are a total of 12 coefficients to be determined for each of the $n-1$ layers of the elastic medium. Each coefficient is a function of the wavenumber k_x and k_y .

Stresses and displacements must be continuous across each interface. This gives six independent conditions for each boundary. There are three stress boundary conditions at the free surface and at the base of the lithosphere. Therefore, the total number of boundary conditions is $6(n-1)$.

The number of constants is twice the number of boundary conditions. This is because Eq. 2-16 is the general solution of Eq. 2-12, which is obtained by taking derivatives of Eq. 2-11. The solution 2-16 does not satisfy equation 2-11 for any arbitrary constants. The additional relationship can be found by substituting Eq. 2-16 into Eq. 2-11,

$$B_x = \frac{r_1 [k_x^2 A_x + k_y k_x A_y + i k k_x A_z]}{k^2} \quad (2-17)$$

$$B_y = \frac{r_1 [k_x^2 A_y + k_y k_x A_x + i k k_y A_z]}{k^2} \quad (2-18)$$

$$B_z = \frac{r_1 [i(k_x A_x + k_y A_y) - k A_z]}{k} \quad (2-19)$$

$$D_x = \frac{r_1 [i k k_x C_z - k_x^2 C_x - k_y k_x C_y]}{k^2} \quad (2-20)$$

$$D_y = \frac{r_1 [i k k_y C_z - k_y^2 C_y - k_x k_y C_x]}{k^2} \quad (2-21)$$

$$D_z = \frac{r_1 [k C_z + i k_x C_x + k_y C_y]}{k} \quad (2-22)$$

where $r_1 = \frac{\lambda + \mu}{\lambda + 3\mu}$

The number of arbitrary constants is reduced to $6(n-1)$.

The six components of the stress and three components of the displacement can then be written as:

$$\begin{aligned} T_{xx} / 2\mu = & -ik_x [r_1 + r_1 k_x^2 z / k] A_x \exp(kz) \\ & - ik_y [r_2 + r_1 k_x^2 z / k] A_y \exp(kz) \end{aligned}$$

$$\begin{aligned}
& + [r_2 k + r_1 k_x^2 z] A_2 \exp(kz) \\
& + ik_x [-r_4 + r_1 k_x^2 z / k] C_x \exp(-kz) \\
& + ik_y [-r_2 + r_1 k_x^2 z / k] C_y \exp(-kz) \\
& + [-r_2 + r_1 k_x^2 z] C_z \exp(-kz)
\end{aligned} \tag{2-23}$$

$$\begin{aligned}
T_{yy} / 2\mu = & - ik_x [r_2 + r_1 k_y^2 z / k] A_x \exp(kz) \\
& - ik_y [r_4 + r_1 k_y^2 z / k] A_y \exp(kz) \\
& + [r_2 k + r_1 k_y^2 z] A_z \exp(kz) \\
& + ik_x [-r_2 + r_1 k_y^2 z / k] C_x \exp(-kz) \\
& + ik_y [-r_4 + r_1 k_x^2 z / k] C_y \exp(-kz) \\
& + [-r_2 + r_1 k_y^2 z] C_z \exp(-kz)
\end{aligned} \tag{2-24}$$

$$\begin{aligned}
T_{zz} / 2\mu = & ik_x[r_1(1 + kz) - r_2] A_x \exp(kz) \\
& + ik_y[r_1(1 + kz) - r_2] A_y \exp(kz) \\
& + k[r_1(1 - kz) + r_3] A_z \exp(kz) \\
& + ik_x[r_1(1 - kz) - r_2] C_x \exp(-kz) \\
& + ik_y[r_1(1 + kz) - r_2] C_y \exp(-kz) \\
& - k[r_1(1 + kz) + r_3] C_z \exp(-kz)
\end{aligned} \tag{2-25}$$

$$\begin{aligned}
T_{xy} / \mu = & - ik_y[2r_1 k_x^2 z / k + 1] A_x \exp(kz) \\
& - k_x[2r_1 k_y^2 z / k + 1] A_y \exp(kz) \\
& + 2r_1 k_x k_y z A_z \exp(kz) \\
& + ik_y[2r_1 k_x^2 z / k - 1] C_x \exp(-kz) \\
& + ik_x[2k_y^2 z r_1 / k - 1] C_y \exp(-kz) \\
& + 2k_x k_y z C_z \exp(-kz)
\end{aligned} \tag{2-26}$$

$$\begin{aligned}
T_{xz} / \mu = & r_1[2k_x^2 z + k_x^2 / k + k / r_1] A_x \exp(kz) \\
& + r_1 k_x k_y [2z + 1 / k] A_y \exp(kz) \\
& + i2k_x [r_1 k z - r_3] A_z \exp(kz) \\
& + r_1 [2k_x^2 z - k_x^2 / k + k / r_1] C_x \exp(-kz) \\
& + r_1 k_x k_y [2z - 1 / k] C_y \exp(-kz) \\
& - i2\mu k_x [r_1 k z + r_3] C_z \exp(-kz)
\end{aligned} \tag{2-27}$$

$$\begin{aligned}
T_{yz} / \mu = & r_1 k_x k_y [2z + 1/k] A_x \exp(kz) \\
& + r_1 [2k_y^2 z + k_y^2 / k + k / r_1] A_y \exp(kz) \\
& + i2k_y [r_1 k_z - r_3] A_z \exp(kz) \\
& + r_1 k_x k_y [2z - 1/k] C_x \exp(-kz) \\
& + r_1 [2k_y^2 z - k_y^2 / k + k / r_1] C_y \exp(-kz) \\
& - i2k_y [r_1 k_z + r_3] C_z \exp(-kz)
\end{aligned} \tag{2-28}$$

$$\begin{aligned}
U_x = & (1 + r_1 k_x^2 z / k) A_x \exp(kz) \\
& + z(r_1 k_x k_y / k) A_y \exp(kz) \\
& + i r_1 k_x z A_z \exp(kz) \\
& + (1 - r_1 k_x^2 z / k) C_x \exp(-kz) \\
& - (r_1 k_x k_y z / k) C_y \exp(-kz) \\
& + i r_1 k_x z C_z \exp(-kz)
\end{aligned} \tag{2-29}$$

$$\begin{aligned}
U_y = & z(r_1 k_x k_y / k) A_x \exp(kz) \\
& + (1 + r_1 k_y^2 z / k) A_y \exp(kz) \\
& + i r_1 k_y z A_z \exp(kz) \\
& - (r_1 k_x k_y / k) C_x \exp(-kz) \\
& + (1 - r_1 k_y^2 z / k) C_y \exp(-kz) \\
& + i r_1 k_y z C_z \exp(-kz)
\end{aligned} \tag{2-30}$$

$$\begin{aligned}
U_z = & ir_1 k_z A_1 \exp(kz) \\
& + ir_2 k_z A_2 \exp(kz) \\
& + (1 - r_1 k) A_2 \exp(kz) \\
& + ir_1 k_z C_1 \exp(-kz) \\
& + ir_2 k_z C_2 \exp(-kz) \\
& + (1 + r_1 z / k) C_2 \exp(-kz)
\end{aligned} \tag{2-31}$$

where $r_1 = \frac{\lambda + \mu}{\lambda + 3\mu}$

$$r_2 = \frac{\lambda}{\lambda + 3\mu}$$

$$r_3 = \frac{\mu}{\lambda + 3\mu}$$

$$r_4 = 2r_2 + 3r_3$$

There are a total of $6(n-1)$ equations for the boundary conditions and the same number of arbitrary constants. Therefore, this is a well defined linear system of $6(n-1)$ equations. If all equations are independent, it admits a unique solution.

Finally, The solution (2-23 to 2-31) is inversely transformed to the space domain by the Fast Fourier Transform technique numerically.

II-3 SIMPLE TESTING MODELS

In three-dimensional Cartesian coordinates, a general closed form solution does not exist for the stress field induced by a surface load in the elastic slab over an inviscid fluid. However, some very simple loading functions are used here to see that the solutions are physically reasonable and quantitatively reliable. The solutions can also be compared with some previous two-dimensional analytical solutions (Artem'jev et al., 1972).

In all these models, the slab is homogeneous, $\lambda = \mu = 0.4 \times 10^{11}$ N/m², $\sigma = 0.25$, ρ (slab) = 2.8 g/cm³, ρ (fluid) = 3.2 g/cm³. The thickness of the elastic slab is H. Other dimensions are expressed in terms of H. In this lithospheric model, H is set as 100 km, which is the assumed thickness of lithosphere. The stresses are computed over a 7H X 7H square and the number of computation points is 8 X 8.

Since the solution is in the form of a Fourier transform, there is no actual boundary condition at the edge of the model. The Fourier Transform assumes that the function will be periodically repeated beyond the edge. In order to reduce any edge effect produced by the periodicity, we first compute the average value of the transform function, then we double the width of the area of definition. On the edge the function must be equal to the average; it is interpolated between the original function and the edge. The stresses and displacements are computed for this enlarged area, but only the result in the original central area will be used and plotted. The following examples indicate that after the boundary condition at the edge is treated in the way discussed above, the edge effect is very small.

II-3-a DISK LOAD AT THE SURFACE

A disk load of radius $2.5 H$ is put on the surface at the center of a square. The magnitude of the load is P . Under such a load, the elastic slab is bent downward at the center as shown by surface displacement contours U_x and U_z (Fig. 2-2-a and 2-2-b). Vertical displacement is about ten times greater than that horizontal displacement at the central area (the displacements are also dependent on the magnitude of P). Stress field (Fig. 2-2-e to 2-2-j) and horizontal displacement contours U_x (Fig. 2-2-c and 2-2-d) show that the slab experiences horizontal compression above the mid-plane (z approximately equal to $0.5H$) and horizontal extension below the mid-plane. Fig. 2-2-e is the Schmidt net projection of principal stress axis (SNPPSA). The convention of this study is that the stress value is positive outward which is different from the engineering convention. The maximum vertical stress T_z is equal to $0.68 P$ at the surface, is equal to about $0.34P$ at $z = 0.5H$ and gradually falls to zero at the base of the slab. Vertical stress is less than horizontal stress at all depths except near the mid-plane. According to bending theory (Timoshenko and Goodier, 1970) maximum horizontal stress should occur at the surface and the base. Horizontal stress and displacement at the mid-plane should vanish. Vertical stress is maximum at the surface and vanishes at the base. The calculations show that the maximum horizontal stress (about $3.0 P$) does occur at the surface and the base, but the horizontal displacement does not vanish at $z = 0.5H$. This is because the boundary conditions at the base are different from the case of pure bending and $z = 0.5H$ does not coincide with the neutral plane. But at $z = 0.5H$ the horizontal displacement in central area is only 6 percent of that of the surface (or base) horizontal displacement, and the maximum horizontal stress is about $0.04P$. The magnitude of the stress field also depends on the wavelength of the load. The relation between load wavelength and stress will be discussed in a later section.

Fig. 2-2-a and 2-2-c illustrate that the magnitude of horizontal movement U_x at $z=0$ and $z=H$ is the same but that the displacement are in opposite directions. The symmetry of the displacements implies that horizontal principal stress at the surface and the base are in opposite way.

II-3-b DIPOLÉ LOAD AT THE SURFACE

Fig. 2-3-a and 2-3-b show the vertical and horizontal displacement due to a surface dipole load in which a positive disk is located in the southwestern quadrant and a negative disk is located in the northeastern quadrant. The stress field (Fig. 2-3-e to 2-3-j) and displacement contours (Fig. 2-3-c and 2-3-d) show that the slab is twisted by the dipole load. Above the mid-plane, the northeastern part is uplifted and stretched away from the negative disk load. The southwestern part is depressed and pulled toward the positive disk load. Vertical displacements change little across the slab, but the magnitude and direction of horizontal displacements change dramatically. In the mid-plane the horizontal displacements drop to minimum. Below the mid-plane, the northeastern quadrant moves toward the negative disk load and the southwestern quadrant is pushed away from the positive load. Under such a dipole load (the maximum value is P) the magnitude of maximum vertical

displacement (below the load) is about $0.01H$ across the slab and horizontal displacements are about $0.0018H$ near the surface and base. Horizontal displacements are extremely small near the mid-plane, and, consequently the horizontal stress is very small. The stress fields show that the positive load acting at the southwestern quadrant induces the local compression above the mid-plane and extension below the mid-plane, meanwhile the negative load acting at the northeastern quadrant causes the opposite effect.

II-3-c STRESS AS A FUNCTION OF WAVELENGTH OF THE LOAD

The stress field is not only dependent on the magnitude of the load but also on its wavelength.

The effect of a two-dimensional surface harmonic load is considered in order to examine how the stress field varies with the wavelength.

$$F(x,y) = P \cos(k_x x) \cos(k_y y)$$

$$\chi = kH = 2\pi H / \lambda$$

where $k = \sqrt{k_x^2 + k_y^2}$, P is the magnitude of the load, λ is its wavelength, k_x and k_y are the wave-numbers and H is the thickness of the slab.

Fig. 2-4-a to 2-4-c show the three-dimensional Fourier transform solutions of maximum horizontal normal stress T_{xx} , vertical normal stress T_{zz} , and shear stress T_{xz} as functions of wavelength of the load and depth. These curves show that when χ is about 0.5 to 0.6, which corresponds to a wavelength approximately equal to 10 times the thickness H , both T_{xx} and T_{zz} reach their maximum value. The mid-plane is a "turning point". At the "turning point", the maximum shear stress occurs for large wavelength (χ is less than or equal to 2.0) and the horizontal normal stress changes sign. Maximum horizontal normal stress occurs near the surface and the base of the slab and reaches up to 5 times that of the given load. At the mid-plane, the maximum shear stress could reach up to $0.92 P$. Vertical normal stress, T_{zz} (Fig. 2-4-c), decays very rapidly with the decrease of wavelength of the load, it reaches the maximum value at the surface, and vanishes at the base. For long wavelength load, maximum vertical stress at the surface equals the load.

Artem'jev et al. (1972) solved a similar problem in two-dimensions; their calculations indicate the same trend as this study but there are large differences in the magnitudes. The magnitudes of the shear and horizontal stress of the three-dimensional model are only about 70 percent of those the two-dimensional model of Artem'jev et al. The reason for the differences in magnitude of the stress may come from the assumption of plane strain for the two-dimensional problem. In order to verify that this difference is explained by the two-dimensional model, a two-dimensional model is simulated by keeping the load constant in the X direction, see Fig. 2-1). The result (Fig. 2-5) is virtually identical to that of Artem'jev et al.

Fig. 2-6 and Fig. 2-7 show behavior of stress in response to a change in elastic parameters. When the Lamé's parameter in the top layer (0 to $0.4 H$) decreases from 0.4 to $0.1 \times 10^{11} \text{ N/m}^2$, stress is concentrated below this weaker layer and the

"turning point" shifts downward to about $0.6H$. Maximum horizontal stress in the top layer decreases 54 percent, maximum shear stress decreases 18 percent (Fig. 2-6).

Alternately, stress will concentrate in the top layer when the λ and μ are increased to $0.8 \times 10^{11} \text{ N/m}^2$. Maximum horizontal stress in the top layer increases 39 percent. The turning point shifts upward to about $0.4H$ (Fig. 2-7).

II-3-d A DISK LOAD AND ITS INTERNAL COMPENSATION

The stress field induced by a mountain and its compensating root may be modeled by the combination of a negative internal disk load with a positive surface disk load. For a given surface load, the state of horizontal stress also depends on the nature of the compensation. Table 2-1 lists the calculated results and compares the stresses in the cases of complete compensation, over compensation and under compensation. In the models given in Table 2-1, a positive disk load is located at the surface and a negative load is located at $z = 0.5H$.

In the state of complete compensation, the negative load bends the slab upward. The bending effect caused by the positive disk load is canceled, but the vertical stress is added. Therefore horizontal displacements are very small. Compared with the vertical stress the horizontal stress is very small (the horizontal stress magnitude is about one sixth to one fourth of the vertical stress in and above the mid-plane) across the entire slab. The vertical stress is almost constant across the slab above the level where the internal load is located, the maximum value equals the given load P . Below the level of compensation, the vertical stress falls to zero.

In contrast, the upper portion of the slab will be in horizontal extension for the case of over compensation, and in horizontal compression for the case of under compensation. Table 2-1 lists cases of 20 percent over compensation and a 20 percent under compensation.

From consideration of over and under compensation, one may deduce that the stress field caused by the combined loads (surface load plus compensation) is quite different from a single surface load.

Generally speaking, the stresses in model A are greater than the stresses in Model B. The great vertical stress in model A is caused by both the surface load of $1.0 P$ and the compensation load of $0.8 P$. It is almost constant across the upper portion of the slab. Model B has a $0.2 P$ load at the surface and induces an extensional horizontal stress field which is comparable to the horizontal stress in the model A, the magnitude of vertical stress is very small.

TABLE 2-1

COMPARING STRESSES FOR DIFFERENT DEGREES OF COMPENSATION

DEPTH	STRESS	MODEL A	MODEL B	MODEL C	MODEL D
0	T_{XX}/P	-2.97	-0.71	-0.14	+0.42
	T_{ZZ}/P	-0.68	-0.94	-1.00	-1.06
	$(S1-S3)/P$	2.34	0.23	0.88	1.51
0.25H	T_{XX}/P	-1.42	-0.42	-1.70	+0.08
	T_{ZZ}/P	-0.57	-0.92	-1.00	-1.08
	$(S1-S3)/P$	1.12	0.51	0.85	1.18
0.5H	T_{XX}/P	-0.03	-0.19	-0.23	-0.27
	T_{ZZ}/P	-0.34	-0.87	-1.00	-1.13
	$(S3-S1)/P$	1.32	0.71	0.78	0.89
0.75H	T_{XX}/P	+1.38	+0.29	+0.03	-0.23
	T_{ZZ}/P	-0.11	+0.02	0	+0.02
	$(S3-S1)/P$	1.54	0.33	0.03	0.27
1.0H	T_{XX}/P	+2.87	+0.53	-0.04	-0.62
	T_{ZZ}/P	0	0	0	0
	$(S3-S1)/P$	2.90	0.57	0.05	0.68

Model A: A disk load P (Fig.2-2) at the surface

Model B: A disk load at the surface with a negative load of 80 per cent (20 per cent under compensation) at $z=0.5H$.

Model C: A disk load at the surface with a negative load of complete compensation at $z=0.5H$.

Model D: A disk load at the surface with a negative load of 120 per cent (20 per cent over compensation) at $z=0.5H$.

DISCUSSION

(1) A single central load applied at the surface (such as an uncompensated mountain) bends the elastic lithosphere downward. The vertical displacement is large but changes little across the slab; meanwhile the magnitude of horizontal displacement is small (compared to vertical displacement) but changes rapidly, both in magnitude and direction. The horizontal flexural stress is greater than the vertical stress at all depths.

(2) A negative central load (such as those that would be caused by overcompensation inside the earth or lower density features at the surface) bends the lithospheric slab upward and causes extensional stress in the crust.

(3) Since the equations are linear, the solutions for different sources can be superposed. The resultant surface topography load and its compensation will cause a nearly constant vertical stress above the compensation level, provided that the compensation is complete. In that case, the magnitude of horizontal stress is less than that of vertical stress.

(4) The simple tests summarized in Table 2-1, show that the stress field calculated from isostatic anomalies alone (such as discussed by Artem'jev et al., 1972) is quite different from the stress computed from the topographic load and its under (or over) compensation indicated by the Bouguer anomaly. In the latter case, the stress is greater.

(5) The stresses calculated from three-dimensional models are formally consistent with the two-dimensional results but less in magnitude. The maximum flexural stress in the elastic slab will be twice as much as the surface load. In the three-dimensional model, the magnitude of stresses is comparable to the regional stresses and there is no need to adjust the material properties in order to reduce the stresses (e.g., Lago and Cazenave, 1981).

(6) Under a surface load of magnitude P , the maximum horizontal stress may reach up to $5.0 P$ near the surface. Shear stress (T_{xz} and T_{yz}) may reach up to $1.0 P$ in the middle of the slab. And the maximum vertical stress is on the order of P .

(7) The magnitude of stress (for both the horizontal normal stress and the shear stress) depends on the ratio between the thickness of the elastic slab and the wavelength of the load. This dependence is not simply a linear relation. A 20 percent variation of the thickness in the elastic slab will cause a 13 percent change in horizontal stress T_{xx} near the surface and less than a 10 percent change in shear stress T_{xz} in the top layer.

(8) A 10 percent change of density contrast between the lithospheric slab and underlying fluid has little effect on the stress field in the top layer.

CHAPTER III

CRUSTAL STRUCTURES OF THE SOUTHEASTERN UNITED STATES

III-1 GEOLOGICAL SETTING

Two areas from the southeastern United States will be studied in this paper: the Southern Appalachian area and the Atlantic Coast-continental margin. The topographic and bathymetric maps are shown in Fig. 3-1 and Fig. 3-2.

The Appalachian mountain belt extends along the east coast of North America. The geological structures of the Southern Appalachians can be divided into several provinces parallel to the trend of the topography (Fig. 3-3). The western-most province, the Appalachian Plateau or Cumberland Plateau, is underlain by nearly horizontal Paleozoic sedimentary rocks. In the Valley and Ridge province, the Paleozoic sedimentary rocks are characterized by long parallel folds and thrust faults. The axes of the folds and the strikes of the thrust faults run generally northeast to southwest and follow the trend of the Southern Appalachians. Those structures are thought to be shallow and without involvement of the Precambrian Grenville basement (Rodgers, 1949; Cook et al., 1979). Geologic evidence (Colton, 1970) indicates that the Basins in eastern Tennessee has more than 10 km of sedimentary cover. Some parallel faults at depths of 10 to 25 km in the Precambrian basement can be seen in the COCORP profile.

The Blue Ridge province is separated from the Valley and Ridge province by a southeastward dipping thrust fault system which consists of the Holston Mountains, Great Smoky, Cartersville and Talladega Thrust faults. The Blue Ridge Province is composed predominantly of extensively metamorphosed rocks. The highest mountains of the Southern Appalachians are the Great Smoky Mountains. They are located in the Blue Ridge Province along the Tennessee-North Carolina state line.

The Brevard zone, a narrowly deformed shear belt, separates the Blue Ridge from the Piedmont province. The Piedmont Province can be further divided into three belts based on the grade of metamorphism and lithology. The Inner Piedmont subprovince is a high-grade metamorphosed crystalline rock belt intruded by plutons.

The Kings' Mountain belt is a narrow band of metamorphosed sedimentary and volcanic rocks. The Charlotte belt consists of remnants of a volcanic arc with metamorphosed sediments (Cook et al., 1980).

The Southern Appalachians are bounded to the southeast by the Atlantic Coastal Plain, which consists of Cenozoic sedimentary rocks that overlap the Piedmont province and cover the crust that was thinned during the Triassic-Jurassic opening of the Atlantic. The average thickness of sedimentary deposits is 2 to 3 km (Marine and Siple, 1974).

The relief of the southeastern continental margin of the United States is complicated. Near South Carolina, the continental margin may be divided seaward into two regions, the Carolina platform and the Carolina trough. The Carolina Platform is approximately 300 km wide and it is bordered by the Atlantic Coastal Plain to the west. The Southeast Georgia Embayment is located in the northwest

portion of the platform and between the Cape Fear Arch and the Peninsula Arch of Florida. The Brunswick Graben is located in the eastern part of the platform, the present continental shelf. The Carolina Trough is about 80 km wide and 400 km long and located between the Blake Fracture zone to the south and the Norfolk Fracture zone to the north. Sykes (1978) proposed that a possible transform fault drawn along the direction of the Blake Fracture zone passes very close to the Charleston area and is nearly coincident with the South Carolina-Georgia seismic zone. In the Carolina Trough the sedimentary deposits are 5 km to 9 km thick, and the depth reaches approximately 2,000 meters (Grow, 1981).

The origin of most of the structures in the southeastern United States can be explained by the closing of the Proto-Atlantic, which was completed 250 million years ago. The subsequent opening of the Atlantic Ocean was accompanied by crustal thinning and the formation of rift basins, many of which are under the present Coastal Plain. Detailed evolutionary models have been proposed by many authors, some of which are Bird and Dewey (1970), Dewey and Kidd (1974), Hatcher (1978), Ross (1979) and Cook et al. (1980).

III-2 GEOPHYSICAL STUDY OF CRUSTAL STRUCTURE

Geophysical surveys, including seismic reflection, seismic refraction, gravity and aeromagnetics, have yielded information on the crustal structure in the Southern Appalachians, Atlantic Coastal Plain and continental margin.

The COCORP (the Consortium for Continental Reflection Profiling) reflection survey in the Southern Appalachians (Cook et al., 1979, 1983) suggested that an allochthonous sheet was thrust westward hundred kilometers during the closure of the Proto-Atlantic Ocean in the late Paleozoic (250 to 500 million years ago) and formed the present Blue Ridge and Inner Piedmont. The COCORP surveys support the thin-skinned tectonics concept which was first recognized by Rich (1934) and supported later by Rodgers (1949) on the basis of geological evidence.

Seismic reflection data in the Southern Appalachians did not resolve the geological structures of the lower crust and the depth to the Moho. The interface between upper and lower crust and the depth to the Moho has been determined by refraction seismic surveys and earthquake travel-time studies.

Warren (1968) shows several seismic refraction profiles across the Southern Appalachians. One of them is perpendicular to the trend of the regional structures. It starts in Campbell, Kentucky near the Tennessee border, and ends in Dahlonega, Georgia. This profile crosses the Appalachian Plateau and the Valley and Ridge province in Tennessee and part of the Blue Ridge in Georgia. The results indicate that the thickness of the upper crust varies between 10 and 18 km with an average P-wave velocity of 6.1 km/s. The Moho depth varies from 38 km to 45 km. The lower crust average P-wave velocity is 6.7 km/s and the upper mantle velocity is 8.0 km/s. Beneath Chattanooga, Tennessee, the Moho depth is 45 km.

After studying the Pn wave arrivals and using time term analysis, Long and Liow (1986) found that the crustal thickness varies from 33 km in the Georgia Piedmont and 35 km in central Alabama to 50 km in the Blue Ridge of eastern Tennessee and northern Georgia.

A refraction profile along the axis of the Piedmont province of Georgia and South Carolina with an extension to the Atlantic Coastal Plain was studied by Kean and Long (1980). It does not clearly show the interface between the upper and lower crust in the Piedmont. The velocity near the Moho discontinuity could be about 6.7 km/s and the depth to the Moho varies from 35 km in the Piedmont to 40 km in the Coastal Plain near the Piedmont and decreases to 29 km near the coast of South Carolina.

On the Basis of synthetic seismogram analysis, Lee (1980) proposed a velocity model for the Coastal Plain. The topmost layer velocity is 5.18 to 5.54 km/s and its thickness is 6 km. The P-wave velocity is 6.6 km/s in the lower crust, and 8.0 km/s in the upper mantle, the depth to the Moho is 33 km.

The refraction investigations of Propes (1985) show that, in the Southern Appalachians, crustal P-wave velocity varies from 5.5 to 5.7 km/s in sedimentary rocks and indicate a gradient from 5.91 to 6.3 km/s in the basement. He suggested that the crustal thickness is 44 to 47 km in the Blue Ridge of eastern Tennessee, 43 km in the Piedmont of central North Carolina and 27 to 36 km in the Coastal Plain.

The magnetic data are characterized by a series of lineaments. Watkins (1964) identified a linear magnetic gradient parallel to the Valley and Ridge Province of the Appalachians extending from the Mississippi Embayment in central Alabama to the Green Mountains in Vermont. King and Zietz (1978) named this 1600 km long lineament the New York-Alabama lineament and suggested that it is an ancient suture zone marking the southeastern boundary of a stable region. The seismicity data show that most earthquake epicenters in southeastern Tennessee are distributed east of the lineament.

The distinctive magnetic features of the continental margin in the southeastern United States are: (1) the Brunswick Anomaly which reflects a buried graben (Brunswick graben), (2) the East Coastal linear anomaly which is related to the transition from continental crust to the oceanic crust, (3) the Blake Spur Anomaly and (4) the Blake Spur fracture zone offset which is the largest offset, of the Blake Spur (Grow, 1981).

The regional Bouguer gravity anomalies in the Southern Appalachians (Fig. 3-4) generally trend NE-SW, apparently following the regional topographic trends. A large negative anomaly appears in the mountain regions of the Blue Ridge, the Valley and Ridge, and the Appalachian Plateau. This negative anomaly suggests that the topography is compensated by crustal thickening, but a negative isostatic anomaly suggests an over-compensation (Ngoddy, 1985). The over-compensation may be caused by erosion of the relatively short-wavelength topography, on a crust that is too rigid to return to isostatic equilibrium at these short wavelengths. Low-density sedimentary deposits in Paleozoic basins, such as the southeast Tennessee rift basin (Long and Liow, 1986) may be the source of some of the shorter wavelength anomalies.

Another notable feature of the gravity field is the Piedmont gravity gradient. The Bouguer anomaly increases rapidly southeastward across the Piedmont province, Changing from -50 mGal to +20 mGal over a distance of 180 to 200 km. Although crustal thinning from the Blue Ridge to the Coastal Plain explains the magnitude of this variation in Bouguer anomaly, additional density changes inside the crust are required in some areas to fully account for the sharpness of the gradient.

Very few seismic refraction data are available for study of the deep crust on the southeastern continental margin. Because the water is deep, the original Bouguer anomalies of the continental margin (Fig. 3-5-a) do not show positive values, even in the deep ocean. After correction for the bathymetry, a large positive value appears at the continental margin (Fig. 3-5-b). The positive value indicates thinning of the crust. Very tight contour lines at the eastern corner indicate that the steep gravity gradient, with gravity increasing from 50 mGal to 150 mGal within 50 km, is probably associated with a rapid rise of Moho. An off-shore negative Bouguer anomaly trough (-40 to -50 mGal) seems associated with the Blake Plateau (Hutchinson et al., 1983a).

The Bouguer anomaly is less than +20 mGal over the Coastal Plain. The crustal thinning in the Coastal Plain, which has been confirmed by many seismic refraction studies, should produce a much larger anomaly. However, the thick, lower-density Coastal Plain sedimentary layer may significantly reduce gravity from the expected high positive anomaly.

Some local negative anomalies, such as those around the Savannah River and along the North Carolina coast, may be related to buried Mesozoic rift basins. Marine Bouguer gravity data for the continental margin off Charleston (Fig. 3-5) and gravity profiles (Hutchinson et al., 1983b, Fig. 3-6) show that: (1) there is a negative anomaly corresponding to the Brunswick Graben and (2) there is a gravity gradient at the Carolina Trough, where the Bouguer anomaly varies southeastward from 0 mGal to -50 mGal within 50 km. It may be caused by thick sediments which overcome the positive effect of the crustal thinning.

III-3 SUMMARY OF CRUSTAL STRUCTURES

In the Southern Appalachians, the Coastal Plain and at the continental margin, seismic refraction studies (discussion above and also, Taylor and Toksoz, 1982; Hutchinson et al., 1983-b) show that the Moho discontinuity could be identified in most refraction profiles with P-wave velocities of the mantle between 8.0 and 8.1 km/s and uniform over the Southern Appalachians and continental margin. Refraction seismic data and gravity data indicate that, in the Appalachian Plateau and the Valley and Ridge provinces, the depth to the Moho varies from 40 to 45 km.

The crust is thickest under the Blue Ridge province where the reported depth to the Moho reaches 50 km. The Moho shallows in the Piedmont to 33 km. In the Coastal Plain, the Moho depth is 29 to 33 km. The crust continually thins toward the sea while the ocean floor deepens. The crustal thickness may be only 10 to 15 km at the eastern edge of the study area (see Fig. 5-9-a).

The transition between the upper and lower crust is not well defined. It varies in depth from 10 to 20 km in some places, but it has not been identified and may not exist in other places. The lower-crustal P-wave velocity in the southeastern United States is around 6.5 to 6.7 km/s. In the Coastal Plain, the lower-crustal P-wave velocity may increase from 6.7 to 7.0 km/s (Hutchinson et al., 1983-b). The average P-wave velocity in the upper crust is 6.1 km/s, and P-wave velocity is less than 5 km/s in the shallow sedimentary rocks. The sedimentary section is 2 to 4 km thick in the Coastal Plain and 7 to 10 km thick on the continental shelf. The P-wave

velocity in the upper unconsolidated sedimentary layers, which are probably water saturated, is 1.7 to 3.0 km/s.

On the basis of multi-channel reflection profiles and magnetic data, Hutchinson et al. (1983-a) suggested that in the continental margin of the southeastern United States, the Moho discontinuity rises in a step-wise manner from a depth of 30 km to 25 km near the Carolina Trough and to 15 km under the Continental Rise.

Mareschal and Kuang (1986) proposed a two-dimensional crustal structure based on an average Bouguer anomaly profile of the Southern Appalachians. In this model, the crust is thickened to 48 km in the Blue Ridge and thinned to 35 km in the Coastal Plain. The density contrast between the crust and mantle is 0.25 g/cm^3 . Some relatively short-wavelength density anomalies are located in the upper and lower crust. The Coastal Plain is a 2 to 3 km thick sedimentary surface layer of density 2.5 g/cm^3 .

CHAPTER IV

SEISMICITY AND STRESS FIELD OF THE SOUTHEASTERN UNITED STATES

IV-1 SEISMICITY

The southeastern United States has fewer earthquakes than the western United States. Most of the epicenters of earthquakes in the southeastern United States are concentrated in two small regions. The Valley and Ridge and Blue Ridge provinces in eastern Tennessee and western North Carolina are part of the Southern Appalachian Seismic Zone identified by Bollinger (1973). The other region of considerable historical seismicity is the Charleston-Summerville area, which is part of the South Carolina-Georgia Seismic Zone (Bollinger, 1973; Tarr, 1977). Other areas are almost aseismic.

Fig. 4-1 shows the location of historical earthquakes and the seismic zones in the southeastern United States. A discussion of the central Virginia Seismic Zone will not be included in this study. Fig. 4-2 shows the epicenter locations of recent (1977-1985) earthquakes. The main difference between the historical and contemporary Southern Appalachian seismicity distribution is that historical events occurred in the Valley and Ridge and Blue Ridge provinces (which include eastern Tennessee and western North Carolina) but contemporary earthquakes have been concentrated in southeastern Tennessee but not in western North Carolina.

The eastern Tennessee seismic region, which is part of the Southern Appalachian seismic zone, is located in the Valley and Ridge and the Blue Ridge province of the the Southern Appalachians, bounded on the northwest by the New York-Alabama lineament and parallel to the trend of the Southern Appalachians. From 1874 to 1928, eight earthquakes with intensities between VII and VIII occurred in this region (Bollinger, 1973). Seismic stations, which have operated since 1928, recorded more than 30 earthquakes of magnitude greater than or equal to 3.0 in this region from 1928 to 1981. Six of them had magnitudes greater than or equal to 4.0, most of the hypocenters are between 6 and 14 km below the earth's surface (Johnston, et al., 1985).

The Georgia-South Carolina seismic zone (Bollinger, 1973) extends through the Atlantic Coastal Plain of South Carolina and is perpendicular to the trend of the Southern Appalachians. The Charleston seismic region (Tarr, 1977) is in the Georgia-South Carolina seismic zone (Fig. 4-3 from Tarr, 1977). A total of 436 earthquakes were reported in South Carolina from 1754 to 1975, of which more than 85 percent occurred in the Charleston-Summerville area. The 1886 Charleston earthquake, with an estimated magnitude of 7.0, is the largest historical event in the southeastern United States. Old records indicate that the seismicity of South Carolina prior to 1886 was at a normal level (Bollinger and Visvanathan, 1977). The 1886 event was followed by aftershocks which account for about 70 percent of all earthquakes recorded between 1754 and 1975, however, most aftershocks were reported during the period 1886 to 1930 (Tarr, 1977). Although the present level of

seismic activity in the Charleston-Middleton Place area is declining, it has not reached the pre-1886 level.

The historical data suggest that Charleston and its vicinity could be a unique seismotectonic region. Paleoseismic analysis of sand liquefaction (Obermeier et al., 1985) suggests that several late Quaternary earthquakes with shaking severity comparable to the 1886 event have occurred in the Charleston area.

IV-2 CONTEMPORARY STRESS FIELD

The orientation of principal stresses near the earth's surface may be determined by in-situ measurements, by geologic methods and by earthquake fault plane solutions.

In-situ stress measurements, which are limited to very shallow depths (at most, a few hundred meters), do not directly indicate stress at great depths. The deep and shallow stresses could be different. Also, *in-situ* stress measurements are sensitive to local geologic structures, topography, anisotropy of rock as well as the experimental uncertainty. Perhaps the most reliable method of in-situ measurement is hydraulic fracturing (McGarr and Gay, 1978) which presently is the only in-situ method for measuring stress at depths down to a thousand meters. The technique consists of isolating a section of borehole over a known depth interval by using inflatable packers. This section is then pressurized by pumping fluid while recording the pressure-time history of the hydraulic fluid. The pumping is continued until a fracture is finally induced. By assuming that the fracture plane is vertical and the fracture is purely tensile, the least horizontal principal compression axis is perpendicular to the fracture. Error in this measurement will be less than 15°.

Surface geological mapping, including the sense of movement of faults, can provide valuable information on regional stress orientation. In a normal-faulting regime, the net horizontal slip is in the direction of the greatest principal stress (least principal compressional stress). Similarly, in a reverse faulting regime, the least principal stress (the greatest principal compressional stress) should be in the direction of the motion. For a pure strike-slip faulting regime, both the greatest and least principal stress axes intersect the pair of fault planes. Usually, if the slip is on a pre-existing fault plane, the calculation of principal stress orientation will involve more complex geometry and require additional information (Angelier, 1979).

The principal stress orientations at substantial depths below the earth's surface may be estimated from the fault plane solutions. The radiation pattern of seismic waves generated by an earthquake in the crust is quadrangular about the source. The initial motion (compression or dilation) at the source will be recorded at the seismic station. The take-off angle (180° minus the dip) and the azimuth can be computed and plotted as a spherical projection which shows the direction of rays and their polarity. The compressional axis "P" and dilatational axis "T" are separated by the two nodal planes which intersect along the intermediate "B" axes.

Theoretically, the angle that the compressional axes should make with the greatest principal stress axis is (Billings, 1972):

$$\theta = 45^\circ + \phi/2$$

where ϕ is the internal friction which depends on the cohesive strength of the rock.

The actual fracture may not be in the direction θ when an earthquake occurs. The failure plane does not necessarily follow the theoretical fracture plane, but in most cases, the plane is along a pre-existing fault. The P, T and B axes do not necessarily coincide with the greatest, least and intermediate principal stress axes, respectively. McKenzie (1969) indicated that the only restriction for the principal stress axes and fault plane relation is that the greatest (compressional) principal stress must lie in the quadrant containing the P axis. Raleigh et al. (1972) found that the P axis could deviate from the greatest (compressional) principal stress axis by 40° or less when an earthquake occurs on a pre-existing fault plane.

Current understanding of plate tectonics (AAPG Plate Tectonic Map, 1985) suggests that the North America Plate moves away from the Mid-Atlantic Ridge at a speed of 2.7 cm per year and that the rotation vector is trending in a northeast direction which is perpendicular to the trace of the New England Seamounts. The calculated direction of tectonic forces is still questionable due to uncertainty in the mechanical models. In the eastern United States, the calculated regional tectonic stress (Richardson et al. 1979; Solomon et al., 1980) of a plate driving force model with basal viscous shear shows the maximum horizontal compression in a northwest direction. Also, other (e.g., Zoback and Zoback, 1980) studies suggest a ridge push force from the northeast direction.

In the Southern Appalachians the earthquake focal mechanisms and other studies of the stress were considered by Sbar and Sykes (1973), Raleigh (1974), McGarr and Gay (1978), Zoback and Zoback (1980), Zoback (1983) and Johnston et al. (1985) among others. Fig. 4-4 (after Zoback, 1983) shows the orientation of the horizontal principal stresses in the southeastern United States.

Sbar and Sykes (1973) combined in-situ stress measurements, geological data, and earthquake fault plane solutions and suggested that much of the eastern United States is experiencing horizontal compression. The maximum compressional axis trends from east to northeast in the mid-continent. They studied the southeastern United States stress regime and used several in-situ measurement data along the Southern Appalachians. The maximum compressional principal stress axes (S_1) are horizontal and orientated $N6^\circ E$ in Rapidan, Virginia, and $N87^\circ E$ in Mt. Airy, North Carolina. In Georgia, the principal stress directions are rather complicated with S_1 varying from northeast to northwest. The magnitude of S_1 in the Southern Appalachians is on the order of tens of MPa. The greatest to least principal stress ratio (S_1/S_3) is over 1.5. Sbar and Sykes (1973) proposed that the Appalachian stress field is complicated by the remnant stress (stress built up during the formation of present structures).

Fault plane solutions of many earthquakes in the Valley and Ridge and the Blue Ridge province were studied by Johnston et al. (1985), Teague (1984), Guinn, (1980), Zelt and Long (1987), among others. Most of the focal mechanisms indicate strike-slip faulting with the nodal plane orientated north-south (right-lateral) or east-west (left lateral) which indicates northeast compression. An analysis of fault plane solutions from 47 events located throughout the Valley and Ridge region of eastern Tennessee (Johnston et al., 1985) shows a single consistent type of motion, strike slip on east-west trending planes with horizontal northeast to southwest compressional axes.

In the eastern Tennessee area, focal mechanisms with a component of normal-faulting are also very common (Zelt and Long, 1987). Among 38 determined earthquake focal mechanisms (with two composite solutions), 22 were strike-slip and 18 were normal faulting events (two earthquakes have composite solutions). Most of the normal focal mechanisms have a horizontal extensional axis trending in a NW-SE direction. The strike slip focal mechanisms are concentrated in the southeastern Tennessee area. A depth analysis indicates that the depths of eastern Tennessee earthquakes depend on the type of faulting. Earthquakes with vertical movements are usually shallower than those with horizontal movement (Zelt and Long, 1987).

Guinn (1980) studied several earthquakes in eastern Tennessee and the Summerville-Charleston region and determined their focal mechanisms. In eastern Tennessee, the focal mechanisms in general, support east to northeast compression. For examples, the February 4, 1976 Conasauga, Tennessee (in the Blue Ridge province) earthquake of magnitude 3.1, implies that the S_1 axis is directed northeast and has a 60° plunge. The July 27, 1977 Englewood, Tennessee (in the Valley and Ridge province) earthquake of magnitude 3.5, implies that the S_1 axis is constrained from north to northeast and varies in plunge from horizontal to vertical. In the Coastal Plain Province, the focal mechanism solutions do not have a consistent direction, but they seem to support a northeast-southwest compressional regional field near the Summerville-Charleston area.

Zoback and Zoback (1980), from the combination of in-situ measurements, focal mechanism solutions and geological observations, proposed that the Atlantic Coastal Plain and the Piedmont province are characterized by northwest to west, rather than northeast compression. The maximum compressional axis appears to be perpendicular to the trend of the Appalachian Mountain belt and the continental margin of the southeastern United States. Another argument in favor of northwest regional compression is that many northeast trending reverse faults along the east coast were active from the Cretaceous to the Cenozoic. The orientation of these faults implies that the contemporary maximum horizontal compression trends in a northwest direction (Wentworth and Merguer-Keefe, 1981; Powell and O'Connor, 1978).

Talwani (1982) suggested a $N60^\circ E$ maximum compressional axis near Charleston based on relocated hypocenters and composite fault plane solutions. But, the focal mechanisms are complicated by the local fault systems. Shallow (4 to 8 km) reverse faulting is associated with the Ashley River Fault and deeper (9 to 15 km) strike-slip faulting is associated with the Woodstock Fault.

Zoback's (1983) recent study, based on the relocated earthquake focal-plane mechanisms and in-situ stress measurements, seems to favor northeast rather than northwest regional maximum compression in the Coastal Plain. Therefore, the east-northeast compressional stress regime of the mid-continental United States can apparently be extended into the Southern Appalachians and the Coastal Plain. Fig. 4-4 shows that the contemporary regional stresses in the middle and eastern North America Plate generally trend north-east. However, the stress in the Coastal Plain area and continental margin is still not consistent with the north-east directions of the mid-continents.

Plate tectonic force is probably the main source of regional stress in the eastern United States (Sbar and Sykes, 1973; Richardson et al., 1979; Zoback and Zoback, 1980). However, whether the direction of ridge push is parallel to that of

regional compression remains questionable. Also, the state of regional stress varies in different geologic provinces. The diverse focal mechanisms suggest that not all earthquakes are responding to regional stress or that the regional stress can not be simplified to a simple pattern in the southeastern United States. Local factors must be considered and additional sources of stress are required in order to interpret the diverse stress directions demonstrated by intraplate events.

CHAPTER V

STRESS FIELD AND SEISMICITY

V-1 PARAMETERS AND LOADS

The elastic parameters which is used for stress computations in the Southern Appalachians and the Atlantic Coastal Plain are determined from geophysical data discussed in Chapter III and are based on several assumptions. The relationship between the P-wave velocity, density and elastic parameters is given by:

$$\alpha = \sqrt{(\lambda + 2\mu) / \rho}$$

or

$$\rho = (\lambda + 2\mu) / \alpha^2$$

where α is the P-wave, velocity which is deduced from seismic data (discussed in Chapter IV), ρ is the density and λ and μ are Lamé's constants, which are used for stress computation.

Rock experiments (Lama and Vutukuri, 1981) give an approximate range of elastic properties under normal temperature and pressure (Table 5-1).

At high pressure and temperature, the rocks in the lower crust and mantle may behave differently than in experiments under surface conditions. The increase in seismic wave velocity suggests that the density and rigidity of the rocks increase with depth. For the purpose of computation, some simplifying assumptions are made: 1) The lithospheric thickness is not critical to the result of stress computation, therefore, it is assumed to be 100 km in the Southern Appalachians and 80 km near the coast and continental margin. The lithosphere is probably thicker than 100 km in the southern Appalachians, the 100 km thickness is used as average value. 2) The normal crustal thickness is 40 km in the Southern Appalachians and 30 km in the Coastal Plain area. 3) The normal boundary between upper and lower crust is assumed to be at a depth of 20 km in the Southern Appalachians, and 15 in the Coast Plain. 4) Elastic parameters and density are as listed in Table 5-2, in which Lamé's constants $\lambda = \mu$.

The theory and technique of computing a stress field induced by surface and internal loads was described in Chapter II. In this chapter, this computing method will be applied to the Southern Appalachians and to the Charleston area, which includes the continental margin.

The lithosphere is considered to be an elastic slab overlying the asthenosphere, which is assumed to be an inviscid fluid. The loads acting on the surface of the lithospheric slab are derived from a combination of the excess mass of topography and the deficit mass of near-surface low-density sediments. In the ocean, the sea level is the zero elevation plane, therefore, the loads are derived from

TABLE 5-1
 AVERAGE VALUE OF
 LABORATORY MECHANICAL PROPERTIES OF ROCKS AND A MINERAL

	POISSON'S RATIO	RIGIDITY MODULUS (10^{11} Pa)	DENSITY (g/cm^3)
GRANITE	0.20-0.23	0.10-0.40	2.6-2.7
BASALT	0.20-0.30	0.30-0.38	2.8-2.9
OLIVINE	0.24	0.87	3.32

TABLE 5-2
ELASTIC PARAMETERS

	P WAVE VELOCITY (km/s)	POISON'S RATIO	LAME'S CONSTANT (10^{11} Pa)	YOUNG'S MODULUS (10^{11} Pa)	DENSITY (g/cm^3)
SEDIMENTS	5.0	0.25	0.38	1.0	2.40
UPPER CRUST	6.0	0.25	0.44	1.1	2.70
LOWER CRUST	6.8	0.25	0.53	1.35	2.85
LITHOSPHERIC- MANTLE	8.1	0.25	0.68	1.70	3.20
ASTHENOSPHERE	7.9	--	--	--	3.10

bathymetry and the negative density contrast between the sea water and the rocks underneath the surface.

The distribution of density anomalies, which are the sources of the internal loads, may be derived from the inversion of gravity data. Other data such as seismic data pertaining to crustal structure can be used to constrain the inversion. Therefore, the internal loads could be deduced in two different ways:

(1) Downward continuation

The downward continuation method utilizes only the spectral characteristics of the gravity anomaly to constrain the interpretation. It assumes that the depths of the sources of gravity anomalies are proportional to these wavelengths. The original surface Bouguer anomaly is Fourier transformed into the frequency domain. Assuming a normal Moho depth, for example, 40 km in the Southern Appalachians, the Fourier components with wavelengths larger than 40 km are multiplied by a downward continuation operator $\text{EXP}(+kh)$, where h is depth (40 km) and k is wavenumber. The result is the downward continued Bouguer anomaly. Assuming that the mass source of the anomaly is concentrated on a thin layer, the load can be obtained as:

$$P = \Delta\rho gh = (g_b / 2\pi G) g = g_b / 4.19$$

where P is the load (in MPa), g_b is the downward continued Bouguer anomaly at that level (in mGal), G is the gravitational constant, g is the acceleration of gravity and $\Delta\rho$ is the density contrast.

The loads on the upper-lower crustal interface, on the Moho discontinuity and on lithospheric-asthenosphere boundaries are computed. The anomalies with very short wavelengths (less than 15 km) are assumed to be caused by shallow density variations and are left at the surface. They are directly transformed to loads.

(2) Crustal Modeling

Alternately, a crustal model can be constructed from seismic refraction data. The gravity anomaly, based on this model, is computed and compared to the observed data. The structural model or density contrast is adjusted until the calculated gravity anomaly fits the observed data. Then, the mass excess (or deficiency), due to the density difference at the undulating interface, is calculated and the load is concentrated on the layer boundary.

In this study, the internal loads are calculated by the downward continuation method. Edge effects caused by the nature of the Fourier transform will be removed as discussed in Chapter II.

Intraplate earthquakes are usually located in the upper crust (Meissner and Strenhlán, 1982). In the southeastern United States, most focal depths are less than 20 km (Fig. 5-1). This is probably due to the following factors: (1) The rock's rheology changes with increasing depth and temperature. At shallow depth, shear stress is released through frictional slip. In the lower crust, steady state creep may

dominate (Bott, 1982). (2) With increasing depth, rock strength increases and the number of fractures decreases. Fig. 5-2 shows the relationship between the rock strengths and depths. In order to be comparable to earthquake focal mechanisms at hypocentral depth, stress analysis in both the Charleston area and the Southern Appalachian area will be presented for a depth of 10 km.

In this study, the "local stress" is defined as the stress induced by the topography and density inhomogeneities inside the lithosphere. Other sources of local stress, (e.g. thermal) are not considered in this study. The "regional stress" is defined as the stress prevailing in a rather large area (e.g., the Southern Appalachians, or the Coastal Plain province) with a generally consistent direction of the maximum compressive axis (this direction may be perturbed locally by geological structures). The trends of the regional maximum compressive axis may not be necessarily parallel to the direction of the plate tectonic force which is considered the main source of the intraplate lithospheric stress. The term "total field" refers to the combination of a local and regional field

V-2 THE SOUTHERN APPALACHIANS

The first area of interest is the Southern Appalachians (Fig. 5-4-a). The calculations were performed on a 1028 km by 1028 km square containing all of South Carolina, and most of Georgia, North Carolina, Tennessee, Virginia, West Virginia and Kentucky. The origin (lower left corner) is at N 31.5 latitude and E 87.5 longitude and the center is in the Blue Ridge of western North Carolina. The analysis and discussion here will be primarily concerned with the Southern Appalachian seismic region, which is in the center of the study area.

The technique and procedure to prepare the surface and internal loads have been discussed in the previous section. To recapitulate briefly, it is assumed that the average Moho depth is 40 km below the surface and the interface between the upper and the lower crust is 20 km below the surface. The internal loads are deduced from the downward continued gravity data and the the surface loads come from the topography and the very short wavelengths of the Bouguer anomaly. Fig. 5-3 shows the calculated loads at depth 0, 20 and 40 km.

LOCAL STRESS FIELD

The local stress and deformation field and the Schmidt Net Projections of the principal stress axes (SNPPSA) of the Southern Appalachians at 10 km depth are shown in Fig. 5-4. The SNPPSA is analogous to spherical projections and usually are used to display earthquake fault plane solutions. The SNPPSA plot can be used to predict the type of faulting and earthquake focal mechanisms resulting from the computed stress field.

Horizontal displacement and SNPPSA (Fig. 5-4-b and 5-4-d), indicate, under the hypotheses above, that the Valley and Ridge and the Blue Ridge provinces are in a NW-SE horizontal extension. The SNPPSA plots suggest a normal faulting mechanism. Meanwhile, the Charlotte Belt and the Atlantic Coastal Plain are subject to NW-SE compression and SNPPSA shows northeast trending reverse faulting. The Inner Piedmont subprovince seems to be a transition zone, its SNPPSA pattern is strike-slip type.

The average differential stress is about 20 MPa and the maximum is 35 MPa. The differential stress contours (Fig. 5-4-c) show that the maximum differential stresses appear in the Blue Ridge area of eastern Tennessee and western North Carolina. Great stresses (more than 20 MPa) are also concentrated in southern West Virginia, northern South Carolina and central western Alabama. The relatively stress-free areas (less than 10 MPa), which may be called stress gaps, are located in the Atlantic Coastal Plain, western Tennessee, northern Alabama, central Georgia (a NE-SW trending gap) and western Virginia (also a NE-SW trending gap).

The historical seismicity of the Southern Appalachians (after Johnston et al., 1985) was shown in Fig. 4-1 and the contemporary (1977-1985) seismicity activity (after Bollinger, 1973) in Fig. 4-2. Comparing the local stress field with the earthquake epicenters of the Southern Appalachians, one may notice that there is a fairly good relation between the local stress field and the seismicity.

SUPERPOSITION OF LOCAL AND REGIONAL STRESS FIELD

Fig. 5-5 shows the total field after combining 20 MPa of $N60^{\circ} E$ regional horizontal compression with the local field. The concentration of stresses in the Valley and Ridge and the Blue Ridge province has been significantly reduced (to less than 20 MPa) when this regional compression is added onto the local field. The differential stresses are concentrated in two seismically inactive regions: eastern Virginia to eastern North Carolina (30 to 35 MPa) and Alabama to western Georgia (30 to 50 MPa). SNPPSA shows that strike-slip faulting would be predicted in Alabama and normal faulting in the Atlantic Coastal Plain. The stress gaps include the Piedmont province, South Carolina and its offshore area.

When 20 MPa of east-west regional compression is added to the local field, the resulting field (Fig. 5-6) shows no concentration of stress west of the Piedmont Province. Stresses are concentrated in the Coastal Plain region including the South Carolina-Georgia Seismic zone. SNPPSA suggests that normal faulting mechanisms would be predicted in the coastal area except near Charleston where the strike-slip focal mechanism (with east-west horizontal compressive axis) is predicted.

The combination of 20 MPa $S75^{\circ} E$ regional compression with the local field (Fig. 5-7) shows no stress concentration in the Southern Appalachian. Stresses are concentrated in the Atlantic Coastal Plain. SNPPSA is interesting in the southeastern portion of the study area: the magnitude of differential stresses in South Carolina is not greater than in other coastal areas such as eastern Georgia and eastern North Carolina but the stress pattern is quite different. It should be noticed now that the results obtained from the Southern Appalachian models are similar to those obtained from the Coastal Plain-Charleston area which will be discussed in the next section. South Carolina seems to be a unique region in the Atlantic Coastal Plain where strike slip type of SNPPSA is predominant while, in other areas, reverse faulting is predicted.

The seismicity in the Southern Appalachians seems to be strongly correlated with the magnitude of local differential stress. The calculated local stress field predicts a normal faulting with a NE-SW horizontal compressional axis and a NW-SE horizontal extensional axis. This result does not predict the strike-slip focal mechanisms for eastern Tennessee, but does show a correlation with the catalog of

normal focal mechanisms which are also prevalent in eastern Tennessee at a relatively shallower depth (Zelt and Long, 1987).

For the total field obtained after superimposing the regional fields on the local field, such correlation is nonexistent in the Valley and Ridge province and the Blue Ridge province of eastern Tennessee and western North Carolina, regardless of the direction of regional compression. The eastern Tennessee and western North Carolina active seismic regions show almost negligibly small stress concentrations.

By contrast, in the South Carolina-Georgia seismic zone as well as elsewhere in the Atlantic Coastal Plain and the Piedmont province, the local stress field does not explain the seismicity. A direction of near east-west regional compression is required to yield a correlation between the total stress field and the regional seismicity (Fig. 5-6). The area of stress concentration and calculated SNPPSA generally predicts the area of seismicity. Previous focal mechanism studies and *in-situ* measurements indicate NE-SW regional compression, although the regional stress computation does not. This study suggests that this inconsistency may result from two aspects:

(1) Focal mechanisms of the events in the eastern Tennessee and western North Carolina seismic zone are strongly affected by local crustal structure and other geologic features; for example, several parallel fault systems in the basement of Valley and Ridge and Blue Ridge provinces. The structure in deep basement rocks is still not well understood. COCORP data show several features located in eastern Tennessee between 9 and 20 km (3.0 to 7.0 seconds two-way travel time). They may indicate deep structural complexities (Cook et al., 1983). Long et al. (1986b) proposed that three major features in eastern Tennessee characterize the crust: first, a northeast trending strike-slip fault which is expressed as the New York-Alabama lineament; second, a sediment thickening in the shallow crust shown by a negative Bouguer Anomaly; and third, a Precambrian rift zone depicted by a north-northeast striking positive gravity anomaly in northern Tennessee. The focal mechanisms of historical as well as contemporary earthquakes are consequently controlled by the nature of the pre-existing fault planes.

(2) Northeast trending compression may correctly describe the stress regime of the southeastern United States (i. e. the mid-continental stress regime). In the Southern Appalachians, the mountain belt, the suture zone, strong folding and faulting, and thick sedimentary basins may locally distort the stress field. The calculations did not include the details of local density anomalies and discontinuities in the crust.

V-3 CHARLESTON AND CONTINENTAL MARGINS

The stresses for the Charleston area were computed in a 1028 km by 1028 km square area rotated 52 degrees from the north and centered at Charleston, South Carolina. Included in this area are the states of Georgia, South Carolina, most of North Carolina and portions of Florida, Alabama, Virginia, West Virginia and Tennessee. This area also covers the southeastern continental margin from North Carolina to northern Florida. The coordinates of the four corners of the study area are in Table 5-3.

The topography and the depth of the ocean floor (bathymetry) are shown in Fig. 3-2 and a Bouguer anomaly contour map is shown in Fig. 3-5(a,b). The highest

TABLE 5-3
COORDINATES OF CORNERS

	LATITUDE (NORTH)	LONGITUDE (WEST)
WEST CORNER	33.6190	87.9710
NORTH CORNER	39.4417	79.2187
EAST CORNER	31.9683	72.7695
SOUTH CORNER	26.5908	81.2183

elevation is about 900 meters near the northwest edge of the study area and the greatest depth to the ocean bottom is about 5000 meters. The Bouguer gravity anomaly (Fig. 3-5-a) in the ocean area contains the effect of the depth of sea water (bathymetry). In order to reveal the structure of the lithosphere, bathymetric correction has been made, in which the density contrast was assumed to be 1.67 g/cm^3 . The Bouguer anomaly after bathymetric correction is shown in Fig. 3-5-b. The loads induced by topography and internal density changes were computed at depths 0, 15 and 30 km (Fig. 5-8).

LOCAL STRESS FIELD

The calculated local stresses and displacements at 10 km depth are shown in Fig. 5-9-b, c and d. Fig. 5-9-b shows the horizontal displacements. The Piedmont Province is under NW-SE compression and the continental margin is in NW-SE extension. Because the Blue Ridge and the Valley and Ridge provinces are located near the edge of the study area, the stress field and displacements were distorted by the edge effect.

The local stresses at 10 km (Fig. 5-9-c) show area of stress concentration in the Southern Appalachians and near the east continental margin. Stress in other areas is relatively small and negligible. The maximum differential stress (S_1-S_3) is about 50 MPa.

SNPPSA (Fig. 5-9-d) shows that local stress would predict reverse faulting in the Piedmont province maximum compressive axis is horizontal and trends northeasterly. Normal faulting would be predicted in the continental margin.

There is very little correlation between the local stress field at 10 km and the seismicity. Neither the magnitude of the differential stress nor SNPPSA predicts the observed earthquakes and their focal mechanisms. The seismic region of South Carolina and Georgia shows a minimal stress whereas the eastern continental margin, an aseismic region, has high stress. The greatest magnitude of the local differential stress is about 60 MPa (at the eastern corner) and the average is about 30 MPa.

SUPERPOSITION OF LOCAL AND REGIONAL STRESS FIELDS

The state of the regional stress in the Atlantic Coastal Plain is not well resolved. Previous studies have shown that the horizontal compressive axis could vary from NE-SW to NW-SE (see the discussion in Chapter IV). However, there must be some connection between the stress field and the seismicity. Adding regional compression of varying directions to the local field could reveal the correlation between the stress and seismicity. The calculated principal stress direction of the total field should best predict the seismicity if the added stress field is parallel to the true regional compressional direction.

Fig. 5-10 shows the total field after combining a $30 \text{ MPa N}60^\circ \text{ E}$ regional compression with the local field. Maximum stress and strike-slip faulting are predicted in the eastern continental margin. Stresses are also concentrated in the Southern Appalachians, and reverse faulting is dominant with the maximum compression axis horizontal and in the NE-SW direction.

Concentrated stress areas and reverse faulting are predominant in the Southeast Georgia Embayment. The South Carolina Seismic Zone is not identified with anomalous stress distribution.

Fig. 5-11 shows the total field after combining a 30 MPa East-West regional horizontal compression field with the local field. The magnitude of stress is significantly reduced in the eastern continental margin (to less than 25 MPa). The stress in the Southern Appalachians remains unchanged (about 50 MPa). The 40 MPa contour line of differential stress includes the South Carolina-Georgia Seismic Zone and the coast of South Carolina, Georgia and northern Florida, but no particular stress concentration occurs in the Charleston area. With east-west regional compression, the study area can be divided in two regions according to SNPPSA: reverse faulting would be predicted in the Southern Appalachians, Georgia and Florida, and strike-slip faulting in the Atlantic Coastal region of northern South Carolina, North Carolina and the continental margin. Most of the South Carolina-Georgia Seismic Zone is in a reverse faulting regime, but the Charleston area is located in the transition zone between these two regimes. The previously mentioned stress concentration offshore of Georgia is reduced. Areas with less concentration of stress include Alabama, western Georgia, Florida, eastern Tennessee and most of the continental margin areas.

Fig. 5-12 shows the total field after combining a 30 MPa S80°E regional horizontal compression field with the local field. The magnitude of the differential stress is further reduced in the eastern continental margin. The maximum differential stress occurs in east central Virginia and central North Carolina and corresponds to reverse faulting. The stress pattern in the South Carolina area clearly indicates that it will gradually change from reverse type faulting (SNPPSA) to strike slip as the regional compressive axis rotates further southeastward. Other areas do not demonstrate this tendency to shift.

Fig. 5-13 shows a total field after combining a 30 MPa S 70° E regional horizontal compression field with the local field. The magnitude of the stress in this area has not been significantly changed. The principal stress pattern in the South Carolina and the North Carolina areas appears to be the strike-slip type of SNPPSA with the S_2 axes in the NW-SE direction.

The total stress field will be significantly changed if the adding regional compression trends further southeastward.

In the Charleston area, there is no indication of correlation between the seismicity and the local stress field caused by the crustal density changes. The earthquake epicenter maps (Fig. 4-1 and 4-3) suggest sparse or no seismicity in the continental margin of the southeastern United States but more activity in the Charleston-Summerville area of South Carolina. However, there is a correlation between the total stress field and seismicity in terms of fault pattern. The calculations indicate that the area of stress concentration roughly follow the earthquake distribution when horizontal compression is added to the local field and this regional compression is orientated in a S80°E (+10°) direction. Total field with other orientation of regional compression does not predict the seismicity pattern of this area. Calculated field does not show a remarkable stress concentration in the Charleston area, but the total field (with a near east-west direction of regional compression) does predict strike slip faulting in South Carolina and predominant

northeast trending reverse faulting for the adjacent areas (i.e., Georgia and North Carolina).

The total field with the S60°E regional compression predicts stress concentration with a northeast trending reverse faulting focal mechanism may occur in central Virginia. A recent focal mechanism study (Munsey, 1984) shows that central Virginia is characterized by strike slip and reverse focal mechanisms. (Among the listed sixteen earthquakes, nine showed strike slip faulting and seven show reverse faulting). The local geological features complicate the interpretation of earthquake focal mechanism. The direction of the regional horizontal compression is also a complex issue, it may be orientated in a northeasterly direction at shallow depth and may shift to northwesterly below the 8 km depth.

Earthquake focal mechanisms as well as *in-situ* stress data in the Atlantic Coastal Plain and the Piedmont province do not show a consistent regional principal stress direction nor a consistent focal mechanism (see Chapter IV). By contrast, reverse faults were formed during the Cretaceous and tend to be predominantly northeast trending (Prowell and O'Connor, 1978; Behrendt et al., 1981) and are widely distributed along the east coast. It may imply that the ridge push from the Mid-Atlantic Ocean Ridge spreading is the regional source.

Following the computation of local stress and the superposition of hypothesized regional stress, it appears very likely that the regional maximum compressive axis in the Atlantic Coastal Plain is in the west-northwest to west direction. The stress pattern and magnitude in Charleston is similar to the other portion of the South Carolina-Georgia Seismic Zone. However, the SNPPSA does show relative stress concentration in South Carolina with strike-slip focal mechanisms. The Charleston area has a unique fault system (for example, Talwani, 1982). Earthquakes may have occurred on a pre-existing fault plane and by so doing they could show such a focal mechanism that differs from the regional stress pattern. This provides the possibility of either reverse or strike-slip faulting in the Charleston area.

CHAPTER VI

CONCLUSIONS AND DISCUSSIONS

Most of our direct knowledge of the mechanical properties and strength of rocks comes from geological observations and experiments (either *in-situ* or in the laboratory) of rock mechanics. Experiments in rock mechanics can simulate the environment of the crust to depths of a few kilometers (Lama and Vutukuri, 1978). Rock strength is influenced in a complex way by the surrounding environment. Many factors, including temperature, confining pressure, elastic inhomogeneity and elastic anisotropy, affect the strength of rocks. In addition, strain history will influence the strength. Experiments have demonstrated that the strength of rocks decreases with an increase in surrounding temperature and the strength intensifies with an increase in confining pressure (Lama and Vutukuri, 1978).

Seismological studies have shown that within the lithosphere, elastic wave velocity as well as density and elastic parameters increase with depth. With increasing depth and lithostatic pressure, rocks become denser, less fractured and stronger.

Lama and Vutukuri (1978) summarized several rock friction experiments which show that although the shear strength of rocks is influenced by a number of factors, e.g. composition, size of sample, moisture, cracks, and the degree of weathering, the *in-situ* cohesion of various rock types varies only from 0.1 to 2.0 MPa. Angles of internal friction vary from 20° to 60° and the coefficients of friction vary from 0.3 to 1.7. Their data reveal that the rock shear-strength parameters derived from laboratory tests are higher than those obtained from field tests.

Byerlee's (1978) friction test on brittle rocks indicates that shear strength depends on the depth where the rock is located. When material is under low pressure (less than 100 MPa, i.e. at a depth less than 3 km), the friction equation can be roughly expressed as

$$\tau = 85 \sigma$$

where τ is the shear stress necessary to break static friction on a surface with normal stress σ .

When the confining pressure is in the 200 to 1700 MPa range (i.e. in the depth between 7 to 60 km), the friction equation becomes (unit MPa):

$$\tau = 80 + 0.6 \sigma$$

For the three-dimensional case, Kirby's experiment (1980) shows that the critical differential stress required to overcome static friction is:

$$\tau = 290 + 2.1 \sigma \quad (\text{for a horizontal compressional case})$$

and

$$\tau = 90 + 0.7 \sigma \quad (\text{for a horizontal extensional case})$$

The above experiments were conducted under the following conditions: relatively short time of force application (up to several minutes), low temperatures (below 500° C) and small rock samples (10-20 cm³). These experimental conditions may not be suitable in natural cases. Meissner and Strenhlau (1982) measured and calculated the strength-depth (confining pressure) relation of rocks under several other situations (Fig. 5-2). The extensional strength of rocks is only about one fourth of the compressive strength. The strength of rocks is reduced if they contain water (see the wet curve in Fig. 5-2).

From the study of maximum shear stress curves and earthquake depth distribution curves, Meissner and Strenhlau (1982) proposed that the upper crust is usually wet and has lower strength. According to these studies, at 10 km depth the shear stress required to break an unfractured rock is about 70 MPa (in the case of extension) and 330 MPa (in the case of compression), respectively. Meissner and Strenhlau's study agrees that the hypocenters of intraplate earthquake are confined to the upper crust. This phenomenon reflects the elastic behavior of the upper crust and implies that the upper crust may have a different rheology and strength than the lower crust.

There are many sources of local stress concentration which could explain intraplate earthquakes, one of which is crustal density anomalies which result from surface topography and the changing crustal thickness. Gravity data provide reliable constraints on the loading function in the lithosphere and the gravity anomaly indicates changes of internal structure. Stress induced by topography and density could reach magnitudes of 10 to 100 MPa. Based on computation the magnitude of stress can be estimated from surface load. For example, one kilometer of surface relief could induce a 30 to 60 MPa vertical stress and 80 to 90 MPa horizontal stress in the upper crust depending on the wavelength of the load. The differential stress, in that case, would reach 40 to 50 MPa. These values are comparable to tectonic forces such as ridge push and slab pull and could possibly trigger earthquakes.

The topographic load and lateral density inhomogeneity in the lithosphere produce a stress concentration in the Southern Appalachians. The calculation of the Southern Appalachian stress field supports the hypothesis tested in this research. The strong and consistent correlation of the Southern Appalachian seismicity with the local stress field suggests that the mass anomalies play an important role in triggering the earthquakes in eastern Tennessee and western North Carolina. The Southern Appalachian local stress field shows that in the Valley and Ridge and Blue Ridge province the maximum compressive axis S_1 is vertical, the intermediate axis S_2 is horizontal and trends northeasterly and the extensional axis is horizontal and perpendicular to the S_2 axis. Therefore, a horizontal projection shows a northeast maximum compressive axis. It is commonly accepted that the regional maximum compressive axis in the Southern Appalachians trends in a northeastern direction. However, neither the calculated local nor the total stress field (with northeast horizontal maximum compression) show the consistency of the earthquake focal mechanisms. How the northeast regional compression, together with the local structures, distorts the stress field, and therefore, controls the earthquake focal

mechanisms is still not well known. The computed stress field indicates that in the Southern Appalachian seismic zone, the regional source (e.g., the ridge push from the mid-Atlantic ocean ridge) may be less important than the local stress field in causing intraplate earthquakes.

Strike-slip focal mechanisms predominate in the Southern Appalachian seismic zone, but normal faulting solutions or high angle P axes are often seen (Zelt et al., 1987; Guinn, 1980). One reason that the horizontal motion predominates over the vertical motion at great depth (≥ 15 km) may be that the horizontal stress is much greater than the vertical stress at these depths. The calculations do not show that southeastern Tennessee (the contemporary seismically active region) has a particular stress anomaly. Some local features which the models are unable to resolve may also be related to this seismic activity. One is an ancient (Precambrian) rift zone which is reflected on the New York-Alabama magnetic lineament; another feature is thick sedimentary in the same area.

The South Carolina-Georgia seismic zone is located in a transition area between two major structures, the Southern Appalachians and the eastern continental margin. The local stress field in the South Carolina-Georgia region shows no correlation with the seismic activity of the area. The topography induced-stress is concentrated in the continental margin and the Appalachian mountain region but not in the South Carolina-Georgia Seismic zone. The calculations did not yield a conclusive result for the relation between the local stress and seismicity. The results point out that neither local nor regional stress fields can be disregarded; both have comparable magnitudes and contribute to the lithospheric stress concentrations and the stress patterns. This study tested different directions of regional compressive axes and combined them with the local field. The results predict the most popular focal solution of the earthquakes in the South Carolina-Georgia Seismic Zone. The computation shows that local field combined with $N80^{\circ}W (+10^{\circ})$ regional compression predicts best the seismicity in the Coastal Plain region. An area of relative stress concentration (differential stress) includes the South Carolina-Georgia seismic zone with strike-slip focal mechanisms prevailing. The calculations do not predict any particular stress anomaly in the Charleston-Summerville seismic region. It may be that besides the local stress, other lithospheric force as well as the local structures and fault systems (Talwani, 1982) play an important role in triggering earthquakes.

Another possibility raised by this study is that the mid-continent region of North America and the Valley and Ridge province and the Blue Ridge province are characterized by a northeast regional maximum compression while the Atlantic Coastal Plain and part of the Piedmont province may belong to another stress regime in which the maximum regional compressive axis trends in a northwest to westerly direction.

The "local stress field", which was defined in Chapter V, does not mean that the stress is induced only by local features. In fact, the local stress field will be affected by long wavelength features (density anomalies, for example) several hundred kilometers away. Also, the Southern Appalachian Mountains affect the stress field in the Charleston, South Carolina area. Therefore, this stress computation technique is more suitable for regional stress analysis. The solution to the problem is controlled by the thickness of the elastic slab: the thinner slab gives more detailed lateral structure; whereas, the thicker slab gives less resolution. For

the lithospheric stress problem in which the thickness of the slab is about 100 km, the proper horizontal spacing should be 20 km to 50 km.

This computing method treats the lateral density variation as an internal load, but is unable to deal with the lateral changes in Lamé's parameters. Another weakness of this method is the difficulty in modeling inclined structures such as faults. The finite element method can be applied to model the local and inclined structure in more detail, but the long wavelength density anomaly and topography must be considered.

Although the upper crust may behave like an elastic medium, the lower crust and the asthenospheric mantle are clearly neither elastic nor brittle. The rheology varies with the lithospheric pressure and temperature. A three-dimensional elastic/visco-elastic solution is believed to be more suitable to real lithospheric cases. Future research should be aimed at this problem.

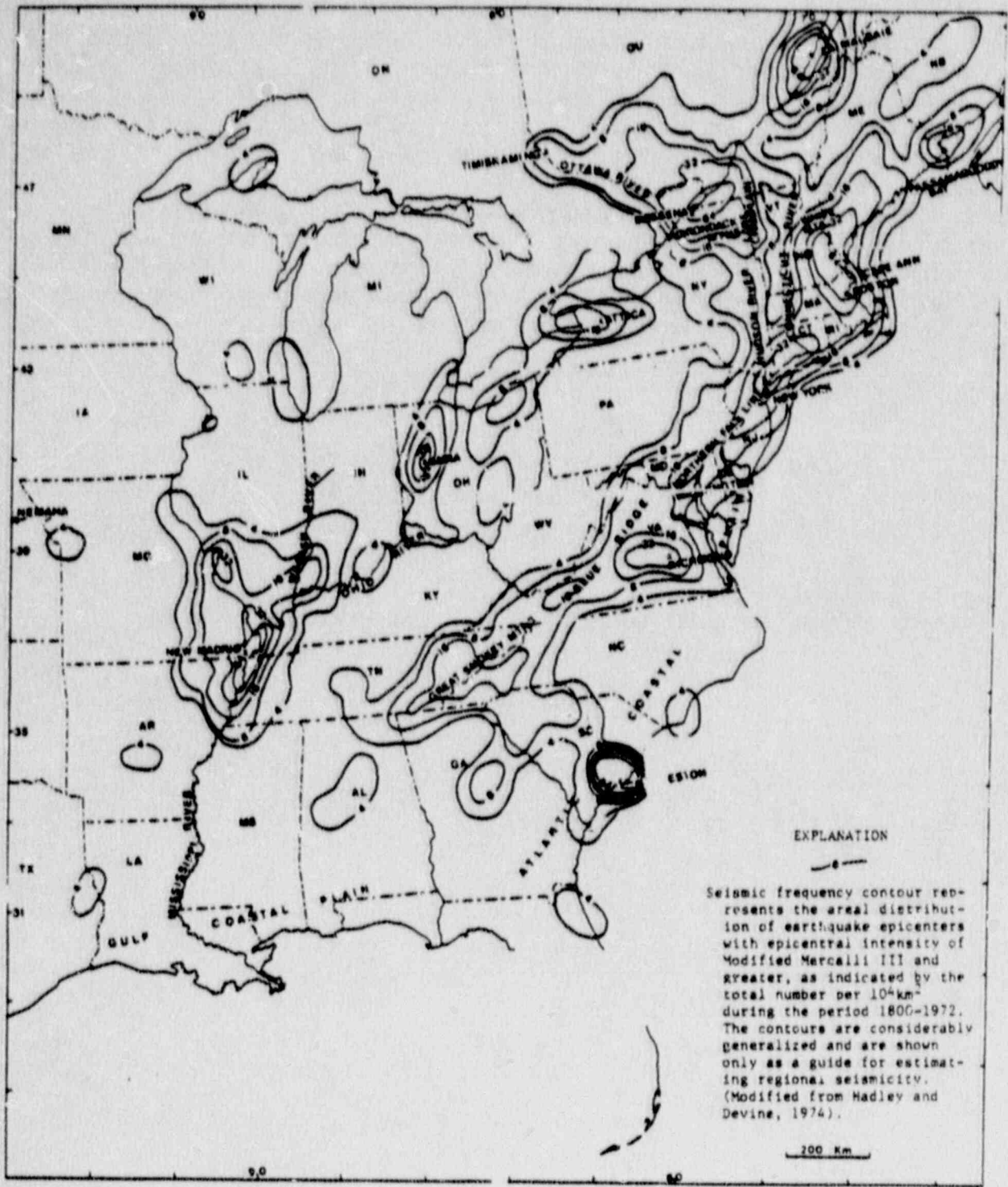


Fig. 1-1. Map of the eastern United States and adjacent Canada showing the seismic frequency for the period 1800-1972 (from Hadley and Devine, 1974).

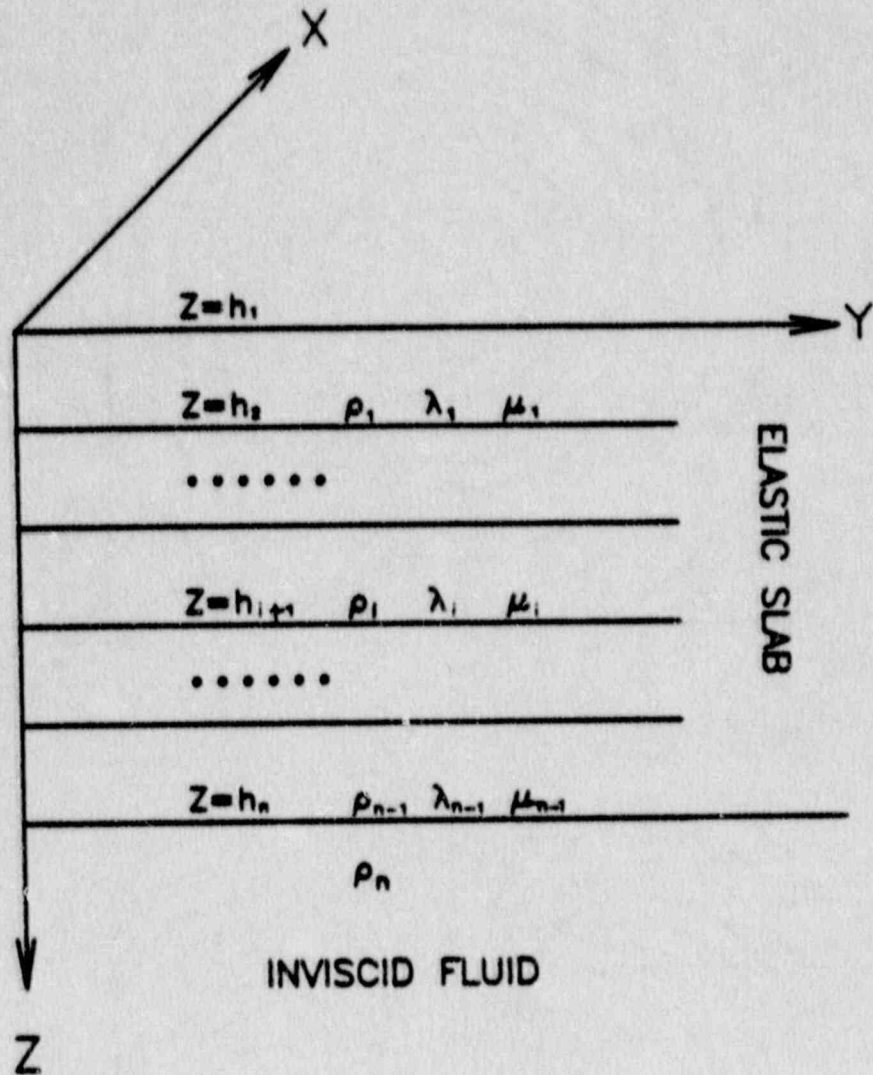


Fig. 2-1. The geometry and coordinate system for calculation of stress in a layered elastic slab (lithosphere) floating on an inviscid fluid (asthenosphere).

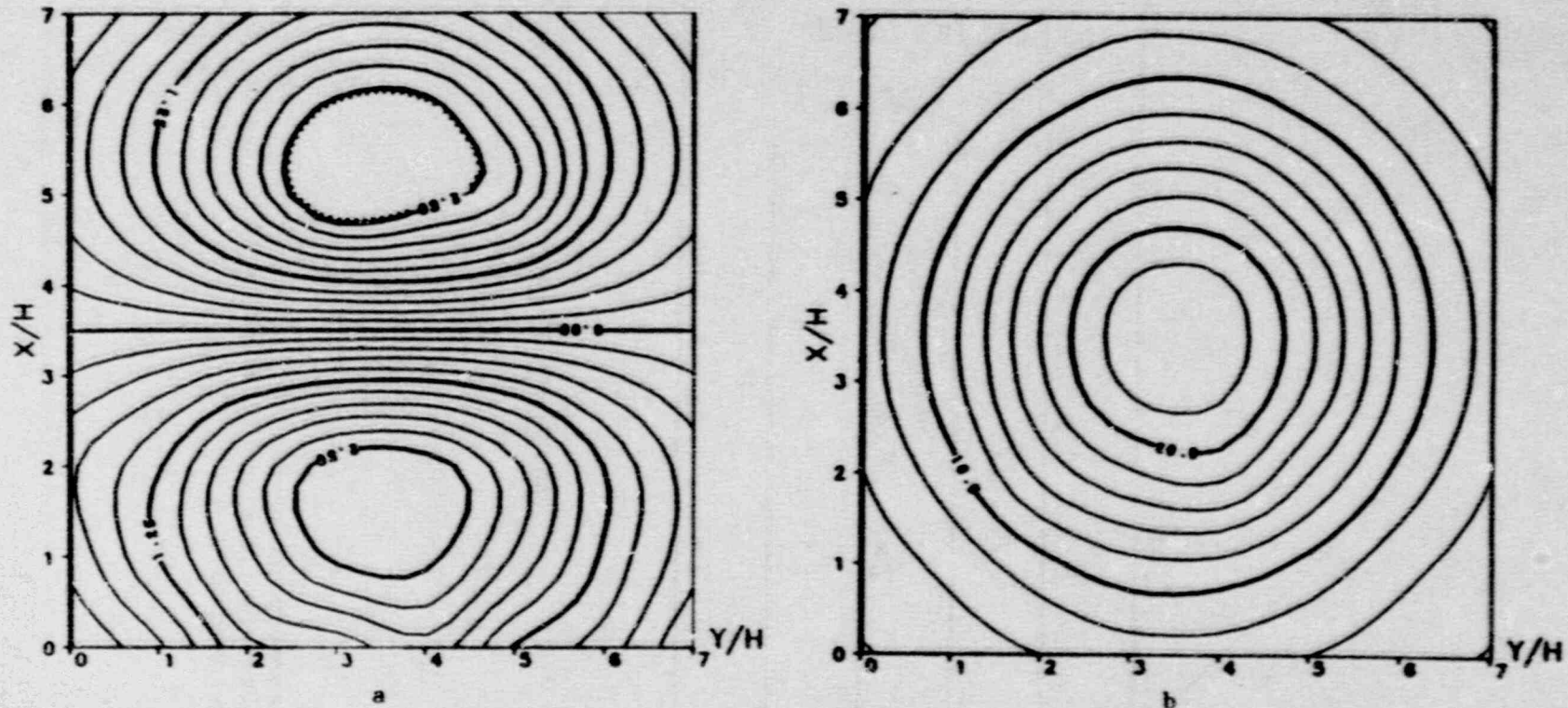
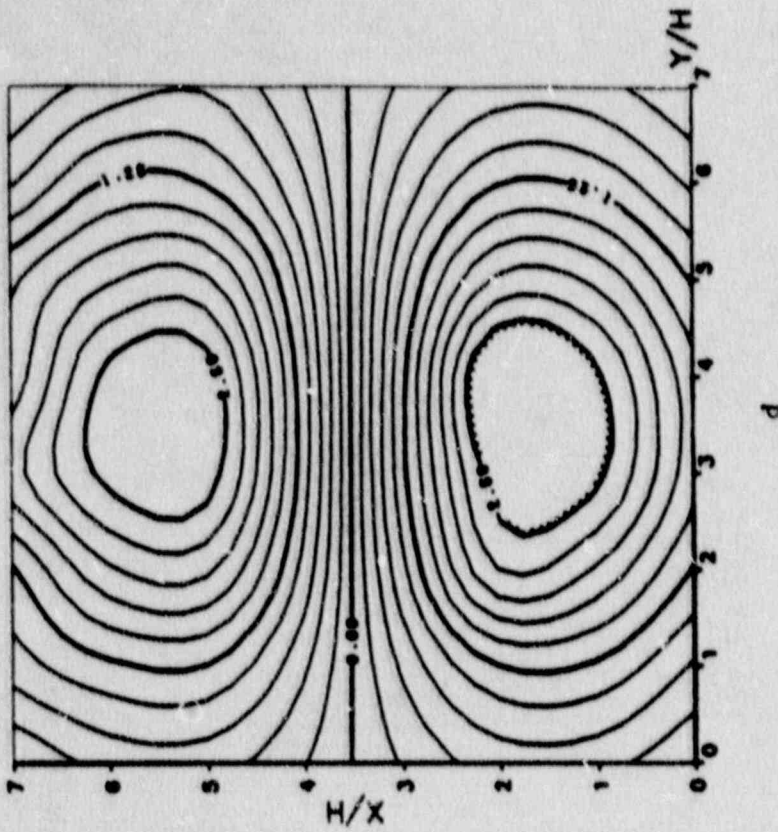
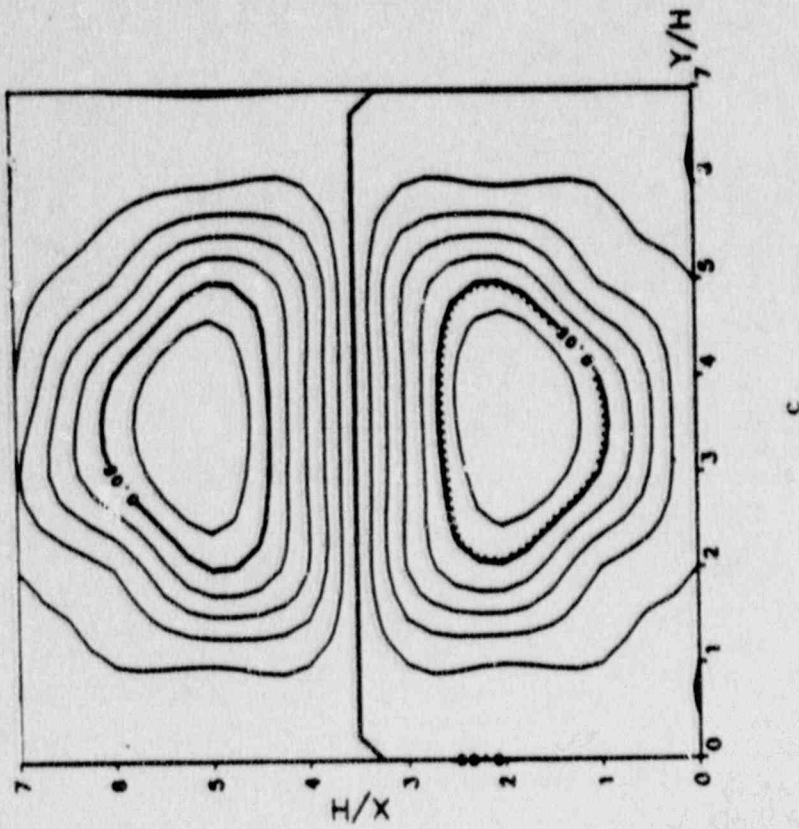


Fig. 2-2. Stresses and displacements under a surface disk load. The unit of displacement is $1/1000 H$, where H is the thickness of the slab. The unit of distance is H . The unit of stress is in P , where P is the magnitude of the given load. (a) Horizontal displacement U_x contours at $z=0$ (surface). (b) Vertical displacement U_z contours at $z=0$.

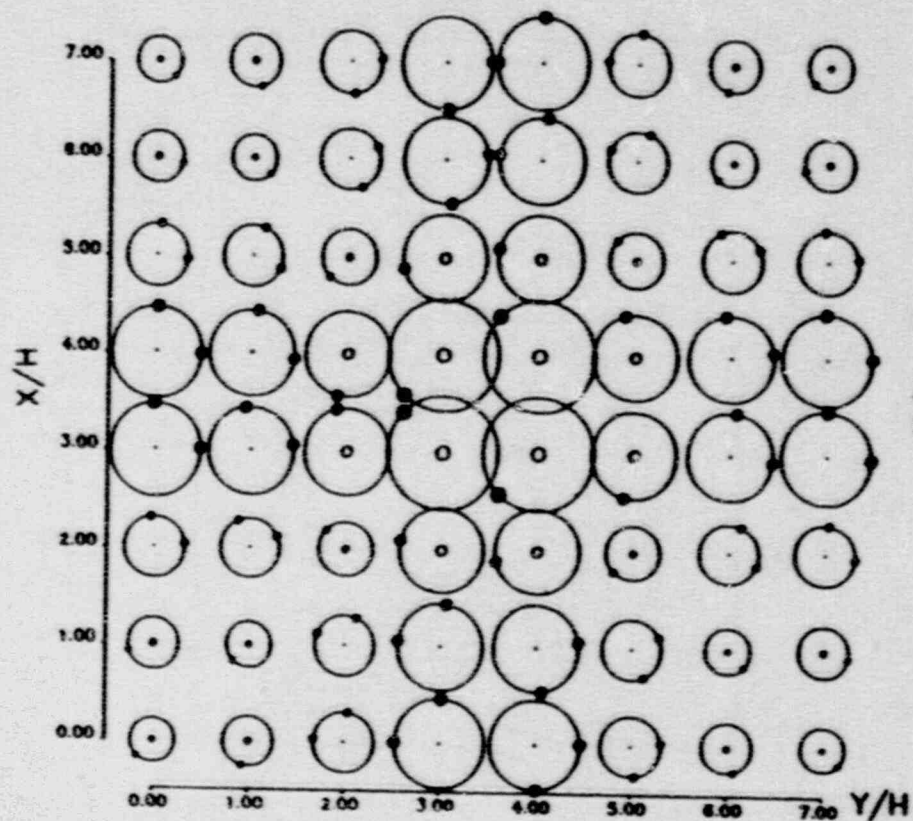


d

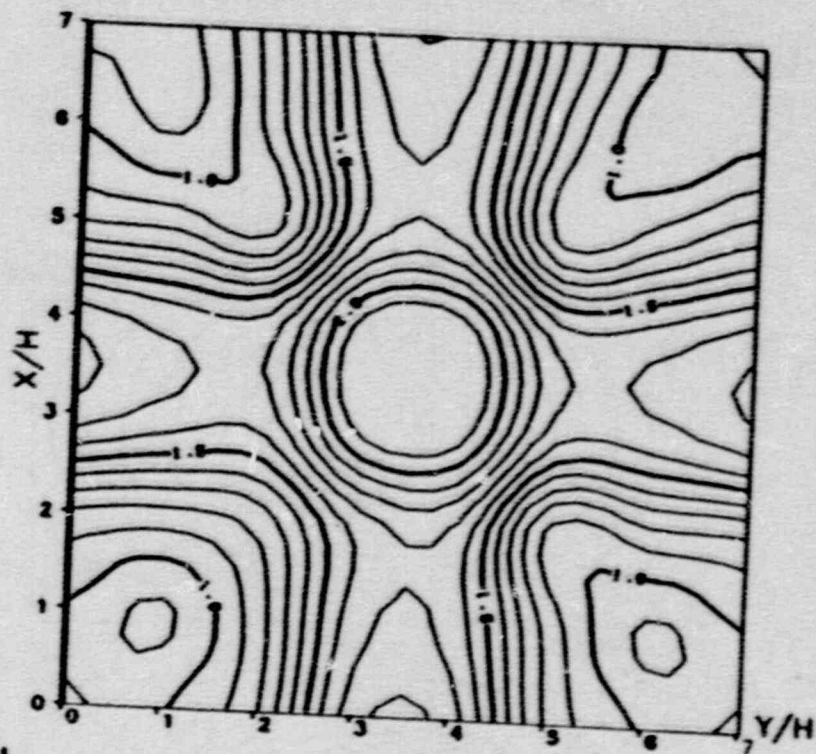


c

Fig.2-2. (c) Horizontal displacement U_x contours at $z=0.5H$. (d) U_x contours at $z=H$.



e



f

Fig. 2-2-e. The SNPPSA at $z=0$. (the Schmidt Net Projection of Principal Stress Axis). The open circle stands for the maximum extensional (S_1 or T) axis, the solid circle represents the maximum compressive (S_3 or P) axis and the dot is the intermediate axis (S_2 or B) axis.

2-2-f. Stress difference (S_1-S_3) contours (SDC) at $z=0$.

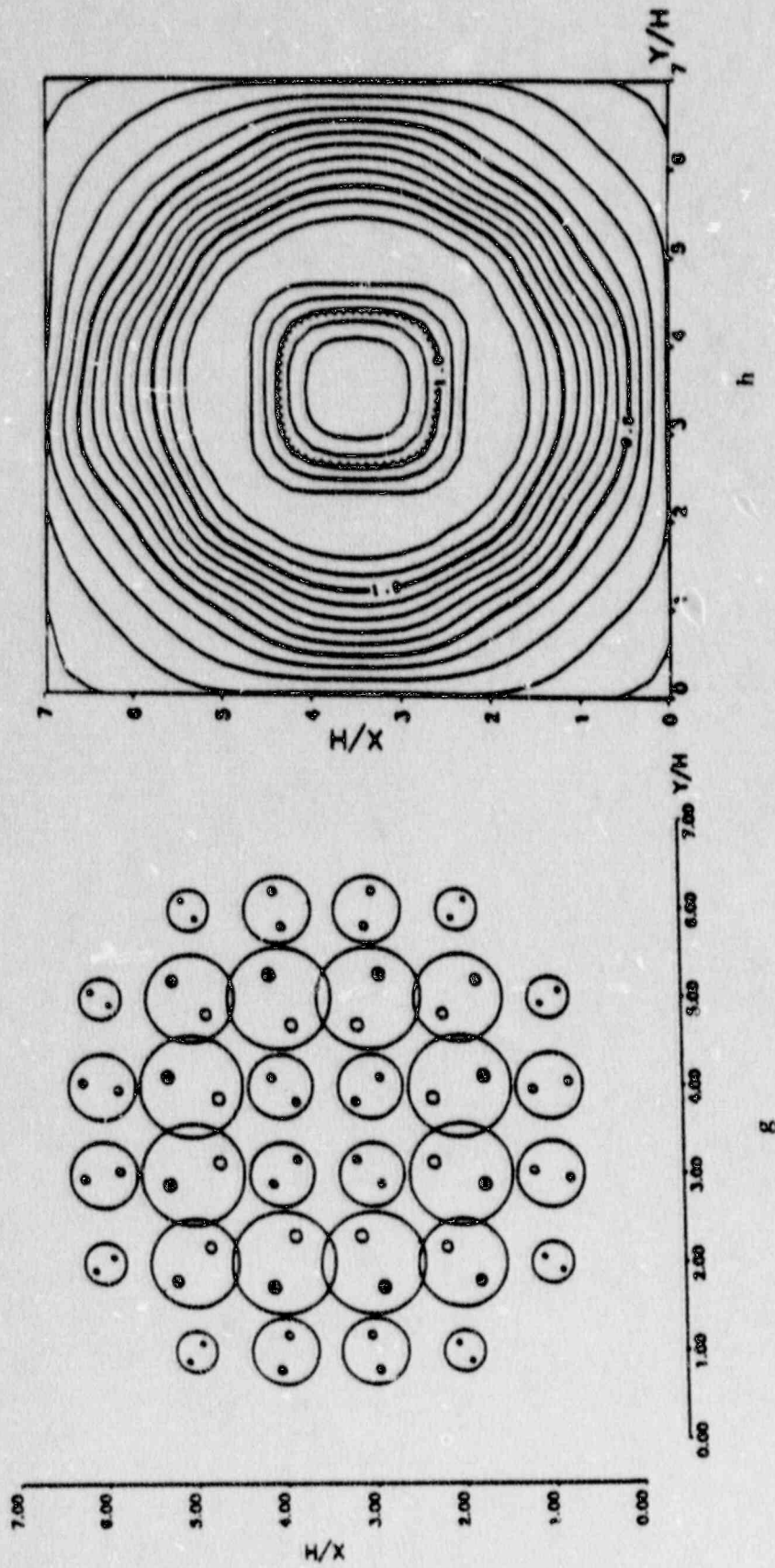


Fig. 2-2-h. SDC at $z=0.5H$

Fig. 2-2-g. SNPPSA at $z=0.5H$.

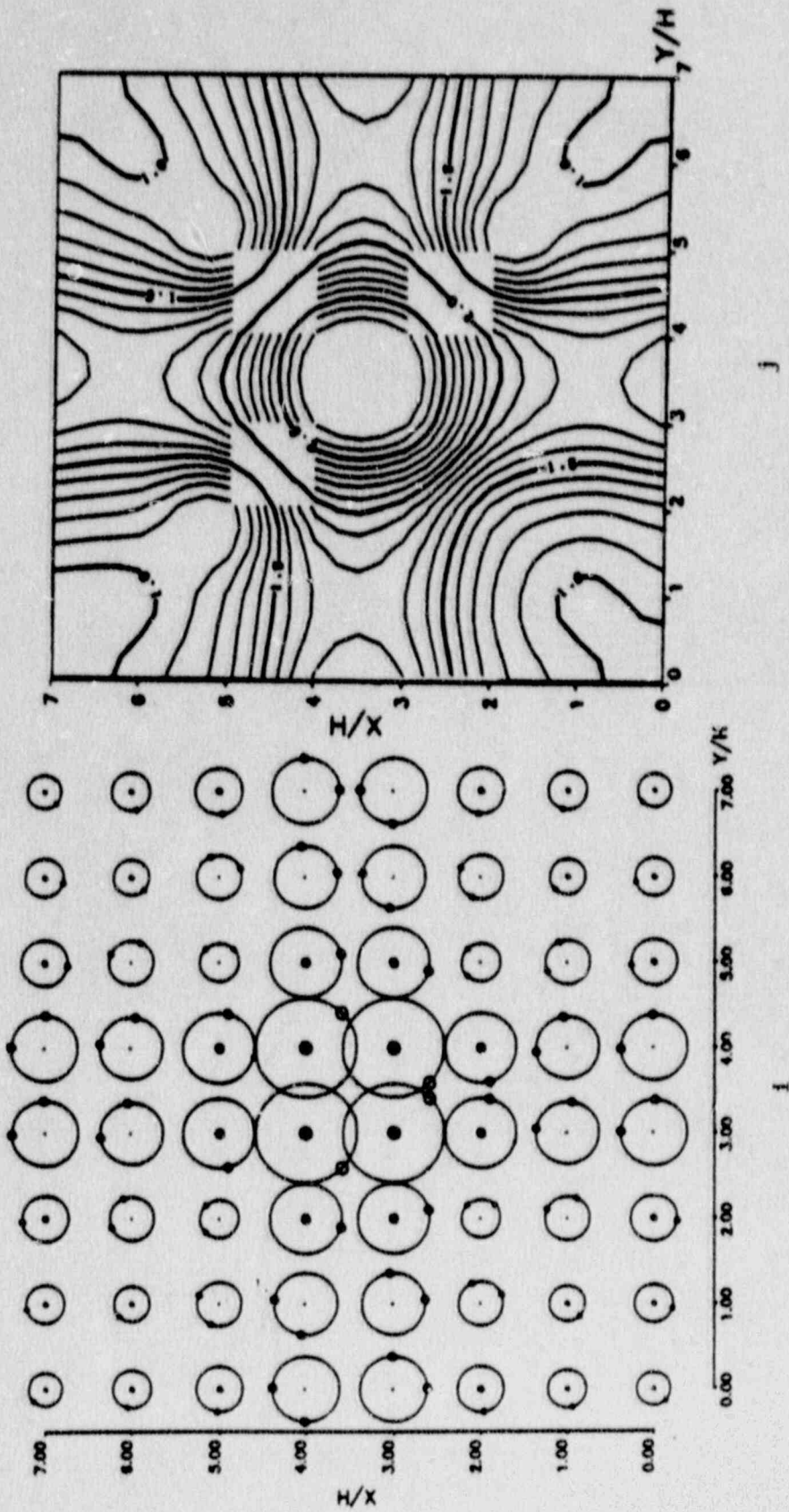


Fig. 2-2-1. SNPPSA at $z=H$.

Fig. 2-2-j. SDC at $z=H$.

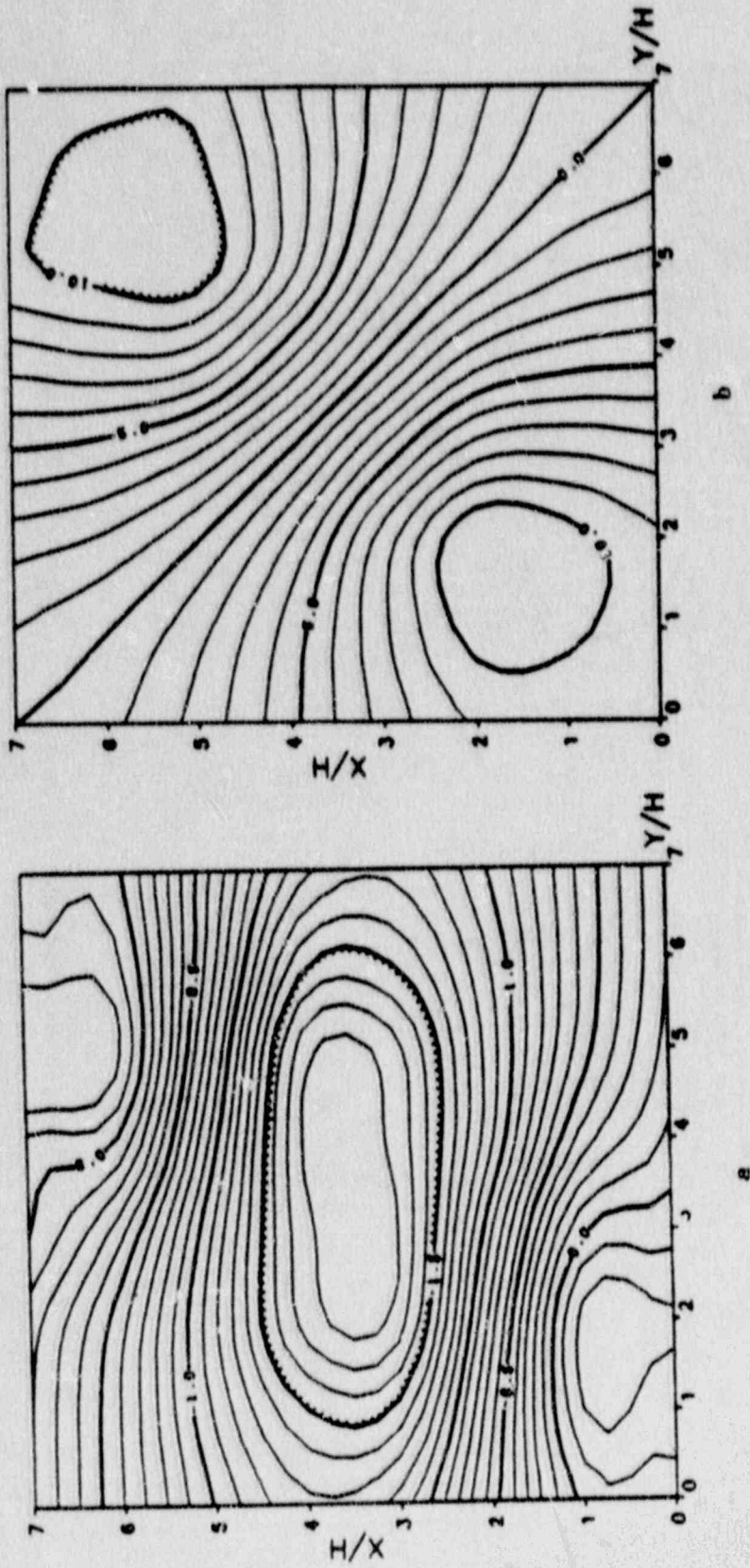
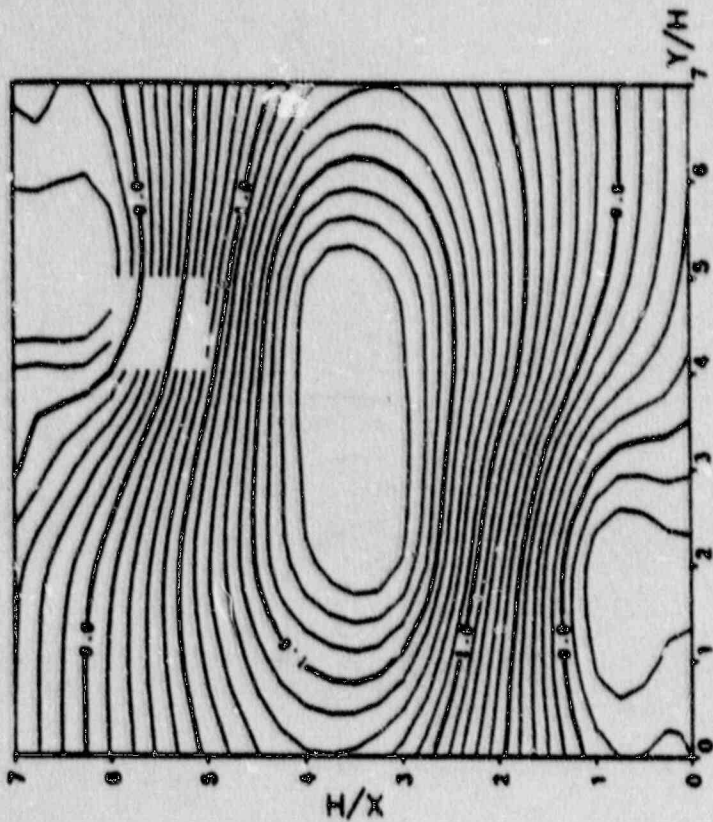
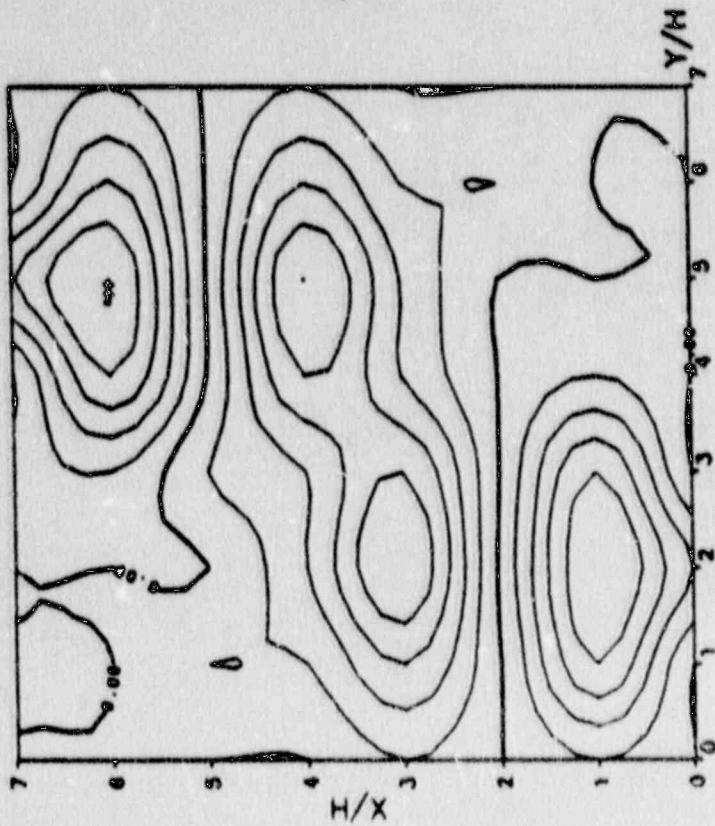


Fig. 2-3-a. Stresses and displacements under a surface dipole load. Horizontal displacement contours at $z=0$. Fig. 2-3-b. Vertical displacement contours at $z=0$.



d



c

Fig.2-3. (c) Horizontal displacement U_x contours at $z=0.5H$. (d) U_x contours at $z=H$.

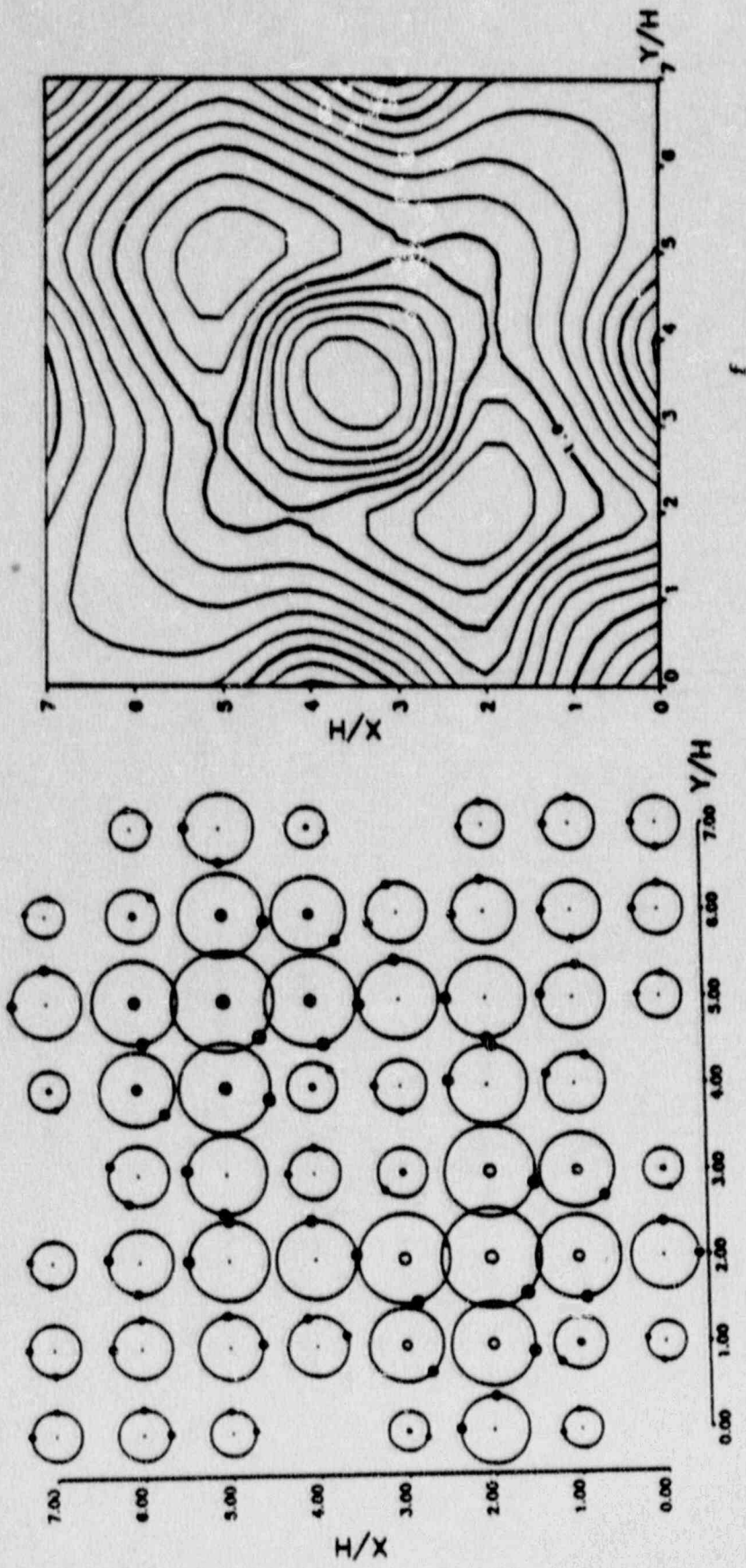


Fig. 2-3-f. Stress difference (SI-S3) contours (SDC) at $z=0$.

Fig. 2-3-e. SNPPSA at $z=0$.

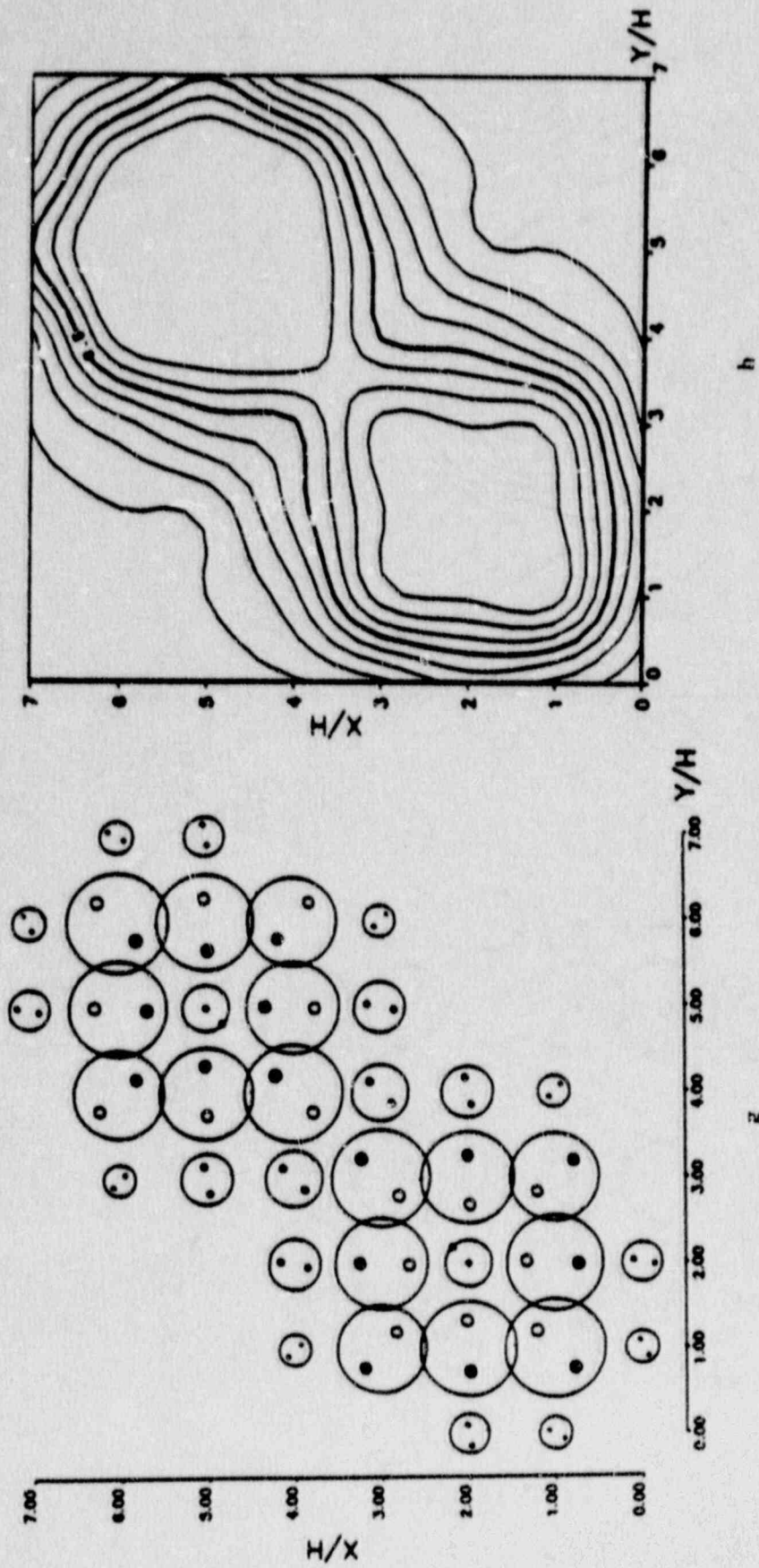


Fig. 2-3-h. SDC at $z=0.5H$.

Fig. 2-3-g. SNPPSA at $z=0.5H$.

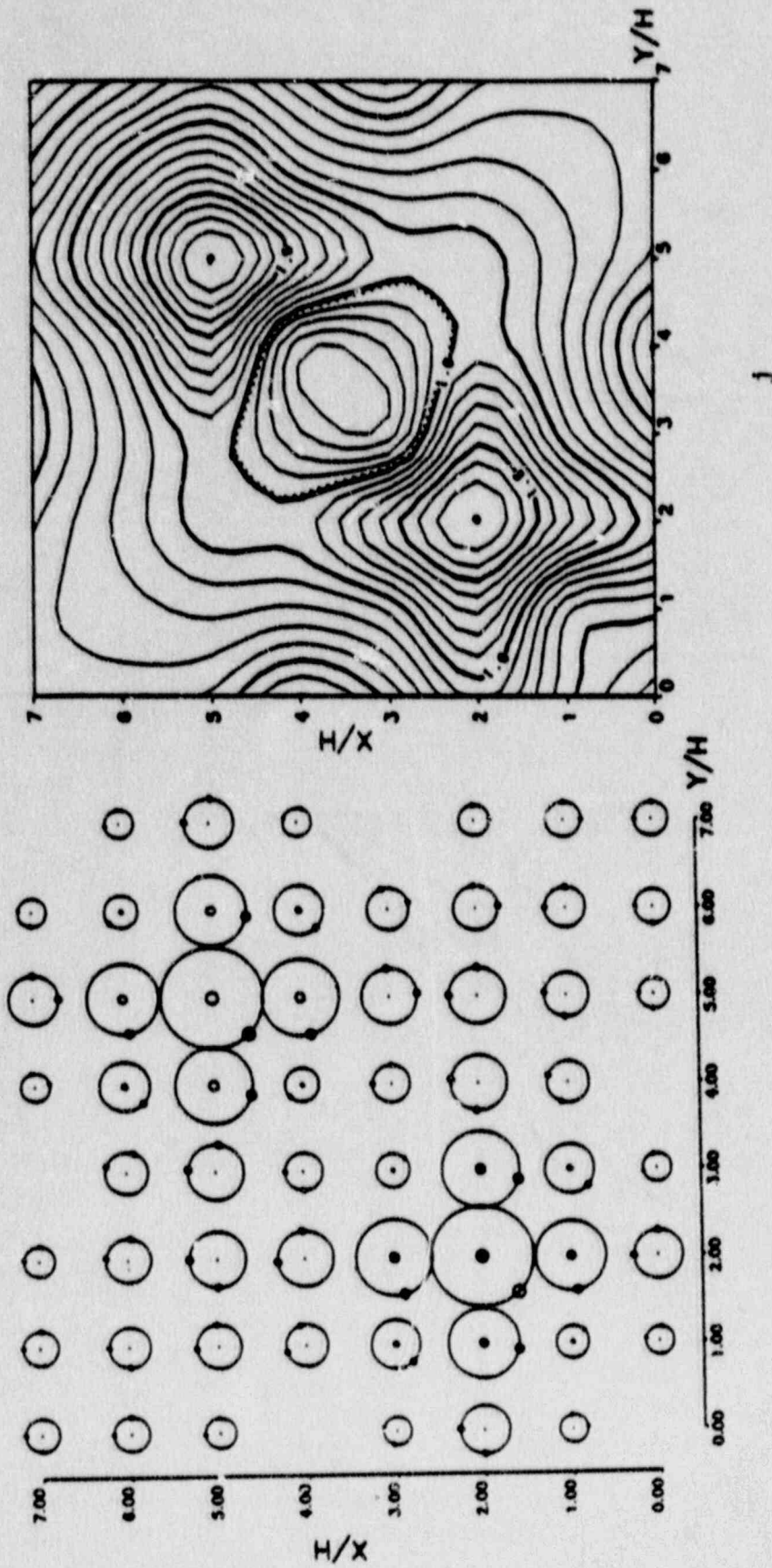


Fig. 2-3-j. SDC at $z=H$.

Fig. 2-3-i. SNPPSA at $z=H$.

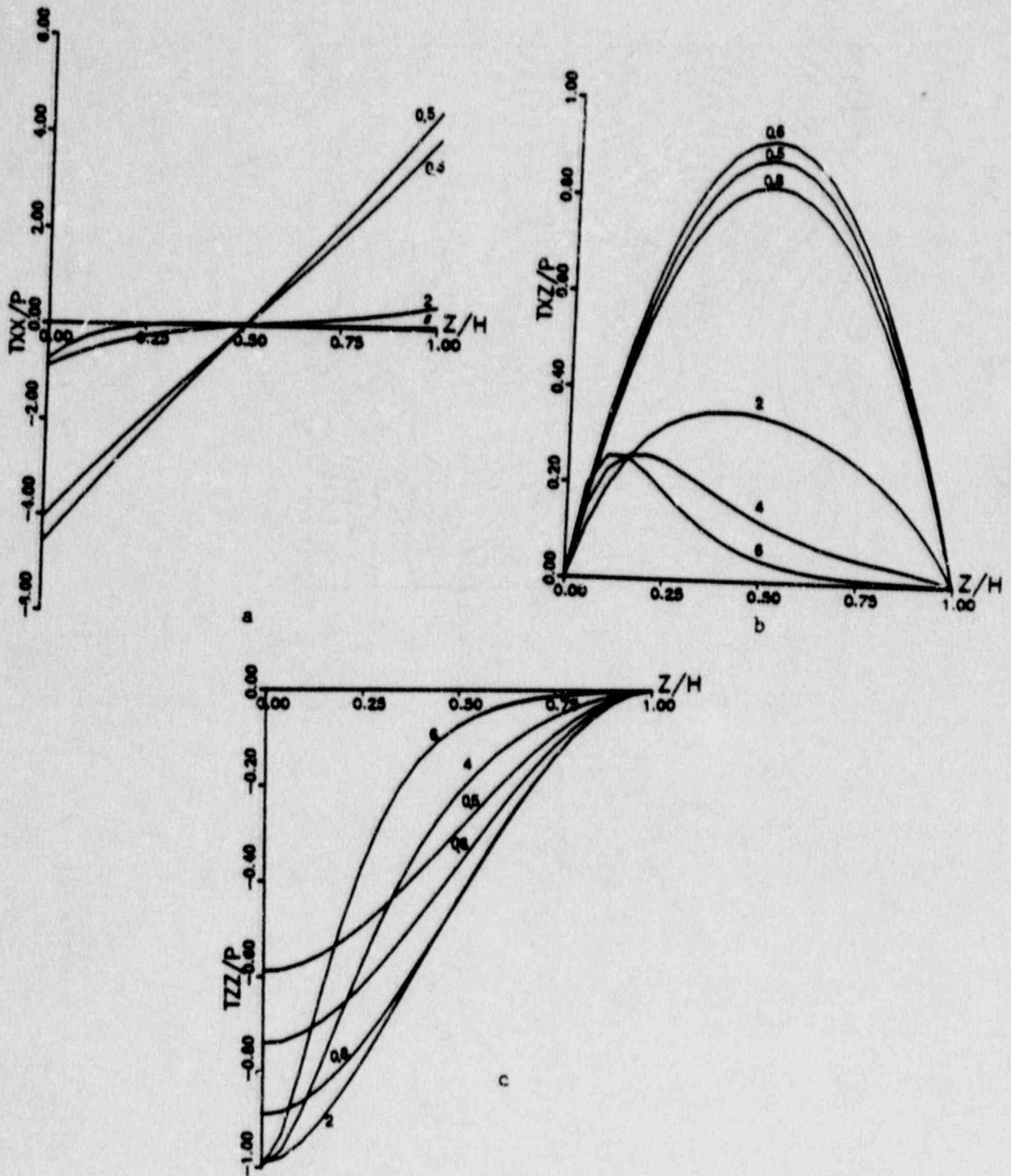
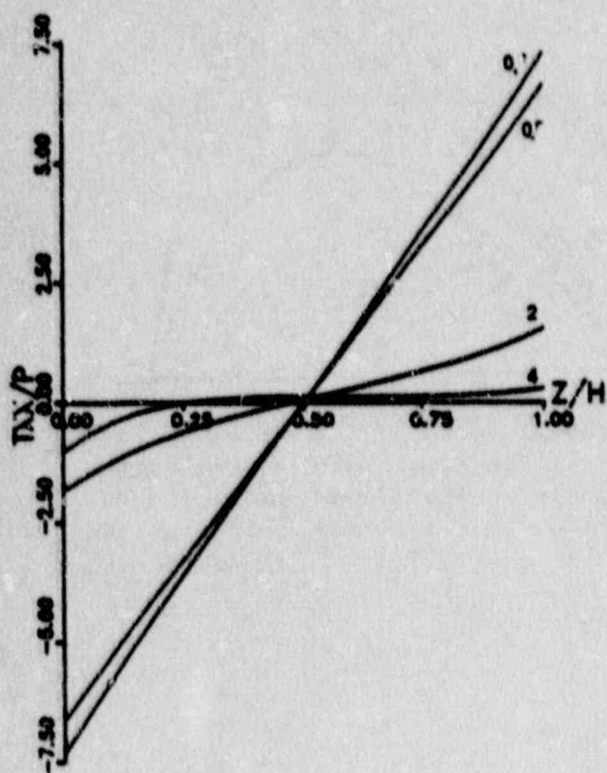
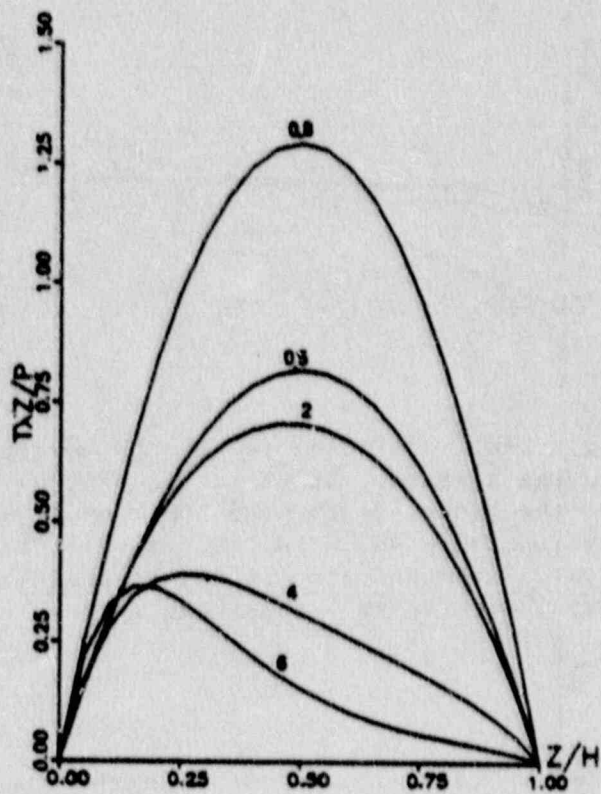


Fig. 2-4. Stresses for the three-dimensional model with a harmonic load on the surface. Stresses are plotted as a function of the wavelengths of the load and depth. Stresses are divided by the amplitude of the load. (a) Shear stress T_{xz} . (b) Horizontal normal stress T_{xx} . (c) Vertical normal stress T_{zz} .



a



b

Fig. 2-5. Stresses for the two-dimensional model with a harmonic load on the surface. Stresses are plotted as a function of the wavelengths of the load and depth. Stresses are divided by the amplitude of the load. (a) Horizontal normal stress T_{xx} . (b) Shear stress T_{xz} .

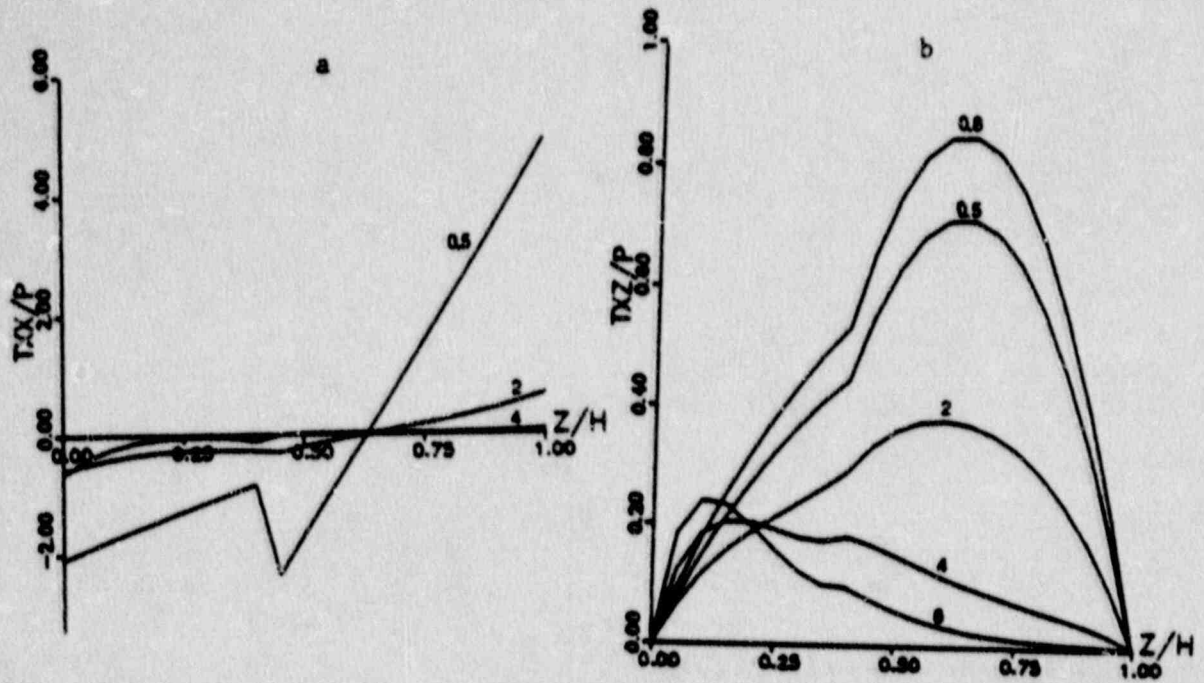


Fig. 2-6. Stresses for the three-dimensional model with a harmonic load on the surface. Stresses are plotted as a function of the wavelengths of the load, depth and the elastic parameters. Lamé's parameter in top layer ($z=0-0.4H$) is 10 GPa which is one quarter of that of second layer. Stresses are divided by the amplitude of the load. (a) Horizontal normal stress T_{xx} . (b) Shear stress T_{xz} .

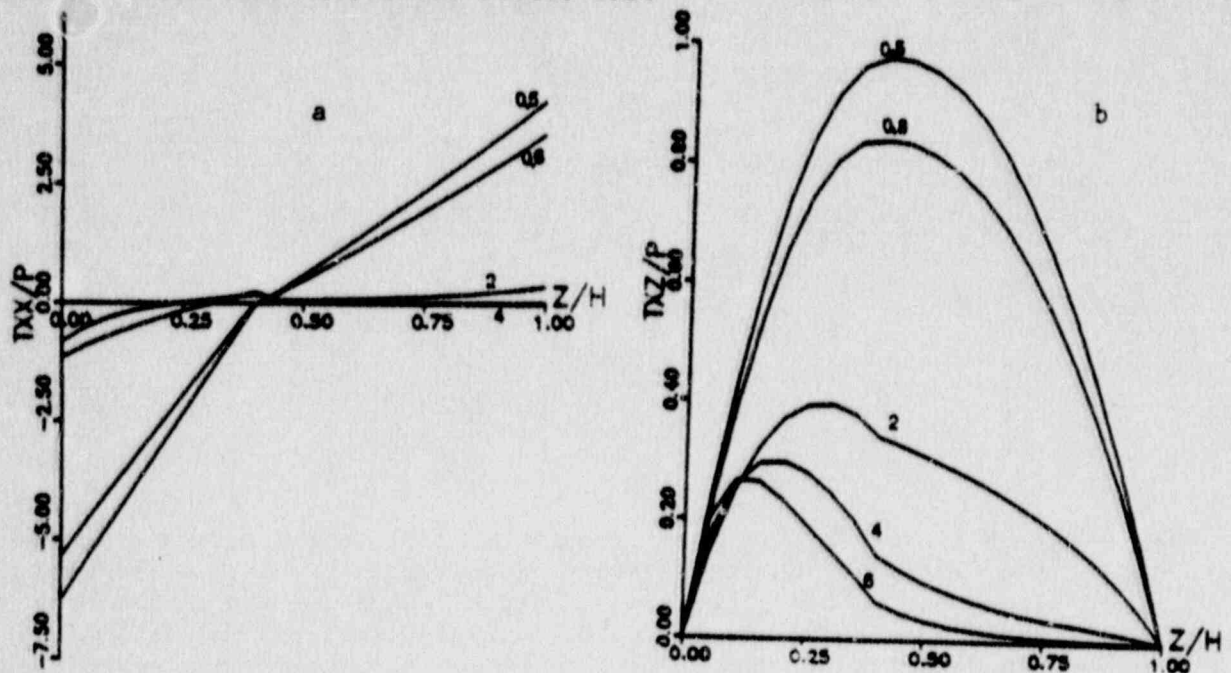


Fig. 2-7. Stresses for the three-dimensional model with a harmonic load on the surface. Stresses are plotted as a function of the wavelengths of the load, depth and the elastic parameters. Lamé's parameter in top layer ($z=0-0.4H$) is 80 GPa which is two times of that of second layer. Stresses are divided by the amplitude of the load. (a) Horizontal normal stress T_{xx} . (b) Shear stress T_{xz} .

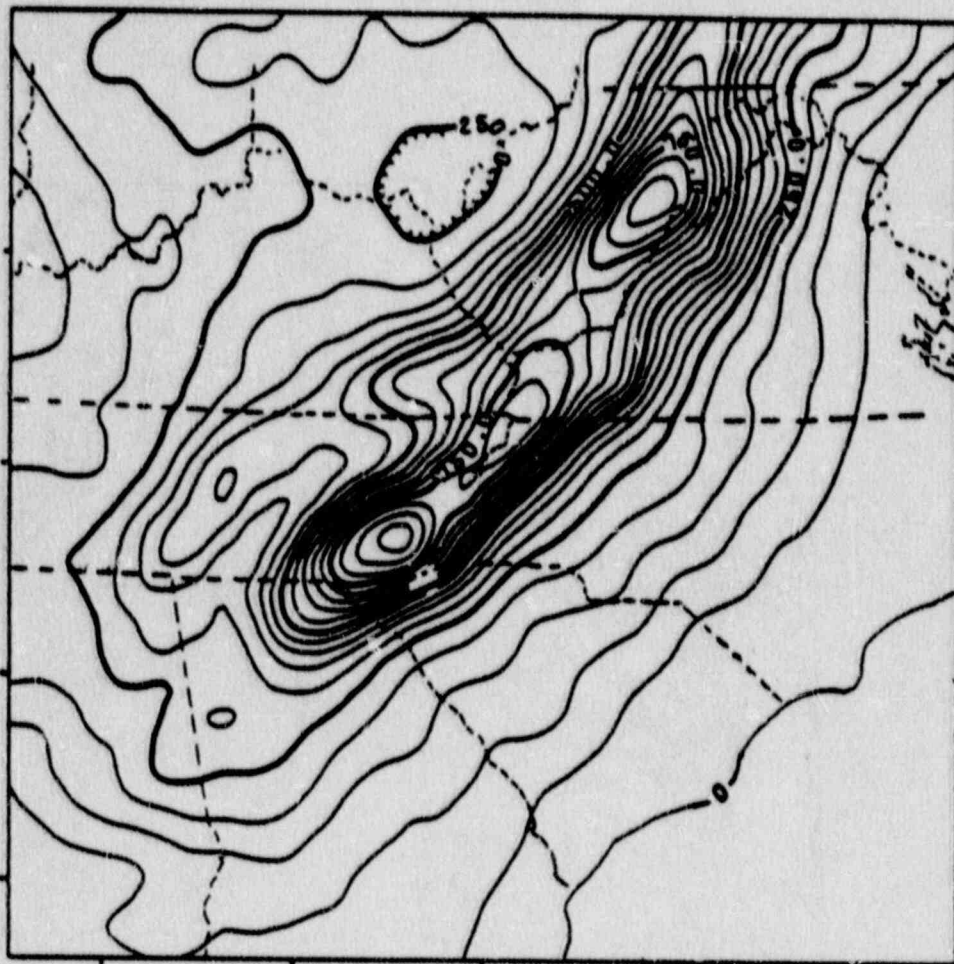


Fig. 3-1. Topographic contours (in meters) of the Southern Appalachians. Contouring interval is 50 meters.



Fig. 3-2. Topographic and bathymetric contours (in meters) of the Coastal Plain and eastern continental margin centered at Charleston, South Carolina. Contouring interval is 100 meters.

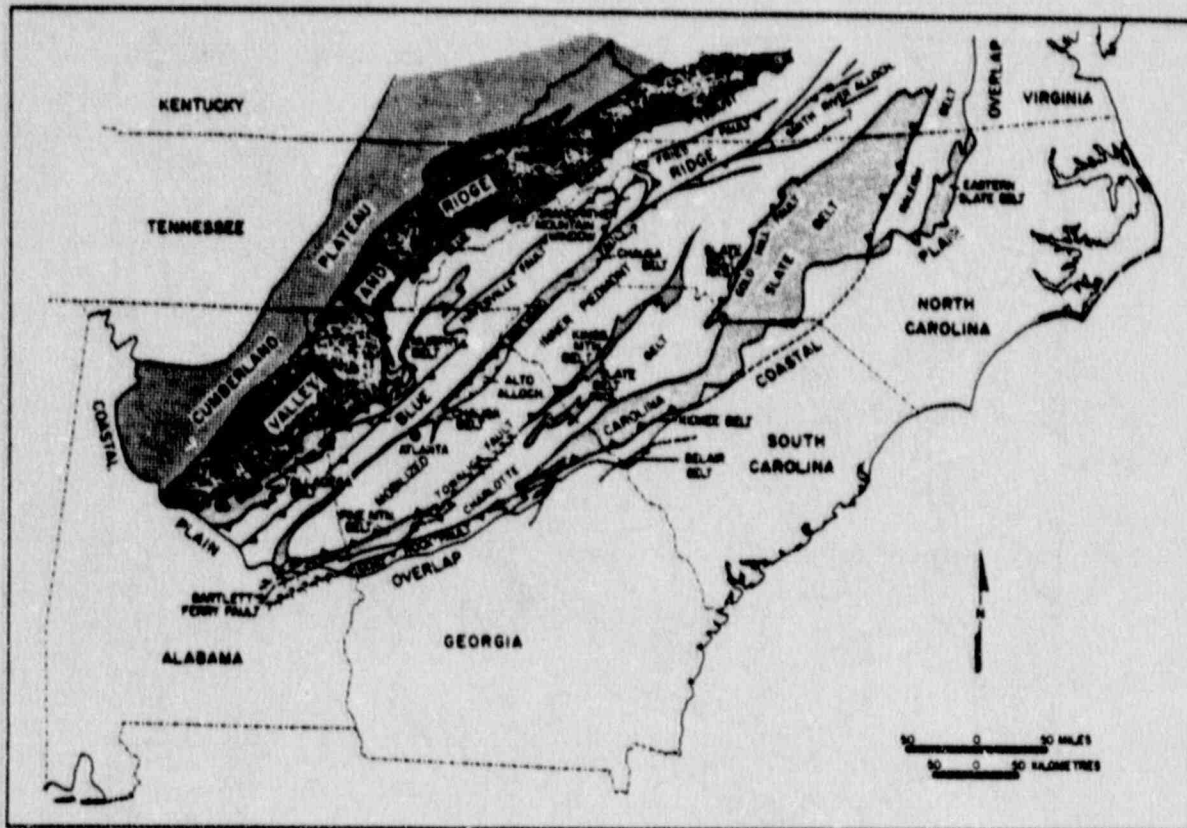


Fig. 3-3. Map of the study area showing the geologic provinces (After Hatcher and Zietz, 1980).

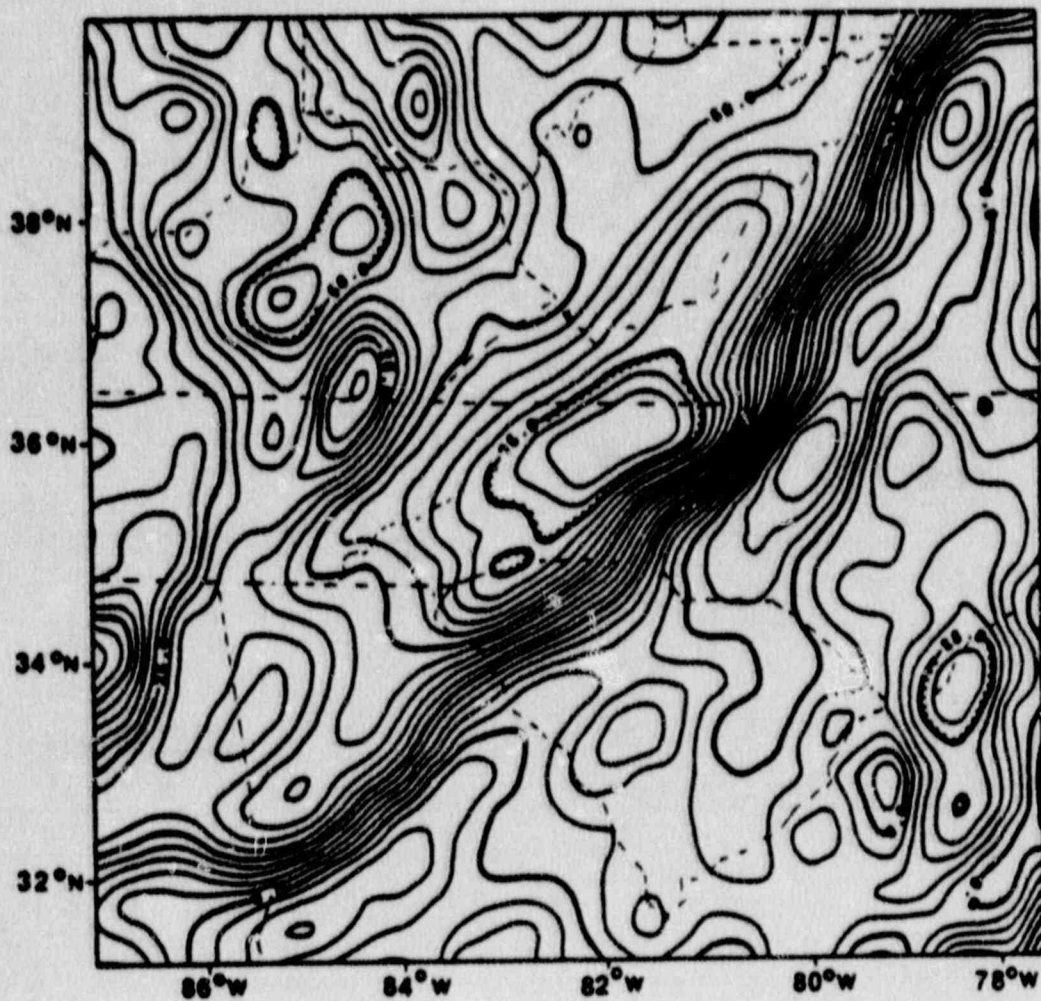


Fig. 3-4. The Bouguer gravity anomalies (in mGal) of the Southern Appalachians. Contouring interval is 5 mGal.

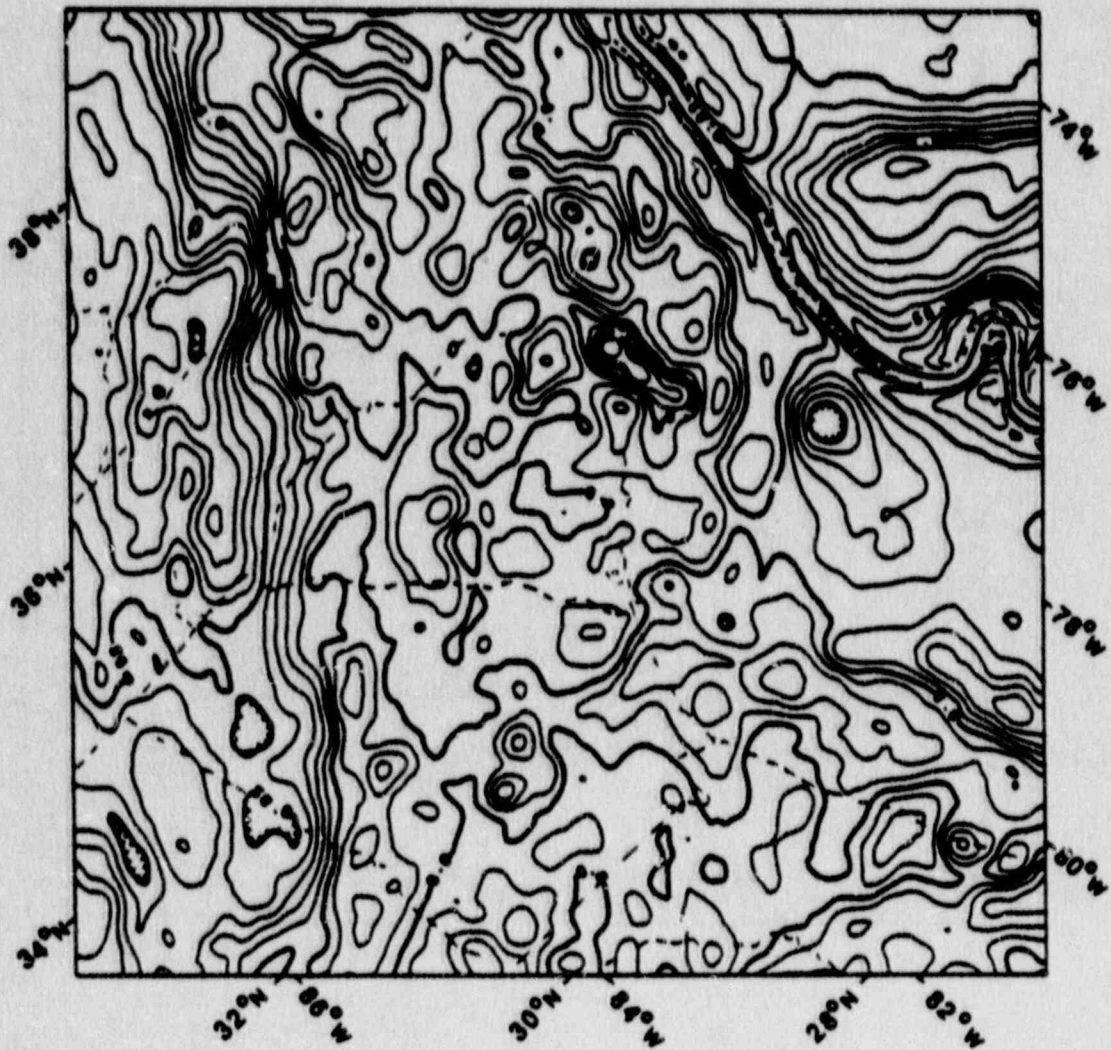


Fig. 3-5-a. The original Bouguer gravity anomalies of the Coastal Plain and the eastern continental margin centered at Charleston, South Carolina (before bathymetric correction). Contouring interval is the same in Fig. 3-4.

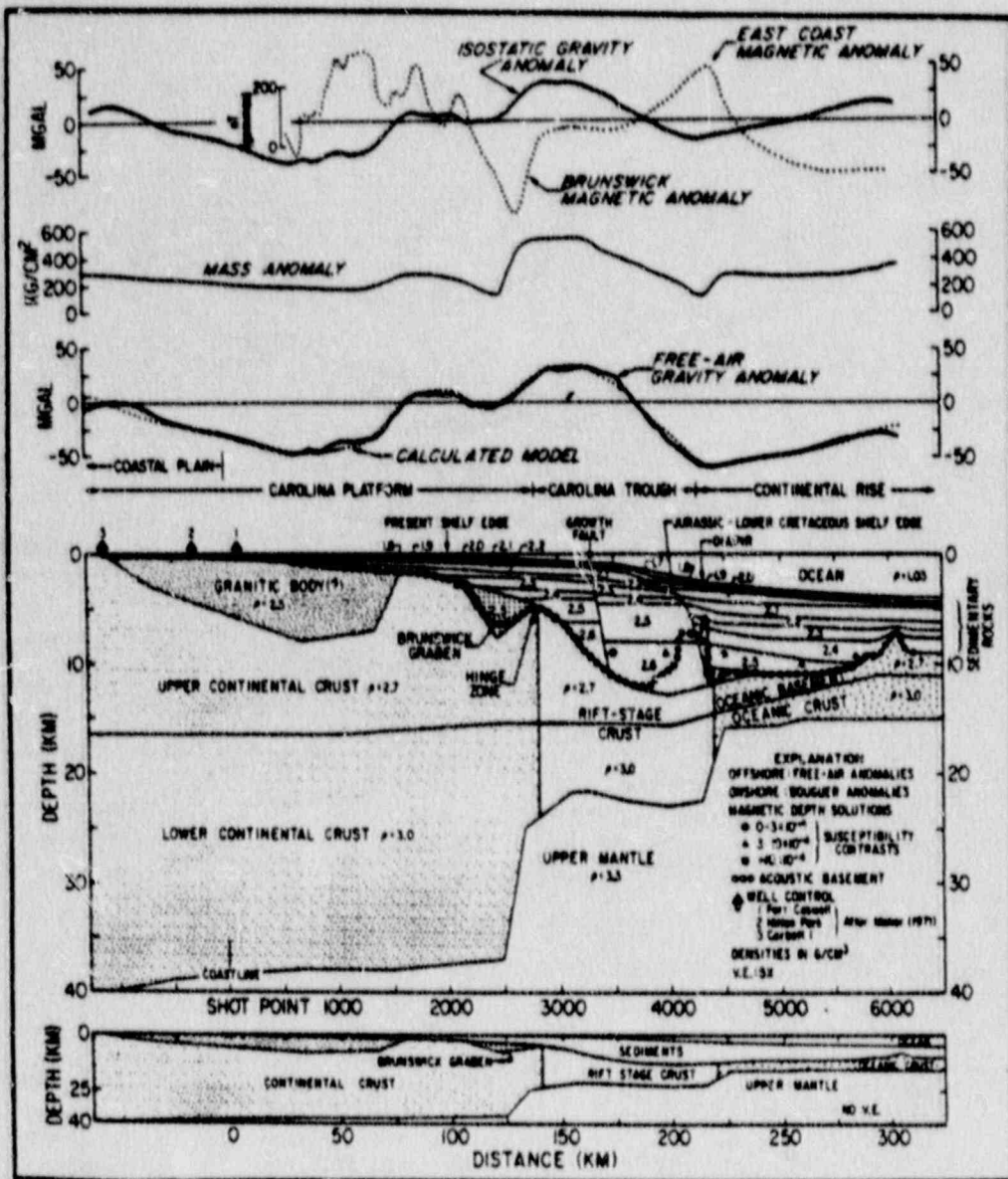


Fig. 3-6. Gravity, magnetic and bathymetric profiles across the southeastern continental margin (From Hutchinson et al., 1983).

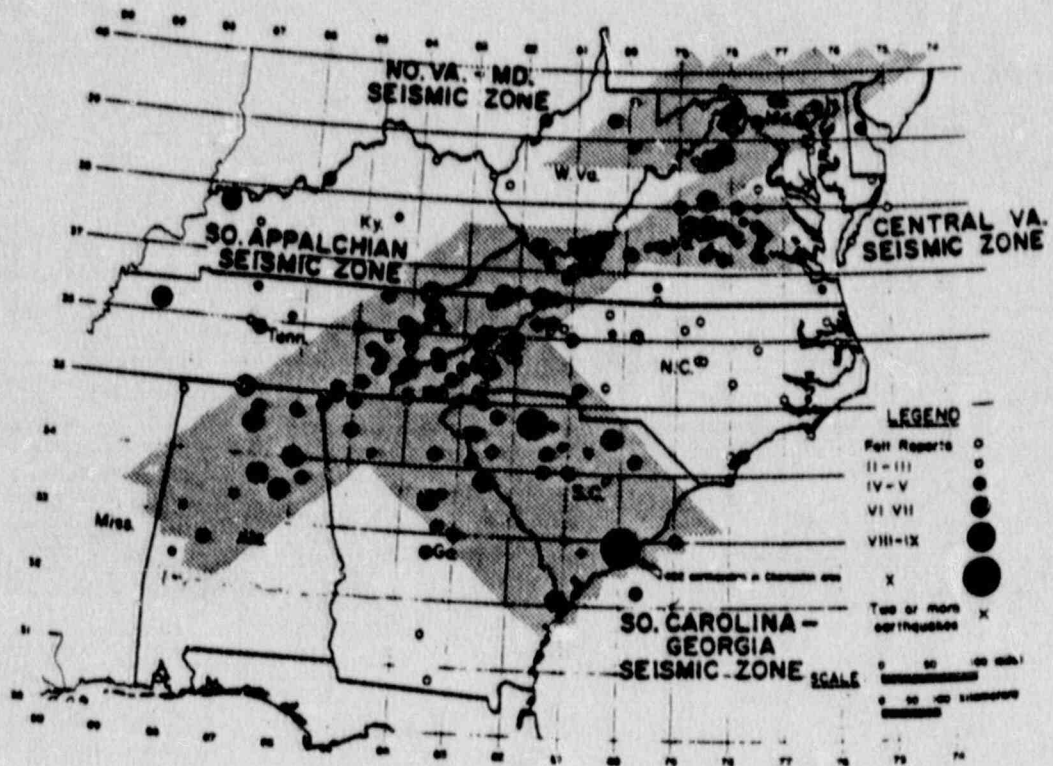


Fig. 4-1. Historical seismicity (1754-1970) and definition of seismic zones in the southeastern United States (From Bollinger, 1973).

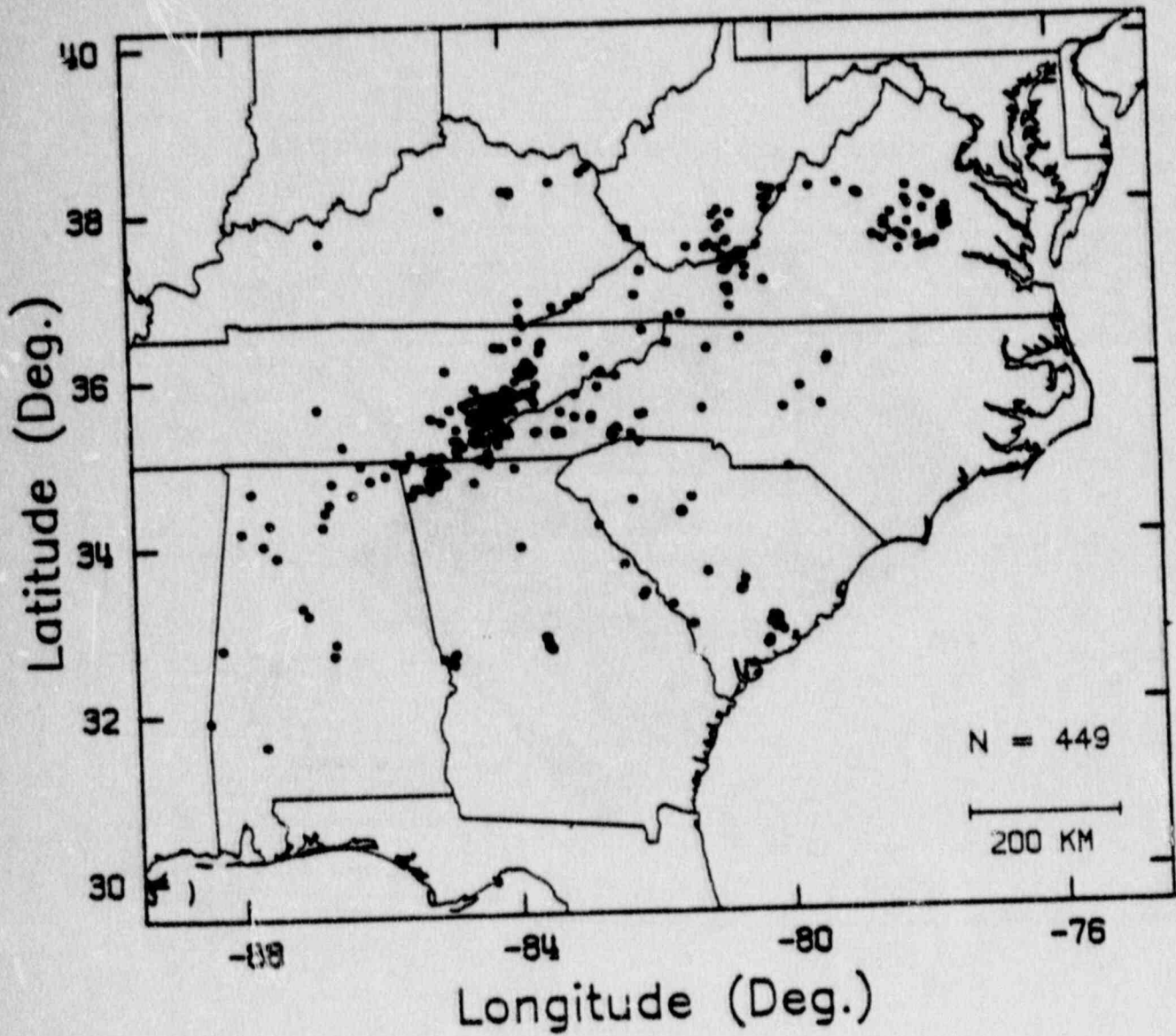


Fig. 4-2. Epicenters for recent earthquakes ($M > 0.0$) in the southeastern United States from July 1977 to 1985 (From Sibol and Bollinger, 1986).

RECENT SEISMICITY AND ITS RELATIONSHIP TO EARTHQUAKE

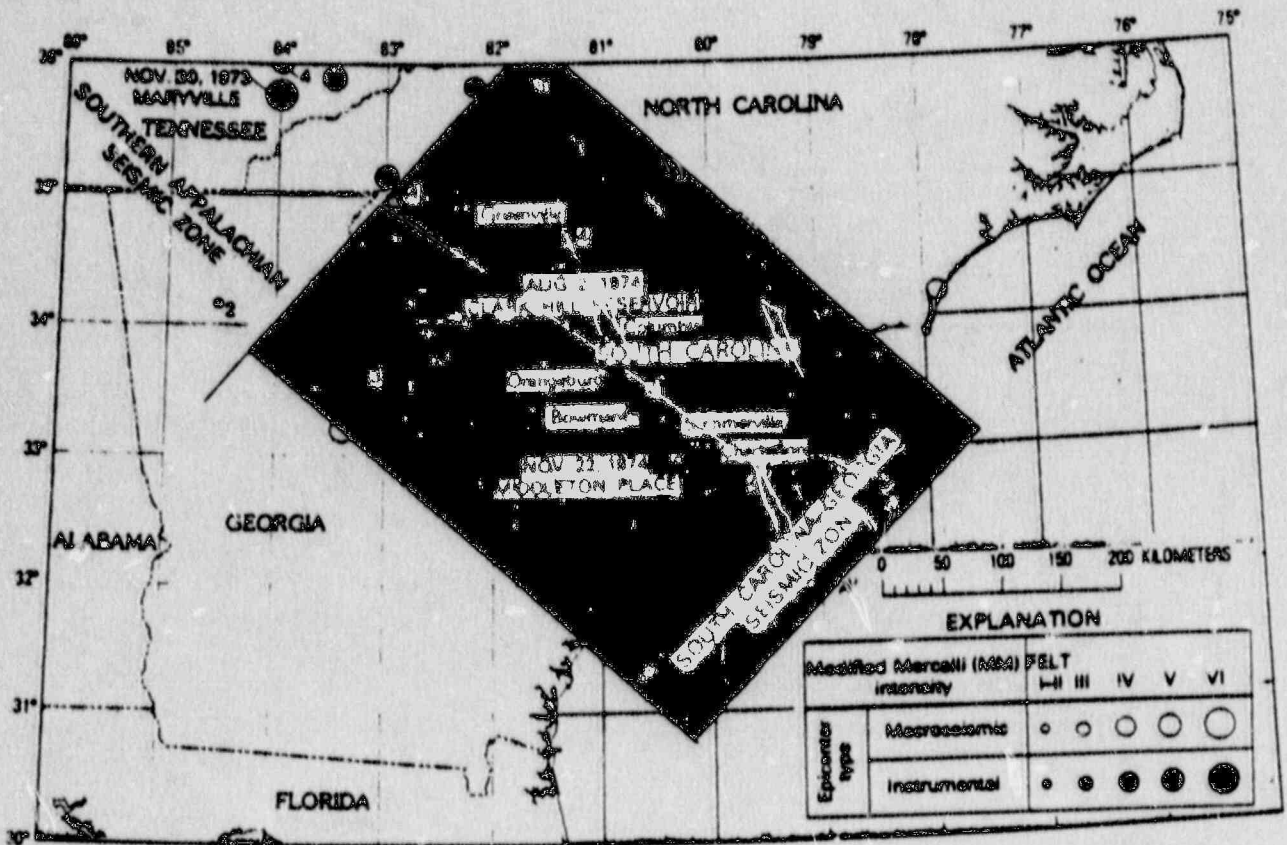


Fig. 4-3. Seismicity (1961-1975) in the South Carolina-Georgia seismic zone (From Tarr, 1977).

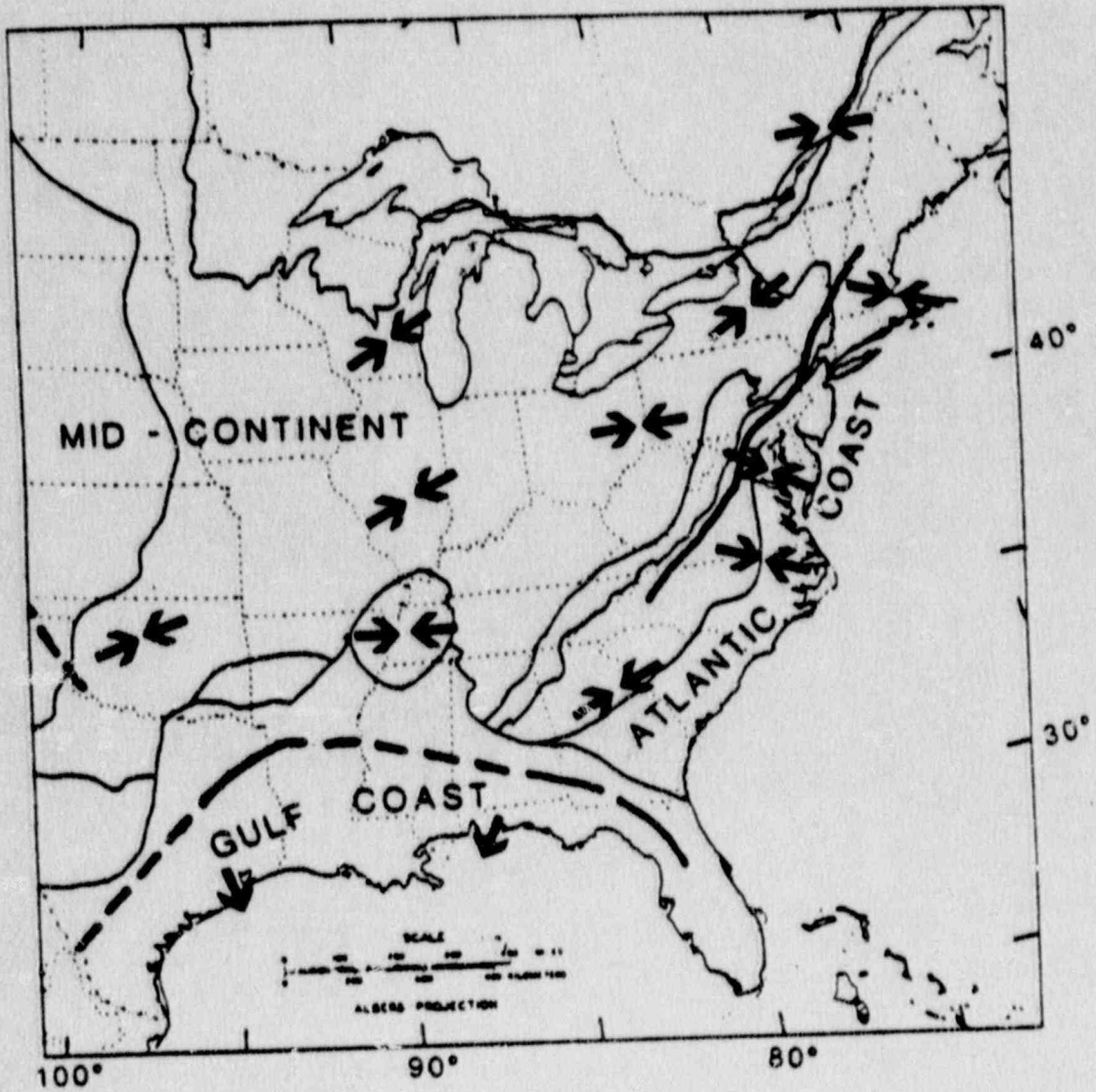


Fig. 4-4. Stress map of the eastern United States (from Zoback, 1983).

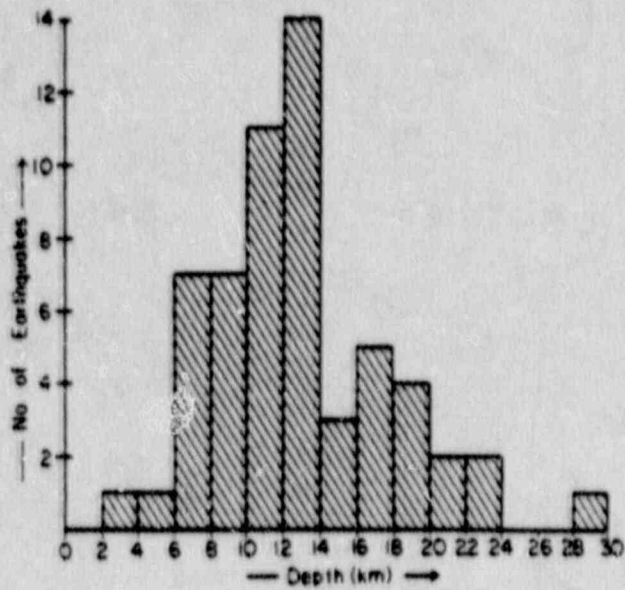


Fig. 5-1. Depth for 58 earthquakes in the Southern Appalachians (from Johnston et al., 1985).

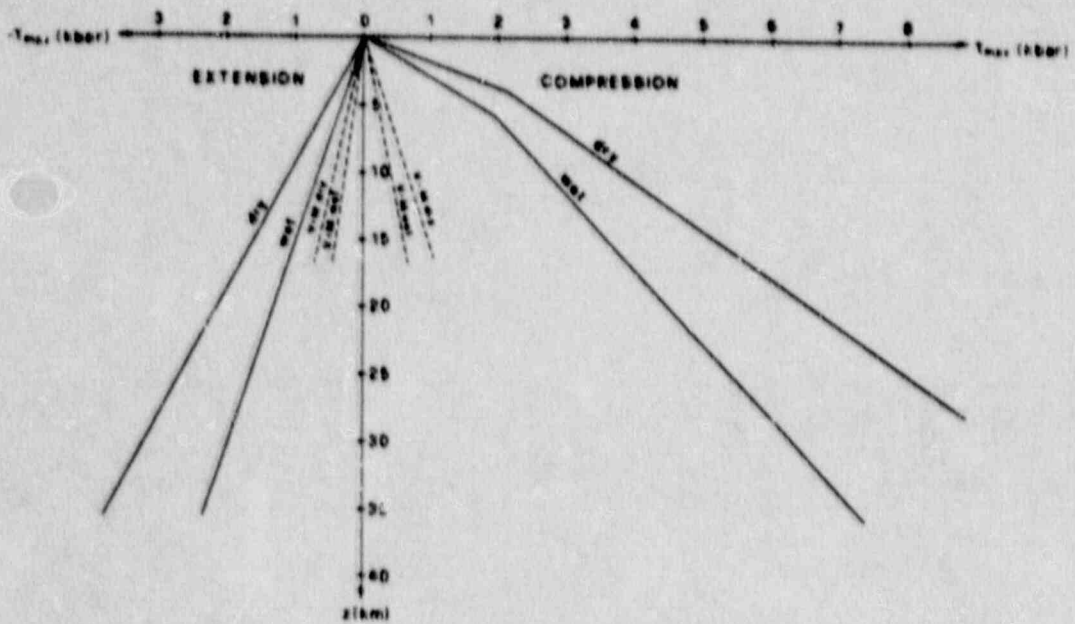
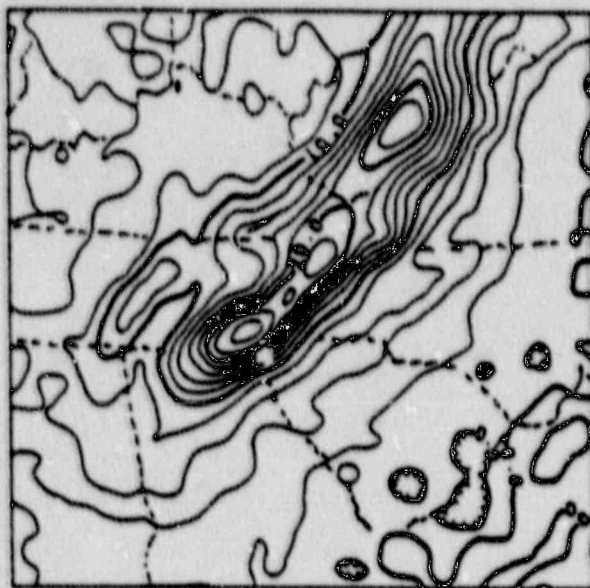
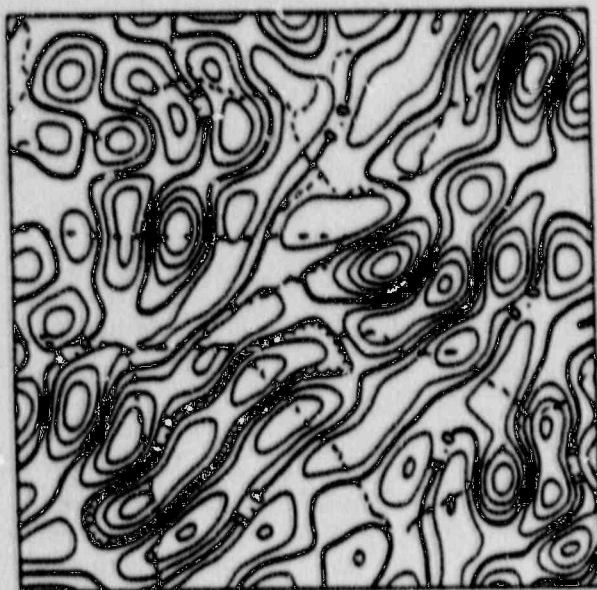


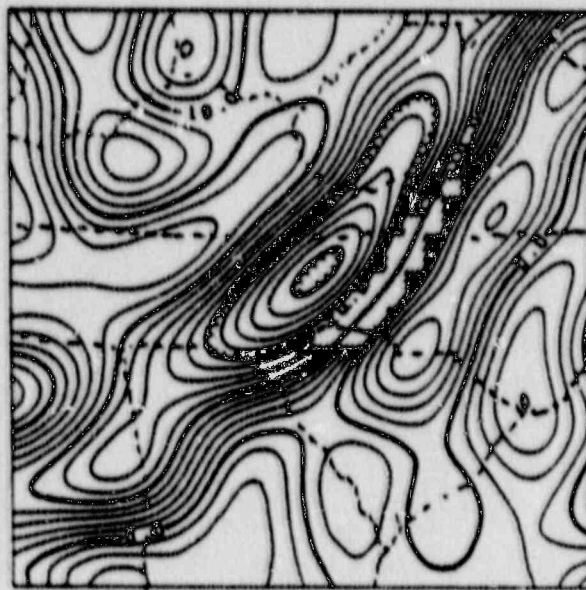
Fig. S-2. Rock strength and depth relations (from Meissner and Strenhlau, 1982). Dry: measurements performed on a great number of dry samples, no pore pressure; wet: pore pressure, assumed to be hydrostatic; V + M: measurement on vermiculite and montmorillonite.



a

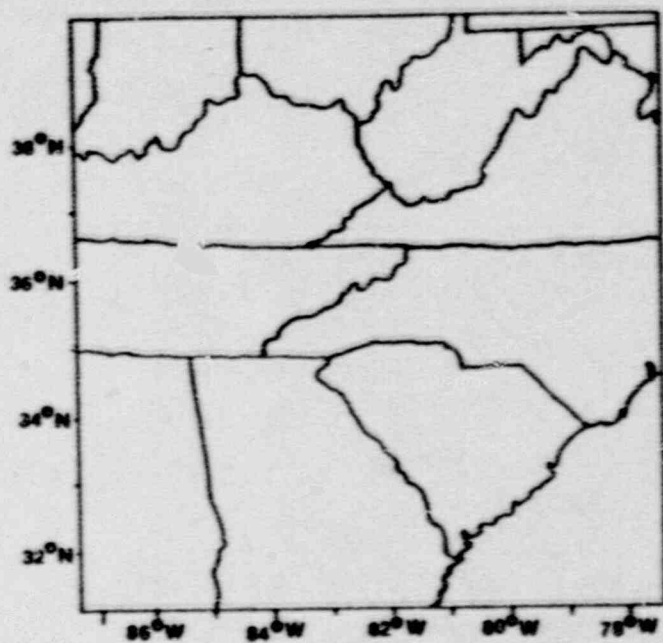


b

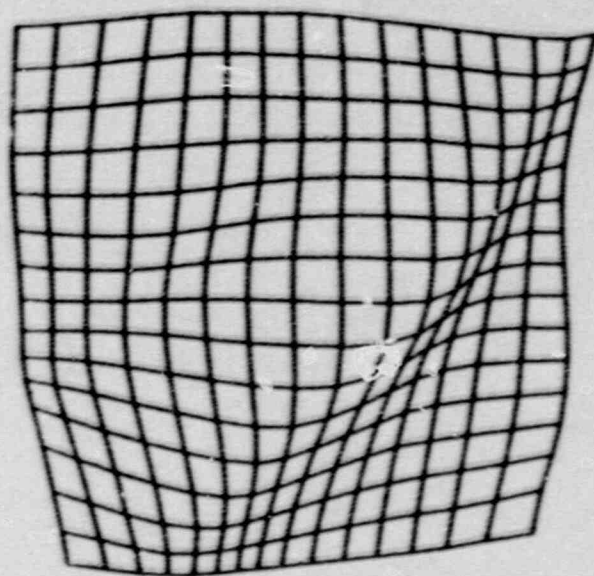


c

Fig. 5-3. Loading for stress calculation in the Southern Appalachians. Contouring interval is 5 MPa. (a) Surface load. (b) Load at upper-lower crustal boundary, $z=20$ km. (c) Load at the Moho, $z=40$ km.



a



b

Fig. 5-4. Local stress field of the Southern Appalachian area at 10 km depth. The unit of stress is in MPa. (a) The coordinates of the study area. (b) Deformation shows the direction of local horizontal stress field.

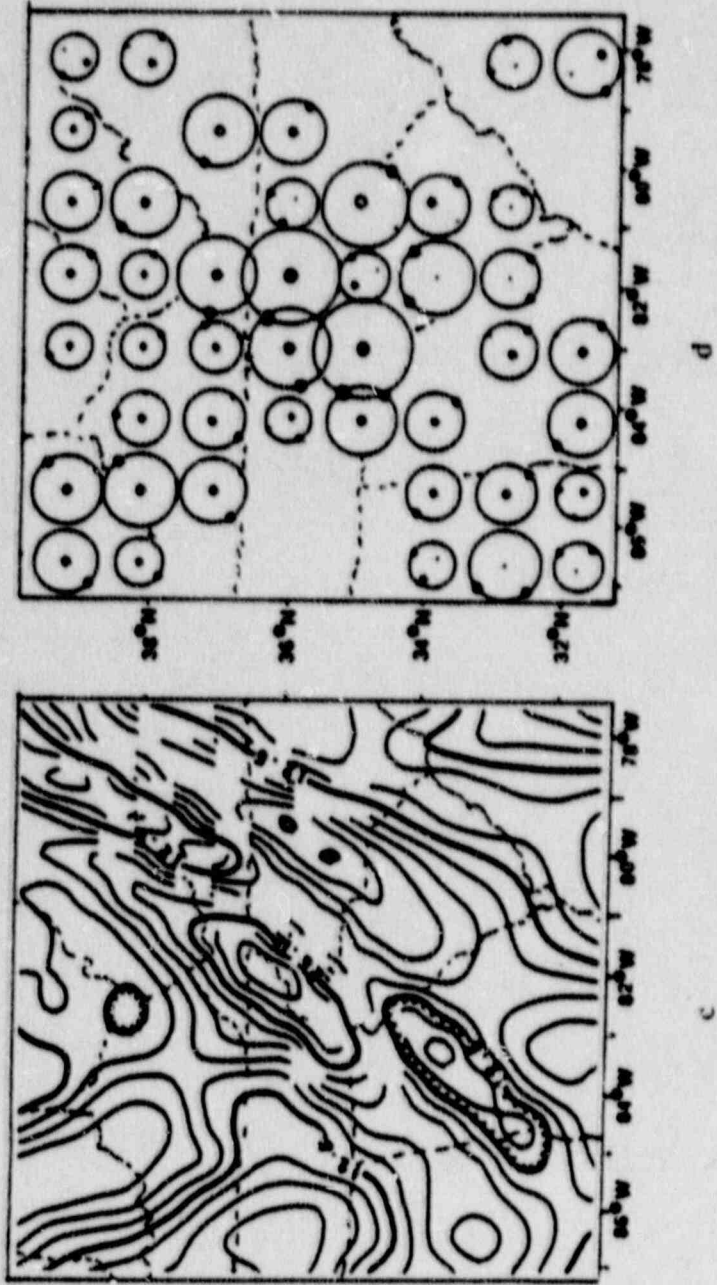


Fig. 5-4-c. Stress difference contours (SDC). The contour interval is 2.5 MPa.
 (d) SNPPSA.

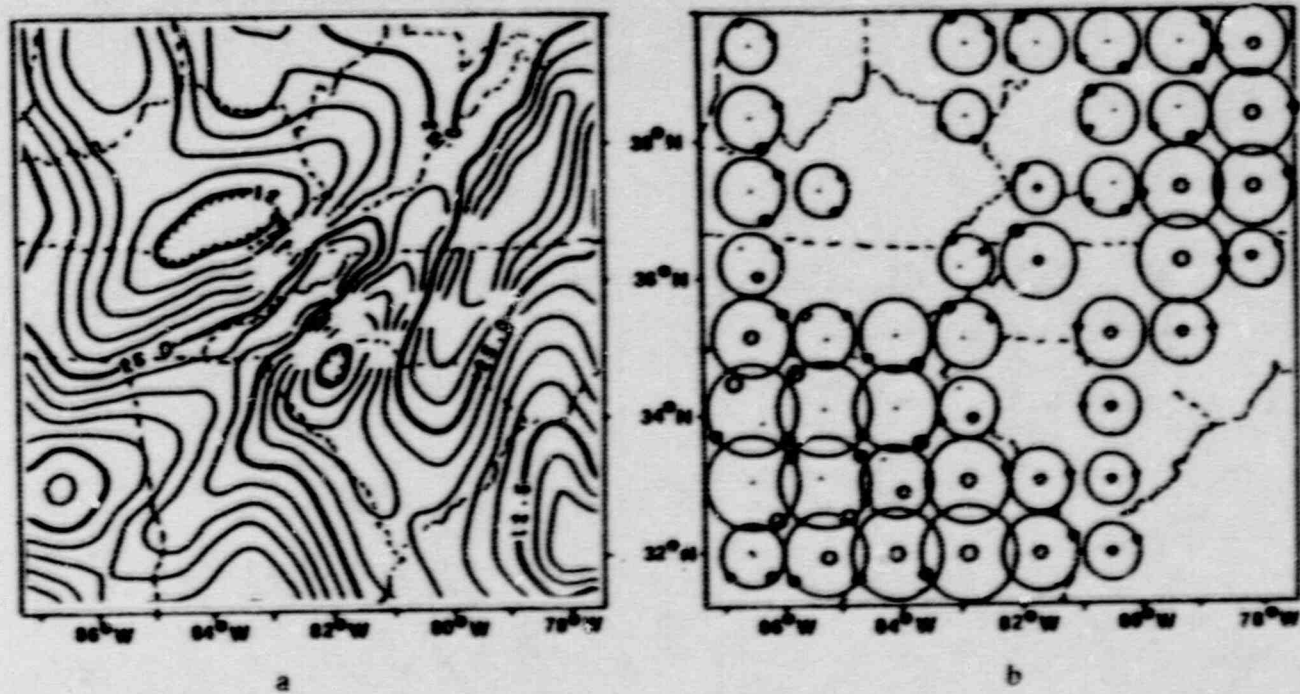


Fig. 5-5. The total stress field which combines the local field (Fig. 5-4) with a 20 MPa N60°E regional horizontal compression. (a) SDC. The contour interval is 2.5 MPa. (b) SNPPSA.

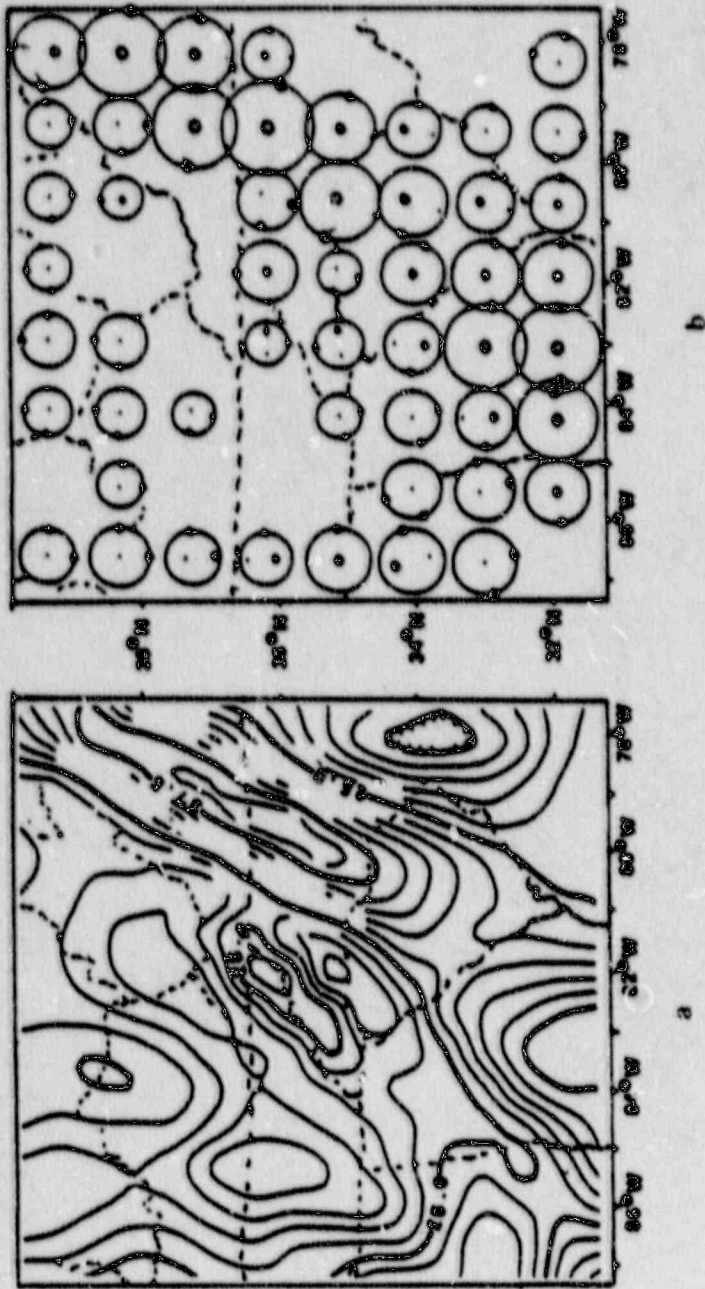


Fig. 5-6. The total stress field which combines the local field (FIG.5-4) with a 20 MPa East-West regional horizontal compression. (a) SIC. The contour interval is 2.5 MPa. (b) SNPPSA.

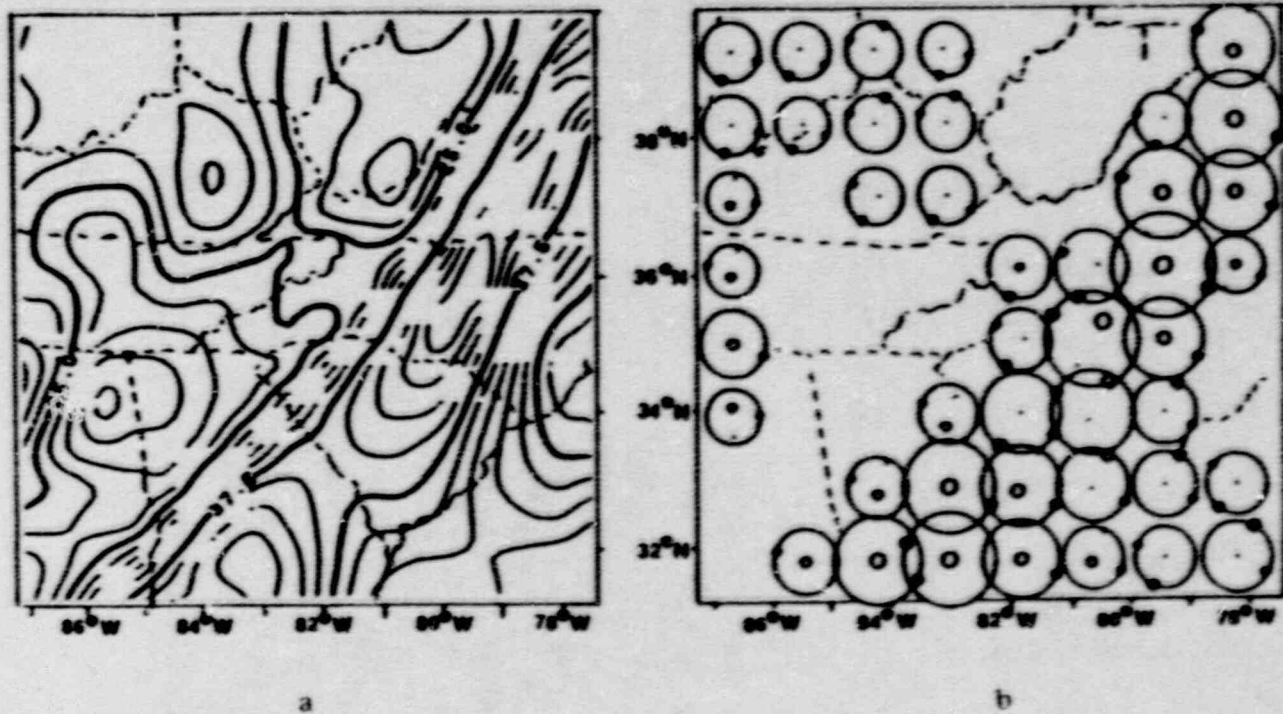
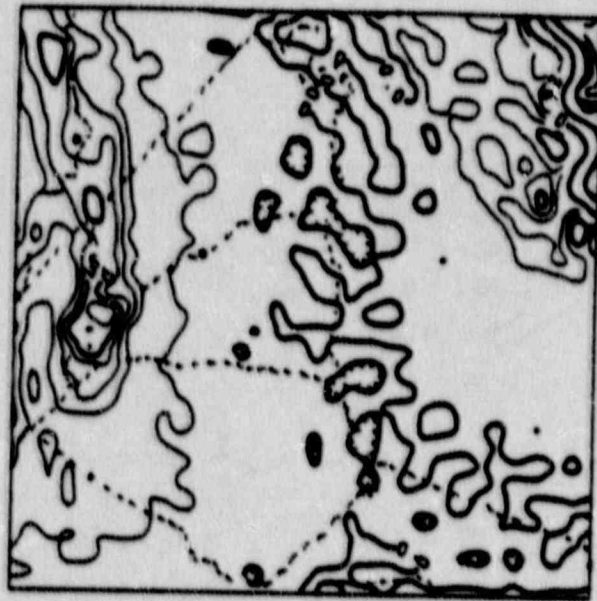
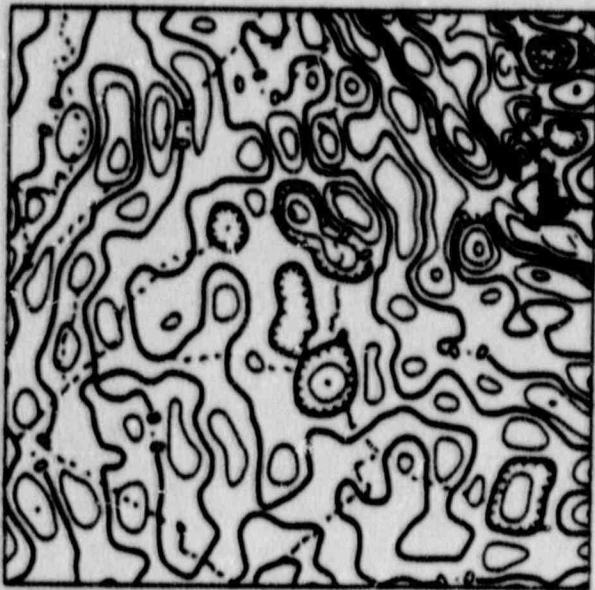


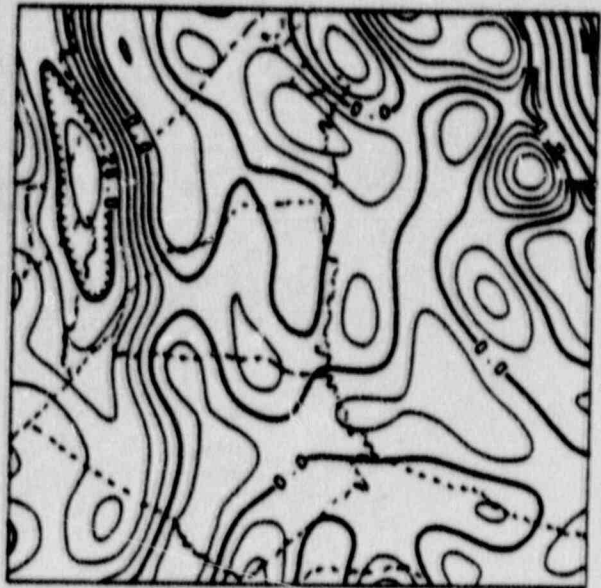
Fig. 5-7. The total stress field which combines the local field (Fig.5-4) with a 20 MPa S75°E regional horizontal compression. (a) SDC. The contour interval is 2.5 MPa. (b) SNPPSA.



a



b



c

Fig. 5-8. Loading for stress calculation in the Coastal Plain and continental margin. Contouring interval is 5 MPa. (a) Load at the surface. (b) Load at the upper-lower crustal boundary, $z=15$ km. (c) Load at the Moho, $z=30$ km.

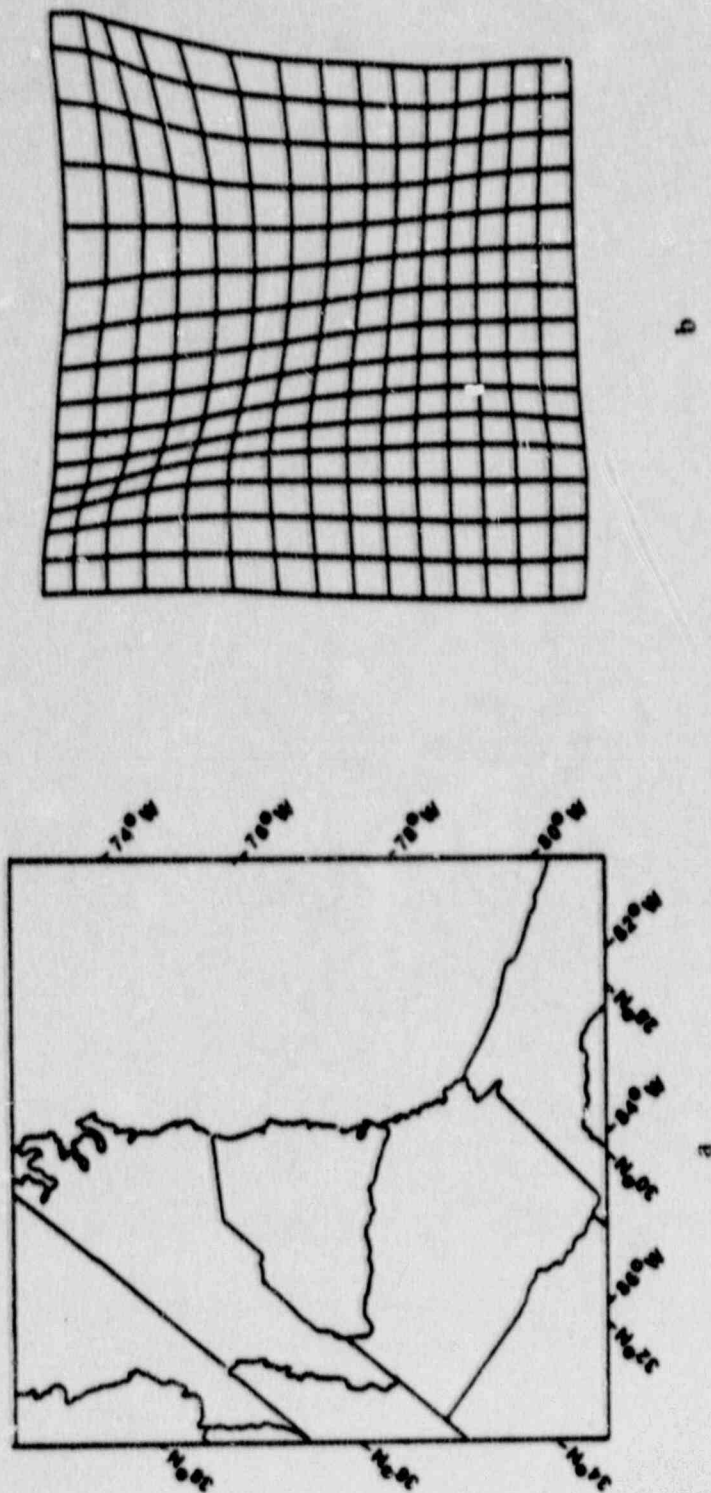


Fig. 5-9. Local stress field of the Coastal Plain and continental margin at 10 km depth. The unit of stress is in MPa. (a) Coordinates of the study area. (b) Deformation shows the direction of local horizontal stress field.

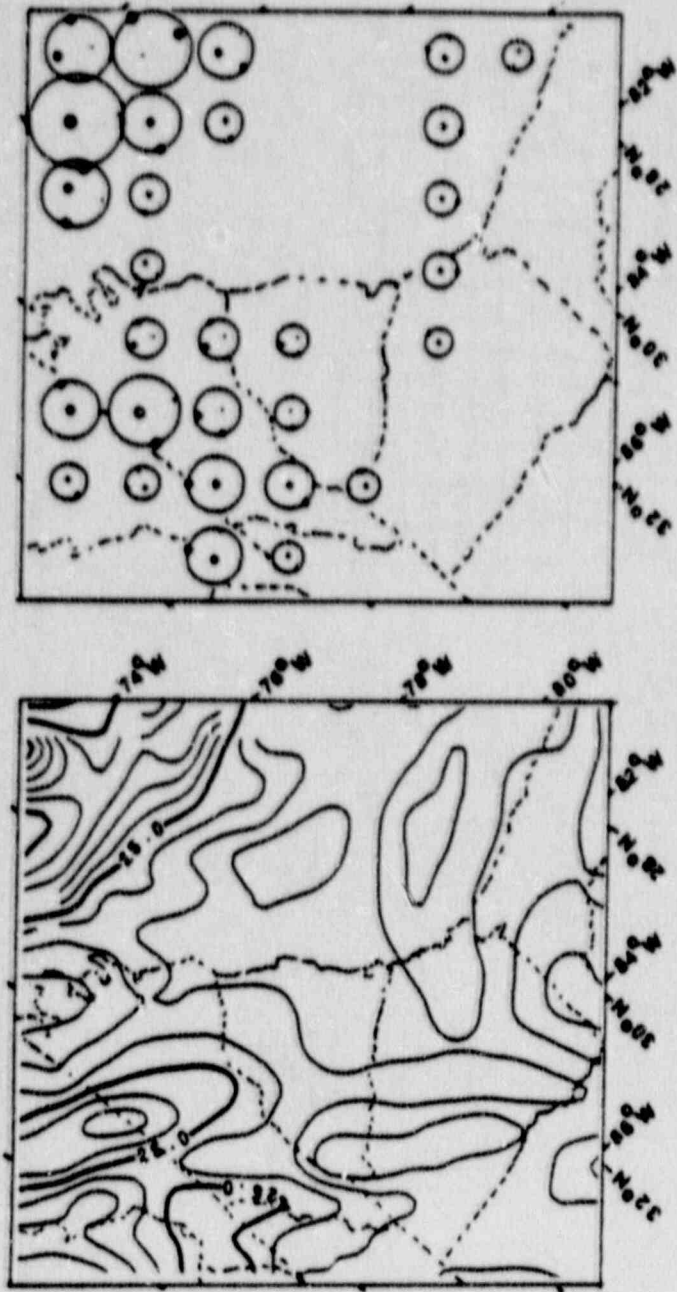


Fig. 5-9. (c) Stress difference contours (SDC). The contour interval is 5.0 MPa. (d) SNPPSA.

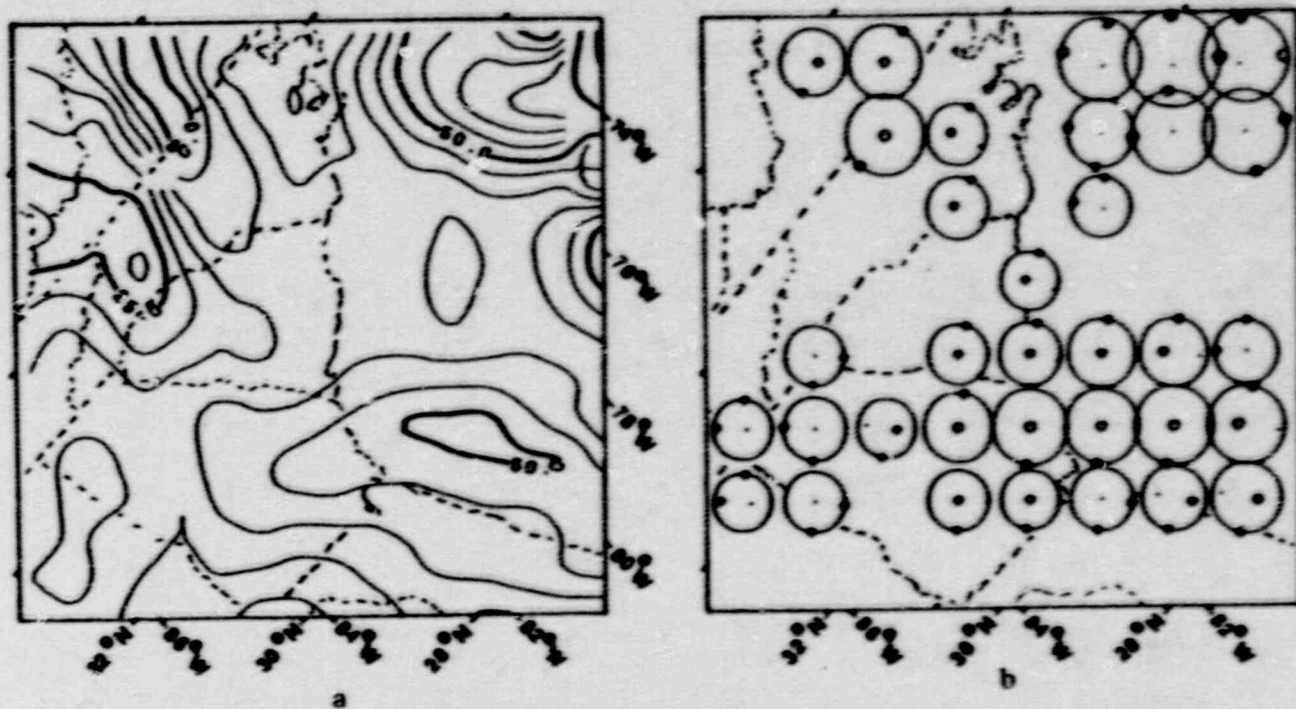


Fig. 5-10. The total stress field which combines the local field (Fig.5-9) with a 30 MPa N60°E regional horizontal compression. (a) SDC. The contour interval is 5.0 MPa. (b) SNPPSA.

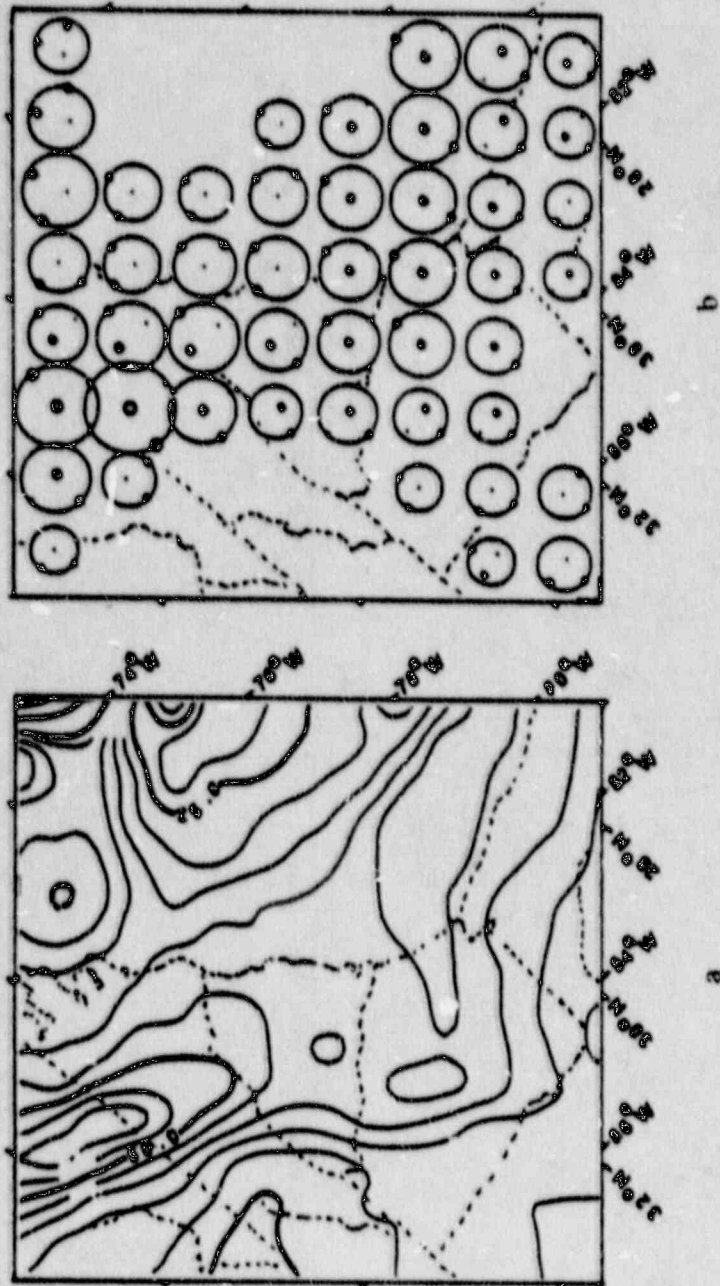


Fig. 5-11. The total stress field which combines the local field (Fig. 5-9) with a 30 MPa East-West regional horizontal compression. (a) SDC. The contour interval is 5.0 MPa. (b) SNPPSA.

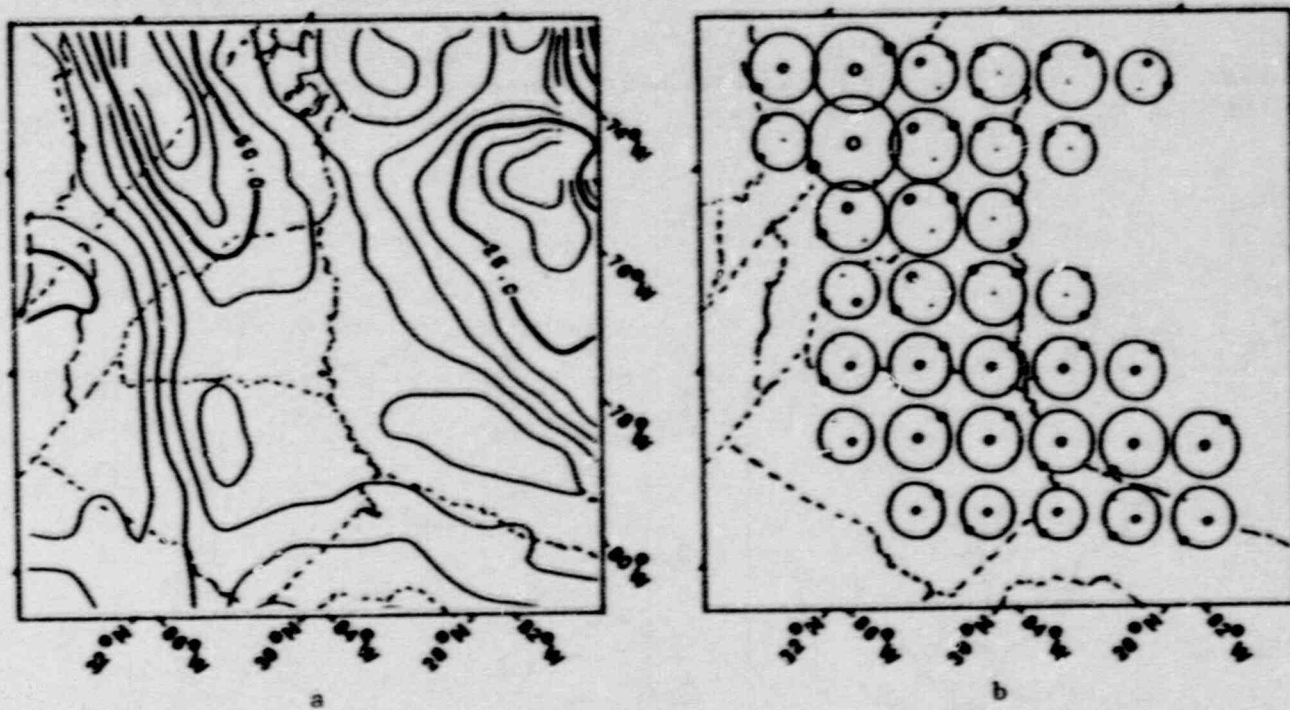


Fig. 5-12. The total stress field which combines the local field (Fig. 5-9) with a 30 MPa S80°E regional horizontal compression. (a) SDC. The contour interval is 5.0 MPa. (b) SNPPSA.

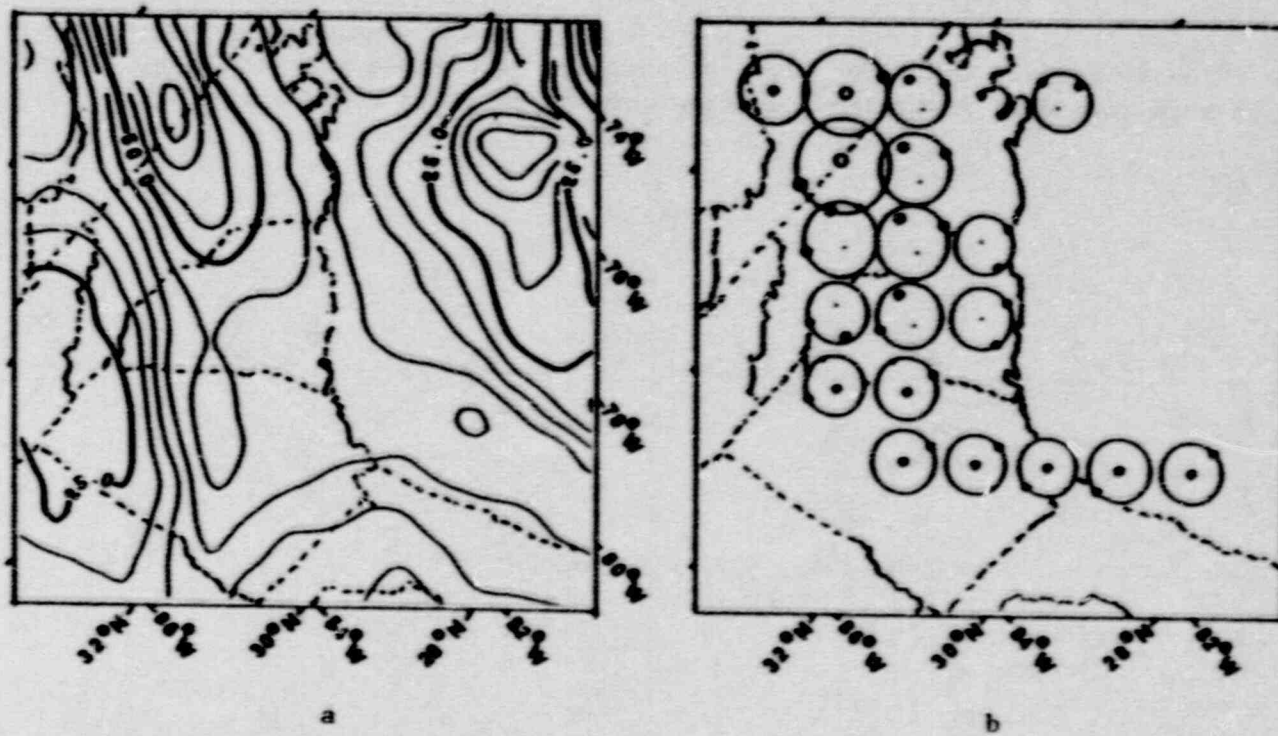


Fig. 5-13. The total stress field which combines the local field (Fig.5-9) with a 30 MPa S70°E regional horizontal compression. (a) SDC. The contour interval is 5.0 MPa. (b) SNPPSA.

BIBLIOGRAPHY

- Angelier, J., Determination of the mean principal directions of stresses for a given fault population, *Tectonophysics*, 56, T17-26, 1979.
- Artem'jev, M.E., V.I. Pune, V.A. Dubrovski and N.S. Kambarov, Seismicity and isostasy, *Phys. Earth Planet. Int.*, 6, 256-262, 1972.
- Artyushkov, E.V., Stresses in the lithosphere caused by crustal thickness inhomogeneities, *J. Geophys. Res.*, 78, 7675-7708, 1973.
- Artyushkov, E.V., Can the earth's crust be in a state of isostasy, *J. Geophys. Res.*, 79, 741-752, 1974.
- Barosh, P.J., Neotectonic movement, earthquakes and stress state in the eastern United States, *Tectonophysics*, 132, 117-152, 1986.
- Behrendt J.C., R.M. Hamilton, H.D. Ackerman and V.J. Henry, Cenozoic reactivation of faulting in the vicinity of the Charleston, S.C., 1886 earthquake, *Geology*, 9, 117-122, 1981.
- Billings, M.P., *Structural Geology*, Third Edition, Prentice-Hall Inc., 1972.
- Bird, J. and J. Dewey, Lithosphere plate continental margin tectonics and the evolution of the Appalachian Orogen, *Geol. Soc. Am. Bull.*, 81, 1031-1059, 1970.
- Bollinger, G.A., Seismicity of the southeastern United State, *Bull. Seis. Soc. Amer.*, 63, 1785-1808, 1973.
- Bollinger, G.A., and Visvanathan, T.R., The seismicity of South Carolina prior to 1886, U.S. Geol. Surv. Prof. Paper 1028-c, 33-42, 1977.
- Bott, M.H.P., and D.S. Dean, Stress at young continental margins, *Nature*, 235, 23-25, 1972.
- Bott, M.H.P., *The Interior of the Earth*, Elsevier Science, 1982.
- Bott, M.H.P., and N.J. Kusznir, The origin of tectonic stress in the lithosphere, *Tectonophysics*, 105, 1-13, 1984.

- Braile, L.W., G.R. Keller, W.J. Hinze and E.G. Lidiak, An ancient rift complex and its relation to contemporary seismicity in the New Madrid Seismic zone, *Tectonics*, 1, 225-237, 1982.
- Braile, L.W., W.J. Hinze and G.R. Keller, Tectonic development of the New Madrid rift complex, Mississippi Embayment, North America, *Tectonics*, 131, 1-213, 1986.
- Byerlee, J., Friction of rocks, *Pure and Applied Geophysics*, 116, 615-626, 1978.
- Campbell, D.L., Investigations of the stress concentration mechanism for intraplate earthquakes, *Geophy. Res. Letters*, 5, 477-479, 1978.
- Colquhoun, D.J. and H.S. Johnson Jr., Tertiary sea-level fluctuation in South Carolina, *Palaeogeography, Palaeoclimatology, Palaeoecology*, 5, 105-126, 1968.
- Colton G.W., The Appalachian Basin-its depositional sequence and their geologic relationships, in *Studies of Appalachian Geology*, edited by Fisher, G.W., F.J. Pettijohn, J.C. Reed Jr. and K.N. Weaver, 1970.
- Condie, K.C., *Plate Tectonics and Crustal evolution*, Pergaman Press, 1982.
- Cook, F.A., D.S. Alrough, L.D. Brown., S. Kaufman, J.E. Oliver, and R. D., Jr. Hatcher, Thin-skinned tectonics. In the crystalline Southern Appalachians-COCORP seismic-refraction profiling of the Blue Ridge and Piedmont, *Geology*, 7, 563-567, 1979.
- Cook, F.A., L.D. Brown, and J.E. Oliver, The Southern Appalachians and the growth of continents, *Scientific American*, 243, 156-168, 1980.
- Cook, F.A., L.D. Brown, S. Kaufman and J.E. Oliver, The COCORP Seismic Reflection Traverse Across the Southern Appalachians, AAPG Studies in Geology, 14, 1983.
- Denham, D., The Tasman Sea earthquake of 25 November 1983 and stress in the Australian Plate, *Tectonics*, 111, 329-338, 1985.
- Dewey, J.W. and W. Kidd, Continental collision of the Appalachians Caledonian orogenic belt, *Geology*, 2, 543-546, 1974.
- Dewey, J.W., A Global Search of Continental Midplate Seismic Regions for Specific Characteristics Bearing on the 1886 Charleston, South Carolina Earthquake, U. S. G. S. Open File Report, 83-843, 391- 426, 1983.
- Erving, C.P. and L.D. McGinnis, Reelfoot Rift: reactivated precursor to the Mississippi Embayment, *Geol. Soc. Am. Bull.*, 86, 1287-1295, 1975.

- Fleitout, L., and C. Froidevaux, Tectonics and topography for a lithosphere containing density heterogeneities, *Tectonics*, 1, 21-56, 1982.
- Fleitout, L., and C. Froidevaux, tectonic stress in the lithosphere, *Tectonics*, 2, 315-324, 1983.
- Grow, J.A., The Atlantic margin of United States. In: *Geology of Passive Continental Margins*, AAPG Eastern Section Meeting and Atlantic Margin Energy Conference, 1981.
- Guinn, S.A., Earthquake Focal Mechanisms in the Southeastern United States, U. S. Nuclear Regulatory Commission Report, NUREG/RG-1503, Washington D.C., 1980.
- Hadley, J.B. and J.F. Devine, Seismotectonic map of the eastern United States, *U.S. Geol. Surv. map, MF-620*, 1974.
- Haskell, N.A., The motion of a viscous fluid under a surface load, Part 1, *Physics*, 6, 235-269, 1935.
- Haskell, N.A., The motion of a viscous fluid under a surface load, Part 2, *Physics*, 7, 56-61, 1936.
- Hatcher, R.D., Jr., Tectonics of the western Piedmont and Blue Ridge, Southern Appalachians: review and speculation, *American J. Sci.*, 278, 276-304, 1978.
- Hatcher, R.D., Jr. and I. Zietz, Tectonic implications of regional aeromagnetic and gravity data from the Southern Appalachians: International Geological Correlation Program-Caledonide Orogen Project Symposium, edited by Wones, D., 235-244, 1980.
- Hutchinson, D.R., J. A. Grow, and K.D. Klitgord, Crustal structure beneath the Southern Appalachians: nonuniqueness of gravity modeling, *Geology*, 11, 611-615, 1983-a.
- Hutchinson, D.R., J.A. Grow, K.D. Klitgord and B.A. Swift, Deep structure and evolution of the Carolina Trough, *AAPG Memo.*, 34, 129-152, 1983-b.
- Illies, J.H., Recent and paleo-intraplate tectonics in stable Europe and the Rhinegraben rift system, *Tectonophysics*, 29, 251-264, 1975.
- Isacks, B., J. Oliver, and L.R. Sykes, Seismology and the new global tectonics, *J. Geophys. Res.*, 73, 5855-5899, 1968.
- Jeffreys, H., *The Earth*, 2nd ed., Cambridge University, 1929.
- Johnston, A.C., D.J. Reinbold and S.J. Brewer, Seismotectonics of the Southern Appalachians, *Bull. Seism. Soc. Am.*, 75, 291-312, 1985.

- Kane, M.F., Correlation of major earthquake centers with mafic/ultramafic basement masses, *U.S. Geol. Survey Prof. Paper 1028-o*, 199-204, 1977.
- Kean, A.E. and L.T. Long, A seismic refraction line along the axis of the southern Piedmont and crustal thicknesses in the southern United States, *Earthquake Notes*, 51, 4, 3-13., 1980.
- King, E.R., and I. Zietz, the New York-Alabama lineament: geophysical evidence for a major crustal break in the basement beneath the Appalachian basin, *Geology*, 6, 312-318, 1978.
- Kirby, S.H., Tectonic stresses in the lithosphere constrains provided by the experimental deformation, *J. Geophys. Res.*, 85, 6336-6363, 1980.
- Kuo, J.T., Static response of a multilayered medium under inclined surface load, *J. Geophys. Res.*, 74, 3195-3207, 1969.
- Lago, B., and A. Cazenave, State of stress in the oceanic lithosphere in response to loading, *Geophys. J. Roy. Astr. Soc.*, 64, 785-799, 1981.
- Lama, R.D. and V.S. Vutukuri, *Handbook on Mechanical Properties of Rocks*, Vol. II, 1978.
- Lambeck, K, and S.M. Nakiboglu, Seamount loading and stress in the ocean lithosphere, *J. Geophys. Res.*, 85, 6403-6418, 1980.
- Lee, C.K., A study of the crustal structure of north central Georgia and South Carolina by analysis of synthetic seismograms, Master's Thesis, Georgia Inst. Tech., Atlanta, GA, 1980.
- Lee, W.H.K., F.T. Wu and S.C. Wang, A catalog of instrumentally determined earthquakes in China (Magnitude ≥ 6) compiled from various sources, *Bull. Seis. Soc. Am.*, 86, 383-398, 1978.
- Lomnitz, C., *Global Tectonics and Earthquake Risk*, Elsevier Science, 1974.
- Long, L.T., Speculations concerning southeastern earthquakes, mafic intrusions, gravity anomalies, and stress amplification. *Earthquake Notes*, 47, No. 4, 29-35, 1976.
- Long, L.T. and J.W. Champion, Jr., Bouguer gravity map of the Summerville-Charleston, South Carolina, epicentral zone and tectonic implications, U.S. Geol. Surv. Prof. Paper 1028-k, 151-166, 1977.
- Long, L.T. and J.S. Liow, Crustal thickness, velocity structure and the isostatic response function in the Southern Appalachians, in *Reflection Seismology: the Continental Crust*, edited by M. Barazangi and L. Brown, AGU, Washington, D.C., 1986(a).

- Long, L.T., J.S. Liow, A. Tie and K.H. Zelt, Seismicity and crustal structure in southeastern Tennessee (Abstract), *EOS Transactions Am. Geophys. Union*, 67, 314, 1986(b).
- McGarr, A., and N.C. Gay, State of stress in the earth's crust, *Ann. Rev. Earth Planet. Sci.* 6, 405-436, 1978.
- McKenzie, D.P., The relationship between fault plane solution for earthquakes and the directions of principal stresses, *Bull. Seis. Soc. Amer.*, 59, 591-601, 1969.
- McKenzie, D.P., Convection in the earth's mantle, *Tectonics*, 12, 267-168, 1972.
- McNutt, M.K., Implications of regional gravity for state of stress in the earth's crust and upper mantle, *J. Geophys. Res.*, 85, 6377-6396, 1980.
- Mareschal, J.C. and J. Kuang, Intraplate stresses and seismicity: the role of topography and density heterogeneities, *Tectonophysics*, 132, 153-162, 1986.
- Marine, I.W. and G.E. Siple, Buried Triassic basin in the central Savannah River area, South Carolina and Georgia, *Bull. Geol. Soc. Am.*, 85, 311-320, 1974.
- Meissner, R. and J. Strenhlau, Limits of stresses in continental crusts and their relation to the depth-frequency distribution of shallow earthquakes, *Tectonics*, 1, 73-89, 1982.
- Mendiguren, J. and F.M. Richter, On the origin of compressional intraplate stress in South America, *Phys. Earth Planet. Int.*, 16, 1978.
- Munsey, J.W., Focal mechanism analysis for recent (1978-1984) Virginia earthquakes, Master's Thesis, Virginia Poly. Inst., 1984.
- Ngoddy, A., Crustal Thickness Across the Southern Appalachians, Master's Thesis, Georgia Inst. Tech., Atlanta, GA, 1985.
- Nuttli, O.W., The Mississippi Valley earthquakes of 1811 and 1812: intensities, ground motion and magnitude, *Bull. Seism. Soc. Am.*, 63, 227-248, 1973.
- Obermeier, S.F., G.S. Gohn, R.E. Weems, R.E. Gelinas, and M. Rubin, Geologic evidence for recurrent moderate to large earthquakes near Charleston, South Carolina, *Science*, 227, 408-411, 1985.
- Propes, R.L., Crustal velocity in the Southern Appalachians, *Master's thesis, Georgia Inst. Tech., Atlanta, GA, 1985.*
- Prowell, D.C. and B.J. O'Connor, Belair fault zone: evidence of Tertiary fault displacement in eastern Georgia, *Geology*, 6, 681-684, 1978.

- Raleigh, C.B., J.H. Healy and J.D. Bredehoeft, Faulting and crustal stress at Rangely, Colorado, in *Flow and Fracture of Rocks*, Geophys. Monogr. Ser., vol. 16, edited by H. C. Heard, et al., 275-284, AGU, Washington, D. C., 1972.
- Raleigh, C.B., Crustal stress and global tectonics, In: *Advances in Rock Mechanics*, Proceedings of the 3rd Congress, International Society of Rock Mechanics, vol. IA, 593-597, National Academy of Sciences, Washinton D. C., 1974.
- Rankin, D.W., Appalachian salients and recesses: Late Precambrian continental breakup and the opening of the Iapetus Ocean, *J. Geophys. Res.*, **81**, 5605-5516, 1976.
- Rankin, D.W., Studies related to the Charleston, South Carolina, earthquake of 1886-introduction of discussion, U.S. Geol. Survey Prof. Paper 1028-a, 1-15, 1977.
- Rich, J., Mechanics of low-angle overthrust faulting as illustrated by Cumberland overthrust block, Virginia, Kentucky and Tennessee, *Am. Assoc. Petro. Geol.*, **18**, 1584-1596, 1934.
- Richardson, R.M., S.C. Solomon, and N.H. Sleep, Tectonic stress in the plates, *Rev. Geophys. Space Physics*, **17**, 981-1019, 1979.
- Rodgers, J., Evolution of thought on structure of middle and Southern Appalachians. *Am. Assoc. Petro. Geol. Bull.*, **33**, 1643-1653, 1949.
- Ross, C., Late Paleozoic collision of North and South America, *Geology*, **7**, 41-44, 1979.
- Savage, W.Z., and H.S. Swolfs, Tectonic and gravitational stress in long symmetric ridges and valleys, *J. Geophys. Res.*, **91**, 3673-3685, 1986.
- Sbar, M.L. and L.R. Sykes, Contemporary compressive stress and seismicity in eastern North America: an example of intraplate tectonics, *Bull. Geol. Soc. Am.*, **84**, 1861-1882, 1973.
- Schubert, G. and A. Yuen, Mantle circulation with partial shallow return flow: effects on stresses in oceanic plates and topography of the sea floor, *J. Geophys. Res.*, **83**, 745-765, 1978.
- Sneddon, I.N., *Fourier Transforms*, McGraw-Hill Co., 1951.
- Solomon S.C., R.M. Richardson, E.A. Bergman, Tectonic stress: models and magnitudes, *J. Geophy. Res.*, **85**, 6086-6092, 1980.
- Sykes, L.R. Mechanism of earthquakes and nature of faulting on the midocean ridge, *J. Geophys. Res.*, **72**, 2131-2152, 1967.

- Sykes, L.R., Intraplate seismicity, reactivation of preexisting zones of weakness, alkaline magmatism, and other tectonism postdating continental fragmentation, *Rev. Geophys. Space. Phys.*, 16, 621-688, 1978.
- Talwani, P., An internally consistent pattern of seismicity near Charleston, South Carolina, *Geology*, 10, 654-658, 1982.
- Tarr, A.C., Recent seismicity near Charleston, South Carolina, and its relationship to the August 31, 1886, earthquake, U.S. Geol. Survey Prof. Paper 1028-d, 43-57, 1977.
- Taylor, S.R. and M.N. Toksoz, Crust and upper-mantle velocity structure in the Appalachian Orogenic belt: implication for tectonic evolutions, *Geol. Soc. Am. Bull.*, 93, 315-329, 1982.
- Teague, A., Focal mechanisms for eastern Tennessee earthquakes, 1981-1983, Master's Thesis, Virginia Poly. Inst., 1984.
- Timoshenko, S.P. and J.N. Goodier, *Theory of Elasticity*, McGraw-Hill Co., 1970.
- Turcotte, D.L., Membrane tectonics, *Geophys. J. Roy. Astron. Soc.*, 36, 33-42, 1974
- Turcotte, D.L. and Oxburgh, E. R., Stress accumulation in the lithosphere, *Tectonophysics.*, 35, 183-199, 1976.
- Walcott, R.I., Flexure rigidity, thickness and viscosity of the lithosphere, *J. Geophys. Res.*, 75, 3941-3954, 1970.
- Walcott, R.I., Late Quaternary vertical measurements in eastern North America: quantitative evidence of glacio-isostatic rebound. *Rev. Geophys. Space Phys.* 10, 894, 1972.
- Warren, D.H., Transcontinental geophysical survey (35°-39°N) seismic refraction profiles of the crust and upper mantle, U.S. Geol. Survey, Map I-535-D, 1968.
- Watkins, J.S., Regional geologic implications of the gravity and magnetic field of a part of eastern Tennessee and southern Kentucky, U. S. Geol. Surv. Prof. Paper, 516A, 1964.
- Watts, A.B. and J.R. Cochran, Gravity anomalies and flexure of the lithosphere along the Hawaiian emperor seamount chain, *Geophys. J. Roy. Astr. Soc.*, 38, 119-141, 1974.
- Wentworth, C.W. and M. Merguer-Keefe, Reverse faulting along the eastern seaboard and the potential for large earthquakes, *Earthquakes and Earthquake Eng. the Eastern United States*, 1, 109-128, 1981.

Zoback, M.L. and M.D. Zoback, State of stress in the conterminous United States, *J. Geophys. Res.*, 85, 6113-6156, 1980.

Zoback, M.D., Intraplate earthquakes, crustal deformation and in situ stress, U.S. Geol. Surv. Open-file Report 83-843, 169-178, 1983.

Zelt, K-H. and L.T. Long, Focal mechanisms of north Georgia and southeastern Tennessee earthquakes (1982-1987), (Abstract), SSA Eastern Section, St. Louis, Oct, 1987.

NRC FORM 308 (2-84) NRCM 1102, 3201, 3202		U.S. NUCLEAR REGULATORY COMMISSION	1. REPORT NUMBER (Assigned by TRS, add Vol. No., if any)
BIBLIOGRAPHIC DATA SHEET		NUREG/CR-5269	
2. TITLE AND SUBTITLE			3. LEAVE BLANK
Evaluation of Hypotheses for the Cause of the 1886 Charleston Earthquake			4. DATE REPORT COMPLETED
5. AUTHOR(S)			MONTH YEAR
			May 1989
R. M. White L. T. Long			6. DATE REPORT ISSUED
			MONTH YEAR
7. PERFORMING ORGANIZATION NAME AND MAILING ADDRESS (Include Zip Code)			8. PROJECT/TASK/WORK UNIT NUMBER
Law Environmental, Inc Subcontractor: 112 Townpark Drive Georgia Institute of Kennesaw, GA 30144 Technology Atlanta, GA 30332			9. PIN OR GRANT NUMBER
			B8291
10. SPONSORING ORGANIZATION NAME AND MAILING ADDRESS (Include Zip Code)			11a. TYPE OF REPORT
Division of Engineering Office of Nuclear Regulatory Research U.S. Nuclear Regulatory Commission Washington, DC 20555			Final
			b. PERIOD COVERED (Include Dates)
			November 1984-May 1989
12. SUPPLEMENTARY NOTES			
13. ABSTRACT (200 words or less)			
<p>This report describes a geophysical/geological investigation in the Charleston, South Carolina, area for the purpose of narrowing the range of theories used to explain the 1886 Charleston earthquake. A comprehensive data set was established by combining existing and new gravity, magnetic and topographic data with seismic, geologic and drilling data. A magnetotelluric survey consisting of 12 soundings, interpreted to depths of over 40 kilometers, was also acquired.</p> <p>A geologic model of the crust in the Charleston area was constructed to define the locations of Triassic/Jurassic basins and Paleozoic plutons in greater detail than has previously been achieved. Three-dimensional regional crustal stress modeling and two-dimensional local stress modeling based on the geologic model were used to analyze earthquake hypotheses. The results of this study strongly support the intersections of Mesozoic basin border faults, whose locations may have been controlled by Paleozoic mafic plutons, as the most likely location for Charleston-type earthquakes. The study infers that the spatial association of seismicity with plutons in the Charleston area may be due to the plutons' role in controlling the location of faults rather than due to stress amplification.</p>			
14. DOCUMENT ANALYSIS -- KEYWORDS/DESCRIPTORS			15. AVAILABILITY STATEMENT
Seismicity Stress Model Tectonics Charleston Crustal Model South Carolina			Unlimited
b. IDENTIFIERS/OPEN-ENDED TERMS			16. SECURITY CLASSIFICATION
			(This page)
			Unclassified
			(This report)
			Unclassified
			17. NUMBER OF PAGES
			18. PRICE

UNITED STATES
NUCLEAR REGULATORY COMMISSION
WASHINGTON, D.C. 20555

OFFICIAL BUSINESS
PENALTY FOR PRIVATE USE, \$300

SPECIAL FOURTH-CLASS RATE
POSTAGE & FEES PAID
USNRC
PERMIT No. G-67

120555139531 1 1AN1RA
US NPC-OADM
DIV FOIA PUBLICATIONS SVCS
TPS PDR-NUREG
P-209
WASHINGTON DC 20555